

C. MØLLER

RELATIVISTIC THERMODYNAMICS

A Strange Incident in the History of Physics

Det Kongelige Danske Videnskabernes Selskab
Matematisk-fysiske Meddelelser 36, 1



Kommissionær: Munksgaard
København 1967

Synopsis

In view of the confusion which has arisen in the later years regarding the correct formulation of relativistic thermodynamics, the case of arbitrary reversible and irreversible thermodynamic processes in a fluid is reconsidered from the point of view of observers in different systems of inertia. Although the total momentum and energy of the fluid do not transform as the components of a 4-vector in this case, it is shown that the momentum and energy of the heat supplied in any process form a 4-vector. For *reversible* processes this four-momentum of supplied heat is shown to be proportional to the four-velocity of the matter, which leads to Ott's transformation formula for the temperature in contrast to the old formula of Planck.

Introduction

In the years following Einstein's fundamental paper from 1905, in which he founded the theory of relativity, physicists were engaged in reformulating the classical laws of physics in order to bring them in accordance with the (special) principle of relativity. According to this principle the fundamental laws of physics must have the same form in all Lorentz systems of coordinates or, more precisely, they must be expressed by equations which are form-invariant under Lorentz transformations. In some cases, like in the case of Maxwell's equations, these laws had already the appropriate form, in other cases, they had to be slightly changed in order to make them covariant under Lorentz transformations. This was, for instance, the case with Newton's equations of mechanics which turned out to hold only for phenomena in which the velocities of the particles are sufficiently small with respect to c the velocity of light.

An investigation of the laws of thermodynamics in relation to the relativity principle was carried through by M. PLANCK and others⁽¹⁾ in the years 1907–1908. In all cases the procedure was the following. One starts by assuming that the usual two laws of thermodynamics hold in the rest system of the body concerned. Then one tries to formulate transformation laws for the transferred heat, the entropy, and the temperature in such a way that the usual laws of thermodynamics are valid also for the transformed quantities belonging to an arbitrary system of inertia. If this should turn out not to be possible, one would have to admit that the classical laws of thermodynamics are not generally valid and one would have to modify them similarly as in the case of Newtonian mechanics. However, such a modification of the classical thermodynamical laws is not necessary.

Let us consider a thermodynamic body in thermal equilibrium at rest in a certain system of inertia \mathfrak{K}^0 . Throughout this paper we shall consider only thermodynamic equilibrium states and (reversible or irreversible) transitions between such equilibrium states. According to the *first law of thermodynamics*, the total energy H^0 in \mathfrak{K}^0 is a unique function of the thermo-

dynamical state of the body. In a process which gives rise to a change of the state, the change ΔH^0 in the energy is given by

$$\Delta H^0 = \Delta Q^0 + \Delta A^0, \quad (1)$$

where ΔQ^0 is the amount of heat transferred to the system in the process and ΔA_0 is the mechanical* work performed on the system by its surroundings, all measured in the rest system \mathfrak{K}^0 of the body in question. Further, according to *the second law of thermodynamics*, the entropy S^0 in the rest system \mathfrak{K}^0 is similarly a function of the thermodynamical state. The change of entropy content by an infinitesimal change of the state is (by definition)

$$dS^0 = \frac{dQ_{\text{rev}}^0}{T^0} = \frac{dH^0 - dA_{\text{rev}}^0}{T^0}, \quad (2)$$

where dQ_{rev}^0 and dA_{rev}^0 represent the amount of heat and the mechanical work, respectively, in a *reversible* process which brings about the change of the state considered, and T^0 is the Kelvin temperature of the system.

Now, consider the same thermodynamical process from the point of view of an observer in a system of inertia \mathfrak{K} with respect to which the body in question moves with the constant velocity \mathbf{v} . Then, on account of the relativity principle, we should have the same relations (1) and (2) between the increases of the energy H , the entropy S , and the transferred heat and mechanical work measured in \mathfrak{K} , i.e.,

$$\Delta H = \Delta Q + \Delta A \quad (3)$$

$$dS = \frac{dQ_{\text{rev}}}{T} = \frac{dH - dA_{\text{rev}}}{T}. \quad (4)$$

The transformation equations for ΔE and ΔA are known from relativistic mechanics. From (3) and (1) we therefore obtain the transformation law for the transferred heat ΔQ . In this way, Planck found the formula

$$\Delta Q = \Delta Q^0 \sqrt{1 - \beta^2}, \quad \beta = \frac{v}{c}. \quad (5)$$

Further he showed that the entropy of a body in thermal equilibrium is a relativistic invariant.

* The word mechanical should not be taken literally, it could also be the work of electromagnetic forces originating from sources in the surroundings.

In order to see this, let us consider a body in some internal equilibrium state which originally is at rest in \mathfrak{K} with an entropy S . If this body is accelerated adiabatically, i.e., infinitely slowly and without heat transfer until it gets the velocity \mathbf{v} , then its internal state is undisturbed and, on account of (4), it has still the same entropy S as before with respect to \mathfrak{K} . On the other hand, it is now with respect to \mathfrak{K}^0 in the same situation as it were initially with respect to \mathfrak{K} . Its entropy S^0 in \mathfrak{K}^0 must therefore be equal to S , i.e. the entropy

$$S = S^0 \quad (6)$$

is a relativistic invariant. From the equations (2)–(6) Planck concluded that the temperature of a body transforms according to the equation

$$T = T^0 \sqrt{1 - \beta^2}. \quad (7)$$

This result has been accepted by all physicists through more than half a century and it is quoted in numerous textbooks including the first edition of my own monograph “The Theory of Relativity”⁽²⁾. Nevertheless, the equations (5) and (7) are wrong, as has been noticed only quite recently. It is a strange and rather unique incident in the history of physics that a fundamental mistake in the original derivation remained overlooked through such a long period of time.

H. OTT⁽³⁾ was the first who pointed out that the formulae (5), (7) of Planck in certain cases lead to unreasonable results and he maintained that they had to be replaced by the equations

$$\Delta Q = \frac{\Delta Q^0}{\sqrt{1 - \beta^2}} \quad (8)$$

and

$$T = \frac{T^0}{\sqrt{1 - \beta^2}} \quad (9)$$

in accordance with (6) which was accepted by him.

However, Ott’s paper remained unnoticed until quite recently. His treatment was also somewhat special in that he mainly considered systems which are closed before and after the process so that the total momentum and energy of the system transform as the components of a 4-vector under Lorentz transformations and this is generally not the case for the systems with which we are dealing in thermodynamics. Take, for instance, the system considered by Planck in his original paper, which is a fluid enclosed in a

container of a changeable volume. Then it is essential that the walls of the container exert a pressure on the fluid before and after the thermodynamical process and, as is well known, the total momentum and energy of the fluid do not transform as the components of a 4-vector in this case.

A few years later, H. ARZÉLIÈS⁽⁴⁾ obviously without knowing Ott's work, considered the case of a fluid anew and came to the same formulae (8) and (9) as Ott; but along with the equations (5) and (7) he also discarded the transformation equations for the momentum and energy of the fluid following from the relativistic mechanics of elastic bodies, which undoubtedly are correct. Therefore, the paper by ARZÉLIÈS caused a whole avalanche of mutually contradicting papers⁽⁵⁾ on the subject, so that the situation regarding this really quite simple problem has become rather confused. Among all these papers the one by KIBBLE⁽⁶⁾ seems to me exceptional. Apart from a few misprints, all his statements seem to be correct. His most important remark is that the work done by the external force in \mathfrak{R} , on account of the relativity of simultaneity, may be different from zero even if the volume is not changed, provided that the pressure is changed during the process. However, in his calculation of this effect, he assumes that the pressure rises suddenly at the beginning of the process, and this is not quite in accordance with the assumption of a reversible change which by definition has to be performed "infinitely" slowly.

In view of the principal importance of the question and hopefully in order to finally remove all doubts about the correctness of Ott's equation (9) and also of his equation (8) for reversible processes, I propose once more in all details to consider arbitrary finite reversible and irreversible changes of a fluid enclosed in a container of changeable volume. For irreversible processes it will be shown that the transformation equation (8) is valid only under the condition that the transferred heat does not carry any momentum in the rest system, and we shall find a generalization of (8) for the case where this condition is not satisfied.

Reversible thermodynamical processes

Let us begin by considering a thermodynamic fluid in an *arbitrary state of motion* which exerts a normal pressure on any surface element. According to the relativistic dynamics of continuous media⁽⁷⁾ we have, if there is no heat conduction, the following transformation laws connecting the pressure p , the energy density h , and the momentum density \mathbf{g} in a fixed system of

inertia \mathfrak{K} with the corresponding quantities p^0 , h^0 , \mathbf{g}^0 measured in the momentary rest system of the fluid at the point and at the time considered.

The pressure is a relativistically invariant scalar, i.e.,

$$p = p^0. \quad (10)$$

If \mathbf{u} is the velocity with respect to \mathfrak{K} of the fluid at the event point considered, we have for the energy- and momentum densities

$$h = \frac{h^0 + p^0 \frac{u^2}{c^2}}{1 - \frac{u^2}{c^2}} \quad (11)$$

$$\mathbf{g} = \frac{h + p}{c^2} \mathbf{u} = \frac{h^0 + p^0}{c^2 - u^2} \mathbf{u}. \quad (12)$$

The latter quantity is connected with the energy current density by Planck's relation

$$\mathbf{S} = c^2 \mathbf{g} = (h + p) \mathbf{u}. \quad (13)$$

The equations (10)–(13) are valid only if we can neglect the contributions from heat conduction. If there is heat conduction, like during a process in which heat is supplied from a reservoir, one has to add to (13) the heat flux vector $\mathbf{S}^{(h)}$ which gives an extra contribution $\mathbf{S}^{(h)}/c^2$ to the momentum density \mathbf{g} in (12).

Next, we consider the case where the fluid is in thermodynamic equilibrium in a cylindrical vessel at rest in a system of inertia \mathfrak{K}^0 , which moves with constant velocity \mathbf{v} with respect to \mathfrak{K} . Then, \mathbf{u} is constant and equal to \mathbf{v} for all elements of the fluid. We can obviously arrange it so that the cylinder axis of the container is parallel to the common x - and x^0 -axis and that the end walls a and b with area F have the coordinates $x_a^0 = 0$, $x_b^0 = l^0$, respectively, in \mathfrak{K}^0 . The latter end wall may be a movable piston so that the volume $V^0 = F^0 l^0$ can be changed by varying l^0 . The area of the walls a and b is the same in \mathfrak{K} and \mathfrak{K}^0 , i.e.,

$$F = F^0, \quad (14)$$

but for the volume we have of course

$$V = V^0 \sqrt{1 - \beta^2}, \quad \beta = \frac{v}{c}. \quad (15)$$

Since the fluid is in an equilibrium state, there is no heat conduction and the pressures p_a^0 and p_b^0 at a and b are equal in \mathfrak{K}^0 , i.e.,

$$p_a^0 = p_b^0 = p^0, \quad (16)$$

and the forces exerted by the walls a and b on the fluid are $p^0 F^0$ and $-p^0 F^0$, respectively, in the direction of the x^0 -axis. In \mathfrak{K}^0 they do not perform any work of course for fixed positions of the walls. However, in \mathfrak{K} the wall a performs a work pFv on the fluid pr. unit time while the force of the wall b has a mechanical effect $-pFv$. This is in accordance with the expression (13), according to which the amount of energy which pr. unit time passes through a into the fluid is $F(S_x - hv) = Fpv$ and equal to the rate at which energy is leaving the fluid through the end wall b . The forces exerted by the cylinder walls do not perform any work because they are perpendicular to the direction of \mathbf{v} .

Since there is no heat conduction in an equilibrium state, we can obtain the total energy $H = hV$ and momentum $\mathbf{G} = \mathbf{g}V$ by integrating (11) and (12) over the volume of the fluid and, by taking account of (15), we get

$$\left. \begin{aligned} H &= \frac{H^0 + \beta^2 p^0 V^0}{\sqrt{1 - \beta^2}} \\ \mathbf{G} &= \frac{H^0 + p^0 V^0}{c^2 \sqrt{1 - \beta^2}} \mathbf{v}, \end{aligned} \right\} \quad (17)$$

which shows that the total momentum and energy of the fluid do not transform like the components of a 4-vector. (For this particular non-closed system it is the momentum and enthalpy $\mathfrak{E} = H + pV$ which together form a 4-vector).

We shall now consider an arbitrary finite *reversible* change of state in which the volume V^0 and the pressure p^0 are changed by the amounts ΔV^0 and Δp^0 . This can be done by keeping the wall a fixed at the position $x_a^0 = 0$ while b is moved from $x_b^0 = l^0$ to $x_b^0 = l^0 + \Delta l^0$, $\Delta l^0 = \Delta V^0 / F^0$. If the expansion starts at $t^0 = 0$ and is finished at $t^0 = \tau^0$, the motion of the wall b is described by an equation

$$x_b^0 = \varphi(t^0) \quad (18)$$

where the function $\varphi(t^0)$ increases slowly from the value l^0 for $t^0 \leq 0$ to the value $l^0 + \Delta l^0$ for $t^0 \geq \tau^0$.

Hence,

$$\varphi(t^0) = \left. \begin{array}{ll} t^0, & t^0 \leq 0 \\ \varphi(t^0), & 0 \leq t^0 \leq \tau^0 \\ t^0 + \Delta t^0, & t^0 \geq \tau^0. \end{array} \right\} \quad (19)$$

The velocity with which the wall b moves in \mathfrak{K}^0 is then $u_b^0 = \varphi'(t^0)$, which is zero for $t^0 \leq 0$ and for $t^0 \geq \tau^0$. For a reversible change the velocity u_b^0 must be small ("infinitesimal") during the whole process, which means that the time τ^0 must accordingly be large. We shall further assume that simultaneously a certain amount of heat ΔQ^0 is *reversibly* supplied to the fluid through the cylinder walls from a heat reservoir comoving with the container. In order to make this heat supply a reversible process, we have to arrange it so that the temperature of the reservoir at each stage of the process is only infinitesimally higher than the temperature of the fluid. Under these conditions we can assume that during the process the fluid goes through a succession of equilibrium states, which means that the pressures $p_a^0(t^0)$ and $p^0(t^0)$ at the walls a and b are equal for equal times t^0 in \mathfrak{K}^0 . Hence,

$$p_a^0(t^0) = p_b^0(t^0) = f(t^0), \quad (20)$$

where $f(t^0)$ is a function (depending on the rate of the heat flux through the cylinder and on the function $\varphi(t^0)$) which rises from the value p^0 for $t^0 \leq 0$ to the value $p^0 + \Delta p^0$ for $t^0 \geq \tau^0$, i.e.,

$$f(t^0) = \left. \begin{array}{ll} p^0, & t^0 \leq 0 \\ p^0 + \Delta p^0, & t^0 \geq \tau^0. \end{array} \right\} \quad (21)$$

Since only the wall b is moving in \mathfrak{K}^0 during the expansion, the total mechanical work done by the surroundings on the fluid during the process is in \mathfrak{K}^0

$$\Delta A^0 = -F^0 \int_0^{\tau^0} p_b^0(t^0) u_b^0 dt^0 = -F^0 \int_0^{\tau^0} f(t^0) \varphi'(t^0) dt^0. \quad (22)$$

We shall now consider the process in question from the point of view of an observer in \mathfrak{K} . According to the Lorentz transformations, we have for any event in x^0, y^0, z^0 at the time t^0

$$t = \frac{t^0 + \frac{vx^0}{c^2}}{\sqrt{1 - \beta^2}}, \quad y = y^0, \quad z = z^0. \quad (23)$$

For a fixed point on a , where x^0 is constantly equal to zero, we have therefore

$$t_a = \frac{t_a^0}{\sqrt{1 - \beta^2}}, \quad dt_a = \frac{dt_a^0}{\sqrt{1 - \beta^2}}. \quad (24)$$

On the other hand, for a point on b for which (18) and (19) hold, we get

$$t_b = \frac{t_b^0 + \frac{v}{c^2} \varphi(t_b^0)}{\sqrt{1 - \beta^2}}, \quad dt_b = \frac{1 + \frac{v\varphi'(t_b^0)}{c^2}}{\sqrt{1 - \beta^2}} dt_b^0. \quad (25)$$

From the relativistic formula for the addition of velocities we get for the velocities u_a and u_b of the walls a and b with respect to \mathfrak{K} , since $u_a^0 = 0$ and $u_b^0 = \varphi'(t_b^0)$,

$$\left. \begin{aligned} u_a &= v \\ u_b &= \frac{v + \varphi'(t_b^0)}{1 + \frac{v\varphi'(t_b^0)}{c^2}} \end{aligned} \right\} \quad (26)$$

Hence, by (24)–(26),

$$\left. \begin{aligned} u_a dt_a &= \frac{v dt_a^0}{\sqrt{1 - \beta^2}} \\ u_b dt_b &= \frac{v + \varphi'(t_b^0)}{\sqrt{1 - \beta^2}} dt_b^0 \end{aligned} \right\} \quad (27)$$

Since the pressure is an invariant scalar, we get from (20) for the pressure at the wall a

$$p_a(t_a) = p_a^0(t_a^0) = f(t_a^0), \quad (28)$$

where t_a and t_a^0 are connected by the equation (24). Similarly, we have for the pressure at the wall b

$$p_b(t_b) = p_b^0(t_b^0) = f(t_b^0), \quad (29)$$

where t_b and t_b^0 here are connected by (25).

Now, equal times $t_a = t_b$ in \mathfrak{K} do not correspond to equal times t_a^0 and t_b^0 , therefore, in general, $p_a(t) \neq p_b(t)$. From (24), (25), and (19) it follows that

$$t_a = t_b = 0 \quad \text{corresponds to} \quad t_a^0 = 0, \quad t_b^0 = -\frac{vt_b^0}{c^2}. \quad (30)$$

Therefore, at this time and at earlier times we have, by (28), (29) and (21),

$$p_a(t) = p_b(t) = p, \quad t \leq 0. \quad (31)$$

Similarly, at the time

$$\left. \begin{aligned} t_a = t_b = \tau, \quad \tau &= \frac{\tau^0 + \frac{v}{c^2}(l^0 + \Delta l^0)}{\sqrt{1 - \beta^2}} \\ t_a^0 = \tau_a^0 \equiv \tau^0 + \frac{v(l^0 + \Delta l^0)}{c^2}, \quad t_b^0 &= \tau^0. \end{aligned} \right\} \quad (32)$$

we have

Since $\tau_a^0 > \tau^0$, it follows from (28), (29) and (21), that

$$p_a(t) = p_b(t) = p^0 + \Delta p^0 \quad \text{for } t \geq \tau. \quad (33)$$

Further, outside the interval $0 \leq t \leq \tau$, the velocities of the walls a and b are equal, viz., $u_a = u_b = v$. Thus the total mechanical force and the corresponding work on the fluid are zero outside the interval $0 \leq t \leq \tau$.

The work ΔA_a performed by the wall a on the fluid during this interval is now, by (14), (28), (27), (30) and (32),

$$\Delta A_a = \int_0^\tau F p_a(t_a) u_a dt_a = \frac{F^0 v}{\sqrt{1 - \beta^2}} \int_0^{\tau_a^0} f(t^0) dt^0. \quad (34)$$

Since $\tau_a^0 - \tau^0 = \frac{v(l^0 + \Delta l^0)}{c^2}$ and $f(t^0) = p^0 + \Delta p^0$ in the interval from τ^0 to τ_a^0 , we get

$$\Delta A_a = \frac{F^0 v}{\sqrt{1 - \beta^2}} \int_0^{\tau^0} f(t^0) dt^0 + \frac{\beta^2 (p^0 + \Delta p^0) (V^0 + \Delta V^0)}{\sqrt{1 - \beta^2}}. \quad (35)$$

Similarly, we get for the work performed by the wall b

$$\Delta A_b = - \int_0^\tau F p_b(t_b) u_b dt_b = - \frac{F^0}{\sqrt{1 - \beta^2}} \int_{-\frac{vl^0}{c^2}}^{\tau^0} f(t^0) (v + \varphi'(t^0)) dt^0, \quad (36)$$

where we have used (27) and (30). In the interval from $-vl^0/c^2$ to zero we have $f(t^0) = p^0$ and $\varphi'(t^0) = 0$. Thus,

$$\Delta A_b = -\frac{\beta^2 p^0 V^0}{\sqrt{1-\beta^2}} - \frac{F^0 v}{\sqrt{1-\beta^2}} \int_0^{\tau^0} f(t^0) dt^0 + \frac{\Delta A^0}{\sqrt{1-\beta^2}} \quad (37)$$

on account of (22). Since again the work performed by the cylinder wall is zero we get in \mathfrak{K} for the total mechanical work performed during the process

$$\Delta A = \Delta A_a + \Delta A_b = \frac{\beta^2 \Delta(p^0 V^0) + \Delta A^0}{\sqrt{1-\beta^2}}, \quad (38)$$

where

$$\Delta(p^0 V^0) = (p^0 + \Delta p^0)(V^0 + \Delta V^0) - p^0 V^0 \quad (39)$$

is the increase of the product of pressure and volume in \mathfrak{K}^0 during the process. This formula (38) is exact for any finite reversible processes. Note that even if $\Delta V^0 = 0$, i.e., when $\Delta A^0 = 0$, we have a finite work in \mathfrak{K} , viz.,

$$\Delta A = \frac{\beta^2 \Delta(p^0 V^0)}{\sqrt{1-\beta^2}} = \frac{\beta^2 V^0 \Delta p^0}{\sqrt{1-\beta^2}} \quad \text{for} \quad \Delta V^0 = 0 \quad (40)$$

which, as we have seen, stems from the relativity of simultaneity.

From (3), (17) and (38) we therefore get, for the amount of heat energy transferred to the fluid in a *reversible* process, since the velocity of the fluid is \mathbf{v} before and after the process,

$$\Delta Q = \Delta H - \Delta A = \frac{\Delta H^0 + \beta^2 \Delta(p^0 V^0) - \beta^2 \Delta(p^0 V^0) - \Delta A^0}{\sqrt{1-\beta^2}}$$

or, on account of (1),

$$\Delta Q = \frac{\Delta Q^0}{\sqrt{1-\beta^2}} \quad (41)$$

which is Ott's formula (8). If this formula is applied to an infinitesimal reversible process we also get, by (4), (2) and (6), Ott's formula (9) for the transformation of the temperature. "Infinitesimal" should here be taken in the physical sense, which means that the increments $\Delta V^0 = dV^0$, $\Delta p^0 = dp^0$ etc. are so small that we can neglect terms depending on the products or higher powers of these increments. In that case, we can put $\varphi'(t^0) = \frac{\Delta l^0}{\tau^0}$ in the interval $0 < t^0 < \tau^0$ and, neglecting terms of higher order, we get from (22)

$$dA^0 = -F^0 \int_0^{\tau^0} f(t^0) \varphi'(t^0) dt^0 = -\frac{F^0 \Delta l^0}{\tau^0} \int_0^{\tau^0} f(t^0) dt^0 = -p^0 dV^0. \quad (42)$$

Further (38) reduces to

$$dA = \frac{\beta^2(p^0 dV^0 + V^0 dp^0) - p^0 dV^0}{\sqrt{1 - \beta^2}} = \frac{\beta^2 V^0 dp^0}{\sqrt{1 - \beta^2}} - p^0 dV^0 \sqrt{1 - \beta^2} \quad (43)$$

which, by (10) and (15), also may be written

$$dA = \frac{\beta^2 V dp}{1 - \beta^2} - p dV. \quad (44)$$

Besides the work $-pdV$ due to the change of volume we have in \mathfrak{K} a work $\frac{\beta^2 V dp}{1 - \beta^2}$ which (apart from a minus sign) is in accordance with the result of KIBBLE (loc. cit.⁽⁶⁾ equation (17)). Since work, energy and time are invariant quantities under purely spatial rotations of the coordinate axes, it is clear that the relations obtained in the preceding developments are independent of the special arrangement of the container with respect to the coordinate axes used in our calculations.

Let us for a moment go back to an arbitrary finite reversible process (with the special arrangements as before). The correct formula (41) or (8) deviates from the earlier equation (5) of Planck and others by a factor $1 - \beta^2$. Where lies the error in the earlier derivation? To see this, let us calculate the total mechanical impulse $\Delta \mathbf{J}$ in \mathfrak{K} which is the time integral of the resultant mechanical force from the walls on the fluid. Since the fluid at any moment during a reversible process is in an equilibrium state, the pressure $p_c(t)$ at the cylinder walls is at any time t equal for all points with the same x -coordinate. Therefore, the impulse caused by the cylinder wall is zero, i.e.

$$\Delta J_y = \Delta J_z = 0. \quad (45)$$

On the other hand, the x -component of $\Delta \mathbf{J}$ is the sum of the impulses ΔJ_a and ΔJ_b of the walls a and b

$$\Delta J_x = \Delta J_a + \Delta J_b. \quad (46)$$

Since the force from a is $K_a(t) = Fp_a(t)$ in the x -direction, we have

$$\Delta J_a = F \int_0^\tau p_a(t_a) dt_a = \frac{F^0}{\sqrt{1-\beta^2}} \int_0^{\tau_a^0} f(t^0) dt^0 = \frac{\Delta A_a}{v} \quad (47)$$

on account of (34). Similarly, we have by (29) and (25),

$$\left. \begin{aligned} \Delta J_b &= -F \int_0^\tau p_b(t_b) dt_b = -F^0 \int_0^{\tau^0} p_b^0(t_b^0) \frac{dt_b}{dt_b^0} dt_b^0 \\ &= -\frac{F^0}{\sqrt{1-\beta^2}} \int_0^{\tau^0} f(t^0) \left(1 + \frac{v\varphi'(t^0)}{c^2}\right) dt^0 \end{aligned} \right\} \quad (48)$$

or, by means of (21) and (22),

$$\Delta J_b = -\frac{vp^0V^0}{c^2\sqrt{1-\beta^2}} - \frac{F^0}{\sqrt{1-\beta^2}} \int_0^{\tau^0} f(t^0) dt^0 + \frac{v\Delta A^0}{c^2\sqrt{1-\beta^2}}. \quad (49)$$

Introducing (47), (49) into (46), and using (35), the x -component of the mechanical impulse becomes

$$\Delta J = \frac{v}{c^2\sqrt{1-\beta^2}} [\Delta(p^0V^0) + \Delta A^0]. \quad (50)$$

Since with our arrangement, $\mathbf{v} = \{v, 0, 0\}$ the three equations (45) and (50) may be comprised in the vector equation

$$\Delta \mathbf{J}_x = \frac{\Delta(p^0V^0) + \Delta A^0}{c^2\sqrt{1-v^2}} \mathbf{v}. \quad (51)$$

According to the dynamical equations for a continuous medium with heat conduction, the change of momentum of the fluid is determined by the ‘‘spatial analogue’’ of the energy equation (3), i.e.

$$\Delta \mathbf{G} = \Delta \mathbf{G}^{(h)} + \Delta \mathbf{J}, \quad (52)$$

where $\Delta \mathbf{G}^{(h)}$ is the increase of momentum due to the conduction of heat to the system. In our case we have, according to (17),

$$\Delta \mathbf{G} = \frac{\Delta H^0 + \Delta(p^0 V^0)}{c^2 \sqrt{1 - \beta^2}} \mathbf{v} \quad (53)$$

which, by (52), (51) and (1), gives

$$\Delta \mathbf{G}^{(h)} = \Delta \mathbf{G} - \Delta \mathbf{J} = \frac{\Delta H^0 - \Delta A^0}{c^2 \sqrt{1 - \beta^2}} \mathbf{v} = \frac{\Delta Q^0}{c^2 \sqrt{1 - \beta^2}} \mathbf{v}. \quad (54)$$

The increase of the momentum due to the heat conduction during the reversible process is, therefore, exactly as if we had added a particle of rest mass $\Delta Q^0/c^2$ and zero velocity in the system \mathfrak{K}^0 . By means of (41), this part of the momentum increase can also be written

$$\Delta \mathbf{G}^{(h)} = \frac{\Delta Q}{c^2} \mathbf{v} \quad (55)$$

in accordance with Einstein's general relation between energy and inertial mass. The total increase of momentum can now be written as a sum of two parts

$$\Delta \mathbf{G} = \Delta \mathbf{G}^{(h)} + \Delta \mathbf{G}^{(m)} \quad (56)$$

where the second part, according to (52), satisfies the equation

$$\Delta \mathbf{G}^{(m)} = \Delta \mathbf{J}. \quad (57)$$

Thus, $\Delta \mathbf{G}^{(m)}$ is that increase of the momentum which is due to the action of the mechanical forces. Only if there is no heat transfer is the mechanical impuls $\Delta \mathbf{J}$ equal to the total increase of the momentum, and here lies the root of the earlier mistake.

Before we come to a closer scrutiny of this point, let us look at the situation in the system \mathfrak{K}^0 . The equations (51)–(57) are valid in any system \mathfrak{K} . If we let $\mathfrak{K} \rightarrow \mathfrak{K}^0$ we have $\mathbf{v} \rightarrow 0$. From (51) we then get in \mathfrak{K}^0 , for the mechanical impulse in a reversible process,

$$\Delta \mathbf{J}^0 = 0 \quad (58)$$

as is also seen immediately from (20). Further, we get from (54) in \mathfrak{K}^0

$$\Delta \mathbf{G}^{(h)0} = 0 \quad (59)$$

i.e. *in reversible processes the momentum transfer due to the heat supply is zero in the system \mathfrak{K}^0* . From (59), (54) and (41) it follows that the quantities

$$\Delta Q_i = \left\{ \Delta \mathbf{G}^{(h)}, \quad \frac{i}{c} \Delta Q \right\} = \frac{\Delta Q^0}{c^2} V_i \quad (60)$$

transform as the components of a 4-vector in any reversible process (V_i is the constant 4-velocity of the fluid).

The scalar product of the mechanical impulse $\Delta \mathbf{J}$ in (51) with the velocity \mathbf{v} is

$$(\Delta \mathbf{J} \cdot \mathbf{v}) = \frac{\beta^2 [\Delta(p^0 V^0) + \Delta A^0]}{\sqrt{1 - \beta^2}}. \quad (61)$$

If we express the mechanical work ΔA in (38) in terms of this quantity, we get

$$\Delta A = (\Delta \mathbf{J} \cdot \mathbf{v}) + \Delta A^0 \sqrt{1 - \beta^2} \quad (62)$$

or, on account of (57),

$$\Delta A = (\Delta \mathbf{G}^{(m)} \cdot \mathbf{v}) + \Delta A^0 \sqrt{1 - \beta^2}. \quad (63)$$

The mistake made in earlier derivations was to replace $\Delta \mathbf{G}^{(m)}$ in this expression by the total increase $\Delta \mathbf{G}$ of the momentum of the fluid. The expression ΔA_P for the work obtained in this way, i.e.,

$$\Delta A_P = (\Delta \mathbf{G} \cdot \mathbf{v}) + \Delta A^0 \sqrt{1 - \beta^2} \quad (64)$$

differs from the correct expression (63) by

$$\Delta A_P - \Delta A = (\Delta \mathbf{G} - \Delta \mathbf{G}^{(m)}) \cdot \mathbf{v} = (\Delta \mathbf{G}^{(h)} \cdot \mathbf{v}) = \frac{\beta^2 \Delta Q^0}{\sqrt{1 - \beta^2}}$$

on account of (54). With (3) and (41) one therefore gets

$$\Delta Q_P = \Delta H - \Delta A_P = \Delta Q - \frac{\beta^2 \Delta Q^0}{\sqrt{1 - \beta^2}} = \Delta Q^0 \sqrt{1 - \beta^2}, \quad (65)$$

which is the equation (5) of Planck.

The philosophy leading to this mistake becomes clearer when we again consider an infinitesimal reversible process. By (42) we get in this case for the mechanical impulse (51)

$$d\mathbf{J} = \frac{V^0 dp^0}{c^2 \sqrt{1 - \beta^2}} \mathbf{v} = \frac{V dp}{c^2 - v^2} \mathbf{v}. \quad (66)$$

Further, for an infinitesimal change of state, the time τ during which the change is reversibly performed is also physically infinitesimal. If we put $\tau = dt$, the equation (52) formally takes the form of an equation of motion

$$\frac{d\mathbf{G}}{dt} = \mathbf{K}, \tag{67}$$

where

$$\left. \begin{aligned} \mathbf{K} &= \mathbf{K}^{(m)} + \mathbf{K}^{(h)} \\ \mathbf{K}^{(m)} &\equiv \frac{d\mathbf{J}}{dt} = \frac{V \frac{dp}{dt}}{c^2 - v^2} \mathbf{v} \\ \mathbf{K}^{(h)} &\equiv \frac{d\mathbf{G}^{(h)}}{dt}. \end{aligned} \right\} \tag{68}$$

Let us for simplicity at the moment consider a process in which the volume is unchanged. Then the change of state is due solely to the heat supply which will increase the pressure, and all parts of the fluid have constantly the same velocity \mathbf{v} in \mathfrak{R} . The old argument was then that \mathbf{K} in (67) is the force which is necessary in order to keep this constant velocity in spite of the increase in proper mass of the system due to the heating up and due to the increased pressure which represents an increase in the elastic potential. This force performs a work

$$dA_P = (\mathbf{K} \cdot \mathbf{v})dt = (d\mathbf{G} \cdot \mathbf{v}) \tag{69}$$

which is just equal to the expression (64) for an infinitesimal process with $dV^0 = 0$, $dA^0 = 0$.

However, (67) is only *formally* an equation of motion. Actually, according to (57) and (68), it consists of the two equations

$$\frac{d\mathbf{G}^{(h)}}{dt} \equiv \mathbf{K}^{(h)} \tag{70}$$

$$\frac{d\mathbf{G}^{(m)}}{dt} = \mathbf{K}^{(m)} \tag{71}$$

of which the first is a *pure identity*. The quantity $\mathbf{K}^{(h)}$ is therefore not a real force, it just describes the rate at which the momentum grows on account of the conduction of heat to the fluid. Physically the increase of proper

mass due to the heat supply is of exactly the same nature as if we add a particle at rest in \mathfrak{K}^0 to the fluid. This particle will then move with the velocity \mathbf{v} with respect to \mathfrak{K} and there is no need for any force to keep up this constant velocity.

The only real equation of motion is (71) and the force $\mathbf{K}^{(m)}$ given by (68) is just the force which is necessary in order to keep \mathbf{v} constant in spite of the increase in elastic potential energy due to the increase of the pressure. There is no mystery about this force $\mathbf{K}^{(m)}$, as we have seen it is a force exerted by the walls in the system \mathfrak{K} . It is the work of this real force which gives us the correct expression

$$dA = (\mathbf{K}^{(m)} \cdot \mathbf{v})dt = \frac{\beta^2 V dp}{1 - \beta^2}. \quad (72)$$

If we have also a change of V we have to add the "internal" work $-pdV$ in order to get the general expression (44).

Irreversible Processes

In the preceding section we have considered only reversible changes of the state of the fluid, and the main result was the transformation equation (38) for the mechanical work, from which the equation (41) for the transformation of the transferred heat energy followed as a consequence. The problem is now if or under which conditions (38) is valid also for irreversible processes. Let us assume that we have the same special arrangement of the cylindrical container with respect to the common x - and x^0 -axis as before. Further, we assume that the change of volume is again obtained by the motion of the piston b which in \mathfrak{K}^0 is described by the equations (18) and (19). But now the function $\varphi(t^0)$ can be completely arbitrary in the interval $0 \leq t^0 \leq \tau^0$. It may even describe an arbitrary oscillatory motion with an amplitude larger than Δl^0 , but we shall assume that it stops at $t^0 + \Delta l^0$ a little time before $t^0 = \tau^0$. Similarly we assume the heat transfer to be stopped a little before τ^0 so as to give the fluid time to reach thermal equilibrium at $t^0 = \tau^0$. As regards the way in which the heat is supplied from the reservoir, we shall not make any assumptions at the moment. The reservoir may for instance have a temperature considerable higher than the temperature of the fluid. Also τ^0 need not be large, and the velocity $\varphi'(t^0)$ of the piston b during the process can be as large as one wants. Since the fluid is in thermal equilibrium before and after the process the equations (17) are valid at $t^0 \leq 0$ and $t^0 \geq \tau^0$ so that we have, as before,

$$\left. \begin{aligned} \Delta H &= \frac{\Delta H^0 + \beta^2 \Delta(p^0 V^0)}{\sqrt{1 - \beta^2}} \\ \Delta \mathbf{G} &= \frac{\Delta H^0 + \Delta(p^0 V^0)}{c^2 \sqrt{1 - \beta^2}} \mathbf{v}. \end{aligned} \right\} (73)$$

Also the equations (23)–(27) are valid here, but the equations (28) and (29) do not hold any more of course. Instead, we have for the pressure $p_a^0(y^0, z^0, t^0)$ in a point at the wall a with coordinates (y^0, z^0) at the time t^0

$$p_a^0 = f(y^0, z^0, t^0), \quad (74)$$

where f is a function about which we know only that it is equal to the constants p^0 and $p^0 + \Delta p^0$ independent of (y^0, z^0) for $t^0 \leq 0$ and $t^0 \geq \tau^0$, respectively, i.e.,

$$f(y^0, z^0, t^0) = \begin{cases} p^0, & t^0 \leq 0 \\ p^0 + \Delta p^0, & t^0 \geq \tau^0. \end{cases} \quad (75)$$

Similarly, we have for the pressure at the wall b

$$p_b^0 = g(y^0, z^0, t^0),$$

where

$$g(y^0, z^0, t^0) = \begin{cases} p^0, & t^0 \leq 0 \\ p^0 + \Delta p^0, & t^0 \geq \tau^0, \end{cases} \quad (76)$$

but we cannot say anything about the functions f and g in the period $0 < t^0 < \tau^0$.

In the system \mathfrak{K}^0 the mechanical work on the fluid is obviously

$$\Delta A^0 = - \int_0^{\tau^0} \int_{F^0} p_b^0 dy^0 dz^0 u_b^0 dt_b^0 = - \int_0^{\tau^0} \int_{F^0} g(y^0, z^0, t^0) dy^0 dz^0 \varphi'(t^0) dt^0. \quad (77)$$

Since the pressure is an invariant scalar, we now have in \mathfrak{K}

$$\text{and} \quad \left. \begin{aligned} p_a(y, z, t_a) &= p_a^0(y^0, z^0, t_a^0) = f(y^0, z^0, t_a^0) \\ p_b(y, z, t_a) &= g(y^0, z^0, t_b^0) \end{aligned} \right\} (78)$$

with the relations (23)–(27) connecting the variables in \mathfrak{K} and \mathfrak{K}^0 . Instead of (34) we then get for the mechanical work performed by the wall a in \mathfrak{K} during the process

$$\left. \begin{aligned}
\Delta A_a &= \int_0^\tau \int_F p_a(y, z, t_a) dy dz u_a dt_a = \int_0^{\tau_a} \int_{F^0} f(y^0, z^0, t_a^0) dy^0 dz^0 \frac{v dt_a^0}{\sqrt{1 - \beta^2}} \\
&= \frac{v}{\sqrt{1 - \beta^2}} \int_0^{\tau^0} \int_{F^0} f(y^0, z^0, t^0) dy^0 dz^0 dt^0 \\
&\quad + \frac{\beta^2 (p^0 + \Delta p^0) (V^0 + \Delta V^0)}{\sqrt{1 - \beta^2}},
\end{aligned} \right\} \quad (79)$$

where we have made use of (27) and (30), (32).

Similarly we get for the work performed by b

$$\left. \begin{aligned}
\Delta A_b &= - \int_0^\tau \int_F p_b(y, z, t_b) dy dz u_b dt_b \\
&= - \int_0^{\tau} \int_{F^0} g(y^0, z^0, t_b^0) \frac{v + \varphi'(t_b^0)}{\sqrt{1 - \beta^2}} dt_b^0 \\
&\quad - \frac{v^2}{c^2} \\
&= - \frac{\beta^2 p^0 V^0}{\sqrt{1 - \beta^2}} - \frac{v}{\sqrt{1 - \beta^2}} \int_0^{\tau^0} \int_{F^0} g(y^0, z^0, t^0) dy^0 dz^0 dt^0 + \frac{\Delta A^0}{\sqrt{1 - \beta^2}},
\end{aligned} \right\} \quad (80)$$

where we again have used (27) and the expression (77) for ΔA^0 . The work performed by the cylinder walls is again zero, since the velocity of the fluid at these walls cannot have a component perpendicular to the wall. The total mechanical work in \mathfrak{R} is therefore

$$\left. \begin{aligned}
\Delta A &= \Delta A_a + \Delta A_b \\
&= \frac{\beta^2 \Delta(p^0 V^0) + \Delta A^0}{\sqrt{1 - \beta^2}} + \frac{v}{\sqrt{1 - \beta^2}} \int_0^{\tau^0} \int_{F^0} [f(y^0, z^0, t^0) - g(y^0, z^0, t^0)] dy^0 dz^0 dt^0,
\end{aligned} \right\} \quad (81)$$

which deviates by the last term from the formula (38) holding for reversible processes.

We shall now calculate the mechanical impulse $\Delta \mathbf{J}$ of the forces from the walls during the period of the irreversible process. The x -component of this vector is composed of the contributions from the walls a and b , i.e.,

$$\Delta J_x = \Delta J_a + \Delta J_b \quad (82)$$

with

$$\left. \begin{aligned} \Delta J_a &= \int_0^\tau \int_F P_a(y, z, t_a) dy dz dt_a \\ &= \int_0^{\tau_a} \int_{F^0} f(y^0, z^0, t_a^0) dy^0 dz^0 \frac{dt_a^0}{\sqrt{1-\beta^2}} = \frac{\Delta A_a}{v}, \end{aligned} \right\} \quad (83)$$

$$\left. \begin{aligned} \Delta J_b &= - \int_0^\tau \int_F p_b(y, z, t_b) dy dz dt_b = - \int_{-\frac{v t^0}{c^2}}^{\tau_0} \int_{F^0} g(y^0, z^0, t_b) dy^0 dz^0 \frac{dt_b}{dt_b^0} dt_b^0 \\ &= - \frac{v p^0 V^0}{c^2 \sqrt{1-\beta^2}} + \frac{v \Delta A^0}{c^2 \sqrt{1-\beta^2}} \\ &\quad - \frac{1}{\sqrt{1-\beta^2}} \int_0^{\tau^0} \int_{F^0} g(y^0, z^0, t^0) dy^0 dz^0 dt^0. \end{aligned} \right\} \quad (84)$$

Here we have used (78), (76), (24), (25), and (77). Thus,

$$\left. \begin{aligned} \Delta J_x &= \Delta J_a + \Delta J_b \\ &= \frac{v[\Delta(p^0 V^0) + \Delta A^0]}{c^2 \sqrt{1-\beta^2}} \\ &\quad + \frac{1}{\sqrt{1-\beta^2}} \int_0^{\tau^0} \int_{F^0} [f(y^0, z^0, t^0) - g(y^0, z^0, t^0)] dt^0. \end{aligned} \right\} \quad (89)$$

If we let $\mathfrak{K} \rightarrow \mathfrak{K}^0$, (89) shows that

$$\Delta J_x^0 = \int_0^{\tau^0} \int_{F^0} [f(y^0, z^0, t^0) - g(y^0, z^0, t^0)] dt^0 \quad (90)$$

so that (89) becomes

$$\Delta J_x = \frac{\frac{v}{c^2} [\Delta(p^0 V^0) + \Delta A^0] + \Delta J_x^0}{\sqrt{1-\beta^2}}. \quad (91)$$

The integral appearing in (81) is just the integral (90), and since

$$\mathbf{v} = \{v, 0, 0\}, \quad (92)$$

we have

$$(\mathbf{v} \cdot \Delta \mathbf{J}^0) = v \Delta J_x^0, \quad (v \cdot \Delta \mathbf{J}) = v \Delta J_x, \quad (93)$$

and (81) may therefore be written in the alternative forms

$$\Delta A = \frac{\beta^2 \Delta(p^0 V^0) + \Delta A^0 + (\mathbf{v} \cdot \Delta \mathbf{J}^0)}{\sqrt{1 - \beta^2}} \quad (94)$$

or

$$\Delta A = (\mathbf{v} \cdot \Delta \mathbf{J}) + \Delta A^0 \sqrt{1 - \beta^2}. \quad (95)$$

In the latter form it is identical with the equation (62) for reversible processes.

For the components of $\Delta \mathbf{J}$ in the y - and z -directions one easily finds that

$$\Delta J_y = \Delta J_y^0, \quad \Delta J_z = \Delta J_z. \quad (96)$$

To prove this one only uses that the pressure at the cylinder wall C is a scalar, i.e.,

$$p_c(x, y, z, t) = p_c^0(x^0, y^0, z^0, t^0) = f_c(x^0, y^0, z^0, t^0) \quad (97)$$

for values of $y = y^0$ and $z = z^0$ corresponding to points on C . In (97) the spacetime coordinates are connected by the Lorentz transformation and

$$f_c(x^0, y^0, z^0, t^0) = \begin{cases} p^0, & t^0 \leq 0 \\ p^0 + \Delta p^0, & t^0 \geq \tau^0 \end{cases} \quad (98)$$

independently of the spatial coordinates. This has the effect that the integrals over the spacetime coordinates, which define ΔJ_y and ΔJ_y^0 or ΔJ_z and ΔJ_z^0 , effectively are over the same domain in spacetime and, since the integrands are invariants, (96) follows.

By (92) the equations (91) and (96) may be comprised in the vector equation

$$\left. \begin{aligned} \Delta \mathbf{J} &= \frac{\Delta(p^0 V^0) + \Delta A^0}{c^2 \sqrt{1 - \beta^2}} \mathbf{v} \\ &+ \frac{(\mathbf{v}/v^2)(\mathbf{v} \cdot \Delta \mathbf{J}^0)(1 - \sqrt{1 - \beta^2}) + \sqrt{1 - \beta^2} \Delta \mathbf{J}^0}{\sqrt{1 - \beta^2}}. \end{aligned} \right\} \quad (99)$$

Now, (52) is of course also valid for irreversible processes with $\Delta \mathbf{G}$ given by (73). In the system \mathfrak{R}^0 this gives

$$\Delta \mathbf{J}^0 = -\Delta \mathbf{G}^{(h)0}. \quad (100)$$

Further, by (52), (73), and (99),

$$\begin{aligned} \Delta \mathbf{G}^{(h)} &= \Delta \mathbf{G} - \Delta \mathbf{J} = \frac{\Delta H^0 - \Delta A^0}{c^2 \sqrt{1 - \beta^2}} \mathbf{v} - \Delta \mathbf{J}^0 \\ &\quad - \mathbf{v} \frac{(\mathbf{v} \cdot \Delta \mathbf{J}^0)(1 - \sqrt{1 - \beta^2})}{v^2 \sqrt{1 - \beta^2}} \end{aligned}$$

or, on account of (100),

$$\Delta \mathbf{G}^{(h)} = \Delta \mathbf{G}^{(h)0} + \mathbf{v} \frac{(\mathbf{v} \cdot \Delta \mathbf{G}^{(h)0})(1 - \sqrt{1 - \beta^2}) + \beta^2 \Delta Q^0}{v^2 \sqrt{1 - \beta^2}}, \quad (101)$$

where

$$\Delta Q^0 = \Delta H^0 - \Delta A^0 \quad (102)$$

is the transferred heat energy in \mathfrak{K}^0 in accordance with the first law (1). When we use the same law (3) in \mathfrak{K} , we now get for the transferred heat energy ΔQ in \mathfrak{K} , by (73) and (94),

$$\Delta Q = \Delta H - \Delta A = \frac{\Delta H^0 - \Delta A^0 - (\mathbf{v} \cdot \Delta \mathbf{J}^0)}{\sqrt{1 - \beta^2}}$$

or, on account of (100) and (102),

$$\Delta Q = \frac{\Delta Q^0 + (\mathbf{v} \cdot \Delta \mathbf{G}^{(h)0})}{\sqrt{1 - \beta^2}}. \quad (103)$$

Thus, if we want the first law of thermodynamics to be valid in its classical form in every Lorentz system \mathfrak{K} , then Ott's formula (8) holds only if we arrange it so that the heat supplied to the fluid does not carry any momentum in the rest system \mathfrak{K}^0 . For a reversible process this is always the case, as we have seen in the preceding section. However, for an irreversible process Ott's equation (8) has in general to be replaced by the formula (103) which together with (101) has the following satisfactory consequence.

If we define a quantity ΔQ_i with the four components

$$\Delta Q_i = \left\{ \Delta \mathbf{G}^{(h)}, \frac{i}{c} \Delta Q \right\}. \quad (104)$$

then the equations (101) and (103) show that the ΔQ_i transform as the components of a 4-vector under arbitrary Lorentz transformations⁽⁸⁾. This is in accordance with a general argument regarding the equivalence of mass and energy⁽⁹⁾. Thus, we have come to the conclusion that the momentum

and energy which are transferred to a system by the supply of heat from outside form the components of a 4-vector. This result which has been obtained here by considering a very special system can be shown to be quite general⁽¹⁰⁾.

On the other hand, it would not be in contradiction with the principle of relativity to change the form of the second law in \mathfrak{K} if only it goes over into (1) for $\mathfrak{K} \rightarrow \mathfrak{K}^0$. This is actually what H. OTT proposes to do. Instead of defining the transferred heat energy ΔQ by (3), he defines a quantity $\Delta \bar{Q}$ in \mathfrak{K} by the following equation

$$\Delta H = \Delta \bar{Q} + \mathbf{v} \left(\Delta \mathbf{G}^{(h)} - \frac{\Delta \bar{Q}}{c^2} \mathbf{v} \right) + \Delta A \quad (105)$$

which is identical with (1) for $\mathfrak{K} \rightarrow \mathfrak{K}^0$, i.e.,

$$\Delta \bar{Q}^0 = \Delta Q^0. \quad (106)$$

By means of (52) and (95), (105) may be written

$$\Delta H - \mathbf{v} \Delta \mathbf{G} = \Delta \bar{Q} (1 - \beta^2) + \Delta A^0 \sqrt{1 - \beta^2} \quad (107)$$

which, by (73) and (1), gives the transformation formula

$$\Delta Q_o = \frac{\Delta Q^o}{\sqrt{1 - \beta^2}} \quad (108)$$

of Ott. For reversible processes and for such irreversible processes where $\Delta \mathbf{G}^{(h)0} = 0$, there is no difference between $\Delta \bar{Q}$ and ΔQ in (41), but in general $\Delta \bar{Q}$ differs from ΔQ .

The definition (105) for $\Delta \bar{Q}$ obviously means a different splitting of the total energy into a "heat-part" and a "mechanical part", a procedure which in many cases may lead to ambiguities. One sometimes even speaks of production of heat in a body without any heat transfer from outside.

As an example of this kind of process, let us assume that the piston b in \mathfrak{K}^0 is moved violently back and forth until it stops after some time, for instance, in the original position. Then the fluid is "heated up" even if there is no heat supply from outside (compare the heating effect when pumping a bicycle). In this case, we have

$$\left. \begin{aligned} \Delta Q_i &= \Delta Q_i^0 = 0 \\ \Delta H &= \Delta A, \quad \Delta \mathbf{G} = \Delta \mathbf{J}. \end{aligned} \right\} \quad (109)$$

In a somewhat loose way of speaking, one then says that a certain amount of heat energy ΔQ_{prod}^0 is produced in \mathfrak{K}^0 which simply is equal to the mechanical work ΔA^0 performed during the process or to the increase of the energy ΔH^0 , i.e.,

$$\Delta Q_{\text{prod}}^0 \equiv \Delta H^0 = \Delta A^0. \quad (110)$$

What is now the heat produced relative to \mathfrak{K} ? Besides performing the “internal work” which in \mathfrak{K}^0 is identified with ΔQ_{prod}^0 , the walls of the container exert extra forces in \mathfrak{K} which are necessary to keep the velocity at the same value \mathbf{v} before and after the process. Their impulse $\Delta \mathbf{J}$ is equal to the increase $\Delta \mathbf{G}$ of the momentum, since we have no supply of heat momentum from outside. These forces perform an “external work” which is equal to $\Delta \mathbf{G} \cdot \mathbf{v}$. Therefore it is natural to define the heat energy produced in \mathfrak{K} by

$$\Delta Q_{\text{prod}} = \Delta H - (\Delta \mathbf{G} \cdot \mathbf{v}). \quad (111)$$

By means of (73) this gives

$$\Delta Q_{\text{prod}} = \Delta H^0 \sqrt{1 - \beta^2} = \Delta Q_{\text{prod}}^0 \sqrt{1 - \beta^2}. \quad (112)$$

The same equation follows from (109), (110) and the equation (95) which in our case reads

$$\Delta A = (\mathbf{v} \cdot \Delta \mathbf{G}) + \Delta Q_{\text{prod}}^0 \sqrt{1 - \beta^2}. \quad (113)$$

The formula (112) corresponds to the equation (5) of Planck, which up to recently was accepted also for the heat transferred from outside, but as we have seen, it is only valid for the heat produced inside a body under the action of external forces. We have here considered a case where the external forces (from the walls of the container) are mechanical forces, but as mentioned earlier, this is not essential. The main thing is only that they are real forces originating from outside the system. They could also be of electromagnetic nature and it would seem, therefore, that the old point of view of v. LAUE⁽¹¹⁾ based on the formula (108) could be maintained in the case of the Joule heat produced in a conducting material under the influence of an external electric field (see also reference 10).

However, it should be emphasized that the notion of heat *produced* in a system during a process in general is a somewhat shady notion. As a matter of fact, it has given rise to many doubtful statements in the past. As is also apparent from the example considered above, the definition of heat production involves a more or less arbitrary splitting up of the increase ΔH

of the total energy in a heat part and a mechanical part. Perhaps it would be better to avoid the use of such ambiguous notions (except in certain well-defined cases). In contrast to the heat produced, the heat transferred to a system during a process, which is clearly defined by the first law of thermodynamics, has an unambiguous meaning, and, as we have seen, the momentum and energy transferred to a system by heat supply transform as the components of a 4-vector under Lorentz transformations.

Acknowledgments

This paper was written during my stay in Leiden as Lorentz Professor in the autumn of 1966. I want to express my sincere thanks to Professor P. MAZUR and his collaborators for the most pleasant and inspiring time spent at the Instituut Lorentz.

References

1. M. PLANCK, Berl. Ber. p. 542 (1907); Ann. d. Phys. **76**, 1 (1908).
F. HASENÖHRL, Wien Ber. **116**, 1391 (1907).
A. EINSTEIN, Jahrb. f. Rad. und El. **4**, 411 (1907).
2. M. VON LAUE, Die Relativitätstheorie, 3rd. ed. (Braunschweig 1952).
W. PAULI, Theory of Relativity (London 1958).
R. C. TOLMAN, Relativity Thermodynamics and Cosmology (Oxford 1950).
C. MØLLER, The Theory of Relativity (Oxford 1952).
W. H. MCCREA, Relativity Physics (New York 1960).
3. H. OTT, Zt. f. Phys. **175**, 70 (1963).
4. H. ARZÉLIÈS, Nuovo Cimento, **35**, 792 (1965).
5. R. PENNEY, Nuovo Cimento **43 A**, 911 (1966).
T. W. B. KIBBLE, Nuovo Cimento **41 B**, 72, 83, 84 (1966).
A. GAMBA, Nuovo Cimento **37**, 1792 (1965); **41 B**, 72 (1966).
H. ARZÉLIÈS, Nuovo Cimento **41 B**, 81 (1966).
6. The first paper by KIBBLE quoted in reference 5.
7. See f. inst. C. MØLLER, The Theory of Relativity, Chap. VI, § 67, Eq. (111).
8. See f. inst. reference 7, Chap. IV, § 36, Eqs. (29).
9. See f. inst. reference 7, Chap. III, § 30.
10. See a paper by I. BREVIK to be published soon.
11. M. VON LAUE, loc. cit., reference 2.

CHR. POULSEN

FOSSILS FROM THE LOWER CAMBRIAN OF BORNHOLM

Det Kongelige Danske Videnskabernes Selskab
Matematisk-fysiske Meddelelser 36, 2



Kommissionær: Munksgaard
København 1967

Synopsis

A Lower Cambrian fauna from Bornholm consisting of 34 species is described. The oldest of the Lower Cambrian rocks, the *Balka quartzite*, contains trace fossils referable to *Diplocraterion*, *Tigillites*, and *Skolithos*, and in addition to these some worm remains comparable to *Byronia* MATTHEW. After a hiatus follows *siltstone* („Green shales” of several authors) and *Rispebjerg sandstone* which represent one single cycle of sedimentation. The siltstone contains a rich fauna which is essentially endemic. Two new genera and seventeen new species are established. The Lower Cambrian age of the siltstone appears clearly from the occurrence of *Fordilla troyensis* WALCOTT and *Hyolithellus micans* BILLINGS. The Rispebjerg sandstone has only yielded a fragment of *Hyolithellus micans* and a single specimen of the trace fossil *Cruziana dispar* LINNARSSON. The conditions of sedimentation and the stratigraphical position of the Bornholm Lower Cambrian are discussed.

CONTENTS

	Page
Preface	5
Introduction	6
The sediments	7
Fossils from the Balka quartzite	13
Annelida	13
Genus et sp. ind. (cf. <i>Byronia</i> MATTHEW)	13
Trace fossils	13
Fossils from the siltstone ("Green shales")	14
Porifera	14
Genus et sp. ind. I (cf. <i>Pyritonema</i> M'COY)	14
- - - II	15
- - - III	15
Pelecypoda	15
<i>Fordilla troyensis</i> WALCOTT	15
Genus et sp. ind.	16
Monoplacophora	17
<i>Proplina?</i> <i>prisca</i> n. sp.	17
<i>Pollicina?</i> <i>cambrica</i> (MOBERG)	18
Gastropoda	19
<i>Prosinuites bornholmensis</i> n. g. et n. sp.	19
Calyptoptomatida	20
<i>Circotheca</i> sp.	20
<i>Orthotheca groedbyensis</i> n. sp.	20
- <i>johnstrupi</i> HOLM	21
- <i>pervilis</i> n. sp.	21
<i>Trapezotheca?</i> <i>pistrinensis</i> n. sp.	22
<i>Hyolithes</i> <i>balticus</i> n. sp.	23
- <i>groenwalli</i> n. sp.	24
- <i>lenticularis</i> HOLM	26
- <i>nathorsti</i> HOLM	27
- sp. I	28
- - II	28
- - ind.	29
<i>Halkieria</i> <i>obliqua</i> n. g. et n. sp.	30
- <i>symmetrica</i> n. sp.	30

Hyolithelloida nov.	31
<i>Hyolithellus micans</i> BILLINGS	31
Genera and species of uncertain systematic position	32
<i>Coleoloides bornholmensis</i> n. sp.	33
– <i>multistriatus</i> COBBOLD	34
– <i>paucistriatus</i> n. sp.	35
– <i>rugosus</i> n. sp.	35
<i>Pseudortholheca danica</i> n. sp.	36
<i>Glauderia mirabilis</i> n. g. et n. sp.	36
Trace fossils	37
<i>Halopoa</i> cf. <i>imbricata</i> TORELL	37
Fossils from the Rispebjerg sandstone	40
Trilobita	40
<i>Cruziana dispar</i> LINNARSSON	40
Hyolithelloida nov.	31
<i>Hyolithellus micans</i> BILLINGS	11
Stratigraphic significance of the fauna	40
Maps, showing outcrops of Lower Cambrian rocks along the streamlets Lilleaa, Læsaa, Grødbyaa, and Øleaa	44
List of fossils and localities	42
References	47
Plates	49

PREFACE

The Lower Cambrian palaeontological material described and discussed in the present paper is a result of the efforts of several collectors during a century. The greater part was collected by F. JOHNSTRUP, K. A. GRÖNWALL, and, particularly, by the present writer. The described and figured specimens are preserved in the Mineralogical and Geological Museum of the University of Copenhagen.

The writer is very grateful to the former Director of the Geological Survey of Denmark, Dr. H. ØDUM, for placing GRÖNWALL'S collections at his disposal for study.

By the courtesy of the Director of the Geological Survey of Denmark, Dr. O. BERTHELTSEN, the writer obtained permission to republish several figures from Danmarks Geologiske Undersøgelse, Ser. 2, No. 62 (K. HANSEN 1936: "Die Gesteine des Unterkambriums von Bornholm").

The writer is much indebted to Dr. H. WIENBERG RASMUSSEN of the Mineralogical and Geological Museum of the University of Copenhagen for permission to use the geological map of Bornholm in the present paper.

Special thanks are due to Dr. A. W. A. RUSHTON, who kindly sent specimens of *Coleoloides multistriatus* from the type locality, Woodlands Quarry, Hartshill, Warwickshire, and placed important information at the writer's disposal.

Last but not least, the writer is most indebted to Mr. C. HALKIER, who undertook the very difficult task of making good photographic prints of the fossils.

INTRODUCTION

The knowledge of the fossil faunas of the Lower Cambrian of Bornholm has hitherto been very incomplete.

From the lower part of the sequence of strata, the Balka quartzite, K. HANSEN (1936) mentions worm burrows. Some of these have proved to be referable to *Skolithos*, *Diplocraterion*, and *Tigillites*.¹

In addition to these trace fossils some carbonized worm tubes, comparable with *Byronia*, have been found. The "genera" mentioned are the only fossils known from the Balka quartzite.

From the overlying siltstone sequence GRÖNWALL (1916) mentions the occurrence of *Hyalithes (Orthotheca) johnstrupi* HOLM, *Hyalithes (sensu stricto) nathorsti* HOLM, *Hyalithes (sensu stricto) lenticularis* HOLM, and *Torellevella laevigata* LINNARSSON.²

In 1935 the present writer visited the siltstone outcrops in order to collect fossiliferous phosphorite nodules. The nodules were broken down to small pieces and studied by means of a binocular microscope. Several new fossils were discovered in this way, and the total number of species from the siltstone now amounts to thirty.

The location of Lower Cambrian sediments appears from the geological map (p. 8). The locality numbers used in the present paper are those introduced by HANSEN (1936).

The trace fossils of the Balka quartzite are easily accessible for study in the localities 229 and 230 on the eastern coast of the island, north and south of Snogebæk harbour, respectively.

The greater number of the fossils from the siltstone originate from outcrops along the streamlets Lilleaa, Læsaa, Grødbyaa, and Øleaa (see figs. 7-9, p. 44-46, and the list of fossils and localities p. 42-43).

¹ STEHMANN (1934) mentions the occurrence of *Monocraterion* (= *Tigillites*) and *Lepocraterion* (= *Tigillites*).

² The specimens of "*Torellevella laevigata*" have turned out to be partly indeterminable, partly referable to *Hyalithellus micans* BILLINGS.

THE SEDIMENTS

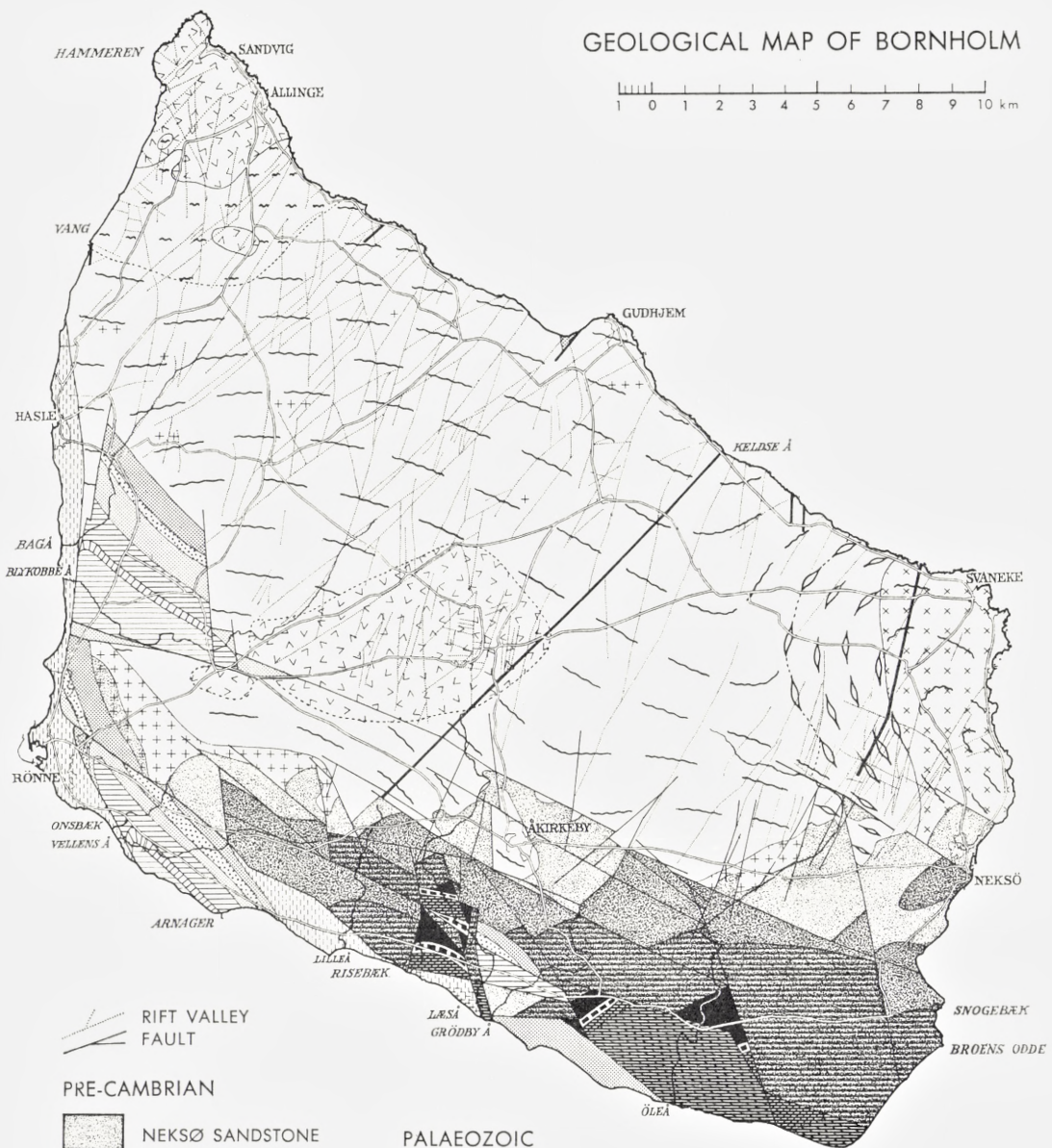
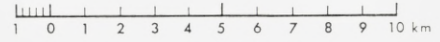
Marine Lower Cambrian sediments, containing the fossils described in the present paper, cover considerable areas in the southern part of the island (see geological map p. 8). The Lower Cambrian series of strata are usually divided into the following units, mentioned in ascending order: Balka quartzite, Siltstone ("Green shales" of several authors), and Rispebjerg sandstone.

These sedimentary rocks have been described and discussed at some length by KAJ HANSEN (1936), and, as far as the petrography of the Bornholm Lower Cambrian is concerned, the reader is referred to HANSEN's paper. A brief account of the general character of the above-mentioned stratigraphic units is considered sufficient here.

The *Balka quartzite* is about 60 m. thick and developed as a fine-grained, more or less thin-bedded, quartzitic sandstone. Coarser beds occur in places, but they are rare. The colour of the quartzite is most frequently white, but the lowermost strata, which were deposited in shallow basins on the surface of the Eocambrian Neksø sandstone, have a greenish tint owing to the presence of a considerable amount of glauconite. In the upper part of the quartzite the rock may here and there be very dark, almost black, owing to the presence of pigment of organic origin. Thin beds of shale, very rich in mica, alternate with quartzite beds in the upper part. The bedding planes of the quartzite show ripple marks and poorly preserved trace fossils. At Snogebæk (Localities Nos. 228, 229, and 230) the quartzite is extremely rich in trace fossils referable to *Diplocraterion*, *Tigillites*, and *Skolithos*.

The Balka quartzite is overlain by about 100 m. of greyish-green *siltstone* known as the "green shales". The basal stratum is a quartz conglomerate of a thickness of about 20 cm. with much glauconite and pebbles of black shale, which may eventually originate from the shale beds of the Balka quartzite. The quartz grains of this basal conglomerate have been pressed into the shale pebbles which apparently must have had the character of

GEOLOGICAL MAP OF BORNHOLM



RIFT VALLEY FAULT

PRE-CAMBRIAN

- NEKSØ SANDSTONE
- DIABASE
- SVANEKE GRANITE
- HAMMER GRANITE
- VANG GRANITE
- GNEISS
- PARADISBAKKE MIGMATITE
- RØNNE GRANODIORITE

PALAEOZOIC

- KAOLIN
- SILURIAN GRAPTOLITE SHALE
- ORDOVICIAN GRAPTOLITE SHALE
- ORDOVICIAN ORTHOCERAS LIMESTONE
- CAMBRIAN ALUM SHALE
- LOWER CAMBRIAN SILTSTONE
- LOWER CAMBRIAN BALKA QUARTZITE

MESOZOIC

- SANTONIAN BAVNODDE GREENSAND
- TURONIAN ARNAGER LIMESTONE
- CENOMANIAN ARNAGER GREENSAND
- NEOKOMIAN CLAY AND SAND
- JURASSIC COAL CLAY AND SAND
- TRIASSIC PARTICOLOURED CLAY



Fig. 1. Quarry 1 km southwest of Aakirkeby. Balka quartzite alternating with thin shale beds. (Phot. C. POULSEN).

soft clay. The following series of strata shows some lithological variation, but the greater part of it has the character of siltstone. The bedding is, as a rule, indistinct, and the bedding planes irregular. Ripple marks have never been observed. Tracks and trails are very common, especially in the middle part of the sequence, where the rock is completely infiltrated by burrows and shows the characters of a typical bioturbidite. This part of the siltstone also contains numerous small, black phosphorite nodules measuring up to five cm. in diameter (text-fig. 3). The fauna of the siltstone is found at this

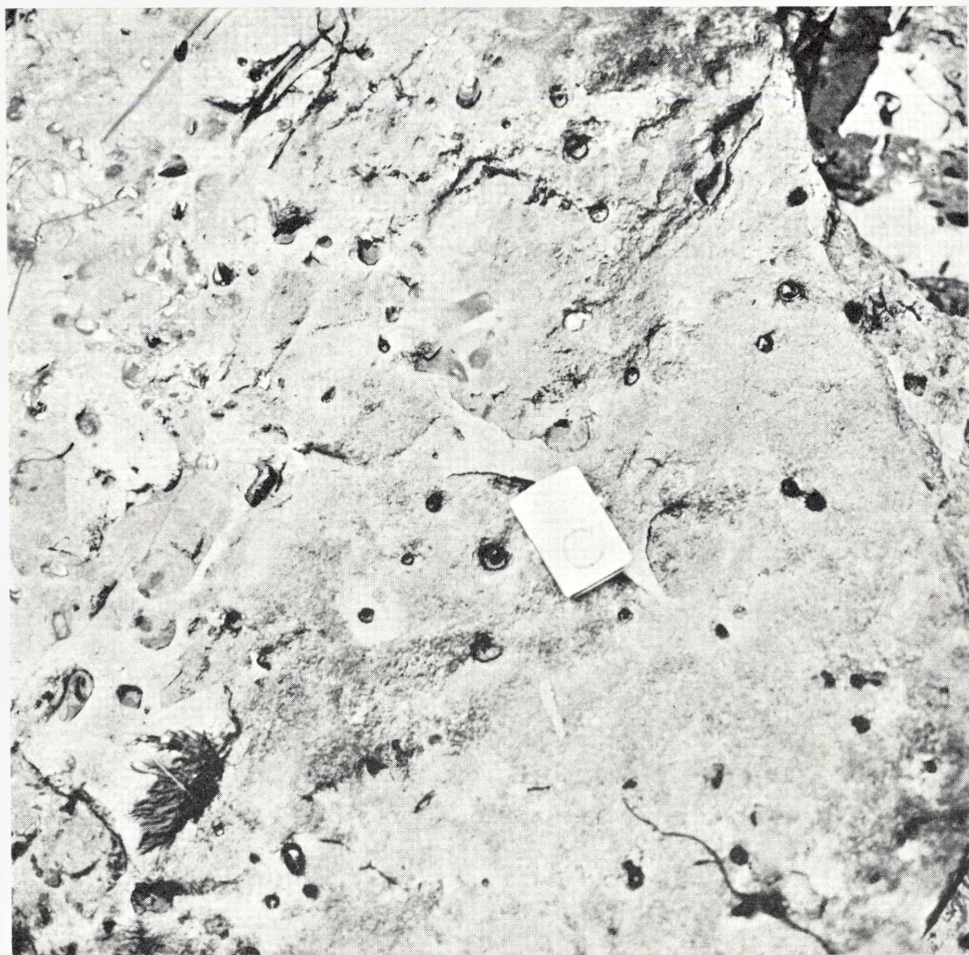


Fig. 2. Exposed bedding plane in Balka quartzite just south of Snogebæk harbour (locality 230), showing trace fossils (*Diplocraterion* and *Tigillites*). (Phot. V. POULSEN).

level and almost exclusively in the phosphorite nodules. Thirty species are now known, the commonest being *Orthotheca johnstrupi* HOLM and *Coleoloides multistriatus* COBBOLD. In the uppermost part of the siltstone sequence a gradually increasing size of the quartz grains has been observed, and the rock grades into the overlying Rispebjerg sandstone.

The *Rispebjerg sandstone* is about 3 m. thick. It is coarse-grained. The lower part (about 2.60 m.) is developed as quartzite, which is, in places, somewhat porous; the upper part has a matrix consisting of black phospho-



Fig. 3. Siltstone with black phosphorite nodules at Broens Odde (locality 232). (Phot. V. POULSEN).

rite. The only fossils known from the Rispebjerg sandstone are a specimen of *Cruziana dispar* LINNARSSON and a specimen of *Hyolithellus micans* BILLINGS, the latter possibly reworked.

In his paper of 1936 (p. 136, fig. 30) HANSEN illustrated his opinion concerning the Lower Cambrian sedimentation by means of his "Epirogenetische Kurve des Unterkambriums von Bornholm". According to HANSEN the Balka quartzite, the siltstone ("Green shales"), and the Rispebjerg sandstone represent one single cycle of sedimentation, the three units

indicating shallow, deeper, and shallow-water conditions, respectively. The present writer, however, is of opinion that the basal conglomerate of the "Green shales" indicates a sedimentary break, and, consequently, the whole Lower Cambrian sequence should represent two cycles of sedimentation. On the other hand, the fossiliferous zone of the "Green shales", containing phosphorite nodules and showing a slight increase in the size of the quartz grains, may indicate a regressive tendency in the environment of the Bornholm region, as shown in HANSEN'S diagram.

The phosphorite nodules in the siltstone have been formed *in situ* as phosphatic impregnations of the sediment around organic remains. The greater part of these organic remains are shells of calyptotomatids which fail to show any special orientation. Accordingly, currents do not appear to have had any essential influence. In his discussion of the occurrence and formation of phosphatic nodules KUENEN (1950) says: "It appears that they are generated under the same conditions as glauconite, that is, mainly in depths less than 1000 m. and where sedimentation is slow or absent". The generally fine-grained nature of the Bornholm Lower Cambrian siltstone may very well indicate slow sedimentation, and the absence of ripple marks on the bedding planes points to a sea bottom beyond the reach of wave action. The Balka quartzite and the Rispebjerg sandstone, however, are shallow-water deposits. The trace fossils *Diplocraterion*, *Skolithos*, and *Tigillites*, which occur in abundance at certain levels in the Balka quartzite, are generally believed to be worm burrows, and, provided that this biotope indicates conditions similar to the recent biotope dominated by *Sabellaria*, it is an obvious conclusion that the quartzite was deposited so close to the coast that the sea bottom was laid bare during low tide.

The above-mentioned sediments constitute the only existing Lower Cambrian on the island of Bornholm, but, as shown by C. POULSEN (1942) and V. POULSEN (1963 and 1965), the occurrence of a considerable amount of Lower Cambrian fossils, i. a. eocystid plates, *Stenothecopsis* spp., and fragments of *Holmia* sp. in the Middle Cambrian *Exsulans* limestone and Kalby clay indicates the former presence of thin, unconsolidated, late Lower Cambrian sediments, which were removed by erosion during a period of emergence.

FOSSILS FROM THE BALKA QUARTZITE

Phylum ANNELIDA

Class Polychaetia GRUBE, 1850

Order Sedentaria LAMARCK, 1818

Family uncertain

Genus et sp. ind. (cf. *Byronia* MATTHEW, 1899)

Pl. 3, fig. 5.

Material: Several tubes preserved as black, glistening, transversely wrinkled films in sandy, micaceous shale from the upper part of the Balka quartzite.

Locality: Graanakkestuen, north of Store Kannikegaard in Bodilsker parish.

Remarks: The genus *Byronia* has been characterized as follows: "Tube curved, horny, wall thin, outer surface bearing concentric annulations" (HOWELL 1962, p. 163, fig. 104 (1)). This description is also adequate with regard to the Bornholm specimens, when the different state of preservation is taken into consideration. The Bornholm species differs from the type species of *Byronia* (*B. annulata* MATTHEW, 1899) in having slender tubes; the apertural width of the Bornholm species is about 2.0 mm. and the corresponding length of the tubes is about 20 mm., whereas the apertural width of *Byronia annulata* is 2.5 mm. corresponding to a tube length of about 17.5 mm. The Bornholm specimens were originally labelled by the writer as *Ottoia* WALCOTT, but they appear to be more in conformity to *Byronia*.

TRACE FOSSILS

In a few localities, 228 (quarry at Hunsemyre), 229 (low coast cliffs at Snogebæk harbour (northern side)), and 230 (low coast cliffs just south of Snogebæk harbour) trace fossils comparable to *Diplocraterion* TORELL and *Tigillites* ROUAULT (text-fig. 2) occur in abundance. In locality 229 some of the strata have the character of "pipe rock" due to the occurrence of a coarse type of *Skolithos* HALDEMAN. All these trace fossils are poorly preserved, and the material does not contribute to the understanding of their origin.

FOSSILS FROM THE SILTSTONE ("GREEN SHALES")

The fossils occur almost exclusively in black phosphorite nodules; the very few fossils found outside the nodules have practically always an internal mould consisting of black phosphorite.

It admits of no doubt whatever that the fauna of the siltstone was benthonic. The writer is of opinion that the horizontal distribution of the fossils may be approximately that of the living individuals on the Lower Cambrian sea bottom.

It is a very remarkable fact that brachiopods and trilobites are entirely lacking. Nevertheless thin-shelled inarticulate brachiopods may have been members of the fauna, and their phosphatic shells may eventually have been engaged in the concentration of phosphate in the sediment resulting in the formation of the black phosphorite nodules.

The fossils are, as a rule, preserved as external and internal moulds, but in one single small, slightly phosphatic limestone lens collected by JOHNSTRUP at "Grødbyaa between Grødby and Grammegaarde", that is between localities 134 and 143, several of the fossils are found with their mineralized exoskeleton preserved; unfortunately, it has been impossible to find more concretions of this type.

Phylum *PORIFERA*

Class Hyalospongea VOSMAER, 1886

Order Lyssakida ZITTEL, 1877

Family uncertain

Genus et species ind. I (cf. *Pyritonema* M'COY, 1850)

Pl. 1, figs. 1-2.

Material: Numerous scattered hexacts in phosphorite nodules.*Localities*: 58 (coast cliff west of Julegaard), 139 (Grødbyaa), 178 and 194 (Øleaa).

Remarks: Only hexacts are known; they are fairly similar to those described and figured by RAUFF (1893-1894, p. 264, Pl. 6, figs. 7-15) as *Pyritonema gracile* (HINDE), from which they differ mainly by having less expanded ray bases. *Pyritonema*, however, is only known from extremely fragmentary specimens, and it can hardly be regarded as a valid genus. Accordingly, a safe determination of the fragmentary Bornholm material must be left out of consideration.

Class uncertain
 Order uncertain
 Family uncertain
Genus et species ind. II

Pl. 1, fig. 3.

Material: *Hyolithellus* tube in siltstone with megascleres of undeterminable types in the interior.

Locality: 194 (Øleaa).

Genus et species ind. III

Pl. 1, fig. 4.

Material: A specimen of *Hyolithes* in siltstone, with burrows containing a few spicule-like bodies which are much obscured by subsequent silicification.

Locality: 194 (Øleaa).

Remarks: In the writer's opinion these burrows may be a result of the activity of some excavating sponge.

Phylum *MOLLUSCA*
 Class Pelecypoda GOLDFUSS, 1820
 Order uncertain
 Family uncertain
 Genus *Fordilla* BARRANDE, 1881
Fordilla troyensis WALCOTT, 1886

Pl. 2, fig. 1.

1873. Bivalve of uncertain class; gen. nov., FORD, Am. Jour. Sci., 3rd ser., vol. 6, p. 139.
 1881. *Fordilla*, BARRANDE, Acéphales. Etudes Loc. et Comp., 8°, p. 391–393, Pl. 361.
 1886. *Fordilla troyensis* WALCOTT, U. S. Geol. Surv., Bull. 30, p. 123–125, Pl. 11, figs. 3, 3a–c.
 1890. *Fordilla troyensis* WALCOTT, U. S. Geol. Surv., 10th Ann. Rep., p. 615, Pl. 73, figs. 2, 2a–c.
 ? 1919. *Fordilla troyensis* (?) COBBOLD, Geol. Mag., dec. 6, vol. 5, p. 156, Pl. 4, fig. 33.
 1931. *Fordilla troyensis*, ULRICH & BASSLER, Proc. U. S. Nat. Mus., vol. 78, Art. 4, p. 97, Pl. 4, figs. 14–15.

1932. *Fordilla troyensis* POULSEN, Meddelelser om Grønland, vol. 87, no. 6, p. 16–17, Pl. 2, figs. 3–5.
1956. *Fordilla troyensis* LOCHMAN, Bull. Geol. Soc., America, vol. 67, p. 1372–1373, Pl. 1, figs. 5–10.

Material: Five specimens in black phosphorite nodules, represented by more or less fragmentary moulds of the interior and exterior of the shell.

Localities: 46 (Lilleaa), 139 (Grødbyaa), and 173 (Oleaa).

Remarks: ULRICH & BASSLER (1931) regarded *Fordilla* as a phyllopod because this genus “has the calcareo-phosphatic structure of the genera here referred to the Limnadiidae”, but WALCOTT’s reasons (WALCOTT 1886) for referring *Fordilla troyensis* to the Pelecypoda rather than to the Crustacea—not least the thickness of the shell, which exceeds that of Cambrian Crustacea except that of the trilobites—cannot be rejected without further ceremony; it should be noticed in this connection that specimens from the Lower Cambrian of East Greenland consist of irregularly grained calcite of the type found in shells where aragonite has been replaced by calcite; phosphate is not met with in the Greenland specimens. LOCHMAN (1956) is of opinion that “the calcareo-phosphatic appearance of the shell may be caused by an outer chitinous layer. Such a layer could be the source of the carbonaceous film retained on many specimens,” and the author mentioned adds that “considering the nature of this material it would seem unwise to arbitrarily reject *Fordilla* as a member of the Pelecypoda”; it should be noticed in this connection that muscle scars comparable to those of pelecypods have not yet been observed. The Bornholm specimens agree fairly well with LOCHMAN’s photographic figures, but the fragmentary state of preservation prevents additions to previous descriptions.

Genus et species ind.

Pl. 2, fig. 2.

Material: A couple of almost complete internal moulds of right and left valve in black phosphorite nodule.

Locality: 46 (Lilleaa).

Description: Shells transversely elongate, subelliptical in outline, somewhat convex, 1.25 times as long as high. Umbones moderately prominent, situated almost in the middle of the dorsal margin. Cardinal margin not visible throughout, but apparently bluntly angular; a row of six poorly developed teeth in front (?) of the umbo of the right (?) valve suggests the

presence of a taxodont hinge. Adductor muscular impressions not preserved. Surface of the interior of the right (?) valve marked with a few broad folds parallelling the ventral margin, whereas such folds are hardly discernible in the left (?) valve; a faintly marked keel extends from the posterior (?) part of the umbonal region to the posterior end of the ventral margin.

Dimensions: Height 1.7 mm., length 2.2 mm.

Remarks: The material is considered too imperfect to permit of any determination. Judging from the nature of the cardinal region, the specimens may be referred to the taxodont group of pelecypods.

Class Monoplacophora WENZ in KNIGHT, 1952
 Order Tryblidioidea LEMCHE, 1957
 Superfamily Tryblidiacea PILSBRY in ZITTEL-EASTMAN, 1899
 Family Tryblidiidae PILSBRY in ZITTEL-EASTMAN, 1899
 Subfamily Proplininae KNIGHT & YOCHELSON, 1958
 Genus *Proplina* KOBAYASHI, 1933
Proplina? prisca n. sp.

Pl. 3, fig. 1.

Material: External mould of right side of a shell in black phosphorite nodule.

Locality: 77 (Læsaa).

Description: Shell small, very high, bilaterally symmetrical, with in-curved, somewhat depressed apex overhanging anterior end. The most elevated point is about 1/6 the distance from the apex to the posterior end; from this point the outline curves regularly to the posterior end and anteriorly to the apex; outline from the apex to the anterior margin concave. Aperture circular. External surface marked by numerous, closely set lines of growth.

Dimensions:

Apertural diameters	2.00 mm.
Distance of apex from anterior margin	1.25 -
- - - - posterior -	2.85 -

Remarks: As mentioned above, the material consists of a single external mould; accordingly, muscle scars have not been observed, and the reference of the species to the genus *Proplina* and the Monoplacophora is questionable; otherwise the agreement with *Proplina* is fairly satisfactory. *Proplina? prisca*

differs from the type species (*Metoptoma cornutaformis* WALCOTT, 1879) in having a much higher shell, a less overhanging apex, and an external surface with finer concentric markings; it shows greater resemblance to *Proplina ampla* KOBAYASHI, 1933, but it is readily distinguished from that species by its higher shell and its less overhanging apex.

Order Archinacelloidea KNIGHT & YOCHELSON, 1958

Superfamily Archinacellacea KNIGHT, 1956

Family Hypseloconidae KNIGHT, 1956

Genus *Pollicina* HOLZAPFEL, 1895

Pollicina? cambrica (MOBERG, 1892)

Pl. 3, fig. 2.

1892. *Dentalium? cambricum* MOBERG, Geologiska Föreningens i Stockholm Förhandlingar, vol. 14, part 5, p. 117, Pl., figs 16–17.

Material: Three specimens in greyish brown phosphatic nodule, preserved as internal and external moulds.

Locality: 137 (Grødbyaa).

Description: Shell bilaterally symmetrical, regularly curved, rapidly tapering, with circular cross-section. The apertural plane appears to be perpendicular to the longitudinal shell axis. The rate of taper is about 1 in 3. Internal and external surfaces smooth.

Dimensions:

Height of shell	about 3 mm.
Apertural diameters	— 1 —

Remarks: The Bornholm material agrees perfectly with MOBERG's description and figures of *Dentalium? cambricum*. The shells of Scaphopoda, however, are open at both ends, and, accordingly, MOBERG's species should be excluded from this class. The species shows considerable resemblance to the genus *Pollicina* HOLZAPFEL. It is distinguished from the type species of that genus (*Cyrtolithes corniculum* EICHWALD, 1860) by its smaller size, less curved shell, and smooth external surface.

Muscle scars have not yet been observed in the shell of *Pollicina*, and the reference of this genus to a family of the Monoplacophora is therefore questionable.

Class Gastropoda CUVIER, 1797

Subclass Prosobranchia MILNE EDWARDS, 1848

Order Archaeogastropoda THIELE, 1925

Suborder Bellerophontina ULRICH & SCOFIELD, 1897

Superfamily Bellerophontacea M'COY, 1851

Family Sinuitidae DALL in ZITTEL-EASTMAN, 1913

Subfamily Sinuitinae DALL in ZITTEL-EASTMAN, 1913

Genus *Prosinuites* n. g. (type species: *Prosinuites bornholmensis* n. sp.)

Diagnosis: Shell bilaterally symmetrical, cap-shaped, with blunt apex overhanging the posterior margin. Anterior and posterior margin with broad shallow sinuses, that of the anterior margin having a tendency to generate a more or less obscure selenizone (pl. 3, figs. 4, 5, and 8).

Remarks: In the writer's opinion the bilateral symmetry and the tendency to develop a selenizone are characters which may indicate that *Prosinuites* should be regarded as a primitive member of the Bellerophontacea, in which development of coils had not yet taken place. The shape of the anterior emargination is fairly similar to that of the genus *Sinuites* KOKEN.

Prosinuites bornholmensis n. sp.

Pl. 3, figs. 3-9.

Material: Four internal moulds from grey limestone lens.

Locality: Grødbyaa between Grødby and Grammegaarde (exact locality unknown).

Description: Shell bilaterally symmetrical, with blunt, somewhat depressed apex overhanging the posterior margin; length (distance from the apex to the anterior margin) about twice the height; the most elevated point is about 1/4 the distance from the apex to the posterior end. Aperture approximately circular, with broad, shallow anterior and posterior emarginations, the posterior one terminating an obscure selenizone.

<i>Dimensions:</i>	I	II (holotype)	III
Length	5.8 mm.	6.6 mm.	6.6 mm.
Height	3.3 —	3.7 —	? —
Diameter of aperture	4.3 —	4.7 —	5.6 —

Remarks: *Helcionella? emarginata* COBBOLD, 1919 from the Lower Cambrian red, sandy limestone of Woodlands Quarry, Hartshill, may belong to the new genus *Prosinuites*; it differs, however, from the Bornholm species in having a lower shell with more strongly overhanging apex.

Class Calyptomatida FISHER, 1962
Order Hyolithida MATTHEW, 1899
Suborder Hyolithina MATTHEW, 1899
Family Orthothecidae SYSSOIEV, 1958
Genus *Circotheca* SYSSOIEV, 1958

Circotheca sp.

Pl. 5, figs. 8–9.

Material: One fragmentary external mould and one fragmentary internal mould in black phosphorite nodules.

Locality: 46 (Lilleaa).

Description: Shell slender, slightly curved, tapering at a rate corresponding to an apical angle of about 13° . Transverse section circular. Judging from the lines of growth, the plane of the apertural margin has a slight ventro-dorsal declination. External surface marked by numerous, crowded, extremely delicate growth lines of equal strength, and spaced about 12–14 to the millimetre; coarser lines of growth occur at irregular intervals.

Dimensions: The fragmentary state of preservation prevents exact information with regard to the size of the shell; in the writer's opinion a shell length of about 25–30 mm. is fairly probable.

Remarks: It is probable that the material represents a new species, but the fragments at hand do not allow of any adequate specific description or use as a holotype. The species appears to be closely related to *Circotheca stylus* (HOLM, 1893), which is the type species of the genus *Circotheca* SYSSOIEV, but it differs clearly from that species in the lack of longitudinal surface markings.

Genus *Orthotheca* NOVAK, 1886

Orthotheca groedbyensis n. sp.

Pl. 6, figs. 7–8.

Material: One fragmentary internal mould of the shell (holotype) and one fragmentary external mould in black phosphorite nodules.

Locality: 137 (Grødbyaa).

Description: Shell apparently straight, tapering at a rate corresponding to an apical angle of about 5° , with semielliptic transverse section. Ventral side slightly concave, with rounded lateral margins. Judging from the external mould, the shell surface is probably smooth.

Dimensions:

Estimated length	25 mm.
Lateral width near aperture	1.8 —
Dorso-ventral diameter near aperture	1.4 —

Affinities: *Orthotheca groedbyensis* is probably closely related to *Orthotheca holmi* COBBOLD¹ from the Lower Cambrian *Protolenus* limestone at Comley in Shropshire; the shell of both species have almost exactly the same semielliptic transverse section; the essential distinguishing character is the apical angle which is 8° in *Orthotheca holmi* and about 5° in *Orthotheca groedbyensis*.

Orthotheca johnstrupi HOLM, 1893

1893. *Hyalolithus (Orthotheca) johnstrupi* HOLM, Sveriges geologiska Undersökning, Ser. C, No. 112, p. 56, Pl. 1, figs. 28–33, 71.

Material: A very large number of fragmentary specimens preserved as internal and external moulds in siltstone and black phosphorite nodules.

Localities: 75, 77, 82², and immediately north of the bridge at Limensgade (Læsaa); 134 (Grødbyaa); 177 (Øleaa).

Remarks: This species is one of the dominant macro-fossils in the siltstone and the black phosphorite nodules, but the new material is not better preserved than that described by HOLM, and, accordingly, it does not allow of any additions to HOLM's description.

Orthotheca pervilis n. sp.

Pl. 6, figs. 1–2.

? 1893. *Hyalolithus (Orthotheca)* sp. No. 1, HOLM, Sveriges geologiska Undersökning, Ser. C, No. 112, p. 108, Pl. 1, figs. 51–52.

Material: One single fragmentary internal mould of the shell with adjoining fragmentary external mould (holotype) in black phosphorite nodule.

Locality: 77 (Læsaa).

Description: Shell apparently straight, tapering at a rate corresponding to an apical angle of about 8°, with almost evenly rounded dorsal side,

¹ In COBBOLD's paper of 1931 (*Quart. Journ. Geol. Soc.* London, vol. 87, pt. 3) *Orthotheca holmi* is regarded as identical with "*Hyalolithus (Orthotheca)* sp. no. 1" figured by HOLM 1893 (Sveriges Geologiska Undersökning, Ser. C, No. 112, Pl. 1, figs. 51–52), but COBBOLD's species from Comley shows a striking difference from the Swedish species with regard to the shape of the transverse section of the shell, that of the former having a much longer dorso-ventral diameter.

² Reworked specimens?

rounded lateral margins, and concave ventral side. Outline of transverse section reniform. External shell surface smooth.

Dimensions:

Estimated length of the shell	33 mm.
Lateral diameter of figured transverse section	6.0 -
Dorso-ventral - - - - -	2.8 -

Remarks: HOLM (1893, p. 108) was of opinion that his "*Hyolithus* (*Orthotheca*) sp. no. 1" differs from other species of his group "Plicati" in having a larger, straight shell with a smaller apical angle, so that it should probably be regarded as an independent species, but, considering the rather poor state of preservation, he did not introduce a specific name. The Bornholm specimen agrees perfectly with HOLM's description and figures, and the present writer is almost sure that it should be referred to the same species. The fact that HOLM's specimen and the Bornholm specimen are of Lower Cambrian age, whereas the closely related species of the group "Plicati" are Middle Cambrian, confirms the view that the Lower Cambrian specimens represent an independent species, for which the present writer proposes the name *Orthotheca pervilis*. The Bornholm specimen is designated as holotype.

Genus *Trapezotheca* SYSSOIEV, 1958

Trapezotheca? pistrinensis n. sp.

Pl. 6, figs. 3-6.

Material: One single fragmentary internal mould of the shell in black phosphorite nodule.

Locality: 77 (Læsaa).

Description: Shell apparently straight, tapering at a rate corresponding to an apical angle of about 9° , with a slight constriction just behind the aperture, strongly arched dorsal side, slightly concave ventral side, and rather narrowly rounded lateral margins. Dorso-lateral part of transverse section approximately parabolic. Aperture almost at right angles to the shell axis. Part of the dorsal crest shows a system of delicate, closely set transversal ridges, which may have a relation to external surface markings.

Dimensions:

Estimated length of the shell	42 mm.
Dorso-ventral width at aperture	4 -
Lateral - - - - -	6 -

Remarks: In the *Treatise on Invertebrate Paleontology*, vol. W, p. 127 FISHER gives the following generic diagnosis of *Trapezotheca*: "Cross section trapezoidal with flat or slightly concave venter. Aperture almost at right angles to shell axis." The type species of *Trapezotheca* (*Hyolithus* (*Orthotheca*) *aemulus* HOLM, 1893) has a subtrapezoidal cross section, although the dorsal angularities have a somewhat rounded appearance. The cross section of *Trapezotheca?* *pistrinensis* differs from that of the type species by having an evenly rounded dorsal crest, and, accordingly, it is not subtrapezoidal, but even a very slight depression of the dorsal crest would immediately result in a cross section similar to that of the typical *Trapezotheca*. The cross section of the Bornholm species appears to be intermediate between that of a specific group of *Orthotheca* (the "Plicati" of HOLM) and that of the type species of *Trapezotheca*, and, accordingly, the present writer is of opinion that maintainance of SYSSOIEV's genus *Trapezotheca* may be questionable.

The apical angle and the cross section serve to distinguish the Bornholm species from similar species of *Trapezotheca* and *Orthotheca*.

Family Hyolithidae NICHOLSON, 1872

Genus *Hyolithes* EICHWALD, 1840

Hyolithes balticus n. sp.

Pl. 3, fig. 10; Pl. 4, fig. 1.

Material: One single fragmentary specimen from black phosphorite nodule, showing the internal mould of the shell and small parts of the external mould.

Locality: 46 (Lilleaa).

Description: Shell straight, tapering almost uniformly at a rate corresponding to an apical angle of about 22° . Dorsal side slightly convex; ventral side slightly concave; lateral margins rounded. Ratio of diameters 1 to 3. Aperture not preserved, but surface markings indicate that it has an evenly rounded, moderately projecting ventral lip and a rectilinear dorso-lateral margin. Surface of internal mould marked by faintly indicated, broadly rounded ridges paralleling the apertural margin and spaced about 6-7 to the millimetre; in the external mould these ridges are very strong and clearly marked.

Dimensions: Neither aperture nor apex is preserved, and, accordingly, it is impossible to estimate the size of the shell. The fragment at hand is about 5.5 mm. long.

Remarks: The apical angle combined with the surface markings and the extremely short dorso-ventral diameter should characterize the species. *Hyalithes balticus* appears to hold a very isolated position; at any rate, the writer has not succeeded in finding any closely related species.

Hyalithes groenwalli n. sp.

Pl. 4, figs. 2-8; Pl. 5, figs. 1-6; text-fig. 4.

Material: Five fragmentary specimens with preserved shell in grey limestone lens and eight associated appendages of the type frequently referred to as *Helenia* by several authors.

Locality: According to the original labels the material was collected by F. JOHNSTRUP in 1869 at the Øleaa between Grødby and Grammegaarde. The exact location is unknown. One appendage has been collected by the present writer from black phosphorite nodule in locality 46 (Lilleaa).

Description: Shell slightly curved towards the dorsal side, tapering at a rate corresponding to an apical angle of about 10° . Aperture with evenly rounded, moderately projecting ventral lip and a slightly concave dorso-lateral margin. Transverse section almost semicircular; ratio of diameters 1 to 2. Ventral side slightly convex, with faintly marked, narrow, concave zone along lateral margins; dorsal side strongly and evenly convex. External surface marked by irregularly spaced longitudinal ridges of unequal strength spaced about 2-3 to the millimetre, and irregularly spaced lines of growth of unequal strength spaced about 7-9 to the millimetre; these surface markings have a tendency to form a reticulate pattern on the dorsal face.

Dimensions: Apertural width of the holotype is 6 mm.; estimated total length about 40 mm.

Affinities: *Hyalithes groenwalli*, which is especially characterized by its small apical angle, semicircular transverse section, and irregularly spaced longitudinal ridges, shows some resemblance to *Hyalithes princeps* BILLINGS from the Lower Cambrian of Newfoundland and Massachusetts with regard to the curvature of the shell and the reticulate pattern of the dorsal side, but it differs clearly from the American species in having a much smaller apical angle, semicircular transverse section, and longitudinal ridges on the ventral face.

The associated appendages (the *Helenia* of some authors) are, as mentioned above, represented by eight specimens. WALCOTT (1889) described the "type species", *Helenia bella* WALCOTT, as follows: "Shell an elongate, narrow, flattened, curved tube. The plane of the flattened surfaces is slightly twisted, so as to throw lateral margins about one quarter of a turn around

and to incline the upper and lower faces nearly 45° at one extremity as compared with the other. The curvature is nearly semicircular. The cross section is an elongated ellipse. The form of the aperture of the larger extremity, as indicated by the striae of growth, has the peristome arching forward on one of the flattened sides and curving slightly backwards on the opposite side. As far I am able to determine, the shell was open at the smaller end, as in *Dentalium*, or the extremity was decollated in all the specimens collected." . . . "Surface marked by irregular, transverse or concentric, im-

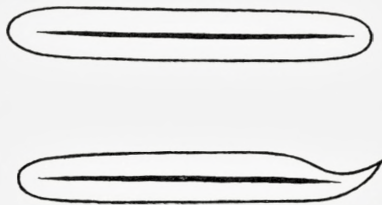


Fig. 4. Appendages of *Hyolithes groenwalli*, n. sp., cross section of a specimen with dorsal furrow (below) and another specimen without furrow ($\times 30$).

bricating lines of growth that vary in number and size on the same specimen and in different specimens."

FISHER (1962) published the following generic diagnosis: "Elongate, narrow, flattened, curved tube, degree of curvature increasing toward closed end; cross section elongate-elliptical. Surface marked by irregular, transverse or concentric imbricating lines that vary in number and size."

MAREK'S (1961) description of material from Bohemia has contributed essentially to the knowledge of appendages; his description runs as follows: "E. L. YOCHELSON describes the shape of the appendages which suggests a curve of logarithmic nature. In the material from Bohemia this shape is also clearly visible. The curvature of the appendages increases towards their narrower distal end, while the part closer to the hyolithid shell is less curved. As established in well-preserved, non-compressed material, the shape of the appendages in cross-section was that of a flattened ellipse. So far it has not been found whether they were compact or hollow, the latter possibility being more probable. In wellpreserved specimens the fine transverse growth lines may be seen on the surface of the appendages; the lines are sometimes curved towards the distal end of the appendage, which is rounded. In addition to it, sculpture formed by very fine transverse furrows has also been established. The coarse longitudinal lines visible in some appendages only, which have also been mentioned by E. L. YOCHELSON,

seem to be due to pressure. The appendages were composed, no doubt, of the same mass as the shells and opercula of *Hyalithes*. Contrary to V. A. SYSOIEV'S (1959) assumption, they were firm structures incapable of coiling and withdrawing into the shell. This means that the appendages projected out of the shell during the animal's life, which was possible due to small openings originating at the contact of the operculum with the shell between the so-called lateral sinuses on the operculum and the insignificant indentation on the sides of the aperture."

The Bornholm material agrees in all essentials with MAREK'S description, but it is now possible to add a few facts. According to BØGGILD (1930), the shell of *Hyalithes* consists of irregularly grained calcite of the type found in shells of molluscs in which primary aragonite has been replaced by calcite; *Hyalithes groenwalli* as well as the associated appendages have the structure mentioned, and it can hardly be doubted that the hyolithid shells and their appendages consisted of aragonite. Transverse sections show that the appendages are hollow, but the walls are thick so that the cavity is very inconsiderable (fig. 4). The appendages here referred to *Hyalithes groenwalli* very clearly show the transverse, imbricating lines of growth, and these lines are spaced about 5–9 to the millimetre. The coarse longitudinal line, regarded by MAREK as a result of pressure, is well-developed in some of the Bornholm specimens which have certainly not been deformed. The longitudinal line has the shape of a broad furrow; it is situated on the dorsal side and extends along the rounded antero-lateral margin apparently to the distal end (Pl. 5, fig. 1); the longitudinal furrow is better developed in some specimens than in others and is sometimes entirely lacking. A few specimens show three indistinctly marked longitudinal furrows on the ventral surface (Pl. 5, fig. 3).

As compared with the appendages of other species, those of *Hyalithes groenwalli* are easily distinguished by their wider, more rapidly tapering body and the location of the dorsal longitudinal furrow close to the antero-lateral margin.

Hyalithes lenticularis HOLM, 1893

1893. *Hyalithus lenticularis* HOLM, Sveriges Geologiska Undersökning, Ser. C, No. 112, p. 79, Pl. 5, figs. 23–28.

Material: Four fragmentary internal moulds of the shell, three specimens in siltstone and one in black phosphorite nodule.

Locality: 77 (Læsaa).

The specimens are poorly preserved, and accordingly nothing can be added to HOLM'S description.

Hyolithes nathorsti HOLM, 1893

Pl. 6, fig. 9.

1893. *Hyolithus nathorsti* HOLM, Sveriges Geologiska Undersökning, Ser. C, No. 112, p. 87, Pl. 1, figs. 65–70.

Material: To the few specimens described and figured by HOLM have been added a few fragmentary internal and external moulds of the shell, partly from black phosphorite nodules, partly from coarse sandstone just below the Rispebjerg sandstone,² and two external moulds of an operculum in black phosphorite nodules possibly belonging to this species.

Localities: 77, 84 (Læsaa), 232 (Broens Odde), 173 (Øleaa (operculum)), 46 (Lilleaa (operculum)).

Description: The poorly preserved fragments of the shell do not allow of any addition to HOLM's description. The opercula, however, are well-preserved; they are tentatively referred to *Hyolithes nathorsti* and may be described as follows:¹ Outline subcircular, with a very broadly rounded triangular tendency. The furrow separating the cardinal shield from the conical shield is shallow. Rooflets indistinctly defined, without any indication of lateral sinuses. Conical shield moderately convex, with an apical angle of about 135°. External surface marked by numerous fine lines of growth paralleling the margin of the operculum and by extremely delicate, faintly marked, rounded riblets radiating from the apex and only visible in the middle portion of the conical shield.

Dimensions:

Length of operculum	3.8 mm.
Width — —	4.6 —
Length — conical shield	3.3 —

Affinities: The operculum here referred to *Hyolithes nathorsti* and that of *Hyolithes tenuistriatus* LINNARSSON as figured by HOLM (1893, pl. 1, fig. 88) have several characters in common, but the former clearly differs from the latter by having a rounded triangular outline, a smaller apical angle of the conical shield, and better developed radiating surface markings on the conical shield.

¹ The morphological terms applied to the operculum are those proposed by MAREK (1963).

² Reworked specimens?

Hyolithes sp. I.

Pl. 6, figs. 10–11.

Material: Three internal moulds of the operculum in black phosphorite nodules.

Locality: 46 (Lilleaa).

Description: Outline subcircular with slightly triangular tendency. Convex main portion entirely surrounded by a very wide, almost flat border delimited by a strong groove; the groove becomes wide in front of the rooflets, where it sinks to deep, triangular pits (natural casts of a bipartite cardinal process) separated from each other by a bridge (natural cast of the central pit). The furrow separating the cardinal shield from the conical shield is shallow. Rooflets fairly well defined, rapidly expanding from the apex of the conical shield to the lateral margin, and without any indication of lateral sinuses. Conical shield moderately convex, with an apical angle of about 100° . Surface of the internal mould marked by relatively coarse, closely set, radiating ridges of varying strength on the conical shield, the rooflets, and the cardinal process, each of the ridges carrying a single row of closely set granules; border smooth.

Dimensions:

Length of operculum	4.7 mm.
Width — —	4.7 —
Length — conical shield	3.8 —

Affinities: The writer is of opinion that the above-described operculum may represent a new species, but it has not been possible to combine it with any of the *Hyolithes* shells at hand, and, accordingly, a specific name for this fossil has been left out of consideration. It shows some resemblance to the operculum of *Hyolithes strettonensis* COBBOLD, 1921, from which it differs by having a much wider border, a smaller cardinal process, and the internal surface marked by radiating ridges.

Hyolithes sp. II.

Pl. 5, fig. 7.

Material: One specimen represented by the external mould of the ventral surface of the shell in black phosphorite nodule.

Locality: 46 (Lilleaa).

Description: Shell straight with exception of the apical end, which is slightly curved towards the dorsal side, rapidly tapering at a rate corresponding to an apical angle of about 20° . Aperture with evenly rounded, moderately projecting ventral lip. Ventral side slightly convex, merging into rounded lateral margins. External surface of ventral side marked by lines of growth of subequal strength, spaced about 14 to the millimetre.

Dimensions: Apertural width about 2 mm.; estimated length of the shell about 6 mm.

Remarks: The specimen described above may represent a new species, the apical angle surpassing that of most Lower Cambrian species, but the fragmentary state of preservation does not allow of any safe identification or use as a type.

Hyolithes sp. ind.

Material: A fragment of the ventral side of the shell in black phosphorite nodule.

Locality: 58 (coast cliff at Julegaard).

Remarks: Judging from the fragment at hand, the shell must have been much larger than those of all the species described above; it is possible that it represents a distinct species, but the material does not allow of any use of it as a basis for description and comparison.

Family Halkieriidae n. fam.

Diagnosis the same as that of the genus *Halkieria*

Genus *Halkieria* n. g.

(Type species *Halkieria obliqua* n. sp.)

Diagnosis: Shell elongate, with slightly convex, almost flat ventral side and moderately convex dorsal side, curved towards the ventral side, tapering towards the apex at an increasing rate, bilaterally symmetrical or slightly twisted so as to show a tendency to form an ascending spiral. External surface markings of the ventral side consisting of delicate, transverse lines of growth and a distinctly marked, median longitudinal groove; external dorsal markings consisting of fairly coarse, transverse lines of growth crossed by strongly marked longitudinal ridges.

Remarks: The affinities of this new genus are uncertain. The general habit of the shell, however, is not very far from that of the *Hyolithina* MATTHEW, 1899, and, accordingly, *Halkieria* and the family Halkieriidae are provisionally placed in that suborder.

Halkieria obliqua n. sp.

Pl. 2, figs. 3-4.

Material: Four external moulds of the dorsal side and two external moulds of the ventral side in black phosphorite nodules.

Localities: 46 (Lilleaa) and 126 (Grødbyaa).

Description: Shell about three times as long as wide, with slightly convex, almost flat ventral side and moderately convex dorsal side, tapering towards the apex at an increasing rate, curved towards the ventral side, slightly twisted so as to form an ascending spiral. External surface markings of the ventral side consisting of delicate, transverse lines of growth and a strongly marked, median, longitudinal groove; those of the dorsal side consisting of rather coarse, transverse lines of growth crossed by strongly marked longitudinal ridges, which are spaced about 10 to the millimetre and provided with minute granules where they cut across the lines of growth.

<i>Dimensions:</i>	I (holotype)	II
Length	about 3.3 mm.	about 4.0 mm.
Maximum width	— 1.15 —	— 1.36 —

Remarks: *Halkieria obliqua* is easily distinguished from the only other known species (*Halkieria symmetrica* n. sp.) by its twisted shell and the larger number of dorsal, longitudinal ridges.

Halkieria symmetrica n. sp.

Pl. 2, fig. 5.

Material: One external mould of the dorsal side and part of the ventral interior in black phosphorite nodule.

Locality: 126 (Grødbyaa).

Description: Shell about 3.6 times as long as wide, bilaterally symmetrical, with slightly convex, almost flat ventral side and strongly convex dorsal side. Dorsal surface markings consisting of indistinctly marked, transverse lines of growth crossed by strongly marked, prominent longitudinal ridges which are spaced about 6 to the millimetre and furnished with minute, closely set granules on their crests.

<i>Dimensions:</i>	
Length	about 4.5 mm.
Maximum width	— 1.1 —

Remarks: Halkieria symmetrica is readily distinguished from the type species (*Halkieria obliqua* n. sp.) by its bilaterally symmetrical shape and by the smaller number of longitudinal ridges.

Phylum *POGONOPHORA* JOHANSSON, 1937 (as class Pogonophora)

The position of the Pogonophora in the animal kingdom has been much discussed and is still a problem. The present writer is not ready to discuss this question here, the more so because the genus *Hyolithellus* BILLINGS mentioned below, which was referred to the Pogonophora by V. POULSEN in 1963, fails to throw light on the problem. The group is here tentatively regarded as a phylum.

Class Hyolithelloida nov.

(Class proposed to include the order Hyolithellida SYSSOIEV, 1957).

Order Hyolithellida SYSSOIEV, 1957 (emend. V. POULSEN, 1963)

Family Hyolithellidae WALCOTT, 1886

Genus *Hyolithellus* BILLINGS, 1871

As mentioned above, V. POULSEN (1963) referred the genus *Hyolithellus* to the Pogonophora. This opinion was supported by several points of resemblance emphasized by that author, e. g. the relatively high content of calcium, nickel, and zinc in the tubes. Furthermore, X-ray fluorescence analysis of extraordinarily well-preserved tubes of *Hyolithellus* shows that no phosphorus is present. The same well-preserved material also shows that the tubes of *Hyolithellus* and those of the recent Pogonophora have several amino acids in common, i. a. Alanin.¹ Finally the length of the tube, as shown by the below-mentioned specimen of *Hyolithellus micans* BILLINGS from northern Sweden, is another point of resemblance. It appears from the above-mentioned paper by V. POULSEN (1963) that *Discinella* HALL and *Mobergella* HEDSTRÖM should not be regarded as opercula of *Hyolithellus*.

Hyolithellus micans BILLINGS, 1871

Pl. 7, figs. 1-2.

1871. *Hyolithellus micans* BILLINGS, Canadian Naturalist, 2nd ser., vol. 6, p. 215, fig. 3a on p. 213.
 1886. *Hyolithellus micans* WALCOTT (pars), Bull. U. S. Geol. Surv., No. 30, p. 142, Pl. 14, figs. 2, 2a-b.

¹ Written communication from Dr. DAVID B. CARLISLE of the Anti-Locust Centre, London.

1888. *Hyolithellus micans* SHALER & FOERSTE, Bull. Mus. Comp. Zool. Harvard, vol. 16, p. 34, Pl. 2, fig. 23.
1890. *Hyolithellus micans* WALCOTT (pars), U. S. Geol. Surv., 10th Annual Report, p. 624, Pl. 79, figs. 1, 1a-b.
1891. *Hyolithellus micans* LAPWORTH, Geol. Mag., p. 522.
1893. *Hyolithellus micans* HOLM, Sveriges Geologiska Undersökning, Ser. C, No. 112, p. 108, Pl. 1, figs. 14-15.
1899. *Hyolithellus micans* MATTHEW, Bull. Nat.-Hist. Soc. New Brunswick, No. 18, p. 192, Pl. 2, figs. 1a-d.
1899. *Hyolithellus micans* MATTHEW, Trans. Roy. Soc. Canada, vol. 5, Sect. 4, p. 109, Pl. 6, figs. 1a-d.
1920. *Hyolithellus micans* COBBOLD, Quart. Journ. Geol. Soc. London, vol. 76, Pl. 24, figs. 19-21.
1925. *Hyolithellus micans* STÖRMER, Fennia, vol. 45, No. 1, p. 16, Pl. 1, fig. 5; Pl. 2, fig. 2 (?).
1932. *Hyolithellus micans* C. POULSEN, Meddelelser om Grønland, vol. 87, No. 6, p. 19; p. 30, Pl. 7, fig. 10.
1945. *Hyolithellus micans* KAUTSKY, Geologiska Föreningens i Stockholm Förhandlingar, p. 138, Pl. 14, figs. 1-5.
1956. *Hyolithellus micans* LOCHMAN (pars), Bull. Geol. Soc. America, p. 1369, Pl. 2, figs. 11-21.
1963. *Hyolithellus micans* V. POULSEN, Biologiske Meddelelser, Kongelige Danske Videnskabernes Selskab, vol. 23, No. 12, p. 1-14, figs. 1b-c.

Material: Two tube fragments with preserved shell in grey limestone lens and 10 external moulds in black phosphorite nodules and siltstone.

Localities: 46 (Lilleaa), 77 (Læsa), an unnumbered locality between Grødby and Grammegaarde (Grødbyaa), 178 (Øleaa), and 232 (Broens Odde).

Description: Tubular shell curved and irregular near the apical end, but straightening towards the aperture. Growth angle of mature specimens varying from 1°-4°. Cross section circular, up to about 3 mm. in diameter. Wall thin at the apical end, increasing gradually in thickness towards the aperture by addition of laminae. Surface markings consisting of a faint irregular annulation and transverse striation. Internal surface of tube smooth. As far as known, complete specimens have never been found. Fragments are usually 5-10 mm. in length; the longest specimen known, a tube fragment from the Lower Cambrian of Aistjakk in northern Sweden, is about 171 mm. long, and its maximum diameter is about 2 mm.

Genera and species of uncertain systematic position.

Family Coleolidae FISHER, 1962

FISHER'S description of the family reads as follows: "Tubuliform calcium-carbonate shells, extremely elongate-conical, almost cylindrical and com-

monly slightly curved towards the apex; cross section circular to elliptical; comparatively thick-walled; laminated, interior surface smooth. Exterior surface smooth or with oblique or longitudinal ornamentation. Opercula and septa unknown. Length 0.5–75 mm., diameter 0.5–2.5 mm. at aperture.”

Remarks: The position of the Coleolidae in the zoological system has been discussed by SANDBERGER (1852), ROEMER (1853), HALL (1879 and 1888), SYSSOIEV (1958), and FISHER (1962). According to the last-mentioned author “much may be said for retaining the coleolids in the Mollusca. Coleolids are possibly ancestral scaphopods but if so, they reveal no evidence of the burrowing habits of living scaphopods. On the other hand, early scaphopods may have been pelagic.” The present writer has had an opportunity of studying fairly well-preserved specimens of *Coleoloides multistriatus* COBBOLD from the Lower Cambrian of Woodlands Quarry at Hartshill in the Nuneaton district, Warwickshire. Two of these are preserved so as to show the laminated nature of the shell, which appears to consist of three distinct layers. This character is in favour of a scaphopod assignment. It deserves notice in this connection that the chemical properties of the shell of *Coleoloides multistriatus* are practically identical with those of the shell of *Dentalium (Antalis) entalis* L. On the other hand, the shells of scaphopods differ from those of the coleolids by having an aperture at each end, and, accordingly, the position of the Coleolidae is still uncertain.

Genus *Coleoloides* WALCOTT, 1889

Coleoloides bornholmensis n. sp.

Pl. 8, figs. 3–4.

Material: Seven external moulds of fragmentary shells in black phosphorite nodules.

Localities: 46 (Lilleaa) and 132 (Grødbyaa).

Diagnosis: A *Coleoloides* with extremely coarse surface markings consisting of longitudinal ridges defined by deep longitudinal grooves.

Description: Shell extremely elongate-conical. Cross sections circular. Surface markings extremely coarse, consisting of about 12–14 deep longitudinal grooves defining prominent longitudinal ridges, which communicate by anastomosis in a few places and are provided with a faintly marked longitudinal furrow on their crest. The initial portion of the shell smooth up to an estimated distance from the apex of about 3 mm., where faint surface markings appear increasing gradually in strength so as to be fully developed at an estimated distance from the apex of about 5 mm.

Dimensions:

Length of figured fragment	7.4 mm.
Anterior diameter of the same	0.25 –

Remarks: *Coleoloides bornholmensis* differs from all species hitherto known, except *Coleoloides rugosus* (p. 35), by having extremely coarse surface markings, and it differs from the last mentioned species by having a more acute apical angle and more regular surface markings.

Coleoloides multistriatus COBBOLD, 1919

Pl. 8, fig. 2; Pl. 9, figs. 1–4.

1919. *Coleoloides typicalis* WALCOTT var. *multistriatus* COBBOLD, Geol. Mag., N. Ser., Decade 6, Vol. 6, p. 154, Pl. 4, figs. 30–32.

Material: Six external moulds in black phosphorite nodules and eight fragmentary shells in grey limestone lens.

Localities: 139 (Grødbyaa) and an unnumbered locality between Grødby and Grammegaarde (Grødbyaa).

COBBOLD's description reads as follows: "Straight tubes of circular section with very slight taper are plentiful in the rock specimens to hand, but very rarely preserve the original surface. In two instances (15 and 38), however, the external surface marks are perceptible; they are very closely set spiral lines, numbering about seventy in the whole circumference of the tube, which is one millimetre in diameter; they are inclined at such an angle as to make one complete circuit of the tube in an length equal to about 10 diameters. . . . The tubes vary in diameter from 1 to 1.3 millimetres."

Remarks: The Bornholm specimens agree very well with the British material. The type locality is Woodlands Quarry, Hartshill, in the Nuneaton district, Warwickshire, where COBBOLD's specimens were collected from a red sandy limestone. Dr. A. W. A. RUSHTON has kindly placed such material from this locality at the writer's disposal and even furnished important supplementary information. It appears from Dr. RUSHTON's studies that some specimens of *Coleoloides multistriatus* show striae at differing slopes at differing points or, in other words, the obliquity of the striae may vary considerably in one and the same specimen. In some specimens the striation is parallel to the longitudinal axis of the shell. It also appears from Dr. RUSHTON's material that the initial portion of the shell, up to a point where the diameter amounts to about 0.25 mm., has a smooth external surface. It

may be added that the striation appears to be sharply marked in some specimens and less so in others, varying from strongly marked striation to practically or absolutely smooth external surfaces.

Pl. 8, figs. 2, shows a normal specimen with preserved shell, collected from a grey limestone lens between Grødby and Grammegaarde (Grødbyaa); Pl. 9, figs. 1–4, shows irregular growth of three specimens in one and the same black phosphorite nodule from locality 139 (Grødbyaa).

Coleoloides paucistriatus n. sp.

Pl. 8, fig. 1.

Material: One single external mould of a shell in black phosphorite nodule.

Locality: 46 (Lilleaa).

Diagnosis: A *Coleoloides* with surface markings consisting of a small number of narrow longitudinal ridges and intervening, wide flat spaces.

Description: Shell extremely elongate-conical. Cross section circular. Surface markings consisting of about 10–12 narrow, slightly oblique longitudinal ridges and intervening spaces twice to three times as wide as the ridges; the ridges communicate by anastomosis in a few places.

Dimensions:

Length of the figured fragment 4.0 mm.
Anterior diameter of the same 0.2 –

Remarks: *Coleoloides paucistriatus* differs from all species of *Coleoloides* hitherto known by having very wide, flat spaces between the longitudinal ridges.

Coleoloides rugosus n. sp.

Pl. 8, fig. 5.

Material: One single external mould of shell fragment in black phosphorite nodule.

Locality: 46 (Lilleaa).

Diagnosis: A *Coleoloides* with rather rapidly tapering shell and extremely coarse surface markings consisting of irregularly undulating longitudinal ridges and intervening grooves of varying width in one and the same specimen.

Description: Shell elongate-conical. Cross section circular. Surface markings extremely coarse, consisting of about 14–16 irregularly undulating ridges, which communicate by anastomosis in a few places, and intervening grooves of varying width. Initial portion of the shell not preserved.

Dimensions:

Length of the figured fragment 1.7 mm.
 Anterior diameter of the same 0.3 -

Remarks: *Coleoloides rugosus* appears to be closely related to *Coleoloides bornholmensis*, from which it differs by having a less acute apical angle and less regular surface markings.

Genus *Pseudorthis* COBBOLD, 1935*Pseudorthis danica* n. sp.

Pl. 7, figs. 3-4.

Material: Five external moulds in black phosphorite nodule.

Localities: 46 (Lilleaa), 142 (Grødbyaa), and 173 (Øleaa).

Diagnosis: A *Pseudorthis* with numerous annulations marked by irregular, engirdling ribs which communicate in places by anastomosis.

Description: Shell tapering at a rate corresponding to an apical angle of about 7°. Cross section circular. Surface markings consisting of sharply defined, closely set, rounded, somewhat irregular, transverse, thread-like ribs, which communicate in places by anastomosis, and are spaced rather regularly 12-13 in a length equal to the diameter of the shell.

Dimensions:

Length of holotype (Pl. 7, fig. 3) about 3 mm.
 Estimated total length of the same - 7 -
 Anterior diameter - - - - 0.7 -

Remarks: The material at hand does not contribute to our knowledge with regard to the systematic position of *Pseudorthis*. The Bornholm species described above differs from the species hitherto described by having more irregular, partly inosculating ribs.

Genus *Glauderia* n. g.¹

(Type species: *Glauderia mirabilis* n. sp.)

Diagnosis: Body slender, subcylindrical (or fusiform?), with subcircular cross section and two deeply impressed longitudinal grooves, which are diametrically opposed to each other and apparently extending along the

¹ Generic name derived from Julegaard, the name of the finding-place, by changing the order of succession of the relevant letters.

greater part (or total length?) of the shell. Shell phosphatic, apparently consisting of one single layer. External surface smooth. Interior of the shell densely granulated and showing two longitudinal ridges corresponding to the external longitudinal grooves.

Glauderia mirabilis n. sp.

Pl. 7, fig. 5.

Material: One single fragmentary specimen in black phosphorite nodule.

Locality: 58 (Coast cliffs at Julegaard, south coast of Bornholm).

Description: Same as that of the genus.

Dimensions:

Length of the figured fragment 6.25 mm.

Maximum diameter of the same 0.55 -

Remarks: Unfortunately the new genus *Glauderia* is only known from a single fragmentary specimen. Both ends of the body are lacking, and accordingly our knowledge of this strange fossil is very incomplete. The specimen, however, is so highly different from other fossils known to the writer that he does not hesitate to use it as the type of a new genus. It deserves notice, as a very rare exception, that the shell is preserved.

Genus *Halopoa* TORELL, 1870

Halopoa cf. *imbricata* TORELL, 1870

Text-fig. 5.

1965. *Halopoa imbricata* MARTINSSON, Geologiska Föreningens i Stockholm Förhandlingar, vol. 87, p. 219–221, text-fig. 29.

Material: Several specimens in fifteen samples of siltstone.

Locality: 232 (Broens Odde).

Remarks: The epichnial trace fossil *Halopoa* is probably present in most of the siltstone beds of the "Green shales".

The Bornholm specimens agree fairly well with the lectotype of *Halopoa imbricata* chosen by MARTINSSON (*op. cit.*, text-fig. 29), but their size is slightly smaller than that of the figured type specimen from the Lower Cambrian of Lugnáas in Västergötland. The "imbricated" nature of the Bornholm specimens is only preserved in a few cases.

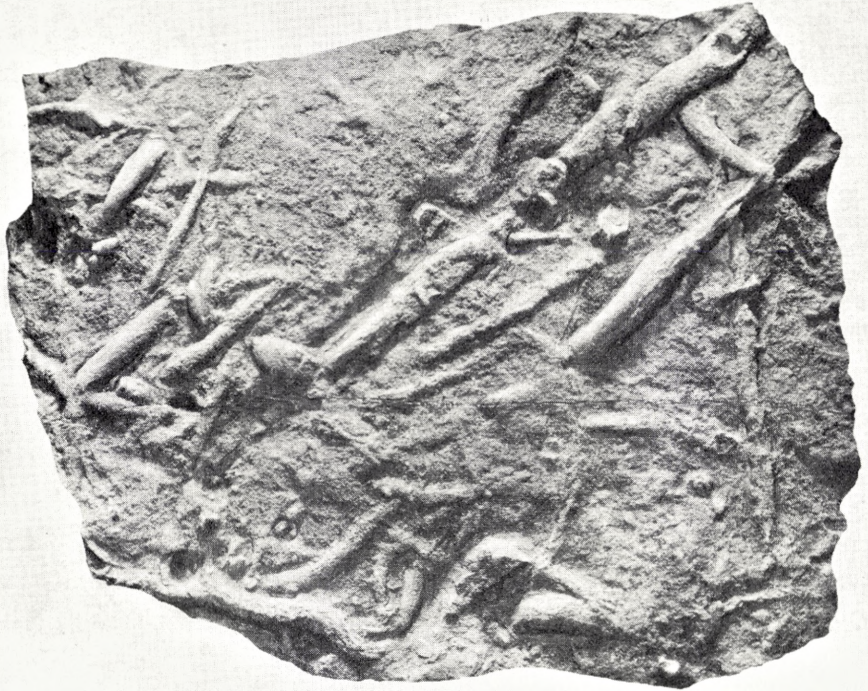


Fig. 5. *Halopoa* cf. *imbricata* TORELL (natural size) in siltstone from Broens Odde (locality 232).

It deserves notice that *Halopoa* shows great resemblance to *Gyrochorte* HEER, 1865 (Cambrian-? Tertiary) and to the Permian *Scoyenia* WHITE, 1929, which may belong to one and the same group of trace fossils, and, as mentioned by MARTINSSON (*op. cit.*, p. 219), "the differences may possibly turn out to be due to differences in lithology and preservation."



Fig. 6. *Cruziana dispar* LINNARSSON (natural size) in Rispebjerg sandstone from Borregaard on Oleaa.

FOSSILS FROM THE RISPEBJERG SANDSTONE

Phylum ARTHROPODA

Class Trilobita WALCH, 1771

Order Reedlichiida RICHTER, 1933?

Suborder Olenellina RESSER, 1938?

Genus et species ind.

Text-fig. 6.

Material: A trace fossil in Rispebjerg Sandstone.*Locality:* Borregaard, Øleaa.

Remarks: The trace fossil agrees very well with that from the Lower Cambrian Sandstone at Lugnås, Sweden, described and figured by LINNARSSON (1871, p. 14–16, Pl. 3, fig. 12) as *Cruziana dispar*. The size of the trace indicates that it was probably made by an olenellid trilobite.

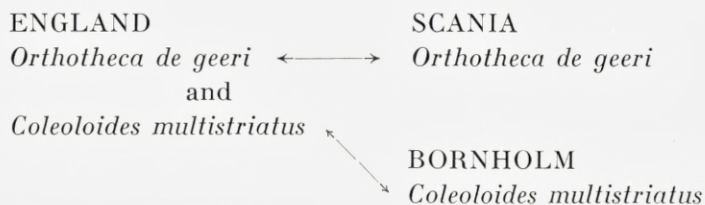
THE STRATIGRAPHIC SIGNIFICANCE OF THE FOSSILS

The occurrence of *Diplocraterion*, *Tigillites*, and *Skolithos* in the Balka quartzite is in favour of a correlation with the Scanian sandstone, which contains the same trace fossils and which has been referred to the *Mobergella holsti* zone (REGNÉLL 1960), although this guide fossil has never been found in Scanian strata. The Balka quartzite has likewise been referred to the *Mobergella holsti* zone (V. POULSEN 1966), but also here the guide fossil is lacking. It seems probable, as already mentioned, that the Balka quartzite is the stratigraphic equivalent of the Scanian sandstone with *Diplocraterion*, etc., but in the writer's opinion the reference of these rocks to the *Mobergella holsti* zone must be regarded as uncertain on account of the lack of palaeontological evidence.

It has been the practice to correlate the Lower Cambrian siltstone and Rispebjerg sandstone of Bornholm with the *Holmia torelli* zone of Scania (GRÖNWALL 1916; C. POULSEN 1935; HANSEN 1937; C. POULSEN 1942; V. POULSEN 1966). This correlation, however, is based on very unsatisfactory material, the fauna of the siltstone being essentially endemic. Only three species are known from other regions, viz. *Fordilla trogensis* WALCOTT, *Coleoloides multistriatus* COBBOLD, and *Hyolithellus micans* BILLINGS.¹

¹ GRÖNWALL (1916) mentions the occurrence of *Torella laevigata* LINNARSSON. The present writer, however, has examined the specimens in question, some of which must be regarded as undeterminable, whereas others proved to be fragments of *Hyolithellus micans* BILLINGS.

Hyalithellus micans appears to have a considerable vertical distribution within the Lower Cambrian, and the stratigraphic range of *Fordilla troyensis* is not yet sufficiently known; accordingly, these widely distributed species are left out of consideration here. *Coleoloides multistriatus* is only known from the Lower Cambrian siltstone of Bornholm and from Lower Cambrian sandy limestone at Hartshill, Warwickshire, England. In the last mentioned locality it is associated with *Orthotheca de geeri* HOLM, which is one of the characteristic species of the Scanian *Holmia torelli* zone. *Orthotheca de geeri*, however, has never been found in the Lower Cambrian siltstone of Bornholm, and accordingly the correlation of the siltstone with the *Holmia torelli* zone of Scania is based on very meagre evidence, as shown in the following scheme:



List of Fossils and Localities	Lilleaa	Julegaard	Laesaa			
	46	58	75	77	82	84
Genus et sp. ind. (cf. <i>Byronia</i> MATTHEW)						
<i>Diplocraterion</i> sp.						
<i>Tigillites</i> sp.						
<i>Skolithos</i> sp.						
Genus et sp. ind. I (cf. <i>Pyritonema</i> M'COY)		+				
- - - - II						
- - - - III						
<i>Fordilla troyensis</i> WALCOTT	+					
Genus et sp. ind. (pelecypod)	+					
<i>Proplina?</i> <i>prisca</i> n. sp.				+		
<i>Pollicina?</i> <i>cambrica</i> (MOBERG)						
<i>Prosinuites bornholmensis</i> n. g. et n. sp.						
<i>Circotheca</i> sp.	+					
<i>Orthotheca groedbyensis</i> n. sp.						
- <i>johnstrupi</i> HOLM			+	+	+	
- <i>pervilis</i> n. sp.				+		
<i>Trapezotheca?</i> <i>pistrinensis</i> n. sp.				+		
<i>Hyalithes balticus</i> n. sp.	+					
- <i>groenwalli</i> n. sp.	+					
- <i>lenticularis</i> HOLM				+		
- <i>nathorsti</i> HOLM	+			+		+
- sp. I	+					
- - II	+					
- - ind.		+				
<i>Halkieria obliqua</i> n. g. et n. sp.	+					
- <i>symmetrica</i> n. sp.						
<i>Hyalithellus micans</i> BILLINGS	+			+		
<i>Coleoloïdes bornholmensis</i> n. sp.	+					
- <i>multistriatus</i> COBBOLD						
- <i>paucistriatus</i> n. sp.	+					
- <i>rugosus</i> n. sp.	+					
<i>Pseudorthotheca danica</i> n. sp.	+					
<i>Glauderia mirabilis</i> n. g. et n. sp.		+				
<i>Halopoa</i> sp.						
<i>Cruziana dispar</i> LINNARSSON						

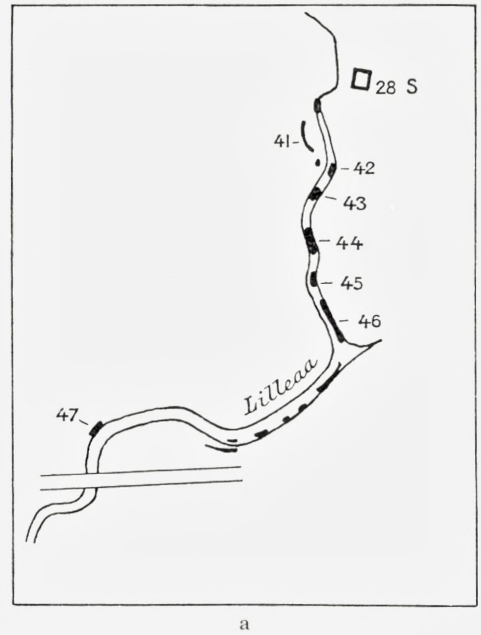
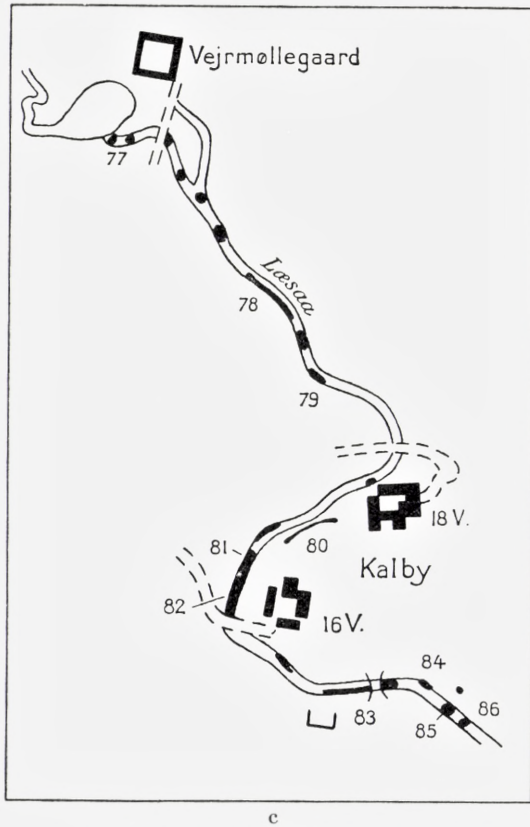
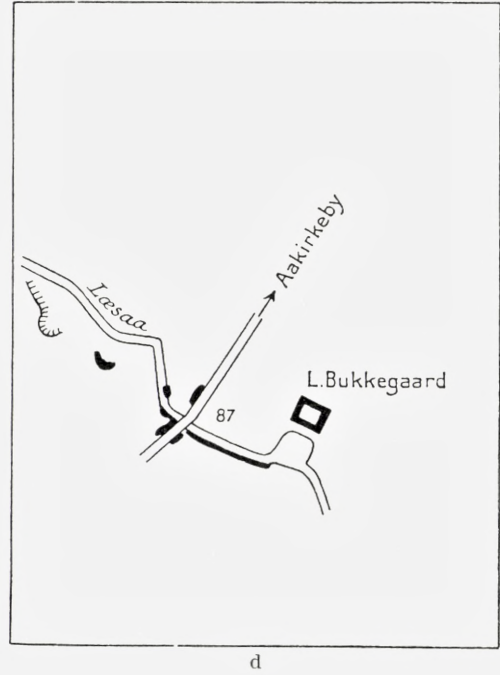
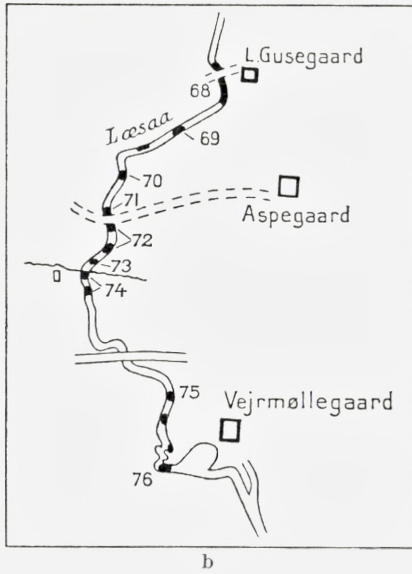


Fig. 7. Outcrops of siltstone along Lilleaa (a) and Læsaa (b-d) (from K. HANSEN 1936).

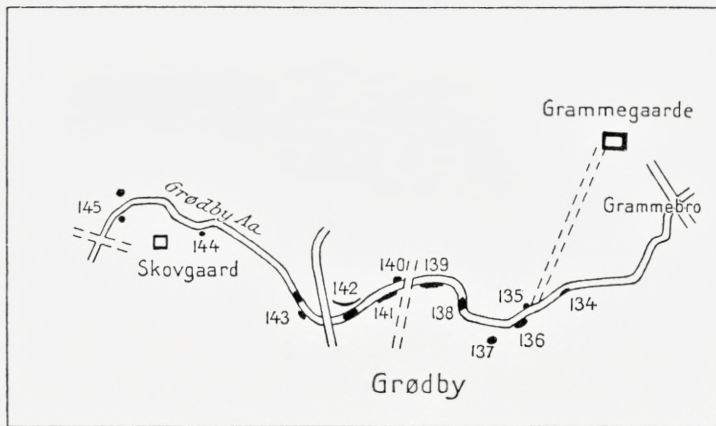
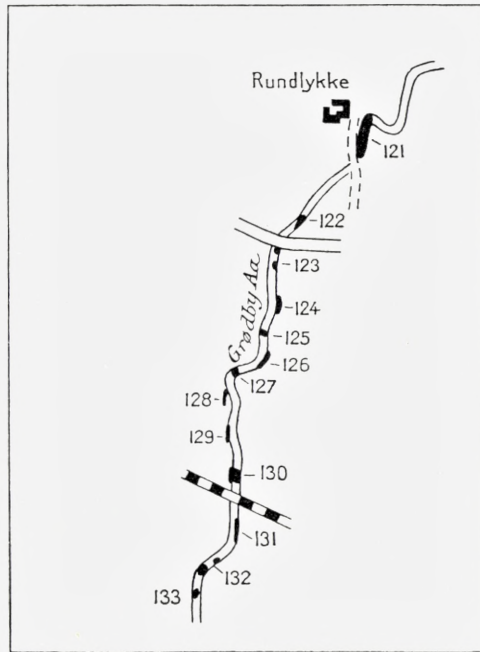


Fig. 8. Outcrops of siltstone along Grødbyaa (from K. HANSEN 1936).

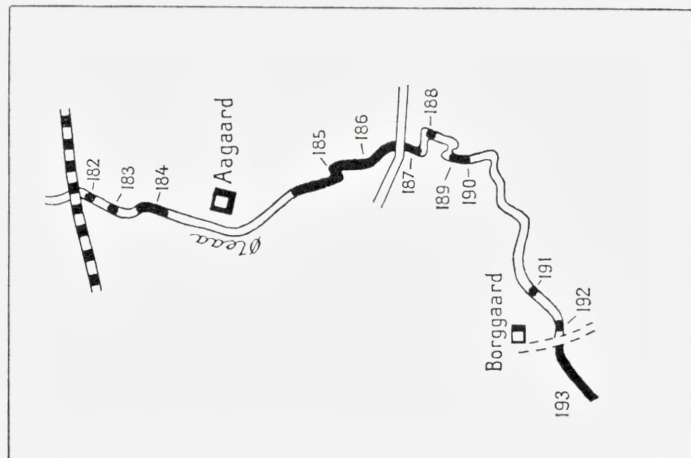
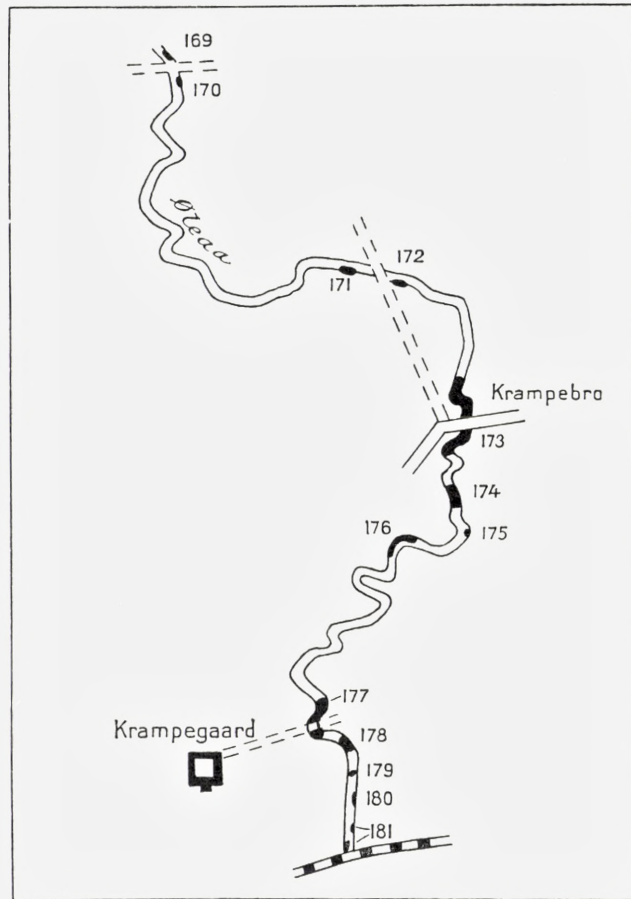


Fig. 9. Outcrops of siltstone along Oleaa (from K. HANSEN 1936).

REFERENCES

- BARRANDE, J., 1881: Acéphales. — Etudes Loc. et Comp. — Prague.
- BILLINGS, E., 1872: On some new genus of Paleozoic fossils. — Canadian Naturalist, vol. 6. — Ottawa.
- COBBOLD, E. S., 1919: Cambrian Hyolithidae etc. from Hartshill in the Nuneaton district, Warwickshire. — Geol. Mag., n. ser., decade 6, vol. 6. — London.
- 1931: Additional fossils from the Cambrian rocks of Shropshire. — Quart. Journ. Geol. Soc. London, vol. 87, part 3. — London.
- EICHWALD, E., 1840: Ueber das silurische Schichtensystem in Esthland. — Zeitschr. Nat. — Heilkunde Med.-chirur. K. Akad. St. Petersburg.
- 1860: Lethaea rossica ou paléontologie de la Russie, décrite et figurée, vol. 1. — Stuttgart.
- FISHER, D. W., 1962 (see TREATISE, etc.).
- GRÖNWALL, K. A., & MILTHERS, V., 1916: Beskrivelse til det geologiske Kortblad Bornholm. — Danmarks Geologiske Undersøgelse, Ser. 1, No. 13. — Copenhagen.
- HANSEN, K., 1936: Die Gesteine des Unterkambriums von Bornholm. — Danmarks Geologiske Undersøgelse, Ser. 2, No. 62. — Copenhagen.
- 1937: Sammenlignende Studier over Kambriet i Skåne og paa Bornholm, I, Nedre Kambrium. — Meddelelser fra Dansk Geologisk Forening, vol. 9. — Copenhagen.
- HOLM, G., 1893: Sveriges Kambrisk-Siluriska Hyolithidae och Conulariidae. — Sveriges Geologiska Undersökning, Ser. C, No. 112. — Stockholm.
- KAUTSKY, F., 1945: Die unterkambrische Fauna von Aistjakk in Lappland. — Geologiska Föreningens i Stockholm Förhandlingar, vol. 67. — Stockholm.
- KUENEN, PH. H., 1950: Marine Geology. — New York & London.
- LINNARSSON, J. G. O., 1871: Geognostiska och palaeontologiska iakttagelser öfver Eophytionsandstenen i Vester götland. — Kgl. Svenska Vet.-Akad. Handlingar, vol. 9, no. 7. — Stockholm.
- LOCHMAN, C., 1956: Stratigraphy, paleontology, and paleogeography of the Elliptoccephala asaphoides strata in Cambridge and Hoosick quadrangles, New York. — Bull. Geol. Soc. America, vol. 67. — New York.
- LYASHENKO, G. P., & SYSSOIEV, V. A., 1958: Tip Mollyuski? Klass Konikonkhii. — Osnovy Paleontologii spravochnik Paleontologov Geologov SSSR (ORLOV, Y. A., LUPPOV, N. P. & DRUSCHCHITS, V. V., eds.), vol. 6.
- MAREK, L., 1963: New knowledge on the morphology of hyolithes. — Sporník Geologických Věd, Paleontologie, řada P, sv. 1. — Prague.
- MARTINSSON, A.: Aspects of a Middle Cambrian Thanatotope on Öland. — Geologiska Föreningens i Stockholm Förhandlingar, vol. 87. — Stockholm.
- MATTHEW, G. F., 1899: Upper Cambrian of Mount Stephen, British Columbia: The trilobites and worms. — Roy. Soc. Canada, Trans., Ser. 2, vol. 5, Sect. 4. — Ottawa.

- MOBERG, J. C., 1892: Om en ny upptäckt fauna i block af kambrisk sandsten, insamlade af Dr. N. O. HOLST. – Geologiska Föreningens i Stockholm Förhandlingar, vol. 14. – Stockholm.
- POULSEN, C., 1932: The Lower Cambrian faunas of East Greenland. – Meddelelser om Grønland, vol. 87, No. 6. – Copenhagen.
- 1935: Nogle hidtil ukendte Forstener fra Bornholms grønne Skifre. – Meddelelser fra Dansk Geologisk Forening, vol. 8. – Copenhagen.
- 1942: Nogle hidtil ukendte Fossiler fra Bornholms Exsulandskalk. – Meddelelser fra Dansk Geologisk Forening, vol. 10. – Copenhagen.
- POULSEN, V., 1963: Notes on *Hyalithellus* BILLINGS, 1871, Class Pogonophora JOHANSSON, 1937. – Biol. Medd. Dan. Vid. Selsk. 23, No. 12. – Copenhagen.
- 1963: The Lower Middle Cambrian Kalby-ler (Kalby clay) on the Island of Bornholm. – Biol. Medd. Dan. Vid. Selsk. 23, No. 14. – Copenhagen.
- 1965: The Oldest Trilobite Remains from Denmark. – Meddelelser fra Dansk Geologisk Forening, vol. 15. – Copenhagen.
- 1966: Cambro-Silurian Stratigraphy of Bornholm. – Meddelelser fra Dansk Geologisk Forening, vol. 16. – Copenhagen.
- RAUFF, H., 1893–1894: Palaeospongeologie – Palaeontographica, vol. 40 – Stuttgart.
- REGNÉLL, G., & HEDE, J. E., 1960: The Lower Paleozoic of Scania – the Silurian of Gotland. – Excursion Guide No. 21, Internat. Geol. Congr., Norden. – Stockholm.
- STEHMANN, E., 1934: Das Unterkambrium und die Tektonik des Paläozoikums auf Bornholm. – Abh. d. geol.-paläont. Inst. d. Univ. Greifswald, 14. – Greifswald.
- SYSSOIEV, V. A., 1957: K morfologii, sistematscheskomu polozhennyv i sistematiike khilolitov. – Akad. Nauk SSSR, Leningrad, Doklady, vol. 116. (On the morphology, systematic position, and systematics of Hyolithoidea).
- 1959: Ekologiya khilolitov. – Akad. Nauk SSSR, Leningrad, Doklady, vol. 127. (Ecology of hyolithids).
- Treatise on Invertebrate Paleontology* edited by R. C. MOORE. – 1960: Part J (Mollusca 1). – 1962: Part W (Miscellanea). – Tulsa.
- WALCOTT, C. D., 1886: Second contribution to the studies on the Cambrian faunas of North America. – U. S. Geol. Surv., Bull. 30. – Washington, D.C.
- 1890: Descriptive notes on new genera and species from the Lower Cambrian or Olenellus zone of North America. – U. S. Geol. Surv., 10th Annual Report. – Washington, D.C.
- YOCHELSON, E. L., 1961: The operculum and mode of life of *Hyalithes*. – Journ. of Paleontology, vol. 35. – Tulsa.
- 1961: Notes on the class Coniconchia. – Ibid.

PLATES

PLATE 1

- Fig. 1. Genus et species ind. (cf. *Pyritonema*), external mould of hexacts ($\times 24$), Locality 178 (Oleaa). (p. 14).
- 2. Genus et species ind. (cf. *Pyritonema*), hexact ($\times 24$), Locality 139 (Grodbyaa).
 - 3. Spicules of indeterminable poriferan genus in the interior of *Hyolithellus* sp. ($\times 15$), Locality 194 (Oleaa). (p. 15).
 - 4. Internal mould of indeterminable hyolithid marked by boring organism; cavities contain indeterminable spicules ($\times 15$), Locality 194 (Oleaa). (p. 15).



1



2



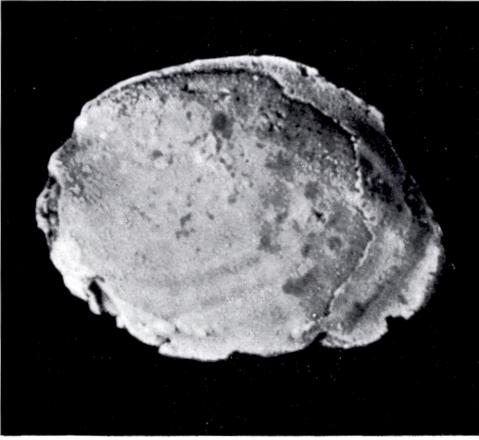
3



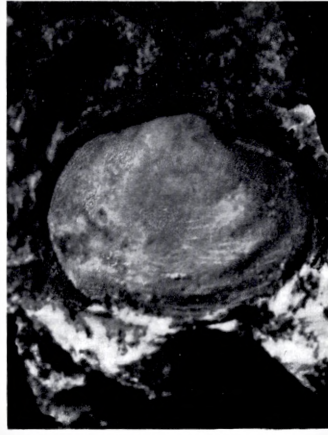
4

PLATE 2

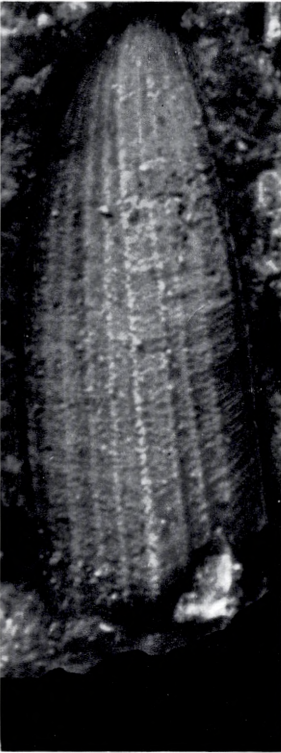
- Fig. 1. *Fordilla troyensis* WALCOTT, internal mould ($\times 16$), Locality 139 (Grødbyaa). (p. 15).
- 2. Genus et sp. ind. (pelecypod), internal mould of right valve ($\times 16$), Locality 46 (Lilleaa). (p. 16).
- 3. *Halkieria obliqua* n. g. et n. sp., cast of dorsal side, *holotype*, ($\times 26$), Locality 46 (Lilleaa). (p. 30).
- 4. *Halkieria obliqua*, n. g. et n. sp., cast of ventral side ($\times 22$), Locality 126 (Grødbyaa).
- 5. *Halkieria symmetrica* n. sp., cast, showing part of dorsal exterior and part of ventral interior, *holotype*, ($\times 22$), Locality 126 (Grødbyaa). (p. 30).



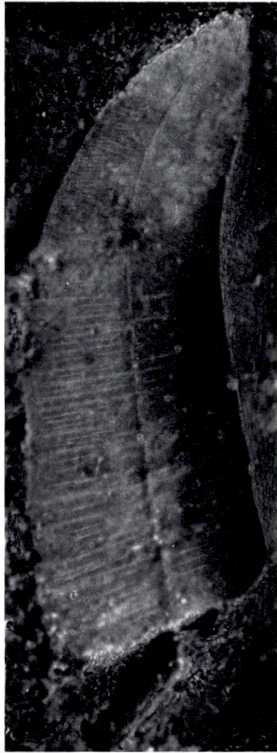
1



2



3



4



5

PLATE 3

- Fig. 1. *Proplina? prisca* n. sp., cast of external mould, *holotype*, ($\times 20$), Locality 77 (Læsaa). (p. 17).
- 2. *Pollicina? cambrica* (MOBERG), specimen figured upside down in order to facilitate comparison with MOBERG's "*Dentalium? cambricum*", ($\times 10$), Locality 137 (Grødbyaa). (p. 18).
 - 3–9. *Prosinuites bornholmensis* n. g. et n. sp. (p. 19).
 - 3–4. Posterior and lateral views of internal mould, ($\times 6$), Locality: the Grødbyaa between Grødby and Grammegaarde.
 - 5–7. Lateral, posterior, and anterior views of internal mould, *holotype*, ($\times 6$), Locality: the Grødbyaa between Grødby and Grammegaarde.
 - 8. Anterior view of internal mould of specimen with clearly indicated selenizone ($\times 6$), Locality: the Grødbyaa between Grødby and Grammegaarde.
 - 9. Half anterior and half top-view of the specimen represented by figs. 3–4, ($\times 6$).
 - 10. *Hyolithes balticus* n. sp., ventral view of internal mould, *holotype*, ($\times 10$), Locality 46 (Lilleaa). (p. 23).



1



3



2



4



5



6



7



8



9



10

PLATE 4

- Fig. 1. *Hyolithes ballicus* n. sp., dorsal view of internal mould, *holotype*, ($\times 10$), Locality 46 (Lilleaa). (p. 23).
- 2-8. *Hyolithes groenwalli* n. sp., fragmentary specimens with partly preserved shell. (p. 24).
 - 2-4. *Holotype*, dorsal, ventral, and lateral views, ($\times 3$), Locality: the Grodbyaa between Grodby and Grammegaarde.
 - 5-8. Another specimen; 5-6, ventral and dorsal views, ($\times 3$); 7-8, external shell surface of ventral side, ($\times 24$), and dorsal side ($\times 16$); Locality: the Grodbyaa between Grodby and Grammegaarde.



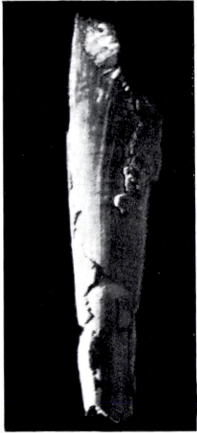
1



2



3



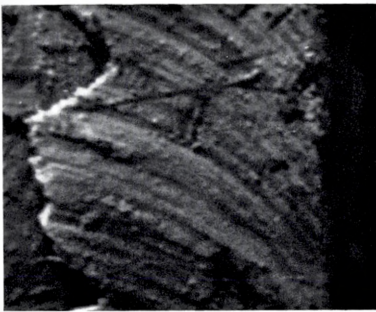
4



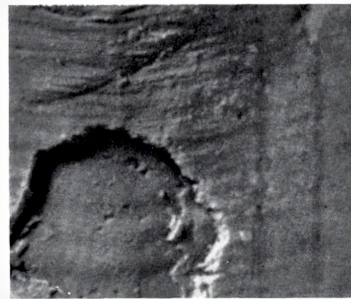
5



6



7



8

PLATE 5

- Fig. 1-4. Appendages ("supports" and "*Helenia*" of some authors) referred to the associated *Hyolithes groenwalli* n. sp.; Locality: the Grodbyaa between Grodby and Gramme-gaarde. (p. 24).
- 1. Left Appendage with well developed longitudinal furrow, dorsal view, ($\times 3$).
 - 2. Proximal part of the same turned 180° to show transversal lines on external mould of ventral side, ($\times 18$).
 - 3. Ventral side of left appendage, showing longitudinal furrows, ($\times 3$).
 - 4. Proximal part of the same turned 180° to show transversal lines, ($\times 18$).
 - 5-6. Cross sections of *Hyolithes groenwalli* n. sp., ($\times 3$), same specimens as those represented by Pl. 4, figs. 6 and 5, respectively. (p. 24).
 - 7. *Hyolithes* sp. II, cast of external mould of the ventral side, ($\times 12$), Locality 46 (Lilleaa). (p. 28).
 - 8-9. *Circotheca* sp., Locality 46 (Lilleaa). (p. 20).
 - 8. Cast, showing external characters of the shell, ($\times 7$).
 - 9. Part of the same ($\times 18$).



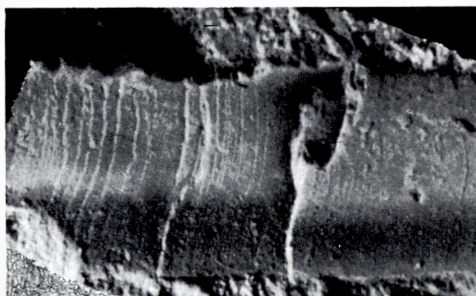
1



4



3



2



5



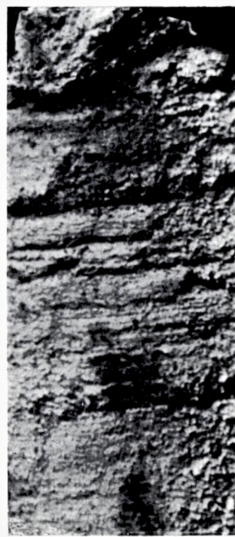
6



7



8



9

PLATE 6

- Fig. 1-2. *Orthotheca pervilis* n. sp., Locality 77 (Læsaa). (p. 21).
- 1. Internal mould, ventral side, *holotype*, ($\times 6$).
 - 2. Cross section of the same, ($\times 6$).
- Fig. 3-6. *Trapezotheca? pistrinensis* n. sp., Locality 77 (Læsaa). (p. 22).
- 3-5. Ventral, dorsal, and lateral views of internal mould, *holotype*, ($\times 3$).
 - 6. Cross section of the same, ($\times 3$).
- Fig. 7-8. *Orthotheca groedbyensis* n. sp., Locality 137 (Grødbyaa). (p. 20).
- 7. Internal mould, dorsal side, *holotype*, ($\times 6.5$).
 - 8. Cross section of the same, ($\times 6.5$).
- Fig. 9. Operculum (possibly belonging to *Hyolithes nathorsti* HOLM), cast of external mould, ($\times 7$), Locality 46 (Lilleaa). (p. 27).
- Fig. 10-11. *Hyolithes* sp. I, internal mould of operculum, topview and lateral view, ($\times 7$), Locality 46 (Lilleaa). (p. 28).



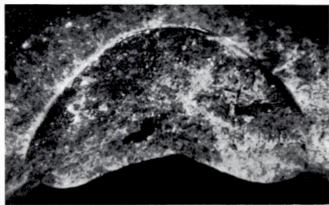
1



3



4



2



7



5



8



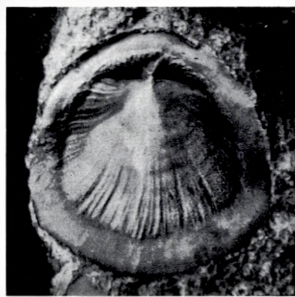
11



9



6



10

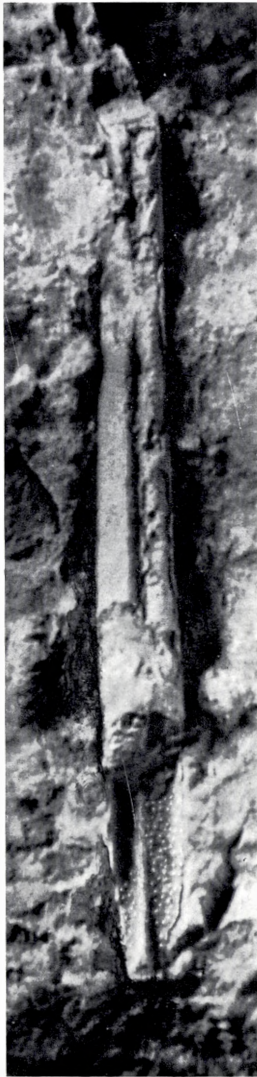
PLATE 7

Fig. 1-2. *Hyolithellus micans* BILLINGS. (p. 31).

- 1. Cast of external mould, ($\times 10$), Locality 178 (Oleaa).
- 2. Specimen with preserved external surface, ($\times 10$), Locality: the Grødbyaa between Grødby and Grammegaarde.
- 3-4. *Pseudorthothea danica* n. sp., casts of external moulds, ($\times 18$), Locality 142 (Grødbyaa). (p. 36).
(The specimen represented by fig. 3 is the *holotype*).
- 5. *Glauderia mirabilis* n. g. et n. sp., *holotype*, ($\times 20$), Locality 58 (coast cliff at Julegaard). (p. 37).



1



5



2



3



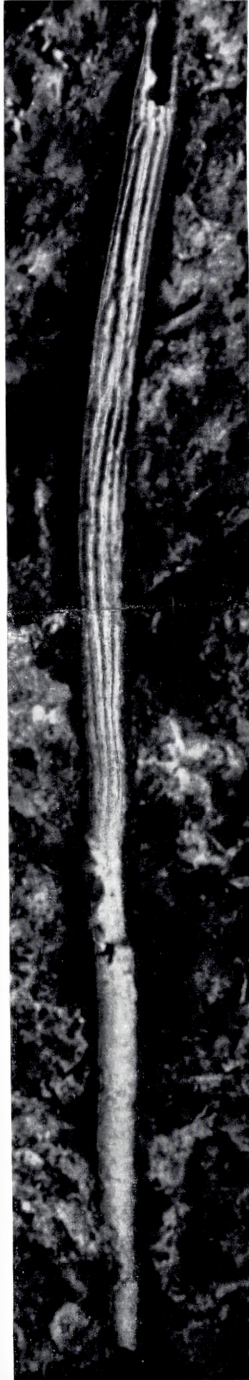
4

PLATE 8

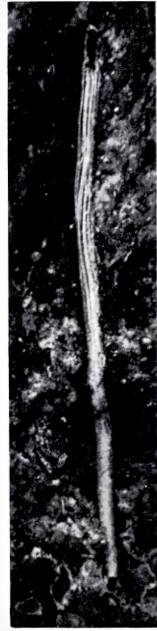
- Fig. 1. *Coleoloides paucistriatus* n. sp., cast of external mould, *holotype*, ($\times 22$), Locality 46 (Lilleaa). (p. 35).
- 2. *Coleoloides multistriatus* COBBOLD, ($\times 16$), Locality: the Grødbyaa between Grødby and Grammegaarde. (p. 34).
 - 3. *Coleoloides bornholmensis* n. sp., cast of external mould, *holotype*, ($\times 10$), Locality 132 (Grødbyaa). (p. 33).
 - 4. The same enlarged to $\times 25$ in order to show details of the external surface.
 - 5. *Coleoloides rugosus* n. sp., cast of external mould, *holotype*, ($\times 27$), Locality 46 (Lilleaa). (p. 35).



1



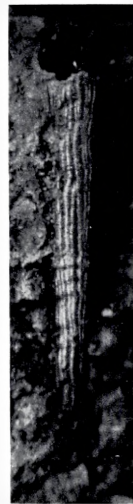
4



3



2



5

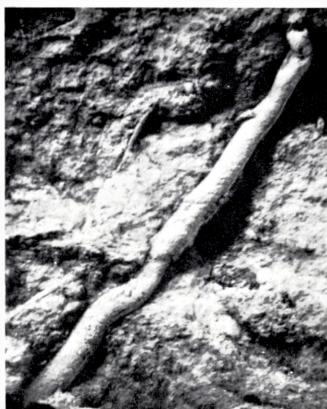
PLATE 9.

Fig. 1–4. *Coleoloides multistriatus* COBBOLD, casts of external moulds of more or less deformed specimens (p. 34).

- 1. Moderately deformed specimen, ($\times 6$), Locality 139 (Grodbyaa).
- 2. The same enlarged $\times 24$ to show the striae.
- 3. Much deformed specimen, ($\times 25$), Locality 139 (Grodbyaa).
- 4. Another much deformed specimen ($\times 11$), Locality 139 (Grodbyaa).
- 5. Genus et sp. ind. (cf. *Byronia* MATTHEW), ($\times 2$), Locality: Graanakkestuen (p. 13).



2



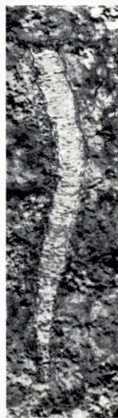
1



3



4



5

I. BREVIK

RELATIVISTIC THERMODYNAMICS

Det Kongelige Danske Videnskabernes Selskab
Matematisk-fysiske Meddelelser **36, 3**



Kommissionær: Munksgaard
København 1967

Synopsis

The covariant conservation laws for a non-closed mechanical system are investigated by emphasizing the interpretation of the work and heat supply as seen from the particular reference frame in which the system is at rest. A distinction is made between the cases where the heat is produced within the system and where it is transferred through the boundary by a convective process. Relativistic transformation formulas for temperature and heat are obtained in general, and the alternative proposals recently put forward in literature are found as corresponding to two special cases. In an appendix, comparisons are made with a result obtained recently by Professor C. MÖLLER.

I. Introduction

Recently, there has been a considerable discussion on the necessity of revising the formerly accepted formulas

$$\Delta Q = \gamma^{-1} \Delta Q^0, \quad T = \gamma^{-1} T^0, \quad (\gamma = (1 - v^2/c^2)^{-\frac{1}{2}}) \quad (1)$$

in relativistic thermodynamics. Instead of (1), ARZELIÈS⁽¹⁾, GAMBA⁽²⁾, KIBBLE⁽³⁾ and OTT⁽⁴⁾ want the following relations

$$\Delta Q = \gamma \Delta Q^0, \quad T = \gamma T^0. \quad (2)$$

In the case of an ideal fluid, eq. (1) may be derived⁽⁵⁾ by means of the thermodynamical laws

$$\Delta E = \Delta Q + \Delta A, \quad \Delta S \geq \Delta Q/T \quad (3)$$

and by means of the following assumption for the mechanical work ΔA exerted on the system (for small displacements)

$$\Delta A = -p \Delta V + \mathbf{v} \cdot \Delta \mathbf{G}, \quad (4)$$

where p is the pressure and \mathbf{G} the total momentum.

From the following investigation it results that the transformation formula for heat is not uniquely determined by the first thermodynamical law but is dependent also on the description of heat supply in the rest inertial system K^0 . Moreover, the transformation formula for temperature is found to be given by (2).

2. General Theory

Consider an elastic body which in K^0 is subjected to some *external* forces with resulting density $\mathbf{f}^0(\mathbf{r}^0, t^0)$ so that each volume element undergoes a

- (1) H. ARZELIÈS, Nuovo Cimento 35, 792 (1965).
- (2) A. GAMBA, Nuovo Cimento 37, 1792 (1965).
- (3) T. W. B. KIBBLE, Nuovo Cimento 41 B, 72 (1966).
- (4) H. OTT, Zeitschr. für Physik 175, 70 (1963).
- (5) C. MÖLLER, The Theory of Relativity (Oxford 1952).

certain displacement with a small velocity $\mathbf{u}^0(\mathbf{r}^0, t^0)$ within the time period $t^0 = 0$ to $t^0 = \tau^0$. The displacement itself is not restricted to be small. When $t^0 = \tau^0$, we suppose all elements to be at rest, so that the momentum change is zero. Now, suppose that the body during the time τ^0 is supplied also with an amount of energy ΔQ^0 of the disordered nature we regard as heat. The components $T_{\mu\nu}^0$ of the mechanical energy-momentum tensor must describe also the effects arising from the heat. The manner in which the heat arises in the body, however, is a crucial point. An amount ΔQ_{conv}^0 may flow *through the boundary* by a process of conduction or radiation. We suppose that this amount originates from sources of different (not necessarily only infinitesimally different) temperatures. ΔQ_{conv}^0 is counted positive when heat flows into the body. This kind of transfer is described by the energy current components $T_{4k}^0 (k = 1, 2, 3)$, while the accompanying momentum density is determined from $T_{k4}^0 = T_{4k}^0$ and the momentum flow from T_{ik}^0 . We demand explicitly no resulting momentum to be transferred to the body by this flow.

Besides, we shall take into account a heat amount ΔQ_{prod}^0 which is assumed to be *produced* within the body, in which case the rate of change $q^0(\mathbf{r}^0, t^0)$ of heat density is described by the fourth component of the four-force extended to read $f_4^0 = i/c(\mathbf{f}^0 \cdot \mathbf{u}^0 + q^0)$. We have then $\Delta Q_{\text{prod}}^0 = \int q^0 dV^0 dt^0$, while $Q_{\text{prod}}^0 = \int q^0 dV^0$ means the rate of produced heat in the total body. (Q_{conv}^0 has the corresponding meaning for the convective heat.) We assume the heat production to be a dissipative effect, caused for instance by electromagnetic fields in a conductor. Actually this is a kind of work exerted on the body, but we find it natural to include it into ΔQ^0 rather than into ΔA^0 in the cases where the amount of energy brought about is clearly connected with a change of entropy.

In order to elucidate this concept of produced heat, let us consider the specific situation where a conductor carries electric current. If $S_{\mu\nu}$ denotes the electromagnetic energy-momentum tensor and $f_{\mu}^{(e)}$ the electromagnetic force density, then we find by integrating the conservation equation $\partial_{\nu}^0 S_{4\nu}^0 = -f_4^{(e)0}$ over the body that the rate of increase of electromagnetic plus heat energy is furnished by a flow of electromagnetic energy through the boundary. However, this energy flow is *not* to be included into T_{4k}^0 on the boundary, since it is not a heat radiation between bodies of different temperatures. Instead, as we have remarked, the heat effect is described as originating from f_4^0 , which again of course may cause changes in the components of $T_{\mu\nu}^0$ as well as in \mathbf{f}^0 . Since f_{μ}^0 is the resulting external force density, we can write $f_{\mu}^0 = f_{\mu}^{(e)0} + f_{\mu}^{(m)0}$, where $f_{\mu}^{(m)0}$ is the mechanical force of non-

electromagnetic origin. $\mathbf{f}^{(m)0}$ will in general include also the reaction force which is necessary in K^0 in order to compensate the electromagnetic force. If the body is kept at rest by external surface forces, then $\mathbf{f}^{(m)0} = 0$ in the interior domain, but the compensation is achieved by means of the stress tensor T_{ik}^0 (this point has been elaborated by OTT⁽⁴⁾).

The described production of heat is in principle an irreversible process. Note that the above considerations are valid only when ΔQ_{prod}^0 is produced by some *external* sources; if this kind of energy is brought about, e.g. by some chemical change in the body itself, our description is inappropriate.

When $t^0 < 0$ and $t^0 > \tau^0$, stationary state is required, i.e. $Q^0 = Q_{\text{conv}}^0 + Q_{\text{prod}}^0 = 0$. Either do then the parts Q_{conv}^0 and Q_{prod}^0 vanish also, or, as may be the case for a body carrying stationary current, heat is flowing out of the system at the same rate as it is produced, as expressed by $Q_{\text{conv}}^0 = -Q_{\text{prod}}^0$.

According to the picture we have now sketched in K^0 , the differential conservation laws may be written $\partial_\nu^0 T_{\mu\nu}^0 = f_\mu^0 = (\mathbf{f}^0, i/c(\mathbf{f}^0 \cdot \mathbf{u}^0 + q^0))$, and the relativistic transformation formulas we obtain for temperature and heat are the consequences of this picture.

Let us investigate the process as seen from an inertial frame K in which K^0 is moving with the velocity v along the x axis. We denote by Σ_1 the part of the world tube of the body bounded by the spacelike surfaces $t^0 = 0$ and $t^0 = \tau^0$, and have then the work ΔA_1 exerted in this domain in K as

$$\Delta A_1 = \int_{\Sigma_1} \mathbf{f} \cdot \mathbf{u} \delta V \delta t, \quad (5)$$

where \mathbf{u} is the velocity of a moving volume element δV . By transforming each factor in the integrand, we obtain

$$\Delta A_1 = \gamma \int \mathbf{f}^0 \cdot \mathbf{u}^0 \delta V^0 \delta t^0 + \gamma v \int f_x^0 \delta V^0 \delta t^0 + \gamma \beta^2 \int q^0 \delta V^0 \delta t^0. \quad (6)$$

In the derivation of this formula, we have ignored terms of the second order in u^0/c and have further ignored a term involving the product $u_x^0 q^0$. If we had permitted u^0 to be arbitrarily large, then the two first terms in (6) would have remained unchanged, but the last term would have been more complicated. Since \mathbf{f}^0 is assumed to carry no momentum to the body, we obtain

$$\Delta A_1 = \gamma \int \mathbf{f}^0 \cdot \mathbf{u}^0 \delta V^0 \delta t^0 + \gamma \beta^2 \Delta Q_{1\text{prod}}^0, \quad (7)$$

where the last term contains the produced heat in Σ_1 . Since we are to use the macroscopic laws (3) in K , the system should be compared at two in-

stants corresponding to the hyperplanes $t = t_1$ and $t = t_2$, so that Σ_1 is located in between them. The work ΔA_2 exerted in K in the domain Σ_2 between $t = t_1$ and $t^0 = O$ is equal to

$$\left. \begin{aligned} \Delta A_2 = \gamma v \int_{\Sigma_2} \left(f_x^0 + \frac{\beta}{c} q^0 \right) \delta V^0 \delta t^0 = \gamma \beta^2 \int_{V_0^*} x^0 f_x^0 \delta V^0 - \\ - \beta^2 t_1 Q_{2\text{prod}}^0 + \frac{\gamma \beta^3}{c} \int_{V_0^*} x^0 q^0 \delta V^0. \end{aligned} \right\} \quad (8)$$

Here we have integrated over time and have taken the integrals over the surface $t^0 = O$ corresponding to the original volume V_0^0 in K^0 . The quantity $Q_{2\text{prod}}^0$ means the rate of produced heat in the total body before the deformation period. We assume $q^0 = q^0(\mathbf{r}^0)$ but $\partial q^0 / \partial t^0 = O$ outside Σ_1 .

A similar expression is obtained for ΔA_3 corresponding to Σ_3 between $t^0 = \tau^0$ and $t = t_2$, and so the total work $\Delta A = \Delta A_1 + \Delta A_2 + \Delta A_3$ takes the form

$$\left. \begin{aligned} \Delta A = \gamma \int \mathbf{f}^0 \cdot \mathbf{u}^0 \delta V^0 \delta t^0 + \beta^2 [\gamma \Delta Q_{1\text{prod}}^0 - t_1 Q_{2\text{prod}}^0 + \\ + (t_2 - \gamma \tau^0) Q_{3\text{prod}}^0] + \gamma \beta^2 \left[\int_{V_0^*} - \int_{V_0^0} \right] x^0 \left(f_x^0 + \frac{\beta}{c} q^0 \right) \delta V^0. \end{aligned} \right\} \quad (9)$$

Here V^0 is the volume in K^0 for $t^0 \geq \tau^0$. Note that q^0 may have different values within the two integrals in the last term.

The total energy after the deformation may readily be obtained by a tensor transformation as

$$E = 2\gamma v \int_{V^0} g_x^0 \delta V^0 + \gamma \beta^2 \int_{V^0} T_{xx}^0 \delta V^0 + \gamma E^0. \quad (10)$$

The first term vanishes, since no total momentum is supplied; moreover, since the energy in K^0 after the deformation is given by

$$E^0 = E_0^0 + \int \mathbf{f}^0 \cdot \mathbf{u}^0 \delta V^0 \delta t^0 + \Delta Q^0, \quad (11)$$

where E_0^0 is the energy before the deformation, we have

$$\Delta E = \gamma \int \mathbf{f}^0 \cdot \mathbf{u}^0 \delta V^0 \delta t^0 + \gamma \beta^2 \left[\int_{V^0} - \int_{V_0^0} \right] T_{xx}^0 \delta V^0 + \gamma \Delta Q^0. \quad (12)$$

From (12) and (9) we can now find ΔQ by the first law. Taking into account that $\int (T_{xx}^0 + x^0 f_x^0) \delta V^0$ is equal to the surface integral $\int x^0 T_{xk}^0 n_k^0 \delta S^0$,

and that $\int x^0 q^0 \delta V^0$ may be substituted by $\int x^0 S_k^0 n_k^0 \delta S^0$, we obtain finally the rather unwieldy expression

$$\Delta Q = \gamma \Delta Q^0 - \beta^2 [\gamma \Delta Q_{1\text{prod}}^0 - t_1 Q_{2\text{prod}}^0 + (t_2 - \gamma \tau^0) Q_{3\text{prod}}^0] + \left. \begin{aligned} & + \gamma \beta^2 \left[\int_{S^0} - \int_{S_0^0} \right] x^0 \left(T_{xk}^0 + \frac{\beta}{c} S_k^0 \right) n_k^0 \delta S^0. \end{aligned} \right\} \quad (13)$$

Here S^0, S_0^0 are the surfaces corresponding to V^0, V_0^0 .

In the following we shall confine ourselves to two cases. In the first place, we consider the situation where no deformation occurs, but where heat is being developed in the body at the same constant rate as it is transferred outwards through the boundary. With $\tau^0 = 0$, we obtain from (13), omitting superfluous indices,

$$\Delta Q = -\beta^2 (t_2 - t_1) Q_{\text{prod}}^0 = -\gamma \beta^2 \Delta Q_{\text{prod}}^0, \quad (14)$$

where ΔQ_{prod}^0 is the heat produced in K^0 during a time $\gamma^{-1}(t_2 - t_1)$. This corresponds to replacing the total integration domain Σ by a domain Σ' bounded by two time-orthogonal surfaces in K^0 lying at a distance $\gamma^{-1}(t_2 - t_1)$ apart from each other. The amounts ΔQ_{prod}^0 corresponding to Σ and Σ' are equal, since q^0 is time-independent at any place.

From (14), (12) and (9) it follows that $\Delta Q < 0$, $\Delta E = 0$, $\Delta A > 0$. Physically this means that the extracted heat must compensate the mechanical work in order to maintain constant energy.

In the second place we assume, as the more interesting case, that both conducted and produced heat is absent in K^0 except in the period $0 \leq t^0 \leq \tau^0$. Again omitting a superfluous index, we then obtain from (13)

$$\Delta Q = \gamma \Delta Q^0 - \gamma \beta^2 \Delta Q_{\text{prod}}^0 = \gamma \Delta Q_{\text{conv}}^0 + \gamma^{-1} \Delta Q_{\text{prod}}^0. \quad (15)$$

We then want to consider the supply of heat as reversible in order to find the transformation formula for temperature from the invariance property of entropy. Since ΔQ_{prod}^0 arises on account of an irreversible process, we have to put this quantity equal to zero and demand ΔQ_{conv}^0 to be transferred reversibly. Assuming the temperature to change negligibly during the process in any reference system, we then obtain the formula

$$T = \gamma T^0. \quad (16)$$

Next, assume the situation corresponding to (15). We want to compare formula (9) in this case with formula (4), commonly accepted as valid for

an ideal fluid. The term $-p\Delta V = -p^0\gamma^{-1}\Delta V^0$ corresponds to $\gamma^{-1}\int \mathbf{f}^0 \cdot \mathbf{u}^0 \delta V^0 \delta t^0$; moreover, we obtain by the same method as led to (12)

$$\Delta G_x = \frac{\gamma\beta}{c} \left[\int \mathbf{f}^0 \cdot \mathbf{u}^0 \delta V^0 \delta t^0 + \left(\int_{V^0} - \int_{V^0_0} \right) T^0_{xx} \delta V^0 + \Delta Q^0 \right], \quad (17)$$

so that for small displacements

$$\Delta A = -p\Delta V + \mathbf{v} \cdot \Delta \mathbf{G} - \gamma\beta^2 \Delta Q^0_{\text{conv}} \quad (18)$$

where ΔA is determined by (9). Eq. (4) is thus found to be valid only in certain cases.

3. Discussion and applications

In some textbooks, when evaluating the work exerted on a fluid in motion, the last term in (4) is claimed to be present since a force $d\mathbf{G}/dt$ should be necessary to maintain constant velocity. However, the total force may be put equal to $d\mathbf{G}/dt$ only when *no momentum* is transferred through the boundary. This is correct only when $\Delta Q^0_{\text{conv}} = 0$, in which case we have already seen that (18) is equivalent to (4). When all heat thus is produced in the body, formula (1) for ΔQ is valid. But the corresponding formula for T is of course not valid.

Horizontal rod.

A uniform rod of length $2L^0$ and width unity is placed parallel to the x axis and is in K^0 subjected to a uniform pressure p^0 in its length direction so that the work done in the period $t^0 = 0$ to $t^0 = \tau^0$ is $\Delta A^0 = -p^0\Delta V^0 = -2p^0\Delta L^0$. This situation, as it appears in K , has been the subject of some discussion. KIBBLE⁽³⁾ calculates the work exerted by the applied forces and finds $\Delta A = -p\Delta V$, which coincides with (9) if one ignores the terms associated with the produced heat. Therefore Kibble attains the result (2), as expected. ARZELIÈS⁽¹⁾ claims that the work exerted in K must be equal to $\gamma\Delta A^0$, that is the quantity which we formerly called ΔA_1 (except from the produced heat term). However, as pointed out by Kibble, by investigating the macroscopic thermodynamical relations, we should work with quantities referring to surfaces of simultaneity in K rather than in K^0 . R. PENNEY⁽⁶⁾ adopts Arzeliès' point of view, but claims additional forces to be present in

(6) R. PENNEY, Nuovo Cimento 43, 911 (1966).

the transient periods in order to maintain constant speed. This way of reasoning, however, means in general that one leaves the expression for the work density per unit time as $\mathbf{f} \cdot \mathbf{u}$, where \mathbf{f} is the real force, obtained by a relativistic transformation from K^0 . We shall mention also another paper by Arzeliès⁽⁷⁾, in which he considers a material particle and claims that a bare supply of heat in K^0 ($\Delta A^0 = 0$) must be equivalent to a bare supply of heat in K . This point of view is implicitly the same as that of Kibble, and leads to the same result as his. We agree that this should be the more normal situation in thermodynamics.

Vertical rod.

When no heat is taken into account, we find in K $\Delta A = \gamma \Delta A^0 = -\gamma^2 p \Delta V$. Of course this should not be compared with the formula $\Delta A = \gamma^{-1} \Delta A^0 + \gamma \beta^2 \Delta(E^0 + p^0 V^0)$, which for vanishing heat is valid for a fluid with *isotropic* pressure and incidently is valid also for the horizontal rod.

PENNEY⁽⁶⁾ wants to exclude the work performed by the horizontal force F_x in K because of its lack of physical reality. This effect is claimed to be balanced by the internal pressure. It therefore seems as desirable to write down the information we can obtain from the energy conservation equation in K in integrated form

$$\int \boldsymbol{\sigma} \cdot \mathbf{n} \delta S + \frac{d}{dt} \int h \delta V = \int \mathbf{f} \cdot \mathbf{u} \delta V \quad (19)$$

Here the integration volume follows the body and contains the part which lies between $y = 0$ and an arbitrary $y < L$. (In K^0 the rod is placed in such a way that $0 \leq y \leq 2L$). h is the energy density and $\boldsymbol{\sigma} = \mathbf{S} - h\mathbf{u}$ the relative energy current. Let the velocity of the lower end in K^0 be denoted by u_0^0 ; by ignoring second order quantities we then obtain

$$\int \boldsymbol{\sigma} \cdot \mathbf{n} \delta S = p^0 u_0^0 (1 - y/L), \quad \frac{d}{dt} \int h \delta V = p^0 u_0^0 y/L, \quad (20)$$

and so the total work $p^0 u_0^0$ per unit time is seen partly to yield an increase of energy, partly to cause an energy flow through the boundary.

Remarks on Ott's work⁽⁴⁾

This long and comprehensive paper deserves special attention, so let us dwell on two essential points.

(7) H. ARZELIÈS, Nuovo Cimento 40B, 333 (1965).

1. Consider a material particle which in K^0 receives a convective supply of heat. In our earlier treatment we have let such a kind of transfer be described by the tensor components T_{Ak}^0 , but Ott lets the change of heat energy be described by an additional term in the fourth component of the four-force. Further, in accordance with the inertia of energy, this heat flow is accompanied by a momentum density whose rate of change in integrated form is represented by extra terms in the ordinary force. Ott obtains the change ΔQ in K by a four-vector transformation from K^0 , and finds that $\Delta Q = \gamma \Delta Q^0$ in general, also when an external force \mathbf{F}^0 present in K^0 supplies the body with the mechanical momentum $\int \mathbf{F}^0 dt^0$ during the actual period τ^0 . The situation considered earlier in our paper corresponds to $\int \mathbf{F}^0 dt^0 = 0$, and with this restriction we see that Ott's result agrees with (15) since the last term in (15) is absent. (See also the end of the appendix).

In his applications, Ott considers extended systems also and obtains the same formula (2) for ΔQ . It is assumed that a transfer of heat into the system is not associated with the occurrence of a mechanical force in a reference frame in which the system is moving. It may be seen readily that with this assumption, Ott's results agree with those we obtained earlier in section 2. For the force density is restricted so as to contain no heat term, and thus produced heat is absent and the formula (15) takes the simplified form (2).

2. As the second point, let us again consider the stationary situation in which a constant electric current is flowing through a conductor and develops heat in K^0 at the same rate as it is transferred outwards through the boundary, i.e. $Q_{\text{prod}}^0 = -Q_{\text{conv}}^0$, q^0 being independent of time at any place. In another reference frame, Ott obtains $q = \gamma q^0$, which seems incompatible with our earlier results for the transformation of produced heat. Let us therefore make a closer investigation on this situation.

The first law may be obtained in general by means of the integrated form of the differential conservation equation involving the fourth line of the mechanical energy-momentum tensor. By adding the produced heat-term to (19) and integrating over time, we obtain

$$\int \boldsymbol{\sigma} \cdot \mathbf{n} \delta S \delta t + \Delta \int h \delta V = -ic \int f_4 \delta V \delta t = \int \mathbf{f} \cdot \mathbf{v} \delta V \delta t + \int q \delta V \delta t, \quad (21)$$

or

$$-\Delta Q_{\text{conv}} + \Delta E = \Delta A + \Delta Q_{\text{prod}}. \quad (22)$$

In the present case $\Delta E = 0$. The essential point here is that we have assumed the form $f_4 = i/c(\mathbf{f} \cdot \mathbf{v} + q)$ in any frame, where $\mathbf{f} \cdot \mathbf{v}$ is interpreted as the mechanical work exerted per unit of volume and time. By this assumption, we obtain at once by Lorentz-transformations from K^0 , $q^0 = -icf_4 - \mathbf{f} \cdot \mathbf{v} = \gamma^{-1}q^0$. If we integrate over a domain Σ in four-space which lies between two constant time-surfaces in K , we obtain $\Delta Q_{\text{prod}} = \gamma^{-1}\Delta Q_{\text{prod}}^0$, where at the right hand side we again have substituted Σ by Σ' as explained in the section following (14). By means of (14) we obtain $\Delta Q_{\text{conv}} = \Delta Q - \Delta Q_{\text{prod}} = -\gamma\Delta Q_{\text{prod}}^0 = \gamma\Delta Q_{\text{conv}}^0$. Note that this transformation formula for the convective heat has the same form as (2).

Let us investigate the possibility of splitting f_4 into two terms in other ways than shown above, corresponding to different interpretations of the mechanical work. An actual possibility might be to put $f_4 = i/c(\mathbf{f}' \cdot \mathbf{v} + q')$, where the four-vector f'_μ is determined by $f'^0_\mu = (\mathbf{f}'^0, 0)$. Thus the mechanical work density per unit time is interpreted as $\mathbf{f}' \cdot \mathbf{v}$, which means that we split off the effect arising from the heat term in f_4^0 . By means of the covariant relation $f_\mu = f'_\mu + q^0 V_\mu/c^2$, where $V_\mu = \gamma(\mathbf{v}, ic)$ is the four-velocity of the medium, we obtain readily $q' = \mathbf{f} \cdot \mathbf{v} - \mathbf{f}' \cdot \mathbf{v} + q = \gamma q^0$, which agrees with Ott's result. The first law can still be written as (21), when \mathbf{f} and q are replaced by \mathbf{f}' and q' .

However, the main obstacle for the present interpretation is apparent from the conservation equations $\partial_\nu T_{i\nu} = f'_i + q^0 V_i/c^2$. A momentum component inside a certain volume element may change on account of a momentum flow (described by T_{ik}) and a mechanical force (described by f'_i). But there is a lack of interpretation of the last term to the right. The common splitting of f_4 —the one used throughout this paper—seems to be preferable from a physical point of view.

Actually, Ott proceeds in another way in order to find the developed heat density. He claims the rate of mechanical work density to be equal to $\mathbf{k} \cdot \mathbf{v}$, where the four-vector k_μ is determined by $k^0_\mu = (\mathbf{k}^0, 0)$, $k^0_i = -\partial^0_k T^0_{ik}$, i.e. \mathbf{k}^0 is the elastic force density which in the interior domain of the body just compensates the electromagnetic force, so that $\mathbf{k}^0 + \mathbf{f}^{(e)0} = 0$. This performance does not seem to be readily incorporated in the above formalism, however, as we have let f_μ denote *external* forces.

Finally, we mention that in order to obtain the transformation formula for q we may consider instead the energy balance equation for the electromagnetic field, $\partial_\nu S_{4\nu} = -f_4^{(e)} = -i/c(\mathbf{f}^{(e)} \cdot \mathbf{v} + q)$, where $S_{\mu\nu}$ is the electromagnetic energy momentum tensor. We obtain of course $q = \gamma^{-1}q^0$ as

before. By adding the equations belonging to the two systems, however, we find $\partial_\nu(T_{4\nu} + S_{4\nu}) = f_4^{(m)}$, where $f_\mu^{(m)0} = (\mathbf{f}^{(m)0}, 0)$ so that the heat terms eliminate each other, and we obtain from this equation neither the first law nor the transformation formula for heat.

I wish to thank Professor C. MØLLER for valuable discussions. The reader is referred also to a paper by Professor MØLLER⁽⁸⁾ on the present subject. That paper was written during his absence from Copenhagen in the autumn of 1966.

- (8) C. MØLLER, Relativistic Thermodynamics. A Strange Incident in the History of Physics
Mat. Fys. Medd. Dan Vid. Selsk. 36, no. 1 (1967).

Nordita, Copenhagen.

Appendix

Let us write down the integrated conservation equations for momentum

$$\int t_{ik} n_k \delta S \delta t + \left(\int_{V^0} - \int_{V^0} \right) g_i \delta V = \int f_i \delta V \delta t, \quad (\text{A. 1})$$

where $t_{ik} = T_{ik} - g_i u_k$. Eq. (A. 1) can also be written as

$$\Delta G_i = \Delta G_i^{(m)} + \Delta G_i^{(h)}, \quad (\text{A. 2})$$

where

$$\Delta G_i^{(m)} = \int f_i \delta V \delta t \quad (\text{A. 3})$$

denotes the increase of momentum due to the external forces and

$$\Delta G_i^{(h)} = - \int t_{ik} n_k \delta S \delta t \quad (\text{A. 4})$$

the increase of momentum due to the heat flow through the boundary. It has been shown by C. MØLLER⁽⁸⁾ that, in the special example considered in his paper, the quantities

$$\Delta Q_{\mu} = \left(\Delta \mathbf{G}^{(h)}, \frac{i}{c} \Delta Q \right) \quad (\text{A. 5})$$

form a four-vector. It therefore seems to be an interesting point to make use of the above formalism to investigate whether the four-vector property of ΔQ_{μ} is more generally valid.

Let us write down the assumptions. In the first place, any produced heat is required to be absent. This means that no heat is supplied except when $0 \leq t^0 \leq \tau^0$. In the second place, the velocity u^0 of a volume element in K^0 is permitted to be arbitrarily large. This is a weaker restriction than we had before in our paper, and means that more general irreversible processes will be included in the description.

Let us now find $\Delta G_i^{(h)}$. The component ΔG_x is still given by (17), and we readily find that

$$\Delta G_y = \frac{\beta}{c} \left(\int_{V^0} - \int_{V^0_0} \right) T_{yx}^0 \delta V^0, \Delta G_z = \frac{\beta}{c} \left(\int_{V^0} - \int_{V^0_0} \right) T_{zx}^0 \delta V^0. \quad (\text{A. 6})$$

Further

$$\Delta G_x^{(m)} = \int_{\Sigma} f_x \delta V \delta t = \gamma \int_{\Sigma} f_x^0 \delta V^0 \delta t^0 + \frac{\gamma \beta}{c} \int_{\Sigma_1} \mathbf{f}^0 \cdot \mathbf{u}^0 \delta V^0 \delta t^0. \quad (\text{A. 7})$$

The first integral on the right hand side is to be evaluated over $\Sigma = \Sigma_1 + \Sigma_2 + \Sigma_3$. The contribution from Σ_1 is $\Delta G_x^{(m)0}$, while the contributions from Σ_2 and Σ_3 may be found by performing the time integrations for each volume element. We obtain

$$\Delta G_x^{(m)} = \frac{\gamma \beta}{c} \left[\Delta A^0 + \left(\int_{V^0_0} - \int_{V^0} \right) x^0 f_x^0 \delta V^0 \right] + \gamma \Delta G_x^{(m)0}, \quad (\text{A. 8})$$

where $\Delta G_x^{(m)0} = -\Delta G_x^{(h)0}$.

Similarly,

$$\Delta G_y^{(m)} = \int_{\Sigma} f_y^0 \delta V^0 \delta t^0 = \frac{\beta}{c} \left[\int_{V^0_0} - \int_{V^0} \right] x^0 f_y^0 \delta V^0 + \Delta G_y^{(m)0} \quad (\text{A. 9})$$

$$\Delta G_z^{(m)} = \frac{\beta}{c} \left[\int_{V^0_0} - \int_{V^0} \right] x^0 f_z^0 \delta V^0 + \Delta G_z^{(m)0}. \quad (\text{A. 10})$$

From (17) and (A. 6–10) we obtain, after some partial integrations,

$$\left. \begin{aligned} \Delta G_x^{(h)} &= \gamma \Delta G_x^{(h)0} + \frac{\gamma \beta}{c} \Delta Q^0 \\ \Delta G_y^{(h)} &= \Delta G_y^{(h)0}, \Delta G_z^{(h)} = \Delta G_z^{(h)0} \end{aligned} \right\} \quad (\text{A. 11})$$

The work ΔA follows from (6)–(9) as

$$\Delta A = \gamma \Delta A^0 + \gamma \beta^2 \left[\int_{V^0_0} - \int_{V^0} \right] x^0 f_x^0 \delta V^0 + \gamma v \Delta G_x^{(m)0} \quad (\text{A. 12})$$

(note that u^0 has been considered small only in the derivation of the last term in (6)). The energy change ΔE is still given by (12), and so

$$\Delta Q = \Delta E - \Delta A = \gamma v \Delta G_x^{(h)0} + \gamma \Delta Q^0. \quad (\text{A. 13})$$

From (A. 13,11) we see that ΔQ_μ transforms like a four-vector between K^0 and K , under the assumptions written down above.

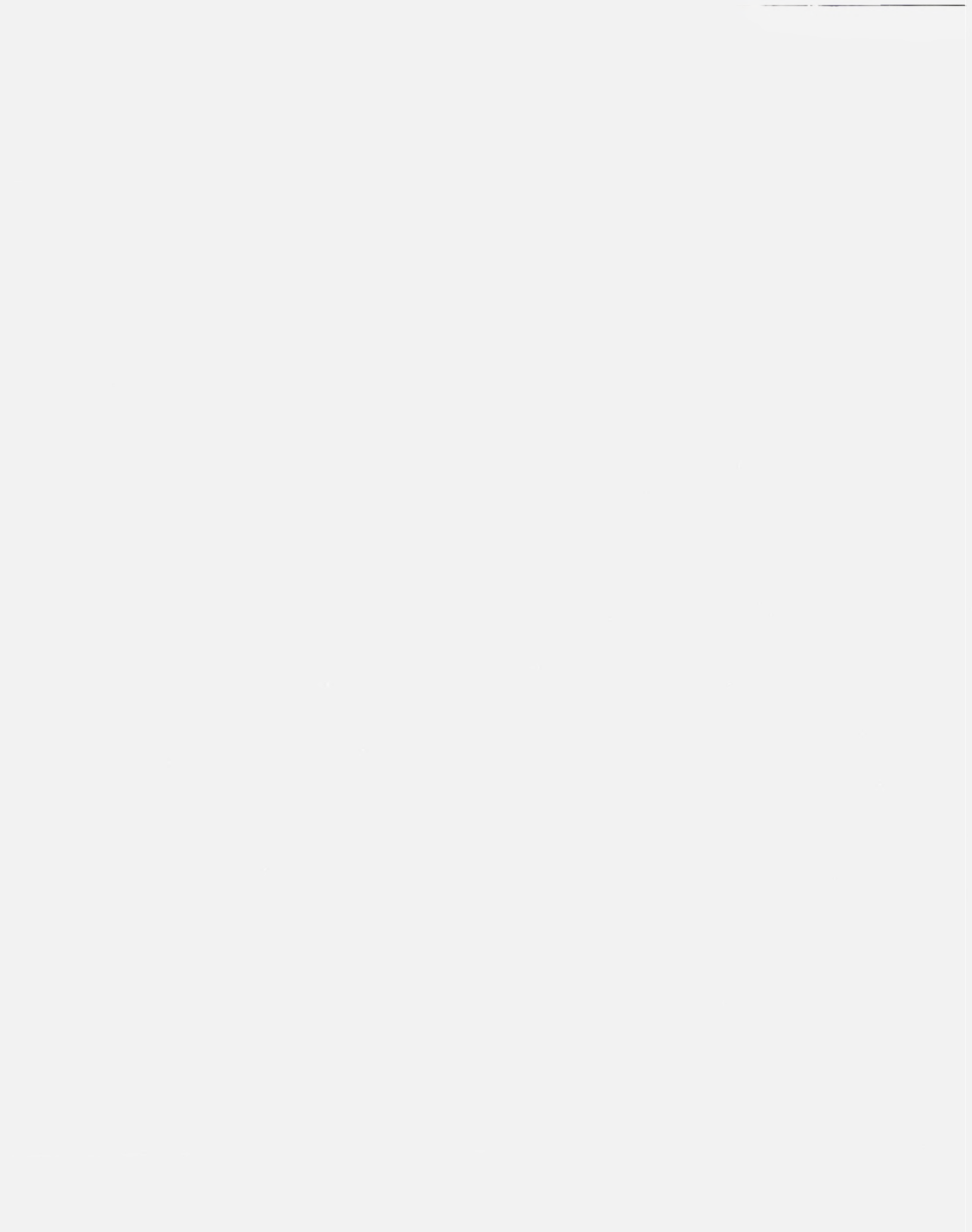
Combining (A. 1) and (21) we may write

$$\Delta G_\mu = \int f_\mu \delta V \delta t - \int t_{\mu k} n_k \delta S \delta t = \Delta G_\mu^{(m)} + \Delta Q_\mu, \quad (\text{A. 14})$$

where $t_{\mu k} = T_{\mu k} - g_{\mu k} u_k$. This equation is in general not a relation between covariant quantities, since only the last term to the right is a four-vector. (The quantity $\Delta G_\mu^{(m)}$ is of course a four-vector as long as we let the integration domain be unchanged under Lorentz transformations. However, when we let the time-orthogonal surfaces in K be substituted by appropriate time-orthogonal surfaces in K^0 upon the transformation $K \rightarrow K^0$, the four-vector property is in general lost). But in the special case where the system is a material particle, then all terms in (A. 14) are four-vectors. Introducing the element of proper time $d\tau = \gamma^{-1} dt$ for the single world line we are considering, we can write

$$\frac{dG_\mu}{d\tau} = F_\mu + \frac{dQ_\mu}{d\tau}, \quad (\text{A. 15})$$

where F_μ is the external total four-force. Eq. (A. 15) is the equation utilized by OTT⁽⁴⁾ in his general proof. However, his result (2) agrees with (A. 13) only when $\Delta G_x^{(h)0} = 0$.



N. O. LASSEN AND N. HORNSTRUP

HALF-LIFE OF ^{208}Tl (ThC')

Det Kongelige Danske Videnskabernes Selskab
Matematisk-fysiske Meddelelser **36**, 4



Kommissionær: Munksgaard
København 1967

Synopsis

The half life of ThC" was measured to be 3.055 ± 0.006 min. or 183.3 ± 0.4 sec., which is 1.5 per cent smaller than the best hitherto known value.

1. Introduction

The half life of ThC'' was determined in 1909 by HAHN and MEITNER¹⁾, who found the value 3.1 min. Later measurements gave the following results: VON LERCH and VON WARTBURG²⁾ (1909) 3.0 min., WOOD³⁾ (1914) 3.1 min., and ALBRECHT⁴⁾ (1919) 3.20 min. More recently, BAULCH, DAVID and DUNCAN⁵⁾ (1957) found the half life to be 3.10 ± 0.015 min. Using a Geiger counter and starting with initial counting speeds of about 10–1000 cpm, they followed the decay of 268 sources which were prepared from ThB + C by a recoil method. The ThC'' nuclei recoiling after the decay of ThC were collected, whereas, by means of an electric field, recoils after β -decay were prevented from reaching the collector.

In a recent paper by MIDDELBOE⁶⁾ on accurate half-life determinations, the importance of having a source free from radioactive impurities was stressed. This gave us the impulse for the present work.

2. Experimental method

A ThC'' source was placed close to a 3×3 inch NaJ-crystal; the amplified pulses from the photo-multiplier fed two scalers. One scaler and a stopwatch were started simultaneously ($t = 0$) by the experimenter; the second scaler was started at $t = T = 600.0$ sec., and both scalers were stopped at $t = 2T = 1200.0$ sec. Hereby the numbers M_1 and M_2 of counts in the time intervals 0–600 and 600–1200 sec., respectively, were obtained. After proper corrections, the numbers of counts N_1 and N_2 corresponding to the decay period of ThC'' yielded the fall-off factor $F = N_1/N_2$. Then, the half life is

$$T_{1/2} = T \log 2 / \log F. \quad (1)$$

By following the decay of the source for a few hours we determined the amount of ThB and ThC impurities in the source; no other radioactive impurities were present.

Originally it was intended to discriminate against energies below 1.3 MeV and to look at the high energy photons from ThC". However, observations of the γ -spectrum from a Cs¹³⁷ standard by means of an RCL 512-channel pulse height analyzer showed that the gain of the photomultiplier tube depended on the counting rate and also on the prehistory of the counter. Counting 45 minutes with a rate of 23000 counts per sec. produced a decrease in gain of about 10 per cent; when the source was removed, a rapid increase of some 4 per cent was observed, followed by a slow exponential increase, so that normal amplification was reached in about a day. Such phenomena are not unknown⁷⁾. Although shorter exposures seemed less fatal, we decided in the half-life measurements to use the whole spectrum. Consequently, the cut-off was put at a value corresponding to a γ -energy of about 0.030 MeV and tests now showed unchanged counting rates before and after exposure to a strong source.

3. Source preparation

Corresponding to three different ways of source production we denote the experiments by the letters A, B, and C.

A.

Active deposit from an emanating source of RdTh was collected on a platinum sphere of about 1 mm in diameter. Sources of ThB and its daughters of about 10–100 μ Curie were used; except for the first few hours, the sources were found to decay with a half life of 10.8 hours (the adopted value for ThB is 10.6 hours) until the counting rate was lower than one count per sec. with the source close to the crystal. Thus, no significant longer lived radioactive impurity was present.

We have no reason to suspect that the RdTh should contain any radio impurities. However, if impurities belonging to the other radioactive series were present, RaB and AcB would be collected together with ThB. Therefore, an α -spectrum of the ThB source was measured by means of a solid-state silicon detector and a 512-channel analyzer; the main α -groups and the less abundant groups with energies 5.60 and 5.76 MeV were seen, but no traces of α -particles with energies 6.28, 7.69, and 8.34 MeV, corresponding to AcC' and Po²¹³, respectively, were found. An upper limit could be set for these impurities; they could at most cause an error in the measured half life of ThC" less than 0.01 per cent.

After removal from the activation chamber, the ThB source was stored for about 20 min. so that possible adhering Tn and ThA decayed. Later, the source was placed in an evacuated tube of 2 cm diameter, the inside wall of which was covered by a thin aluminum foil, and the source was

held at a potential of -300 V with respect to the surrounding aluminum foil. For about 3–10 min., the recoiling ThC''-atoms created in the α -decay of ThC were collected on the aluminum foil. The purpose of the potential difference was to prevent recoils from β -decay of ThB to be collected; however, complete separation was never obtained; the ThC'' sources always contained small amounts of both ThB and ThC, but no longer living activities.

B.

In another attempt at producing pure ThC'' sources, the starting material was $120 \mu\text{Curie}$ RdTh dissolved in HNO_3 . By means of a Dowex 1 ion-exchange column, a source of about $5 \mu\text{Curie}$ of ThX + descendants was prepared. This source, after drying, was dissolved in $0.1 n$ HCl and put on a Dowex 50 column, from which a ThB + C source was obtained by eluting with $1 n$ HCl.

Tl was then oxidized to stage III by means of chlorine and the solution was made $6 n$ with respect to HCl. By shaking the solution with an equal volume of ethylether for 30 sec., we transferred the ^{208}Tl to the ether phase, thereby separating it from Pb and Bi (ThB and ThC).

However, also this source was found to contain small amounts of ThB and ThC, and in addition it would sometimes contain ThX. It was thought to be too risky to correct for ThX and all its successors, especially because one of them is a gas and because it has a half life comparable to the half life of ThC''. The results were therefore only used when a very low limit for possible ThX contamination of the source could be set.

C.

A ThB + C source was prepared in the way described under A. This source was placed in a vacuum box approximately one mm from a glass plate covered by a thin polysterene film prepared in a way similar to that described by BJØRNHOLM⁹⁾. The thickness of the film was $3\text{--}5 \mu\text{g}/\text{cm}^2$ so that some recoil atoms from α -decay would penetrate to the glass plate, whereas ThB and ThC atoms were supposed to be caught in the film. After exposure for some 3–5 min., the polysterene film was removed by washing the glass plate in an acetone bath.

4. Measurement of ThB and ThC impurities

Fig. 1 shows the well-known decay scheme for ThB. Let A , B , and C denote the number of atoms of ThB, ThC and ThC'' respectively, λ_A , λ_B , and λ_C the corresponding total decay constants, and λ_{B1} the partial decay constant for $\text{ThC} \rightarrow \text{ThC}''$. Then,

$$A = A_0 e^{-\lambda_A t} \quad (2a)$$

$$B = \frac{A_0 \lambda_A}{\lambda_B - \lambda_A} e^{-\lambda_A t} + \left(B_0 - \frac{A_0 \lambda_A}{\lambda_B - \lambda_A} \right) e^{-\lambda_B t} \quad (2b)$$

$$C = \left. \begin{aligned} & \frac{A_0 \lambda_A \lambda_{B1}}{(\lambda_C - \lambda_A)(\lambda_B - \lambda_A)} e^{-\lambda_A t} + \left[\frac{B_0 \lambda_{B1}}{\lambda_C - \lambda_B} - \frac{A_0 \lambda_A \lambda_{B1}}{(\lambda_C - \lambda_B)(\lambda_B - \lambda_A)} \right] e^{-\lambda_B t} \\ & + \left[C_0 - \frac{B_0 \lambda_{B1}}{\lambda_C - \lambda_B} + \frac{A_0 \lambda_A \lambda_{B1}}{(\lambda_C - \lambda_B)(\lambda_C - \lambda_A)} \right] e^{-\lambda_C t}. \end{aligned} \right\} \quad (2c)$$

The activity at the time t is $A\lambda_A + B\lambda_B + C\lambda_C$, and the counting rate is $A\lambda_A \varepsilon_A + B\lambda_B \varepsilon_B + C\lambda_C \varepsilon_C$, where for example ε_A is the probability that a transformation from ThB to the ground state of ThC is registered by the counter, and where ε_B includes the decay $\text{ThC} \rightarrow \text{ThC}''$ as well as the decay $\text{ThC} \rightarrow \text{ThC}'$ ($\rightarrow {}^{208}\text{Pb}$).

If no counts are lost due to random coincidences, the counting rate may be written

$$R_s(t) = \beta_1 e^{-\lambda_A t} + \beta_2 e^{-\lambda_B t} + \beta_3 e^{-\lambda_C t} + D, \quad (3)$$

where D is the natural background and β_1 , β_2 , and β_3 are constants depending on the initial amounts of ThB, ThC, and ThC''.

For $t > 5000$ s, $e^{-\lambda_C t} = 0$. β_1 and β_2 were determined such as to give the best fit to six values of $R_s(t) - D$ in the interval $5000 < t < 10000$.

If we had wanted to correct M_1 and M_2 for the influence of the impurities of ThB and ThC, the corrections would have been

$$-G_1 = -\int_0^T (\beta_1 e^{-\lambda_A t} + \beta_2 e^{-\lambda_B t} + D) dt - \int_0^T (\beta_3 - \varepsilon_C C_0 \lambda_C) e^{-\lambda_C t} dt = -G'_1 - G''_1. \quad (4a)$$

$$-G_2 = -\int_T^{2T} (\beta_1 e^{-\lambda_A t} + \beta_2 e^{-\lambda_B t} + D) dt - \int_T^{2T} (\beta_3 - \varepsilon_C C_0 \lambda_C) e^{-\lambda_C t} dt = -G'_2 - G''_2. \quad (4b)$$

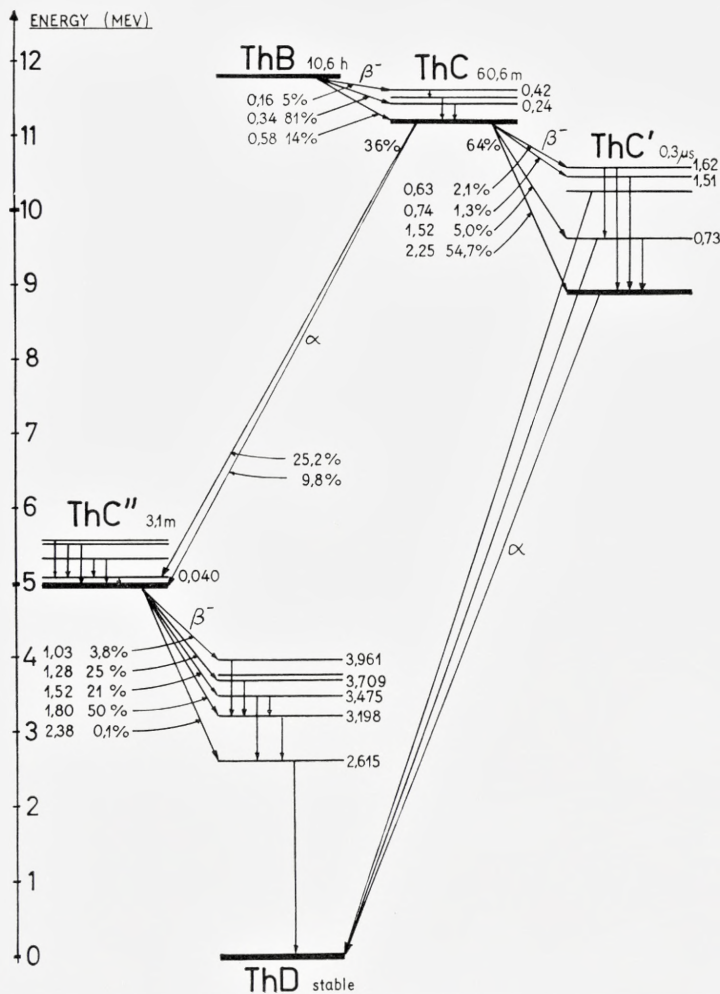


Fig. 1. Decay scheme for ThB.

However, since $G_2''/G_1'' = e^{-\lambda_1 t} = N_2/N_1$, we need only apply the corrections $-G_1'$ and $-G_2'$. To determine the half life $T_{1/2}$, M_1 and M_2 need only be corrected with the integrals of that part of the count rate which does not decay with the period $T_{1/2}$.

It should be noticed that, to determine β_1 and β_2 , we must know λ_A and λ_B , but no knowledge of the efficiencies is required.

It is unnecessary to find the actual amounts of impurities; however, if we do want them, we have to know the efficiencies. Replacing the source with a ^{32}P source an efficiency of 0.07 was found. We estimate the probability to observe a β -particle from a decay to be 0.00, 0.07 and 0.07 for ThB, ThC, and ThC", respectively. For ThC", for example, we find $\varepsilon_c = 0.07 + 0.93 \cdot \varepsilon_{\gamma c}$, where $\varepsilon_{\gamma c}$ is the probability that the decay is registered through any of the photons. Using known curves¹⁰⁾ for counter efficiency as a function of distance and energy, and taking into account the decay scheme and the known conversion coefficients¹¹⁾, we find the total efficiencies to be

$$\varepsilon_A \sim 0.18, \quad \varepsilon_B \sim 0.09, \quad \text{and} \quad \varepsilon_C \sim 0.44.$$

β_1 and β_2 may be expressed in terms of λ_A , λ_B , λ_{B1} , ε_A , ε_B , A_0 , and B_0 . From these expressions we find, with the above mentioned efficiencies,

$$\varepsilon_A A_0 \lambda_A \sim 2.5 \beta_{12}; \quad \varepsilon_B B_0 \lambda_B \sim 0.3 \beta_2 + 0.2 \beta_1,$$

which may be used to calculate the amount of impurity atoms from the values for β_1 and β_2 given in Table 2 (p. 10).

5. Corrections for deadtime losses and impurities

When determining β_1 and β_2 from the counting rate for large t -values we may safely neglect losses due to random coincidences. With the high initial counting rates, however, appreciable deadtime corrections must be applied to M_1 and M_2 . Deadtime and impurity corrections are coupled, and both have been taken care of by the following procedure. If we assume the deadtime τ of the counter arrangement to be a constant, we have

$$R_m = \frac{R_s}{1 + \tau R_s}, \quad (5)$$

where R_m and R_s are the measured and the "true" counting rates. For $0 < t < T$ we put $e^{-\lambda_A t} = 1$ and $e^{-\lambda_B t} = e^{-\lambda_B T/2} = 0.95$. Then, from (3),

$$R_s(t) = E_1 + \beta_3 e^{-\lambda_c t} = \beta_1 + 0.95 \beta_2 + D + \beta_3 e^{-\lambda_c t} \quad (6a)$$

which, introduced in (5), gives

$$M_1 = \int_0^T R_m dt = \int_0^T \frac{E_1 + \beta_3 e^{-\lambda_c t}}{1 + \tau E_1 + \tau \beta_3 e^{-\lambda_c t}} dt. \quad (7a)$$

Integrating and rearranging, one finds

$$\beta_3 = \frac{(1 - e^{-U_1})(1 + \tau E_1)}{\tau(e^{-U_1} - e^{-\lambda_c T})} = \frac{(U_1 - \frac{1}{2}U_1^2 + \frac{1}{6}U_1^3)(1 + \tau E_1)}{\tau(1 - U_1 + \frac{1}{2}U_1^2 - \frac{1}{6}U_1^3 - 0.10346)}, \quad (8a)$$

where

$$U_1 = [M_1(1 + \tau E_1) - E_1 T] \tau \lambda_c. \quad (9a)$$

Similarly,

$$M_2 = \int_0^{2T} \frac{E_2 + \beta_3 e^{-\lambda_c t}}{1 + \tau E_2 + \tau \beta_3 e^{-\lambda_c t}} dt = \int_0^T \frac{E_2 + \beta_3 e^{-\lambda_c T} e^{-\lambda_c t'}}{1 + \tau E_2 + \tau \beta_3 e^{-\lambda_c T} e^{-\lambda_c t'}} dt', \quad (7b)$$

where

$$E_2 = 0.99 \beta_1 + 0.846 \beta_2 + D. \quad (6b)$$

Now, $\beta_3' = \beta_3 e^{-\lambda_c T}$ may be found from expressions similar to (8a) and (9a). Finally, introducing $F = \beta_3/\beta_3'$ in (1), we obtain the half life $T_{1/2}$ corrected for deadtime losses and impurities.

Since $\tau \sim 6 \cdot 10^{-6} s$, one has $\tau E_1 \ll \ll 1$. Also $E_1 T \ll \ll M_1$. Hence, $U_1 \ll 1$ for $M_1 \ll (\tau \lambda_c)^{-1} \sim 40 \cdot 10^6$. This justifies the use of the series expansion in (8), and furthermore shows that no very accurate value for λ_c need be used in (9a) since, to first order in U_1 , the factor λ_c nearly cancels out in the ratio β_3/β_3' . Actually, iteration is used.

6. Determination of deadtime τ

Shortly before or shortly after each half life measurement the dead-time was measured. Two standard sources, ^{22}Na and ^{60}Co , were used. The counting rates m_1 , m_2 , m_{12} , and m_b , corresponding to one source in a standard position, the other source in another standard position, both sources in their respective positions, and no sources, respectively, were measured. Then⁸⁾,

$$\tau = \tau_1 \left[1 + \frac{\tau_1}{2} (m_{12} - 3m_b) \right]$$

with

$$\tau = \frac{m_1 + m_2 - m_{12} - m_b}{2(m_1 - m_b)(m_2 - m_b)}.$$

When counting one source, the other source was removed, but a "dummy" was used to secure identical conditions in the various measurements. The counting times were so as to give a statistical error in τ of about 0.3%. The half life determinations were carried out in two periods, separated by several months. τ was found to be constant within each period, but slightly different for the two periods (5.60 and 5.70 μs , respectively). Table 1 gives the results for the first period.

TABLE 1.

	m_1	m_{12}	m_2	m_b	τ
A1.....	9 988	28 494	20 675	16.2	5.62
A2.....	18 333	33 799	19 066	15.0	5.58
A3.....	17 836	33 434	19 117	15.0	5.59
A4.....	17 858	33 384	19 055	14.8	5.62
A5.....	13 687	26 751	15 259	11.9	5.60
A6.....	15 732	29 465	16 422	12.9	5.58
A7.....	18 471	32 865	17 805	21.0	5.60

7. Results

Disregarding two B-measurements, because the source contained ThX, the first 12 measurements are summarized below.

In Table 2, M_1 and M_2 are the actually registered numbers of counts in the first two 10 min.-periods. The fourth column gives approximate values for β_3 (approximately the initial count rate). The background was always found to be between 7.2 and 7.5 c/s. For example, for A1: $D = 7.38 \pm 0.05$ c/s. The deadtime τ is given in § 6.

The mean value of the twelve measurements is $T_{1/2} = (3.055 \pm 0.002)$ min., where the stated error covers only statistical errors.

TABLE 2.

	M_1 counts	M_2 counts	β_3	β_1	β_2	$\frac{(\beta_1 + \beta_2)}{\beta_3}$	$T_{1/2}$	$\Delta T_{1/2}$ stat. error
	0-600s	600s-1200s	c/s	c/s	c/s	‰	min	‰
A1....	2 679 523	293 064	11 600	1.0	3.4	0.38	3.060	1
A2....	2 447 774	267 815	10 600	1.8	5.0	0.64	3.056	1
A3....	2 877 098	313 071	12 500	0.6	4.4	0.40	3.051	1
A4....	1 139 344	134 599	4 800	1.6	24	5.3	3.049	4
A5....	2 001 459	222 650	8 600	2.1	9.5	1.35	3.064	1.5
A6....	1 684 836	185 540	7 200	0.4	9.2	1.35	3.051	1.5
A7....	1 296 647	145 292	5 500	1.3	11.6	2.4	3.048	2
B1....	396 506	45 704	1 650	1.3	-0.4	0.55	3.060	3
C1....	706 550	80 186	2 900	1.8	3.9	2.0	3.055	2.5
C2....	981 243	107 501	4 100	0.5	1.4	0.45	3.056	2
C3....	1 059 091	115 065	4 500	0.05	1.2	0.38	3.051	2
C4....	429 359	48 762	1 800	-0.02	0.34	0.18	3.059	2.5

8. Discussion

The fluctuation of the twelve values for the half life, defined by $\sigma^2 = \langle (T - \langle T \rangle)^2 \rangle$, is found to be $\sigma = 0.005$ min., in agreement with the statistical uncertainty of a single measurement.

By plotting the values of $T_{1/2}$ against M_1 no correlation is found. Plotting $T_{1/2}$ against the fractional amount of impurities may possibly show a slight tendency towards lower $T_{1/2}$ values for high impurities, but the variation is not outside the limits of error.

First, when discussing a possible error due to an error in τ , we may disregard the impurities and the background. Then, according to (5) and (6a),

$$\begin{aligned}
 N_1 &= \int_0^T R_s dt = (\beta_3/\lambda_c) (1 - e^{-\lambda_c T}) \\
 M_1 &= \int_0^T \frac{R_s dt}{1 + \tau R_s} \approx \int_0^T R_s dt - \tau \int_0^T R_s^2 dt. \\
 \Delta M_1 &= N_1 - M_1 \approx \tau \int_0^T R_s^2 dt = \tau \int_0^T \beta_3^2 e^{-2\lambda_c t} dt \\
 &= \frac{1}{2} \tau \lambda_c \frac{1 - e^{-2\lambda_c T}}{(1 - e^{-\lambda_c T})^2} \left[\frac{\beta_3}{\lambda_c} (1 - e^{-\lambda_c T}) \right]^2. \\
 \Delta M_1 &\approx 2.4 \cdot 10^{-3} N_1^2 \tau.
 \end{aligned}$$

An error $\delta\tau$ causes an error in N_1 ($\delta N_1 = \delta(\Delta M_1)$), which is

$$\delta N_1/N_1 \sim 2.4 \cdot 10^{-3} M_1 \tau (\delta\tau/\tau)$$

and, since $F \sim 10$ and since the relative error in N_2 (due to $\delta\tau$) may be disregarded,

$$\delta T_{1/2}/T_{1/2} \sim -(1/2)\delta F/F \sim -(1/2) \delta N_1/N_1 \sim -1.2 \cdot 10^{-3} M_1 \tau (\delta\tau/\tau).$$

Introducing $\tau \sim 6 \cdot 10^{-6}$ s we find

$$\text{for } M_1 \sim 2 \cdot 10^6 \qquad \delta T_{1/2}/T_{1/2} \sim -0.015 \delta\tau/\tau$$

$$\text{for } M_1 \sim 7 \cdot 10^5 \qquad \delta T_{1/2}/T_{1/2} \sim -0.005 \delta\tau/\tau.$$

The statistical uncertainty in τ is insignificant. But the value used for τ might be erroneous, because τ may depend on the energy spectrum. However, the mean values of $T_{1/2}$ for A1-2-3-5-6 and for B1-C1-2-3-4, are 3.057 and 3.056 min., respectively, with a statistical uncertainty of about 0.002 min. and these two groups of measurements happen to correspond roughly to the above mentioned values of M_1 . If the error in τ were as much as 20 per cent, the two mean values should differ by 0.006 min. – which they

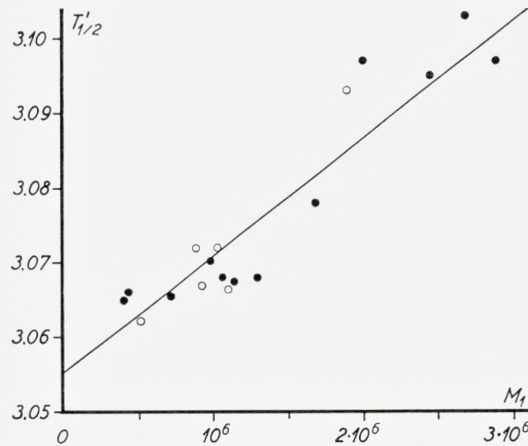


Fig. 2. $T'_{1/2}$ is the measured half life of ThC'', corrected for ThB and ThC impurities, but not for deadtime losses. M_1 is the number of counts in the first 10 min.-period. The closed circles refer to the measurements summarized in Table 2, and the straight line represents a least square fit to these points. The open circles refer to the measurements of Table 3.

do not – and in this case the error in the last mean value would be 0.003 min. It seems safe to conclude that $\delta T_{1/2} < 0.006$ min.

The experimental data may be treated in a different way. When F is replaced by $F' = (M_1 - E_1 T)/(M_2 - E_2 T)$, formula (1) gives values $T'_{1/2}$ for the uncorrected half life. Plotting $T'_{1/2}$ against M_1 should be expected to give a straight line with a slope determined by τ and intersecting the Y-axis at $T_{1/2}$. Such a plot is shown in Figure 2, where the straight line is drawn by means of the method of least square deviations. Again we find $T_{1/2} = 3.055$ min. and the slope of the line corresponds to a value of the deadtime $\tau \sim 5.6 \mu\text{s}$.

Next, when discussing errors due to erroneous impurity corrections, we may disregard deadtime losses and background. Statistical errors of the impurity corrections have already been included in $\Delta T_{1/2}$ given in Table 2.

Assuming, for the sake of simplicity, only two $R_s(t)$ values used for the determination of β_1 and β_2 , we have

$$\begin{aligned} R_1 &= \beta_1 e^{-\lambda_A t_1} + \beta_2 e^{-\lambda_B t_1} \\ R_2 &= \beta_1 e^{-\lambda_A t_2} + \beta_2 e^{-\lambda_B t_2}. \end{aligned}$$

Solving for β_1 and β_2 and differentiating, we obtain $\delta\beta_1/\delta\lambda_A$, etc. Further,

$$G'_2 = \beta_1 e^{-\lambda_A T} \frac{1 - e^{-\lambda_A T}}{\lambda_A} + \beta_2 e^{-\lambda_B T} \frac{1 - e^{-\lambda_B T}}{\lambda_B}.$$

By differentiation, $\frac{\delta G'_2}{\delta \lambda_A} = \frac{\delta N_2}{\delta \lambda_A}$, etc., are obtained. For example, $\delta N_2 \sim 2.5 \cdot 10^6 \beta_2 \delta \lambda_B$, which shows that an error of 5 per cent in λ_B will only for A4 produce an error in the half life of more than about 0.5⁰/₀₀.

Now, let us consider errors due to time measurement. Repeated checks showed the stopwatch time to be in error by less than 0.1⁰/₀₀. The half life is found from the expression $T_{1/2} = 600 \log 2 / \log F$ and, therefore,

$$\delta T_{1/2} = -T_{1/2} \delta(\log F) / \log F \sim -(1/2) T_{1/2} \delta F / F.$$

One scaler worked in T_2' seconds, the other scaler in $(T_2'' - T_1)$ seconds, where $T_1 \sim 600$, $T_2' \sim T_2'' \sim 1200$. Then,

$$\begin{aligned} N_1 &= \frac{\beta_3}{\lambda_c} [1 - e^{-\lambda_c T_2'} - (e^{-\lambda_c T_1} - e^{-\lambda_c T_2''})] \\ N_2 &= \frac{\beta_3}{\lambda_c} (e^{-\lambda_c T_1} - e^{-\lambda_c T_2''}). \end{aligned}$$

Differentiating, putting the numerical values $\delta T_1 \sim \delta T_2' \sim \delta T_2''$, and assuming the worst possible signs, one gets $\delta T_{1/2} \sim \delta T_1$. T_1 is the important time interval, i.e., the interval from the start of the first to the start of the second scaler. δT_1 is supposed to be smaller than 0.2 sec. ~ 0.003 min. for the mean value.

The stability of the counter arrangement was checked occasionally. The power supply was stabilized, and a change of 10 volts of the main 220 Volt A.C. supply would produce a change of only 3⁰/₀₀ in counting rate. Supervising the main supply for long periods never revealed so large

changes, and the possibility that the average half life should be significantly in error due to spurious changes is vanishingly small.

We consider it safe to state that $T_{1/2} = 3.055 \pm 0.006$ min.

To account for the disagreement with the result of BAULCH, DAVID and DUNCAN⁵⁾, we are inclined to believe that their sources may have contained ThB+C impurities. This would have been difficult to observe due to the small counting rates involved in their experiments; furthermore, in spite of various efforts using different retarding potentials, we were never able to produce a pure source by means of method A, which is similar to their source preparation techniques.

9. Supplementary measurements

As a further check, six measurements of the half life of ThC'' were performed by another experimenter. These measurements are summarized in Table 3.

TABLE 3.

	M_1	M_2	β_3	β_1	β_2	$\frac{\beta_1 + \beta_2}{\beta_3}$	$T_{1/2}$		$\Delta T_{1/2}$
	c/600s	c/600s	c/s	c/s	e/s	‰	uncorr.**	corr.	stat. error
							min	min	‰
C5 ...	508 738	57 007	2 150			0.15 ± 0.15	3.057	3.053	3
C6 ...	881 877	96 945	3 750	0.45	1.0	0.40	3.067	3.057	2
C7 ...	1 102 386	120 661	4 700	0.03	3.5	0.75	3.068	3.047	2
C8 ...	923 117*	85 310*	3 800	1.4	6.2	2.0	3.117	3.053	2
C9 ...	1 942 335	251 181	8 200	49	33	10	3.325	3.061	4
C10 ..	1 032 474	114 223	4 400	0.80	3.2	0.9	3.079	3.055	2

* Counts in 660 s.

** These values are corrected for deadtime losses, but not for impurities of ThB+C.

Here, $\tau = 5.90 \cdot 10^{-6}$ s. $D \sim 7.5$ c/s as before. The mean value of the six measurements is again 3.055 min.

When preparing the source for C7, the polysterene film was removed from the glass plate in a bath of acetone to which had been added carriers of Pb and Bi. As seen, the purity of the source was not improved. In C8, no polysterene film was used; the idea was to investigate whether the im-

purity correction would work for high impurities. The same applies to C9, in which experiment the bare glass plate was exposed to the ThB + C source for two hours with the aim to increase the amounts of both ThB and ThC in the ThC" source. Also in C10 no polystyrene film was used. Furthermore, in this experiment the counter arrangement was changed; the β -particles from the source were stopped in a second inactive glass plate and the bremsstrahlung photons were filtered away with one mm of lead; thus the efficiencies were radically changed.

Auxiliary deadtime measurements, using sources of ^{60}Co and ^{22}Na , gave the same value for τ with counting rates m_{12} of 30 000 and 15 000 c/s, and within the statistical error also for $m_{12} = 2\,500$ c/s. The deadtime was about 2 per cent higher for $^{60}\text{Co} + ^{137}\text{Cs}$ sources or for $^{22}\text{Na} + ^{137}\text{Cs}$ sources, and some 5 per cent higher when two ^{137}Cs sources were used. Using sources of ^{60}Co and ^{241}Am , τ was found to be $11.5\ \mu\text{s}$, but the radiation from ^{241}Am is very soft (~ 60 keV).

10. Half life of $^{137}\text{Ba}^m$

As a further check of our procedure we measured the half life of $^{137}\text{Ba}^m$, previously determined by MIDDELBOE⁶⁾. Ba was separated from the parent ^{137}Cs by means of a KCFC-ion exchange column¹²⁾ with particle sizes 35–60 standard mesh size; the background count rate due to radioimpurities was about 10^{-5} times the initial count rates of $^{137}\text{Ba}^m$. Using count rates of 3 000–30 000 c/s at the start of the measurements, our mean value from ten determinations was 2.559 ± 0.006 min., in good agreement with the value 2.5577 ± 0.0032 min. given by MIDDELBOE.

These experiments were carried out at the Niels Bohr Institute, University of Copenhagen. The authors wish to express their heartiest thanks to Mr. N. O. ROY POULSEN, mag. scient., for many valuable discussions. We gratefully acknowledge the help of Mr. T. OSTENFELD who with much skill carried out the measurements mentioned in § 9. We are furthermore indebted to the leader of the radiochemistry group, Mrs. M. L. ANDERSEN, cand. polyt., and to Mrs. H. BORK for the preparation of the ThB + C source used for the B-experiment and the KCFC ion-exchange column used for milking the ^{137}Cs source.

References

1. O. HAHN and L. MEITNER: Verh. Deutsche Phys. Ges. **11** (1909) 55.
2. F. v. LERCH and E. v. WARTBURG: Sitzb. Akad. Wiss. Wien **118**, **2a** (1909) 1575.
3. A. B. WOOD: Phil. Mag. **28** (1914) 808.
4. E. ALBRECHT: Sitzb. Akad. Wiss. Wien **128**, **2a** (1919) 925.
5. D. L. BAULCH, H. A. DAVID and J. F. DUNCAN: Austr. J. Chem. **10** (1967) 85 and 112.
6. V. MIDDELBOE: Mat. Fys. Medd. Dan. Vid. Selsk. **35**, no. 8, 1966.
7. I. CANTARELL: Nucl. Sc. & Eng. **18** (1964) 31.
I. CANTARELL and I. ALMODOVAR: Nucl. Instr. Meth. **24** (1963) 353.
8. E. BLEULER and G. J. GOLDSMITH: Experimental Nucleonics, Rinehart & Co., New York 1952.
9. S. BJØRNHOLM, E. R. JOHANSEN and H. NØRDBY: Nucl. Instr. Meth. **27** (1963) 243.
10. R. L. Heath: Scintillation Spectrometry Gamma-Ray Spectrum Catalogue, Phillips Petroleum Co., Atomic Energy Division, Idaho Falls, Idaho. July 1, 1957.
11. Nuclear Data Sheets, Nat. Acad. Sc., NRC, Wash. DC.
12. W. E. PROUT, E. R. RUSSELL and H. J. GROH: J. Inorg. Nucl. Chem. **27** (1965) 473.

JOHN BRAMMER PETERSEN, JØRGEN LEI,
NIELS CLAUSON-KAAS AND KJELD NORRIS

THE CHEMISTRY OF ENDIALONE

Det Kongelige Danske Videnskabernes Selskab
Matematisk-fysiske Meddelelser **36**, 5



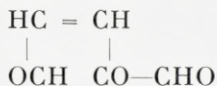
Kommissionær: Munksgaard
København 1967

Synopsis

29 pyridine compounds, 26 of which are new, have been prepared by oxidation of furfural with one or two moles of chlorine in water followed by reaction with amino compounds.

I. Introduction

cis-Oxoglutaconaldehyde (I) has never been prepared pure. But all existing knowledge indicates⁽¹⁾ that a solution of hydrates of I is formed in a high-yield reaction, when furfural is oxidized with chlorine or bromine in aqueous, acidic solution under certain reaction conditions.



I

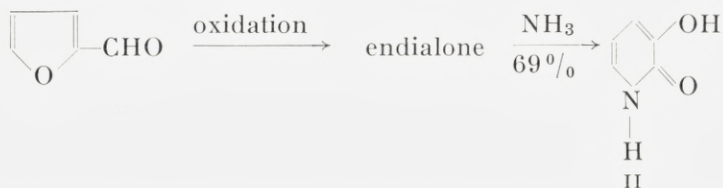
Such solutions are reasonably stable and have here been used to prepare a number of new compounds. The reactions leading to these compounds are in part general. Representative examples of the reactions are reported in this communication.

Solutions of *cis*-oxoglutaconaldehyde, as obtained by oxidation of furfural in water, are colourless. This means that molecules which contain two or more free carbonyl groups in conjugation cannot be present. No other information as to the structure of *cis*-oxoglutaconaldehyde in an aqueous solution is available. We believe such solutions contain a number of different molecular species, the concentrations of which depend upon the reaction conditions during their formation, as well as upon temperature, pH, concentration, and storage conditions of the solutions. Examples of the influence of age of a certain solution upon the yields of two different reactions, both with sulfamic acid, are given in the experimental part.

cis-Oxoglutaconaldehyde is, together with the corresponding *trans*-derivative, the simplest possible straight-chain compound having one double bond, two aldehyde groups, and one keto group. We use the trivial name endialone for the compound in whatever form it may exist in aqueous solution.

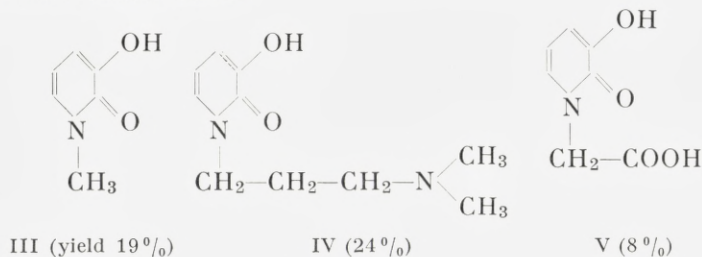
II. Endialone and Amino Compounds

(a) *Endialone and ammonia* give the known 3-hydroxy-2(1*H*)-pyridone (2,3-pyridinediol) (II). The experimental part of this paper contains a recipe according to which II is precipitated pure directly from the reaction mixture in a 45 per cent yield. Another, less convenient procedure describing isolation of II in a 69 per cent yield through prolonged continuous extraction of the reaction mixture with ether is also given.



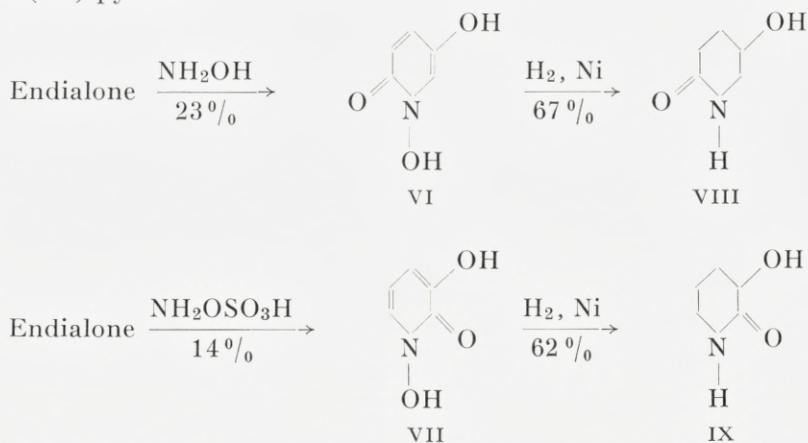
No detailed picture of the reaction leading to II can be given, since the exact structures of reactants and intermediates are unknown. The overall reaction consists of a connection of the two aldehyde groups of endialone through one ammonia molecule, followed by aromatization.

(b) *Endialone and primary aliphatic amines* similarly give 1-substituted 3-hydroxy-2(1*H*)-pyridones. Compounds III–V were prepared in this way. Attempts to prepare 1-substituted phenyl compounds from endialone and anilines were unsuccessful.

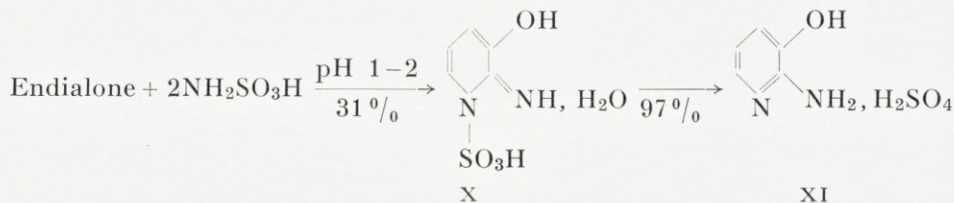


III is a known compound. It gives, as does the parent 3-hydroxy-2(1*H*)-pyridone, a strong and characteristic blue colour with ferric chloride. In Part III thirteen other 3-hydroxy-2(1*H*)-pyridones, all of which give similar blue ferric chloride reactions, are described. We therefore believe this reaction to be characteristic of the 3-hydroxy-2(1*H*)-pyridone structure (*cf.* Ref. 2). Since IV and V, which are new, also give the same blue ferric chloride reactions, we regard this as proof of the structures proposed for these two compounds.

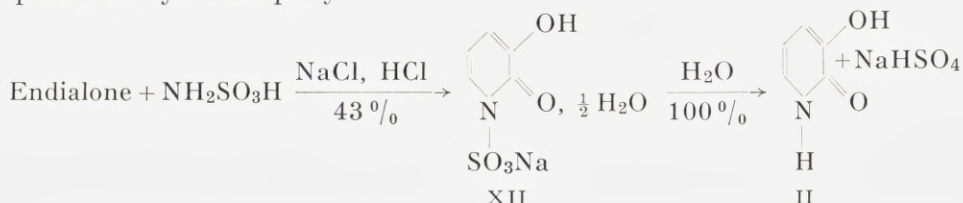
(c) *Endialone and hydroxylamine* give, by reaction at pH 2, the known 1,5-dihydroxy-2(1*H*)-pyridone (VI). With hydroxylamine-*O*-sulfonic acid in strongly acidic solution the new 1,3-dihydroxy-2(1*H*)-pyridone (VII) is formed. Both compounds were identified by catalytic hydrogenation to the corresponding hydroxypiperidones (VIII, respectively IX), which are known. VI is the only compound so far prepared from endialone and amino compounds, which is a 5-hydroxy-2(1*H*)-pyridone and not a 3-hydroxy-2(1*H*)-pyridone.



(d) *Endialone and sulfamic acid* give a mixture of two crystalline compounds, which in part precipitate from the reaction mixture. One of these compounds is predominantly formed in a rather slow reaction at pH 1–2, and may under these conditions be isolated pure from the reaction mixture by filtration and washing of the filter cake. The monohydrate structure X is proposed for this compound. It is slightly soluble in water, but forms a soluble sodium salt, which may be isolated pure as a semihydrate on evaporation of its solution. The sodium salt of X is stable, but the parent compound is, on standing, transformed slowly, on heating, rapidly, into 2-amino-3-pyridinol sulfate (XI) in a quantitative reaction.

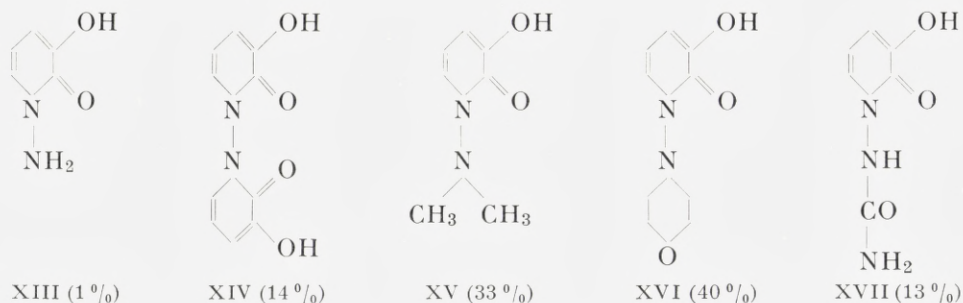


The second compound, which precipitates from mixtures of endialone and sulfamic acid containing sodium ions, is predominantly formed in a rapid reaction in a strongly acidic solution, and may under these conditions precipitate pure from the reaction mixture. The semihydrate structure XII is proposed for this compound. It is rather soluble in water and is stable in an alkaline solution. On standing, it is in part slowly transformed into 3-hydroxy-2(1*H*)-pyridone (II), on heating in an acidic aqueous solution, quantitatively and rapidly.



Both compounds prepared from endialone and sulfamic acid are new. The structures given (X and XII) are only to be regarded as proposals accounting for their formation, and for their transformation into 2-amino-3-pyridinol and 3-hydroxy-2(1*H*)-pyridone, respectively.

(e) *Endialone and hydrazino compounds* give the corresponding N-substituted 1-amino-3-hydroxy-2(1*H*)-pyridones, five of which



(XIII–XVII) have been prepared. Of these Compound XVII can, as expected, be hydrolyzed to XIII (yield 75%).

All five hydrazino compounds are new. They give a blue ferric chloride reaction proving the proposed structures. An acetate (XVIII) and a benzoate (XIX) of XV were prepared by conventional methods. Both are new and, as expected, give no ferric chloride reaction.

III. Endialone and Chlorine

When a strongly acidic solution of endialone is treated with chlorine, one mole is added to the double bond and a stable solution of hydrated 2,3-dichloro-4-oxoglutaraldehyde (XX) is formed. Proof of this is obtained by reaction of the solution with a number of amino compounds. Representative examples of such reactions, which are in part general, are given below.

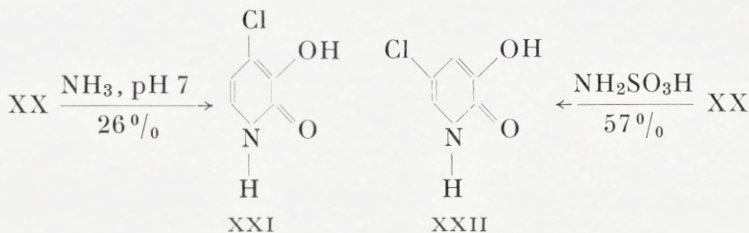


XX

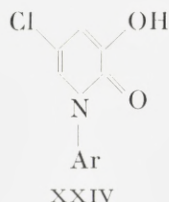
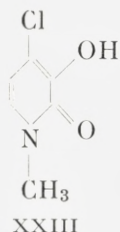
Solutions of hydrated 2,3-dichloro-4-oxoglutaraldehyde are colourless. This means that molecules which contain two free neighbouring carbonyl groups cannot be present. No other information as to the structure of XX in aqueous solution is available.

XX, like endialone, gives 2(1*H*)-pyridones by reactions with amino compounds. Altogether sixteen compounds, all of which are new, have been prepared. Again the overall reaction in each case consists of a connection of the two aldehyde groups through an amino group, followed by aromatization. All reaction products contain one chlorine atom, which must be situated in a β - or in γ -position. The positions of the chlorine atom as well as of the oxygen functions were in each case chosen on the basis of the NMR spectrum.

XX and ammonia give 4-chloro-3-hydroxy-2(1*H*)-pyridone (XXI) by reaction at pH 7. XX and sulfamic acid give the isomeric 5-chloro-3-hydroxy-2(1*H*)-pyridone (XXII) by reaction in strongly acidic solution. Both compounds give a blue ferric chloride reaction.

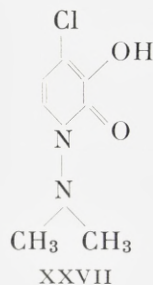
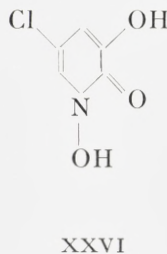
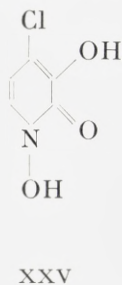


XX and methylamine give 4-chloro-3-hydroxy-1-methyl-2(1*H*)-pyridone (XXIII) (yield 21 %) by reaction at pH 7.5. The compound gives a blue ferric chloride reaction.



Similarly XX and anilines give 1-aryl-5-chloro-3-hydroxy-2(1*H*)-pyridones (XXIV) by reaction in strongly acidic solution. Ten such compounds have been prepared in yields varying from 6 to 36 per cent. They all give a blue ferric chloride reaction.

XX and hydroxylamine give 4-chloro-1,3-dihydroxy-2(1*H*)-pyridone (XXV) (yield 15%) by reaction at pH 4. The same reactants in a more acidic solution give the isomeric 5-chloro-1,3-dihydroxy-2(1*H*)-pyridone (XXVI) (yield 17%).



XX and *N,N*-dimethylhydrazine give 4-chloro-1-(dimethylamino)-3-hydroxy-2(1*H*)-pyridone (XXVII) by reaction in acidic solution. The compound gives a blue ferric chloride reaction.

It will be noted that all compounds mentioned in this part are 3-hydroxy-2(1*H*)-pyridones. Furthermore, that reactions carried out in neutral or slightly acidic solution give γ -chloro compounds, while, with one exception (XXVII), reactions carried out in more acidic solutions give β -chloro compounds.

IV. Discussion of Results

The new syntheses of pyridine compounds described here are as a rule sensitive to slight changes of the reaction conditions, and low-yield syntheses always give a corresponding large amount of dark resinous or solid polymeric

material. This behaviour, which is typical of reactions with furan compounds, is understandable, considering the structures of the compounds involved and the complexity of the reactions. Each preparation consequently requires much experimental work in order to find reaction conditions which give a good yield. If, however, such conditions have first been found for any particular compound, then the actual preparation is both cheap and simple, since in each case, from a preparative point of view, it is a one-step reaction from furfural.

As mentioned in the introduction, most of the syntheses are representative examples of general reactions. They exemplify and extend the principle of using furans as a source for the production of 1,4-dicarbonyl compounds as recommended in a former publication in these communications⁽³⁾.

V. Summary

29 pyridine compounds, 26 of which are new, have been prepared by oxidation of furfural with one or two moles of chlorine in water followed by reaction with amino compounds.

VI. Experimental

Preparation of a molar solution of endialone. Chlorine (70.9 g, 1.00 mole) is passed into a well-stirred emulsion of furfural (96.1 g, 1.00 mole) in water (700 ml) at 0° over a period of 30 min. Furfural dissolves during the reaction. At the same time a minor amount of an oily precipitate, which sticks to the wall of the reaction vessel, is formed. 40% Sodium hydroxide solution (about 200 g, 2.00 mole) is added dropwise with stirring, until pH of the solution is 2.0. The mixture is decanted from the oily precipitate and diluted with water to 1000 ml and stored at -25°.

The almost colourless solution, assuming that a quantitative reaction has taken place, is molar with respect to endialone and two-molar with respect to sodium chloride. Where nothing else is stated, the solution has been used in the following preparations and been described as being molar with respect to endialone.

Preparation of 3-hydroxy-2(1H)-pyridone (II) (yield 45%). Furfural (139 g, 1.45 mole), sodium bromide (20 g), water (400 ml), t-butyl alcohol (200 ml), and concentrated hydrochloric acid (60 ml) are mixed in a two

litre reaction flask to give a clear solution. Sodium hypochlorite solution (about 700 ml, 1.45 mole of chlorine) is added dropwise with stirring and cooling at 0° over a period of 45 min. During addition the pH of the reaction mixture rises due to sodium hydroxide present in the hypochlorite solution. If the value 1.0 should be reached, then 40 ml of concentrated hydrochloric acid is added in one portion. A few minutes after the addition of hypochlorite solution is completed, powdered ammonium chloride (200 g) is added in one portion, and the pH immediately afterwards brought as rapidly as possible to 7.5 by the addition of concentrated ammonium hydroxide solution, and automatically kept there for 20 min. by the further addition of concentrated ammonium hydroxide solution (use a thin-walled, rapidly indicating glass electrode). During this time the temperature of the reaction mixture is regulated by external cooling in such a way that it rises to $6-8^{\circ}$ in 2-4 min. (precipitation of II begins), remains there for another 2-4 min., and finally drops to 5° , and remains there for the rest of the time. After this period of 20 min. the pH of the reaction mixture is brought to 5 by the addition of concentrated hydrochloric acid, and the mixture then cooled to 0° in 5 min. The precipitate of yellowish brown crystals is isolated by rapid filtration, washed with water (700 ml), t-butyl alcohol (100 ml), and ether (250 ml), and dried at 120° . 70-75 g (about 45%) of II is in this way obtained as a light brown powder, m.p. $251-253^{\circ}$ (in an evacuated tube, corr.).

Preparation of 3-hydroxy-2(1H)-pyridone (II) (yield 69%). Furfural (9.61 g, 0.100 mole) was dissolved in N hydrochloric acid (150 ml). Sodium hypochlorite solution (about 56 ml, 0.105 mole of chlorine) was added dropwise with stirring and cooling at 0° over a period of 15 min. The resulting solution of endialone was then added dropwise with stirring over a period of 1 hour to an emulsion of ether (50 ml) and aqueous ammonium chloride (25 g in 70 ml) at 20° . During the addition the pH of the reaction mixture was automatically kept at 7.5 by the addition of concentrated ammonium hydroxide solution. After the reaction the mixture was continuously extracted with ether, whereby 7.8 g of crude II was isolated as a brown powder. Sublimation gave 7.67 g (69%) of an almost white product, m.p. $246-254^{\circ}$.

3-Hydroxy-1-methyl-2(1H)-pyridone (III). A solution containing 0.10 mole of endialone was prepared from furfural and sodium hypochlorite solution as described in the preceding experiment. A 33% aqueous solution of methylamine (14.1 g, 0.15 mole) was added during 1 min. with stirring, whereby the temperature of the reaction mixture rose from 0° to about 15° . The pH of the solution was brought to 7.5 and kept there for 30 min. by the

addition of 40% sodium hydroxide solution (4.9 ml in all). During this time the temperature was kept at 15°. The very dark reaction mixture was then heated to 75°, cooled to room temperature, brought to pH 4 by the addition of concentrated hydrochloric acid (about 2 ml), and continuously extracted with ether overnight. 2.90 g of material, m.p. 123–127°, was isolated in this way. Sublimation (115°, 0.1 mm) followed by crystallization from carbon tetrachloride (35 ml) gave 2.38 g (19%) of white crystals of III, m.p. 130–132°; previously found 131°⁽⁴⁾. [Found: C 57.3; H 5.7; N 10.9. Calc. for C₆H₇NO₂ (125.1); C 57.6; H 5.6; N 11.2]. The product gave a strong blue ferric chloride reaction.

1-[3-(Dimethylamino)propyl]-3-hydroxy-2(1H)-pyridone (IV). A solution containing 0.100 mole of endialone was prepared as in the preceding experiment. 3N hydrochloric acid (17 ml) and then N,N-dimethyl-1,3-propanediamine (10.2 g, 0.100 mole) were added, both in one portion, whereby the temperature of the reaction mixture rose from 0° to about 20°. After a few minutes the red mixture was cooled to 10°. The pH of the solution was brought to and kept at 7.5 for 15 min. by the addition of 40% sodium hydroxide solution (6.2 ml in all). During this time the temperature rose to 20°. The very dark reaction mixture was heated to 70°, kept there for 10 min., cooled to room temperature and brought to pH 9 by the addition of 40% sodium hydroxide solution (about 3 ml). Continuous extraction with ether (48 hours) and distillation of the ethereal extract gave 5.65 g of an oil, b_{0.2} 112–117°, which rapidly turned yellowish red on exposure to air. The oil was dissolved in 99% ethanol (40 ml). A solution of 85% phosphoric acid (3.34 g) in ethanol (10 ml) was added dropwise with stirring over 5 min., whereby a white precipitate was formed. The mixture was heated under reflux (15 min.), cooled and filtered. The filter cake was washed with ethanol and dried. 7.01 g (24%) of almost white crystals of the phosphate of IV m.p. 210–212° was obtained in this way. [Found: C 40.8; H 6.8; N 9.5; P 10.4. Calc. for C₁₀H₁₉N₂O₆P (294.3): C 40.8; H 6.5; N 9.5; P 10.5]. Another crystallization from 80%-ethanol gave 6.28 g of material melting at 213–214°. Further crystallization did not change the melting point. The product gave a strong blue ferric chloride reaction.

3-Hydroxy-2-oxo-1(2H)-pyridineacetic acid (V). This compound was prepared from furfural (0.100 mole), sodium hypochlorite solution (0.105 mole), and glycine (7.50 g, 0.100 mole), as described in the pre-

paration of III. The final reaction mixture (pH 7.5) was acidified with concentrated hydrochloric acid (15 ml) and continuously extracted with ether (48 hours). The ethereal extract (about 75 ml) was a suspension of crystals, which were filtered off (4.3 g) and recrystallized from dioxane (45 ml). 2.4 g of crystals, m.p. 213–216° was obtained in this way. Two further crystallizations gave 1.32 g (8%) of V, m.p. 217–219°. [Found: C 49.6; H 4.3; N 8.4. Calc. for $C_7H_7NO_4$ (169.1): C 49.7; H 4.2; N 8.3]. The product gave a strong blue ferric chloride reaction.

A sodium salt monohydrate was prepared in the usual way, m.p. 280–283° (dec.). Water is given off at about 180°. [Found: C 40.2; H 4.0; N 6.6. Calc. for $C_7H_8NNaO_5$ (209.1): C 40.2; H 3.9; N 6.7].

1,5-Dihydroxy-2(1H)-pyridone (VI). Hydroxylamine hydrochloride (7.0 g, 0.100 mole) was dissolved in a stirred solution of freshly prepared endialone (100 ml, 0.100 mole) at 0°. 40% Sodium hydroxide solution was automatically added to the clear solution at 0°, pH being kept at 2.0. Crystals began to separate after 5–10 min. After 1 hour practically no more sodium hydroxide was consumed by the reaction. In all 6.5 ml (0.093 mole) had been added at this time. The precipitate was filtered off, washed with water, and crystallized from water (330 ml) with carbon black. The crystals were filtered off, washed with water, and dried (0.1 mm, 20°, overnight). 2.88 g (23%) of VI was obtained in this way. [Found: C 47.2; H 4.0; N 10.9. Calc. for $C_5H_5NO_3$ (127.1): C 47.3; H 4.0; N 11.0]. The product, as described previously⁽⁵⁾, melted partially with destruction around 220° (in an evacuated tube), and gave a strong violet ferric chloride reaction.

1,3-Dihydroxy-2(1H)-pyridone (VII). 90% Hydroxylamine-*O*-sulfonic acid⁽⁶⁾ (12.5 g, 0.10 mole) was dissolved in a stirred solution of freshly prepared endialone (100 ml, 0.100 mole) at 0°. After 7 min. concentrated hydrochloric acid (50 ml) of room temperature was added in one portion with cooling. The temperature rose immediately to 15°. The mixture was now kept at 15° for 2 hours, during which time the solution became dark red, but remained practically clear. Neutralization at 20° to pH 3.5 with 40% sodium hydroxide solution (about 60 ml), continuous extraction with ether for 2 days, and evaporation of the ethereal suspension to dryness gave a very dark semi-solid residue, which after washing with two 5 ml portions of methanol gave 2.05 g of impure VII. Sublimation (150°, 0.5 mm) gave 1.96 g of slightly yellow crystals, m.p. 183–187°. Crystallization from *n*-butanol finally gave 1.74 g of pure VII (14%), m.p. 188–190°. Further

crystallization did not change the melting point. [Found: C 47.4; H 4.0; N 11.1. Calc. for $C_5H_5NO_3$ (127.1): C 47.3; H 4.0; N 11.0]. The product gave a strong red ferric chloride reaction.

5-Hydroxy-2-piperidone (VIII). 0.64 g of VI was hydrogenated as described in the literature⁽⁵⁾. The yield of crystallized VIII was 0.39 g (67%), m.p. 144–146°. [Found: C 52.1; H 7.9; N 12.0. Calc. for $C_5H_9NO_2$ (115.1): C 52.2; H 7.9; N 12.2]. The identity with the product described in the literature⁽⁵⁾ was established spectroscopically (IR in KBr).

3-Hydroxy-2-piperidone (IX). 0.64 g of VII was hydrogenated as described for the hydrogenation of 3-hydroxy-2(1*H*)-pyridone⁽⁷⁾. The reaction product was sublimated (100–110°, 0.1 mm), yielding 0.36 g of IX (62%) as white crystals, melting point and mixed melting point with an authentic sample 133–135°, mixed melting point with VIII 107–115°. [Found: C 52.4; H 7.9; N 11.9. Calc. for $C_5H_9NO_2$ (115.1): C 52.2; H 7.9; N 12.2]. The product was furthermore identified spectroscopically (IR in KBr).

Reaction of endialone and sulfamic acid at pH 1–2. A solution of sodium sulfamate is prepared by dissolving sulfamic acid (194 g, 2.00 mole) in water (500 ml) and 40% sodium hydroxide solution (200 g). A solution of freshly prepared endialone (1000 ml, 1.00 mole) is added in one portion at 10°. pH of the solution is adjusted to 1.7 by the addition of 3 N hydrochloric acid (about 50 ml) and the resulting clear, slightly yellow solution left standing at 10° with stirring. After about 15 min. X begins to precipitate as an almost white powder. After 3 hours the precipitate is isolated by filtration, washed with water (300 ml), methanol (200 ml), and ether, and dried (20°, 1 mm, 2 hours). The yield of almost white crystals of X is 64.5 g (31%). [Found: C 29.0; H 4.0; N 12.9; S 15.5; H₂O (Karl Fischer) 8.2. Calc. for $C_5H_6N_2O_4S \cdot H_2O$ (208.2): C 28.8; H 3.9; N 13.4; S 15.4; H₂O 8.7]. Repetition of the experiment gave 66.6 g (32%) of X.

Addition of concentrated hydrochloric acid (40 ml) to the mother liquid from X, heating under reflux for 5 min., addition of sodium hydroxide solution to pH 4.5, and continuous extraction with ether gave 10.0 g of 3-hydroxy-2(1*H*)-pyridone (9%).

*Properties of 3-hydroxy-2-imino-1(2*H*)-pyridinesulfonic acid hydrate (X)*. X is practically insoluble in cold water and in organic solvents. It melts at 70–90°, dependent on the rate of heating. At 10–20° above the melting point

it crystallizes (formation of 2-amino-3-pyridinol sulfate), to melt again at 124–125°. It gives a blue ferric chloride reaction.

X (1.0 g) was crystallized very rapidly from water (50 ml) in an 85% yield. The crystallized product was white and gave only one spot when investigated by thin layer chromatography (on "Kieselgel G" in methanol). After standing for four days at room temperature, it was apparent from the chromatogram that the product had been partly transformed into 2-amino-3-pyridinol and sulfuric acid.

A preparative, almost quantitative transformation of X (64.5 g) into 2-amino-3-pyridinol was carried out by heating with water (200 ml) under reflux (5 min.), cooling to room temperature, adding 40% sodium hydroxide solution, until pH of the mixture was 8.0 (about 65 g), and continuously extracting the resulting suspension of crystals with ether. 32.8 g (97%) of 2-amino-3-pyridinol was obtained in this way. The product melted in an evacuated tube at 172–174° (polymorphic changes of the crystals appear to take place at temperatures near the melting point).

3-Hydroxy-2-imino-1(2H)-pyridinesulfonic acid sodium salt semihydrate. Freshly prepared X (3.40 g, 0.0163 mole), 98% sodium hydroxide (0.665 g, 0.0163 mole), and water (10 ml) were mixed to give an almost clear, slightly yellow solution, which was evaporated to dryness under 15 mm from a water bath (100°). 3.43 g of a greyish-white powder was scratched out of the flask. [Found: C 27.3; H 2.8; N 12.6; S 14.5; H₂O (Karl Fischer) 3.7. Calc. for C₅H₅N₂NaO₄S, $\frac{1}{2}$ H₂O (221.2): C 27.2; H 2.7; N 12.7; S 14.4; H₂O 4.1].

The product was stable to heating under reflux for 20 min. in N sodium hydroxide solution. It formed no precipitate with barium chloride.

Reaction of endialone and sulfamic acid in 3 N acid solution. Powdered sulfamic acid (30.0 g, 0.31 mole), water (100 ml), and concentrated hydrochloric acid (60 ml) are placed in a one litre reaction flask, and the suspension cooled to -5°. A four week old solution (stored at -25°) of endialone (200 ml, 0.200 mole) of -10° is added in one portion. The mixture is stirred efficiently at 10° for 1 hour. Precipitation of XII begins after 5 min., whereby the mixture is rapidly transformed into a thin paste. Ethanol (350 ml) is added, the suspension cooled with stirring to -10°, and filtered through a sintered glass disk. The cake of white crystals is washed on the filter (without stirring) with ethanol (80 ml) and ether. The crystals are dried in a thin layer on paper at room temperature. The yield of XII is 19.2 g (43%).

[Found: C 26.8; H 2.5; ashes in CH determination 32.1; N 6.2; S 14.1; H₂O (Karl Fischer) 4.6. Calc. for C₅H₄NNaO₅S, $\frac{1}{2}$ H₂O (222.2): C 27.0; H 2.3; ashes if Na₂SO₄ 31.9; N 6.3; S 14.4; H₂O 4.1].

Boiling of the mother liquor from XII for a few minutes, followed by cooling and addition of sodium hydroxide solution to pH 4.5, and continuous extraction with ether gave 2.2 g of 3-hydroxy-2(1*H*)-pyridone (10%).

Properties of 3-hydroxy-2-oxo-1(2H)-pyridinesulfonic acid sodium salt semihydrate (XII). XII shows no sharp melting point. It is rather soluble in water. The solution shows pH 5, gives a blue ferric chloride reaction, and no precipitate with barium chloride. After heating to 100° the solution is more acid (pH 1–2) and gives a precipitate with barium chloride (formation of 3-hydroxy-2(1*H*)-pyridone and sodium hydrogen sulfate).

If XII is dissolved in N sodium hydroxide and the solution heated to boiling, no precipitate of barium sulfate is formed after cooling, acidification, and addition of barium chloride.

A preparative, quantitative transformation of XII (15.0 g, 0.068 mole) into 3-hydroxy-2(1*H*)-pyridone was carried out by heating with water (75 ml) under reflux (15 min.), cooling to room temperature, adding 98% sodium hydroxide pellets (2.75 g, 0.068 mole), and continuously extracting the resulting suspension of crystals with ether. 7.56 g (100%) of 3-hydroxy-2(1*H*)-pyridone was obtained in this way, m.p. in an evacuated tube 253–254°.

Experiments on the change of endialone solutions with time. Apart from the experiments described above, compounds X and XII were also prepared from endialone solutions stored at –25° for various lengths of time. The yields of all preparations are summarized in Table 1.

1-Amino-3-hydroxy-2(1H)-pyridone (XIII) from endialone. To a freshly prepared solution of endialone (50 ml, 0.050 mole) of 0° concentrated hydrochloric acid (25 ml) was added in one portion with cooling and stirring.

TABLE 1. Experiments on the change of endialone solutions with time.

Age of endialone solution, days	Yield of X %	Yield of XII %
0	31, 32	37
4	28	
15	28	
28		43

The temperature was allowed to rise to 10° . Finely powdered hydrazine sulfate (6.5 g, 0.050 mole) was added and the mixture kept at 10° for 30 min., heated to 50° and kept there for another 30 min. The reaction mixture was cooled to 20° , brought to pH 4.5 with a 40% sodium hydroxide solution (cooling), and continuously extracted with ether overnight. Evaporation of the ether and washing of the semi-solid residue with a small amount of methanol gave a crystalline product, which was purified by sublimation (130° , 0.2 mm) to give 90 mg of white crystals, m.p. $150-158^{\circ}$. Crystallization from methanol gave 45 mg (1%) of XIII, m.p. $161-163^{\circ}$. The product, which gave a strong blue ferric chloride reaction, was identified by means of its infrared spectrum (in KBr, see below).

3,3'-Dihydroxy-2,2'-dioxo-1(2H),1'(2'H)-bipyridine (XIV). To a freshly prepared solution of endialone (100 ml, 0.100 mole) of 0° concentrated hydrochloric acid (50 ml) was added in one portion with cooling and stirring. The temperature was allowed to rise to 10° . Finely powdered hydrazine sulfate (5.2 g, 0.040 mole) was added, and the mixture kept at 10° with stirring for 2 hours, during which time it turned brownish red. Precipitation of crude XIV began after a few minutes. The product was filtered off, washed with water and methanol, and dried (100° , 1 hour). The yield was 2.72 g (brown powder). Crystallization from water (500 ml) with carbon black gave 1.25 g (14%) of XIV as white needles, which decomposed above 300° . [Found: C 54.8; H 3.7; N 12.7. Calc. for $C_{10}H_8N_2O_4$ (220.2): C 54.6; H 3.7; N 12.7]. The product gave a strong blue ferric chloride reaction.

1-(Dimethylamino)-3-hydroxy-2(1H)-pyridone (XV). To a freshly prepared solution of endialone (200 ml, 0.200 mole) was added concentrated hydrochloric acid (20 ml), and then N,N-dimethylhydrazine (12.0 g, 0.20 mole) at 0° with cooling and stirring. The mixture was heated to 60° , and kept there for 1 hour. The colour of the mixture gradually changed from orange through deep red to dark brown. The mixture was cooled to 20° , neutralized with a 40% sodium hydroxide solution (about 20 ml), and continuously extracted with ether overnight. After removal of the ether the resulting residue was distilled. The fraction boiling at $113-123^{\circ}$ under 15 mm (12.2 g) was collected, dissolved in boiling cyclohexane (30 ml), and the solution cooled to 10° with shaking. The resulting crystals were filtered off and washed with 5 + 10 ml of cyclohexane. 10.2 g (33%) of white crystals of XV were obtained in this way, m.p. $81-83^{\circ}$. [Found: C 54.7; H 6.7; N 18.1. Calc. for $C_7H_{10}N_2O_2$ (154.2): C 54.5; H 6.5; N 18.2]. The product gave a strong blue ferric chloride reaction.

4-[3-Hydroxy-2-oxo-1(2H)-pyridyl]morpholine (XVI). A solution of pH 1 of 4-aminomorpholine (5.1 g, 0.050 mole) in hydrochloric acid (volume about 100 ml) was added to a freshly prepared solution of endialone (50 ml, 0.050 mole). The mixture was heated to 60°, while the pH was automatically kept at 1.0 by the addition of 40% sodium hydroxide solution. The mixture, which darkened more and more, was kept at pH 1.0 and 60° for 30 min., cooled to room temperature, adjusted to pH 3.5, and continuously extracted with ether overnight. Evaporation of the ether gave 5.73 g of brown material, which after sublimation (150°, 0.1 mm) gave 4.49 g (46%) of slightly yellow crystals of XVI, m.p. 174–177°. Crystallization from toluene (25 ml) gave 3.92 g (40%) of white crystals, m.p. 177–179°. Further crystallization did not change the melting point. [Found: C 55.1; H 6.1; N 14.1. Calc. for C₉H₁₂N₂O₃ (196.2): C 55.1; H 6.2; N 14.3]. The product gave a strong blue ferric chloride reaction.

1-[3-Hydroxy-2-oxo-1(2H)-pyridyl]urea (XVII) was prepared from equimolar amounts of endialone and semicarbazide hydrochloride by reaction at 10–50°. The best yield of analytically pure material obtained in one among 22 experiments was 13%, but no reproducible directions for the synthesis have been found so far; white crystals from water, m.p. 233–235° (decomp.). [Found: C 42.7; H 4.3; N 24.9. Calc. for C₆H₇N₃O₃ (169.1): C 42.6; H 4.2; N 24.9]. The product gave a strong blue ferric chloride reaction.

1-Amino-3-hydroxy-2(1H)-pyridone (XIII) from XVII. XVII (1.34 g) was dissolved and heated under reflux (80 min.) in 6 N hydrochloric acid (100 ml). The reaction mixture was cooled to room temperature, brought to pH 5.0 by the addition of a 40% sodium hydroxide solution (about 42 ml), and continuously extracted with ether overnight. 0.75 g (75%) of XIII, m.p. 161–163°, was obtained in this way. [Found: C 47.7; H 4.7; N 22.2. Calc. for C₅H₆N₂O₂ (126.1): C 47.6; H 4.8; N 22.2]. The IR spectrum in KBr was identical with that of the sample of XIII prepared from endialone and hydrazine.

1-(Dimethylamino)-3-hydroxy-2(1H)-pyridone acetate (XVIII). XV (1.00 g) was dissolved in a mixture of acetic anhydride (5 ml) and pyridine (5 ml), and the solution left at room temperature overnight. After removal of the solvent, the oily residue (1.25 g) was distilled, yielding 1.17 g (92%) of XVIII, b_{0,4} 102°, slightly yellow oil, n_D²⁵ 1.5232. The oil crystallized on

standing to white crystals melting at 48–49°. [Found: C 55.3; H 6.1; N 14.2. Calc. for $C_9H_{12}N_2O_3$ (196.2): C 55.1; H 6.2; N 14.3].

The product may be crystallized from ether-benzine (40–65°) at –20° (m.p. of crystallized product 49–50°). Its aqueous solution gave no ferric chloride reaction. The infrared spectrum in KBr showed absorption bands at 1665 cm^{-1} (amide-carbonyl) and at 1767 cm^{-1} (ester-carbonyl).

1-(Dimethylamino)-3-hydroxy-2(1H)-pyridone benzoate (XIX). XV (5.00 g, 0.0325 mole) was dissolved in pyridine (30 ml). Benzoyl chloride (7.05 g, 0.0500 mole) was added dropwise at room temperature with stirring. The mixture was left overnight, and then poured on ice-water (200 ml). The white precipitate formed was filtered off, washed with water, and dried (20°, 0.1 mm). 8.43 g of white crystals, m.p. 121–131°, were obtained in this way. Crystallization from cyclohexane (250 ml) gave 6.75 g (81%) of XIX, m.p. 137–138°. [Found: C 65.1; H 5.5; N 10.9. Calc. for $C_{14}H_{14}N_2O_3$ (258.3): C 65.1; H 5.5; N 10.9].

The product gave no ferric chloride reaction. The infrared spectrum in KBr showed absorption bands at 1660 cm^{-1} (amide-carbonyl) and at 1740 cm^{-1} (ester-carbonyl).

Preparation of a molar solution of 2,3-dichloro-4-oxoglutaraldehyde (XX). Chlorine (70.9 g, 1.00 mole) is passed through a cylindrical sintered glass tube into a vigorously stirred emulsion of freshly distilled furfural (48.0 g, 0.500 mole) in water (350 ml) over a period of 1 hour 40 min. at 0°. After half of the chlorine has been added (40 min.), concentrated hydrochloric acid (42 ml, 0.50 mole) and polypropyleneglycol (5 drops of No. 2025 from Union Carbide) are added, the latter to prevent foaming. After the addition of all chlorine the reaction mixture is stirred for 30 min. at –5° to 0°, filtered from a small amount of a sticky precipitate, diluted with water to 500 ml, and stored at –25°, at which temperature the solution is stable for at least six months.

Assuming that a quantitative reaction has taken place, the solution is molar with respect to XX, and 3 N with respect to hydrochloric acid. It has been used in the following preparations and been described as being molar with respect to XX.

4-Chloro-3-hydroxy-2(1H)-pyridone (XXI). Concentrated ammonium hydroxide solution (about 25 ml) was added rapidly to a solution of XX

(100 ml, 0.100 mole) at 0° (external cooling), until pH of the reaction mixture was 7.0. The reaction flask was removed from the cooling bath, and the pH kept at 7.0 by automatic addition of ammonium hydroxide solution. After about 5 min. a yellow precipitate was formed. During the reaction the temperature of the reaction mixture rose to around 35°, and the mixture turned very dark. When, after about 30 min., a total amount of about 42 ml of ammonium hydroxide had been added, the reaction was complete. The dark suspension was cooled to 15° and brought to pH 4.0 by the addition of concentrated hydrochloric acid (1–2 ml). After a few minutes the precipitate was filtered off, washed twice with water, and dried (80°, 15 hours). The yield was 10.0 g of a black powder.

2.00 g was crystallized from acetic acid (80 ml) with carbon black (0.5 g), giving 0.76 g (26% based upon furfural) of light grey plates of XXI, melting in an evacuated tube with darkening decomposition at 290–295°. Further crystallizations did not change the IR spectrum (in KBr). [Found: C 41.5; H 2.9; Cl 24.3; N 9.5. Calc. for C₅H₄ClNO₂ (145.6): C 41.3; H 2.8; Cl 24.4; N 9.6]. The product gave a strong blue ferric chloride reaction.

5-Chloro-3-hydroxy-2(1H)-pyridone (XXII). Sulfamic acid (75 g, 0.77 mole) was added to a solution of XX (500 ml, 0.500 mole), and the resulting slurry heated to 50° during 10 min. with stirring. The acid dissolved, and the reaction mixture turned orange red. After a few minutes at 50°, XXII began to separate as a light yellow precipitate. The mixture was kept at 50° for 1 hour, cooled to 10°, kept there for 15 min., and the precipitate filtered off and dried at 80° overnight. 48 g of a light brown powder was obtained in this way.

Sublimation (200°, 0.2 mm, 90 min.) of 250 mg gave 215 mg of XXII as white crystals, melting in an evacuated tube with darkening and decomposition at 290–295°. The amount corresponds to a yield of 57%, based upon furfural. The IR spectrum (in KBr) was radically different from that of 4-chloro-3-hydroxy-2(1H)-pyridone (XXI). [Found: C 41.5; H 2.9; Cl 24.3; N 9.4. Calc. for C₅H₄ClNO₂ (145.6): C 41.3; H 2.8; Cl 24.4; N 9.6]. The product gave a strong blue ferric chloride reaction.

Crystallization from acetic acid may be used to purify larger amounts of crude material. Thus 5.00 g gave 3.34 g of analytically pure XXII when crystallized from acetic acid (70 ml) with carbon black (1 g). The amount corresponds to a yield of 44%, based upon furfural.

An identical preparation made from a 6 months old solution of XX, stored at –25°, gave a 53% yield of XXII.

4-Chloro-3-hydroxy-1-methyl-2(1H)-pyridone (XXIII). A 33% aqueous solution of methylamine (21.0 ml, 0.20 mole) was added dropwise with stirring over a few minutes to a solution of XX (200 ml, 0.20 mole) of -20° . The temperature rose to -5° . pH of the faintly yellow mixture was brought to 7.5 by dropwise addition of 40% sodium hydroxide solution, and automatically kept at this value for 45 min. by further addition of sodium hydroxide solution. The reaction temperature was at the same time kept at 0° . The temperature of the dark brown reaction mixture was now raised to room temperature in an hour, pH still being kept at 7.5. The total amount of sodium hydroxide solution added was 34.5 ml. Concentrated hydrochloric acid (about 9 ml) was added dropwise until pH 3, and the mixture then continuously extracted with ether overnight. Evaporation of the ethereal extract, sublimation of the residue (150° , 0.5 mm), and two crystallizations from absolute ethanol gave 6.86 g (21%) of XXIII, m.p. $186-187^{\circ}$. [Found: C 45.1; H 3.9; Cl 22.2; N 8.9. Calc. for $C_6H_6ClNO_2$ (159.6): C 45.2; H 3.8; Cl 22.2; N 8.8]. The product gave a strong blue ferric chloride reaction.

1-Aryl-5-chloro-3-hydroxy-2(1H)-pyridones (XXIV). The appropriate aniline (0.1 mole) (solid anilines were crushed to a fine powder before use) was added to a solution of XX (100 ml, 0.1 mole) of -20° . The resulting solution or suspension (in some cases the hydrochlorides of the anilines may not be soluble in the reaction mixture at lower temperature) was heated with stirring to 90° and kept there for 30 min. During this time the reaction mixture turned dark, and a sticky black tar was usually formed. The reaction mixture was cooled to 55° , and extracted several times with chloroform at this temperature. The solvent was removed from the combined chloroform extracts by distillation, and the residue sublimated at $175-200^{\circ}$ under 0.5 mm. The sublimate was crystallized from 99% ethanol or from ethanol-water (1:1) to yield the pure 2(1H)-pyridones. These all gave a strong blue ferric chloride reaction. Data for the ten compounds prepared are given in Table 2.

4-Chloro-1,3-dihydroxy-2(1H)-pyridone (XXV). Hydroxylamine hydrochloride (34.8 g, 0.500 mole) was added in one portion to a solution of XX (500 ml, 0.500 mole) of -20° . The resulting solution was brought to pH 4.0 by dropwise addition of 40% sodium hydroxide solution. At the same time the temperature of the reaction mixture was allowed to rise to 0° . pH of the mixture was now automatically kept at 4.0 by further addition of sodium hydroxide solution, while the temperature was brought to 60° and kept

TABLE 2. 1-Aryl-5-chloro-3-hydroxy-2(1*H*)-pyridones.

Substituents in the phenyl group (Ar) of structure XXIV	Yield %	m. p., °C	Formula (M)	Analyses				
					C	H	Cl	N
None.....	21	147—149°	C ₁₁ H ₈ ClNO ₂ (221.6)	Found	59.5	3.7	16.1	6.3
				Calc.	59.7	3.6	16.0	6.3
2-Methyl.....	6	172—173°	C ₁₂ H ₁₀ ClNO ₂ (235.7)	Found	61.2	4.4	15.1	6.1
				Calc.	61.2	4.2	15.1	5.9
3-Methyl.....	16	158—160°	—	Found	61.4	4.4	15.0	6.0
4-Methoxy.....	14	172—174°	C ₁₂ H ₁₀ ClNO ₃ (251.7)	Found	57.4	4.2	14.0	5.6
				Calc.	57.3	4.0	14.1	5.6
2-Chloro.....	6	164—165°	C ₁₁ H ₇ Cl ₂ NO ₂ (256.1)	Found	51.5	2.9	27.6	5.5
				Calc.	51.6	2.8	27.7	5.5
3-Chloro.....	23	185—186°	—	Found	51.7	2.9	27.6	5.5
2,3-Dichloro.....	15	222—223°	C ₁₁ H ₆ Cl ₃ NO ₂ (290.5)	Found	45.3	2.3	36.6	4.8
				Calc.	45.5	2.1	36.6	4.8
2,5-Dichloro.....	13	145—146°	—	Found	45.4	2.2	36.6	4.8
3,4-Dichloro.....	15	193—194°	—	Found	45.4	2.2	36.5	4.9
3-Nitro.....	36	235—236°	C ₁₁ H ₇ ClN ₂ O ₄ (266.7)	Found	49.0	2.6	13.0	10.3
				Calc.	49.4	2.6	13.3	10.5

there for 1 hour. The mixture turned dark brown, and a dark precipitate was formed. At this point a total amount of about 210 ml of sodium hydroxide solution had been added. The mixture was cooled to room temperature, and evaporated to dryness under vacuum from a water bath. 99% ethanol was added, and again evaporated to remove traces of water. The remaining dark cake was extracted with dioxane in a Soxhlet apparatus. Evaporation of the dioxane extract to dryness, and sublimation (150°, 0.5 mm) gave 16.5 g of slightly yellow crystals, which after two crystallizations from ethanol-water (1:4) gave 12.4 g (15%) of XXV. The product showed no well-defined melting point. [Found: C 37.3; H 2.8; Cl 22.2; N 8.7. Calc. for C₅H₄ClNO₃ (161.6): C 37.2; H 2.5; Cl 22.0; N 8.7]. The product gave a red ferric chloride reaction.

5-Chloro-1,3-dihydroxy-2(1H)-pyridone (XXVI). A solution of XX (100 ml, 0.100 mole) was brought to pH 2.5 by dropwise addition of 40% sodium hydroxide solution (about 21 ml) at 0°. Hydroxylamine hydro-

chloride (7.0 g, 0.10 mole) was added in one portion. The mixture was heated to 75°, and kept there for 2 hours. The dark brown reaction mixture was cooled to room temperature, and brought to pH 4.0 with 40% sodium hydroxide solution (about 15 ml). During this neutralization a black tar was precipitated together with some crystalline material, and stirring became difficult. The mixture was continuously extracted with ether for 3 days. Evaporation of the ethereal extract, and sublimation of the residue (150°, 0.5 mm) gave 3.85 g of slightly yellow crystals. Crystallization from water gave 2.70 g (17%) of XXVI. [Found: C 37.1; H 2.4; Cl 21.8; N 8.5. Calc. for C₅H₄ClNO₃ (161.6): C 37.2; H 2.5; Cl 22.0; N 8.7]. The product showed no well defined melting point, but decomposed slowly above 180°. The IR spectrum was radically different from that of XXV. Another crystallization did not change the analytic values. The product gave a strong red ferric chloride reaction.

4-Chloro-1-(dimethylamino)-3-hydroxy-2(1H)-pyridone (XXVII). A solution of XX (500 ml, 0.500 mole) was brought to pH 3 by dropwise addition of 40% sodium hydroxide solution (110 ml) at 0°. A solution of N,N-dimethylhydrazine (30 g, 0.50 mole) and concentrated hydrochloric acid (50 ml) in water (250 ml) was added in one portion. The temperature of the clear mixture rose to about 10°, and the colour turned red. The mixture was heated to 85°, and kept there for 2 hours. The colour hereby changed from dark red into brown, and some black material was precipitated. The mixture was cooled to 20°, stirred at this temperature for 10 min., and filtered. The dark precipitate on the filter was washed with water, until the washings only gave a faint blue colour on addition of a solution of ferric chloride. The pH of the combined filtrate and washings was adjusted to 6.3 by dropwise addition of 40% sodium hydroxide solution (85 ml), and the mixture continuously extracted with ether overnight. Evaporation of the ethereal extract to dryness gave 21.7 g of a brownish crystalline residue. Crystallization with carbon black (1.25 g) from ethanol-water (1:2) (100 ml) gave 14.6 g of slightly brown needles of XXVII, m.p. 132–135°. Two further crystallizations from ethanol-water (1:2) gave 11.0 g (12%) of constant melting material (m.p. 135–137°). [Found: C 44.1; H 4.8; Cl 18.8; N 15.0. Calc. for C₇H₉ClN₂O₂ (188.6): C 44.5; H 4.8; Cl 18.8; N 14.9]. The product gave a strong blue ferric chloride reaction.

NMR spectra. The spectra were measured in solution in DMSO with TMS as an internal standard. 5-Chloro-3-hydroxy-2(1H)-pyridones (XXII and all ten XXIV) showed $\tau = 2.50\text{--}2.80$ for α -protons and 3.11–3.18 for

TABLE 3. τ -values for protons of 1, β -dihydroxy-2(1*H*)-pyridones.

Compound	τ for protons in positions		
	α	β	γ
VI	2.50	3.37	2.71
VII	2.54	3.81	3.15
XXV	2.50	3.66	
XXVI	2.32		3.22

γ -protons. 4-Chloro-3-hydroxy-2(1*H*)-pyridones (XXI, XXIII and XXVII) showed $\tau = 2.78-2.82$ for α -protons and $3.70-3.74$ for β -protons. Values for α -, β -, and γ -protons of 1, β -dihydroxy-2(1*H*)-pyridones are given in Table 3.

VII. Acknowledgement

We are greatly indebted to our colleagues J. RASTRUP ANDERSEN and K. SCHAUMBURG, Department of Chemical Physics, University of Copenhagen, for carrying out all spectroscopic work reported here, and for all deductions based thereon.

28 Rugmarken, Farum, Denmark.

VIII. References

- (1) DUNLOP and PETERS: The Furans. Reinhold Publishing Corporation, New York 1953, pp. 385-395.
- (2) H. J. DEN HERTOOG, J. P. WIBAUT, F. R. SCHEPMAN, and A. A. VAN DER WAL, *Rec. Trav. Chim.* **69** (1950) 700.
- (3) N. CLAUSON-KAAS: Reactions of the Furan Nucleus; 2,5-Dialkoxy-2,5-dihydrofurans and 2,5-Diacetoxy-2,5-dihydrofuran. *Mat. Fys. Medd. Dan. Vid. Selsk.* **24**, No. 6 (1947).
- (4) A. F. BICKEL and J. P. WIBAUT, *Rec. Trav. Chim.* **65** (1946) 65.
- (5) J. T. NIELSEN, N. ELMING, and N. CLAUSON-KAAS, *Acta Chem. Scand.* **9** (1955) 30.
- (6) R. GÖSL and A. MEUWSEN, *Chem. Ber.* **92** (1959) 2521.
- (7) N. ELMING, *Acta Chem. Scand.* **11** (1957) 914.

D. G. BURKE AND B. ELBEK

A STUDY OF ENERGY LEVELS IN
EVEN-EVEN YTTERBIUM ISOTOPES
BY MEANS OF
(d,p), (d,t), AND (d,d') REACTIONS

Det Kongelige Danske Videnskabernes Selskab
Matematisk-fysiske Meddelelser **36**, 6



Kommissionær: Munksgaard
København 1967

CONTENTS

	Page
1. Introduction	3
2. Theoretical Considerations	5
3. Experimental Details and Presentation of Results	7
4. Interpretation of the Data	7
4.1. Ground State Rotational Bands	7
4.2. Quadrupole γ -vibrations	18
4.3. Octupole Vibrations	26
4.4. Low-lying $K = 0$ Bands	30
4.5. Other Levels in ^{170}Yb	34
4.6. Other Levels in ^{172}Yb	35
4.7. Other Levels in ^{174}Yb	38
5. Summary	40
References	43

Synopsis

Targets prepared from separated isotopes of all the stable ytterbium nuclei have been bombarded with 12 MeV deuterons from a tandem Van de Graaff accelerator. The reaction products were analyzed with a broad range, single-gap, magnetic spectograph with an overall resolution of 0.1% . In order to study the levels in even nuclei, the triton and proton spectra from ^{171}Yb and ^{173}Yb targets and the inelastic deuteron spectra from ^{168}Yb , ^{170}Yb , ^{172}Yb , ^{174}Yb , and ^{176}Yb targets were recorded. The systematics of the (d,d') population of vibrational bands are discussed and utilized for the identification of γ - and octupole vibrational levels in nuclei in which these had not previously been observed. The (d,p) and (d,t) cross sections are compared with the predictions of stripping theory of deformed nuclei calculated with empirical values of the single-particle cross sections obtained from experiments on even-even targets. The populations of ground states are in agreement with these predictions as modified by pairing theory. The (d,p) and (d,t) populations of several rotational bands show patterns which resemble those expected for two-quasiparticle states, although in many cases the absolute cross sections were smaller than predicted for a pure configuration. The stripping and pick-up data for the vibrational bands offer strong experimental evidence that these states can be considered as superpositions of two-quasiparticle states. The predicted components are found to be present, but the theoretical amplitude often shows only qualitative agreement with the observed cross sections.

1. Introduction

The energy spectra of deformed even-even nuclei have mostly been studied in radioactive decay or by Coulomb excitation. These studies have provided evidence for the occurrence of low-lying quadrupole vibrational states and some rather scattered information about octupole vibrational states. In addition, it has been possible to identify certain levels as two-particle states, but the basis for the assignments has often been scanty and very little is known about the purity of such configurations.

The microscopic descriptions¹⁾ of nuclear vibrational motions have made the distinction between "collective" and "single-particle" excitations less sharp. In the simplest approach, a state in an even nucleus is considered to be a superposition of two-quasiparticle states. The "single-particle" excitations have only one such component, whereas the "collective" states are characterized by the presence of many components, each with a small amplitude. However, it is to be expected that states with structure intermediate to those mentioned can occur.

The microscopic treatment of nuclear states is an excellent guide for the interpretation of the results of single-particle transfer reactions and, conversely, the experimental cross sections for such reactions are measures of the amplitudes for certain configurations. Thus, the measurements can be compared directly to theoretical predictions.

It should be stressed that, for even-even final nuclei, only amplitudes involving the odd target ground-state particle can be measured by single-particle transfer reactions. Furthermore, only fairly large amplitudes can be observed by transfer processes. Even if the experimental spectrum is clean and well resolved so that small cross sections can be detected, there will always be considerable uncertainties about other mechanisms which could result in such intensities. This is in contrast to the situation for several types of decay processes in which rather small admixtures often cause appreciable effects.

Collective vibrational states based on the ground state are most easily localised by Coulomb excitation or by various inelastic scattering processes. In many cases, the cross section for such reactions also measures to a good approximation the reduced electric multipole transition probability between the ground state and the excited state.

In the present work, the (d, p) , (d, t) , and (d, d') reactions are used to investigate the energy levels in the even isotopes of ytterbium. A previous report²⁾ describes the results of similar measurements in the odd ytterbium isotopes. The present investigations are largely based on the earlier findings, and it might therefore be appropriate to present a summary of some of the results for the odd final nuclei.

At lower excitation energies, the cross sections for the neutron transfer processes were consistent with the nuclear states representing almost pure single-particle motion in a deformed well. The cross sections were well accounted for on the basis of the stripping theory developed by SATCHLER³⁾, the NILSSON⁴⁾ wave functions, and single-particle cross sections obtained from a DWBA (Distorted Wave Born Approximation) calculation⁵⁾. The absolute cross sections for the low-lying states clearly showed the effects of a partial filling of the states near the Fermi surface in the target nuclei. These results are in quantitative agreement with the predictions of the pairing theory.

At higher excitation energies, there were several indications of a considerable mixing of states, the most noticeable being the absence of cross sections as large as those predicted for pure single-particle states. This breakdown of the single-particle description seemed to take place at an energy approximately corresponding to the quadrupole phonon energy. A related phenomenon was a considerable spreading of quadrupole vibrational strength. This was indicated by the absence, in any single band populated by the (d, d') process, of a cross section comparable to that found in the even nuclei.

Although many of the low-lying states of deformed odd nuclei are well described by the Nilsson wave functions, it appears that the odd nuclei of Yb offer particularly favourable examples of pure single-particle motions. This is partly related to the fact that, in these nuclei, the collective vibrational modes are weak and are found at high excitation energies and partly to the absence of close-lying single-particle levels with K differing by 0 or 1 unit.

The present study of the levels in the even isotopes of Yb has largely profited from the knowledge of the single-particle states in the odd isotopes. Also the general confidence in methods and procedures which have been subject to an experimental test has been important for the experimental study of levels in even-even final nuclei, which is more difficult for several

reasons. The transferred particle can couple with the odd-target particle to form two different configurations, that is two rotational bands, as compared to one band for the odd final nucleus. The level density above the energy gap in an even-even nucleus is thus greater than that near the ground state in an odd nucleus, which means that better resolution is desirable. There are additional experimental difficulties because each particle group can contain contributions with different l -values. The intensity patterns for rotational bands populated in a given single-particle transfer process are characteristic of the intrinsic states on which the bands are based. However, these patterns are often not as unique as in the case of odd final nuclei because of the averaging effects introduced by the summation of several components to form the cross section for each final state. Finally, there is the practical consideration that only one or two stable odd targets exist for a given atomic number, a fact which limits the number of single-particle transfer processes that can be used to populate states in even-even nuclei.

On the other hand, for the study of the even nuclei, empirical values of the single-particle cross sections obtained from the studies of odd nuclei could be used to improve the predictions for the single-particle cross sections. This method has been widely applied in the present paper. The interpretation of the inelastic deuteron scattering data is also much simpler for even than for odd nuclei and has been helpful in locating the collective quadrupole and octupole vibrations.

2. Theoretical Considerations

SATCHLER³⁾ has given an expression for the cross section of the reaction which transfers a nucleon with angular momentum j to or from a target nucleus of spin I_i to a final state I_f , where I_f is a member of a rotational band in a deformed nucleus. It has been found that the populations of many levels in odd Yb nuclei by (d,p) and (d,t) reactions are well accounted for by this simple description of the process.

For the even target nuclei, the effects of pairing were taken into account simply by multiplying the cross section $(d\sigma/d\Omega)_s$ predicted by Satchler (cf. Eq. 1 of ref. 2) by a factor of U^2 for a (d,p) process and a factor of V^2 for a (d,t) process. These factors are in agreement with the intuitive picture that the cross section for putting a particle into a given state is proportional to the probability for the state being empty and, correspondingly, the cross section for removing a particle is proportional to the probability for the state being full.

The same factors apply for reactions on odd targets except when the transferred neutron is in the same Nilsson orbit as the ground-state particle in the odd target. As an example of this exception, one can consider the (d, t) reaction leading into the ground state of an even-even nucleus. The probability of finding the unpaired neutron in the ground-state orbital, ν , of the odd target nucleus is unity, and the cross section for picking up this neutron is $(d\sigma/d\Omega)_g$. Following this process there is a condition of no neutrons in the state ν which, however, is not the ground state of the even nucleus, since the latter has only a probability $U^2(\nu)$ of state ν being empty. Hence, the cross section $(d\sigma/d\Omega)_g$ should be multiplied by the factor $U^2(\nu)$ which is the overlap of the two cases. Similar reasoning will yield a factor $V^2(\nu)$ in the (d, p) cross section leading to the ground state of an even-even nucleus. One can also invoke the principle of detailed balance to show that these are the appropriate factors to be used for transitions of the ground states of even-even nuclei. For example, the cross section for the (d, p) reaction between the ground states of the even-even nucleus A and the odd nucleus $A + 1$ has a factor $U^2(\nu)$. The (d, t) reaction between the same two ground states can be regarded as the inverse reaction and thus should also be proportional to $U^2(\nu)$. A more formal derivation of these factors is outlined below.

Let us assume that an even-even nucleus has the Bardeen-Cooper-Schrieffer ground state

$$|v = 0\rangle = \prod_{\nu} (U(\nu) + V(\nu)a^{+}(\nu)a^{+}(\bar{\nu})) |0\rangle, \quad (1)$$

where $|0\rangle$ and $|v = 0\rangle$ represent the vacuum states for particles and quasiparticles, respectively. Here, ν and $\bar{\nu}$ represent conjugate nucleons while $a(\nu)$ and $a^{+}(\nu)$ are annihilation and creation operators for particles in the state ν . The quasiparticle annihilation and creation operators $\alpha(\nu)$ and $\alpha^{+}(\nu)$ are related to the operators $a(\nu)$, $a^{+}(\nu)$ by the unitary transformation

$$\left. \begin{aligned} \alpha^{+}(\nu) &= U(\nu)a^{+}(\nu) - V(\nu)a(\bar{\nu}) \\ \alpha^{+}(\bar{\nu}) &= U(\nu)a^{+}(\bar{\nu}) + V(\nu)a(\nu). \end{aligned} \right\} \quad (2)$$

If one starts with an odd target nucleus with one quasiparticle in the state ν

$$\alpha^{+}(\nu)|v = 0\rangle$$

and removes a nucleon from the same state by means of a pick-up reaction, the result is

$$a(\nu)\alpha^{+}(\nu)|v = 0\rangle. \quad (4)$$

Thus, the cross section for performing this process and arriving at the ground state of the final nucleus is

$$|\langle v = 0 | a(v)\alpha^+(v) | v = 0 \rangle|^2 \left(\frac{d\sigma}{d\Omega} \right)_s = U^2(v) \left(\frac{d\sigma}{d\Omega} \right)_s. \quad (5)$$

The cross sections for stripping and pick-up reactions of this type can be summarized⁶⁾ by the relationships

$$\left[\frac{d\sigma}{d\Omega}(j + I_1(v = 0) \leftrightarrow I_2(v = 1)) \right]^{1/2} = U(v) \left(\frac{d\sigma}{d\Omega} \right)_s^{1/2} \quad (6a)$$

$$\left[\frac{d\sigma}{d\Omega}(j + I_1(v = 1) \leftrightarrow I_2(v = 0)) \right]^{1/2} = -V(v) \left(\frac{d\sigma}{d\Omega} \right)_s^{1/2} \quad (6b)$$

where the single nucleon with angular momentum j is transferred between two nuclear states with spins I_1 and I_2 . The mass of the nucleus with I_2 is one unit greater than that with I_1 . The quantity v represents the number of unpaired nucleons of the type being transferred.

3. Experimental Details and Results

The beam of 12 MeV deuterons for the present experiments was obtained from the Niels Bohr Institute's tandem Van de Graaff accelerator. The technique of target preparation and operation of the broad-range magnetic spectrograph has been outlined previously²⁾. No attempt has been made to measure angular distributions of the reaction products, but exposures were made at two or three different angles for each reaction studied. Triton and proton spectra from targets of ^{171}Yb and ^{173}Yb are shown in Figs. 1–4, and Figs. 5–9 show inelastic deuteron spectra. The energies and cross sections for population of the levels observed are given in Tables 1–5. For a discussion of the uncertainties involved in these measurements, see ref. 2. The Q-values for stripping and pick-up processes leading to the ground states of the daughter nuclei have already been reported²⁾. Proposed level schemes for 168 , 170 , 172 , 174 , ^{176}Yb are shown in Figs. 10–14. The assignments given to the levels in these diagrams are discussed in the following section.

4. Interpretation of the Data

4.1. Ground State Rotational Bands

The energies of levels in the ground state rotational bands of these nuclei have been well established up to spin values of eight or ten^{8, 14)}. In the present (d, d') experiments, the states up to and including the spin six member are

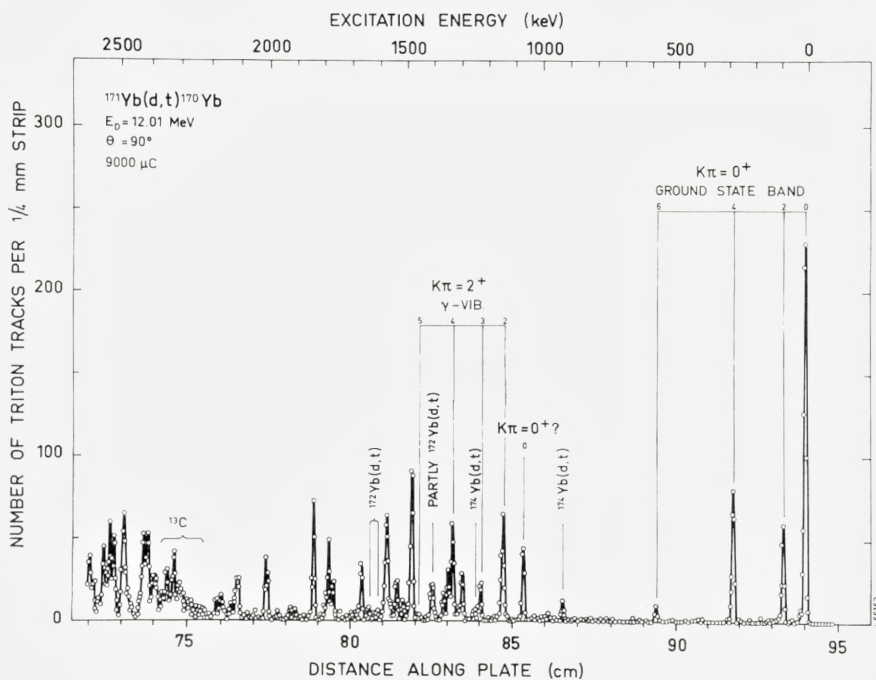


Figure 1. Triton spectrum for the reaction $^{171}\text{Yb}(d,t)^{170}\text{Yb}$ at $\theta = 90^\circ$.

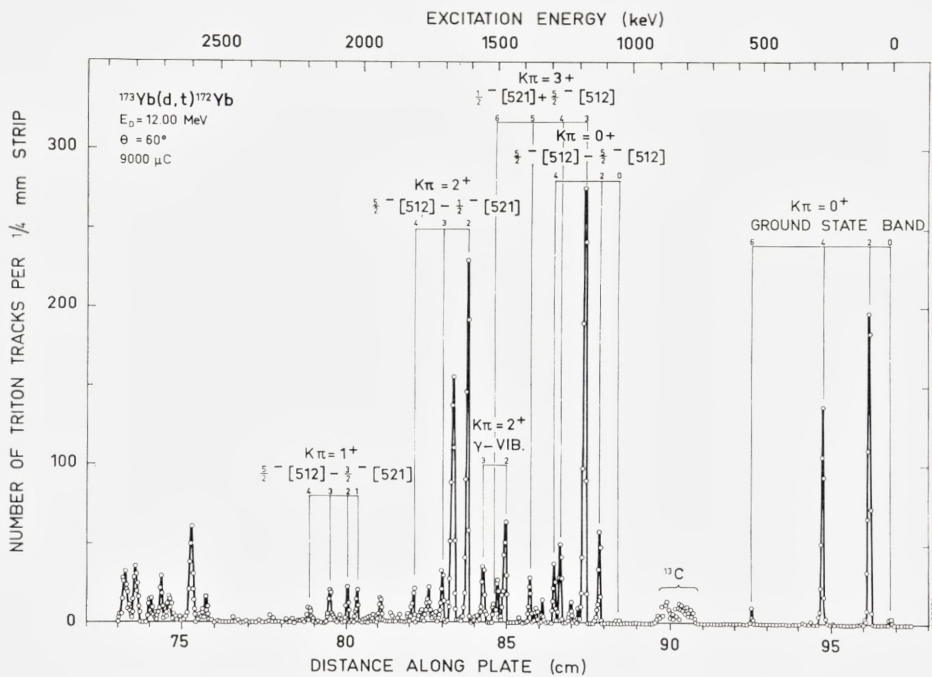


Figure 2. Triton spectrum for the reaction $^{173}\text{Yb}(d,t)^{172}\text{Yb}$ at $\theta = 60^\circ$.

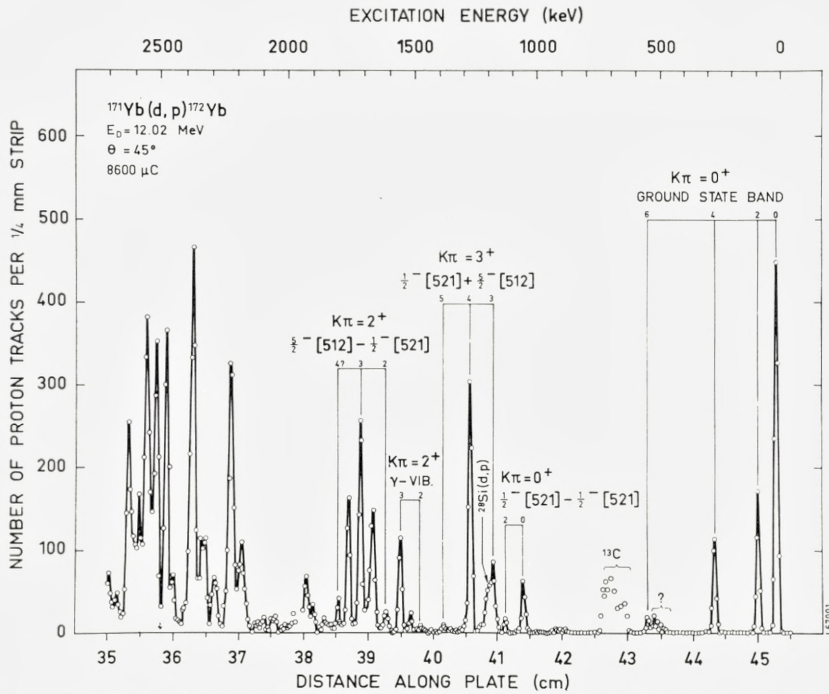


Figure 3. Proton spectrum for the reaction $^{171}\text{Yb}(d,p)^{172}\text{Yb}$ at $\theta = 45^\circ$.

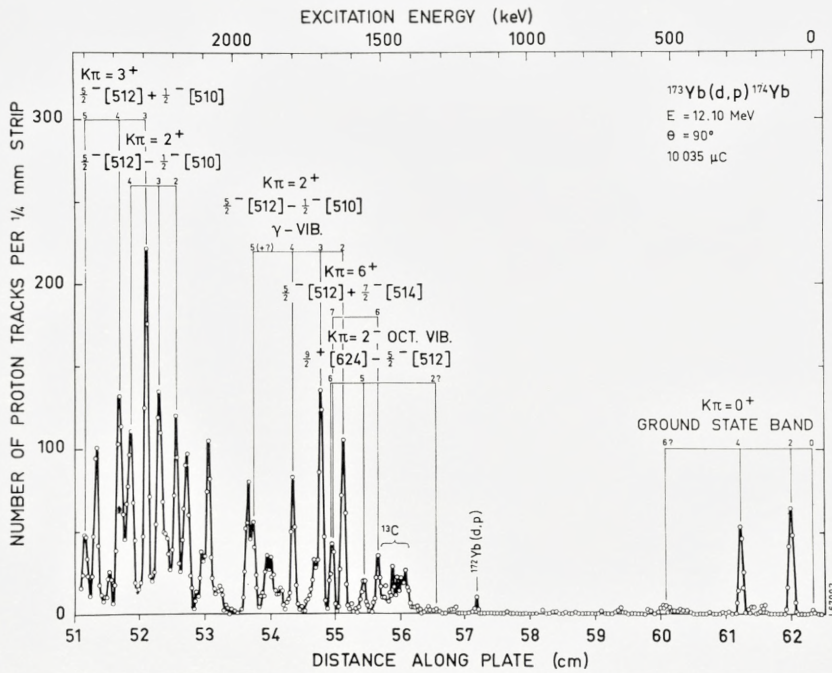


Figure 4. Proton spectrum for the reaction $^{173}\text{Yb}(d,p)^{174}\text{Yb}$ at $\theta = 90^\circ$.

TABLE 1. Levels in ^{168}Yb .

Energy		$d\sigma/d\Omega$ ($\mu\text{b}/\text{sr}$)		R^*	$I, K\pi$	Comments
Previous value ^{7, 8)}	(d, d')	$\theta = 85^\circ$	$\theta = 125^\circ$			
0	0	82600	13000		0,0+	Ground state rotational band
87.9	87	6300	3090	2.0	2,0+	
286.9	287	61	69	0.9	4,0+	
585.7	582	4.3	7.9	0.6	6,0+	
986	981	127	54	2.3	2,2+	γ -vibration
	1150	3.3	3.1	1.1	0,0+	β -vibration
1174	1167	18	27	0.7	4,2+	γ -vibration
1233	1230	32	8.3	3.9	2,0+	β -vibration
1391	1387	6.8	7.7	0.9	4,0+	β -vibration
	1433	2.6	3.0	0.9		
	1475	84	65	1.3	3,? -	Octupole vibration
	1547	11	12	0.9		
	1595	42	35	1.2	3,? -	Octupole vibration
	1725	5.1	5.6	0.9		
	1860	12	8.0	1.5		
	1969		5.9			
	1997		3.3			
	2058		13			
	2122		16			

* In this work, R denotes the ratio of (d, d') cross section at $\theta = 90^\circ$ to that at 125° . However, in the case of ^{168}Yb only, the values shown are actually ratios of data at $\theta = 85^\circ$ and $\theta = 125^\circ$. For all levels except the ground state, this will have a very small effect on R due to the slow variation of the (d, d') cross section with θ .

strongly populated. The systematics of the relative populations of the ground state rotational levels in the even rare earth nuclei have been described earlier¹⁵⁾. It was suggested that the population of the 4+ states could take place in part by a direct E4-transition from the ground state. The Yb-nuclei show particularly low cross sections for the 4+ states, which could indicate that the population is mainly by multiple excitation. In this connection it might be significant that the values of the ratio, R , of the 90° yield to the 125° yield for the Yb-nuclei is less than unity in all cases. In the beginning of the rare earth region where the 4+ cross sections are large, this ratio is^{15, 16)} approximately 1.20. The 6+ states are also weakly populated in the Yb-nuclei. Strangely enough, in most cases the 90° cross section is larger than the 125° cross section.

The cross sections for the population of levels in the ground state rota-

TABLE 2. Levels in ^{170}Yb .

Energy		$d\sigma/d\Omega (d, t) \mu\text{b}/\text{sr}$					$d\sigma/d\Omega (d, d') \mu\text{b}/\text{sr}$		R	$I, K\pi$	Comments
Prev. value ref ^s)	(d, t)	(d, d')	$\theta = 45^\circ$	$\theta = 60^\circ$	$\theta = 90^\circ$	$\theta = 125^\circ$	$\theta = 90^\circ$	$\theta = 125^\circ$			
0	0	0	305	222	130	48	63000	13000	4.8	0,0+	Gr. state rot. band
84.3	84	84	30	45	30	15	5600	2700	2.0	2,0+	
277.7	275	278	36	60	47	35	37	64	0.6	4,0+	
	573	577			~ 5	5.6	7.1	5.0	1.4	6,0+	
	1065		16	25	22	7.1				0,0+?	F - F*
	1138	1145	31	47	45	20	77	35	2.2	2,2+	γ -vib.
	1221		10		14	6.0				3,2+	γ -vib.
	1289	1300	8.7	19	16	8.7	19	12	1.6		
	1324	1330	8.8	31	32	21	16	22	0.7	4,2+	γ -v b.
	1341		4.9		16	9.6					
	1358		3.3	12	10	6.1					
	1398	1400	11	17	19	~ 7.5	54	60	0.9	3,? -	Oct. vib.
	~ 1445				~ 3	2.3				5,2+	γ -vib.
	1473		43	66	56	29					
	1508		2	13	~ 6	4.4					
	1529		6.5		15	7.8					
	1552			26	~ 5	2.5					
	1564		14		45	35					
		1586						2.3			
	1655		4.7	14	16	11					
	1690			~ 2	~ 2						
	1757			26	12	12					
	1774		~ 6		27	14					
		1783					46	53	0.8	3,? -	Oct. vib.
	~ 1789		~ 2			~ 3					
	1829		13	25	32	19					
	1911		~ 0.6		4.5						
	1963	1968	1.8		~ 3	~ 1.6	0.8	1.6			
	2000		4.2		24	9.3					
	2106		5.4		21	14					
		2115						7.5			

* The notation is patterned after that of ref. 20. The letter F indicates the single-particle state nearest to the Fermi level. The level order is as in Fig. 21 of ref. 2, and the key to Tables 2-4 is as follows: F-4: 3/2-[521], F-3: 5/2+[642], F-2: 5/2-[523], F-1: 7/2+[633], F: 1/2-[521], F+1: 5/2-[512], F+2: 7/2-[514], F+3: 9/2+[624], F+4: 1/2-[510], F+5: 3/2-[512].

TABLE 3. Levels in ^{172}Yb .

Prev. value ref. ^{9,10)}	Energy			$d\sigma/d\Omega (d,t)$ $\mu\text{b/sr}$		$d\sigma/d\Omega (d,p)$ $\mu\text{b/sr}$		$d\sigma/d\Omega (d,d')$ $\mu\text{b/sr}$		R	I, K π	Comments
	(d, t)	(d, p)	(d, d')	$\theta = 60^\circ$	$\theta = 90^\circ$	$\theta = 45^\circ$	$\theta = 90^\circ$	$\theta = 90^\circ$	$\theta = 125^\circ$			
0	0	0	0	3	~ 4	106	37	63000	13000	4.8	0,0+	Gr. state rot. band
79	78	80	79	170	136	34	17	6400	3200	2.0	2,0+	
260	260	260	260	110	87	26	20	61	68	0.9	4,0+	F-F, (F+1)-(F+1)
540	539	542	543	5			2	8.4	6.4	1.3	6,0+	
1043	1045	1046		weak		14	~ 3				0,0+	F+(F+1)
1119	1114	1116	1116	44	56	4	~ 4	2.2	1.0	~ 2.2	2,0+	
1172	1170	1170		230	209	²⁸ Si*	5				3,3+	
	(1195)			~ 5**								
	1224		1222	9	~ 13			29	26	1.1	3,?-	Oct. vib.
1263	1261	1263	1262	39	~ 35	70	49	22	26	0.9	4,3+	F+(F+1)
	1283			26	~ 41						4,0+	F-F, (F+1)-(F+1)
	1333			~ 6	~ 12							
	1352	1349	1355	~ 8	~ 16	~ 1	~ 2	4.9	0.9			
1376	1374	~ 1373		22	~ 32	~ 2					5,3+	F+(F+1)
	(1415)			2								
1466	1465	1466	1465	58	46	~ 2		35	18	2.0	2,2+	γ -vib.
	1497			~ 19								
1510	1507	1508		~ 8**	27	5	~ 2				6,3+	F+(F+1)
	1544			39	60							
1549		1550				26	20				3,2+	γ -vib.
1609	1607	1604	1605	184	167	8	~ 3	4.5	3.2	1.4	2,2+	(F+1)-F
		~ 1634	1631				~ 2	2.2	3.5			
			1660					1.0	1.7	0.6	4,2+	γ -vib
1663	1659	1661		154	158	42	20					
1702	1699	1702		29	~ 34	64	33				3,2+	(F+1)-F
			1708					15	12	1.2	(3,?-)	(Oct. vib.)
1749	1752	1750	1747	22	~ 14	38	32	2.1	1.3			
	1775			~ 8								
1803	1803	1793	1789	19	~ 30	10	~ 6		3.3		4,2+	(F+1)-F
			1820					54	53	1.0	3,?-	Oct. vib.
	1859	~ 1853		~ 2	~ 7	~ 6	~ 3					
	1886	1893		~ 2		~ 7	4					
	1925	1921		16	18	≥ 20 ***	12					
		1967				≥ 4 ***	12					
	2008			15	~ 12						1,1+	(F+1)-(F-4)
			2032					21	20	1.0	3,?-	Oct. vib.
	2046			13	~ 11						2,1+	(F+1)-(F-4)
			2050					7.0	11	0.6		
		2097				4	2					
	2109			~ 18	20						3,1+	(F+1)-(F-4)
		2121				3	6					
	2179	2173		6		40	5					
	2193			4							4,1+	(F+1)-(F-4)
	2228	2218		***	10	105	38					
		2279				24	24					
		2325					~ 8					
		2344				46	19					
		2371				144	80					

* Intensity not reliable due to presence of peaks from target impurity indicated.

** Approximately 40% of the intensity quoted is due to ^{174}Yb target impurity.

*** Intensity not reliable due to joint in photographic plates at this point.

TABLE 4. Levels in ^{174}Yb .

Prev. value ref. $^{11, 12, 13}$	Energy		$d\sigma/d\Omega (d, p)$ $\mu\text{b/sr}$		$d\sigma/d\Omega (d, d')$ $\mu\text{b/sr}$		R	$I, K\pi$	Comments
	(d, p)	(d, d')	$\theta = 60^\circ$	$\theta = 90^\circ$	$\theta = 90^\circ$	$\theta = 125^\circ$			
0	0	0	~ 0.6	~ 0.7	63000	13000	4.8	0,0+	Gr. state rot. band
76.5	77	79	62	29	5400	3300	1.7	2,0+	
252	251	252	38	20	71	108	0.7	4,0+	
527		523			5.7	3	1.9	6,0+	Oct. vib.
1316				≤ 2				2,2-	
		1348			14				Oct. vib.
		1380			45	39	1.2	3,2-	
~ 1520	1509			17				(6,6+)	((F+2)+(F+1))
	1559			11				5,2-	Oct. vib.
	1630	1629	73	44	38	29	1.4	2,2+	γ -vib.
	1667		24	18				6,2-	Oct. vib. ((F+2)+(F+1))
		1696			16	19	0.8	(7,6+)	
	1702		99	67				3,2+	γ -vib.
~ 1723			~ 12	~ 12					
		1760				2			
		1778			15	19	0.8		
	1799	1801	56	35	14	15	0.9	4,2+	γ -vib.
	1841		~ 30*	~ 8					
		1846			55	55	1.0	3,?-	Oct. vib.
	1876		~ 15	~ 15					
	1926		~ 10	24				5,2+	γ -vib.
	1947		~ 15	35					
	2039		~ 19	10					
	2080		79	51					
	2101		~ 40	14					
	2150		~ 40	58					
	2189	2178	79	51	9	10		2,2+	(F+1)-(F+4)
	2213			19					
	2237	2230	144	78		2		3,2+	(F+1)-(F+4)
	2284		144	95				3,3+	(F+1)+(F+4)
	2333		110	69				4,2+	(F+1)-(F+4)
	2370		100	67				4,3+	(F+1)+(F+4)
	2407		~ 40	11					
	2450		~ 80	47					
	2482			26				5,3+	(F+1)+(F+4)

* Contains impurities?

TABLE 5. Levels in ^{176}Yb .

Energy		$\frac{d\sigma}{d\Omega}(d,d')\mu\text{b/sr}$		R	$I, K\pi$	Comments
Previous value	(d, d')	$\theta = 90^\circ$	$\theta = 125^\circ$			
0	0	63000	13000	4.8	0,0+	Ground state rotational band
82.1	82	4500	2700	1.7	2,0+	
270	270	75	117	0.6	4,0+	
564	565	4.4	1.8	2.4	6,0+	
1270	1254	57	27	2.2	2,2+	
	1340		3.2			
	1429	13	9.3	(1.4)	4,2+	γ -vibration
	1491	30	19	1.6	(3,? -)	Octupole vibration?
	1692	8.5	4.7	(1.8)		
	1767	13	12	1.1		
	1790	39	50	0.8	3,? -	Octupole vibration

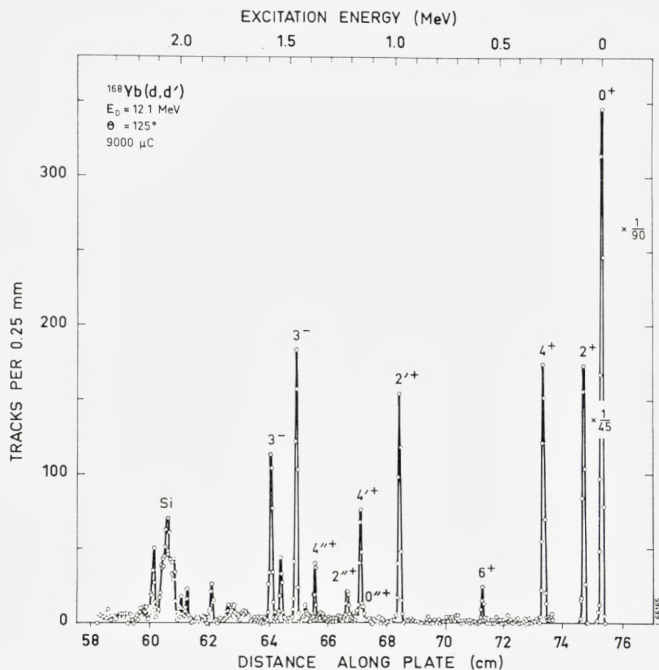
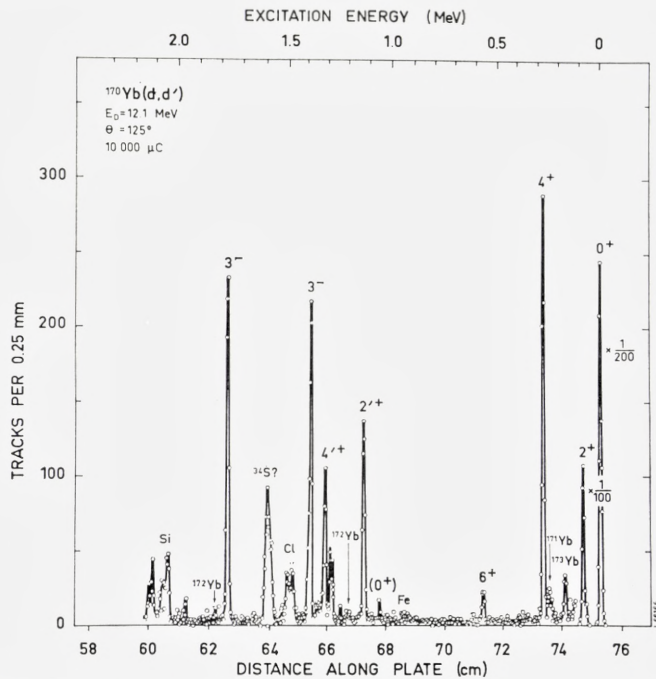
tional bands by means of (d, p) and (d, t) reactions can be calculated from equations (6) if one knows the quantities $C_{j'l}^2\varphi_l$ and $U(v)$ or $V(v)$. Empirical values of these parameters can be obtained from the stripping and pick-up reactions on even targets²⁾. Theoretical values could be used, although they do differ slightly from the experimental ones. For the Yb-nuclei there is good evidence that several of the single-particle states are quite pure. For such cases it might be more reasonable to use empirical values of $C_{j'l}^2\varphi_l$ for predictions of the cross sections to states in even-even nuclei. This would compensate for some uncertainties in the theoretical wave functions and in the DWBA calculations. If the states in the odd nuclei are not pure, such a procedure should of course not be applied.

Table 6 shows some of the experimental values of $C_{j'l}^2\varphi_l$ for several Nilsson states, obtained from (d, p) and (d, t) reactions²⁾ at $\theta = 90^\circ$. These data are normalized such that they correspond to Q-values of 4 MeV and -1.5 MeV for the (d, p) and (d, t) processes, respectively. Predictions for the intensities of the ground-state rotational bands have been made by inserting the values of $C_{j'l}^2\varphi_l$ from Table 6 into equations (6). Such results are shown in columns 2, 4, 6 and 8 of Table 7 where the values presented are $(d\sigma/d\Omega)_g$. The alternate columns of Table 7 show the experimentally observed values and, thus, the ratios between values in the corresponding columns should yield the U^2 or V^2 for the particular state in the final nucleus. The last two columns of Table 8 show estimates of U^2 and V^2 obtained in this way for the four possible ground-state reactions with the two stable odd

TABLE 6. Empirical values of $C_{j_l}^2 \varphi_j$, $\theta = 90^\circ$ (microbarns per steradian).

Spin j	$C_{j_l}^2 \varphi_l(d, p), Q = 4.0 \text{ MeV}$			$C_{j_l}^2 \varphi_l(d, t), Q = -1.5 \text{ MeV}$		
	1/2 - [521]	5/2 - [512]	1/2 - [510]	1/2 - [521]	5/2 - [512]	3/2 - [521]
1/2	75	—	4	270	—	—
3/2	7	—	124	16	—	140
5/2	29	4	64	50	12	Not obs.
7/2	40	115	26	92	270	150
9/2	5	4	6	9	7	19
11/2	4	4	Not obs.	5	8	Not obs.

targets. These are to be compared with the corresponding values in the third and fourth columns, which were obtained from studies of the transfer of neutrons into and out of the same Nilsson states in experiments with even-even targets²⁾. It is seen that there is acceptable agreement between corresponding values of V^2 obtained from the different reactions. However, in both cases measured, the values of U^2 obtained from experiments with odd targets are appreciably lower than the corresponding values from experiments with even targets. As an example, one can consider the two values for the U^2 of the $1/2 - [521]$ orbital in ^{170}Yb (cf. Table 8) which have been determined from the ground-state transitions in the $^{171}\text{Yb}(d, t)^{170}\text{Yb}$ and the $^{170}\text{Yb}(d, p)^{171}\text{Yb}$ reactions. As mentioned in sect. 2, the same factor U^2 must apply to both reactions because of the principle of detailed balance. Although the (d, p) and (d, t) reactions are not exactly inverse, the use of the empirical values of $C_{j_l}^2 \varphi_l$ in the cross section comparisons should ensure quite close agreement between the reduction factors U^2 , and the observed discrepancy of more than a factor of two is therefore surprising. It should, however, be remembered that the ground-state Q-values for the (d, t) reactions on odd targets are approximately 1.5 MeV higher than those on even targets. The predicted experimental cross sections therefore depend on the Q-dependence obtained from the DWBA calculations (Fig. 11 of ref. 2). More complete calculations with improved triton potentials²³⁾ give a Q-dependence less steep than the one used here. An estimate shows that the values for U^2 in Table 8 obtained from odd targets consequently should be increased by approximately 25 %. This correction is, however, not sufficient to remove the discrepancy with the values obtained from even targets, and the origin of this discrepancy is therefore still unknown. In order to be consistent with the earlier work, no correction has been applied to the values in Tables 7 and 8.

Figure 5. Deuteron spectrum for the reaction $^{168}\text{Yb}(d,d')$ at $\theta = 125^\circ$.Figure 6. Deuteron spectrum for the reaction $^{170}\text{Yb}(d,d')$ at $\theta = 125^\circ$.

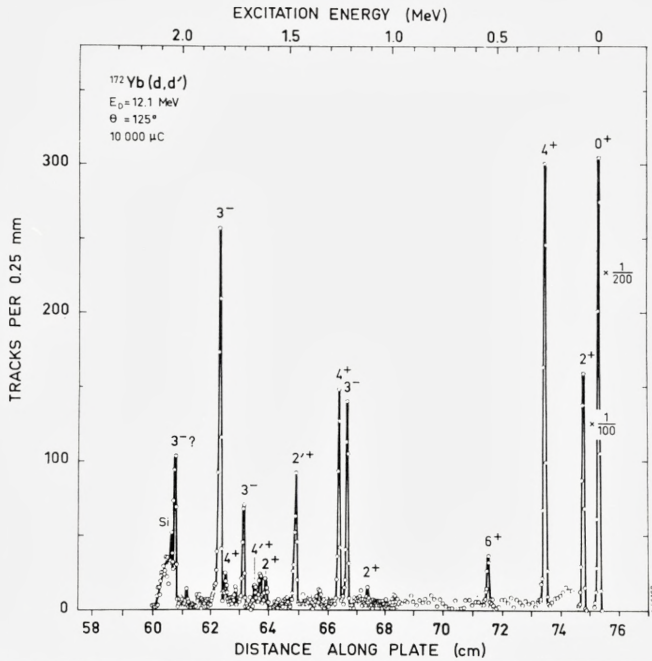


Figure 7. Deuteron spectrum for the reaction $^{172}\text{Yb}(d,d')$ at $\theta = 125^\circ$.

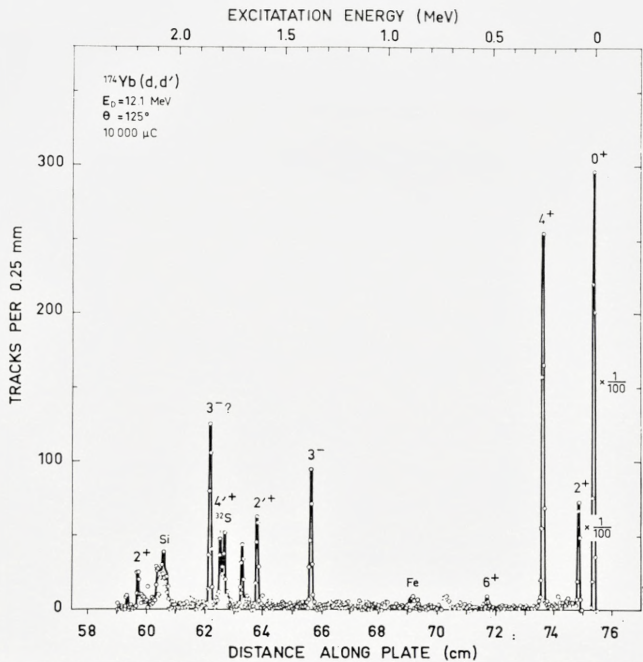


Figure 8. Deuteron spectrum for the reaction $^{174}\text{Yb}(d,d')$ at $\theta = 125^\circ$.

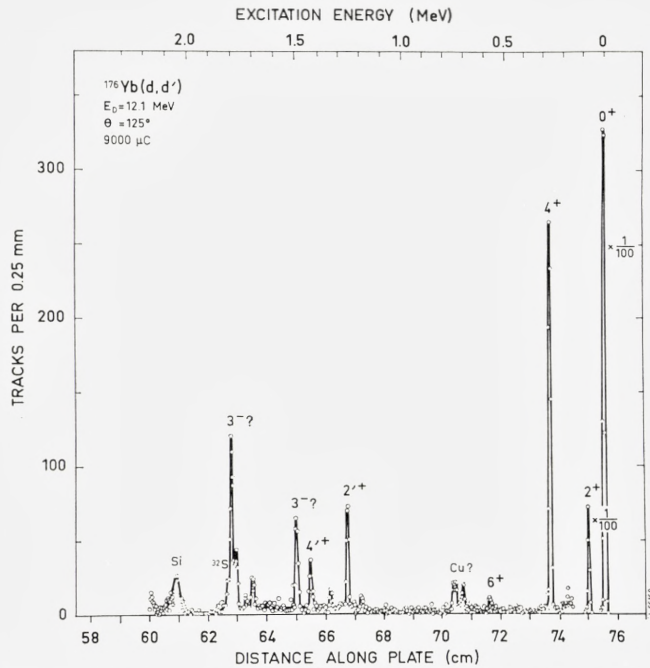


Figure 9. Deuteron spectrum for the reaction $^{176}\text{Yb}(d,d')$ at $\theta = 125^\circ$.

4.2. Quadrupole γ -vibrations

The $K = 2$ quadrupole vibrational states in deformed rare earth nuclei have been the subject of many investigations. There are good theoretical predictions of the observed systematics of excitation energies and transition probabilities to the ground states^{17, 18}). Due to the nature of the states near the Fermi surface in the ytterbium region, the γ -vibrations occur at rather high excitation energies and the $B(E2)$ values connecting them with the ground states are small¹⁷). As a result, most of these states were not observed in a recent survey of vibrational states in rare earth nuclei by means of the Coulomb excitation process¹⁹). The energies of the γ -vibrational states in ^{168}Yb , ^{170}Yb , ^{172}Yb , and ^{176}Yb were previously known^{7, 17, 11}) although there has been some uncertainty concerning the assignment of the 1.468 MeV state in ^{172}Yb as a γ -vibrational state²⁰).

It has been shown that the collective vibrational states in the even nuclei of samarium and gadolinium were strongly excited by the (d,d') process. The quadrupole excitations could with reasonable certainty be identified on

TABLE 7. Comparison of ground state rotational band populations with predictions $\theta = 90^\circ$.

Spin	Transfer of 1/2 - [521] neutron				Transfer of 5/2 - [512] neutron			
	$^{171}\text{Yb} (d, t) \ ^{170}\text{Yb}$		$^{171}\text{Yb} (d, p) \ ^{172}\text{Yb}$		$^{173}\text{Yb} (d, t) \ ^{172}\text{Yb}$		$^{173}\text{Yb} (d, p) \ ^{174}\text{Yb}$	
	Predicted	Exp.	Predicted	Exp.	Predicted	Exp.	Predicted	Exp.
	$\left(\frac{d\sigma}{d\Omega}\right)_s$	$\frac{d\sigma}{d\Omega}$	$\left(\frac{d\sigma}{d\Omega}\right)_s$	$\frac{d\sigma}{d\Omega}$	$\left(\frac{d\sigma}{d\Omega}\right)_s$	$\frac{d\sigma}{d\Omega}$	$\left(\frac{d\sigma}{d\Omega}\right)_s$	$\frac{d\sigma}{d\Omega}$
0	520	130	36	36	8.5	4	0.8	0.7
2	118	30	20	16	344	136	45.4	29
4	162	47	27	20	213	87	34.0	20
6	7	5	3	2	10	Not obs.	3.5	Not obs.

the basis of the ratio of the yields at two angles. Furthermore, the inelastic scattering cross section at 90° was, within the experimental error, proportional to the reduced transition probability $B(E2)$.

The inelastic scattering spectra shown in Figs. 5-9 contain several strong groups for which the ratio, R , of the 90° yield to that at 125° is in the range 2.0-3.0, which is typical for quadrupole excitations. In each spectrum, one such group was found which could be ascribed to the $K = 2$ γ -vibrational state. The γ -vibrational bands seem to be characterized by fairly strong populations of the $2+$ and $4+$ states, whereas the $3+$ states, which have unnatural parity, were never observed with certainty.

The above mentioned properties definitely establish the 1468 keV state in ^{172}Yb as the γ -vibrational $2+$ state. A similar state was observed at 1630 keV in ^{174}Yb .

Some of the properties of the γ -vibrational states have been collected in Table 9. The reduced transition probabilities, $B(E2)$, given there are based

TABLE 8. Experimental values of U^2 and V^2 .

Nilsson state	Ground state of isotope	From experiments with even-even targets ^a		From experiments with odd targets	
		U^2 (%)	V^2 (%)	U^2 (%)	V^2 (%)
1/2 - [521].....	^{170}Yb	54 ± 8	44 ± 7	26 ± 4	-
1/2 - [521].....	^{172}Yb	30 ± 4	74 ± 11	-	86 ± 13
5/2 - [512].....	^{172}Yb	74 ± 11	28 ± 4	40 ± 6	-
5/2 - [512].....	^{174}Yb	27 ± 4	75 ± 11	-	62 ± 9

2*

TABLE 9. Properties of $K = 2 +$ gamma-vibrational states.

Isotope	E_{2+}	$\hbar^2/2\mathfrak{J}$	B(E2) ^{a)}	B(E2) _{s.p.u.} ^{b)}
¹⁶⁸ Yb	981	13.4	0.15	5.2
¹⁷⁰ Yb	1145	13.2	0.094	3.2
¹⁷² Yb	1465	13.9	0.044	1.5
¹⁷⁴ Yb	1629	12.2	0.050	1.7
¹⁷⁶ Yb	1254	12.5	0.070	2.4

a) $B(E2)e^2$ in units of $10^{-48} \text{ cm}^4 = 1.18 \times (d\sigma/d\Omega)_{90^\circ}$ in mb/sr .

b) $1B(E2)_{s.p.u.} = 0.029 \times 10^{-48} e^2 \text{ cm}^4$.

upon the semi-empirical fact that the inelastic cross sections are proportional to the reduced transition probability between the ground state and the excited state. The proportionality constant was obtained by interpolation from (d, d') data for the even isotopes of Sm, Gd, Th and U. Furthermore, for ¹⁷⁶Yb, the B(E2) value was already known¹⁹⁾. The value obtained here is in good agreement with the earlier value. The 90° (d, d') cross sections were used for the evaluation of the B(E2) values because it was felt that they were less affected by multiple excitations involving the $4+$ states.

Fig. 15 shows some of the systematic features of the γ -vibrational states as functions of the mass number. For the nuclei ¹⁷²Yb and ¹⁷⁴Yb the energies are high and the transition probabilities low. Thus, for these nuclei, typical collective properties are less well developed than for other nuclei in the rare earth region.

Additional information concerning these levels is obtained from the (d, p) and (d, t) reactions in the ¹⁷⁰Yb, ¹⁷²Yb, and ¹⁷⁴Yb nuclei. Current theories consider the collective vibrations to consist of superpositions of quasiparticle states and the decomposition of the $K = 2$ γ -vibrations has been calculated^{17, 18)}. These two-particle states can be populated in the stripping and pick-up reactions by coupling the transferred neutron (or hole) with the unpaired nucleon in the odd mass target. There is an obvious selection rule that one can populate only the two-particle states for which one of the particles is the ground state of the odd target nucleus.

In most cases, the calculations show that only one or two components of the vibrational states have appreciable amplitude¹⁷⁾ and also satisfy the above selection rule. Thus, it is easy to calculate the predicted intensities for the population of a vibrational state by a (d, p) or (d, t) reaction from its theoretical composition. However, it should be remembered that, when more than one component is present, the amplitudes $\theta_{j\lambda}$ in the expression for the spectroscopic factor add coherently—that is, they must be added for

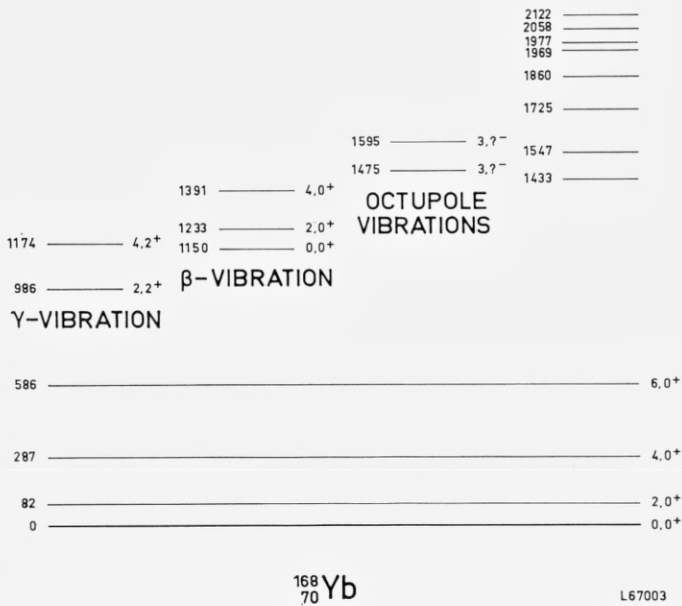


Figure 10. Level scheme for ^{168}Yb . The numbers on the left side of each level indicate the excitation energy in keV, and those on the right are the quantum numbers $I, K\pi$.

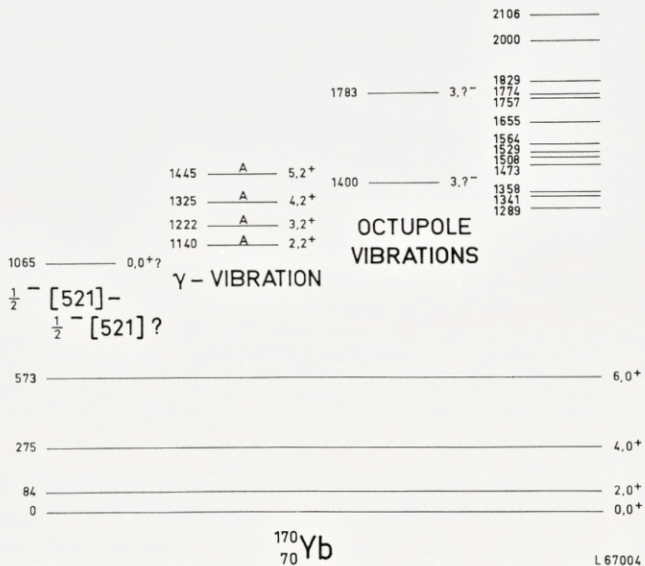


Figure 11. Level scheme for ^{170}Yb . See caption to Figure 10.

a given j before being squared. Only the magnitude of $C_{j\ell}^2 \varphi_\ell$ and not its sign was obtained from the experiments with even-even targets. Therefore, in all calculations of mixed states which follow, each term has been given the same sign as the theoretical value of $C_{j\ell}$.

The $1/2 - [521]$ Nilsson orbital forms the ground state of ^{171}Yb . For the γ -vibrational state in ^{170}Yb , Bès et al.¹⁷⁾ predict two components which should be populated in the (d, t) reaction. These are the $1/2 - [521] + 3/2 - [521]$ state with amplitude 0.45 and the $1/2 - [521] - 5/2 - [523]$ state with amplitude 0.52. Empirical values of $C_{j\ell}^2 \varphi_\ell$ for the $3/2 - [521]$ and $5/2 - [523]$ states from (d, t) experiments on even Yb targets²⁾ then predict the cross sections^{*)} for the $2+$, $3+$, $4+$, and $5+$ members of the $K = 2$ γ -vibration to be 33, 14, 13, and $10 \mu\text{b}/\text{sr}$, respectively. The experimental cross sections for these states are 45, 14, 32, and $\sim 3 \mu\text{b}/\text{sr}$. As we shall see later, there is a good possibility that the experimental value quoted for the $2+$ member actually is that for a closely spaced doublet, the other state having a cross section of $\sim 5 \mu\text{b}/\text{sr}$. This would reduce the observed population of the $2+$ state to $\sim 40 \mu\text{b}/\text{sr}$. Similarly, the cross section of the $4+$ state may be reduced by $\sim 8 \mu\text{b}/\text{sr}$ to $\sim 24 \mu\text{b}/\text{sr}$.

The agreement between prediction and experiment is not very good for the $4+$ and $5+$ states. One might try to account for the high cross section of the $4+$ state by considering the possibility that the observed value pertains to additional unresolved levels. Of course, this line of argument cannot be applied to the $5+$ level where the observed strength is only about $3 \mu\text{b}/\text{sr}$ compared to a predicted value of $10 \mu\text{b}/\text{sr}$. It is possible, however, to calculate which set of amplitudes, if any, for the above mentioned two-quasi-particle components would yield the experimental cross sections. One can calculate, first, the effect of varying the relative amplitudes of the two components to reproduce the relative intensities of the different members of the rotational band and, then, normalize both amplitudes to obtain agreement with the absolute values of the observed cross sections. Let I_2, I_3, I_4 , and I_5 be the intensities of the $2+, 3+, 4+$, and $5+$ states, respectively, and let "a" and "b" be the respective amplitudes of the $1/2 - [521] + 3/2 - [521]$ and $1/2 - [521] - 5/2 - [523]$ components. In Fig. 16, the solid curves show the predicted intensity ratios $I_2/I_3, I_4/I_3$, and I_5/I_3 as a function of the ratio b/a . The cross-hatched areas show the experimentally observed relative intensities. It is seen that the predicted and the experimental values of I_2/I_3 are in good agreement if b/a is less than 0.8, and for I_4/I_3 the value of b/a must be less than about 0.6. The experimental ratio I_5/I_3 places a still lower

* All comparisons of cross sections in the present work are based on the 90° data.

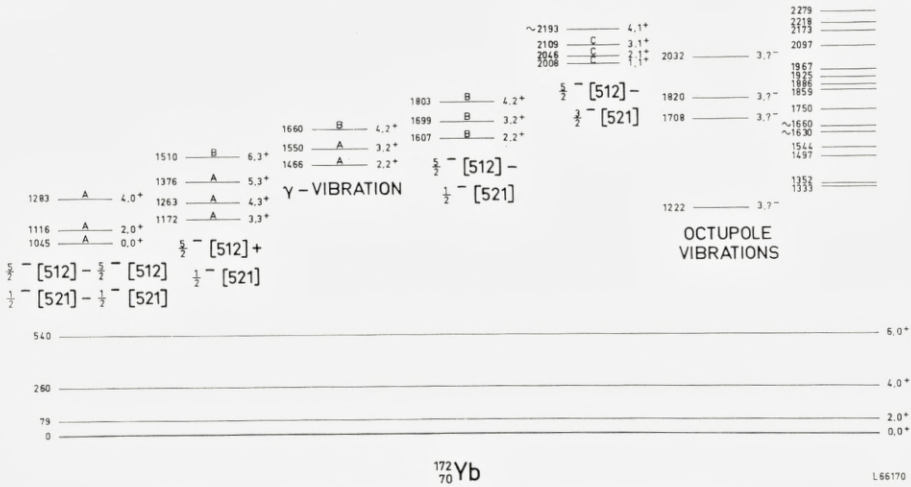


Figure 12. Level scheme for ^{172}Yb . See caption to Figure 10.

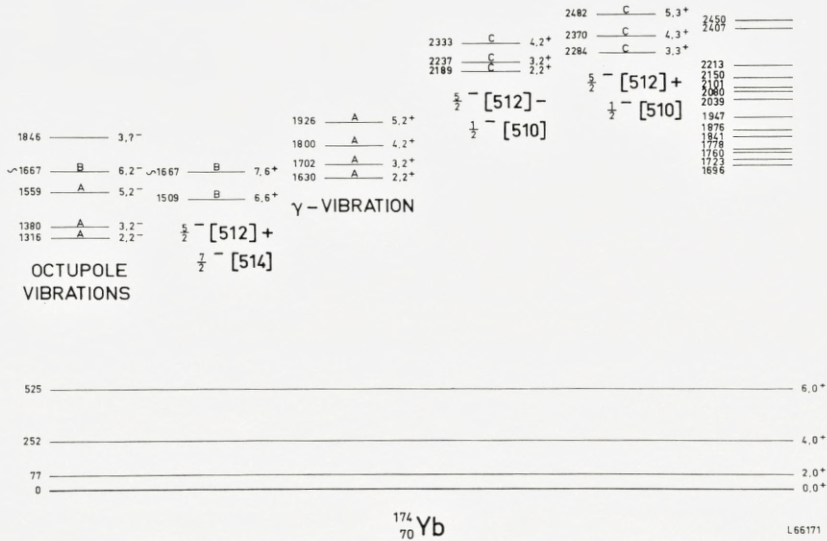


Figure 13. Level scheme for ^{174}Yb . See caption to Figure 10.

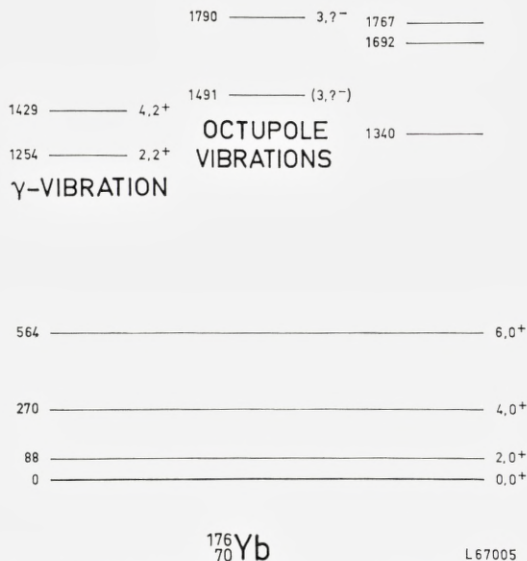


Figure 14. Level scheme for ^{176}Yb . See caption to Figure 10.

limit on b/a . The relative uncertainty in I_5 is large as the cross section is weak, but even the generous relative error of 100% would limit the ratio b/a to less than 0.4. The absolute values of the cross sections give $a \approx 0.53$ and $0.05 \lesssim b \lesssim 0.2$. The amplitude of the $1/2 - [521] + 3/2 - [521]$ component is seen to be in good agreement with the theoretical value of 0.45, but that of the $1/2 - [521] - 5/2 - [523]$ component is less than about one half of the theoretical value 0.52.

In ^{172}Yb , the only component of the 1.468 MeV, $K = 2$, γ -vibration which can be populated in either the (d, p) or the (d, t) reaction is a fragment of the $1/2 - [521] - 5/2 - [512]$ state. According to BÈS et al.¹⁷⁾, this component should have an amplitude of 0.20. On the other hand, the calculations of SOLOVIEV¹⁸⁾ suggest that the state at 1.468 MeV is almost a pure $1/2 - [521] - 5/2[512]$, $K = 2$ two-quasiparticle state. From the (d, d') systematics discussed above it is seen that most likely the band is the $K = 2$ γ -vibration. The stripping and pick-up reactions can provide an empirical estimate of the amplitude of the above two-quasiparticle configuration which forms a part of this vibration. As this band was not strongly populated in either the (d, p) or (d, t) process, the weaker peaks were not observed. Hence, in this discussion, only the member of the band with the largest cross section is considered. In the (d, t) reaction the $2+$ member of the band is expected

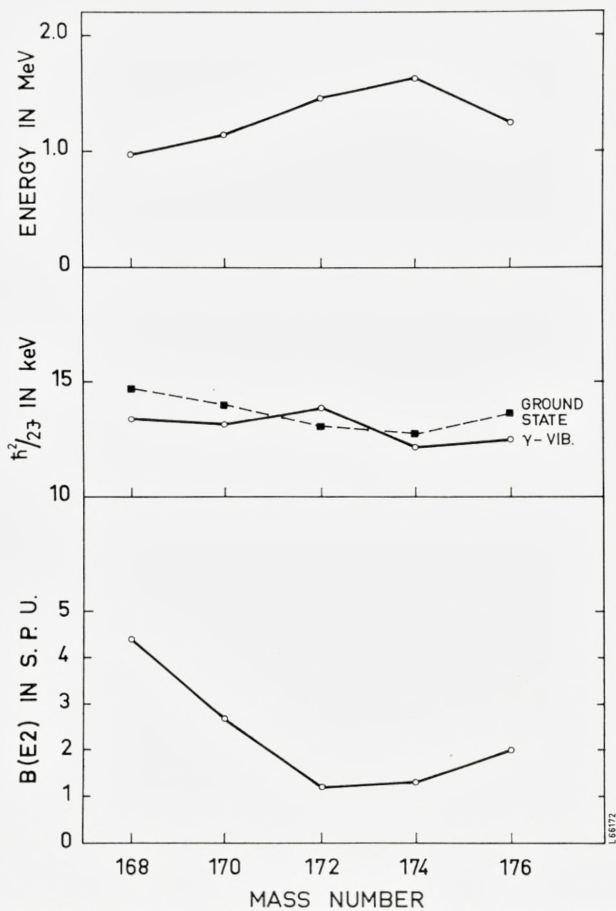


Figure 15. Properties of γ -vibrational states in even Yb nuclei. The top graph shows the energy of the $I, K\pi = 2, 2+$ state. The centre figure shows the inertial parameter $\hbar^2/2I$ for the rotational bands based on the γ -vibrations (solid lines) compared with values for the ground state rotational bands (dashed lines). In the bottom graph are found the reduced transition probabilities which connect the γ -vibrational states to the ground states.

to be populated most strongly. For the pure two-quasiparticle configuration, this state would be expected to have a cross section of $185 \mu b/sr$ if one assumed a reasonable value of $V^2 \approx 0.8$ for the $1/2 - [521]$ orbital in ^{173}Yb . This estimate of V^2 was obtained from an interpolation of the results of ref. 2. The experimental cross section for the $2+$ state at 1.468 MeV is $46 \mu b/sr$, which implies that the state is about 25% $1/2 - [521] - 5/2 - [512]$. An independent estimate of the amplitude of this component can be obtained

from the (d, p) spectra where the $3+$ member of the band is the most strongly populated. Again using the values of $C_{j'l}^2 \varphi_l$ of Table 6, and $U^2 \approx 0.8$ for the $5/2 - [512]$ orbital in ^{171}Yb , the pure two-quasiparticle state would be expected to have a cross section of $62 \mu\text{b}/\text{sr}$. The experimental cross section is $20 \mu\text{b}/\text{sr}$ so that the vibrational state contains $\sim 32\%$ of the two-quasiparticle state. The two estimates of the admixture are consistent, within experimental error, and indicate that the amplitude for the $1/2 - [521] - 5/2 - [512]$ component of the $K = 2$ γ -vibration in ^{172}Yb is about 0.50 or 0.55 as compared to the theoretical estimate of 0.20¹⁷⁾.

In ^{174}Yb , there is again only one two-quasiparticle state which is predicted to have a large component in the γ -vibration. This is the $5/2 - [512] - 1/2 - [510]$ state with a theoretical amplitude of 0.56¹⁷⁾. The $1/2 - [521] - 5/2 - [512]$ state is also expected to contribute an amplitude of 0.07, but, coupled with a low value of U^2 for the $1/2 - [521]$ state in ^{173}Yb , this is found to result in a negligible correction to the cross sections. The $2+$, $3+$, $4+$, and $5+$ members of the rotational band based on the $K = 2$ γ -vibration are then expected to have (d, p) cross sections of 27, 32, 17, and $6 \mu\text{b}/\text{sr}$, respectively. The experimental values are 44, 67, 35, and $< 22 \mu\text{b}/\text{sr}$. It is seen that the observed cross sections are almost twice as large as those predicted, which would suggest that the amplitude of the $1/2 - [510] - 5/2 - [512]$ state is closer to 0.75 or 0.80 than the theoretical value of 0.56. It is also noted that the predicted ratios of the cross sections to the $2+$, $3+$, $4+$, and $5+$ states are 0.85:1.00:0.53:0.19 as compared with experimental values of 0.66:1.00:0.52: < 0.33 , respectively. These ratios agree reasonably well, although the intensity of the $2+$ state is a little weaker than expected, compared to the other members of the band. However, if the amplitude of the $1/2 - [521] - 5/2 - [512]$ state were ~ 0.5 instead of 0.07, the predicted intensity ratios would be in agreement with the experimental data.

4.3. Octupole Vibrations

Just as in the case of the quadrupole excitations discussed in the previous section, the collective octupole vibrations are strongly excited by the (d, d') process. The ratios R of the 90° yield to the 125° yield for the Sm and Gd nuclei were found to be in the range of 1.2—1.6, with some tendency toward a decrease with increasing mass numbers.

The inelastic scattering spectra shown in Figs. 5—9 contain several strong deuteron groups with R in the range of 1.0—1.3. Although the absolute intensities of these groups are considerably smaller than those observed in

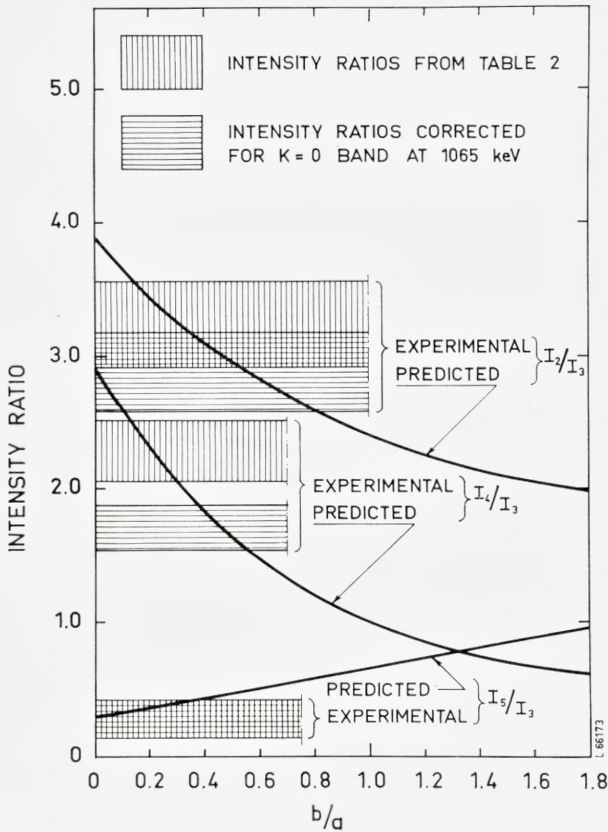


Figure 16. Intensity ratios for members of the γ -vibrational band in ^{170}Yb populated by the (d,t) reaction. The letters a and b are the amplitudes of the $1/2- [521] + 3/2- [521]$ and $5/2- [523] - 1/2- [521]$ components, respectively. The experimental values shown by vertical cross-hatching were obtained with the assumption that no other unresolved states contribute to the observed cross sections. However, it is possible that the $2+$ and $4+$ states are actually unresolved doublets (see text), in which case the present interpretation indicates that the adjusted intensity ratios shown by horizontal cross-hatching are applicable.

the lighter deformed rare earth nuclei, it is natural to associate at least some of them with excitations of collective octupole states. Some of the properties of states believed to be of this nature are collected in Table 10.

On the basis of the (d, d') results it has been possible to identify the spin 1, 3, and 5 members of rotational bands based on $K\pi = 0^-$ octupole vibrations in the Sm and Gd nuclei^{16, 21}). In ^{152}Sm , these rotational members have also been found in a vibrational band known to be $K\pi = 1^-$. The absence of any deuteron groups which can be assigned to possible spin 1 members

TABLE 10. Properties of octupole vibrational states

Isotope	$E_3 - K$	$\hbar^2/2\mathfrak{I}$ keV	B(E3) ^{b)}	B(E3) _{s.p.u.} ^{c)}
¹⁶⁸ Yb	1475		0.077	6.2
–	1595		0.039	3.1
¹⁷⁰ Yb	1400		0.049	3.9
–	(1783) ^{a)}		(0.045)	(3.6)
¹⁷² Yb	1222 (2)		0.026	2.1
–	(1708)		(0.015)	(1.2)
–	1820		0.053	4.2
–	2032		0.022	1.8
¹⁷⁴ Yb	1380 2	10.0	0.041	3.3
–	1846		0.051	4.1
¹⁷⁶ Yb	1491		0.027	2.2
–	(1790)		(0.038)	(3.0)

- a) Brackets indicate that the assignment is doubtful.
b) B(E3)/e² in units of 10⁻⁷²cm⁶ = 0.85 (dσ/dΩ)_{90°} in mb/sr.
c) 1 B(E3)_{s.p.u.} = 1.25 × 10⁻⁷⁴e²cm⁶.

associated with most of the lower levels in Table 10 suggests that these are not members of the $K = 0$ or $K = 1$ bands. From the following discussion it will be seen that there is evidence supporting the assignment of $K = 2$ to one of these states. The appearance of $K\pi = 2^-$ states at the lowest energy is also in agreement with the fact that the lowest lying octupole state in ¹⁶⁶Er has recently ^{22, 23, 24)} been established to have a K -value of 2.

In Table 10, columns 5 and 6 contain B(E3) values for these octupole states. These values were obtained from the (d, d') intensities in a manner similar to that described for the quadrupole excitations. It is believed that this procedure will yield B(E3) values within an uncertainty of 40 %₀. A slight correction for Q -dependence of the proportionality constant was obtained from a DWBA calculation.

The largest E3 transition probabilities found in the Yb nuclei are approximately five single-particle units. This number can be compared to values of 20 to 30 single-particle units for nuclei at the beginning of the deformed rare earth region. Thus, there is a very considerable decrease in the strength of the octupole levels below approximately 2 MeV as one increases in mass from the Sm and Gd regions.

As in the case of γ -vibrations, the single-particle transfer reaction can sometimes provide important additional information. The lowest 3⁻ state in ¹⁷⁰Yb is at 1400 keV. A peak corresponding to this energy is also observed

in the (d, t) spectrum. Of the $19 \mu b/sr$ observed approximately $7 \mu b/sr$ are ascribed to the ^{172}Yb impurity in the target. The peaks in the triton spectra at 1289, 1341, and 1358 keV might possibly be associated with lower spin members of an octupole rotational band. In the (d, d') spectrum, there is a multiple group at ~ 1300 keV, part of which might correspond to a $1-$ state. If this is indeed the case, it is impossible on the basis of the present data to decide whether this band has $K = 0$ or $K = 1$. Both of these possibilities would involve small amplitudes of states¹⁸⁾ found by the transfer of the $1/2+[400]$ or the $3/2+[402]$ neutrons and are consistent with the weak triton groups observed.

For ^{172}Yb , the lowest energy $3-$ state seen in the (d, d') process is at 1222 keV. This level is also weakly populated in the (d, t) reaction, but as in the case of ^{170}Yb , the data do not give a unique determination of the K -value. Any possible band members with spin less than 3 could be weakly populated or could be obscured by the large triton groups at 1119 and 1172 keV.

The wave functions for the octupole states in this region are likely to contain components involving the $1/2+[400]$ and $3/2+[402]$ Nilsson orbitals¹⁸⁾ which have (d, t) cross sections of the order of $\sim 100 \mu b/sr$ for the population of a spin 3 state at this Q -value. The observed cross section of $\sim 13 \mu b/sr$ thus gives an upper limit of $10-15 \%$ for the admixture of either of these states into the octupole vibration.

The state at 1222 keV is not observed in the (d, p) reaction, which is consistent with the fact that there are no nearby Nilsson states above the Fermi surface connected to the $1/2-[521]$ orbital with large octupole matrix elements.

As seen from Table 10, there are three other states in ^{172}Yb which have large (d, d') cross sections, and R values which would suggest they are octupole excitations. The state at 1707 keV coincides, within the experimental error, with a state assigned as $I, K\pi = 3, 2+$ (see section 4.6). It is highly improbable that this is the same state as that observed in the (d, d') spectrum, because experience has shown that the latter process populates only natural parity states. The remaining $3-$ states have no corresponding peaks in the (d, p) or (d, t) spectra with cross sections greater than $\sim 5 \mu b/sr$.

The lower energy $3-$ state observed in the (d, d') spectrum of ^{174}Yb is at 1380 keV. It is interesting to speculate that this might be one member of a $K = 2$ band based on the $2-$ state at 1320 keV. This $2-$ level was previously assigned to be the $9/2+[624]-5/2-[512]$ two-neutron configuration¹¹⁾, which is consistent with the present suggestion if one considers that

the $9/2 + [624] - 5/2 - [512]$ combination is predicted¹⁸⁾ to make up a large fraction of the $K\pi = 2 -$ octupole vibration. Further evidence for this assignment is obtained from the results of the (d, p) reaction in which this two-quasiparticle component can be populated by the transfer of a $9/2 + [624]$ neutron. The energies given above for the spin 2 and 3 members indicate that the inertial parameter $\hbar^2/2\mathfrak{J}$ is 10 keV, which suggests the 4, 5, and 6 spin members should be at approximately 1460, 1560, and 1680 keV. The expected cross sections for the spin 2, 3, 4, 5, 6, 7, 8, and 9 spin members of the rotational band are 2, ~ 1 , 8, 11, 8, 3, ~ 1 and ~ 0 $\mu b/sr$, respectively. Thus, the proton groups corresponding to the spin 2 and 3 members should hardly be observable and would be lost in the small background seen in these regions of the spectrum. The spin 4 state is unfortunately obscured by protons from the ^{13}C impurity in Fig. 4. However, the group at 1559 keV with ~ 11 $\mu b/sr$ can be ascribed to the spin 5 member, and part of the 18 $\mu b/sr$ in the peak corresponding to 1667 keV can be due to the 6 - state. (The remainder of the 1667 keV group will be explained later). Thus it is seen that all the available data are consistent with the possibility that the $K = 2$ octupole vibration exists at 1320 keV and that this collective state contains a large admixture of the $9/2 + [624] - 5/2 - [512]$ two-neutron configuration.

4.4. Low-Lying $K = 0$ Bands

It is known that a number of low-lying bands with $K\pi = 0 +$ exist in deformed rare earth nuclei. In particular, low-lying collective states which are connected to the ground-state band with fairly large electric quadrupole matrix elements have been found in some cases. These states are often called β -vibrations, although their character is not entirely clear. In addition, several other $K = 0$ bands have been identified at excitation energies less than 2 MeV. The present experiments add to our knowledge of the nature of these states in two ways. Firstly, the transfer reactions enable us to determine the amplitudes of certain two-quasiparticle components in the state, and secondly, the excitation by (d, d') of the $2 +$ states allows an estimate of the reduced transition probabilities to the ground state.

As for the ground-state bands, special attention is required when the transferred neutron is in the same Nilsson orbital as the unpaired target nucleon. It has been seen that a state filled with a pair of nucleons $(\nu, \bar{\nu})$ is present in the correlated ground state of a nucleus with the probability $V^2(\nu)$. Hence, there must be a probability $1 - V^2(\nu)$ or $U^2(\nu)$ that this state

is distributed among $K = 0 +$ excited states in the spectrum. One would expect that these $K = 0$ bands in the (d, t) and (d, p) processes are populated in the same way as the ground-state rotational bands. For instance, with a (d, t) reaction on a ^{173}Yb target one could remove the single $5/2 - [512]$ neutron. This process should take place with a cross section $\left(\frac{d\sigma}{d\Omega}\right)_s$, but it has been seen that only a fraction U^2 of this strength leads to the ground state of ^{172}Yb . Therefore, a cross section $V^2\left(\frac{d\sigma}{d\Omega}\right)_s$ must lead to the population of other $K = 0 +$ states which have admixtures of the $5/2 - [512] - 5/2 - [512]$ configuration. This can also be shown by considering the wave function of the component of state $(\nu, \bar{\nu})$ which is orthogonal to the ground state (i.e., is in excited states) and is⁶⁾

$$|v = 2, (\nu, \bar{\nu})\rangle = \{V(\nu) - U(\nu)\alpha^+(\nu)\alpha^+(\bar{\nu})\} \prod_{\nu' \neq \nu} \{U(\nu') + V(\nu')\alpha^+(\nu')\alpha^+(\bar{\nu}')\} |0\rangle. \quad (7)$$

The probability of populating this component in, say, a (d, p) reaction from an odd target nucleus in a state $\alpha^+(\bar{\nu}) |v = 0\rangle$ is

$$|\langle v = 2, (\nu, \bar{\nu}) | \alpha^+(\bar{\nu})\alpha^+(\nu) | v = 0 \rangle|^2 \left(\frac{d\sigma}{d\Omega}\right)_s = U^2(\nu) \left(\frac{d\sigma}{d\Omega}\right)_s. \quad (8)$$

Similarly, the (d, t) cross section to the portion of the state $(\nu, \bar{\nu})$ orthogonal to the ground state is

$$|\langle v = 2, (\nu, \bar{\nu}) | \alpha(\nu)\alpha^+(\nu) | v = 0 \rangle|^2 \left(\frac{d\sigma}{d\Omega}\right)_s = V^2(\nu) \left(\frac{d\sigma}{d\Omega}\right)_s. \quad (9)$$

In these expressions, $U^2(\nu)$ and $V^2(\nu)$ pertain to the filling of the ground state of the final nucleus. Of course, the relative intensities for the populations of the various members of the rotational bands based on these states are expected to be the same as those in the ground-state band in any one reaction.

In the (d, p) and (d, t) spectra for reactions leading to ^{172}Yb , one sees particle groups corresponding to states at excitation energies of 1045, 1115, and 1283 keV in ^{172}Yb . The energy spacings of these levels are reasonable for the $0 +$, $2 +$, and $4 +$ members of a $K = 0 +$ band with a slightly greater moment of inertia than that of the ground state. It is also seen that, in both processes, the relative intensities for the rotational members are strikingly similar to those observed for the ground-state band. This is particularly noticeable for the 1045 keV level which should be populated by $l = 1$

TABLE 11. Comparison of (d,p) and (d,t) populations of the $K = 3$ band at 1172 keV in ^{172}Yb . Intensities shown are cross sections in $\mu\text{b}/\text{sr}$ at $\theta = 90^\circ$.

Spin	Predicted intensities for $1/2 - [521] + 5/2 - [512]$ state		Predicted intensities for $1/2 - [521] - 7/2 - [514]$ state		Experimental intensities	
	(d,t)	(d,p)	(d,t)	(d,p)	(d,t)	(d,p)
3	270	11	0	6	209	5
4	54	66	0	15	35	49
5	42	3	0	4	32	< 2
6	~ 13	1	0	0.1	~ 5	~ 2

stripping in the (d,p) process. In order to enhance the intensity of the proton group corresponding to this state, an exposure was made at $\theta = 45^\circ$ where a maximum in the angular distribution for $l = 1$ stripping is expected for the Q -value and beam energy used in this work²⁵). It is seen that the 1045 keV state is populated quite strongly in this spectrum. This test was considered as an important verification of the existence and nature of the state, as the 1045 keV level itself is populated only very weakly in the (d,t) process.

It is interesting to note that, except for the ground-state rotational band, no excited states below 1174 keV have previously been reported in ^{172}Yb . The present assignment of $K\pi = 0+$ gives a good explanation. A $K = 0$ band would not be expected to be strongly populated in the electron capture decay of ^{172}Lu which has $K\pi = 4-$. In the β^- -decay of ^{172}Tm , which has $K\pi = 2-$, the transitions to the 1045 keV band would have much smaller Q -values than those leading to the ground-state band and could easily have been missed. However, a careful study should reveal the β^- -feeding of these levels and, in fact, the 1044 and 1119 keV states have recently been observed in a study of the β^- -decay of ^{172}Tm , using lithium-drifted germanium γ -ray detectors¹⁰).

On the basis of the absolute values of the cross sections, it is possible to make some comments about the $1/2 - [521] - 1/2[521]$ and $5/2[512] - [512]$ components of the 1045 keV state. If all the components of the wave function orthogonal to the ground state appear in one excited band, the above expressions give the expected cross sections for levels in that band. If only a fraction of this component appears in a given $K = 0$ excited band, the cross sections will be correspondingly reduced.

In the reaction $^{173}\text{Yb}(d,t)^{172}\text{Yb}$, the population of the band based on

the 1045 keV level is $\sim 30\%$ of the value $\left(\frac{d\sigma}{d\Omega}\right)_s$ calculated from the data in Table 6. The value of V^2 for the $5/2 - [512]$ orbital in the ground state of ^{172}Yb is $\sim 30\%$ according to Table 8. Thus, it seems that most of the $5/2 - [512] - 5/2 - [512]$ amplitude which is not in the ground state is found in the band based on the 1045 keV state.

For the (d, p) reaction, the cross section to the 1045 keV level at $\theta = 90^\circ$ is too weak to be reliable. However, one can make use of the data at $\theta = 45^\circ$. There, the cross section for the 1045 keV level is $\sim 13\%$ of that for the ground state. This value can be used to estimate that the cross section for the 1045 keV level is $0.09 \left(\frac{d\sigma}{d\Omega}\right)_s$. Thus, the value of U^2 for the $1/2 - [521]$ orbital in the ground state of ^{172}Yb is at least 0.09. This is also consistent with the data given in Table 8.

A state with a similar nature may also have been observed in ^{170}Yb at an excitation energy of 1065 keV. This assignment is not nearly as certain as the one in ^{172}Yb , but it does give a good explanation of the (d, t) data. Although complete angular distributions have not been measured, the variation of the (d, t) cross section for the 1065 keV state over the four angles measured closely resembles that for other states populated by $l = 1$ pick-up. This aspect of the reaction has not been well studied, but it is possible to say that this state is not populated by a pick-up process with high angular momentum transfer. This excludes the possibility that the 1065 keV level could be one of the four possible two-quasiparticle states formed by picking up a $7/2 + [633]$ or $5/2 - [523]$ neutron, as these states are populated predominantly by processes involving the transfer of 4, 5, or 6 units of angular momentum. Furthermore, the spectrum does not show a rotational band based on the 1065 keV state with an intensity pattern consistent with pick up of a $3/2 - [521]$ neutron to form a $K = 1$ band. If this band had the same relative intensities as the ground-state band, the $2+$ and $4+$ states would be expected to have cross sections of 5 and $8 \mu\text{b}/\text{sr}$, respectively. These states would be at almost the same excitation energies as the $2+$ and $4+$ members, respectively, of the γ -vibrational band discussed earlier and give rise to the estimated $\sim 5 \mu\text{b}/\text{sr}$ and $8 \mu\text{b}/\text{sr}$ which might have to be subtracted from the cross sections to those states.

The (d, t) cross section to the 1065 keV state is $\sim 8\%$ of the value $\left(\frac{d\sigma}{d\Omega}\right)_s$ expected for a pure $1/2 - [521] - 1/2 - [521]$ state. This means that V^2 for the $1/2 - [521]$ orbital in the ground state of ^{170}Yb is at least 0.08. From experiments with even targets it appears that the V^2 is actually about 0.44.

Thus, a large component of this $K = 0$ configuration is yet to be assigned or some other hindrance occurs.

There is empirical evidence from the lighter rare earth nuclei that the (d, d') reaction populates the $0+$, $2+$, and $4+$ members of excited $K = 0$ bands^{15, 16}. The cross sections for these states are approximately equal at 125° , but at 90° the $2+$ state is usually dominant.

The (d, d') spectrum obtained for ^{168}Yb (Fig. 5) gives evidence for the population of a $K = 0$ band based at a level at 1150 keV. This band has been observed earlier⁷). The estimated $B(E2)$ value for the $2+$ state is given in Table 9.

It will be difficult to observe the $2+$ and $4+$ members of the suggested $K = 0$ band in ^{170}Yb with the (d, d') process, because these states occur at almost the same energies as strongly populated members in the γ -vibrational band. In the 125° spectrum, there is weak evidence for a peak corresponding to the $0+$ state.

The (d, d') spectra for ^{172}Yb show a small population of the $2+$ member of the $K = 0$ band based on the 1045 keV state discussed above. The cross section is an order of magnitude smaller than for the ^{168}Yb case, which indicates that this band has a different nature than those usually classified as β -vibrations.

4.5. Other Levels in ^{170}Yb

There are a number of states below an excitation energy of 2 MeV in ^{170}Yb which have not been discussed. Unfortunately, in this case the only one-neutron transfer process which can be studied with the use of stable targets, is the pick-up process, and a considerable ambiguity exists concerning the interpretation of the data. For the largest unassigned peaks in the (d, t) spectrum of Fig. 1, several possible combinations of rotational bands exist. For instance, the state at 1473 keV could be a $K\pi = 1+, 3/2 - [521] - 1/2 - [521]$ configuration or a $K\pi = 0+$ state with a large $1/2 - [521] - 1/2 - [521]$ component similar to the levels discussed in section 4.4. The level at 1564 keV could be the spin 3 member of the possible $K\pi = 1+$ band mentioned above, or a $K = 2+$ state which contains the remainder of the $1/2 - [521] + 3/2 - [521]$ strength which was not found in the γ -vibration. Considering energies and cross sections at only one angle, one cannot exclude any of the above suggestions. However, (d, t) spectra have been recorded at four different angles for this particular reaction, and considerations of the cross section ratios at these angles suggest that the population of the 1564 keV state takes place with an l -value of three or more, whereas

that of the 1473 keV level involves less than three units of angular momentum transfer. This would eliminate the assignment of spin 2 to the 1564 keV level and thus favour the choice of a $K\pi = 1 +$ band at 1473 keV. The levels at 1473, 1508, 1564, and 1655 keV could be spin 1, 2, 3, and 4 rotational members. If this state were the $3/2 - [521] - 1/2 - [521]$ configuration, the intensities for these four states would be expected to be 87, 27, 74, and 50 $\mu b/sr$, respectively, at $\theta = 90^\circ$. The observed cross sections are 56, ~ 6 , 45, and 16 $\mu b/sr$, respectively, which indicates that, if this is a $K\pi = 1 +$ band, it consists of only slightly more than half of the $3/2 - [521] - 1/2 - [521]$ state.

In view of the uncertainty of the nature of the strongly populated states discussed above, there is little use in making speculations concerning the weaker peaks. Many levels are expected in this region of excitation which can be populated by the transfer of $7/2 + [633]$ or $5/2 - [523]$ neutrons. As these orbitals have low values of $C_{jl}^2 \varphi_l$, many weakly populated states are expected, which may be the explanation for many of the small peaks in Fig. 1.

4.6. Other Levels in ^{172}Yb

There has been a great deal of discussion concerning the $K\pi = 3 +$ level at 1172 keV in ^{172}Yb . GALLAGHER and SOLOVIEV²⁰⁾ have considered the early experimental information and assigned the level to be the $K = 3 +, 1/2 - [521] + 5/2 - [512]$ two-quasiparticle state. More recently, GÜNTHER et al.²⁶⁾ have measured the magnetic dipole moment of this state and concluded that only the $1/2 - [521] - 7/2 - [514]$ two-neutron configuration was consistent with their results. The present measurements show clearly that the $1/2 - [521] - 5/2 - [512]$ state is indeed present at this excitation energy. This is seen most easily from the data in Table 11 which compare the predicted cross sections for the two configurations with the experimental values. The state formed by coupling the $1/2 - [521]$ and $5/2 - [512]$ neutrons can be populated by both the (d, p) and (d, t) reactions because these orbitals are the ground states of the ^{171}Yb and ^{173}Yb target nuclei, respectively. However, the $1/2 - [521] - 7/2 - [514]$ state is not expected to be populated by the (d, t) reaction because neither component of this two-quasiparticle configuration is present in the ground state of ^{173}Yb . The $1/2 - [521] + 5/2 - [512]$ state is the only one which should occur at such a low excitation energy and have such high cross sections in the (d, t) process.

A closer look at these data shows that the experimental (d, t) cross sections are only about 75 % of the predicted values. Although the expected uncertainty on each of these values is about 15 %, it is noted that the expe-

rimental (d, p) cross section is also less than the predicted value by about the same factor. This could be an indication that only about three quarters of the state at 1172 keV is made up of the $1/2 - [521] + 5/2 - [512]$ combination.

It is interesting to speculate on the significance of the measured value of the magnetic moment. For instance, it has been suggested that both of the two-quasiparticle states mentioned above might be present at almost the same excitation energy near 1172 keV. This, of course, would make no difference to the (d, t) measurements and would make only a small difference for the (d, p) results as the transfer of a $7/2 - [514]$ neutron takes place with a cross section much smaller than that of a $5/2 - [512]$ neutron. Although the experimental (d, p) cross section to the band agrees more closely with that expected for the $1/2 - [521] + 5/2 - [512]$ state alone than with that expected for the sum of the two states, the agreement is not good enough to exclude the possibility that both bands are present at almost the same energy.

Another possibility is that the 1172 keV level might have some admixtures of two-proton states. The measured magnetic moment is 0.64 ± 0.04 n.m. The calculated magnetic moments for several two-quasiparticle states are as follows²⁶⁾

Two-neutron	$1/2 - [521] + 5/2 - [512]$	$\mu = -0.126$	n.m.
	$1/2 - [521] - 7/2 - [514]$	$\mu = +0.59$	n.m.
Two-proton	$7/2 + [404] - 1/2 + [411]$	$\mu = +2.19$	n.m.
	$5/2 + [402] - 1/2 + [411]$	$\mu = +2.87$	n.m.

The two-proton states listed consist of orbitals near the Fermi surface and are expected to have rather low excitation energies (1.4 and 1.7 MeV²⁰). If the 1172 keV state contains only about three quarters of the $1/2 - [521] + 5/2 - [512]$ state as discussed above, and if the other 1/4 of the state is one of the two-proton configurations, a magnetic moment of $\sim +1/2$ n.m. could easily be explained.

This suggestion implies that the 1172 keV state has an admixture of more than one two-quasiparticle state, somewhat similar to the vibrational states discussed above, though with the amplitude of the $1/2 - [521] + 5/2 - [512]$ being ~ 0.9 . The inelastic deuteron scattering results may indicate a slightly collective nature for this state. It is seen that in the (d, d') population of vibrational levels only the transitions to the states of natural parity in the rotational bands are observed. In the ¹⁷²Yb(d, d') spectrum, the 1263 keV level, which is the 4+ member of the rotational band based on the 1172 keV state, is seen. The exact mechanism of this process is not understood,

but it is interesting to consider the possibility that small admixtures of other two-quasiparticle states could give rise to a collective hexadecapole moment which could cause the excitation of the $4+$ state from the ground state by a direct E4-transition.

It was shown in section 4.2. that only about 25 % of the $K\pi = 2+$ two-quasiparticle state $5/2 - [512] - 1/2 - [521]$ was involved in the γ -vibration at 1466 keV. This means that a large fraction of this state should be observed elsewhere in the spectrum. The state under discussion is expected to have a large cross section, and one could perhaps make an attempt to associate it with some of the large peaks observed in the spectra. However, on the basis of the present stripping and pick-up reactions alone, it is not easy to identify this band with certainty, since it is difficult to decompose the observed spectra into clearly defined rotational bands. If this state were at an excitation of ~ 1.6 MeV, the $2+$, $3+$, and $4+$ members of the rotational band would be expected to have cross sections of 133, 48, and $28 \mu b/sr$ in the (d, t) reaction and 2, 48, and $17 \mu b/sr$ in the (d, p) reaction, respectively, assuming an admixture of only 75 % for the $1/2 - [521] - 5/2 - [512]$ component. There is no unique group of levels which meets all the requirements exactly, but there are two sets of levels which fit roughly into bands and have cross sections comparable to those expected. Three states at approximately 1607, 1699, and 1803 keV have cross sections of 167, ~ 34 , and $\sim 30 \mu b/sr$ in the (d, t) reaction and ~ 3 , 33, and $\sim 6 \mu b/sr$ in the (d, p) process, respectively. Another set of levels found at 1660, 1750, and 1855 keV has (d, t) cross sections of 158, ~ 14 , and $\sim 7 \mu b/sr$ and (d, p) cross sections of 20, 32, and $\sim 3 \mu b/sr$, respectively. As stated above, these states do not fit exactly the expectations, but it is noted that they are the only ones with reasonable intensities for the state in question. The levels at 1607 and 1660 keV are the only ones with (d, t) cross sections greater than $\sim 20 \mu b/sr$ until an excitation energy of ~ 2.5 MeV is reached. The peak in the (d, t) spectrum corresponding to a level at 1660 keV is broader than others nearby and thus probably includes more than one group. Therefore the first set of levels mentioned above is in better agreement with expectations than the second. However, there are also other reasons for choosing the 1607 keV band for the $K\pi = 2+$ band in question.

If there is some of the $K\pi = 2+$ two-quasiparticle state $5/2 - [512] - 1/2 - [521]$ mixed into the γ -vibration, some of the γ -vibration could be mixed into the two-neutron state. Hence, one might expect a small (d, d') population for the spin 2 member of the band at 1607 keV. It is seen that there is a small peak in the (d, d') spectrum at about this energy, which supports the assign-

ment. It is also noted that OTTESON¹⁰⁾ has studied the ^{172}Tm decay and found a $K\pi = 2+$ band where the $2+$, $3+$, and $4+$ members coincide, within errors, with those discussed above. On the basis of transitions seen in the decay, this band was assigned to be the $5/2 - [512] - 1/2 - [521]$ configuration. The rotational energies in the band deviate considerably from the simple $I(I+1)$ dependence, but this might not be too surprising when one considers that there are several rotational bands with positive parity in this region of excitation energies.

There are four triton groups in the spectrum of Fig. 3, which correspond to levels at energies of 2008, 2046, 2109, and 2193 keV. These groups resemble the pattern expected for the $K\pi = 1+$, $5/2 - [512] - 3/2 - [521]$ band for which the spin 1, 2, 3, and 4 members have predicted cross sections of 50, 50, 47, and 40 $\mu\text{b}/\text{sr}$, respectively. The observed intensities are 12, ~ 11 , 20, and < 14 $\mu\text{b}/\text{sr}$ and thus, if this set of levels is due to the configuration suggested, only a fraction of the single-particle strength is present.

As seen in the spectrum of Fig. 3, there are many strongly populated states above an excitation energy of 2 MeV. It is reasonable to expect that some of the lowest of these are states formed by stripping a $1/2 - [510]$ or $3/2 - [512]$ neutron, as these are the next lowest Nilsson states which have large values of $C_{j\ell}^2\varphi_l$. However, if one tries to compare the observations with predictions, it immediately becomes clear that the situation is complex. For instance, the stripping of a $1/2 - [510]$ neutron should yield a $K\pi = 1+$ band with cross sections for the $1+$, $2+$, $3+$, and $4+$ members of approximately 45, 150, 70, and 30 $\mu\text{b}/\text{sr}$, respectively, and a $K\pi = 0+$ band whose $0+$, $1+$, $2+$, $3+$, $4+$, $5+$, and $6+$ spin members should have cross sections of 2.5, 120, 135, 34, 14, 1, and 0.2 $\mu\text{b}/\text{sr}$, respectively. The transfer of neutrons into states which lie higher in the Nilsson scheme takes place with similar, or larger, cross sections. However, the large peaks in Fig. 3 corresponding to ~ 2.5 MeV excitation have cross sections of 50 to 80 $\mu\text{b}/\text{sr}$ and are much too weak to represent a pure state of this nature. Hence, it appears that a situation similar to that observed in the odd Yb nuclei²⁾ prevails, whereby the states become strongly mixed and the intensity for a particular transfer process is distributed over several levels, resulting in a corresponding increase in the density of levels populated.

4.7. Other Levels in ^{174}Yb

The data pertaining to ^{174}Yb are more ambiguous than those for ^{172}Yb because only the (d, d') and (d, p) reactions were used. The ground state of ^{173}Yb is the $5/2 - [512]$ orbital and thus all two-quasiparticle states in ^{174}Yb

which are populated by the (d, p) reaction involve this neutron. The stripping cross sections to rotational bands based on states at 0, 1320, and 1630 keV have already been discussed. Another level at ~ 1518 keV has previously been observed^{11, 12, 13)} in the decays of ^{174}Lu and ^{174}Tm , and there are differences of opinion as to whether it is the $K\pi = 6+, 5/2 - [512] + 7/2 - [514]$ or the $K\pi = 7-, 5/2 - [512] + 9/2 + [624]$ state. One positive piece of information which favours the first choice is that the 994 keV gamma transition leading to the $6+$ member of the ground state rotational band has an internal conversion coefficient which indicates that its multipolarity is $E2^{13)}$. However, it is possible that both states may exist at ~ 1520 keV excitation and are populated differently in the two decay processes.

If the $6+$ assignment is correct, one would expect to observe (d, p) cross sections to the spin 6 and 7 members of the rotational band of approximately 20 and $16 \mu\text{b}/\text{sr}$, respectively. There is a proton group populating a state at ~ 1509 keV with an intensity of $17 \mu\text{n}/\text{sr}$, which could be the $6+$ state, although the energy deviation from the previous value is slightly larger than the expected experimental error. The proton group populating the level at ~ 1667 keV has been partly ascribed to the spin 6 member of the band based at 1320 keV. However, there is $\geq 10 \mu\text{b}/\text{sr}$ of this peak left unassigned, which could be due to the spin 7 member of the $K\pi = 6+$ band. This choice would correspond to an inertial parameter $\hbar^2/2 \mathfrak{J}$ of ~ 11.5 keV, which would be quite reasonable for the $5/2 - [512] + 7/2 - [514]$ state.

If the $K\pi = 7-$ state were found at ~ 1520 keV, one would expect (d, p) cross sections to the spin 7, 8, and 9 members of $\sim 5, 10,$ and $16 \mu\text{b}/\text{sr}$, respectively. If the peak at ~ 1723 keV were due to the spin 8 member and part of that at 1947 keV due to the spin 9 member, the value of $\hbar^2/2 \mathfrak{J}$ would be ~ 12.5 keV, which is rather high for this two-quasiparticle state. One cannot, however, exclude the possibility that the spin 8 member is unresolved from the strongly populated state at 1702 keV and the spin 9 member is included in the peak at ~ 1926 keV. Thus it is seen that the (d, p) data give some support to the assignment of the $K\pi = 6+$ state at ~ 1520 keV, but do not exclude the possibility that the $K\pi = 7-$ state may be present at about the same excitation energy.

It was seen that about half the intensity of the $K\pi = 2+, 5/2 - [512] - 1/2 - [510]$ two-quasiparticle state was found in the γ -vibration at 1630 keV. This combination involves the stripping of a $1/2 - [510]$ neutron which occurs with large cross sections. It should therefore be easy to find the remainder of the strength to the $K\pi = 2+$ band and also to the $K\pi = 3+$ band which is formed by coupling the same two neutrons with their spins parallel to

each other. In the spectrum of Fig. 4, a number of strong proton groups are seen with excitation energies between 2.1 and 2.5 MeV. The expected cross sections for a pure $K = 2$ state formed by stripping a $1/2 - [510]$ neutron in this region of excitation energies are 111, 129, and $69 \mu b/sr$ for the spin 2, 3, and 4 members, respectively. The $K = 3$ band would be expected to have cross sections of 154, 133, and $41 \mu b/sr$ to the 3, 4, and 5 spin members, respectively. As about half of the strength of the $K = 2$ state is found in the γ -vibration, the $K = 3$ band is expected to have the largest peaks. It is seen that none of the peaks is quite as large as the predicted intensities for the $K = 3$ band, but the states at 2284, 2370, and 2482 keV have cross sections of 95, 67, and $26 \mu b/sr$, respectively. These levels probably represent the 3, 4, and 5 spin members of a band which contains about 60 % of the $K\pi = 3+, 5/2 - [512] + 1/2 - [510]$ configuration.

There are remaining peaks corresponding to states at 2189, 2237, and ~ 2333 keV which have an intensity pattern resembling that of the spin 2, 3, and 4 members based on the γ -vibration. The absolute cross sections to these levels are consistent with those one would expect for a band containing approximately one-half of the $5/2 - [512] - 1/2 - [510]$ state. Further evidence for this suggested assignment is presented by the (d, d') spectrum which, in analogy to ^{172}Yb , shows small peaks at the excitation energies of the proposed spin 2 and 4 members.

The assignments discussed in this section must be regarded as being rather tentative. Some of the ambiguities could be removed by a careful study of the angular distributions of the strong peaks preferably with better resolution.

Summary

The low-lying levels in even-even Yb nuclei have been studied by the single-neutron transfer processes (d, p) and (d, t) , and by the inelastic scattering process (d, d') . The characteristics of these reactions are fairly well known from studies on other nuclei and therefore the main effort in the present work was directed toward the extraction of a maximum amount of information about the levels in the even Yb nuclei from the observed cross sections. Particular emphasis has been placed on the decomposition of the nuclear states in terms of two-quasiparticle excitations. For this purpose it was important that the collective states built on the ground state could be identified from the (d, d') experiments.

In some cases, the absolute values of the cross sections for stripping

reactions leading to the ground state in the even nuclei did deviate from those calculated on the basis of the cross sections for the inverse transfer process leading to the odd nucleus. The origin of this discrepancy is not clear, but it might partly be connected with imperfections in the DWBA procedure used in the comparison of the cross sections. In other cases, however, the populations of ground state $K = 0$ bands yielded values of $U^2(v)$ and $V^2(v)$ for orbitals involved in the paired ground state, which were in good agreement with the corresponding values obtained from reactions on even target nuclei.

The (d, d') reaction systematically populated the $2+$ and $4+$ members of the $K = 2$ quadrupole vibrations, although the reduced transition probabilities were quite low. In a few cases, a weak population by (d, d') was observed for bands with $K\pi = 0+$. One of the most interesting aspects of the present work is that the (d, p) and (d, t) cross sections to the vibrational bands confirm the validity of considering such states to consist of superpositions of two-quasiparticle states. The present results lend convincing support to the calculated decomposition^{17, 18)} of the vibrations, although the predicted amplitudes often show only qualitative agreement with the measurements.

In all the nuclei, states were observed in the (d, d') reaction which were assigned as octupole vibrations. The collective octupole strength, however, appears to be weak in the Yb-region. In ^{174}Yb , it was possible to identify a two-quasiparticle component in one of the octupole bands, which indicated that the octupole state with lowest energy has $K\pi = 2-$.

In ^{172}Yb , the nature of several states has been definitely established. These include states with $K\pi = 0+$ at 1045 keV, $K\pi = 3+$ at 1172 keV, and $K\pi = 2+$ at 1607 keV. In addition, several other states whose assignments are not so certain have been observed, including a possible $K\pi = 1+$ level at 2008 keV. In ^{170}Yb and ^{174}Yb , several levels have been tentatively assigned as two-quasiparticle states, sometimes with the assistance of previous investigations. It was found that the possibility of using both neutron transfer reactions to populate levels in ^{172}Yb was of considerable importance in eliminating ambiguities in the assignments and, therefore, it was more difficult to study the levels in ^{170}Yb and ^{174}Yb . For these nuclei it would be very helpful to carry out a detailed study of the angular distributions, preferably using better resolution than was employed in the present work.

Acknowledgements

The authors express their gratitude to B. HERSKIND and M. C. OLESEN for assistance in performing some of the measurements and to Mrs. ANNA GRETHE JØRGENSEN for counting the tracks in the photographic emulsions. One of the authors (D. G. B.) wishes to acknowledge financial support in the form of fellowships from the N.A.T.O. and the Alfred P. Sloan Foundation, and is grateful to many staff members at the Niels Bohr Institute for the hospitality which he received during his stay there as a guest.

*The Niels Bohr Institute
University of Copenhagen*

and

*McMaster University
Hamilton, Ontario*

References

- 1) For a recent survey, see e.g. O. NATHAN and S. G. NILSSON, in Alpha-, Beta- and Gamma-Ray Spectroscopy, Vol. 1, K. Siegbahn, Editor, North-Holland Publishing Company, Amsterdam (1965).
- 2) D. G. BURKE, B. ZEIDMAN, B. ELBEK, B. HERSKIND and M. OLESEN, Mat. Fys. Medd. Dan. Vid. Selsk., **35**, no. 2 (1966).
- 3) G. R. SATCHLER, Ann. Phys. **3**, 275 (1958).
- 4) S. G. NILSSON, Mat. Fys. Medd. Dan. Vid. Selsk. **29**, no. 16 (1955).
- 5) R. H. BASSEL, R. M. DRISKO and G. R. SATCHLER, ORNL Report 3240.
- 6) A. BOHR and B. MOTTELSON, Lecture Notes (unpublished) Copenhagen (1963).
- 7) R. GRAETZER, G. B. HAGEMANN and B. ELBEK, Nuclear Physics **76**, 1 (1966).
- 8) Nuclear Data Sheets, Edited by K. WAY. National Academy of Sciences, Washington.
- 9) G. KAYE and R. L. GRAHAM, Bulletin, American Physical Society, Series 2, **9**, 498 (1964).
- 10) O. H. OTTESSEN (unpublished data) private communication from C. W. Reich.
- 11) L. FUNKE, H. GRABER, K. H. KAUN, H. SODAN and L. WERNER, Nuclear Physics **61**, 465 (1965).
- 12) J. KANTELE, Phys. Letters **11**, 59 (1964) and private communication.
- 13) J. PEDERSEN, Thesis, University of Copenhagen (unpublished, 1965).
- 14) H. MORINAGA, Nuclear Physics **75**, 385 (1966).
- 15) B. ELBEK, M. KREGAR and P. VEDELSBY, Nuclear Physics **86**, 385 (1966).
- 16) R. BLOCH, B. ELBEK and P. O. TJÖM, Nuclear Physics A **91**, 576 (1967).
- 17) D. R. BÈS, P. FEDERMAN, E. MAQUEDA and A. ZUKER, Nuclear Physics **65**, 1 (1965).
- 18) V. G. SOLOVIEV, Dubna preprint no. D-2157 (1965).
- 19) Y. YOSHIKAWA, B. ELBEK, B. HERSKIND and M. C. OLESEN, Nuclear Physics **73**, 273 (1965).
- 20) C. J. GALLAGHER, JR. and V. G. SOLOVIEV, Mat. Fys. Skr. Dan. Vid. Selsk. **2**, no. 2 (1962).
- 21) E. VEJE, B. ELBEK, B. HERSKIND and M. C. OLESEN, to be published.
- 22) J. ZYLICZ, M. H. JØRGENSEN, O. B. NIELSEN and O. SKILBREID, Nuclear Physics **81**, 88 (1966).
- 23) P. O. TJÖM and B. ELBEK, Mat. Fys. Medd. Dan. Vid. Selsk. **136**, no. 8 (1967).
- 24) D. G. BURKE et al., to be published.
- 25) M. N. VERGNES and R. K. SHELINE, Phys. Rev. **132**, 1736 (1963).
- 26) C. GÜNTHER, H. BLUMBERG, W. ENGELS, G. STRUBE, J. VOSS, R.-M. LIEDER, H. LUIG and E. BODENSTEDT, Nuclear Physics **61**, 65 (1965).

J. U. ANDERSEN

AXIAL AND PLANAR DIPS IN
REACTION YIELD FOR ENERGETIC
IONS IN CRYSTAL LATTICE

Det Kongelige Danske Videnskabernes Selskab
Matematisk-fysiske Meddelelser **36**, 7



Kommissionær: Munksgaard
København 1967

CONTENTS

	Page
Introduction	3
§ 1. Emission of Particles from a String	3
§ 2. Emission of Particles from a Plane.....	7
§ 3. Thermal Vibrations.....	9
§ 4. Numerical Calculations	11
§ 5. Results of the Numerical Calculations	12
§ 6. Discussion of Results.....	21
References	26

Synopsis

Computer programs have been developed to calculate numerically the dips in yield along low-index directions and planes of energetic positively charged particles emitted isotropically from substitutional sites in a crystal lattice. The calculations are based on Lindhard's theoretical treatment of directional effects and include effects of thermal vibrations of the emitting atoms. The obtained intensity distributions also give the nuclear reaction yield as a function of the direction of an incident beam.

Introduction

During the last few years, directional effects connected with the passage of swift charged particles through a crystal lattice have been studied intensively in a number of laboratories, both experimentally and theoretically. Perhaps the most interesting effect observed is the almost complete extinction of nuclear reactions for positively charged particles incident on a single crystal parallel to a low-index direction¹⁾ or plane²⁾. This shadow phenomenon has already been shown to be a very useful tool in solid state investigations³⁾. The present work contains numerical evaluations of some of the related formulas derived in the comprehensive theoretical treatment⁴⁾* given by LINDHARD. Although the main purpose is to give quantitative theoretical estimates, the results of the numerical calculations may also serve as an illustration of the fundamental qualitative aspects of Lindhard's theoretical treatment.

The calculations to be presented in the following are directly concerned with the emission of positively charged particles from lattice sites. The obtained probability distributions for the direction of emergence of the particles from the crystal, however, also give the probability for particles incident on the crystal to hit a lattice atom as a function of the direction of incidence. This may easily be verified by direct calculation, but may also be regarded as a consequence of the reversibility rule discussed in I, § 5.

The first two paragraphs contain the formulas on which the calculations are based. The reader is referred to I for derivation and further discussion of these formulas.

§ 1. Emission of Particles from a String

The basic approximation in I is that of an isolated string of atoms, i.e. the interaction of a particle moving at a small angle to a low-index direction is treated as the interaction of the particle with isolated strings or rows of atoms. This simplifies very much the theoretical description. Furthermore,

* In the following referred to as I.

it is shown in I that this interaction may be treated essentially by classical mechanics*.

As a first approximation (the continuum approximation), the atomic potentials are replaced by an average potential $U(r)$ given by

$$U(r) = \int_{-\infty}^{\infty} \frac{dz}{d} V(\sqrt{r^2 + z^2}), \quad (1)$$

where r is the distance from the string, $V(R)$ the atomic potential, and d the distance between atoms in the string. In this approximation, the transverse energy of a particle $E_{\perp} = E\varphi^2 + U(r)$ is conserved in a collision with a string.

In I, Appendix A, this description is refined by considering the transverse energy at the planes perpendicular to the string half-way between atoms. It is shown in a direct way that the transverse energy defined in this way is approximately conserved when the angle between the particle path and the string is small.

On the basis of this approximation, the emission of a particle from a string atom is considered in I, § 6. The particle motion is divided into three stages:

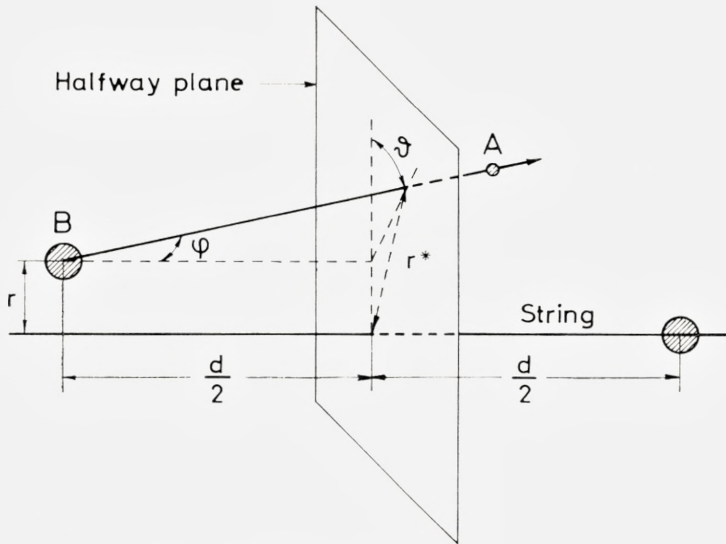
- a) Emission from the string atom
- b) Passage through the crystal lattice
- c) Transmission through the crystal surface.

Figure 1 illustrates the calculation of the distribution in transverse energy after stage a). The particle A with energy E is emitted from atom B. The angle of emission is φ and ϑ is the azimuthal angle of emission. At the moment of emission, the atom is at a distance r from an otherwise perfect string. Thus, the thermal vibrations of all string atoms except the emitting atom are neglected, whereas the thermal vibrations of the emitting atom are represented by a probability distribution for r , $dP(r)$, which is taken as a Gaussian:

$$dP(r) = e^{-r^2/\varrho^2} \frac{d(r^2)}{\varrho^2} \cdot \alpha, \quad (2)$$

where $\alpha \simeq 1$ is a normalization constant and ϱ^2 the mean square displacement perpendicular to the string.

* For a general quantum mechanical treatment, the reader is referred to ref. 5).



$$E_{\perp} = E\varphi^2 + U(r^*)$$

$$r^{*2} = r^2 + \left(\frac{\varphi d}{2}\right)^2 + r\varphi d \cos \vartheta$$

Fig. 1. Emission of particle from string atom.

The emission is assumed to be isotropic. Consequently, the probability distribution for φ is proportional to φ (for small angles φ) and for ϑ a constant. The transverse energy of the emitted particle is calculated at the half-way plane as the sum of the transverse kinetic energy $E\varphi^2$, and the transverse potential energy $U(r^*)$.

From this, an expression for the distribution in transverse energy after stage a) is derived*:

$$\Pi_{\text{out}}(E_{\perp}) = \int_{r=0}^{r_0} dP(r) \int d(E\varphi^2) \int_0^{2\pi} \frac{d\vartheta}{2\pi} \cdot \delta(E_{\perp} - U(r^*) - E\varphi^2). \quad (3)$$

Here, r_0 is given by $\pi r_0^2 = (Nd)^{-1}$, where N is the number of atoms per cm^3 and d the distance between the atoms on the string. The other parameters are indicated in Fig. 1.

* Here, and in the following, the probability distributions are normalized to the random case, i.e. to $U(r) \equiv 0$.

According to I, Appendix A, the transverse energy of the particle is not changed by collisions with perfect strings. In the following, we neglect the change in transverse energy during stage b) of the motion caused by thermal vibrations of the atoms on the strings and assume strict conservation of transverse energy in stage b).

Stage c) of the particle motion is the transmission through the crystal surface. The transverse energy $E\psi_e^2$ of a particle, which has been transmitted through the crystal surface at a distance r from a string, is given by $E\psi_e^2 = E_\perp - U(r)$, where E_\perp is the transverse energy before the transmission. Consequently, the distribution in transverse energy outside the crystal surface $P_e(E\psi_e^2)$ becomes

$$P_e(E\psi_e^2) = \int dE_\perp \Pi_{\text{out}}(E_\perp) T(E\psi_e^2, E_\perp), \quad (4)$$

where the transmission factor $T(E\psi_e^2, E_\perp)$ is given by

$$T(E\psi_e^2, E_\perp) = \int_0^{r_0} \frac{d(r^2)}{r_0^2 - \hat{r}^2(E_\perp)} \delta(E_\perp - E\psi_e^2 - U(r)). \quad (5)$$

Here, $\hat{r}(E_\perp)$ is defined by $U(\hat{r}(E_\perp)) = E_\perp$.

The transmission factor $T(E\psi_e^2, E_\perp)$ is analogous to I, eq. (6.1), the transmission factor for particles incident on a crystal surface. The only difference is that r_0^2 in the denominator is replaced by $r_0^2 - \hat{r}^2(E_\perp)$ because the particle motion is restricted to that part of the transverse plane where $E_\perp > U(r)$.

From (4) and (5) we get

$$P_e(E\psi_e^2) = \int_0^{r_0} \frac{d(r^2)}{r_0^2 - \hat{r}^2(E\psi_e^2 + U(r))} \Pi_{\text{out}}(E\psi_e^2 + U(r)). \quad (6)$$

Formula (3) is in I treated analytically in the continuum approximation: $r^* = r$, and an explicit expression for $\Pi_{\text{out}}(E_\perp)$ is derived, using the standard potential I, eq. (2.6):

$$U(r) = \frac{1}{2} E\psi_1^2 \cdot \log \left(\left(\frac{Ca}{r} \right)^2 + 1 \right), \quad (7)$$

where

$$\psi_1 = \left(\frac{2Z_1 Z_2 e^2}{d \cdot E} \right)^{1/2};$$

a is the Thomas-Fermi screening radius and $C \simeq \sqrt{3}$. The result is

$$I_{\text{out}}(E_{\perp}) = \exp \left\{ -\frac{C^2 a^2}{\varrho^2} (e^{E\psi_1^2} - 1)^{-1} \right\} - \exp \left\{ -\frac{r_0^2}{\varrho^2} \right\}. \quad (8)$$

Furthermore, a qualitative estimate, I, eq. (6.12), of the integrated dip is given:

$$\Omega \simeq \pi \cdot \frac{\psi_1^2}{2} \cdot \log \frac{\gamma C^2 a^2 + \varrho^2}{\varrho^2}, \quad (9)$$

where $\gamma = 1.78$ is Euler's constant.

Except at low energies, where $\psi_1 \gtrsim a/d$, formula (8) gives a good approximation for the width of the dip and its dependence on the vibrational amplitude ϱ . The important feature of compensation, however, is missing in this continuum description. The accuracy of the formulas (8) and (9) is further discussed in § 5.

§ 2. Emission of Particles from a Plane

A similar, but weaker correlation of successive small angle scattering events exists for a particle moving at a small angle to a low-index crystal plane. The scattering of the particle by a plane of atoms may, as a first approximation, be treated as the motion in an average planar potential:

$$Y(y) = N \cdot d_p \int_0^{\infty} 2\pi r dr V(\sqrt{y^2 + r^2}), \quad (10)$$

where $N \cdot d_p$ represents the atomic density in the plane, N being the number of atoms per cm^3 and d_p the distance between planes. In this approximation, the transverse energy $E_{\perp} = E\varphi^2 + Y(y)$ of a particle with respect to a plane is conserved.

In the string case, the continuum description was improved by measuring the transverse energy at the half-way planes. A similar refinement is not straightforward in the planar case because of the less well-defined correlation between successive scattering events. The need for such a refinement is, however, smaller in the planar case since the planar potential decreases more slowly with distance than the string potential, and the critical angles for planes are smaller. Furthermore, the compensation of the dip is already contained in the continuum description of the planar case as may easily

be seen by integrating formula (12) with respect to E_{\perp} . Consequently, in the following, the planar case is treated in the continuum approximation.

Formulas for the distribution in transverse energy of particles emitted from a planar atom are not given explicitly in I but may easily be derived in analogy to the string case. Again, zero-point and temperature vibrations are represented by a Gaussian distribution of the distance y of the emitting atom from the plane at the moment of emission:

$$dP(y) = \frac{2}{\sqrt{\pi}} e^{-y^2/\varrho^2} dy \frac{\alpha}{\varrho}, \quad (11)$$

where α is a normalization constant, $\alpha \simeq 1$, and ϱ^2 is the mean square displacement perpendicular to the plane. If the emission is assumed to be isotropic, the probability distribution for the angle of emission φ is a constant (for small angles φ).

The transverse E_{\perp} of the emitted particle is the sum of the transverse kinetic energy $E\varphi^2$, where E is the energy of the emitted particle, and the transverse potential energy $Y(y)$. Thus, the distribution in transverse energy $\Pi_{\text{out}}(E_{\perp})$ after stage a) becomes

$$\left. \begin{aligned} \Pi_{\text{out}}(E_{\perp}) &= \int_0^{a_p/2} dP(y) \int d(E\varphi^2) \left(\frac{E_{\perp}}{E\varphi^2} \right)^{1/2} \delta(E_{\perp} - E\varphi^2 - Y(y)) \\ &= \int_{\hat{y}(E_{\perp})}^{a_p/2} dP(y) \left(\frac{E_{\perp}}{E_{\perp} - Y(y)} \right)^{1/2}, \end{aligned} \right\} \quad (12)$$

where $\hat{y}(E_{\perp})$ is given by $Y(\hat{y}(E_{\perp})) = E_{\perp}$ for $E_{\perp} < Y(0)$ and $\hat{y}(E_{\perp}) = 0$ for $E_{\perp} > Y(0)$.

Again, we neglect the redistribution in transverse energy in stage b) and only consider stage c), the transmission through the crystal surface. This is complicated by the fact that in statistical equilibrium, the probability distribution $P_0(E_{\perp}, y)$ for the distance y of a particle with given transverse energy E_{\perp} from a plane is not constant as in the two-dimensional string case, but inversely proportional to the square root of the transverse kinetic energy (I, eq. (3.2)):

$$P_0(E_{\perp}, y) = \left. \begin{cases} \frac{K}{d_p} \cdot \left(\frac{E_{\perp}}{E_{\perp} - Y(y)} \right)^{1/2} & \text{for } E_{\perp} > Y(y) \\ 0 & \text{for } E_{\perp} < Y(y) \end{cases} \right\} \quad (13)$$

where K is a normalization constant, $K = K(E_{\perp})$, given by

$$K(E_{\perp}) = \left(\int_{\hat{y}}^{\hat{a}_p/2} \frac{dy}{d_p} \left(\frac{E_{\perp}}{E_{\perp} - Y(y)} \right)^{1/2} \right)^{-1}. \quad (14)$$

The transmission factor $T(E\psi_e^2, E_{\perp})$ thus becomes:

$$\left. \begin{aligned} T(E\psi_e^2, E_{\perp}) &= \int_0^{\hat{a}_p/2} dy P_0(E_{\perp}, y) \delta(E_{\perp} - E\psi_e^2 - Y(y)) \\ &= K \cdot \int_{\hat{y}(E_{\perp})}^{\hat{a}_p/2} \frac{dy}{d_p} \left(\frac{E_{\perp}}{E_{\perp} - Y(y)} \right)^{1/2} \delta(E_{\perp} - E\psi_e^2 - Y(y)). \end{aligned} \right\} \quad (15)$$

From this we get the distribution in transverse energy outside the crystal:

$$\left. \begin{aligned} P_e(E\psi_e^2) &= \int dE_{\perp} \Pi_{\text{out}}(E_{\perp}) T(E\psi_e^2, E_{\perp}) \\ &= \int_0^{\hat{a}_p/2} \frac{dy}{d_p} K(E\psi_e^2 + Y(y)) \cdot \left(\frac{E\psi_e^2 + Y(y)}{E\psi_e^2} \right)^{1/2} \Pi_{\text{out}}(E\psi_e^2 + Y(y)). \end{aligned} \right\} \quad (16)$$

§ 3. Thermal Vibrations

In the above formula, an Einstein model of independently vibrating lattice atoms is assumed. Furthermore, the vibrations of all atoms except the emitting atom are neglected. This may be a reasonable first approximation since the vibrations of the other atoms are averaged out when many atoms contribute to the scattering.

The mean square amplitude $\langle R^2 \rangle$ may be estimated from the Debye model (see e.g. ref. 6):

$$\langle R^2 \rangle = \frac{9\hbar^2}{M\kappa T_D} \left\{ \frac{1}{4} + \frac{1}{X_D} \Phi(X_D) \right\}, \quad (17)$$

where M is the atomic mass of the crystal atoms, \varkappa is Boltzmann's constant, T_D the Debye temperature, and X_D defined by $X_D = T_D/T$. The function $\Phi(X_D)$ is defined by

$$\Phi(X_D) = \frac{1}{X_D} \int_0^{X_D} \frac{x dx}{e^x - 1}. \quad (18)$$

Φ is tabulated in e.g. ref. 7).

From (17), $\langle R^2 \rangle$ may be calculated as a function of the absolute temperature T . For $T < T_D$, the term $1/4$ from zero-point vibrations dominates, and for $T > T_D$, $\langle R^2 \rangle$ is proportional to T .

For the mean square vibration perpendicular to a string or a plane, we have $\langle r^2 \rangle = 2/3 \langle R^2 \rangle$ and $\langle y^2 \rangle = 1/3 \langle R^2 \rangle$, respectively. From these relations, and from (17), the parameter ϱ in formulas (2) and (11) may be estimated.

Since the nearest neighbour plays a dominating part in the interaction of the emitted particle with the string or plane, it may be of interest to estimate the correlation between the vibrations of neighbouring atoms. This may be done⁸⁾ on the basis of a formalism as developed in ref. 6). If $u_\alpha(\vec{r})$ is the α -component of the displacement operator at the position \vec{r} , a correlation coefficient β for the α -components of the vibrations of the neighbouring atoms is defined by:

$$\beta = \frac{\langle u_\alpha(\vec{r}) u_\alpha(\vec{r} + \vec{d}) \rangle}{\langle u_\alpha(\vec{r})^2 \rangle}, \quad (19)$$

where \vec{d} is the distance vector between the two neighbouring atoms. As usual, $\langle \rangle$ denotes the expectation value.

In ref. 8), this correlation coefficient is estimated in two limits: $T \ll T_D$ and $T \gg T_D$, in the Debye approximation:

$$T \ll T_D: \beta \simeq 2(1 - \cos(k_D \cdot d)) / (k_D \cdot d)^2 \quad (20)$$

$$T \gg T_D: \beta \simeq \frac{\pi}{2} \cdot (k_D \cdot d)^{-1} \quad (21)$$

Here, k_D is defined by $k_D = (6\pi^2/V_0)^{1/3}$, where V_0 is the volume of the unit cell.

If we set $d = V_0^{1/3}$ and disregard the cosine term in (20), we get in the two limits $\beta \simeq 0.13$ and $\beta \simeq 0.40$, respectively. It is seen that, despite the correlation, the mean square relative displacement in both limits is larger than the mean square absolute displacement. In consequence, it seems justified to neglect the correlation in the present approximation.

§ 4. Numerical Calculations

String case

The intensity distribution (6) is calculated by simulating emission of particles from a vibrating string atom. First, the intensity distribution (3) is calculated. The three parameters (cf. Fig. 1), r , ϑ , and φ are varied independently in steps: $r : (1-25) \cdot \varrho/10$, $\vartheta : (1-10) \cdot \pi/10$, $\varphi : (1-50) \cdot \psi_1/10$. For each set of parameter values, the transverse energy E_{\perp} of the particle is calculated from the relation $E_{\perp} = E\varphi^2 + U(r^*)$. (Lindhard's standard potential (7) has been applied with $C = \sqrt{3}$). Thereby, the emission angle ψ is determined through the relation $E\psi^2 = E_{\perp}$, and ψ is approximated by an integral multiple of $\psi_1/10$. The emission spectrum is obtained, each event being weighted by a factor $2\varphi \cdot r/\varrho \cdot \exp\{-r^2/\varrho^2\}$, which accounts for the probability distribution of the parameters r , ϑ , and φ .

In the last part of the program, the change in the angular distribution in stage c) – the transmission through the surface – is calculated from (6). For simplicity, $r_0^2 - \hat{r}^2$ has been replaced by r_0^2 in the program. This introduces an error of at most a few per cent for some values of the emission angle. The angle of emergence ψ_e is also approximated by an integral multiple of $\psi_1/10$.

The program contains four external parameters: $P1 = Ca/d$, $P2 = \varrho/d$, $P3 = \psi_1$, and $P4 = \pi r_0^2/d^2$. The last parameter only influences the second part of the calculation, transmission through the surface. Furthermore, the intensity distribution before this transmission has an important similarity property. As a function of ψ/ψ_1 , the distribution only depends on the two parameters $P1/P2 = Ca/\varrho$ and $P2/P3 = \varrho/d\psi_1$. This may be compared to the probability distribution (8) obtained in the continuum approximation. This distribution depends only on one parameter, Ca/ϱ .

The program has been used at the GIER computer at the University of Aarhus. For one set of external parameters, the calculation takes ~ 5 minutes.

Planar case

In this case, the integrals in (12), (14), and (16) are calculated directly. The potential used is the continuum planar potential obtained by introducing Lindhard's standard potential I, eq. (2.6'') in (10):

$$Y(y) = 2\pi Z_1 Z_2 e^2 N d_p [(y^2 + C^2 a^2)^{1/2} - y] \quad (22)$$

with $C = \sqrt{3}$.

It would have been more correct to use a potential

$$\hat{Y}(y) = Y(y) + Y(d_p - y). \quad (23)$$

However, the two potentials only differ appreciably for $y \approx d_p/2$, and the correction will therefore be of minor importance.

If a distance d is introduced by

$$N \cdot d_p \cdot d^2 = 1 \quad (24)$$

and an angle ψ_p by

$$\psi_p = \left(\frac{2Z_1 Z_2 e^2}{d \cdot E} \right)^{1/2} \cdot \sqrt{\frac{Ca}{d}}, \quad (25)$$

(22) is transformed into

$$Y(y) = \pi \cdot E \cdot \psi_p^2 \cdot \left[\left(\frac{y^2}{(Ca)^2} + 1 \right) - \frac{y}{Ca} \right]. \quad (26)$$

It is easily seen from formulas (24), (25), (26) and from (10), (12), (14), and (16) that the shape of the intensity distribution only depends on two parameters: $p1 = Ca/\rho$ and $p2 = Ca/d_p$. For fixed values of these two parameters, the planar dips are similar with scaling factor ψ_p . Essentially, the parameter $p2$ only influences the surface transmission so that, analogously to the continuum description of the string case (8), the intensity distribution as a function of ψ/ψ_p before transmission through the surface only depends on one parameter Ca/ρ .

This program has also been used at the GIER computer at the University of Aarhus. For one set of parameter values, the calculation takes ~ 10 minutes.

§ 5. Results of the Numerical Calculations

String case

As mentioned above, the string dip is essentially determined by the relative magnitude of the three parameters, $P1$, $P2$, and $P3$. The influence of the fourth parameter, $P4 = \pi r_0^2/d^2$ is illustrated in Fig. 2, which shows how the transmission through the surface of the crystal changes the angular distribution. It is seen that the transmission almost exclusively influences the intensity at the bottom of the dip.

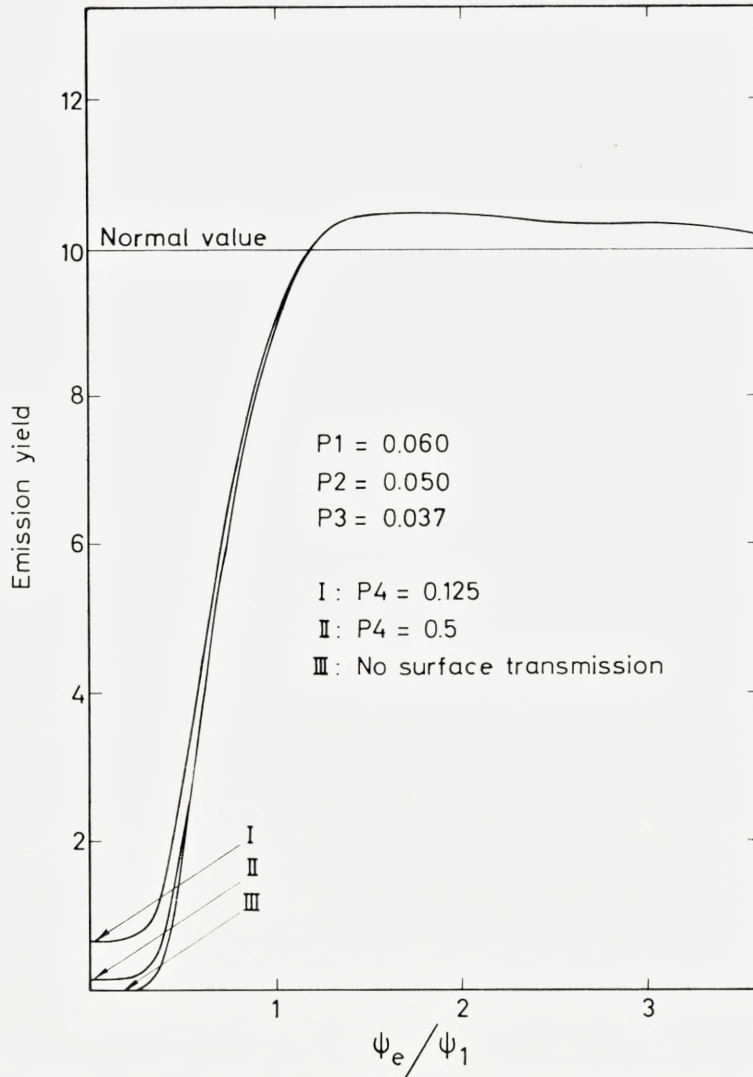


Fig. 2. Influence of the surface transmission on the angular distribution illustrated by the emission of 500 keV protons from a $\langle 100 \rangle$ string in tungsten at 1470°K . Actual value of $P4$ is 0.5.

The most important parameter is $P3 = \psi_1$. In the continuum approximation (8), angular distributions for different values of ψ_1 are similar, with scaling factor ψ_1 . In the present calculation, the similarity is broken. This

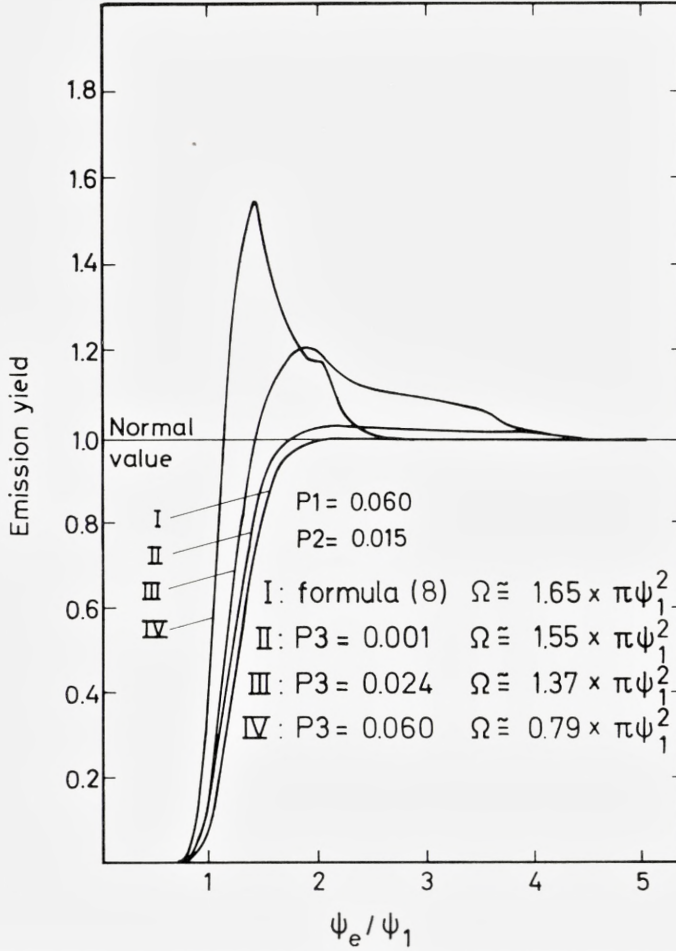


Fig. 3. Illustration of the deviations from similarity of angular distributions for varying $P3 = \psi_1$. Values of $P1$ and $P2$ correspond to emission of protons from a $\langle 100 \rangle$ string in tungsten at $\sim 100^\circ$ K. Values II, III, and IV of ψ_1 correspond to proton energies of 700 MeV, 1.2 MeV, and 0.2 MeV, respectively. Ω is the integrated (two-dimensional) dip.

is illustrated in Fig. 3, which shows angular distribution before surface transmission for fixed values of $P1 = Ca/d$ and $P2 = q/d$ and varying $P3$. Also shown in the figure is the curve calculated from (8). It is seen that the numerically calculated curves approach this curve for $P3 \rightarrow 0$. In order to compare with the approximation (9) for the integrated dip Ω , this has been calculated for each curve.

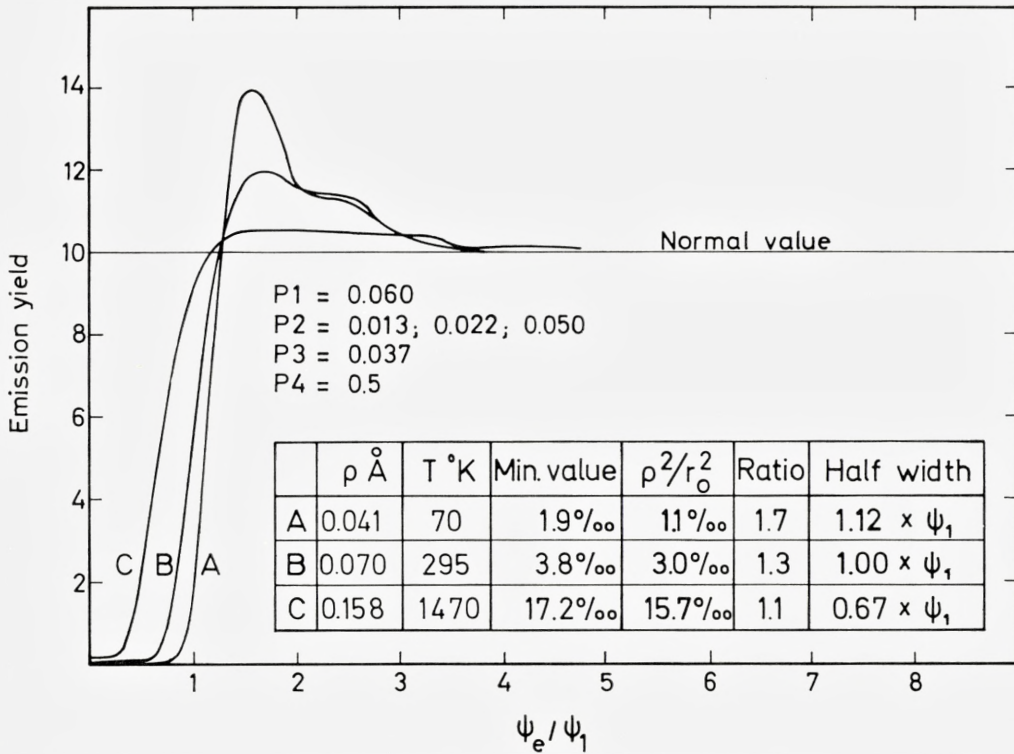


Fig. 4. Influence of vibrational amplitude ϱ on angular distribution of 500 keV protons emitted from a $\langle 100 \rangle$ string in tungsten at different temperatures.

Figure 4 shows how the calculated string dips depend on $P2 = \varrho/d$. The parameters $P1$, $P3$, and $P4$ correspond to 500 keV protons incident on a tungsten crystal along a $\langle 100 \rangle$ direction. The first column in the table in the figure shows the ϱ -values, and the second column the temperatures which, in this case, correspond to the values of the parameter $P2$. The ϱ -dependence of the minimum yield is shown in the third column and compared with the value ϱ^2/r_0^2 , which is the minimum yield calculated in the continuum approximation (I, eq. (6.13)). As expected, the agreement is best for large values of ϱ . The last column in the table shows the variation with ϱ of the width at half minimum of the dip.

Figures 3 and 4 also illustrate the compensation of the dip by an increase in yield at angles slightly larger than the width. The compensation is analogous to the compensation of the classical Rutherford shadow behind an atom

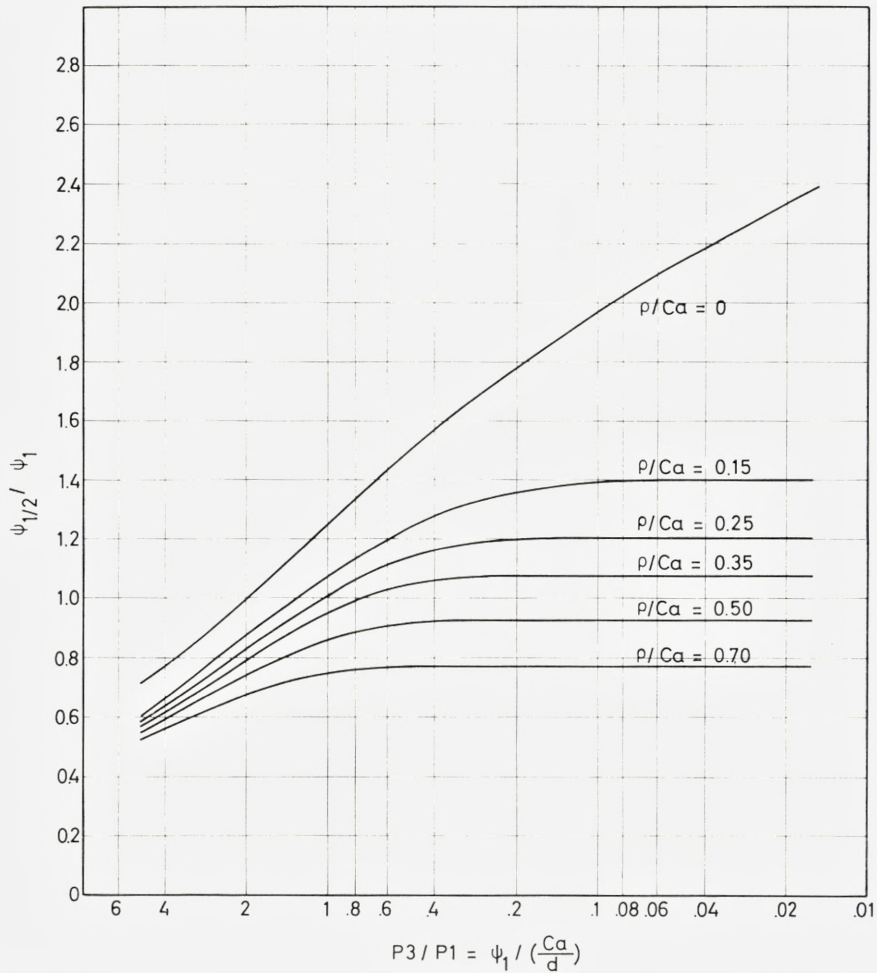


Fig. 5. Semi-logarithmic plot of the calculated half width $\psi_{1/2}$ as a function of the two parameters $\psi_1/(Ca/d)$ and ρ/Ca .

(treated in I, §2). In that case, half the compensation is found at angles $\sim Ca/d$. This feature is easily recognized in Figs. 3 and 4. Another qualitative feature of the compensation is seen. The high and narrow compensating shoulder found at small values of ρ is rapidly smeared out when ρ increases relative to $\psi_1 \cdot d$.

An important parameter, which may be extracted from the calculated curves, is the width at half dip as a function of the relative magnitude of

the three parameters $P1 = Ca/d$, $P2 = \varrho/d$, and $P3 = \psi_1$. In most cases, the surface transmission does not influence the half width very much (cf. Fig. 2). It was therefore not included in the calculations on which Fig. 5 is based. The results are plotted as a family of curves, each characterized by a fixed value of $P1/P2 = \varrho/Ca$. The curves give the half width $\psi_{1/2}$ in units of ψ_1 as a function of $P3/P1 = d\psi_1/Ca$. This family of curves is compared to the curve obtained from I, eq. (A. 19), corresponding to $\varrho = 0$. It is interesting to note that for $\psi_1 < Ca/d$, the ratio $\psi_{1/2}/\psi_1$ is almost constant and close to unity when thermal vibrations are included. As a rule of thumb, the full width at half dip may be taken to be $2\psi_1$ for $\psi_1 \lesssim Ca/d$.

The region $\psi_1 \gg Ca/d$ has not been investigated in detail, mainly because few experiments are performed at very low energies. The calculations may, however, easily be extended to cover this region.

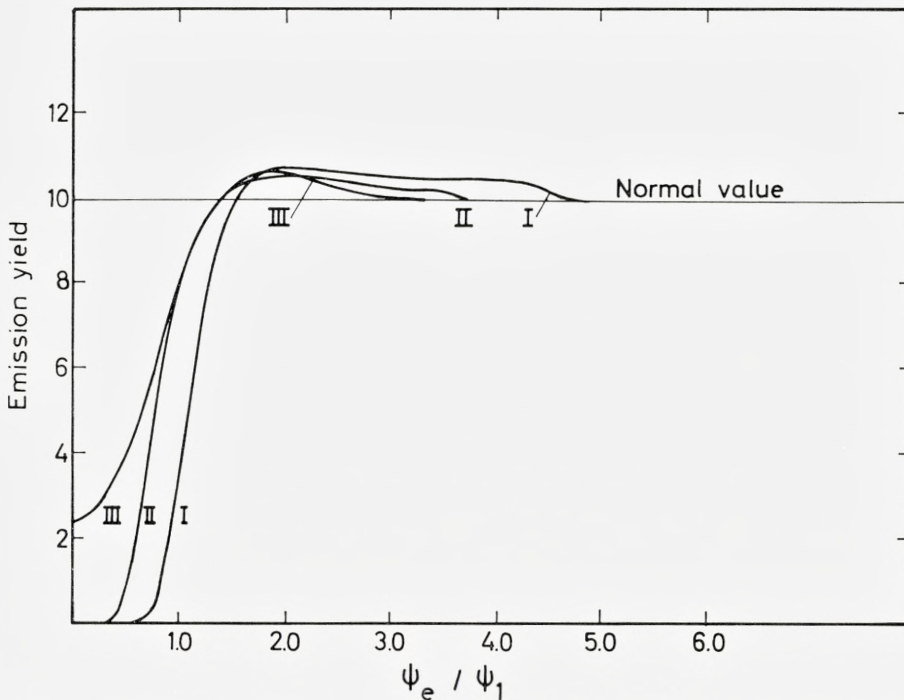


Fig. 6. Comparison of different calculations of the angular distribution of 5.49 MeV alpha particles emitted from a $\langle 111 \rangle$ string in tungsten. Curves I and II are calculated numerically with Lindhard's standard potential and a Bohr potential, respectively. Curve III is calculated by OEN⁹⁾ on the basis of a two-particle model. In all calculations, the value $\varrho = 0.054 \text{ \AA}$ has been used.

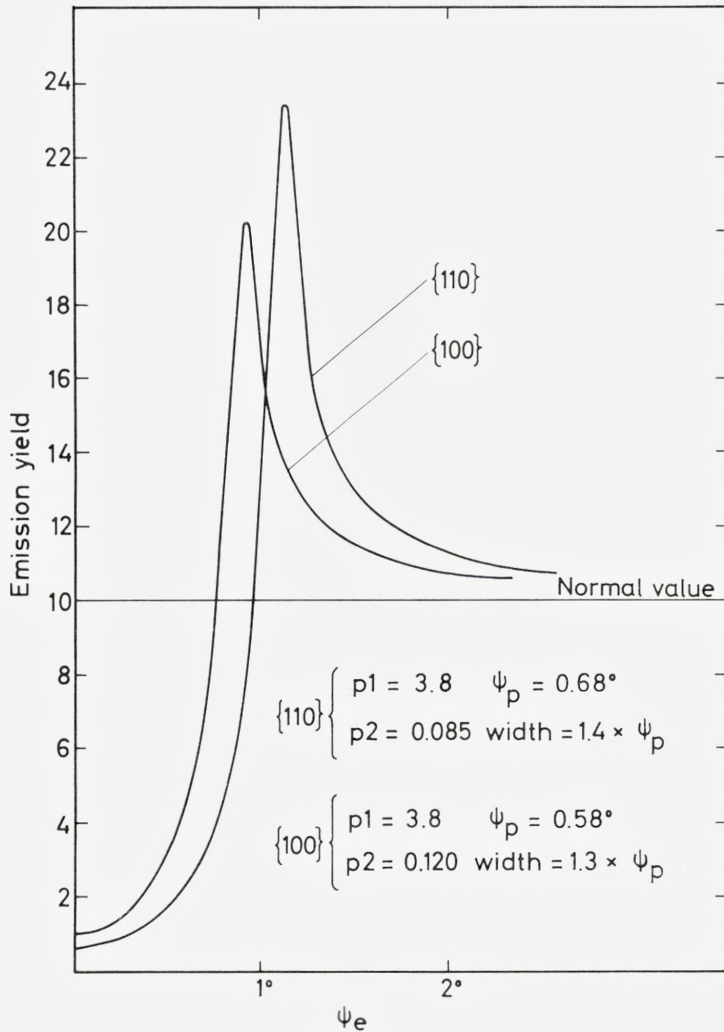


Fig. 7. Angular distribution of 400 keV protons emitted from $\{100\}$ and $\{110\}$ planes in tungsten at room temperature.

Comparison with numerical calculations on the basis of a two-particle model

The influence of thermal vibrations on the classical shadow behind an atom has been numerically evaluated by OEN⁹⁾. In Fig. 6, his results for the shadow behind a single atom are compared to the present results for the shadow behind a string of atoms. The comparison is complicated by the

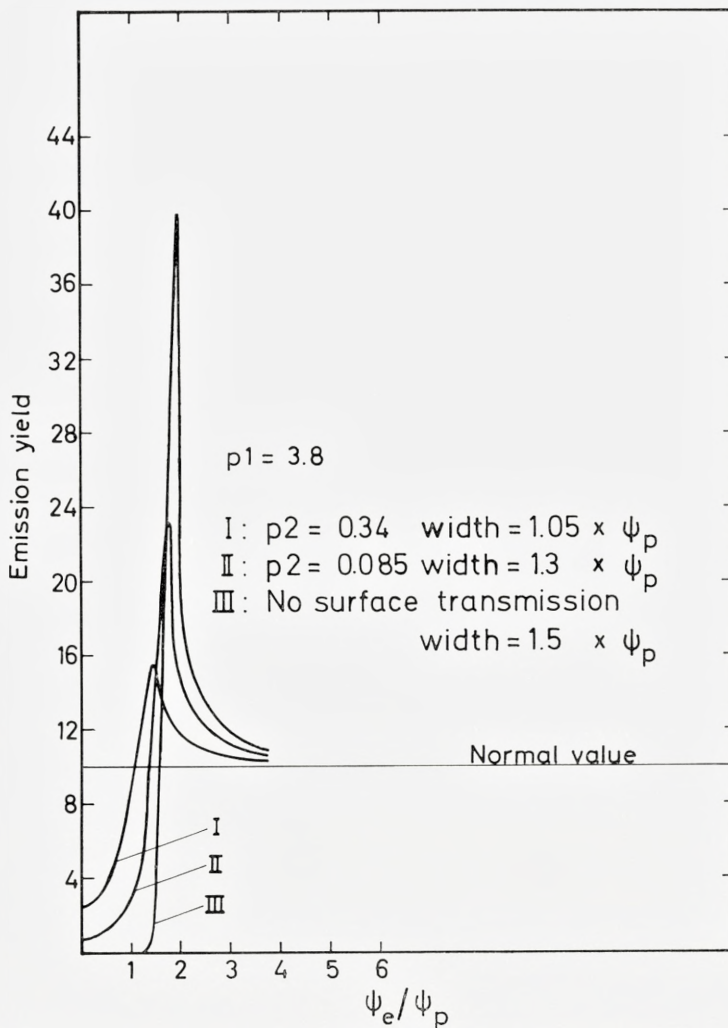


Fig. 8. Influence of the surface transmission on a planar dip illustrated by angular distribution of protons emitted from $\{110\}$ plane in tungsten at room temperature. Actual value of p_2 is 0.085.

difference of the potentials used in the two calculations (OEN uses an exponentially screened potential). The string calculation has therefore been repeated with an exponentially screened potential. The resulting curve is also shown in Fig. 6. It is seen that the width of the dip obtained with a Bohr potential is much smaller than that of the dip obtained with Lindhard's

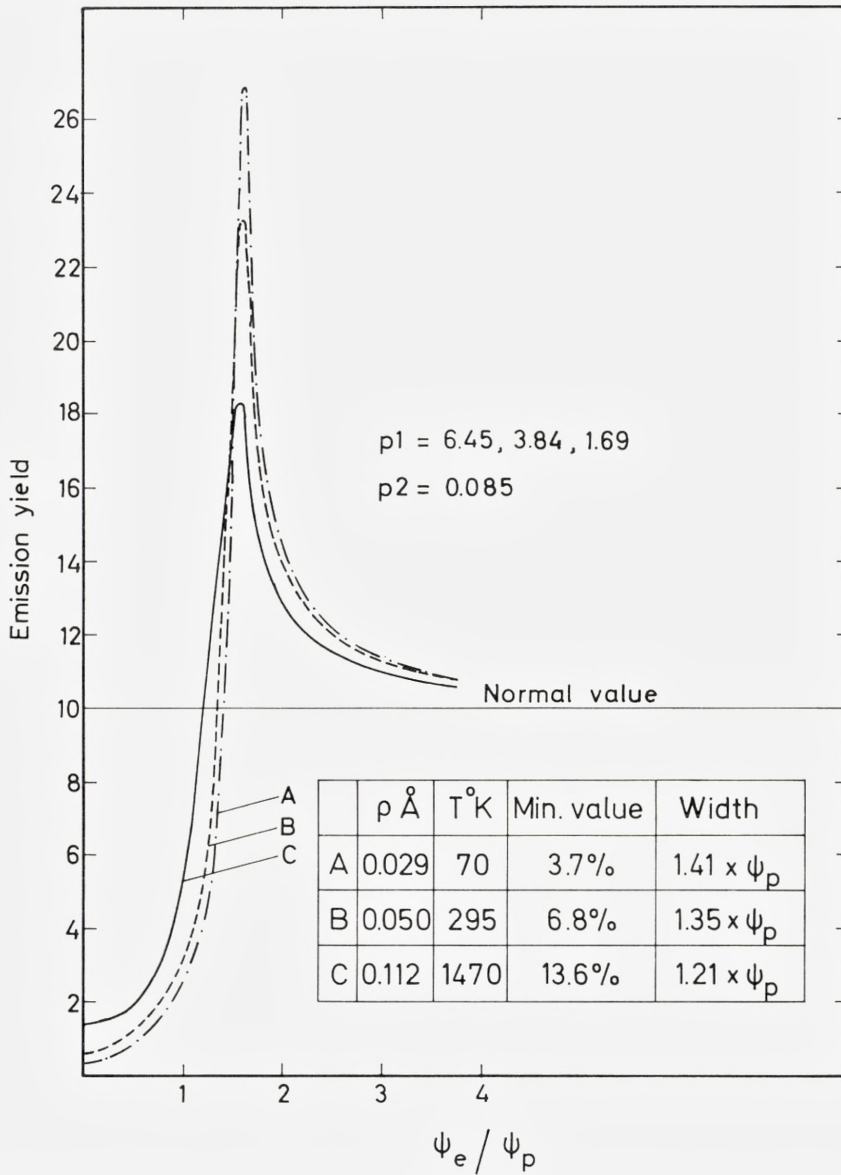


Fig. 9. Dependence on the vibrational amplitude ϱ of a $\{110\}$ planar dip in tungsten.

standard potential. This is not surprising since in the actual case $\psi_1 \sim a/d$, i.e. scattering of the emitted particles at distances $\gtrsim a$ plays an important part, and in this region, the Bohr potential is known to decrease too rapidly.

The difference between curves II and III may be attributed to the scattering from the second, third, etc., neighbour on the string. As expected, the difference is largest for small angles.

Planar case

Two typical planar dips are shown in Fig. 7. We may compare the width at normal value with the respective values of ψ_p given by (25). This comparison is made in the figure. It is seen that ψ_p is a fairly good measure of the width.

Figure 8 illustrates the influence of the transmission through the surface and of the parameter $p2 = Ca/d$. It is seen that the influence of the transmission — as expected — is much larger than in the string case.

Figure 9 shows the dependence on ϱ of a planar dip. The planar dip shows a somewhat weaker ϱ -dependence than does the string dip. The minimum value is changing by a factor of 3.7 compared to a factor of 14.3 in Fig. 4. The width changes with a factor of 0.86 compared to a factor of 0.60 in Fig. 4.

§ 6. Discussion of Results

String case

Before comparing the results of the calculations with experiments, it may be appropriate to discuss briefly the kind of agreement to be expected. For this purpose, we may divide the string dip roughly into three regions:

- 1) The bottom of the dip
- 2) The side of the dip, i.e. the region where the yield rises rapidly to the normal value
- 3) The shoulder, i.e. the region just outside the dip where the dip is compensated by a yield higher than normal.

The main physical interest is concentrated on region 1), where the large dip in yield occurs. This dip may be characterized by the minimum yield χ_{\min} . The value of χ_{\min} found in experiments depends critically on the experimental conditions. First of all, χ_{\min} is sensitive to all kinds of crystal defects, especially surface defects such as an oxide layer or even small deviations of the crystal structure near the surface from the bulk structure.

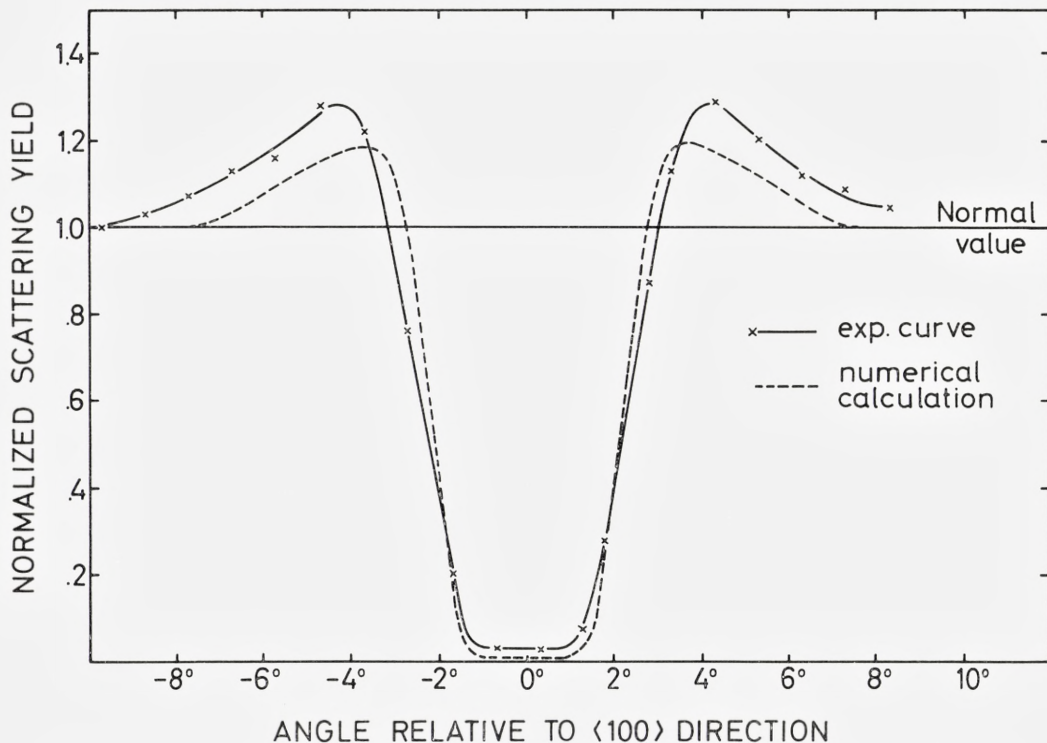


Fig. 10. Experimental¹³⁾ and calculated string dip in Rutherford scattering yield for 480 keV protons incident along a $\langle 100 \rangle$ direction on a tungsten crystal at 390° K.

Furthermore, under normal experimental conditions it is not possible to resolve the yield due to the first layer of the crystal from which the yield is normal. In most cases, some multiple scattering is also included in measurements of χ_{\min} . A quantitative agreement between the numerically calculated value of χ_{\min} and the experimentally found value is therefore not to be expected. In favourable cases it has, however, been possible^{10, 11)} to measure χ_{\min} values of the same order as Lindhard's qualitative estimate, $\chi_{\min} = Nd\pi(q^2 + a^2)$ (I, eq. (6.14))*.

Region 2) may be characterized by the width at half minimum of the dip. The width is not very sensitive to experimental conditions and should therefore show good agreement between calculation and experiment.

* In cases with very high depth resolution, more detailed information about the minimum yield and its variation with depth may be obtained as recently demonstrated by BOGH¹²⁾. For such cases, theoretical estimates considering the specific experimental conditions may be developed.

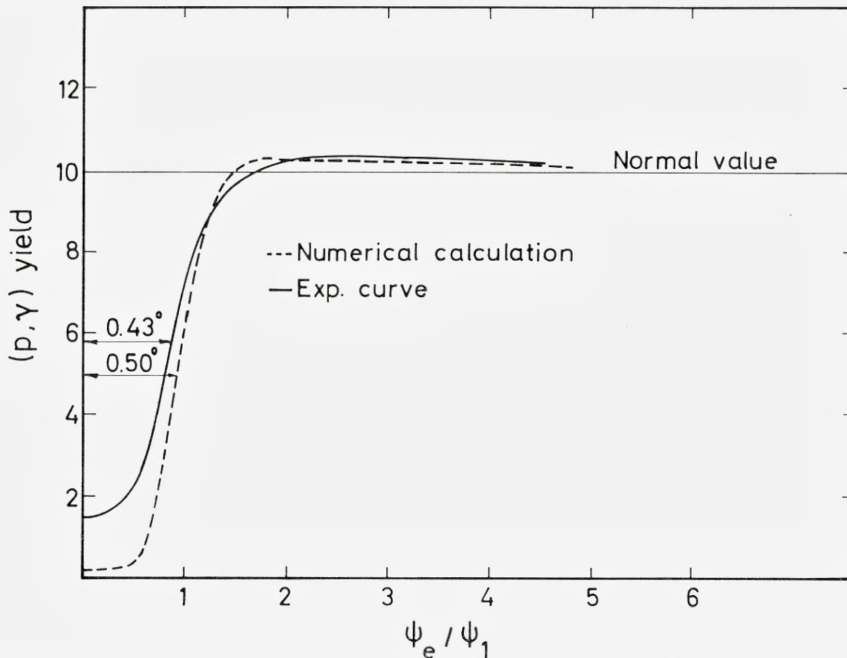


Fig. 11. Experimental¹⁰⁾ and numerically calculated string dip in (p, γ) yield for 1400 keV protons incident along a $\langle 110 \rangle$ direction on an aluminium crystal at room temperature.

Region 3) cannot be expected to show quantitative agreement, the main reason being that in most cases, the yield in this region is strongly influenced by planar effects. Clear experimental evidence of this influence is found in e.g. ref. 13). Measurements may, however, be expected to exhibit the qualitative features of the compensation mentioned in connection with Figs. 3 and 4.

Here, we shall not give a comprehensive comparison between the available experimental results and corresponding numerical calculations. A considerable amount of experimental results is found in refs. 11) and 13). In these references, the corresponding results of the numerical calculations are also given. To illustrate the kind of agreement found in most cases, two experimental and calculated string dips are compared in Figs. 10 and 11. As seen in these figures, the width of the experimental dip is well reproduced in the calculation.

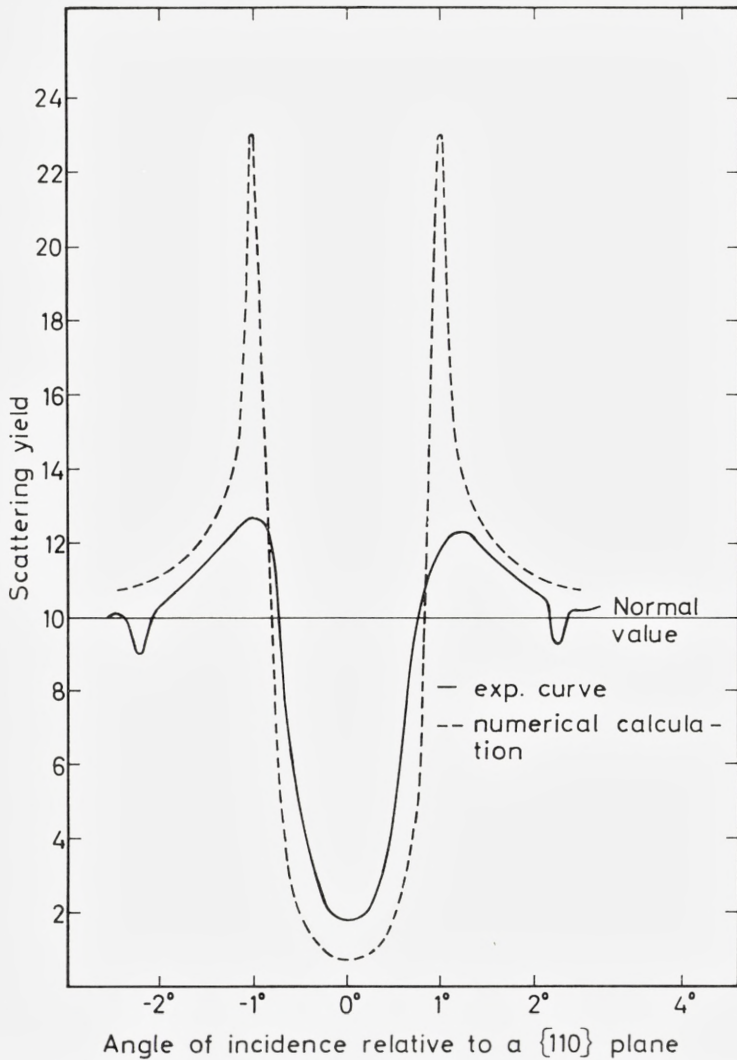


Fig. 12. Comparison between measured and calculated planar dip in Rutherford scattering yield for 480 keV protons incident along a {110} plane on a tungsten crystal at room temperature.

Planar case

The theoretical description of the planar case is not expected to be as accurate as the description of the string case and consequently, a less quantitative agreement is expected. The agreement obtained in the planar case is

illustrated in Fig. 12. The widths at normal value are in fair agreement but the minimum values differ by a factor of two, and the very high shoulder found in the calculation is not reproduced by experiment. This is not surprising since very little multiple scattering is required to smear out the extremely narrow shoulders.

Acknowledgements

The author is indebted to J. LINDHARD for stimulating interest and criticism, and also to J. A. DAVIES for numerous discussions. K. O. NIELSEN and P. JESPERGAARD are thanked for a special effort to spur the writing of this paper.

*Institute of Physics, University of Aarhus
Aarhus C, Denmark*

References

- 1) E. BØGH, J. A. DAVIES and K. O. NIELSEN, Phys. Lett. **12**, 129 (1964).
- 2) J. U. ANDERSEN, J. A. DAVIES, K. O. NIELSEN and S. L. ANDERSEN, Nucl. Instr. & Meth. **38**, 210 (1965).
- 3) E. BØGH, Proceedings of the Cairo Solid State Conference, September 1966 (Plenum Press).
L. ERIKSSON, J. A. DAVIES, J. DENHARTOG, H. J. MATZKE and J. L. WHITTON, Can. Nucl. Techn. **5**, no. 6 p. 40 (1966).
- 4) J. LINDHARD, Mat. Fys. Medd. Dan. Vid. Selsk. **34**, no. 14 (1965).
- 5) P. LERVIG, J. LINDHARD and V. NIELSEN, Nucl. Phys. A **96**, 481 (1967).
- 6) R. J. GLAUBER, Phys. Rev. **98**, 1692 (1955).
- 7) Internationale Tabellen zur Bestimmung von Kristallstrukturen **2**, 574 (1935).
- 8) R. S. NELSON, M. W. THOMPSON and H. MONTGOMERY, Phil. Mag. **7**, 1385 (1962).
- 9) O. S. OEN, Phys. Lett. **19**, 358 (1965) and private communication.
- 10) E. BØGH and E. UGGERHØJ, Phys. Lett. **17**, 116 (1965) and Nucl. Instr. & Meth. **38**, 216 (1965).
- 11) J. A. DAVIES, J. DENHARTOG and J. L. WHITTON, submitted to Phys. Rev.
- 12) E. BØGH, Phys. Rev. Letters **19**, 61 (1967).
- 13) J. U. ANDERSEN and E. UGGERHØJ, to appear in Can. J. Phys. (1968).

P. O. TJØM AND B. ELBEK

A STUDY OF ENERGY LEVELS IN
ODD-MASS GADOLINIUM NUCLEI
BY MEANS OF
(*d,p*) AND (*d,t*) REACTIONS

Det Kongelige Danske Videnskabernes Selskab
Matematisk-fysiske Meddelelser **36**, 8



Kommissionær: Munksgaard
København 1967

CONTENTS

	Page
1. Introduction	3
2. Theoretical Cross Sections	4
3. Experimental Procedures	7
4. Results and Discussion	8
4.1. <i>Q</i> -Values	8
4.2. General Features of the Spectra	19
4.3. Detailed Interpretation of the Spectra	22
4.3.1. The $3/2 - [521]$ Orbital	23
4.3.2. The $5/2 + [642]$ and the $3/2 + [651]$ Orbitals	25
4.3.3. The $1/2 + [660]$ Orbital	28
4.3.4. The $11/2 - [505]$ Orbital	29
4.3.5. The $3/2 + [402]$ and the $1/2 + [400]$ Orbitals	31
4.3.6. The $3/2 - [532]$ Orbital	34
4.3.7. The $1/2 - [530]$ Orbital	36
4.3.8. The $7/2 + [404]$ Orbital	39
4.3.9. The $5/2 - [523]$ Orbital	40
4.3.10. The $1/2 - [521]$ Orbital	42
4.3.11. The $7/2 + [633]$ Orbital	43
4.3.12. The $5/2 - [512]$ Orbital	44
4.3.13. The $1/2 - [510]$ Orbital	45
4.3.14. The $1/2 + [651]$ Orbital	46
4.3.15. Other Levels in the Deformed Nuclei	46
4.3.16. Levels in ^{153}Gd and ^{151}Gd	48
5. Comparison of Intensities with Predicted Values	48
6. Conclusions	52
References	54

Synopsis

The energy levels of ^{151}Gd , ^{153}Gd , ^{155}Gd , ^{157}Gd , ^{159}Gd , and ^{161}Gd have been investigated by means of (*d,p*) and (*d,t*) reactions on the stable even gadolinium isotopes. The deuteron energy was 12.1 MeV and the charged reaction products were analyzed in a magnetic spectrograph at 60°, 90°, and 125°. Application of theoretical and semi-empirical rules for the cross sections allowed the identification of states belonging to 16 different Nilsson orbitals, most of them in several nuclei. In the lighter gadolinium nuclei, the onset of deformation gives rise to complicated level structures which only in part can be explained by the Nilsson model. The spectra of these nuclei also show several effects which can be ascribed to the crossing of levels with the same spin and parity, but belonging to different oscillator shells. The experimental level scheme based on the observation of the $7/2 + [404]$ and $1/2 + [651]$ Nilsson orbitals in ^{159}Gd is compressed by approximately a factor of two compared to the theoretical level scheme.

Introduction

In an earlier investigation¹⁾, the energy levels of the odd isotopes of ytterbium were studied by means of (d,p) and (d,t) reactions induced by 12 MeV deuterons. The main results of this investigation were the systematic localization of a number of Nilsson states as a function of the neutron number and the experimental proof that the cross sections for population of these states by single-neutron transfer reactions to a surprising accuracy were obtained from the Nilsson²⁾ wave functions, the distorted wave Born approximation (DWBA) formalism³⁾, and the pairing theory. It was therefore indicated that the low lying levels in ytterbium represent relatively pure single-particle motions. However, in a few cases, significant deviations from the simple scheme outlined above were observed. Some of the deviations could be related to the coupling of the single particle to the collective gamma vibration, and a microscopic treatment⁴⁾ of this coupling gave qualitative agreement with the experimental results. At higher excitation energies, the presence of other couplings became evident, but no detailed analysis of the relevant experimental material was attempted.

This work extends the earlier investigation into the odd Gd nuclei in the beginning of the region of deformed rare earth nuclei.

For several reasons, the situation in the Gd nuclei is expected to be more complex than it was the case for the Yb nuclei. In the beginning of the deformed region, the deformation is rapidly changing with the neutron number. In fact, the lightest nuclei investigated here, ^{151}Gd and ^{153}Gd , cannot be assumed to possess any stable deformation. Furthermore, the even Gd nuclei show low lying, strongly collective excitations⁵⁾ of quadrupole and octupole type, in contrast to the even Yb nuclei where these excitations are high lying and weak⁶⁾. Finally, the single-particle spectrum in the Gd nuclei contains several near lying states with the same parity and a K -quantum number differing by zero or one unit. Such states are probably strongly mixed.

On the other hand, the low-energy spectrum of the Gd nuclei is expected to show the presence of single-particle levels from the $N = 4$ oscillator shell.

These states have large components of the $s_{1/2}$, $d_{3/2}$ or $g_{7/2}$ shell-model orbitals and are predicted to have large cross sections for the neutron transfer processes. Especially large (d, t) cross sections can be expected in the Gd nuclei, as the $N = 4$ states there will occur as hole excitations.

Some assistance in the analysis of the (d, t) spectra was provided from the measurement of the triton angular distributions for the $^{160}\text{Gd}(d, t)^{159}\text{Gd}$ reaction⁷⁾. The relatively simple spectrum of the ^{159}Gd nucleus made it possible to obtain angular distributions for triton groups where the orbital angular momentum, l , of the neutron picked up had values of 0, 1, 2, 3, 4, 5 or 6. These distributions could then be used as references for the analysis of more complicated cases in other nuclei.

Finally, the (d, d') spectra for the odd nuclei ^{155}Gd and ^{157}Gd have been useful in the analysis of levels with collective admixtures. A detailed account of the (d, d') experiments will be published separately⁸⁾.

2. Theoretical Cross Sections

For reference, we here list a few formulae which have been used in the comparison of the experimental cross sections to those obtained from theory.

The theory of stripping and pick-up for a deformed target nucleus has been given by SATCHLER⁹⁾. When the target nucleus is even and has spin 0, the cross section for stripping leading to a rotational level with spin $I_f = j$ can be written

$$\frac{d\sigma}{d\Omega} = 2C_{j,l}^2 \varphi_l(\theta) U^2, \quad (1)$$

where the factor U^2 approximately takes into account the effect of the partial filling of the neutron orbital in the target nucleus. The $C_{j,l}$ is the expansion coefficient of the Nilsson wave function on the spherical wave functions. These coefficients have been tabulated by several authors^{10, 11, 12)}. The angular function $\varphi_l(\theta)$ is obtained from the DWBA calculation for the transfer of a neutron with orbital angular momentum l . For the present work, the $\varphi_l(\theta)$ functions were obtained from a GIER ALGOL computer code¹³⁾ similar to the well-known code SALLY³⁾. The optical model parameters for the deuteron, proton and triton potentials used in the calculations are listed in table 1. The deuteron and proton potentials are essentially the same as those used for the analysis of the Yb data¹⁾, whereas the triton potentials are those found from the analysis of the $^{160}\text{Gd}(d, t)$ angular distributions⁷⁾.

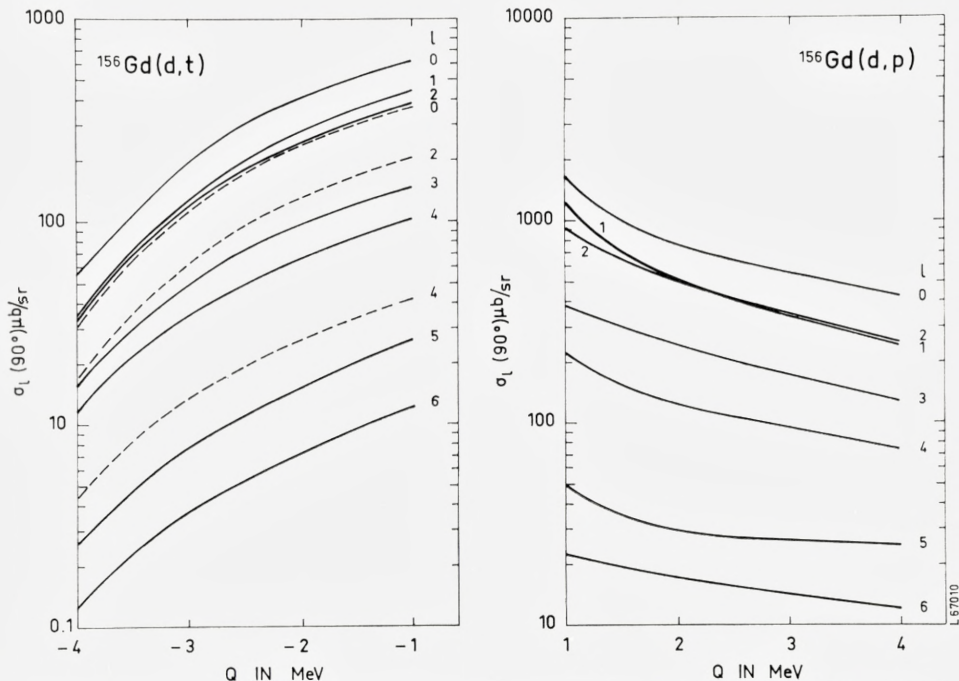


Fig. 1. Q -dependence of the single-particle cross section $\sigma_l(\theta)$. The odd l -values correspond to the $N = 5$ oscillator shell. For the even l -values the curves for $N = 6$ are drawn full, those for $N = 4$ dotted.

The $\varphi_l(\theta)$ function in eq. (1) differs from that obtained from the DWBA calculation by a normalization factor N . If $\sigma_l(\theta)$ is the result of the DWBA calculation, we use the normalization $\varphi_l(\theta) = 1.5 \sigma_l(\theta)$ for the (d, p) reactions, which is in agreement with common practice. For the (d, t) reaction we use the empirical relationship $\varphi_l(\theta) = 3.0 \sigma_l(\theta)$.

The $\varphi_l(\theta)$ functions depend on the Q -value of the transfer reaction. For a comparison of the data obtained for the different nuclei it was found useful to reduce all the experimental cross sections to a standard Q -value by means of the theoretical Q -dependence which is shown in fig. 1. The (d, p) cross sections were reduced to $Q = 3.0$ MeV, whereas the (d, t) cross sections were reduced to $Q = -2.0$ MeV. For cases in which the l -values were not known, the Q -dependence for $l = 2$ was used. When the data were compared for levels with definite assignments, calculations for the proper values of l and the oscillator quantum number N were used.

Equation (1) applies only to pure Nilsson states. The experimental

material presented here contains several cases where strong mixing of the wave functions for two or more levels is indicated. If the wave function for a level contains admixtures with amplitudes a_i of other levels, then the stripping cross section for the n 'th level is taken to be

$$\frac{d\sigma_n(\theta)}{d\omega} = 2\left(\sum_i C_{j,l}^{(i)} U_i a_{in}\right)^2 \varphi_l(\theta), \quad (2)$$

where the $C_{j,l}^{(i)}$ refers to the expansion coefficient for the i 'th level and U_i to the corresponding pairing factor. The pick-up cross section is obtained by replacing U_i by the pairing factor V_i .

An especially important coupling is the Coriolis coupling between rotational bands differing by one unit in K -quantum number. If we limit ourselves to two bands, K and $K+1$, then the Coriolis matrix¹⁴⁾ element is

$$A_K = -\frac{\hbar^2}{2\mathfrak{J}} \langle K|j_-|K+1\rangle (U_K U_{K+1} + V_K V_{K+1}), \quad (3)$$

where \mathfrak{J} is the nuclear moment of inertia and j_- denotes the usual total angular momentum lowering operator. The last factor in (3) takes into account the pairing¹⁵⁾. The matrix elements j_- can be expressed in terms of the $C_{j,l}$ coefficients

$$\langle K|j_-|K+1\rangle = \sum_{j,l} C_{j,l}^{(K)} C_{j,l}^{(K+1)} \sqrt{(j-K)(j+K+1)}. \quad (4)$$

The admixed amplitudes can be calculated according to KERMAN¹⁴⁾. However, in order to avoid ambiguities in the relative signs of the expansion coefficients, we here give a consistent set of formulae for the case $E_{K+1} - E_K > 0$, where E refers to the unperturbed level energy. The perturbed wave functions, u , of level 1 or 2 can then be expressed by

$$u^{(1,2)} = a_K^{(1,2)} u_K + a_{K+1}^{(1,2)} u_{K+1} \quad (5)$$

and the perturbed energies as

$$E^{(1,2)} = \frac{1}{2}(E_{K+1} + E_K) \pm \frac{1}{2} \sqrt{(E_{K+1} - E_K)^2 + 4A_K^2(j-K)(j+K+1)}. \quad (6)$$

The amplitudes, a , are determined by

$$a_K^{(1,2)} = \left\{ 1 + \left[\pm R + \sqrt{1 + R^2} \right]^2 \right\}^{-\frac{1}{2}}; \quad a_K^2 + a_{K+1}^2 = 1, \quad (7)$$

where

$$R = \frac{E_{K+1} - E_K}{2A_K \sqrt{(j-K)(j+K+1)}}. \quad (8)$$

The signs are determined by the rules

$$\left. \begin{array}{l} \text{if } A_K < 0, \text{ then } a_K^{(1)}/a_{K+1}^{(1)} < 0 \text{ and } a_K^{(2)}/a_{K+1}^{(2)} > 0 \\ \text{if } A_K > 0, \text{ then } a_K^{(1)}/a_{K+1}^{(1)} > 0 \text{ and } a_K^{(2)}/a_{K+1}^{(2)} < 0. \end{array} \right\} \quad (9)$$

If $E_{K+1} - E_K < 0$, a_K and a_{K+1} are interchanged in equation (7) and the signs determined by (9) are reversed.

3. Experimental Procedures

The experimental methods closely follow those of ref.¹⁾. A 12.1 MeV deuteron beam was obtained from the Niels Bohr Institute tandem accelerator. The reaction products from a thin target were analyzed in a broad-range magnetic spectrograph and recorded on photographic plates which were scanned manually to obtain the particle intensity as a function of the distance along the plate.

The targets for this investigation were prepared by the University of Aarhus isotope separator group by direct deposition of the separated isotopes on carbon foils, about 40 $\mu\text{g}/\text{cm}^2$ thick. The exposures in the magnetic spectrograph, which here are analyzed for proton tracks and triton tracks, are identical to those analyzed for deuteron tracks in ref.⁵⁾.

A few improvements in the experimental techniques described in ref.¹⁾ have been introduced for the present series of measurements. In most cases, three angles, 60°, 90° and 125°, were measured immediately after each other. For the 60° and 90° exposures, the target was left in the same position (transmission geometry) whereas the target was turned for the 125° exposure (reflection geometry). The use of the same target and identical beam conditions for all angles greatly improved the accuracy of the relative cross section determinations and has made it possible to draw some conclusions about angular momenta on the basis of intensity changes with angle.

The magnetic spectrograph was carefully recalibrated over the full energy range. The role of partial saturation in the iron was evaluated, but the effects were found to be negligible for the field strengths used in the present work ($B_{\text{max}} \sim 10.000$ Gauss).

The intensity of the beam obtainable from the tandem accelerator has gradually been improved, which made it possible to use smaller beam de-

TABLE 1. Optical model parameters for deuterons, tritons, and protons.

	V MeV	W MeV	r_0 fm	a fm	r'_0 fm	a' fm	r_c fm
(d,p) deuteron parameters	86	12	1.15	0.87	1.37	0.70	1.25
proton parameters	54	15	1.25	0.65	1.25	0.47	1.25
(d,t) deuteron parameters	86	12	1.15	0.87	1.37	0.70	1.25
triton parameters	154	12	1.10	0.75	1.40	0.65	1.25

fining apertures. As a rule, beams of $0.7 \mu A$ through two $0.55 \times 3 \text{ mm}^2$ apertures were used. The resulting resolution (FWHM) was approximately 9 keV for the (d,t) spectra, whereas the (d,p) spectra, which mostly were recorded at the low dispersion part of the photographic plate, rarely showed resolutions better than about 13 keV.

Somewhat improved excitation energy determinations were obtained by the use of the center-of-gravity of a peak for position definition instead of the usual 1/3 intensity point on the high energy side of the peak. The accuracy of the Q -values is estimated to be ± 10 keV, whereas the accuracy of the excitation energies is ± 3 keV below 1 MeV of excitation, and otherwise ± 5 keV.

4. Results and Discussion

Gadolinium has five stable even isotopes which all were used as targets in the present investigation. Thus, the energy levels in the odd nuclei from ^{151}Gd to ^{161}Gd could be investigated by at least one of the reactions (d,p) and (d,t) .

A spectrum for each of the ten different reactions is shown in figures 5–14. The level energies obtained as the average of the determinations at three angles are listed in tables 2–7, which contain also the measured differential cross sections and the suggested Nilsson assignments for some of the levels. The basis for these assignments will be discussed in detail in the following sections.

4.1. Q-Values

The localization of the ground state poses no problem in the final nuclei from ^{161}Gd to ^{155}Gd where the low energy spectrum is well known. For ^{153}Gd , it is possible uniquely to relate the spacings of levels observed by the transfer reactions to spacings of levels known from decay studies. Thereby

TABLE 2. Levels populated in ^{151}Gd .

Energy average (d,t) keV	Assignment	$d\sigma/d\Omega$ (d,t) $\mu\text{b/sr}$		
		60°	90°	125°
0	(f7/2)	387	358	
108		7	6	
375		10	25	
394		99	119	
424		23	21	
584		72	66	26
616		26	21	13
666		48	54	34
697		4	6	5
707		1	2	5
806		14	11	3
835		41	28	16
847		7	7	8
882		1	2	
907		3	2	
977	(d3/2)	138	190	129
1047	(s1/2)	137	178	124
1083		12	5	3
1156		21	14	15
1190		22	30	15
1204		14	29	25
1357			19	13

the ground state is also established. A similar correspondence can be obtained for ^{151}Gd , but for fewer energy levels. The Q -values for the ground states are collected in table 8 which also lists the neutron separation energies derived from the data by means of the expressions

$$\left. \begin{aligned} S_n(A) &= 6.258 \text{ MeV} - Q_{d,t} \text{ for } A \rightarrow A-1 \\ S_n(A) &= 2.225 \text{ MeV} + Q_{d,p} \text{ for } A-1 \rightarrow A. \end{aligned} \right\} (10)$$

Table 8 includes also the data for the odd target nuclei of Gd, which will be discussed separately¹⁶⁾. It should be noted that the independent determinations of the separation energies by (d,p) and (d,t) reactions are in good agreement with each other, which gives some confidence in the accuracy of the absolute values of Q . Also the agreement with the most recent mass spectroscopic two-neutron separation energies¹⁷⁾ is satisfactory.

TABLE 3. Levels populated in ^{153}Gd .

Energy average		Assignment	$d\sigma/d\Omega(d,p)$ $\mu\text{b/sr}$			$d\sigma/d\Omega(d,t)$ $\mu\text{b/sr}$		
(d,p) keV	(d,t) keV		60°	90°	125°	60°	90°	125°
0	0		94	39	12	100	94	41
43	43		~ 6	~ 1	~ 1	~ 1		~ 2
93	94		630	405	171	178	197	118
110	110		60	36	22	42	50	27
138	140	11/2 11/2 - [505]?	52	53	40	14	28	26
	172					21	49	41
182	183		23	16	2	14	18	13
217	213	3/2 3/2 + [402]	110	72	55	326	385	273
	251					10	13	13
	304					9	16	12
315	315		31	15	6	22	9	7
328	328	1/2 1/2 + [400]	25	12	6	346	390	260
363	363	3/2 1/2 - [530]	445	232	97	155	144	24
	394					2	8	25
435	431		369	148	65	25	15	18
	441					7	26	21
	483						10	11
507	504		189	78	40	38	50	44
530	533		136	64	29	4	6	
548	546		65	46	22	2	4	
575			10	6	4			
	580					10	17	19
606	606		24	15	10	2	3	
634			14	18	11			
648	646		29	27	7	4	3	
678			37	34	11			
721			71	41	20			
736			11	4				
772	773		147	103	59	11	16	14
856		1/2 1/2 - [521]	427	189	65			
876			27	25	19			
	883					6	13	9
889			28	26	17			
905			52	38	21			
943		3/2 1/2 - [521]	55	30	14			
960		5/2 1/2 - [521]	175	63	25			
	983					3	4	
994			89	39	21			

(continued)

TABLE 3 (continued).

Energy average		Assignment	$d\sigma/d\Omega(d,p) \mu b/sr$			$d\sigma/d\Omega(d,t) \mu b/sr$		
(d,p) keV	(d,t) keV		60°	90°	125°	60°	90°	125°
1034			19	10	4			
1052			64	35	15			
1081			9	5				
1099			22	16	7			
1115			8	6	3			
	1116					12		23
1143			24	21	9			
1155	1151	7/2 1/2 - [521]	82	39	25	15		36
1171			193	94	37			
1194		9/2 1/2 - [521]	12	6	3			
1235			27	14	10			
1251			27	9	5			
	~ 1287	7/2 7/2 + [404]				~ 49		
1296			60	23	15			
1339			19	7	8			
1361			139	62	32			
1384			76	35	15			
1400			67	35	15			
1421			65	36	18			
1448			58	25	8			
1482			49	31	20			
1496			37	20	12			
1509			43	25	32			
1533			42	25	13			
1548			71	48	26			
1564			39	15	7			
1584			51	37	15			
1597			28	19	9			
1615			47	26	14			
1631			13	10	8			
1655			51	31	13			
1669			22	13	5			
1686			34	13	10			
1701			18	13	8			
1720			65	30	13			
1738			47	26	12			
1755			69	36	15			
1772			34	25	9			

TABLE 4. Levels populated in ^{155}Gd .

Energy average		Assignment	$d\sigma/d\Omega(d,p)$ $\mu\text{b/sr}$			$d\sigma/d\Omega(d,t)$ $\mu\text{b/sr}$		
(d,p) keV	(d,t) keV		60°	90°	125°	60°	90°	125°
0	0	3/2 3/2 - [521]	118	43	33	78	58	22
~ 60	~ 60	5/2 3/2 - [521]	~ 4	~ 3		~ 2	~ 1	
~ 81	~ 83		~ 4	~ 3		~ 8	~ 12	~ 7
107	106		114	83	35	239	241	129
	119	11/2 11/2 - [505]				84	97	49
145	145	7/2 3/2 - [521]	227	138	64	100	92	41
213	214		59	48	37	31	56	35
247	250	9/2 3/2 - [521]	28	10	5	5	10	6
267	267	3/2 3/2 + [402]	74	59	28	340	343	210
287	282		16	9		30	32	9
321	322	5/2 5/2 - [523]	50	28	20	108	95	40
	345					2	4	8
367	367	1/2 1/2 + [400]	129	56	28	608	594	319
392	393	7/2 7/2 - [523]	117	90	42	23	49	22
422	~ 423	1/2 1/2 - [530]	20	9	8		~ 16	~ 16
	~ 428					34	~ 32	~ 25
450	451	3/2 1/2 - [530]	170	89	34	405	328	129
485		9/2 5/2 - [523]	29	25	20			
	489	5/2 1/2 - [530]				77	101	80
	556	7/2 1/2 - [530]				57	50	14
556		1/2 1/2 - [521]	401	200	95			
	594	β -vib, 3/2 3/2 - [521]				20	12	11
614		3/2 1/2 - [521]	75	36	13			
	617	9/2 1/2 - [530]				8	7	4
658	659	5/2 1/2 - [521]	81	36	23	5	4	
692			19	8	13			
	721	β -vib, 7/2 3/2 - [521]				13	24	12
751	753		31	17	3	23	25	7
784	787	7/2 1/2 - [521]	153	98	46	4	5	4
	813	β -vib, 9/2 3/2 - [521]				8	4	4
866	867	9/2 1/2 - [521]	12	11		5	4	
1005			38	21				
1025			48	41				
1082			28	7				
1110			26	21				
	1118					1	4	
1131			51	42				
1160*			13	16				

* Several unresolved peaks from 1160 keV to 1250 keV.

(continued)

TABLE 4 (continued).

Energy average		Assignment	$d\sigma/d\Omega(d,p)$ $\mu b/sr$			$d\sigma/d\Omega(d,t)$ $\mu b/sr$		
(d,p) keV	(d,t) keV		60°	90°	125°	60°	90°	125°
1191		7/2 7/2 + [404]	14	7				
	1239					4	4	
1241			16	8				
	1267					7	2	
	1295					67	~ 95	80
1303			60	33				
	1331					2	3	
1339			44	16				
	1357					~ 1	4	
1362			44	26				
1408			31	21				
1438			69	66				
1472			70	38				
1518			40	21				
1548			65	41				
1563			31	14				
1587			32	9				
1604			83	37				
1626			233	125				
1653			41	18				
1704		28	20					
1745		63	53					
1794		66	41					
1822		42	31					
1843		175	84					
1869		55	20					
1899		53	33					
1932		79	42					

In fig. 2 the neutron separation energies are shown as function of the mass number. The most noticeable feature is the decrease in $S_n(A)$ for the lighter nuclei. This effect is undoubtedly related to the onset of deformation.

It is also noted that the differences in S_n between even and odd nuclei are largest for the most neutron deficient nuclei. A similar trend has been observed for other series of isotopes in the rare earth region and implies an increase in the neutron pairing energies as the number of neutrons is reduced. The occurrence of strongly collective states in the neutron deficient nuclei⁵⁾ may probably be related to a corresponding increase in the energy gap.

TABLE 5. Levels populated in ^{157}Gd .

Energy average		Assignment	$d\sigma/d\Omega(d, p) \mu\text{b/sr}$			$d\sigma/d\Omega(d, t) \mu\text{b/sr}$	
(d, p) keV	(d, t) keV		60°	90°	125°	60°	90°
0	0	3/2 3/2 - [521]	146	55	23	205	100
	~ 53	5/2 3/2 - [521]					~ 2
~ 62	~ 63	5/2 5/2 + [642]		~ 2	~ 3	~ 1	~ 2
	~ 115	7/2 5/2 + [642]				4	3
133	132	7/2 3/2 - [521]	236	132	69	232	150
181	181	9/2 5/2 + [642]	55	25	18	75	65
228	227	9/2 3/2 - [521]	23	9	11	10	13
~ 276		11/2 5/2 + [642]	4	3	2		
315			6	3			
~ 346	~ 349	11/2 3/2 - [521]		5	8	4	9
360	361	13/2 5/2 + [642]	62	50	40	38	49
	~ 372					~ 3	~ 3
	426	11/2 11/2 - [505]				36	69
435	435	5/2 5/2 - [523]	51	28	21	25	24
478	475	3/2 3/2 + [402]	75	31	21	554	404
	513					44	46
518	523	7/2 5/2 - [523]	206	103	64	5	9
617	618	9/2 5/2 - [523]	44	20	20	5	11
665	665		18	6	5	49	37
686	684	1/2 1/2 + [400]	117	70	45	1080	844
	700	3/2 3/2 - [532]?				58	59
704		1/2 1/2 - [521]	359	128	60		
	718					85	45
745	744	3/2 1/2 - [521]	21	20	6	6	9
	751	5/2 3/2 - [532]?				6	13
	770					8	10
	792					104	66
795		5/2 1/2 - [521]	116	70	44		
812	809	3/2 1/2 - [530]	178	84	26	346	260
	813	7/2 3/2 - [532]?				190	143
834			84	38	25		
	837	5/2 1/2 - [530]				65	43
	850					8	20
	901	7/2 1/2 - [530]				22	20
903		7/2 1/2 - [521]	78	39	23		
	918	9/2 3/2 - [532]?				6	7
	962	9/2 1/2 - [530]				11	~ 12
965			78	51	36		
	981					8	6

(continued)

TABLE 5 (continued).

Energy average		Assignment	$d\sigma/d\Omega(d,p) \mu b/sr$			$d\sigma/d\Omega(d,t) \mu b/sr$	
(d,p) keV	(d,t) keV		60°	90°	125°	60°	90°
~ 988		9/2 1/2 - [521]		~ 4			
1039			9	~ 4	3		
	~ 1060	11/2 1/2 - [530]				2	
	1093					21	
	1113					3	
1117			61	43	27		
	1141					31	22
1142			38	14	17		
	1175					3	6
1185				5	2		
	1203					~ 1	3
1206				5	5		
	1246					5	3
1289			5	3	3		
	1296					21	11
	1305					9	7
1312			37	13	7		
	1316					2	3
1331			9	7	4		
	1339					4	5
	1352					2	4
1354			14	11	7		
1391		7/2 5/2 - [512]?	114	95	54		
	1396					4	6
	1414					5	3
1437			10	2			
	1466					3	6
1472			38	19	14		
1487			52	19	15		
1519			24	5	7		
	1524					4	4
1555			11	11	7		
	1556					27	23
	1569					5	11
	1589					30	31
1593			112	50	38		
	1611					6	4
1614			22	17	14		
	1635					3	4

(continued)

TABLE 5 (continued).

Energy average		Assignment	$d\sigma/d\Omega(d,p) \mu b/sr$			$d\sigma/d\Omega(d,t) \mu b/sr$		
(d,p) keV	(d,t) keV		60°	90°	125°	60°	90°	
1660		7/2 7/2 + [404]	43	34	20			
	1670					2	4	
	1720					4	6	
	1731					8	7	
	1738					12	19	
1744				123	62	27		
1767				21	11	8		
1793				68	19	18		
1809				39	15			
	1811						9	6
	1825						56	61
1833				47	35			
1845				81	35			
1869				80	40			
1906			206	188				
1929			45	27				

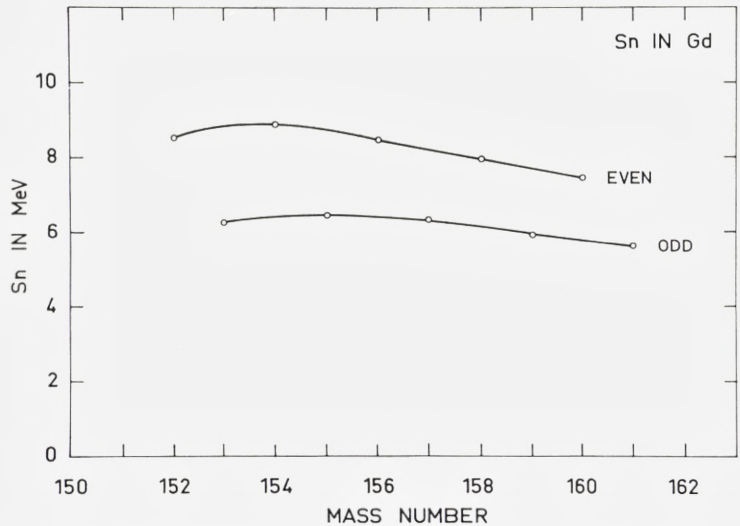


Fig. 2. Neutron separation energy as a function of the mass number.

TABLE 6. Levels populated in ^{159}Gd .

Energy average		Assignment	$d\sigma/d\Omega(d,p) \mu\text{b/sr}$			$d\sigma/d\Omega(d,t) \mu\text{b/sr}$		
(d,p) keV	(d,t) keV		60°	90°	125°	60°	90°	125°
0	0	3/2 3/2 - [521]	155	66	24		191	73
	~ 50	5/2 3/2 - [521]				~ 4	~ 4	~ 2
	67	5/2 5/2 + [642]				~ 3	~ 4	~ 2
122	120	7/2 3/2 - [521]	148	88	39	298	219	91
147	146	5/2 5/2 - [523]	47	22	12	42	27	10
185	184	9/2 5/2 + [642]	49	29	13	112	86	38
	211	9/2 3/2 - [521]				17	22	12
227	226	7/2 5/2 - [523]	242	136	49	140	118	45
~ 275	~ 272	11/2 5/2 + [642]	7	~ 3	~ 2	~ 2	~ 3	~ 1
330	327	11/2 3/2 - [521]	27		17	11	25	11
		9/2 5/2 - [523]						
373	371	13/2 5/2 + [642]	50		33	58	71	47
457	455	11/2 5/2 - [523]	22	18	13	10	18	16
507	506	1/2 1/2 - [521]	525	199	81	146	80	20
559	557	3/2 1/2 - [521]	34	25	11	12	7	2
589	588	5/2 1/2 - [521]	100	67	28	24	17	5
	598					4	4	2
680	681	11/2 11/2 - [505]	4	4	7	55	102	86
706	704	7/2 1/2 - [521]	202	136	62	32	26	16
746	743	3/2 3/2 + [402]	45	31	13	747	613	297
761		9/2 1/2 - [521]	25	18	21			
783	780	1/2 1/2 + [660]	33	13	4	265	195	77
	799					27	29	17
	816						17	17
837			3	8	4			
	855	9/2 1/2 + [660]				18	23	6
~ 875		5/2 5/2 - [512]		~ 3	~ 4			
	876					7	26	20
	924					12	13	3
950	945	7/2 5/2 - [512]	230	141	76	15	12	
977	973	1/2 1/2 + [400]	40	20	10	680	584	290
1000	999	3/2 1/2 + [660]	11	6	2	114	114	74
1044		9/2 5/2 - [512]	10		4			
*	1057	13/2 1/2 + [660]				43	52	49
	1077					13	15	
	1109	3/2 3/2 - [532]				85	54	33
	1126					46	26	7
	1143	3/2 1/2 - [530]				310	219	77
1138			234	103	59			

* Several unresolved (d,p) levels from 1044 keV to 1140 keV.

(continued)

TABLE 6 (continued).

Energy average		Assignment	$d\sigma/d\Omega(d,p)$ $\mu\text{b/sr}$			$d\sigma/d\Omega(d,t)$ $\mu\text{b/sr}$		
(d,p) keV	(d,t) keV		60°	90°	125°	60°	90°	125°
~ 1182	1158	5/2 3/2 - [532]				115	90	28
	1176	5/2 1/2 - [530]				7	8	2
		11/2 5/2 - [512]		~ 4	~ 5			
	1200				28	25	4	
1204			24	15	18			
	1238	7/2 1/2 - [530] 7/2 3/2 - [532]				38	37	16
1237			23	8	9			
	1250					6	8	
	1282	7/2 1/2 + [660]				36	28	4
1287			31	16	7			
	1301	9/2 1/2 - [530]				10	13	4
	1341	9/2 3/2 - [532]				43	34	24
	1356					3	4	
	1390	11/2 1/2 - [530]				2	9	6
1396			49	28				
	1415					12		8
	1423					37		13
1430			157	78	28			
1474			18	10	5			
1493			31	19	9			
	1506					15		4
1521			104	39	15			
	1536					15		3
	1550					7		6
	1561					31		28
	1573					11		8
	1600					13	7	2
1602	**	3/2 1/2 - [510]	617	278	132			
1638		5/2 1/2 - [510]	171	92	45			
1693			135	60	70			
1718			41	22	18			
1751		7/2 1/2 - [510]	63	44	27			
1780			86	58	35			
1808			85	52	22			
	1810					9	7	
	1839					25	26	5
1840			53	26	16			
1887			86	39	21			

** Several unresolved (d,t) levels from 1600 keV to 1800 keV.

(continued)

TABLE 6 (continued).

Energy average		Assignment	$d\sigma/d\Omega(d,p) \mu b/sr$			$d\sigma/d\Omega(d,t) \mu b/sr$		
(d,p) keV	(d,t) keV		60°	90°	125°	60°	90°	125°
1909			29	18	13			
1925			71	32	15			
1953			79	25	18			
1977	1960	7/2 7/2 + [404]				98	104	95
	1991	1/2 1/2 + [651]	265	131	37	19	14	11
1993		3/2 1/2 + [651]	254	118	60			
2040		5/2 1/2 + [651]	320	154	28			
2053			86	74	80			
2081		7/2 1/2 + [651]	71	47	27			
2106			80	34	13			
2134			123	61	42			
2168			92	47	12			
2193			52	39	17			

4.2 General Features of the Spectra

As for the Yb nuclei, the basis for the interpretation of the (d,p) and (d,t) spectra has mostly been the systematic occurrence of characteristic intensity patterns for the rotational bands based on the different Nilsson states and the absolute cross sections for population of these bands. In many cases, this basis has been sufficient for a unique assignment but, as it will become evident from the discussion below, the spectra often show structures which in no simple manner can be accounted for by the Nilsson model. This is, of course, especially so for the nuclei which are not expected to have a stable equilibrium deformation, but also nuclei which possess all the characteristics of deformation show significant deviations from the expected scheme.

For the analysis of the more complicated cases, it has been of importance to utilize additional information, such as the rate of intensity change with angle, the cross sections for inelastic scattering, and the evidence available from decay scheme studies. Still, for a considerable number of levels, it has not been possible to give a satisfactory explanation.

This being the case, it is interesting to investigate whether the single-particle description is a sound basis for the analysis of the spectra. There

TABLE 7. Levels populated in ^{161}Gd .

Energy average (d, p) keV	Assignment	$d\sigma/d\Omega(d, p) \mu\text{b/sr}$		
		60°	90°	125°
0	5/2 5/2 - [523]	30	20	8
73	7/2 5/2 - [523]	44	~ 20	11
163	9/2 5/2 - [523]	35	22	17
276	11/2 5/2 - [523]	12	7	6
313	3/2 3/2 - [521]	122	52	19
356	1/2 1/2 - [521]	387	168	57
397	3/2 1/2 - [521]	25	15	7
438	5/2 1/2 - [521]	313	195	87
510	7/2 3/2 - [521]			
	9/2 7/2 + [633]	33	24	10
529	7/2 1/2 - [521]	101	67	34
~ 585	11/2 7/2 + [633]	~ 2		~ 2
604	9/2 1/2 - [521]	23	13	11
645	11/2 3/2 - [521]	14	15	11
681	13/2 7/2 + [633]	48	51	38
~ 753	11/2 1/2 - [521]		~ 2	
~ 809	5/2 5/2 - [512]	10	~ 3	~ 2
834		188	82	32
889	7/2 5/2 - [512]	478		152
925		56	28	23
972	13/2 9/2 + [624]?	64	64	31
994	9/2 5/2 - [512]	9	16	12
1049		10	16	13
1097		12	9	7
1123	11/2 5/2 - [512]	7	11	8
1177		54	35	21
1309	1/2 1/2 - [510]	9	5	
1339	3/2 1/2 - [510]	538	300	
1378		192	79	
1403	5/2 1/2 - [510]	136	98	
1413		213	93	
1466	7/2 1/2 - [510]	77	46	29
1489	1/2 1/2 + [651]	242	157	48
1501	3/2 1/2 + [651]	151	137	59
1520		29	33	14
1556	5/2 1/2 + [651]	680	309	106
1591	7/2 1/2 + [651]	39	37	20
1615		91	50	16
1643		23	19	7
1664		46	27	14

TABLE 8. Q -values and neutron separation energies for Gd nuclei.

Mass A	$Q(d,t)$ A \rightarrow A - 1 keV	$Q(d,p)$ A - 1 \rightarrow A keV	$S_n(d,t)$ keV	$S_n(d,p)$ keV
152	-2338 ± 10		8596 ± 10	
153		4015 ± 10		6240 ± 10
154	-2642 ± 10		8900 ± 10	
155	-190 ± 10	4217 ± 10	6448 ± 10	6442 ± 10
156	-2287 ± 10	6319 ± 10	8545 ± 10	8544 ± 10
157	-112 ± 10	4136 ± 10	6370 ± 10	6361 ± 10
158	-1688 ± 10	5724 ± 10	7946 ± 10	7949 ± 10
159		3717 ± 10		5942 ± 10
160	-1200 ± 10		7458 ± 10	
161		3411 ± 10		5636 ± 10

is ample evidence for a considerable spreading of intensity, and it is not easy to see how distant single-particle levels one should consider in the analysis. Some light might be shed on this problem by the size of the integrated cross section for all levels in the low energy spectrum.

Let us first consider the levels populated by the (d,t) reaction. In the deformed nuclei ^{159}Gd , ^{157}Gd , and ^{155}Gd , the level assigned as $7/2 + [404]$ gives a natural limit for the summation of cross sections. A possibly related level in ^{153}Gd is found at 1287 keV and the summation can be carried to this energy. For experimental reasons, the (d,t) spectrum in ^{151}Gd was not recorded above 1400 keV. The summed cross sections with these limits are plotted in fig. 3 as a function of the mass number. All cross sections have been reduced to $Q = -2$ MeV, as explained in sect. 2. For the deformed nuclei, there is surprisingly good agreement between the experimental cross sections and the summed theoretical cross sections for all Nilsson levels from the $7/2 + [404]$ level to the $3/2 - [521]$ level. The latter is ground state in three of the nuclei and can therefore be assumed to represent the Fermi surface. Although this agreement may be fortuitous, it is indicated that the expected strength for the hole states by and large is observed. The total (d,t) cross section is only about half that expected for a pure shell model including the $N = 4$ $g_{7/2}$, $s_{1/2}$, and $d_{3/2}$ levels, the $N = 5$ $h_{11/2}$ levels and half of the $N = 5$ $f_{7/2}$ levels.

A similar comparison for the (d,p) cross sections is considerably more uncertain because of the lack of suitable summation limits. Fig. 3 shows the summed (d,p) cross section between the ground state and a somewhat

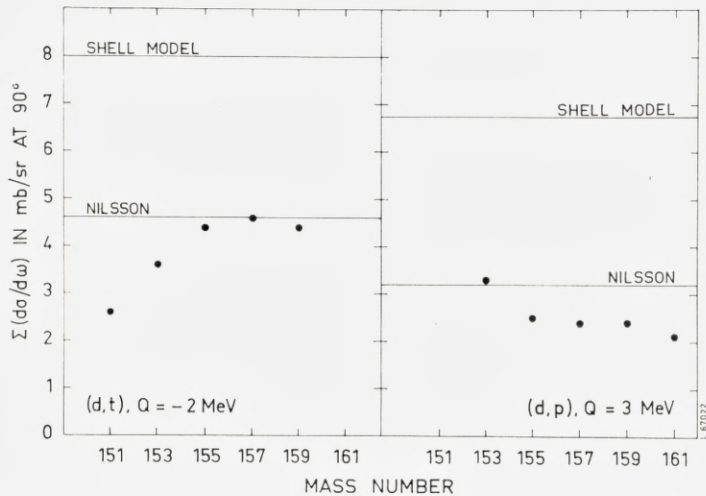


Fig. 3. Summed cross section as a function of the mass number.

arbitrarily chosen limit at 2 MeV of excitation. The theoretical Nilsson cross section sum from the $3/2 - [521]$ orbital to the $1/2 + [651]$ orbital is in reasonably good agreement with the experimental sum. The increase in the summed cross section for ^{153}Gd probably reflects the lowering of the states as the spherical shell-model configurations are approached.

A comparison can also be made for the densities of levels observed in the transfer reactions. Couplings between the individual single-particle levels as, e.g., the Coriolis coupling will redistribute the intensities. This will not greatly affect the number of levels observed in the spectrum although, in some cases, a weakly populated level in one band can get admixtures of a strongly populated level in another band and thereby contribute to the observed level density. Couplings of the single-particle states to the vibrational states will increase the number of levels populated compared to what is predicted from the Nilsson scheme. Fig. 4 shows the results of a comparison of this type for the levels in the Gd nuclei. The energy regions included are the same as those used for the comparison of cross sections in fig. 3. The moderate increase in level density indicates that the number of levels strongly coupled to additional degrees of freedom (vibrations) is rather small.

4.3. Detailed Interpretation of the Spectra

This section contains a detailed discussion of the features of the spectra, which it has been possible to describe in terms of single-particle levels in a deformed well and the couplings of such levels to each other or to elementary

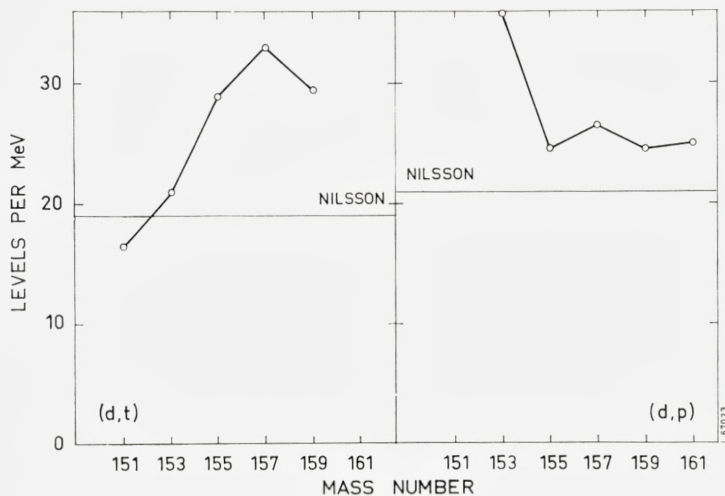


Fig. 4. The density of levels as a function of the mass number.

vibrational modes. The individual Nilsson orbits are discussed separately below. Tables 9 and 10 list the theoretical cross sections for the (d,t) and (d,p) reactions, respectively, for the pure single-particle states. The observed energies of the band heads are plotted in fig. 15, and the complete level schemes for the six nuclei investigated are shown in figs. 16–21.

4.3.1. The $3/2-[521]$ Orbital

This orbital is the ground state in ^{155}Gd , ^{157}Gd , and ^{159}Gd . In ^{161}Gd , a group at 313 keV has a cross section and angular dependence as expected for the $3/2-$ level of this band. The $7/2-$ state, however, must then coincide with the assigned $5/2\ 1/2-[521]$ state and the $9/2-$ state with the $7/2\ 1/2-[521]$ state. A possible $11/2-$ state is then observed at 645 keV.

The $3/2-$, $7/2-$, $9/2-$, and $11/2-$ members of the band are all observed in the three nuclei where this band occurs as ground state, except in ^{155}Gd where the $11/2-$ member coincides with another group. The intensities are roughly in agreement with those given in table 9. The $5/2-$ member of the band, which is not expected to be observed for the pure Nilsson state, is weakly populated in the bands considered here. This may be mostly a result of the Coriolis coupling to the $5/2-[523]$ band and will be discussed later.

The occurrence of the same band as ground state in three consecutive nuclei is a somewhat remarkable fact which must be associated with the crossings of the $3/2+[651]$ and $5/2+[642]$ states with the $3/2-[521]$ state. The considerable change in deformation with increasing neutron number is

TABLE 9. The theoretical cross sections in $\mu b/sr$ for (d, t) reactions in the Gd isotopes.
 $Q = -2 \text{ MeV}$, $\theta = 90^\circ$, $V^2 = 1$.

J Nilsson orbital	1/2	3/2	5/2	7/2	9/2	11/2	13/2
1/2 + [411]	126	336	154	36	6	–	–
5/2 + [402]	–	–	71	12	5	–	–
7/2 + [404]	–	–	–	157	3	–	–
1/2 + [400]	858	189	90	6	1	–	–
3/2 + [402]	–	678	56	12	1	–	–
1/2 – [541]	183	233	171	24	25	14	–
7/2 – [523]	–	–	–	20	2	89	–
1/2 – [530]	10	357	35	137	30	14	–
1/2 + [660]	12	4	81	1	104	0	27
3/2 – [532]	–	65	126	48	53	10	–
3/2 + [651]	–	1	32	2	83	0.4	33
9/2 – [514]	–	–	–	–	1	93	–
5/2 + [642]	–	–	6	1	55	0.6	37
3/2 – [521]	–	176	~ 0	315	24	11	–
5/2 – [523]	–	–	44	45	74	6	–
11/2 – [505]	–	–	–	–	–	94	–
1/2 – [521]	420	41	108	147	25	4	–
7/2 + [633]	–	–	–	0.5	28	0.7	40
1/2 + [651]	171	195	249	92	24	9	6
5/2 – [512]	–	–	6	465	13	6	–
7/2 – [514]	–	–	–	26	87	3	–

apparently large enough to ensure that the $3/2 - [521]$ state stays above the two $N = 6$ states (see fig. 23). This seems to require that the crossings of the energy levels occurs at somewhat larger deformation than indicated by the newest Nilsson diagrams¹⁸⁾.

The (d, t) cross sections for the $3/2 -$ and $7/2 -$ states, which are plotted in fig. 22, clearly show the increased filling of the $3/2 - [521]$ orbital as the neutron number is increased. A corresponding variation can be traced in the (d, p) cross sections, but the behaviour is less regular.

The moments of inertia for the $3/2 - [521]$ bands are listed in table 11. It should be remarked that the rotational energies of this band show an alternating energy term similar to that observed in the ^{159}Tb spectrum¹⁹⁾. The analysis of the rotational energies will be published later⁸⁾.

TABLE 10. The theoretical cross sections in $\mu b/sr$ for (d,p) reactions in the Gd isotopes.

$$Q = +3 \text{ MeV}, \theta = 90^\circ, U^2 = 1.$$

J Nilsson orbital	1/2	3/2	5/2	7/2	9/2	11/2	13/2
11/2 - [505]	-	-	-	-	-	69	-
3/2 + [651]	-	1	23	1	78	0.4	34
3/2 - [521]	-	107	~ 0	275	17	8	-
5/2 + [642]	-	-	4	1	39	0.6	37
5/2 - [523]	-	-	39	40	54	4	-
1/2 - [521]	255	25	95	120	18	3	-
7/2 + [633]	-	-	-	0.3	20	0.7	40
1/2 + [651]	120	137	171	65	16	10	6
5/2 - [512]	-	-	5	408	10	4	-
7/2 - [503]	-	-	-	482	4	2	-
7/2 - [514]	-	-	-	22	63	2	-
9/2 + [624]	-	-	-	-	6	0.6	42
1/2 + [640]	52	3	210	34	49	15	5
3/2 + [642]	-	29	83	67	9	20	5
1/2 - [510]	10	414	151	100	6	1	-
3/2 - [512]	-	82	333	62	10	0.8	-
3/2 - [501]	-	784	72	40	~ 1	~ 0	-

4.3.2. The 5/2 + [642] and the 3/2 + [651] Orbitals

The identification of the 5/2 + [642] orbital in the deformed Gd nuclei is somewhat doubtful. The predicted pattern consists of two lines with $j = 9/2$ and $j = 13/2$, respectively. A similar pattern is expected for the 3/2 + [651] orbital where the 5/2 + state, however, is also populated (cf. tables 9 and 10). The situation is further complicated by the strong Coriolis matrix element between these two bands and by the abnormal order of filling of the Nilsson orbitals. The latter is illustrated in fig. 23, which is drawn to explain the persistent occurrence of the 3/2 - [521] state as ground state in the Gd nuclei.

With the reservations necessitated by the complications discussed above, plausible 5/2 + [642] bands have been found in the ^{159}Gd and ^{157}Gd nuclei. The assignment in ^{157}Gd is in agreement with earlier decay scheme work. For ^{159}Gd , the (d,t) spectrum is relatively clear in the region of the band proposed and the study of the angular distributions supports the assignments⁷⁾.

In ^{155}Gd , the 5/2 + level at 105 keV which has been proposed for the 5/2 5/2 + [642] level¹¹⁽²⁰⁾ is strongly populated in both the (d,p) and the

TABLE 11. Inertial parameters and decoupling parameters. Numbers in brackets are decoupling parameters for $K = 1/2$ bands.

Nilsson orbital	161	159	157	155	153
3/2 - [521]	10.4	10.0	11.0	12.0	
5/2 - [523]	10.3	11.5	11.8	10.2	
5/2 + [642]		7.7	7.5		
1/2 + [660]		13.3 (4.51)			
3/2 - [532]		9.8	10.2		
1/2 - [530]		7.7 (0.15)	7.7 (0.16)	8.6 (0.12)	
1/2 - [521]	10.9 (0.25)	11.6 (0.49)	12.2 (0.27)	13.9 (0.32)	16.0 (0.74)
7/2 + [633]	7.1				
5/2 - [512]	11.5	10.7			
1/2 - [510]	11.3 (-0.12)	11.6 (0.38)			
1/2 + [651]	7.6 (-0.47)	7.3 (-0.27)			

(d, t) reactions and can therefore not be the band head of the $5/2 + [642]$ orbital, unless this orbital is heavily mixed with orbitals which have strong components of $j\pi = 5/2 +$. Inspection of table 9 shows that such components are found for the $1/2 + [400]$, $3/2 + [402]$, $1/2 + [660]$, and $3/2 + [651]$ orbitals which all are expected as low lying states in the Gd nuclei. However, the (d, t) cross section for the 106 keV level is considerably larger than expected for any $5/2 +$ component and a $5/2 +$ assignment is therefore untenable. A more likely explanation for the 106 keV level is that it represents a fraction ($\sim 40\%$) of the strong $3/2 + [402]$ state. A splitting of this intensity could result from the coupling of the $3/2 + [651]$ and the $3/2 + [402]$ levels which are expected to cross for deformations $\delta \sim 0.3$. A similar phenomenon is discussed in sect. 4.3.3 for the $1/2 + [660]$ orbital. If indeed the 106 keV is a $3/2 +$ level related to the $3/2 + [651]$ orbital, it is reasonable to suggest that the level at 86 keV seen in the decay studies²⁰⁾, which is weakly populated in the transfer reactions, is a $5/2 +$ level related to the $5/2 + [642]$ orbital. This would be consistent with all the information available. Furthermore, the angular distribution for the level at 214 keV is similar to that observed for the $13/2 + [642]$ level in ^{159}Gd and is therefore possibly the $13/2 +$ level of this or the $3/2 + [651]$ band. Unfortunately, this observation does not make the structures of these strongly Coriolis mixed bands in ^{155}Gd much clearer. Further mixing is caused by the large Coriolis matrix elements which connect several of the positive parity states mentioned above. It is exceedingly difficult to comprehend the result of the simultaneous operation of all the couplings, and it is therefore not surprising that it has been impossible to

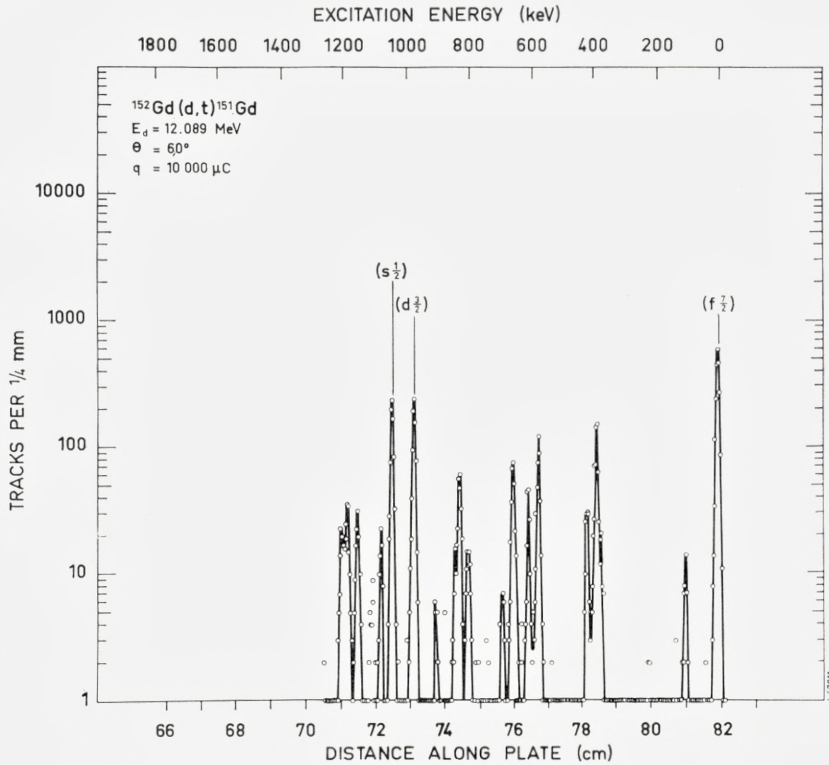


Fig. 5. Triton spectrum for the reaction $^{152}\text{Gd}(d,t)^{151}\text{Gd}$ $\theta = 60^\circ$.

identify with certainty the $3/2 + [651]$ band in any of the Gd nuclei, although this band is expected to occur at quite low excitation energies.

It should be remarked that the occurrence of crossing energy levels in the Gd nuclei is intimately connected with the onset of deformation, and a discussion of the resulting coupling phenomena is of interest for our whole understanding of the Nilsson model. We therefore plan to return to this problem which can be attacked, partly, by improvements in the experimental material and, partly, by the construction of computer programmes which allow a rapid evaluation of the expected energy levels and their population by the transfer reactions. An angular distribution study for the $^{156}\text{Gd}(d,t)^{155}\text{Gd}$ reaction which presently is being analyzed²¹⁾ could add considerably to our understanding of the crucial ^{155}Gd spectrum.

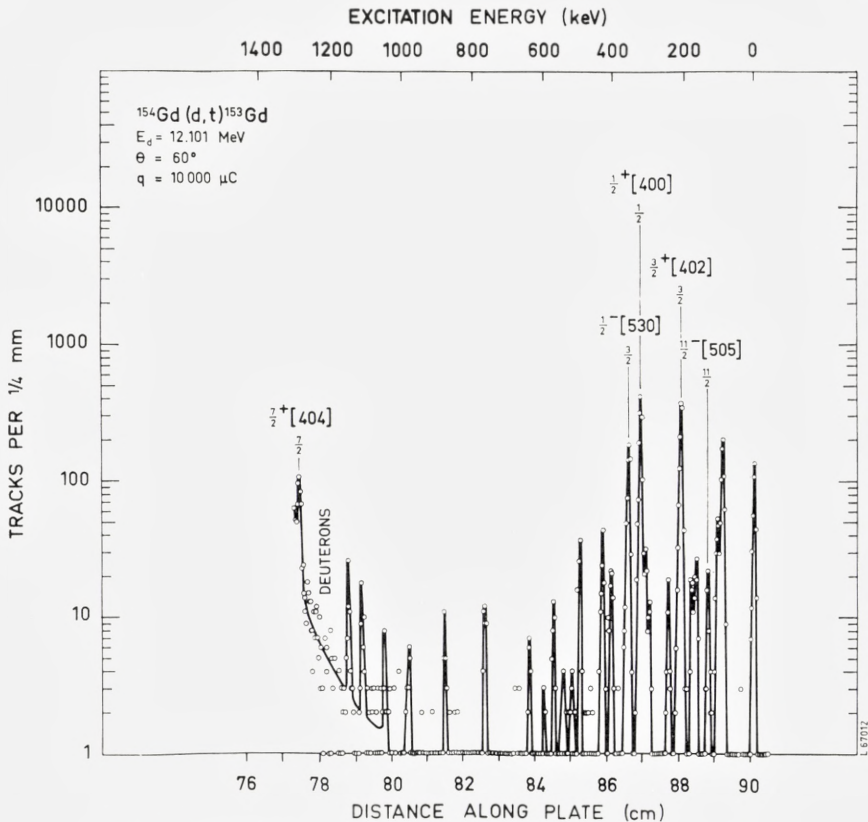


Fig. 6. Triton spectrum for the reaction $^{154}\text{Gd}(d,t)^{153}\text{Gd}$ $\theta = 60^\circ$.

4.3.3. The $1/2 + [660]$ Orbital

The $^{160}\text{Gd}(d,t)^{159}\text{Gd}$ spectrum has a strong group corresponding to a level energy of 780 keV. The angular distribution for this group⁷⁾ strongly suggests $l = 0$. Apart from that of the $1/2 \ 1/2 + [400]$ level, no strong $l = 0$ groups are expected and the only reasonable explanation for the 780 keV group is that it represents a fraction of the $1/2 \ 1/2 + [400]$ intensity, the bulk of which is found in the group at 973 keV (cf. sect. 4.3.5). A possible mechanism for such a splitting of intensity is the coupling between the orbitals $1/2 + [660]$ and $1/2 + [400]$ which, as discussed above, are expected to cross each other.

The theoretical decoupling parameter of the $1/2 + [660]$ band is $a = 6.0$, and it is interesting that it has been possible (cf. fig. 20) to construct a band of levels with reasonable intensities and l -values, which corresponds to

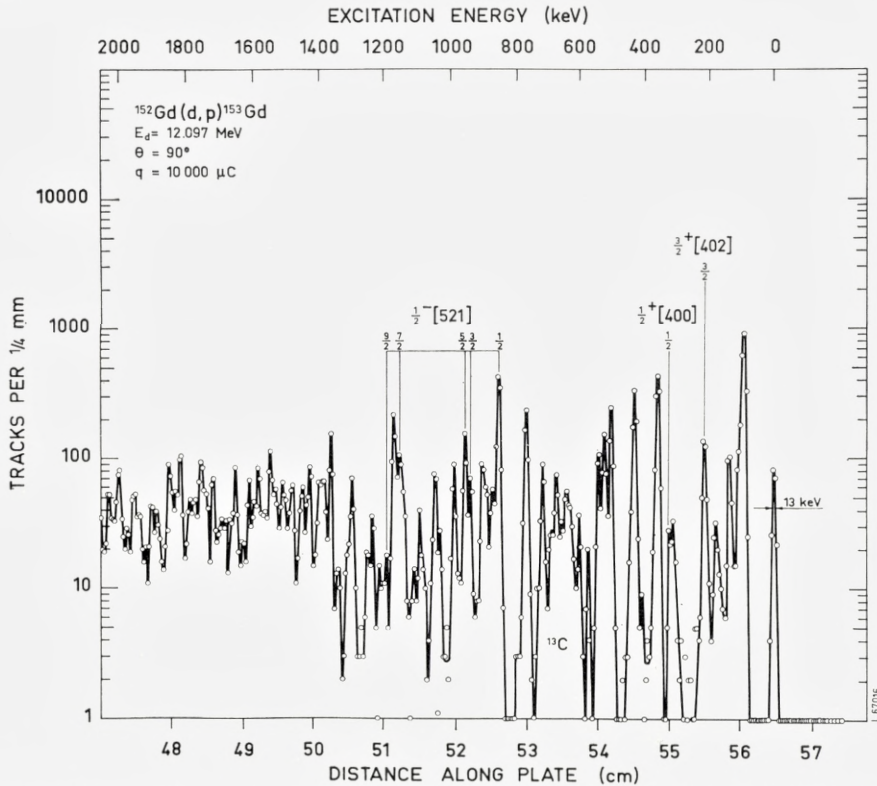


Fig. 7. Proton spectrum for the reaction $^{152}\text{Gd}(d,p)^{153}\text{Gd}$ $\theta = 90^\circ$. In this and in the following figures, groups ascribed to reactions on target impurities are indicated by the symbol of the impurity. Thus, the broad group marked ^{13}C is due to the $^{13}\text{C}(d,p)^{14}\text{C}$ reaction.

$\alpha = 4.51$ and $A = 13.3$ keV. Unfortunately, there are several other solutions with the same $1/2+$ and $13/2+$ states as shown in fig. 20. Nevertheless, this identification is the most convincing observation of the $1/2+$ [660] orbital made up to now.

4.3.4. The $11/2-$ [505] Orbital

Only the $11/2-$ member of this band is expected to be populated in the transfer reactions. Still, it has been possible to identify this orbital in ^{159}Gd , ^{157}Gd , ^{155}Gd , and ^{153}Gd on the basis of the characteristic angular dependence of the $l = 5$ transitions. Furthermore, an isomer in ^{157}Gd has been observed⁽²²⁾ at 423 keV, which is in agreement with the energy of the $11/2-$ level observed here.

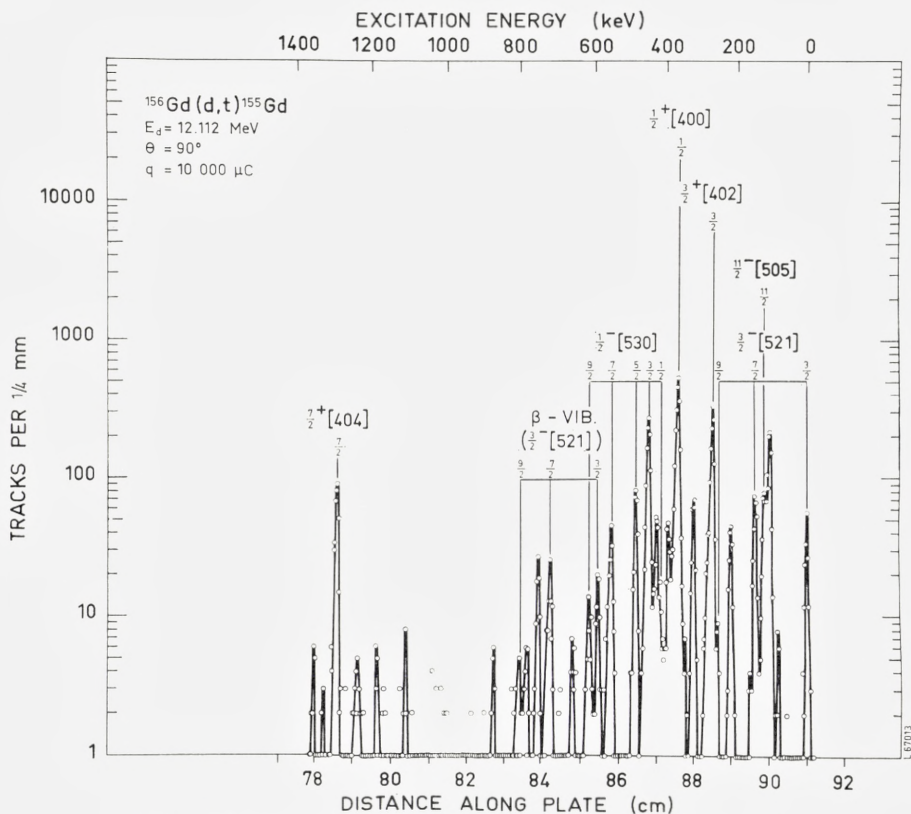


Fig. 8. Triton spectrum for the reaction $^{156}\text{Gd}(d,t)^{155}\text{Gd}$ $\theta = 90^\circ$.

In ^{155}Gd , the levels at 119 keV and 214 keV are possible candidates for a $11/2^-$ [505] assignment. Recent angular distribution measurements²¹⁾ slightly favour the 119 keV level for the $11/2^-$ [505] assignment, but this level can then hardly be identical to a known level²⁰⁾ at 118 keV. A possible explanation for the 214 keV level was discussed in sect. 4.3.2.

For the above mentioned nuclei, the ratios of the triton intensities at 90° , $Q = -2$ MeV to the calculated intensities are 1.02, 0.79, 1.27, and 0.51, respectively, which indicates a slowly decreasing filling of this orbital as the neutron number is reduced. In ^{159}Gd and ^{157}Gd , the level is weakly populated in the (d,p) reaction (cf. tables 6 and 5), as expected for a hole state. In ^{155}Gd and ^{153}Gd , somewhat stronger (d,p) groups occur at the positions for the $11/2^-$ levels. The excitation energy for this orbital shows a smooth dependence on the neutron number (fig. 15).

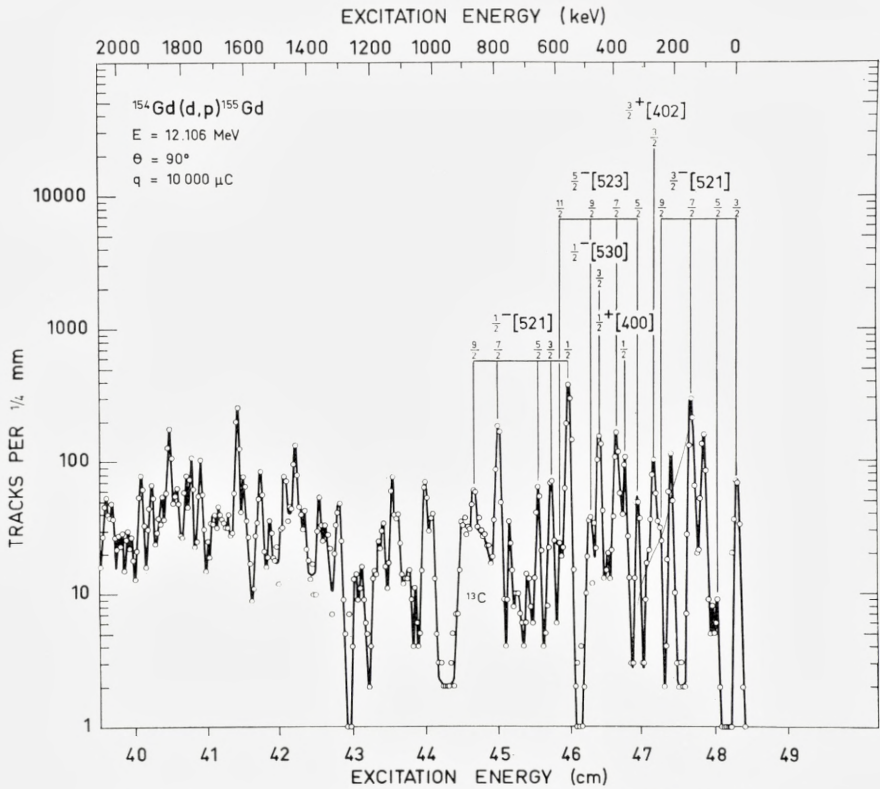


Fig. 9. Proton spectrum for the reaction $^{154}\text{Gd}(d,p)^{155}\text{Gd}$ $\theta = 90^\circ$.

4.3.5. The $3/2 + [402]$ and the $1/2 + [400]$ Orbitals

Table 9 shows that very strong lines are expected in the (d,t) spectra from the $3/2 + [402]$ and the $1/2 + [400]$ orbitals which originate in the $d_{3/2}$ and $s_{1/2}$ shell model states. Indeed, all the (d,t) spectra show two strong lines fairly close to each other, which could be the $3/2 +$ and $1/2 +$ states of these bands, but it has been difficult to decide which group belongs to which orbital and, in all cases, one must accept considerable deviations between the theoretical rotational patterns and those observed. For a general discussion of the various coupling phenomena which could cause such deviations see sect. 4.3.2.

In the ^{159}Gd spectrum the angular distributions⁷⁾ unambiguously show that the group at 734 keV has $l = 2$, whereas the group at 973 keV has $l = 0$. In view of the large cross sections for these lines, the assignments to the

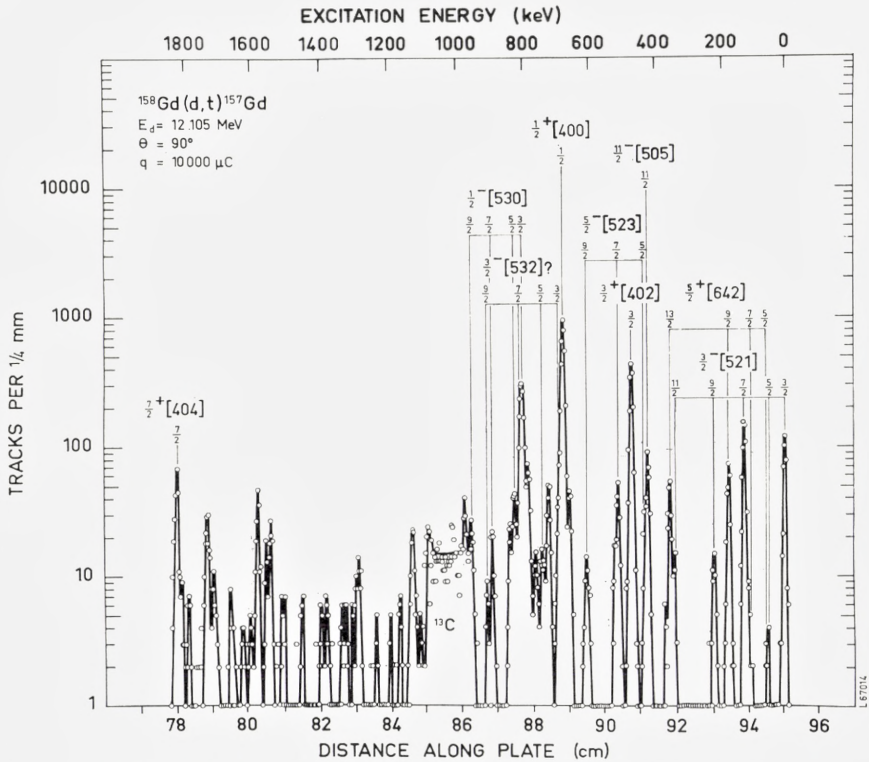


Fig. 10. Triton spectrum for the reaction $^{158}\text{Gd}(d,t)^{157}\text{Gd}$ $\theta = 90^\circ$.

states $3/2 \ 3/2 + [402]$ and $1/2 \ 1/2 + [400]$, respectively, are certain. The level order is then in agreement with that of the Nilsson model²⁾. The same level order has then been assumed for the deformed nuclei ^{157}Gd , ^{155}Gd , and ^{153}Gd . In the ^{151}Gd spectrum, there are two strong lines at 977 keV and 1047 keV. Although the nature of these states is not clear, it is natural to assume that they contain large components of the $d_{3/2}$ and $s_{1/2}$ shell-model states, respectively.

As mentioned above, there are considerable difficulties connected with the assignment of rotational bands for the $N = 4$ states. Table 9 shows that the $3/2 +$ and $5/2 +$ states in the $1/2 + [400]$ band and the $5/2 +$ state in the $3/2 + [402]$ band are expected to have appreciable (d, t) cross sections. Again, the ^{159}Gd spectrum is the most favourable case to discuss. As mentioned in sect. 4.3.3, the level at 780 keV seems to be populated mainly by $l = 0$ and can therefore not to any appreciable extent be the $5/2 +$ state of the

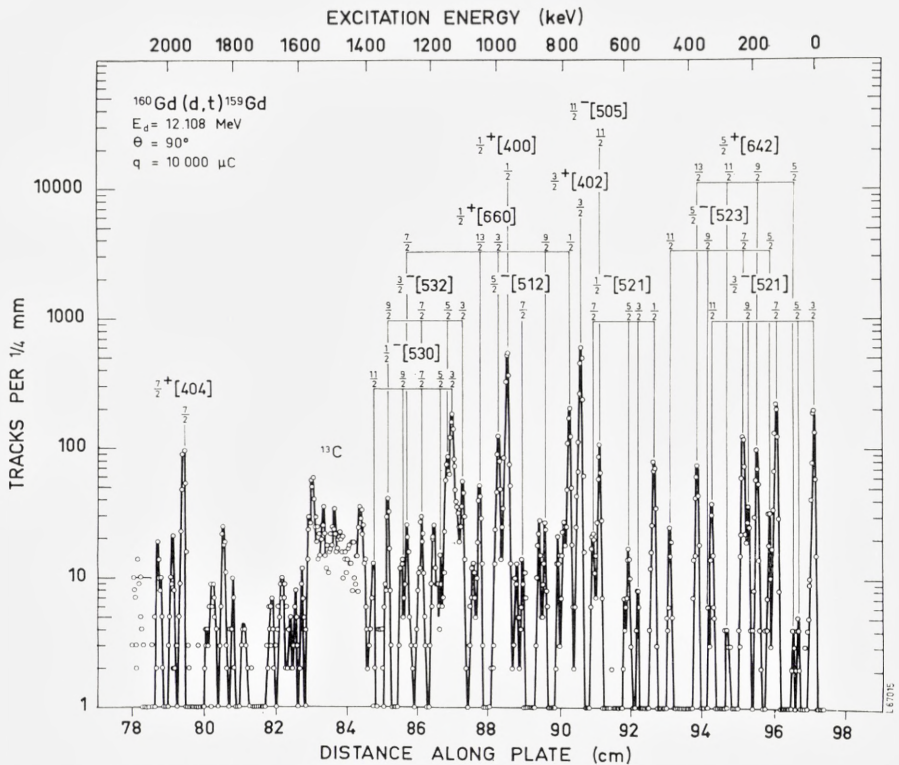


Fig. 12. Triton spectrum for the reaction $^{160}\text{Gd}(d,t)^{159}\text{Gd}$ $\theta = 90^\circ$.

is then at 1057 keV, but this group has an angular distribution which indicates a high angular momentum, possibly $l = 6$. This group is tentatively assigned to the $13/2+$ member of the $1/2+ [660]$ band (cf. sect. 4.3.3), but could of course contain some contribution from the $5/2$ $1/2+ [400]$ state. If this is the case, the parameters for this band are $a = -0.15$ and $A = 10.0$ keV. This is somewhat surprising as the pure band is expected to have a slightly positive decoupling parameter. Also the admixture of the $1/2+ [660]$ band indicated by the intensity of the state assigned $1/2$ $1/2+ [660]$ would yield a large positive decoupling parameter.

The other Gd nuclei show no structures which can be ascribed to simple rotational bands based on the $1/2+ [400]$ state.

4.3.6. The $3/2- [532]$ Orbital

This orbital is expected to occur as a hole state between the $1/2+ [400]$ orbital and the $1/2- [530]$ orbital to be discussed in the following section.

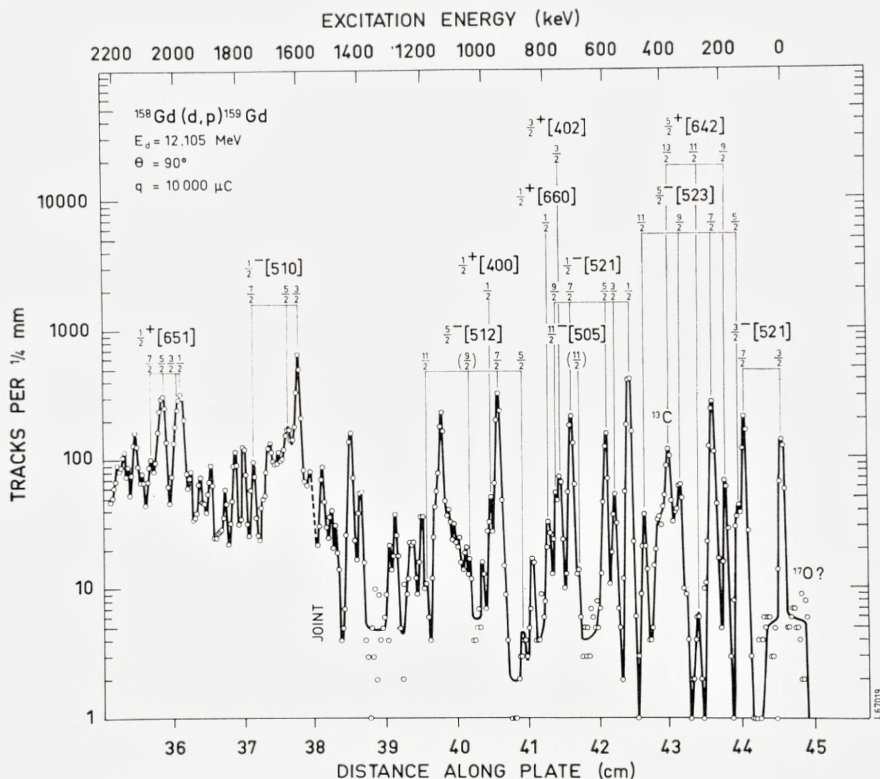


Fig. 13. Proton spectrum for the reaction $^{158}\text{Gd}(d,p)^{159}\text{Gd}$ $\theta = 90^\circ$.

The pattern consists of rather strongly populated $3/2$, $5/2$, $7/2$, and $9/2$ levels and a somewhat weaker $11/2$ level. Some deviations from the pattern can be expected because of couplings to the large number of $K\pi = 1/2 -$ and $3/2 -$ bands in this region of the Nilsson diagram.

In ^{159}Gd , the $3/2 -$ level has been placed at 1109 keV where a group with $l = 1$ is observed⁷⁾. The intensities of the rotational states agree well with the theoretical intensities, but the rotational spacings are somewhat irregular. In ^{157}Gd , there are several possible positions for the $3/2 - [532]$ band, the most likely being the one indicated in fig. 19. The intensities are, however, not in good agreement with those calculated and again the rotational spacings show some deviations. The band has not been identified in ^{155}Gd .

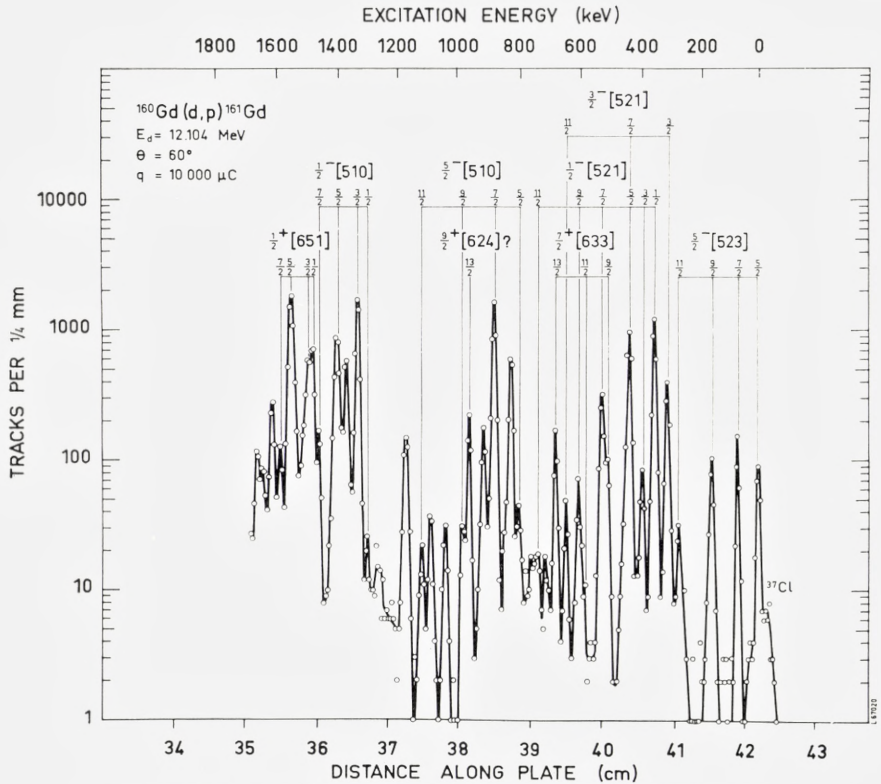


Fig. 14. Proton spectrum for the reaction $^{160}\text{Gd}(d,p)^{161}\text{Gd}$ $\theta = 60^\circ$.

4.3.7. The $1/2-[530]$ Orbital

The $1/2-[530]$ orbital is characterized by a strong population in the (d,t) reaction of the $3/2-$ state and a somewhat smaller population of the $7/2-$ state. The theoretical decoupling parameter is $a = -0.31$, but this value is quite sensitive to changes in the deformation.

For all the Gd nuclei, a strong group is observed in the (d,t) spectra at an excitation energy slightly higher than that of the $1/2+[400]$ orbital. In ^{159}Gd , this group occurs at 1143 keV and has an $l = 1, j = 3/2$ distribution⁷⁾. The assignment $3/2\ 1/2-[530]$ is therefore quite certain, but there are several possibilities for the associated rotational band. The band shown in fig. 20 corresponds to $a = 0.15$ and $A = 7.7$ keV. The intensities are in good agreement with those calculated from the theoretical wave functions, except for the $7/2-$ state where the observed intensity is less than 50% of the

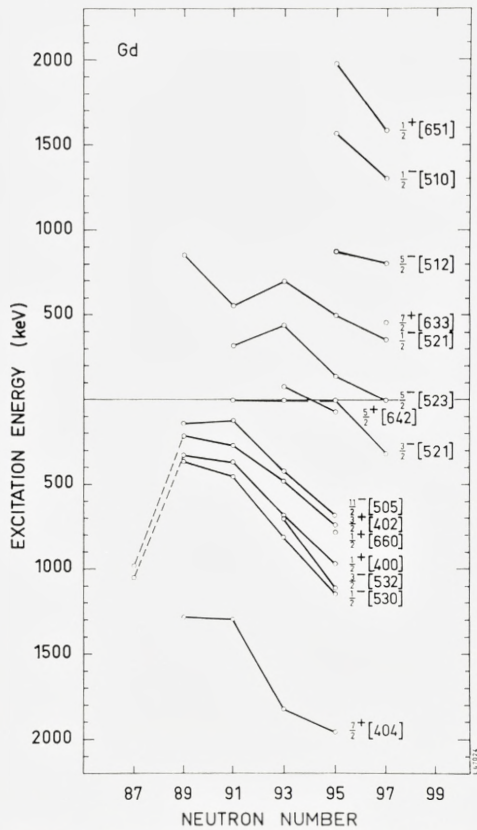


Fig. 15. Energies of the band heads for the Nilsson states observed. Points at negative energies indicate hole states.



Fig. 16. Level scheme for ^{151}Gd .

calculated intensity. This discrepancy is furthermore increased, because the state assigned as $7/2\ 3/2 - [532]$ within the experimental resolution occurs at the same energy. The only other possible choice for the $7/2\ 1/2 - [530]$ group is that at 1282 keV which, however, has only about 30% of the theoretical cross section. The $5/2 -$ and $9/2 -$ groups could then be those at 1200 keV and 1390 keV, which yields $\alpha = 0.014$ and $A = 11.6$ keV. A closer analysis including the effects of the Coriolis coupling to several nearby bands is necessary to choose between the bands proposed, but the one given in fig. 20 may be preferable because of its similarity to the $1/2 - [530]$ bands suggested in ^{157}Gd and ^{155}Gd .

In ^{157}Gd , the $3/2 -$ state is undoubtedly found at 809 keV. The band sug-

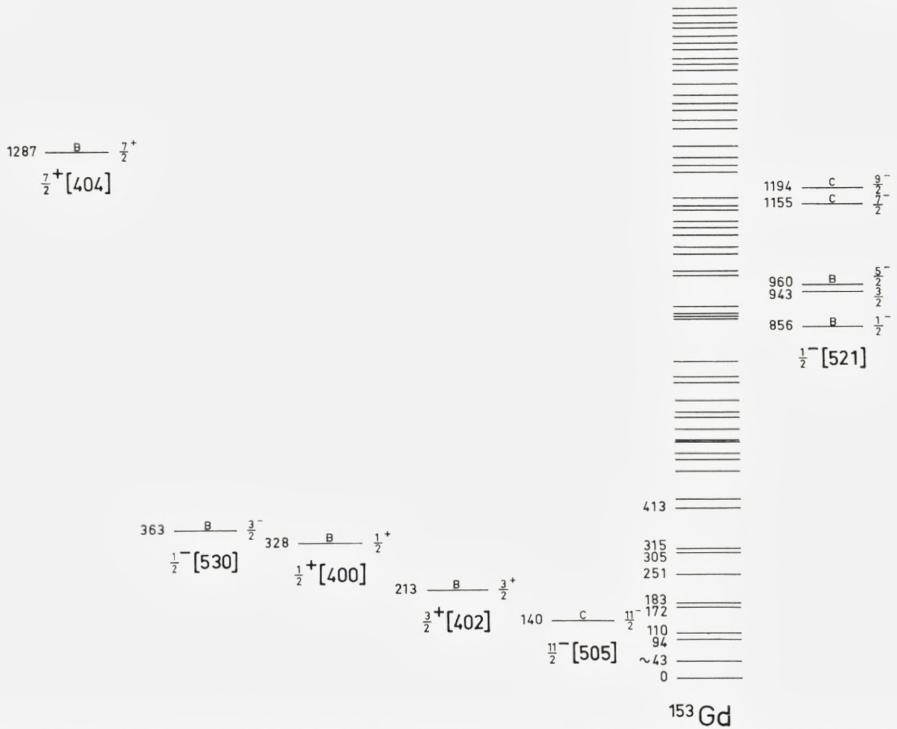
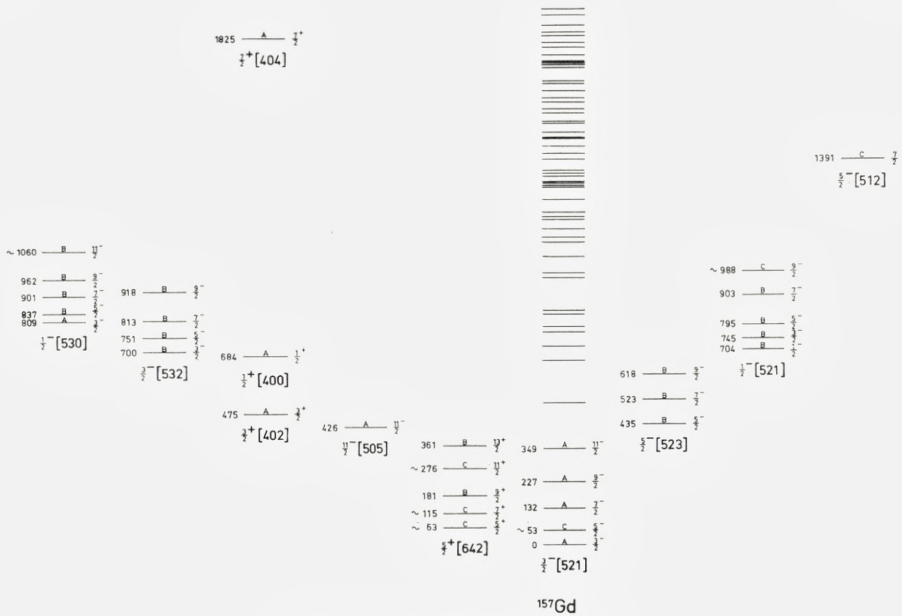


Fig. 17. Level scheme for ^{153}Gd . Nilsson states to the left are hole excitations, those to the right particle excitations. The letter *A* indicates that all the available data suggest the assignment, *B* an assignment consistent with the observations, but where lack of resolution or intensity prevents a definite assignment. Finally, *C* indicates that a group was observed at the position expected, e.g., for a rotational level but with an intensity considerably different from the theoretically predicted intensity.

gested in fig. 19 yields $a = 0.16$ and $A = 7.7$ keV, but, as it was the case in ^{159}Gd , the intensity of the $7/2^-$ state is weaker than expected, whereas the $5/2^-$ state is too strong. In ^{155}Gd , the $3/2^-$ state is found at 451 keV, and an acceptable band with $a = 0.12$ and $A = 8.6$ keV is shown in fig. 18. Also here the $7/2^-$ intensity is too weak and the $5/2^-$ intensity too large. The group at 426 keV could correspond to the $1/2^-$ state of this band. The band is excited quite strongly in the (d, d') reaction, which indicates a Coriolis coupling to the $3/2^- [521]$ ground-state band⁸⁾.

In ^{153}Gd , the group at 363 keV is probably related to the $3/2^- 1/2^- [530]$ states in the nuclei discussed above. The groups at 436 keV and 504 keV can be incorporated as $5/2^-$ and $7/2^-$ states in a band with $a = -0.2$ and $A = 12.2$ keV, but the existence of rotational spectra in this nucleus is by no means well established.

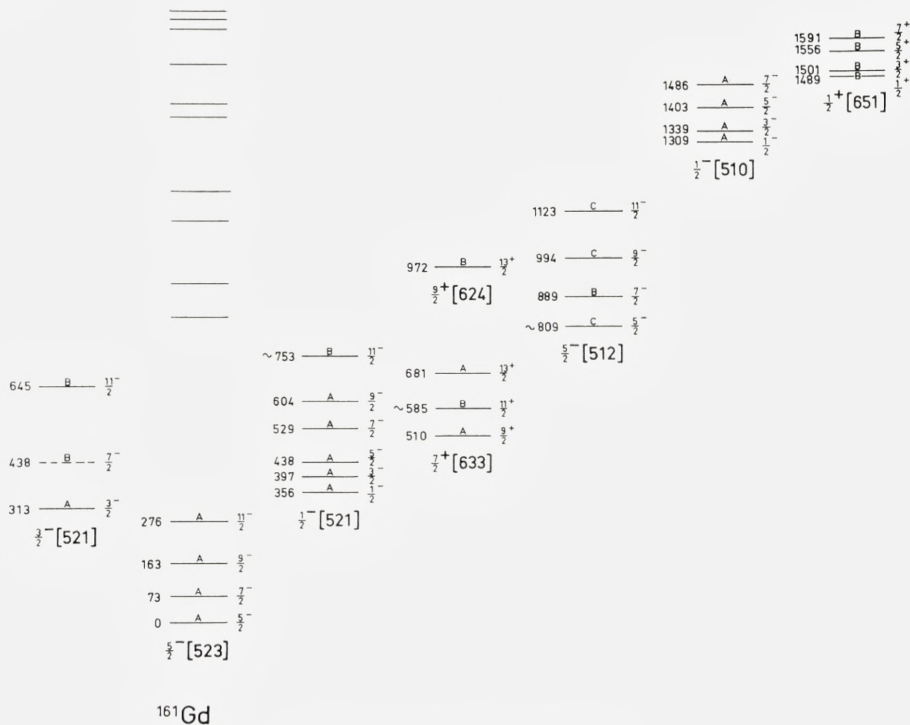
Fig. 19. Level scheme for ^{157}Gd .

certain. However, the absolute intensity of this state is somewhat larger than expected from the Nilsson wave functions.

4.3.9. The $5/2-[523]$ Orbital

This and the following sections discuss orbitals which are observed as particle excitations in the gadolinium nuclei. Most of the information comes therefore from the (d, p) spectra.

The $5/2-[523]$ orbital forms the ground state in ^{161}Gd . In this nucleus, all the rotational states up to the $11/2-$ state are observed with relative intensities in agreement with theoretical predictions. In ^{159}Gd , the band is expected as a low lying particle excitation, but no pattern similar to that in ^{161}Gd is observed below 700 keV. However, if the band head is placed at 146 keV, the 226 keV, the 327 keV and possibly the 455 keV levels form an acceptable $K = 5/2$ band. The $7/2$ member of this band has a cross section approximately five times larger than expected for the $7/2-5/2-[523]$ state. This deviation can be explained qualitatively by Coriolis coupling to the $3/2-[521]$ band which has a large cross section for the $7/2-$ state. Application of the formulae of sect. 2 shows that about 50% of the observed

Fig. 21. Level scheme for ^{161}Gd .

states are populated in the (d, d') reaction⁸⁾ as expected from the Coriolis coupling to the ground state band. The latter band has therefore been preferred here and is shown in fig. 18.

4.3.10. The $1/2^- [521]$ Orbital

This orbital should occur as a particle excitation in all the gadolinium nuclei. All the rotational states are expected to be populated with most of the intensity in the $1/2^-$, $5/2^-$, and $7/2^-$ states. The theoretical decoupling parameter is 0.9 and the resulting pattern is highly characteristic of the orbital. The identification of the band is therefore quite certain in spite of significant differences between the observed and calculated absolute cross sections.

The cross sections for the rotational states in the $1/2^- [521]$ show violent fluctuations, but the average values are in reasonable agreement with the theoretical predictions (fig. 24). Several effects can be responsible for this

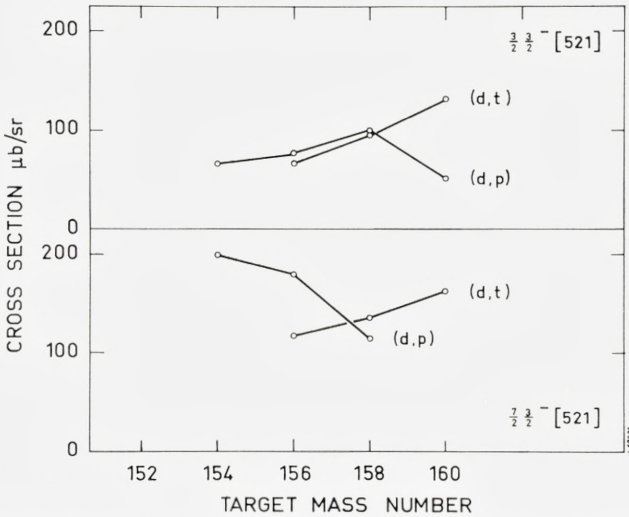


Fig. 22. Cross section for the $3/2 \ 3/2^- [521]$ and $7/2 \ 3/2^- [521]$ states as a function of the final mass number. The (d,p) cross sections are reduced to $Q = 3$ MeV and the (d,t) cross sections to $Q = -2$ MeV.

behaviour, the most important probably being the coupling to the gamma-vibrational states. Calculations by SOLOVIEV²³⁾ show that, in ^{155}Gd , the lowest $1/2^-$ state is $42\% \ 1/2^- [521]$, 37% gamma vibration based on the $3/2^- [521]$ state, and 18% gamma vibration based on the $5/2^- [523]$ state. The (d,p) cross section obtained here seems to indicate a somewhat larger single-particle amplitude than given by SOLOVIEV; on the other hand, the predicted contribution from the gamma vibration based on the ground state is in very good agreement with the results obtained for ^{155}Gd in the (d,d') experiment⁸⁾. The low cross section for the $1/2^- [521]$ band in ^{157}Gd is somewhat surprising in view of the fact that this band is weakly populated in the (d,d') reaction. The decoupling parameters for the $1/2^- [521]$ bands in the gadolinium isotopes are considerably smaller than the theoretical value, which is in agreement with observations for other bands with vibrational admixtures¹⁹⁾.

In addition to the coupling to the gamma vibration, the Coriolis coupling to the various $K = 1/2^-$ and $3/2^-$ bands can be expected to be of importance.

4.3.11. The $7/2^+ [633]$ Orbital

The $7/2^+ [633]$ orbital is expected to be weakly populated and only in ^{161}Gd it has been possible to identify the band with some degree of certainty.

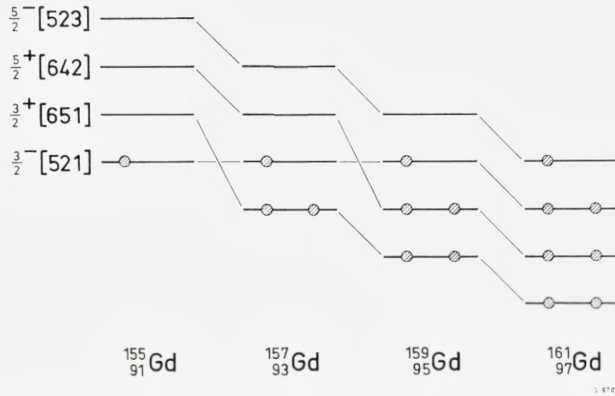


Fig. 23. Expected order of filling of Nilsson states in deformed Gd isotopes.

The groups corresponding to the $9/2$ and $13/2$ states shown in fig. 21 have reasonable intensities, and high l values are indicated by the angular intensity variations. The inertial parameter is $A = 6.4$ keV, in agreement with the generally high moment of inertia for this orbital.

4.3.12. The $5/2- [512]$ Orbital

This orbital is characterized by a strong $l = 3$ group to the $7/2-$ state. The ^{161}Gd spectrum has a strong proton group at 889 keV which appears to have $l = 3$; unfortunately, the group at 90° coincided with a plate joint. Nevertheless, this group has been assigned to the $7/2$ $5/2- [512]$ state, and a reasonable rotational band has been constructed (fig. 21). In ^{159}Gd , there is no single group with the expected intensity, but three groups at 950 keV, 1138 keV, and 1430 keV seem to have $l = 3$ and a combined reduced intensity corresponding to approximately 80% of the intensity of the $7/2-$ group in ^{161}Gd . It is therefore indicated that, in ^{159}Gd , the strength in the $5/2- [512]$ orbital is shared between several levels. In ^{157}Gd , there is a single group at 1391 keV with $l = 3$, but the intensity is there only about 30% of that in ^{161}Gd . It has not been possible to trace the $5/2- [512]$ orbital in the lighter gadolinium nuclei.

It is interesting to note the breakdown of the single-particle description for the $5/2- [512]$ orbital and also for the $1/2- [521]$ orbital in the gadolinium nuclei. In the ytterbium nuclei, these states occur near the ground state and show excellent agreement¹⁾ with the predictions based on pure Nilsson wave functions.

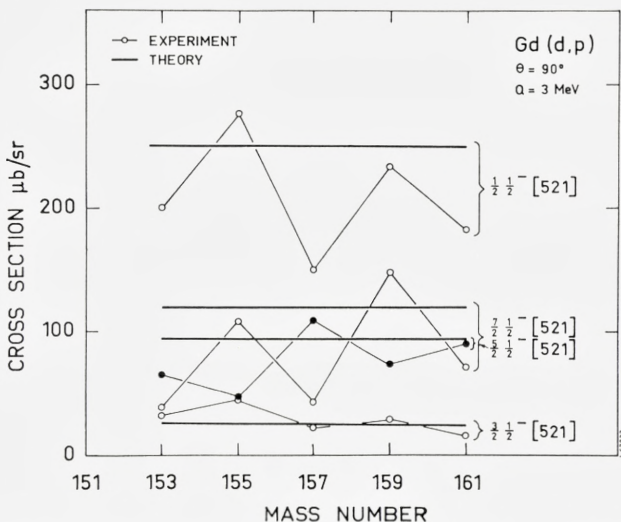


Fig. 24. Cross section for the (d,p) reaction of the $1/2^- [521]$ state as a function of the final mass number. The cross section is reduced to $Q = 3$ MeV.

4.3.13. The $1/2^- [510]$ Orbital

For this orbital, a strong $l = 1$ group is expected to the $3/2^-$ level and relatively strong $l = 3$ groups to the $5/2^-$ and $7/2^-$ levels. The theoretical decoupling parameter is $a = -0.34$, but the experimentally determined decoupling parameters for this band in other nuclei are slightly positive.

In ^{161}Gd , the strong group at 1339 keV which has an $l = 1$ distribution is assigned to the $3/2^-$ level of the $1/2^- [510]$ band. The rotational band shown in fig. 21 is constructed from groups with nearly correct relative intensities (cf. table 19) and yields $a = -0.12$ and $A = 11.3$ keV. The total absolute cross section of the band is about 60% of that expected for a pure state.

The ^{159}Gd spectrum has an intense peak at 1602 keV with an $l = 1$ angular dependence. If this peak is assigned to the $3/2^-$ level, the rotational band shown in fig. 20 can be constructed from groups with reasonable intensities and angular distributions; however, the solution is not unique, since other groups are present in the same energy region. The band shown in fig. 20 corresponds to $a = 0.38$ and $A = 11.6$ keV. The total intensity is approximately 50% of the calculated intensity.

In the (d,p) spectra of lighter nuclei, there are no single groups with as large intensities as those discussed above and it has therefore not been possible to identify the $1/2^- [510]$ band or fractions thereof.

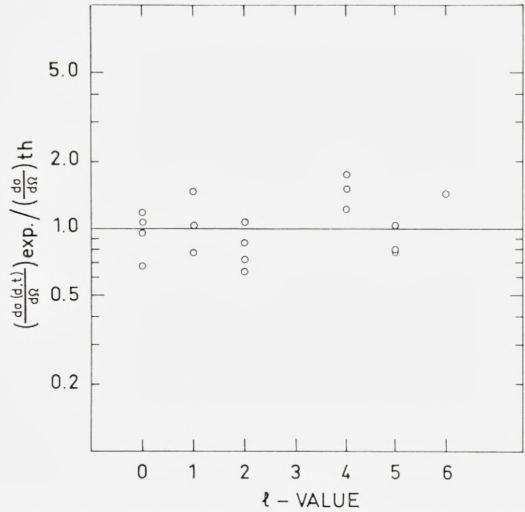


Fig. 25. Ratio of experimental to theoretical cross sections for states populated by (d,t) reactions.

4.3.14. The $1/2 + [651]$ Orbital

On the basis of the Nilsson diagram this orbital can be expected as a fairly low lying particle state in the well deformed nuclei. It is characterized by large cross sections (cf. table 10) to the $1/2$, $3/2$, $5/2$, and $7/2$ states and a decoupling parameter of -0.6 and should therefore be fairly easy to identify in the spectra. The band is not expected to be much affected by mixing, because the quantum numbers are different from those of the neighbouring levels.

The $1/2 + [651]$ orbital has been tentatively identified in ^{161}Gd and ^{159}Gd . In both nuclei, the four levels which are expected to be strongly populated have been observed with large cross sections, although the agreement with the predicted values is not perfect (cf. table 20). The parameters of the band in ^{161}Gd are $a = -0.47$ and $A = 7.6$ keV and, in ^{159}Gd , $a = -0.27$ and $A = 7.7$ keV.

The $1/2 + [651]$ band is expected at approximately 2.5 MeV in ^{157}Gd , but at this excitation energy the spectra are complicated and have not been analyzed.

4.3.15. Other Levels in the Deformed Nuclei

The level schemes, figs. 18–21, show a considerable number of levels for which it has not been possible to give a definite assignment to a single-particle orbital. Most of these levels are found at high excitation energies,

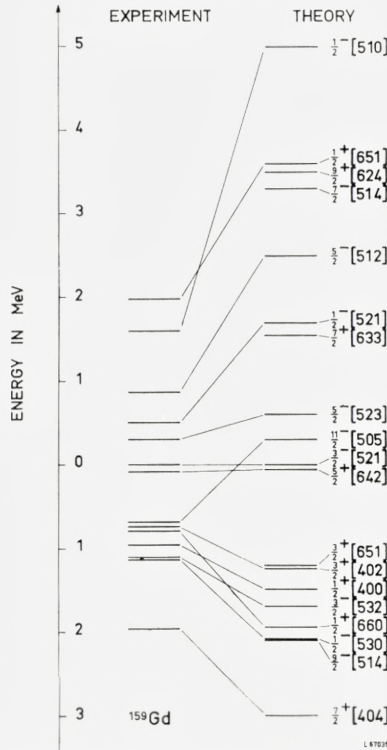


Fig. 26. Experimental and theoretical Nilsson levels in ^{159}Gd .

but especially the ^{155}Gd and the ^{157}Gd spectra show several low lying levels in this category, which are strongly populated by the transfer reactions. The discussion in the preceding sections has repeatedly touched upon the various types of couplings which can spread the single-particle intensity of several levels, and we shall here just mention a few unassigned levels for which it seems reasonable to make more definite statements.

The level at 972 keV in ^{161}Gd appears to have a high l -value, perhaps $l = 6$. In this region of the spectrum, the $9/2 + [624]$ orbital is expected, and it is possible that the 972 keV level is the $13/2 +$ level of this band. If this is the case, the $7/2 - [514]$ orbital is the only particle excitation below the $1/2 + [651]$ orbital which has not been identified in ^{161}Gd .

It has recently been suggested²⁰⁾ that a beta-vibrational band with energies 592.6 keV ($3/2 -$) and 647.8 keV ($5/2 -$) occurs in ^{155}Gd . This suggestion is mostly based on the observation of an E0 component in the decay of these states. The present (d, t) data lend some support to the band pro-

posed. The groups at 594 keV, 721 keV, and 813 keV which could correspond to the $3/2^-$, $7/2^-$, and $9/2^-$ members show intensity ratios of 1.00:1.89:0.37. These can be compared to the corresponding ratios 1.00:1.92:0.22 for the ground-state band. The total (d, t) intensity to the excited band is approximately 25% of that to the ground-state band. It should be remarked that the $7/2^-$ state suggested here is different from the 706 keV state proposed in ref.²⁰. The moment of inertia parameter A for the beta band is 10.6 keV compared to 12.1 keV for the ground-state band. The reduction in A is in agreement with the data for the beta vibrations in the even nuclei. The beta-vibrational band in ^{155}Gd is also observed in the (d, d') spectra⁸).

4.3.16. Levels in ^{153}Gd and ^{151}Gd

On the basis of the present data, very little can be said about the nature of the levels in ^{153}Gd and ^{151}Gd .

It has been proposed²⁴) that the $3/2 + [651]$ orbital forms the ground state in ^{153}Gd . This assignment is difficult to reconcile with the strong population observed here for the ground state and the 93 keV state. If indeed the ground-state spin²⁵) of ^{153}Gd is $3/2$, then the present data rather point to a connection to the $3/2 - [521]$ state. The properties of the level at 93 keV in ^{153}Gd resemble those of the mysterious level at 105 keV in ^{155}Gd (cf. sect. 4.3.2). The levels at 140 keV, 213 keV, 328 keV, 363 keV, and 1287 keV seem to be related to the $11/2 - [505]$, $3/2 + [402]$, $1/2 + [400]$, $1/2 - [530]$, and $7/2 + [404]$ orbitals, respectively, and are discussed in the previous sections. Similarly, the 856 keV level has been assigned as the band head of a band related to the $1/2 - [521]$ orbital.

In ^{151}Gd , even the ground-state spin is unknown. The ground state in the isotope ^{149}Sm has been assigned to the $f7/2$ shell-model state and the (d, t) data are consistent with the same assignment for the ^{151}Gd ground state. The levels at 977 keV and 1047 keV have been associated with the $d3/2$ and $s1/2$ shell-model states and are discussed in sect. 4.3.5.

5. Comparison of Intensities with Predicted Values

It is of considerable interest to compare the observed absolute intensities with those predicted from theory as outlined in sect. 2. A comparison of this kind was performed for the ytterbium isotopes which, on the average, showed good agreement between the (d, p) cross sections, whereas the calculated (d, t) cross sections were somewhat lower than the experimental

TABLE 12. (d, t) population of the $3/2 - [521]$ band.

Spin	$d\sigma/d\Omega, \theta = 90^\circ, Q = -2 \text{ MeV}$				Relative values of C_{jt}^2			
	Theory	^{155}Gd	^{157}Gd	^{159}Gd	Theory	^{155}Gd	^{157}Gd	^{159}Gd
3/2	176	68	84	132	0.10	0.11	0.10	0.14
5/2	~ 0	~ 1	2	4	~ 0	~ 0.005	0.006	0.01
7/2	315	117	135	164	0.53	0.54	0.46	0.50
9/2	24	12	12	17	0.26	0.35	0.26	0.32
11/2	11	—	8	2	0.11	—	0.17	0.04

TABLE 13. (d, t) population of the $11/2 - [505]$ band.
 $d\sigma/d\Omega, \theta = 90^\circ, Q = -2 \text{ MeV}$.

Spin	Theory	^{153}Gd	^{155}Gd	^{157}Gd	^{159}Gd
11/2 -	94	48	119	74	96

TABLE 14. (d, t) population of the $N = 4$ states.
 $d\sigma/d\Omega, \theta = 90^\circ, Q = -2 \text{ MeV}$.

Level	Theory	^{153}Gd	^{155}Gd	^{157}Gd	^{159}Gd
3/2 3/2 + [402]	678	717	488	435	586
1/2 1/2 + [400]	858	820	922	1015	642
7/2 7/2 + [404]	157	$\sim 270^*$	277	194	235

* Estimated from the yield at 60° .

TABLE 15. (d, t) population of the $1/2 - [530]$ band.

Spin	$d\sigma/d\Omega, \theta = 90^\circ, Q = -2 \text{ MeV}$				Relative values of C_{jt}^2			
	Theory	^{155}Gd	^{157}Gd	^{159}Gd	Theory	^{155}Gd	^{157}Gd	^{159}Gd
1/2	10	27	—	—	0.006	0.02	—	—
3/2	357	554	365	275	0.21	0.35	0.40	0.29
5/2	35	165	58	10	0.06	0.30	0.18	0.03
7/2	137	100	29	48	0.23	0.18	0.07	0.14
9/2	30	13	18	18	0.35	0.15	0.35	0.31
11/2	14	—	—	13	0.15	—	—	0.24

TABLE 16. (d, p) population of the $3/2 - [521]$ band.

Spin	$d\sigma/d\Omega, \theta = 90^\circ, Q = 3 \text{ MeV}$					Relative values of C_{jl}^2				
	Theory	^{155}Gd	^{157}Gd	^{159}Gd	^{161}Gd	Theory	^{155}Gd	^{157}Gd	^{159}Gd	^{161}Gd
3/2	107	64	76	91	53	0.10	0.10	0.12	0.30	0.11
5/2	0	—	—	—	—	0	—	—	—	—
7/2	275	192	177	105	120	0.53	0.59	0.57	0.70	0.47
9/2	17	13	12	—	—	0.26	0.32	0.32	—	—
11/2	8	—	—	—	14	0.11	—	—	—	0.42

TABLE 17. (d, p) population of the $5/2 - [523]$ band.

Spin	$d\sigma/d\Omega, \theta = 90^\circ, Q = 3 \text{ MeV}$					Relative values of C_{jl}^2				
	Theory	^{155}Gd	^{157}Gd	^{159}Gd	^{161}Gd	Theory	^{155}Gd	^{157}Gd	^{159}Gd	^{161}Gd
5/2	39	37	34	48	22	0.07	0.11	0.11	0.10	0.08
7/2	40	113	124	112	~ 21	0.08	0.33	0.39	0.28	0.08
9/2	54	25	20	~ 14	22	0.79	0.56	0.50	0.27	0.64
11/2	4	—	—	18	7	0.06	—	—	0.35	0.20

TABLE 18. (d, p) population of the $1/2 - [521]$ band.

Spin	$d\sigma/d\Omega, \theta = 90^\circ, Q = 3 \text{ MeV}$						Relative values of C_{jl}^2					
	Theory	^{153}Gd	^{155}Gd	^{157}Gd	^{159}Gd	^{161}Gd	Theory	^{153}Gd	^{155}Gd	^{157}Gd	^{159}Gd	^{161}Gd
1/2	255	200	252	151	213	171	0.25	0.39	0.35	0.32	0.23	0.25
3/2	25	31	43	22	27	15	0.02	0.06	0.06	0.05	0.03	0.02
5/2	95	63	43	110	68	~ 85	0.18	0.24	0.12	0.46	0.15	0.24
7/2	120	38	110	43	135	86	0.23	0.15	0.25	0.18	0.29	0.19
9/2	18	6	11	—	18	13	0.27	0.17	0.23	—	0.30	0.29
11/2	3	—	—	—	—	—	0.05	—	—	—	—	—

TABLE 19. (d, p) population of the $1/2 - [510]$ band.

Spin	$d\sigma/d\Omega, \theta = 90^\circ, Q = 3 \text{ MeV}$			Relative values of C_{jl}^2		
	Theory	^{159}Gd	^{161}Gd	Theory	^{159}Gd	^{161}Gd
1/2	10	—	4	0.01	—	0.01
3/2	414	198	210	0.41	0.50	0.50
5/2	151	67	70	0.29	0.34	0.33
7/2	100	31	33	0.19	0.16	0.15
9/2	6	—	—	0.09	—	—
11/2	1	—	—	0.02	—	—

TABLE 20. (d, p) population of the $1/2 + [651]$ band.

Spin	$d\sigma/d\Omega, \theta = 90^\circ, Q = 3 \text{ MeV}$			Relative values of C_{Jl}^2		
	Theory	^{159}Gd	^{161}Gd	Theory	^{159}Gd	^{161}Gd
1/2	120	82	111	0.070	0.16	0.17
3/2	137	70	81	0.13	0.22	0.20
5/2	171	88	191	0.17	0.28	0.40
7/2	65	29	26	0.23	0.34	0.23
9/2	16	—	—	0.06	—	—
11/2	10	—	—	0.22	—	—
13/2	6	—	—	0.13	—	—

values. As the cross-section systematics strongly indicated that the states in Yb did correspond to almost pure single-particle excitations, it was concluded that the DWBA results for the (d, p) reaction were quite accurate, whereas the particular DWBA calculation used for the (d, t) reaction was not entirely satisfactory.

For the gadolinium isotopes considered here, a comparison of experimental and theoretical (d, p) cross sections is not very meaningful as a check on the DWBA results. The discussion in sect. 4 shows that almost none of the states observed as particle excitations corresponds to pure configurations. However, the optical model parameters used in the calculations are identical to those used for ytterbium, and there is good reason to believe that they should work well for gadolinium too. The ratios of observed to calculated (d, p) cross sections can then be taken as measures of the purities of the particle states observed.

Tables 16 to 20 compare the reduced (d, p) cross sections to those obtained from the theoretical wave functions and the DWBA results with the parameters listed in table 1. It is evident that, in most cases, the observed cross sections are lower than predicted, in agreement with the discussion in sect. 4. Apart from the cases where strong Coriolis couplings significantly affect the cross sections, the relative intensities to the rotational states within a band are in reasonable agreement with the theory.

The situation with respect to the (d, t) cross sections is somewhat different because of the poor agreement between the experimental and theoretical cross sections for the ytterbium isotopes. The parameters used for gadolinium (table 1) are probably superior to the earlier ytterbium parameters, but again, in the gadolinium isotopes there is a lack of states which can be assumed to be pure single-hole excitations. Nevertheless, a comparison of

the cross sections for selected cases shows reasonable agreement between experimental and theoretical values. These cases are listed in tables 12 to 15. Fig. 25, which corresponds to fig. 24 of ref.¹⁾, shows that the agreement between experiment and theory for the low l values is considerably better than for ytterbium. However, the cross sections for the high l -values appear to be somewhat too high, in agreement with the observations for ytterbium.

As a further check on the accuracy of the DWBA results, the (d, t) parameters listed in table 1 were used for the ytterbium nuclei. The ratios of experimental to theoretical cross sections thus obtained were considerably closer to unity than the earlier results, but the procedures are still too uncertain to allow a precise determination of spectroscopic factors from the (d, t) reaction.

6. Conclusions

The present survey of the single-neutron transfer reactions to the odd gadolinium isotopes identifies rotational bands which correspond to 16 different Nilsson orbitals. Most of these bands or parts thereof have been observed in several final nuclei.

In many cases, it is indicated that the rotational bands based on the single-particle excitations are considerably mixed with each other and with bands based on collective states. In all the nuclei, several levels are observed for which no assignment can be made.

The single-particle levels observed span a considerable range of energies. Fig. 26 shows the theoretical Nilsson levels for a deformation of $\beta = 0.3$ and $\hbar\omega = 8.8$ MeV together with the experimentally observed levels in ¹⁵⁹Gd. The observed level order in general agrees with the theoretical one, except for the $11/2 - [505]$ level which occurs considerably lower than expected. The experimental energy scale is compressed almost a factor of two compared to the theoretical scale. This effect has been observed earlier and can, at least in part, be ascribed to the pairing interaction which can be estimated to reduce the energy span by $\sim 2\Delta$ or approximately 2.5 MeV. If one considers that the $1/2 - [510]$ level is lowered by the gamma vibration, this expectation is in reasonable agreement with the observations.

It should be remarked that fig. 26 includes levels from the $N = 4, 5,$ and 6 oscillator shells. Especially important is the simultaneous observation of the $7/2 + [404]$ and the $1/2 + [651]$ orbitals, which fixes the relative positions of the $1g7/2$ and $2g9/2$ shell-model states. The observation of components of these distant single-particle levels in one nucleus reflects the tremendous change in the single-particle levels caused by the deformation.

Acknowledgements

The authors want to thank R. BLOCH for assistance in some of the measurements and ANNA GRETE JØRGENSEN and GUNVER DAMM JENSEN for careful plate scanning. This work has greatly profited from the excellent targets prepared by G. SØRENSEN, J. THORSAGER, and V. TOFT at the University of Aarhus Isotope Separator. Finally, P. O. TJØM acknowledges support from Norges Teknisk-Naturvitenskapelige Forskningsråd.

*The Niels Bohr Institute
University of Copenhagen*

References

- 1) D. G. BURKE, B. ZEIDMAN, B. ELBEK, B. HERSKIND and M. C. OLESEN, Mat. Fys. Medd. Dan. Vid. Selsk. **35**, nr. 2 (1966).
- 2) S. G. NILSSON, Mat. Fys. Medd. Dan. Vid. Selsk, **29**, nr. 16 (1955).
- 3) R. H. BASSEL, R. M. DRISKO and G. R. SATCHLER, ORNL Report **3240** (unpublished).
- 4) D. R. BÈS and CHO YI-CHUNG, Nuclear Physics **86** (1966) 581.
- 5) R. BLOCH, B. ELBEK and P. O. TJØM, Nuclear Physics A **91** (1967) 576.
- 6) D. G. BURKE and B. ELBEK, Mat. Fys. Medd. Dan. Vid. Selsk. to be published.
- 7) M. JASKOLA, K. NYBØ, P. O. TJØM and B. ELBEK, Nuclear Physics A **96** (1967) 52.
- 8) F. STERBA, P. O. TJØM and B. ELBEK, to be published.
- 9) G. R. SATCHLER, Ann. Phys. **3** (1958) 275.
- 10) M. N. VERGNES and R. K. SHELINE, Phys. Rev. **132** (1963) 1736.
- 11) C. W. REICH and M. E. BUNKER, unpublished.
- 12) B. E. CHI, Nuclear Physics **83** (1966) 97.
- 13) R. K. COOPER and J. BANG, The Niels Bohr Institute, G.A.P. **2** (1965).
- 14) A. K. KERMAN, Mat. Fys. Medd. Dan. Vid. Selsk. **30**, no. 15 (1956).
- 15) A. BOHR and B. R. MOTTELSON, Lecture Notes (Copenhagen 1966).
- 16) P. O. TJØM and B. ELBEK, to be published.
- 17) S. WHINERAY, private communication (1967).
- 18) S. G. NILSSON, private communication (1966).
- 19) R. M. DIAMOND, B. ELBEK and F. S. STEPHENS, Nuclear Physics **43** (1963) 560.
- 20) M. FINGER, P. GALAN, J. URBANZC (Dubna), private communication (1966).
- 21) M. JASKOLA, B. ELBEK and P. O. TJØM, to be published.
- 22) J. BORGGREEN, L. WESTGAARD and N. J. S. HANSEN, Nuclear Physics A **95** (1967) 202.
- 23) V. G. SOLOVIEV, private communication (1966).
- 24) B. HARMATZ, T. H. HANDLEY and J. W. MIHELICH, Phys. Rev. **128** (1962) 1186.
- 25) D. ALI, Nuclear Physics **71** (1965) 441.
- 26) I. J. SPALDING and K. F. SMITH, Proc. Phys. Soc. (London) **79** (1962) 787.

N. O. LASSEN AND ARNE OHRT

MULTIPLE SCATTERING OF α -PARTICLES

Det Kongelige Danske Videnskabernes Selskab
Matematisk-fysiske Meddelelser **36**, 9



Kommissionær: Munksgaard
København 1967

Synopsis

The distributions in the projected angle of α -particles having passed thin foils of Be, Al, Ni or Au, respectively, were measured. For 20 MeV α -particles, both the shape of the distributions and the half widths were found to agree with Molière's theory. Also for 8.8 and 6.0 MeV α -particles the half widths agree with his theory.

1. Introduction

Multiple scattering of α -particles is caused by collisions between the particles and the atomic nuclei in the stopping substance. Such collisions may result in scattering at large angles, but events of this kind are very rare, whereas each α -particle may suffer hundreds of small deflections even in a moderately thin foil. The direction of these deflections are random, and therefore the resulting deflection does not become large and it only increases slowly with the number of collisions.

The multiple scattering was observed by RUTHERFORD in the first decade of this century⁽¹⁾. Although the concept of the atomic nucleus did not exist at that time, RUTHERFORD, using a theory by LORD RAYLEIGH for the addition of randomly oriented vectors⁽²⁾, correctly explained the phenomenon as being due to numerous soft collisions with the atoms. Shortly after the discovery by RUTHERFORD, the multiple scattering of α -particles was observed by LISE MEITNER⁽³⁾.

More detailed studies of the multiple scattering were performed by GEIGER (1910)⁽⁴⁾ and by MAYER (1913)⁽⁵⁾, both using the scintillation method and α -particles from RaC' and from Po, respectively. In 1932, MAURER⁽⁶⁾, using a Geiger counter and ThC' α -particles, performed measurements very similar to Geiger's and compared his results with a theory by BOTHE⁽⁷⁾. In 1951, HUUS⁽⁸⁾ measured the multiple scattering of protons and deuterons accelerated in a Van de Graaff. So did later BICHSEL⁽⁹⁾, and for protons of 1–5 MeV he found very close agreement with a theory by MOLIÈRE^{(14) (15)}.

NIELS BOHR⁽¹⁰⁾ took great interest in the stopping phenomena and he stressed the intimate relationship between multiple scattering and nuclear stopping. Also BETHE⁽¹¹⁾ has given several contributions to the theory of multiple scattering. The first more detailed theory, also discussing the way in which the central multiple scattering Gaussian distribution joins the distant single scattering Rutherford distribution, was given by E. J. WILLIAMS^{(12) (13)} in 1940. In 1947, MOLIÈRE advanced his famous theory^{(14) (15)},

and since then many other theoretical papers on this subject have appeared. The interest has, however, been mostly directed towards high energy particles, and with the above mentioned exceptions also the scanty experimental investigations have been confined to high energy particles. References may be found in a recent paper by W. SCOTT⁽¹⁶⁾. Most recently, MARION and ZIMMERMAN⁽¹⁷⁾ have discussed the theories of MOLIERE and of NIGAM, SUNDARESAN and WU⁽¹⁸⁾ and have carried out numerical calculations on the multiple scattering.

It is well known that, in the study of cosmic rays by photographic emulsions, the multiple scattering together with other stopping effects has been used as a means for determining particle properties.

2. Short survey of theoretical results

A. Elementary theory

Assuming a Coulomb potential between the α -particle and the nucleus, the scattering angle Θ in the Laboratory system for small angles is

$$\Theta = b'/p = Z_1 Z_2 e^2 / pE, \quad (1)$$

where p is the impact parameter, b' is defined by the second equation, Z_1 and Z_2 are the charge numbers of the particle and the nucleus, respectively, E is the Laboratory energy, and e the electronic charge. To a first approximation the screening of the nuclear charge by the atomic electrons may be taken into account by introducing a minimum angle

$$\Theta_{\min} = b'/p_{\max} = b'Z_2^{1/3}/a, \quad (2)$$

where $a = 0.885 \cdot a_0$. Here, a_0 is the hydrogen Bohr radius ($5.29 \cdot 10^{-9}$ cm).

The distribution in the projected angle x of a beam of α -particles having passed a foil of thickness t g cm⁻² is approximately a Gaussian with a standard deviation

$$\sigma(x) = \sqrt{\frac{\pi N_0 t Z_1 Z_2 e^2}{A E}} \sqrt{\ln \frac{\Theta^*}{\Theta_{\min}}}, \quad (3)$$

where N_0 is Avogadro's number $6.0 \cdot 10^{23}$, A is the mass number of the target nucleus, and Θ^* is a cut-off angle given by

$$\Theta^* = \sqrt{\frac{\pi N_0 t Z_1 Z_2 e^2}{A E}}. \quad (4)$$

In the derivation of this result, only collisions giving deflections smaller than Θ^* are taken into account. On the average just one collision for each α -particle has been neglected, whereas the number of collisions taken into consideration is

$$n = \Theta^{*2}/\Theta_{\min}^2, \quad (5)$$

which must be much larger than one in order that we can talk about multiple scattering.

For larger angles the projected distribution goes over in the Rutherford distribution $W(x)dx \propto x^{-3}dx$.

B. Molière's theory

MOLIÈRE assumes a Thomas-Fermi potential. He introduces a reduced angle φ defined by

$$\varphi = x/(\Theta^*\sqrt{B}), \quad (6)$$

where x is the projected angle, Θ^* is defined by (4), and B is another parameter depending on the stopping substance and the foil thickness and also slightly on the energy. We have

$$B - \ln B = \ln[\Theta^*/\Theta_a]^2 - 0.15 \quad (7)$$

where

$$\Theta_a = \frac{\hbar Z_2^{1/3}}{0.885 \alpha_0 m_1 v} \sqrt{1.13 + 3.76 \alpha^2} \quad (8)$$

$$\alpha = Z_1 Z_2 e^2 / (\hbar v). \quad (9)$$

Here m_1 and v are the mass and the velocity of the α -particle. In most cases (where v is not too large or Z_2 not too small) Θ_a is approximately equal to Θ_{\min} . As seen, B is essentially a measure of the number of collisions.

The distribution in reduced angle is given by a series expansion

$$f(\varphi)d\varphi = f^{(0)}(\varphi)d\varphi + \frac{1}{B} f^{(1)}(\varphi)d\varphi + \frac{1}{B^2} f^{(2)}(\varphi)d\varphi + \dots \quad (10)$$

where $f^{(0)}(\varphi)$ is a Gaussian

$$f^{(0)}(\varphi) = \frac{2}{\sqrt{\pi}} e^{-\varphi^2} \quad (11)$$

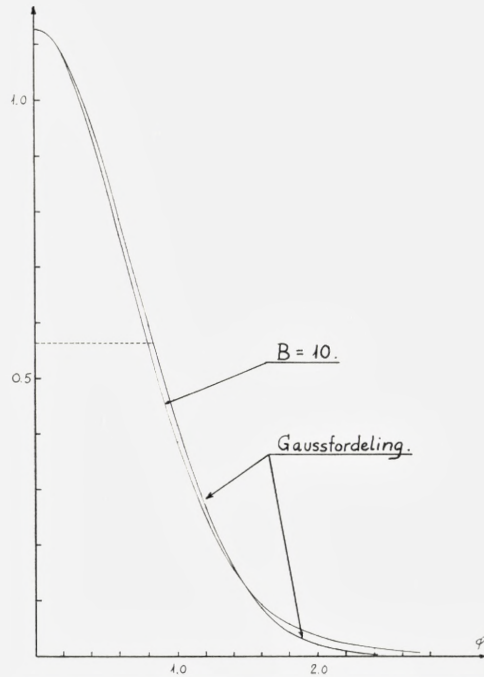


Fig. 1. The Molière distribution for a typical case ($B = 10$) and the function $f^{(0)}(\varphi)$, in the figure denoted "Gaussfordeling".

whereas $f^{(n)}(\varphi)$ are more complicated, oscillating functions. They are tabulated in refs. ⁽¹⁵⁾ and ⁽¹⁶⁾.

Fig. 1 shows the Molière distribution for a case with $B = 10$, and in the same figure the corresponding $f^{(0)}$ -distribution is shown. The half width for the $f^{(0)}$ -distribution is $\Delta_G = 2.35/\sqrt{2} = 1.66$. The half width $\Delta(\varphi)$ for

TABLE 1.*

	$\Theta^* \cdot E/\sqrt{t}$	Θ_a^{-1}/E	$\Theta^*/(\Theta_a \sqrt{t})$
Be.....	$1.67 \cdot 10^{-2}$	(2200)	(36.8)
Al.....	$3.13 \cdot 10^{-2}$	540	16.9
Ni.....	$4.57 \cdot 10^{-2}$	197	9.00
Au.....	$7.05 \cdot 10^{-2}$	49.5	3.49

* Here, E is in MeV, t in mg cm^{-2} , Θ^* and Θ_a in radians. The table is good for Al, Ni and Au. For Be, the values are correct at 10 MeV, whereas Θ_a^{-1} and Θ^*/Θ_a should be corrected by about $+8\%$ and -13% at 5 and 20 MeV, respectively.

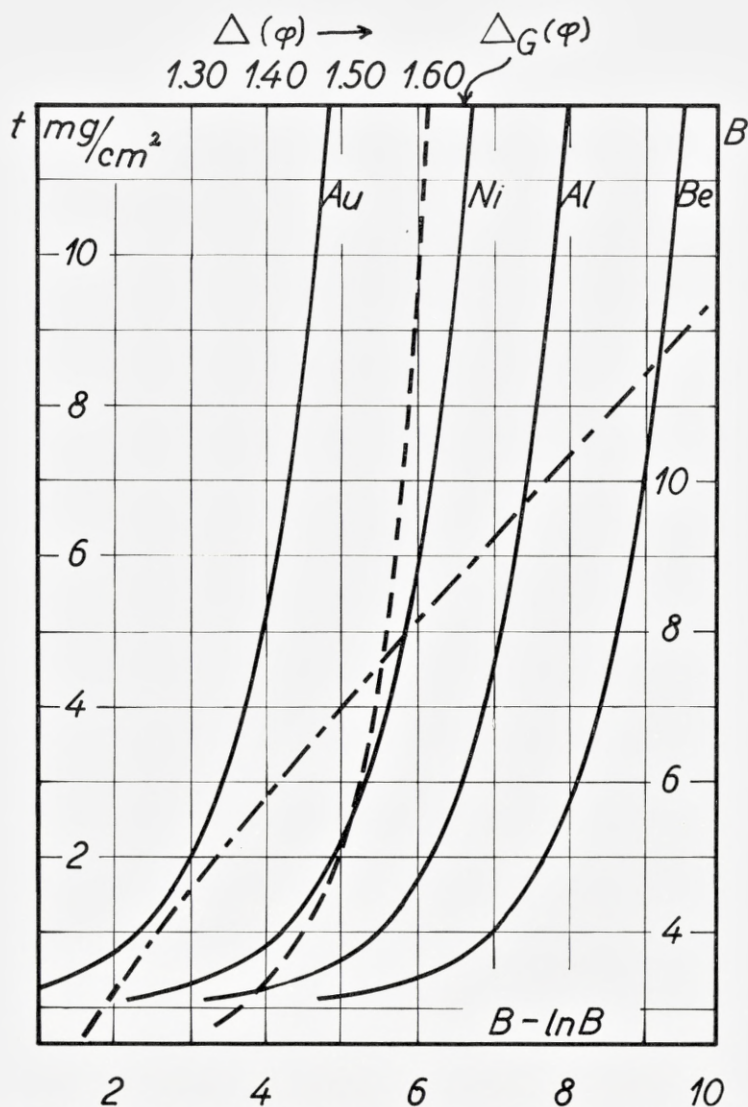


Fig. 2. B and $\Delta(\varphi)$ for different foil thicknesses $t \text{ mg/cm}^2$ (and for α -particles 5–20 MeV). The left-hand scale of ordinates, the full-drawn curves and the lower scale of abscissae give the relation between the foil thickness t and $B - \ln B$. From the latter, B may be obtained by means of the dot-and-dash curve and the right-hand scale of ordinates. Finally, the dashed line connects B and $\Delta(\varphi)$ (upper scale of abscissae). The dashed curve may be slightly incorrect for the smallest B -values, because in formula (10) only terms until the term with B^{-2} were included; anyhow, the use of the Molière theory is not well justified for the smallest B -values. The full-drawn curve for Be should be correct at 10 MeV, and only very slightly off at 5 and at 20 MeV.

the Molière distribution is about 5 per cent smaller. $\Delta(\varphi)$ is a function of B , and by drawing distributions for other B -values we have determined this function, which is shown in Fig. 2. This figure may also be used to find B for a known foil thickness. Values of Θ^* and approximate values of Θ_a may be obtained from Table 1 (for α -particles 5–20 MeV).

3. Experiments with 20 MeV α -particles

The beam from the Copenhagen cyclotron was passed through two slits, each of width ξ . The second slit was placed 50 cm behind the first, and 20 cm behind the second slit a target was placed; it consisted of a pile of copper plates, each of thickness ξ . The plates were 10×40 mm² with the long edge, parallel to the slits, facing the beam; they were pressed hard against each other. In most experiments, $\xi = 0.45$ mm; in four cases, corresponding to the four bottom rows in Table 2, $\xi = 0.1$ mm. Foils could be placed immediately behind the second slit.

With no foil only two of the copper plates were hit by the beam, and they alone became radioactive. When a foil was inserted in the beam, however, the beam was scattered, and several plates became active. Among the produced radioisotopes only Ga⁶⁶ emits γ -quanta of energy higher than 1.5 MeV. Using a 3×3 inch NaI-crystal and discriminating against lower energy quanta, we obtained distribution curves like that shown in Fig. 3. Corrections for decay with the known half life 9.6 hours have been applied.

The figure refers to a Ni-foil 8.1 mg/cm². The curve is the Molière distribution calculated for a thickness 7.9 mg/cm². The agreement between the experimental points and the theoretical curve is as good as could be expected, both as regards the shape of the distribution and the half width. The latter is found to be $\Delta' = 6.06$ mm, in agreement with the Molière value (for 8.1 mg/cm² $\Delta_{\text{Mol}} = 6.16$ mm). Correcting in the usual way for the influence of the finite slit sizes ξ , we obtain for the corrected half width the value $\Delta'' = ((\Delta')^2 - (1.4\xi)^2)^{1/2} = (6.06^2 - 0.63^2)^{1/2} = 6.03$ mm. In this case the correction is negligible, and actually the proper correction is even smaller (see next chapter). The corrections used to obtain the values Δ_{exp} given in Table 2 are $-(2/3)(\Delta' - \Delta'')$, and they are, even for the thinnest foils, smaller than five per cent; in the example, $\Delta_{\text{exp}} = (6.06 - 0.02)/200 = 3.02 \cdot 10^{-2}$ rad.

Fig. 4 shows a probability plot of the same distribution. The ordinates for the open points are the ratio $\sum_{i=1}^j n_i / \sum n_i$ in per cent (right-hand scale of

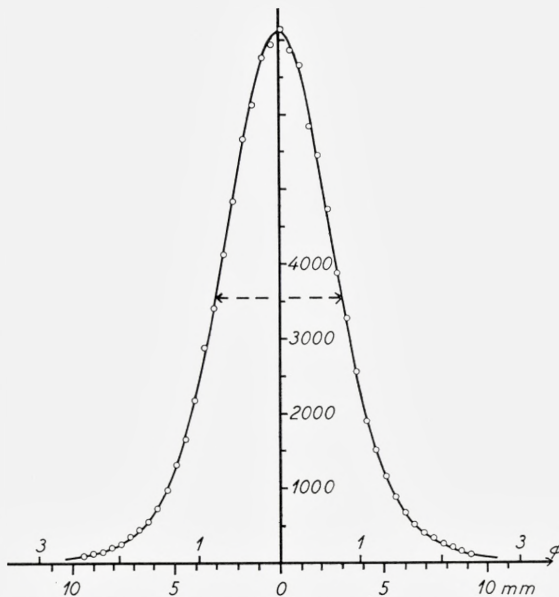


Fig. 3. Projected distribution of the beam of 20 MeV α -particles after multiple scattering in a nickel foil, 8.1 mg/cm² thick. The points are the experimentally measured activities in counts per min. of the copper plates. The lower scale of abscissae is the distance along the target in mm; to obtain the projected angle divide by 200 mm. The upper scale of abscissae is the reduced angle φ . The full-drawn curve is the Molière distribution.

ordinates), where n_i is the number of counts per min. for the i 'th copper plate, and $\sum n_i$ is the total area below the curve in Fig. 3. The closed points are obtained after a correction for lacking measurements at large angles, i. e., when $0.0035 \sum n_i$ is added to $\sum_{i=1}^j n_i$ and $0.0070 \sum n_i$ is added to $\sum n_i$.

The Molière distribution deviates from the Gaussian $f^{(0)}(\varphi)$; the difference is only small in the central region, but quite large in the wings of the distribution. This can also be seen in Fig. 4, and it can easily be shown that the middle part of the probability plot of the Molière distribution is very nearly a straight line which corresponds to the $f^{(0)}$ -function⁽¹⁹⁾. For all distributions measured with 20 MeV α -particles we found the characteristic appearance of the probability plot shown in Fig. 4: A straight line in the middle and deviations from this line at both ends. In an attempt at expressing in a brief way the sign and the magnitude of the deviation from a Gaussian, we have adopted the following procedure. From a plot like Fig. 3, the half

width Δ' of the distribution itself was obtained; the middle part of the probability distribution gave the half width Δ'_G of the $f^{(0)}$ -distribution. The fractional difference $\delta = (\Delta'_G - \Delta')/\Delta'_G$ is taken as a measure for the size of the wings and compared to the value obtained from the Molière theory. Plots like Fig. 4 were used only for illustrative purposes; a simple calculation from the values n_i gives a more accurate value of Δ'_G than can be obtained

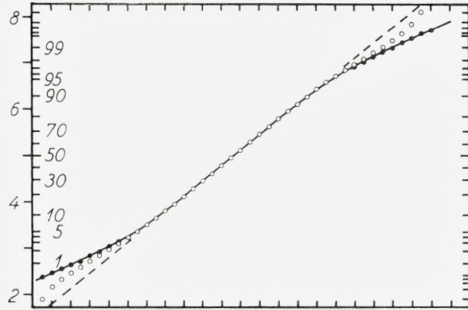


Fig. 4. The projected distribution in Fig. 3 transformed to probability paper. The ordinate is the number of "probits". A division on the axis of abscissae is 0.9 mm on the target. Open points are obtained directly from the points in Fig. 3, closed points after correction for jacking measurements at great distances from the central ray. The full-drawn curve represents the Molière distribution, the dotted line the $f^{(0)}$ -function.

from a plot. For the measurements listed in Table 2, with the exception of the last four values, Δ'_G could be determined with an accuracy of about one per cent, and in most cases the same applies for Δ' ; only for a few of the narrower distributions the drawing of curves through the measured points was slightly more ambiguous. Thus, the absolute uncertainty of δ is about one per cent (for example: $\delta = (4 \pm 1) \%$ for the beryllium foils) and, as seen from Table 2, the agreement with the Molière values is good. It should here be noted that errors in α -energy E , foil thickness t and in any geometrical measures cancel out and do not contribute to the error in δ .

From Table 2 it is also seen that the experimental half widths agree well with the Molière theory. Taking into account the uncertainty of Δ_{exp} , which is estimated to about 4 per cent, the only deviations from the Molière theory which may (or may not) be significant appear in the results for aluminium foils of 1.8 and 3.1 mg/cm². It is interesting to note that BICHSEL (9) for 1–5 MeV protons also found excellent agreement with the Molière theory, just with the exception of thin aluminium foils.

For the thin Ni-foils, 0.1–0.9 mg/cm², the geometry was changed, the slit widths being reduced to 0.1 mm. The activities obtained were much

TABLE 2. Multiple Scattering of 20 MeV α -particles.*

Substance	t mg/cm ²	E MeV	B	Θ^* 10 ⁻³ rad	Θ^*/Θ_a	Δ_{ET} 10 ⁻² rad	Δ_{Mol} 10 ⁻² rad	Δ_{exp} 10 ⁻² rad	δ_{Mol} %	δ_{exp} %
Be.....	5,0	19,4	11,1	1,92	70	0,92	1,01	0,97	4	4
„.....	10,0	18,6	11,9	2,84	100	1,43	1,56	1,49	4	4
Al.....	1,8	19,8	8,2	2,11	23	0,87	0,94	0,80	6	6
„.....	3,1	19,6	8,8	2,82	30	1,22	1,31	1,39	5	5
„.....	5,8	19,3	9,5	3,90	41	1,76	1,88	1,84	5	5
„.....	7,1	19,2	9,8	4,34	45	1,99	2,15	2,16	5	4
„.....	10,2	18,8	10,1	5,32	54	2,50	2,68	2,64	5	5
Ni.....	1,8	19,8	6,7	3,10	12	1,15	1,23	1,20	7	7
„.....	3,6	19,7	7,5	4,40	17	1,74	1,87	1,87	6	5
„.....	6,3	19,4	8,1	5,90	23	2,44	2,62	2,57	6	6
„.....	8,1	19,3	8,4	6,76	26	2,86	3,08	3,02	5	5
„.....	10,8	19,1	8,8	7,88	30	3,40	3,66	3,59	5	5
Ni.....	0,1	20	3,0	0,72	3	0,17	0,18	0,21	17	14
„.....	0,22	20	4,1	1,07	4	0,30	0,32	0,35	12	8
„.....	0,45	20	5,0	1,53	6	0,48	0,51	0,51	10	12
„.....	0,90	19,9	5,8	2,17	8,5	0,74	0,80	0,79	8	14

* The first column in this table gives the stopping substance, column 2 the foil thickness and column 3 the mean energy of the α -particles inside the foil. The next three columns give parameters from the Molière theory. Δ_{ET} is the half width calculated from the elementary theory, i. e., using formula (3) in which, however, Θ_{min} has been replaced by Θ_a , Θ^*/Θ_a being taken from Table 1. $\Delta_{\text{Mol}} = \Delta(\varphi)\Theta^*/\sqrt{B}$ is obtained by means of Table 1 and Fig. 2. As for δ , see text.

smaller and hence the uncertainties larger, in $\Delta_{\text{exp}} \sim 10$ per cent and in $\delta_{\text{exp}} \sim 4$ per cent. At least for the two thinnest foils the number of collisions made by the α -particles is quite small and one can hardly talk about multiple scattering; therefore, the theories do not apply. Nevertheless, the calculated and the measured half widths agree fairly well.

Fig. 5 shows the result for nickel foils of various thickness; it may be noted that the half width Δ increases roughly, but not exactly, proportional to the square root of the foil thickness t .

4. Experiments with ThC + C' α -particles

A source of ThB and its daughters was prepared in the usual way. A piece of a platinum wire with a one mm sphere at one end was placed in a small chamber containing thoron, emanating from radiothorium. This source emits α -particles of energies 8.8 and 6.0 MeV, which were detected

by a silicon solid-state detector. During the measurements a slit was placed close to the source, a second slit which could be covered by a foil was placed 10 cm away, and a third slit 20 cm from the first slit. All three slits were placed parallel, and each was 0.52 mm in width. The third slit and the counter behind it could be moved sideways by means of a micrometer screw, and for each setting the α -spectrum was recorded on a 100 channel

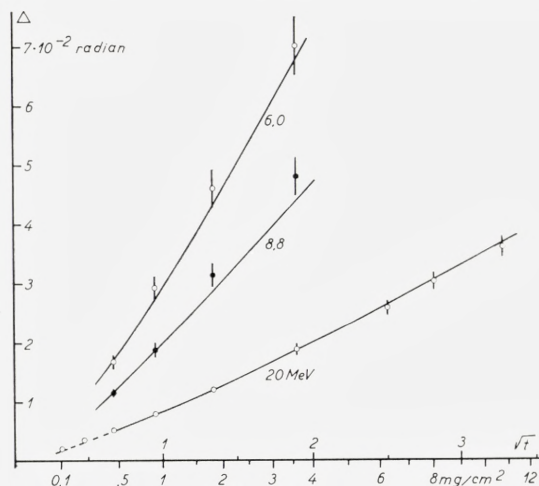


Fig. 5. The half width Δ of the projected distribution after multiple scattering in nickel foils of various thickness t mg/cm² for α -particles with incoming energies 6.0, 8.8, and 20 MeV. The points are experimental values, the curves are calculated from Molière's theory.

pulse height analyzer. From the spectra the angular distribution of the 8.8 and 6.0 MeV α -particles, respectively, could be obtained. Fig. 6 shows an example.

In these experiments the geometry was not as good as in the experiments reported in the preceding paragraph, and it is essential to correct the measured half widths for the influence of the finite slit widths. With no foil the distribution is a curve composed of parabolic arcs⁽¹⁹⁾; this curve and corresponding experimental measurements are shown in Fig. 7, and it should be noted, that the distribution deviates from a Gaussian in a way opposite to the Molière distribution. Therefore, and since the geometrical corrections are not negligible, we cannot measure the shape of the distribution sufficiently accurate for a close comparison with the Molière distribution, and we cannot determine the quantity δ .

Naturally, by lengthy calculations it would be possible to find for any foil

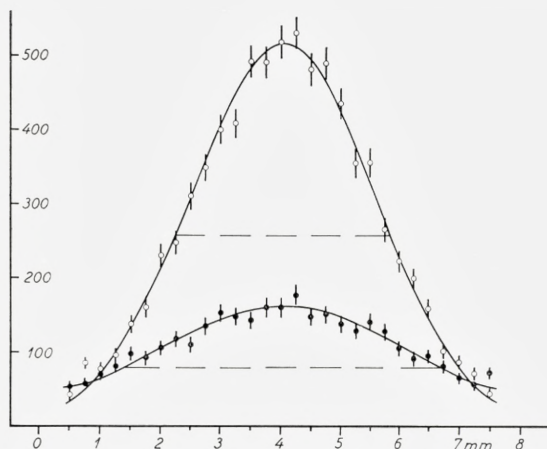


Fig. 6. Projected distribution after multiple scattering in an aluminum foil, 4.0 mg/cm^2 in thickness, for α -particles with incoming energies 8.8 and 6.0 MeV (open and closed points, respectively). The ordinate is the number of α -particles per 30 min., the abscissa is the displacement of the third slit and the counter. To obtain the projected angle divide by 94 mm, the distance from the foil to the counter slit. All slit widths are 0.52 mm. The curves are Gaussians with half widths, 3.6 and 5.3 mm, respectively.

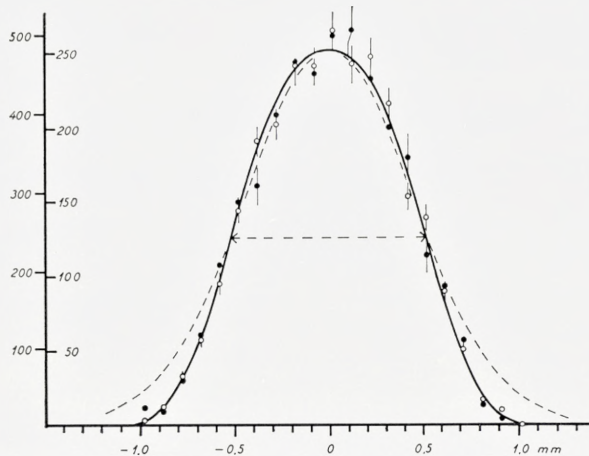


Fig. 7. Projected distribution without foil. Open points refer to 8.8 MeV α -particles (left-hand scale of ordinates), closed points to 6.0 MeV α -particles (right-hand scale of ordinates). The full-drawn curve is the expected distribution (see text). For comparison, the dotted line shows a Gaussian with the same half width.

TABLE 3. Multiple Scattering of ThC + C' α -particles.*

Substance	t mg/cm ²	E MeV	B	Θ^* 10 ⁻³ rad	Θ^* / Θ_a	Δ_{ET} 10 ⁻² rad	Δ_{Mol} 10 ⁻² rad	Δ_{exp} 10 ⁻² rad
Be.....	5,0	7,46	11,1	5,00	70	2,42	2,65	2,45
Al.....	1,8	8,41	8,2	4,97	23	2,06	2,23	2,18
.....	..	5,54	8,2	7,55	23	3,14	3,38	3,29
.....	4,0	7,87	9,1	7,96	34	3,52	3,76	3,68
.....	..	4,80	9,1	13,0	34	5,73	6,18	5,6
Ni.....	0,45	8,71	5,0	3,51	6	1,11	1,18	1,14
.....	..	5,96	5,0	5,14	6	1,62	1,72	1,67
.....	0,9	8,63	5,9	5,03	8,5	1,73	1,87	1,87
.....	..	5,87	5,9	7,39	8,5	2,54	2,74	2,92
.....	1,8	8,49	6,7	7,20	12	2,67	2,88	3,13
.....	..	5,68	6,7	10,8	12	4,04	4,32	4,6
.....	3,6	8,18	7,5	10,6	17	4,20	4,40	4,8
.....	..	5,28	7,5	16,4	17	6,50	6,82	7,0
Au.....	0,39	8,75	2,2	5,03	2,2	1,05	(0,9)	0,8
.....	..	6,02	2,2	7,32	2,2	1,53	(1,3)	1,51
.....	0,45	8,74	2,4	5,40	2,3	1,17	(1,1)	1,36
.....	..	6,01	2,4	7,86	2,3	1,70	(1,5)	1,86
.....	0,54	8,74	2,8	5,92	2,6	1,35	1,30	1,37
.....	..	6,00	2,8	8,64	2,6	1,97	1,94	1,93
.....	0,70	8,72	3,1	6,76	2,9	1,64	1,65	1,69
.....	..	5,99	3,1	9,83	2,9	2,39	2,40	2,40
.....	0,92	8,71	3,5	7,76	3,4	2,00	2,08	2,27
.....	..	5,97	3,5	11,3	3,4	2,92	3,02	3,17
.....	1,07	8,69	3,7	8,39	3,6	2,24	2,33	2,23
.....	..	5,95	3,7	11,2	3,6	3,25	3,38	3,40
.....	1,31	8,68	4,0	9,30	4,0	2,56	2,71	2,68
.....	..	5,93	4,0	13,6	4,0	3,77	3,96	3,84

* For further explanation, see Table 2.

the distribution to be expected according to Molière's theory. In view of the rather limited number of counts, of course especially in the wings of the distributions, such calculations would hardly be reasonable. We have used the GIER electronic computer of the Niels Bohr Institute to calculate the total half width to be expected if the multiple scattering distribution were a Gaussian with standard deviation σ ; the result is shown in Fig. 8. It is found that the proper correction to apply to the measured half width is smaller than would correspond to a quadratic addition of the multiple scattering half width and the "zero-thickness" half width; this is the justification for the correction used in the preceding paragraph.

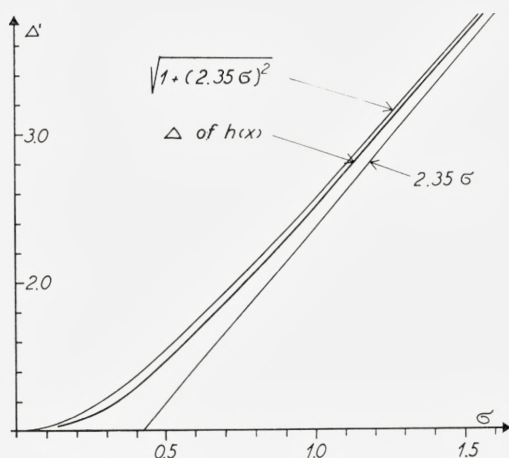


Fig. 8. Correction of the measured half width due to finite slit widths. The ordinate is the measured half width, the abscissa the standard deviation of the (here assumed) Gaussian distribution of the multiple scattering. The lower curve with zero correction. The upper curve is obtained by quadratic addition of half widths. The middle curve gives the half width of the distribution curve $h(x)$ to be expected with the above mentioned assumption (and as found by numerical calculations). The unit for abscissae and ordinates is 2ξ , where ξ is the common width for the three slits.

The results obtained for Th α -particles are summarized in Table 3. The uncertainty in Δ_{exp} is estimated to about 7 per cent, perhaps slightly higher for the broadest distributions, where the lack of good statistics is most pronounced. No significant departures from the Molière theory are observed.

The beryllium, aluminum and nickel foils were obtained commercially. The gold foils were made by evaporation *in vacuo* onto a glass plate covered by a thin layer of sugar, and afterwards they were floated off in water. Their thickness was determined from the energy loss by the α -particles, a 512 channel pulse-height analyzer being used to record the α -spectra. Of course, the foils are thinner than corresponding to the limit of validity of the Molière theory; nevertheless, the theory gives results closely agreeing with the experimental values.

These experiments were carried out at the Niels Bohr Institute, The University of Copenhagen. For valuable help our thanks are due Mr. N. O. Roy Poulsen, mag. sc., and the cyclotron group.

References

1. E. RUTHERFORD: Phil. Mag. **12**, 143, 1906.
2. LORD RAYLEIGH: Theory of Sound, 2. Ed. 1894, p. 39.
3. LISE MEITNER: Phys. Zeitschr. **8**, 489, 1907.
4. H. GEIGER: Proc. Roy. Soc. A **83**, 492, 1910.
5. F. MAYER: Ann. d. Phys. **41**, 931, 1913.
6. G. MAURER: Zs. f. Phys. **78**, 395, 1932.
7. W. BOTHE: Zs. f. Phys. **4**, 161 und 300, 1921.
8. T. HUUS: Mat. Fys. Medd. Dan. Vid. Selsk. **26**, no. 4, 1951.
9. H. BICHSEL: Phys. Rev. **112**, 182, 1958.
10. N. BOHR: Mat. Fys. Medd. Dan. Vid. Selsk. **18**, no. 8, 1948.
11. H. A. BETHE: Phys. Rev. **70**, 821, 1946.
12. E. J. WILLIAMS: Phys. Rev. **58**, 292, 1940.
13. E. J. WILLIAMS: Revs. Mod. Phys. **17**, 217, 1945.
14. G. MOLIÈRE: Zs. f. Naturf. **2a**, 183, 1947.
15. G. MOLIÈRE: Zs. f. Naturf. **3a**, 78, 1947.
16. W. J. SCOTT: Revs. Mod. Phys. **35**, 231, 1963.
17. J. B. MARION and BARBARA A. ZIMMERMAN: The Lemon Aid Preprint Series in Nuclear Physics, October 1966.
18. B. P. NIGAM, M. K. SUNDARESAN and T.-Y. WU: Phys. Rev. **115**, 491, 1959.
19. N. O. LASSEN og ARNE OHRT: Fysisk Tidsskrift **65**, 65, 1967.

J. LINDHARD, VIBEKE NIELSEN AND M. SCHARFF(†)

APPROXIMATION METHOD IN CLASSICAL SCATTERING BY SCREENED COULOMB FIELDS

(Notes on Atomic Collisions, I)

Det Kongelige Danske Videnskabernes Selskab
Matematisk-fysiske Meddelelser **36**, 10



Kommissionær: Munksgaard
København 1968

CONTENTS

§ 1. Introduction	3
§ 2. General Considerations	4
§ 3. Power Law Potentials and Wide Angle Extrapolation	12
§ 4. Scattering Formula for Screened Coulomb Potentials	16
§ 5. Magic Formula for Scattering	24
References	31

Synopsis

The paper presents a comprehensive approximation formula for classical scattering of fast ions by atoms. The formula has been applied in previous papers.

We discuss at first the simplifications and the errors resulting from the use of a Thomas-Fermi type potential in scattering calculations. The accuracy of classical mechanics in such scattering problems is treated briefly.

We study scattering by power law potentials for low angle deflections and derive a wide angle extrapolation in terms of a one-parameter formula. The formula is applied to Thomas-Fermi potentials, where the reduced scattering cross section is found numerically as a function of a single scattering parameter. The stopping cross section is obtained as a function of reduced energy. We derive the magic formula, which leads to easy estimates of scattering in any potential, and compare scattering by several types of screened potentials. Comparison is also made with more precise computations of scattering.

§ 1. Introduction

The present paper is subtitled "Notes on Atomic Collisions, I", and belongs to a group of four papers. Although the publication of the paper has been delayed, some of its results were quoted and utilized in a summarizing article¹¹⁾ and in the already published Notes II¹²⁾ and III¹³⁾, as well as in other associated papers^{14, 15, 16, 17)}. In point of fact, the essential parts of the paper were worked out in the years 1958–59 as a necessary basis for our studies of slowing-down of heavy ions. At that time, little was known about details of the collisions in question, but during later years experimental and theoretical results have improved the knowledge in this field. Nevertheless, we adhere to the original treatment. The reason for doing this is partly that we want to state the precise basis of the formulae used in later work, and partly that attempts at improvement of the general framework would hardly be physically justified at present.

The main point in this paper, as in Notes IV (unpublished), is that collisions between ions and atoms may be described approximately in terms of similarity properties, where, at first, merely one parameter suffices to embrace all scattering processes. In Notes II and III, these extremely simple similarity properties are found to lead to significant simplifications in the theory of particle radiation effects.

More definitely, the purpose of the paper is to find comprehensive approximation methods for treating elastic scattering of ions by atoms. The scattering problem is comparatively simple since we disregard the inelastic effects, which are studied in Notes IV. In the following, we shall therefore mainly discuss approximation methods from a formal point of view, with less emphasis on their physical justification or on their application to studies of ranges and radiation damage. It may be appropriate, however, to sketch at first the background for the introduction of the present scattering method. This is done in § 2, where we consider the various approximations involved in the use of a simple interaction potential in scattering calculations. The magnitude of the potential is also discussed, and we consider briefly the

justification for the use of classical mechanics in ion-atom scattering. After this preamble, we study in § 3 scattering by power law potentials, and find that low angle deflections may be extrapolated to wide angles in terms of a one-parameter formula, retaining a fair accuracy. This treatment is applied to Thomas-Fermi type potentials in § 4, where the reduced scattering cross section is given as a function of a single scattering parameter. In § 5 we derive the magic formula which leads to easy estimates of scattering in any potential, and we compare scattering by several types of screened potentials. The present scaling formulae are compared with more precise scattering calculations.

§ 2. General Considerations

Ion-Atom Collisions at Low Velocities

Consider an ion, with charge number Z_1 and velocity v , colliding with an atom at rest with charge number Z_2 . We disregard excitations and ejection of electrons from ion or atom during the collision. Although such inelastic effects are important in many respects, they may in first approximation be disregarded when we ask for the deflection in the centre of mass system. The reason for this is, briefly, that electrons can take over little momentum but often a considerable amount of energy, because of their low mass.

We are interested in just the deflection of the ion and the recoil of the atom in the idealized elastic encounter, a so-called nuclear collision. If the ion comes close to the atom, the force is an unscreened Coulomb force and scattering is essentially given by the Rutherford formula. At larger distances of separation, however, the Coulomb force is screened, and the scattering is influenced by the field from atomic and ionic electrons.

When an ion penetrates a medium at a high velocity v , the scattering of the ion by atoms is not large and is mainly of type of Rutherford scattering. At decreasing velocity, however, the nuclear collisions at first lead to considerable multiple scattering and finally become important also in the stopping. The latter dominance occurs when the velocity v is quite low compared to the orbital velocities of electrons which could be carried by the ion, i. e. according to Thomas-Fermi estimates¹⁷⁾,

$$v < v_1 = Z_1^{2/3} v_0,$$

where $v_0 = e^2/\hbar$. In fact, electronic and nuclear stopping are of the same order of magnitude when¹²⁾ $v \sim 0.1v_1$.

This implies that the problems of deviations from Rutherford scattering arise primarily when we have to do with an ion where the nuclear charge to a considerable extent is compensated by electrons carried by the ion. The nuclear charge of the atom is apparently completely screened at large distances by atomic electrons. However, the outermost electrons do not, for swift particles, compensate at the static atomic screening radius, but at slightly larger distances, because the screening contains dynamic features. We therefore envisage the interaction as a screened Coulomb field, where the screening may depend moderately on velocity. With reservations for velocity dependence, the ion-atom field is similar to the static interaction between two atoms of charge numbers Z_1 and Z_2 .

Classical Scattering by Screened Potentials

Suppose that the force is known, and that the scattering is classical. The angle of scattering in the centre of mass system might then be a function of five variables, $\theta = \theta(Z_1, Z_2, v, M_0, p)$, where M_0 is the reduced mass and p the impact parameter. We are normally concerned with a conservative and central force, implying conservation of angular momentum. The classical equation of motion is then

$$\frac{d^2(R^{-1})}{d\varphi^2} + R^{-1} + \frac{R^2}{M_0 v^2 p^2} F(R) = 0, \quad (2.1)$$

where φ is the polar angle, $M_0 = M_1 M_2 / (M_1 + M_2)$ the reduced mass, $F(R)$ the outward force, and $R = R(\varphi)$ the distance of separation. The initial condition, corresponding to impact parameter p , is $R^{-1} = 0$ and $d(R^{-1})/d\varphi = p^{-1}$ for $\varphi = 0$. When integrating eq. (2.1), we find that $R^{-1}(\varphi)$ increases with φ and has a maximum, whereupon it decreases and becomes zero at a certain angle, φ_1 . The total deflection θ , in the centre of mass system, is then $\theta = \pi - \varphi_1$.

If the force depends on Z_1, Z_2 and distance R , the deflection θ will be a function of four variables, the velocity v and the mass M_0 having combined to one variable, $M_0 v^2$,

$$\theta = \theta(Z_1, Z_2, M_0 v^2, p). \quad (2.2)$$

The problem confronting us is whether this complicated dependence may be simplified. In the following chapters we attempt to show that, with good approximation, the number of independent variables reduces from four to one.

The first two steps in the reduction are obtained through simplifying approximations in the interaction potential.

To this end, let us consider similarity properties of interaction potentials; an approximate estimate of the potential function is given below. The ion-atom potential must be of type of

$$V(\vec{R}) = \frac{Z_1 Z_2 e^2}{R} u, \quad (2.3)$$

where the function u must tend to unity when $R \rightarrow 0$, and must vanish when $R \rightarrow \infty$, because the Coulomb potential is screened at large distances. A velocity-independent conservative potential corresponds to

$$u = u(Z_1, Z_2, R). \quad (2.4)$$

Thus, eq. (2.4) would result from a static Hartree calculation of the ground state energy of two atoms as a function of distance of separation, R . For the present purposes, however, formula (2.4) would hardly do, because the two parameters Z_1 and Z_2 correspond to an embarrassing large number of cases, of order of 10^4 .

In a Thomas-Fermi treatment the static interaction between two atoms is given by

$$u = u\left(\frac{Z_1}{Z_2}, \frac{R}{a}\right), \quad (2.5)$$

where a is a characteristic screening length (cf. pp. 8–9). Formula (2.5) has one parameter less than eq. (2.4), and is therefore much simpler. When eq. (2.5) is introduced in eq. (2.1), the angle of deflection depends on three variables only,

$$\theta = \theta(Z_1/Z_2, b/a, p/a), \quad (2.6)$$

where $b = 2Z_1 Z_2 e^2 / (M_0 v^2)$ is the familiar collision diameter. The parameter a/b in eq. (2.6) is used repeatedly in the following. We denote it as ε , since it is a reduced energy,

$$\varepsilon = \frac{a}{b} = \frac{a}{Z_1 Z_2 e^2} \cdot \frac{1}{2} M_0 v^2. \quad (2.7)$$

One final simplification of u may be made without introducing undue errors. Consider a simplified Thomas-Fermi potential

$$u = u\left(\frac{R}{a}\right), \quad (2.8)$$

where the dependence of u on the ratio Z_1/Z_2 in eq. (2.5) is disregarded. This simplification is actually a fairly good approximation, as discussed below (pp. 8–10).

Eq. (2.8) implies similarity of all ion-atom potentials. As a consequence, the angle of deflection obtained from eq. (2.1) becomes a function of two variables only

$$\theta = \theta\left(\varepsilon, \frac{p}{a}\right). \quad (2.9)$$

Since the differential cross section is $d\sigma = d(\pi p^2)$, it may, according to eq. (2.9), be written as

$$d\sigma = \pi a^2 \cdot F\left(\varepsilon, \sin \frac{\theta}{2}\right) d\Omega, \quad (2.10)$$

where we have introduced the variable $\sin\theta/2$ in place of θ , and where $d\Omega$ is the differential solid angle. Numerical computations of cross sections corresponding to eq. (2.10) have been made by several authors. Thus, EVERHART et al.⁴⁾ calculated scattering by the exponentially screened potential of BOHR, eq. (2.11).

The formula (2.9) shows that classical scattering by screened potentials (2.8) has comparatively simple similarity properties. Thus, suppose that in two different cases the reduced energies, ε , are the same, as well as the reduced impact parameters, p/a . We are then concerned with corresponding collisions: not only are the two deflections the same, but so are the orbits in space and time, when measured in reduced variables.

In applications of scattering formulae like (2.9), we are usually concerned with integral equations^{12, 13)}, the integration being over the differential cross section $d\sigma$. It is then desirable to have still simpler properties, i.e. only one reduced variable instead of two in eq. (2.10). In the following, we attempt to show that this simplification may be made, retaining an accuracy which is satisfactory for most purposes. In this connection it should be remembered that already eq. (2.9) contains several consecutive approximations. If, in specified cases, one wants to improve upon standard results obtained from the simplest possible similarity description, one should not always turn to eq. (2.9), but may instead consider, e.g., the details of the Hartree treatment and of the inelastic effects.

Estimate of Ion-Atom Interaction

We shall now describe briefly the reasons for our use of an ion-atom interaction containing only one screening length, a . This type of interaction is basic to the similarity approach in the present paper, cf. the preceding section and § 4. The actual magnitude of a and its dependence on the atomic numbers Z_1 and Z_2 , however, is immaterial to the similarity treatment.

In his well-known survey paper²⁾, NIELS BOHR discussed qualitatively many basic aspects of ion-atom collisions, and for this purpose he introduced an exponentially screened ion-atom interaction, i. e. eq. (2.3) with

$$u = \exp(-R/a_B). \quad (2.11)$$

This potential has been widely used but, when $R > a_B$, it decreases much more rapidly than do actual ion-atom interactions. For the purpose of more detailed estimates of deflections it was therefore necessary to look for a better potential. Clearly, it is possible to find a more accurate interaction, but the question is whether one can retain the simplicity of Bohr's potential, where there is only one screening parameter and similarity of all ion-atom interactions.

Before going further, we may again emphasize that the proper ion-atom interaction is a screened field containing inelastic parts and being dependent on the relative velocity. In point of fact, velocity dependence and inelastic terms are always directly connected and cannot occur independently of each other. Moreover, we have already mentioned that we are concerned mainly with cases of low velocity, where the nuclear charge of the ion is approximately neutralized by electrons. For these reasons, it would seem consistent to consider a velocity-independent, elastic interaction, and use as a guidance the static interaction between two atoms.

When asking for a potential described by one screening length, we disregard the shell structure belonging to a Hartree treatment, which again emphasizes that the static interaction obtained is to be used only as a guidance.

With these preliminaries, we can readily find the approximate shape of the potential. A static Thomas-Fermi treatment is easily seen to lead to potentials of type of (2.5), i. e. $u = u(Z_1/Z_2, R/a)$, where u is symmetric in Z_1, Z_2 , and where a , at fixed ratio Z_1/Z_2 , is proportional to $Z_1^{-1/3}$ (or to $Z_2^{-1/3}$)*. If one of the atomic numbers is small compared to the other, e. g.

* The proof is as follows. Suppose that the Thomas-Fermi equations are solved for atomic numbers Z_1, Z_2 , and distance of separation R . We ask whether another case, $Z'_1 = \alpha Z_1, Z'_2 = \alpha Z_2$, can be solved by scaling all lengths by a factor β , e. g. $R' = \beta R$. The local potential energy of an electron is changed by α/β . The local kinetic energy is changed by $\alpha^{2/3} \beta^{-2}$, being proportional to the density to the power two thirds. Scaling is obtained when the two energies change by the same factor, i. e. for $\beta = \alpha^{-1/3}$.

$Z_1 = 1$, $Z_2 \gg 1$, the potential must be approximately the Thomas-Fermi potential of a single atom, so that in this extreme the screening function u becomes

$$u = \varphi_0(R/a), \quad (2.12)$$

where φ_0 is the Fermi function ⁷⁾, and $a = 0.8853 \cdot a_0 \cdot Z_2^{-1/3}$, the number 0.8853 being a familiar Thomas-Fermi convention ($a_0 = \hbar^2/m\epsilon^2$).

In order to see whether a suitable choice of a can be introduced in eq. (2.12) so as to fit approximately all cases, one need only estimate the static Thomas-Fermi interaction in the other extreme, i.e. $Z_1 = Z_2$. For this purpose, we made a detailed derivation of the potential on the basis of the perturbation method described by GOMBÁS ⁷⁾. We need not reproduce the lengthy calculations here, which also would indicate an unwarranted importance of these static calculations*. We further compared with numerical Thomas-Fermi-Dirac calculations by SHELDON ²¹⁾ for $Z_1 = Z_2 = 7$, which did not deviate from the perturbation calculation by more than $\sim 10\%$.

When trying to see whether these numerical results for $Z_1 = Z_2$ may be approximated by eq. (2.12) with a suitable choice of $a = a(Z_1, Z_2)$, we considered Bohr's screening length as a starting-point. On the basis of qualitative considerations, BOHR suggested that the reciprocal square of the total screening length was the sum of the reciprocal squares of the screening lengths of the two atoms. It turns out that this choice reproduces fairly accurately the above-mentioned numerical results, i.e., eq. (2.12) may be applied for any pair Z_1, Z_2 , with

$$a = 0.8853 a_0 \cdot (Z_1^{2/3} + Z_2^{2/3})^{-1/2}, \quad (2.13)$$

which quantity differs from Bohr's choice only by a constant factor close to unity, $a = 0.8853 a_B$. The formula (2.13) in (2.12) begins to deviate from the numerical estimates (cf. footnote) when R/a becomes large ($\gtrsim 5$), but this is the least important and most dubious part of the potential. The error might be remedied by not using exactly the Fermi function φ_0 at large distances.

In the following we represent the ion-atom interaction by eq. (2.12) together with eq. (2.13). We shall use various simple approximations to u , besides the Fermi function φ_0 .

It is important to note that, for practical purposes, several other choices of a do not differ from eq. (2.13). Thus, suppose that we choose a screening

* The perturbation treatment, with $Z_1 = Z_2$, leads in first approximation to the interesting formula $u = \varphi_0^2(R/[2 \cdot 0.8853 \cdot a_0 \cdot Z_2^{-1/3}])$, i.e. the square of the Fermi function belonging to a single atom, but taken at half the distance of separation.

length a' proportional to $(Z_1^{1/2} + Z_2^{1/2})^{-2/3}$, instead of a in eq. (2.13). When Z_1/Z_2 changes, the ratio a'/a also changes, but this variation of a'/a is by less than $\pm 4\%$, and usually considerably less. We therefore found no reason to deviate from Bohr's choice of dependence on atomic numbers.

We later learned about the ingenious Thomas-Fermi estimates by FIRSOV⁶⁾, who derived both upper and lower limits for the potential. The reader is referred to Firsov's papers for a more detailed understanding of the static Thomas-Fermi estimates. With the qualifications mentioned above, Firsov's results are in accord with the present estimates.

In order to emphasize the uncertainties of potentials, we may quote one example. In Fig. 4 is shown the deflection by the Lenz-Jensen potential relative to that by the Thomas-Fermi potential, θ_{LJ}/θ_{TF} , as a function of impact parameter p . When p exceeds $2a$, the ratio θ_{LJ}/θ_{TF} begins to drop, and is ~ 0.75 for $p = 4a$. The Lenz-Jensen potential belongs to an isolated atom, or to $Z_1 \ll Z_2$, where it is often a better approximation to actual potentials than is the Thomas-Fermi potential, for large values of R/a^7 . This indicates the magnitude of one type of uncertainty.

Validity of Classical Estimates

The problem arises whether it is permissible to use classical mechanics in the present scattering phenomena. Usually, when posing a problem of this kind, we would have to specify completely the scattering measurement in question, in order that a well-defined answer may be given. In the present case, however, the phenomena are often classical to such a wide extent that practically all relevant calculations may be performed on the basis of classical mechanics.

To be more specific, let us consider the question whether a given total deflection, $|\theta| < 1$, may be associated with a certain impact parameter p and a classical path during the collision. For elastic collisions, this problem was discussed in a general way on the basis of wave packets in ref. 19, appendix B, in analogy to the discussion by BOHR²⁾. It was shown that if we attempt to obtain a given impact parameter p and corresponding classical deflection $\theta(p)$, the minimum uncertainties in these quantities become

$$(\delta p)^2 = \frac{\hbar}{2|\theta'(p)|} \quad \text{and} \quad (\delta\theta)^2 = \hbar \cdot |\theta'(p)|. \quad (2.14)$$

If we demand that the relative uncertainty in deflection be small, $(\delta\theta)^2 < \theta^2$, we find the following condition for a classical path

$$\left| \lambda \cdot \frac{d}{dp} \frac{1}{\theta(p)} \right| < 1, \quad (2.15)$$

where $\lambda = \hbar/M_0v$ is the wave length of the relative motion.

For a Coulomb potential, the deflection is $\theta = b/p$; when introduced in eq. (2.15), this leads to Bohr's condition

$$\varkappa = \frac{2Z_1Z_2e^2}{\hbar v} > 1, \quad (2.16)$$

and if e.g. $v \ll Z_1^{2/3}e^2/\hbar$ (cf. p. 4), the condition (2.16) is amply fulfilled. For the Coulomb potential, the minimum uncertainty in impact parameter is $\delta p/p \sim (2\varkappa)^{-1/2}$, according to eq. (2.14).

In order to illustrate the general behaviour for screened Coulomb potentials, let us consider the analytically simple standard potential (4.13), where the deflection is $\theta = (b/p)(1 + p^2/C^2a^2)^{-1}$, $C^2 \sim 3$, i.e. according to eq. (2.15),

$$\varkappa > 1 + \frac{3p^2}{C^2a^2}, \quad (2.17)$$

which inequality indicates that at sufficiently large p , or small θ , the classical approximation becomes doubtful. In the usual case of large \varkappa , the inequality (2.17) is violated only at very low values of θ .

As a general result, we have found that at sufficiently high velocities, or sufficiently low angles of deflection, a quantal treatment is necessary. For several reasons, however, classical estimates may remain more reliable than indicated above. First, we often need not ask for classical trajectories, but want instead to estimate integrals of type of $\int (\sin \theta/2)^{2n} d\sigma$, $n = 1, 2$. These integrals are usually approximated well by a classical calculation when $\varkappa > 1$. Second, even at high velocities where $\varkappa < 1$, classical integrals of the above type are not completely in error, because the major part of the scattering is of Rutherford type, which formula obtains both in classical and quantal calculations. Third, we are always concerned with repulsive fields, where simple estimates are more reliable than for attractive fields.

These cursory remarks may indicate both that classical estimates are valid to a wide extent and also how, in a specified case, the error of a classical calculation can be estimated. It should be noted that we have here discussed elastic collisions only.

§ 3. Power Law Potentials and Wide Angle Extrapolation

Perturbation Calculation

We ask for a classical scattering formula with the least possible number of independent variables, with the hope to retain a reasonable accuracy. It is then tempting to consider first the familiar perturbation treatment, corresponding to forward scattering and to an approximately rectilinear path with constant velocity. Let the path be parallel to the z -axis, and let the impact parameter be p . If $K_{\perp}(p, z)$ denotes the force perpendicular to the path, the deflection in the centre of mass system becomes the transverse momentum transfer divided by the total momentum, i. e.*:

$$\theta = \frac{1}{M_0 v^2} \int_{-\infty}^{\infty} K_{\perp}(p, z) dz = -\frac{1}{M_0 v^2} \frac{\partial}{\partial p} \int_{-\infty}^{\infty} V([p^2 + z^2]^{1/2}) dz, \quad (3.1)$$

if $\theta \ll 1$. The angle θ is therefore obtained from the potential V by one integration and one differentiation. Consider a screened Coulomb potential (2.3) of type of eq. (2.8), where the potential is a function containing only one parameter, R/a . We then find from formula (3.1)

$$\theta = \frac{b}{p} g\left(\frac{p}{a}\right), \quad (3.2)$$

where $b = 2Z_1 Z_2 e^2 / M_0 v^2$ is the collision diameter, and

$$g(\zeta) = \int_0^{\pi/2} \cos \varphi d\varphi \left\{ u\left(\frac{\zeta}{\cos \varphi}\right) - \frac{\zeta}{\cos \varphi} u'\left(\frac{\zeta}{\cos \varphi}\right) \right\}. \quad (3.3)$$

The formulae (3.1) and (3.2) may also be obtained from eq. (2.1), if the last term on the left in eq. (2.1) is considered as a perturbation. Note that in the case of an unscreened Coulomb potential, one has $u(R/a) = 1$ and therefore $g = 1$.

As to the number of variables necessary in a perturbation treatment, we find from eq. (3.2), since $a/b = \varepsilon$,

$$\varepsilon \cdot \theta = \frac{a}{p} \cdot g\left(\frac{p}{a}\right). \quad (3.4)$$

* The reader may notice that the integrated potential on the right-hand side of eq. (3.1) is of importance also in small angle quantal scattering¹⁸⁾, and in directional effects for crystal lattices¹⁹⁾, where it is proportional to the continuum potential, $U(r) = d^{-1} \int_{-\infty}^{\infty} V((r^2 + z^2)^{1/2}) dz$, the constant d being the distance between atoms along the particle path.

The number of independent variables is therefore reduced by one in the perturbation treatment, i.e. from two in eq. (2.9) to one— p/a —in eq. (3.4), because the dependent scattering variable has become $\varepsilon\theta$. This similarity in dependence of scattering on energy for $\theta \ll 1$ we now wish to extend to scattering by finite angles θ .

If the scattering potential depends also on Z_1/Z_2 , i.e. if eq. (2.5) holds, we find that $g = g(Z_1/Z_2, p/a)$, so that $\varepsilon \cdot \theta$ in eq. (3.4) depends on two variables, which again is one variable less than in the exact solution (2.6) belonging to the potential (2.5).

Power Law Potentials

In order to see whether scattering by finite angles may also permit a reduction in the number of variables, we study at first in some detail the case of power law potentials, $V(R) \propto R^{-s}$, or

$$u\left(\frac{R}{a}\right) = \frac{k_s}{s} \cdot \left(\frac{a}{R}\right)^{s-1}, \tag{3.5}$$

where k_s is a constant. One of the advantages of power law potentials is that, for several integer values of s , there are simple exact scattering formulae, so that it becomes easy to estimate the accuracy of approximate solutions.

In limited intervals of R , screened Coulomb potentials like eq. (2.3) may be represented by power law potentials, i.e. $s = -\partial \log V / \partial \log R$. For low values of R , the power s must approach the value 1 belonging to an unscreened Coulomb potential. In a considerable region of R -values, s is of order of 2 or 3.

From eqs. (3.5), (3.2) and (3.3) we find for the deflection

$$\theta = \gamma_s \cdot b \cdot a^{s-1} k_s \frac{1}{p^s}, \quad \text{if } \theta \ll 1, \tag{3.6}$$

where

$$\gamma_s = \int_0^{\pi/2} \cos^s \varphi d\varphi = \frac{\Gamma\left(\frac{1}{2}\right) \Gamma\left(\frac{s+1}{2}\right)}{2\Gamma\left(\frac{s}{2} + 1\right)} = \frac{1}{2} B\left(\frac{1}{2}, \frac{s+1}{2}\right), \tag{3.7}$$

$B(x, y)$ being the beta function³⁾. From the explicit formula for γ_s in terms of gamma functions, one derives the useful relation $\gamma_s \cdot \gamma_{s-1} = \pi/(2s)$. It

follows then that $s \cdot \gamma_s = (s-1) \cdot \gamma_{s-2}$. Table 1 gives values of γ_s in a number of representative cases; we are only interested in cases where $s \geq 1$. In § 5 we attempt to approximate γ_s by simple functions.

TABLE 1. Values of $\gamma_s = \frac{1}{2} B\left(\frac{1}{2}, \frac{s+1}{2}\right)$.

s	1	1.5	2	2.5	3	4	5	∞
γ_s	1	0.874	$\pi/4$	0.719	$2/3$	$3\pi/16$	$8/15$	$\sqrt{\pi/2s}$

Wide Angle Extrapolation

At small angles of deflection, it is not important to select carefully the variables which are to characterize the scattering. In the above, we chose as variables the angle θ and the impact parameter p . In the case of finite angles of deflection, we may note, first, that the differential cross section $d\sigma = d(\pi p^2)$ is preferable to the variable p . Second, we usually want to integrate functions of T times the probability of scattering, where T is the energy transfer in the laboratory system²⁾, $T = T_m \cdot \sin^2 \theta/2$, T_m being the maximum energy transfer in elastic collisions. In terms of T , the differential cross section (2.10) becomes, according to eq. (3.6),

$$d\sigma = -\pi \left\{ \frac{b^2}{4} \alpha^{2s-2} k_s^2 \gamma_s^2 T_m \right\}^{1/s} \cdot \frac{1}{s} \frac{dT}{T^{1+1/s}}, \quad (3.8)$$

and we expect this formula to be more appropriate than eq. (3.6), at wide angles of deflection. It so happens that for Coulomb potentials the formula (3.8) is exactly the Rutherford law (cf. below), and it is therefore worth while to consider the consequences of (3.8) in some detail.

Even though eq. (3.8) is derived from the perturbation formula (3.6), there is considerable difference between the two, at finite angles θ . Firstly, in eq. (3.8) θ is replaced by $2 \sin \theta/2$, as described above. Secondly, eq. (3.8) is obtained from formula (3.6) by differentiation of p^2 , so that p^2 in eq. (3.6) might contain an arbitrary additive constant, $p^2 \rightarrow p^2 + p_0^2$, and still lead to eq. (3.8). Therefore, eq. (3.8) is equivalent to

$$2 \sin \frac{\theta}{2} = \gamma_s \cdot b \cdot \alpha^{s-1} k_s \cdot (p^2 + p_0^2)^{-s/2}, \quad (3.9)$$

where p_0^2 , so far, is an arbitrary constant. The obvious demand that $T \leq T_m$ in eq. (3.8), or that $\sin \theta/2 \leq 1$ in eq. (3.9), leads to fixation of p_0 . For

repulsive potentials we have $\sin\theta/2 = 1$ for $p = 0$, so that, according to eq. (3.9), $p_0^2 = (\gamma_s \cdot b \cdot a^{s-1} k_s / 2)^{2/s}$ *. The introduction of p_0 implies, qualitatively, that for a given impact parameter p we have introduced an effective closest distance of approach, $\sim (p^2 + p_0^2)^{1/2}$. We describe eq. (3.9), or eq. (3.8) with $0 \leq T \leq T_m$, as the wide angle extrapolation.

Accuracy of Wide Angle Extrapolation

It remains to study the accuracy of eq. (3.9). Let us consider $s = 1$, i.e. an unscreened Coulomb potential. In this case, $u = 1$ in eq. (3.5) and therefore $k_1 = 1$. Since also $\gamma_1 = 1$, we find that $p_0 = b/2$. Thus, eqs. (3.8) and (3.9) are seen to contain the exact Rutherford formula.

Let us next compare eq. (3.8) with exact scattering in another potential of considerable interest, i.e. a repulsive R^{-2} -potential. A straightforward comparison shows that in this case the differential cross section (3.8) agrees well with the exact classical scattering (cf. BOHR, ref. 2, eq. (1.5.5)), the error increasing from 0 at $T = 0$, to -3% at $T = T_m$, corresponding to backward scattering.

More generally, it turns out that—independently of the value of s —the relative error in eq. (3.8) is largest at $T = T_m$, and decreases towards zero when T tends to zero. Let us therefore consider the error belonging to backward scattering as a function of s . When s increases from 1, the relative error in eq. (3.8) for backward scattering rises slowly from 0 to $\sim 15\%$ at $s = 3/2$, whereupon it decreases to 0 at $s \approx 2$, and becomes -20% at $s = 5/2$. For higher s -values it becomes increasingly negative. As a result, we find that in the region $1 < s < 5/2$ the formula (3.8) is sufficiently accurate for our purposes, even for large energy transfers T . For values of s higher than $\sim 5/2$, the accuracy is not good in the limit of extreme backward scattering.

The power law potentials give only a first guidance, since we wish to study screened Coulomb potentials, where the effective power s increases slowly from 1 at small values of R/a , to $s \sim 2$ when $R/a \sim 1$ and, finally, to $s \sim 3-4$ at large distances where $R/a \gg 1$. At low energies, the collisions become less penetrating, and the scattering by screened Coulomb potentials is determined by regions with high values of s . Since the present method underestimates the backward scattering in such regions, it might seem as

* We have thus found that θ is a function of only one variable $\xi_s = b \cdot a^{s-1} k_s / p^s$. This is also correct in an exact description of scattering by R^{-s} -potentials. The exact formulae for the dependence of θ on ξ_s deviate from the comprehensive formula (3.9), but deviations are quite small at low s -values, as shown in the text.

if scattering integrals are seriously underestimated at low energies. For several reasons, however, we expect that such errors are much reduced. First, at any given energy the backward scattering concerns the closest collisions, i. e. the lowest effective power s . Second, a reduced accuracy merely in the region $\theta \approx \pi$ does not impair most estimates of scattering integrals. In this connection, it is also important that backward scattering events can remain rare even during the whole process of slowing-down, and thus need not contribute much to the dominating part of the probability distribution of, e. g., energy loss. Third, it should be remembered that inelastic effects can be important just in the case of backward scattering, so that here we may not need the highest possible accuracy in the approximation of elastic collisions. It seems therefore worth while to accept the procedure of extrapolation to wide angles used in eqs. (3.8) and (3.9), and apply it to actual potentials with the hope that, by and large, errors are less than, say, $10^0/0$.

§ 4. Scattering Formula for Screened Coulomb Potentials

Before treating actual examples of screened potentials, we introduce a terminology suitable for the similarity treatment belonging to the wide angle extrapolation. If we apply the wide angle extrapolation to eq. (3.4), its left-hand side becomes $\varepsilon \cdot 2 \sin \theta / 2$, so that in the differential cross section, (2.10), the function $\varepsilon^{-2} F$ depends only on this variable. We therefore introduce a parameter t given by

$$t = \varepsilon^2 \cdot \sin^2 \theta / 2, \quad \varepsilon = a/b. \quad (4.1)$$

The parameter t is proportional to the energy transfer T times the particle energy E , $t = T \cdot E \cdot (M_2/M_1) \cdot (2Z_1Z_2e^2/a)^{-2}$.

We may now rewrite the differential cross section (2.10) in the following form

$$d\sigma = -\pi a^2 \frac{dt}{2t^{3/2}} f(t^{1/2}), \quad (4.2)$$

whereby we have defined a scaling function $f(t^{1/2})$. We have introduced the factor $t^{3/2}$ in the denominator for practical purposes: the case of power law scattering with $s = 2$ then corresponds to $f = \text{const}$. In the inner parts of the atom where $s < 2$, the function f therefore decreases for increasing t ; in the outer parts of the atom, where $s > 2$, f increases with increasing t . Now, t in itself is a measure of the depth of penetration into the atom, large values of t corresponding to small distances of approach. We therefore

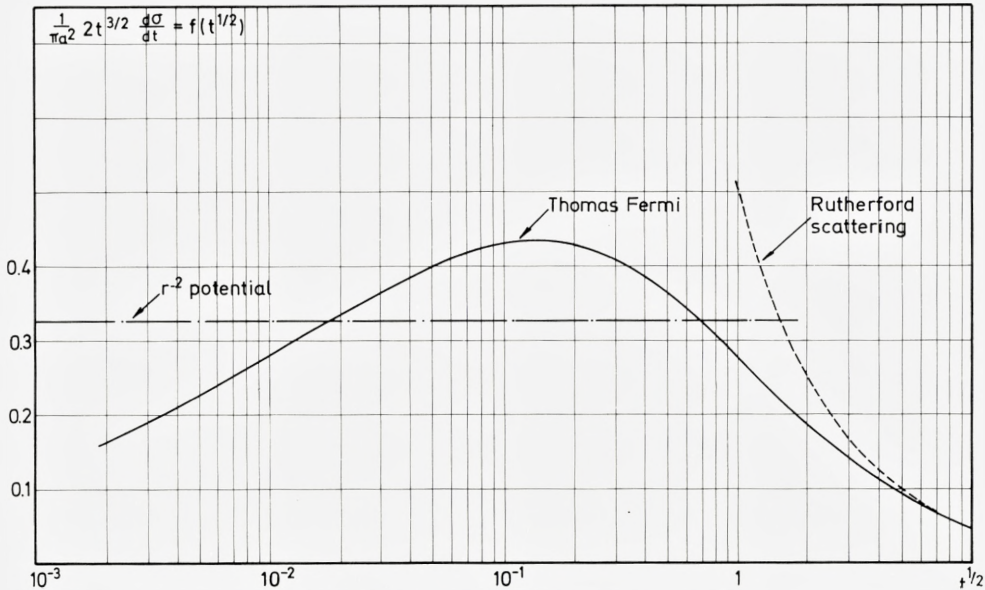


Fig. 1. Reduced differential cross section, calculated from Thomas-Fermi potential and eqs. (4.3) and (4.4). Ordinate is $f(t^{1/2}) = 2t^{3/2}(d\sigma/dt) \cdot (\pi a^2)^{-1}$; abscissa is $t^{1/2} = \varepsilon \sin \theta/2$. For large values of $t^{1/2}$, curve approaches Rutherford scattering, indicated by dashed curve. Horizontal line represents f for R^{-2} -potential.

expect that f increases for small values of t until it reaches a maximum, and decreases for large values of t .

In order to treat scattering by a screened Coulomb potential, we must specify the wide angle extrapolation of the general perturbation formula (3.4). By means of the procedure leading to eq. (3.9), we find directly

$$t^{1/2} = \varepsilon \cdot \sin \theta/2 = \frac{1}{2} \frac{a}{(p^2 + p_0^2)^{1/2}} g\left(\frac{1}{a} (p^2 + p_0^2)^{1/2}\right), \tag{4.3}$$

where $p_0 = p_0(\varepsilon, a)$ has become a redundant parameter, which need not be determined. If we know the screening function u , we can compute g from eq. (3.3) by one differentiation and one integration. Next, we solve eq. (4.3) with respect to $p^2 + p_0^2$, i.e. $p^2 + p_0^2(\varepsilon, a) = a^2 \cdot G(t^{1/2})$. Having obtained $G(t^{1/2})$, we derive $f(t^{1/2})$ in (4.2) by differentiation

$$f(t^{1/2}) = -t \cdot G'(t^{1/2}). \tag{4.4}$$

This calculation of the universal scattering function f is normally done numerically.

TABLE 2a.

Thomas-Fermi scattering
function $f(t^{1/2})$, cf. text and
Fig. 1.

$t^{1/2}$	$f(t^{1/2})$
0.002	0.162
0.004	0.209
0.01	0.280
0.02	0.334
0.04	0.383
0.10	0.431
0.15	0.435
0.20	0.428
0.40	0.385
1	0.275
2	0.184
4	0.107
10	0.050
20	0.025
40	0.0125

TABLE 2b.

Thomas-Fermi $s(\varepsilon)$ and $w(\varepsilon)$, cf. text and
Figs. 2 and 3.

ε	$s(\varepsilon)$	$w(\varepsilon)$
0.002	0.120	0.000097
0.004	0.154	0.00025
0.01	0.211	0.00085
0.02	0.261	0.00206
0.04	0.311	0.00479
0.10	0.372	0.0138
0.15	0.393	0.0214
0.20	0.403	0.0287
0.40	0.405	0.0542
1	0.356	0.105
2	0.291	0.152
4	0.214	0.189
10	0.128	0.228
20	0.0813	0.245
40	0.0493	0.249

In our basic numerical computation of f , we have chosen the Thomas-Fermi potential ($u(\xi) = \varphi_0(\xi)$). It turns out that for very low values of t the function $f(t^{1/2})$ behaves asymptotically as $\sim 1.43 \cdot (t^{1/2})^{0.35}$. The results are shown in Table 2a and Fig. 1, the latter representing $f(t^{1/2})$ as a function of $t^{1/2}$. In the figure is also shown the asymptotic Rutherford scattering, $f = 1/(2t^{1/2})$, as well as a horizontal line corresponding to power law scattering with $s = 2$, and $k_2 = 2/(0.8853e)$, i.e. the value of k_2 chosen by BOHR²⁾.

It is apparent that the treatment is inaccurate at low values of ε , e.g. $\varepsilon < 10^{-2}$. In particular, at such low values of ε the case of low atomic numbers Z_1 and Z_2 corresponds to particularly low energies, where deviations from Thomas-Fermi estimates may be considerable.

Stopping Cross Sections and Fluctuations¹²⁾

Having obtained the scattering cross section in terms of $f(t^{1/2})$, we may next calculate the stopping cross section S for nuclear collisions given by

$$S = \int T d\sigma = T_m \cdot \int \sin^2 \frac{\theta}{2} d\sigma, \quad (4.5)$$

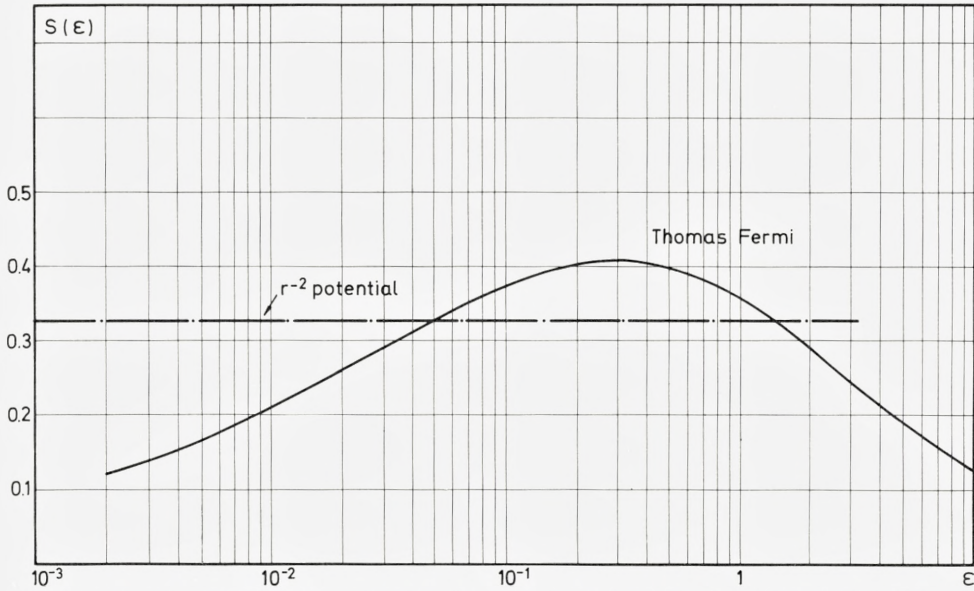


Fig. 2. Reduced nuclear stopping cross section s , (4.7), as function of ϵ . Curve obtained by integration (4.8) of Thomas-Fermi curve in Fig. 1. Horizontal line represents s for R^{-2} -potential.

where T is the energy transfer to an atom at rest, and $T_m = E \cdot 4M_1M_2 \cdot (M_1 + M_2)^{-2}$ is the maximum value of T . The stopping cross section S may be associated with the specific energy loss, $S(E) = (dE/dR) \cdot N^{-1}$, where N is the number of atoms per unit volume and dR the differential path length, R being the range measured along the path. It is seen that if we define a reduced range, ϱ , by

$$\varrho = RN M_2 \cdot 4\pi a^2 \frac{M_1}{(M_1 + M_2)^2}, \tag{4.6}$$

we may introduce a reduced stopping cross section $s(\epsilon)$ by means of the equation

$$s(\epsilon) = \frac{dE}{dR} \cdot \frac{\epsilon}{E} \cdot \frac{R}{\varrho}. \tag{4.7}$$

We consider only nuclear stopping in (4.7), and find from (4.2) and (4.5)

$$s(\epsilon) = \frac{1}{\epsilon} \int_0^\epsilon f(\zeta) d\zeta. \tag{4.8}$$

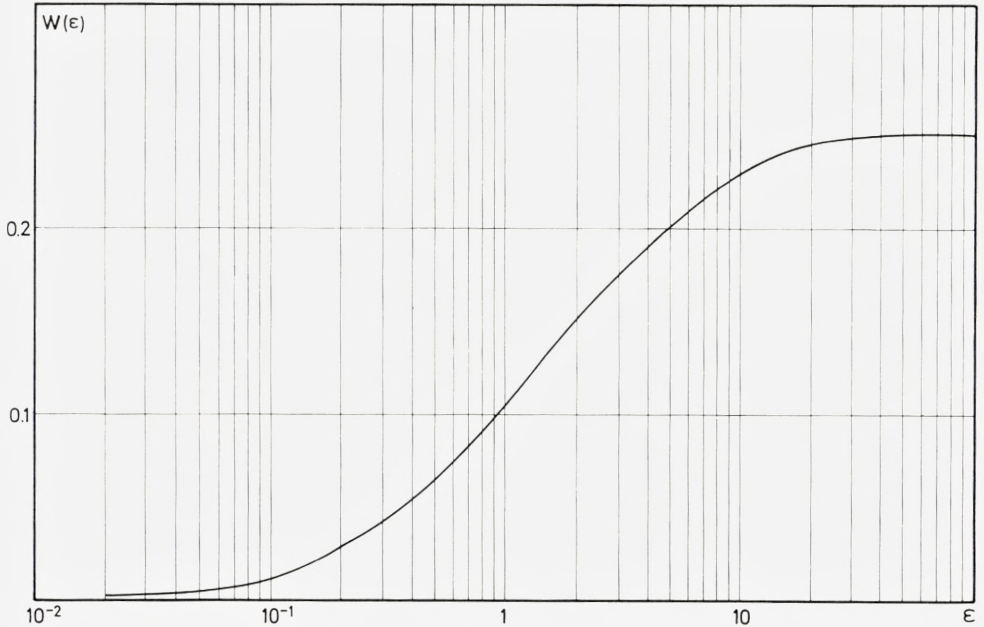


Fig. 3. Reduced square fluctuation in energy loss $w(\varepsilon)$, obtained from eq. (4.9) and Thomas-Fermi $f(t^{1/2})$.

In Fig. 2 and Table 2b is shown the reduced stopping cross section (4.8) as a function of ε , computed from the Thomas-Fermi estimate of f given in Fig. 1 and Table 2a; for $\varepsilon \gtrsim 10$ one finds approximately $s = (2\varepsilon)^{-1} \log(1.294\varepsilon)$. The corresponding square fluctuation in reduced energy loss,

$$w(\varepsilon) = \frac{1}{\varepsilon^2} \int_0^\varepsilon \zeta^2 f(\zeta) d\zeta, \quad (4.9)$$

is shown in Fig. 3 and Table 2b.

It may be noted that a stopping cross section depending on the variable ε obtains not only from the one-parameter cross section (4.2), but also from the two-parameter cross section (2.10). If so desired, we would in fact—by differentiation of $\varepsilon \cdot s(\varepsilon)$ in eq. (4.8)—be able to find a function $f(t^{1/2})$ in eq. (4.2) which gives exactly the same stopping cross section as a two-parameter scattering formula, (2.10).

It should be appreciated that in many cases one is not concerned with the total nuclear stopping cross section (4.8). Since the probability of the closest collisions is low, these collisions may correspond to a tail in the energy loss

distribution. If one then observes the most probable energy loss, this quantity may be obtained from the integration in eq. (4.8) with an upper limit smaller than ε . The simplicity of the present description in such cases was utilized by FASTRUP et al.⁵⁾

Power Law Scattering

In the case of power law potentials, eq. (3.5), the formula (3.8) leads to

$$f(t^{1/2}) = \lambda_s \cdot t^{\frac{1}{2} - \frac{1}{s}}, \quad (4.10)$$

where the constant $\lambda_s = (2/s)(k_s \gamma_s / 2)^{2/s}$ depends on γ_s given by eq. (3.7). In particular, $\lambda_1 = k_1^2 / 2$, so that $f = t^{-1/2} / 2$ for Rutherford scattering, and for $s = 2$ we find $f = \lambda_2$, where $\lambda_2 = k_2 \pi / 8$. It turns out that $0.3 \lesssim \lambda_s \lesssim 1.5$, and $1 \leq s \lesssim 3$, in the important regions of screened Coulomb interactions*.

Whereas the power law scattering (3.8) was derived as an approximate description of scattering by power law potentials, we may turn the tables and consider the power law scattering as a basic approximation without bothering about the question of an associated potential. Power law scattering has proved useful in analytic treatments of integral equations^{12, 13, 22)}. The only restriction we put on the power law scattering is that $s \geq 1$, so that it is never more strongly peaked in the forward direction than corresponding to Rutherford scattering. Thus, according to eq. (4.10) or (3.8), the differential cross section $d\sigma/dT$ is proportional to T to a power between T^{-1} and T^{-2} . The present scattering by screened Coulomb fields must therefore always remain quite different from isotropic scattering, where $d\sigma/dT$ is constant.

For power law scattering the reduced stopping cross section (4.8) becomes

$$s_s(\varepsilon) = \frac{\lambda_s}{2 \left(1 - \frac{1}{s}\right)} \cdot \varepsilon^{1 - \frac{2}{s}}. \quad (4.11)$$

Again, the case of power law scattering for $s = 2$ is particularly simple, since $s_2(\varepsilon) = \lambda_2 = \text{const.}$

Comparison of Deflections by Various Potentials

A comparison between deflections by various screened potentials is shown in Fig. 4. The deflections are measured relative to the corresponding

* For small t , the asymptotic behaviour of the Thomas-Fermi scattering function in Table 2a corresponds to $s \approx 3.1$ and $\lambda \approx 1.43$, whereas the standard potential, (4.13), leads to $s \rightarrow 3$, $\lambda \rightarrow 0.87$.

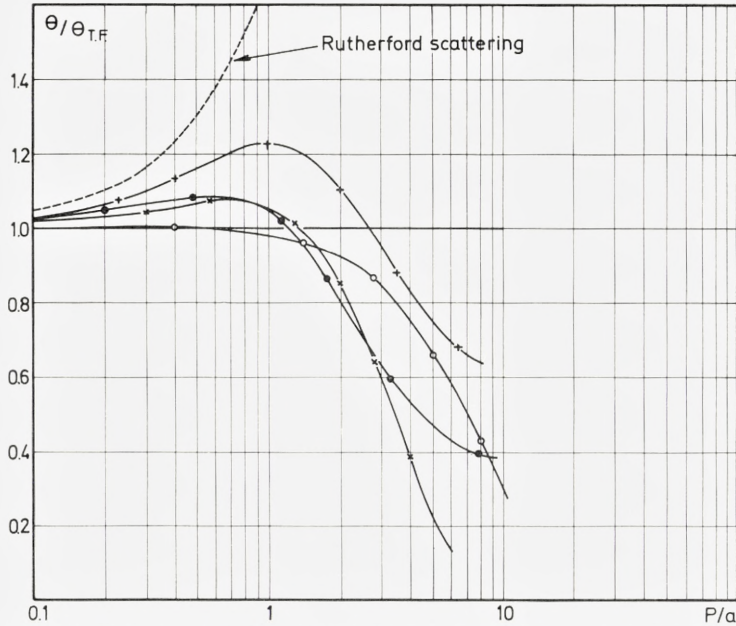


Fig. 4. Comparison between deflections by various screened potentials. At a given energy ε , ordinate θ/θ_{TF} represents deflection measured relative to deflection for Thomas-Fermi potential. Abscissa is reduced impact parameter p/a . The curves shown are Lenz-Jensen potential: \circ , Bohr potential: \times , standard potential, $C^2 = 3$: $+$, and $C^2 = 1.8$: \bullet .

deflection in a Thomas-Fermi potential at the same energy E , so that the ordinate is the ratio θ/θ_{TF} . The abscissa is the reduced impact parameter, p/a . The comparison in Fig. 4 therefore belongs to the perturbation case, where deflections are small. The curves were calculated from the magic formula, cf. § 5. It may be added that the curves in Fig. 4 are actually applicable at all angles of deflection, if the ordinate is interpreted as $(t/t_{TF})^{1/2}$ and the abscissa as $(p^2 + p_0^2)^{1/2}/a$.

The curve with open circles represents the Lenz-Jensen potential. It follows the Thomas-Fermi potential rather well until $p/a \sim 2$, and then drops considerably below it. Although the Lenz-Jensen potential belongs to single atoms, the curve indicates that the Thomas-Fermi potential may overestimate scattering at large impact parameters. The curve for the Bohr potential (\times) is slightly too high when $p/a < 1$, but is much too low when $p/a > 2$.

The figure also indicates the relative deflection by the 'standard potential'. For several purposes it has been useful to approximate the screened ion-

atom interaction by a simple function, which we have called standard potential^{18, 19)},

$$u(R/a) = 1 - \frac{R}{(R^2 + C^2 a^2)^{1/2}} \quad (4.13)$$

The standard potential contains one adjustable parameter, C . A fairly good over-all fit is obtained for the usual choice, $C^2 = 3$. The standard potential is much simpler analytically than the Bohr potential and also a better approximation to the Thomas-Fermi potential.

In Fig. 4, the curve for the standard potential with $C^2 = 3$ (+) is too high when $p/a \sim 1$, but at high values of p/a it has the merit of being between Thomas-Fermi and Lenz-Jensen. For comparison is also shown a curve for the standard potential with $C^2 = 1.8$ (full circles). It follows the Bohr potential rather closely when $p/a < 2$, but for higher values of p/a it is less in error than is the Bohr potential.

Wide Angle Extrapolation for Attractive Potentials

In the perturbation case, eq. (3.1), the magnitude $|\theta|$ of the deflection is independent of the sign of the potential. This holds no longer at finite angles—except for unscreened Coulomb potentials—and the wide angle approximation (3.9) and (4.3) is applicable only for repulsive potentials. It may be worth while to indicate that a similar wide angle approximation may be introduced for attractive potentials, but it does not possess the accuracy belonging to repulsive potentials. Consider the extrapolation of eq. (3.6) for attractive potentials, and demand again that Rutherford scattering is obtained exactly. We are then led to the substitution $\theta \rightarrow 2tg\theta/2$, i.e. instead of eq. (3.9) we get $2tg\theta/2 = \gamma_s \cdot b \cdot a^{s-1} k_s \cdot p^{-s}$. For general screened potentials we therefore introduce, instead of t in eq. (4.1), the parameter $t^* = \varepsilon^2 \cdot tg^2\theta/2$, with $\varepsilon = a/b$. The differential cross section is determined by eq. (4.2), where t is replaced by t^* , the function f being given e.g. in Fig. 1. This simple approximation may sometimes be useful (for large ε), but as a general rule it is not particularly accurate.

Approximations by Other Authors

During later years, several authors have discussed approximation methods in elastic scattering by screened repulsive Coulomb fields (cf. e.g. refs. 1, 6, 8, 9, 10, 23). HEINRICH⁸⁾ has suggested an interesting interpolation between forward and backward scattering which has some resemblance to our treatment. His results may be more accurate than ours, but do not contain the similarity property which is the main simplification in the present work. Both LEIBFRIED et al.⁹⁾ and SMITH et al.²³⁾ have studied a series expansion valid at small angles only and an expansion valid only for θ in the neighbourhood of π . BIERSACK¹⁾ has made scattering calculations where he comments on some of the present results.

§ 5. Magic Formula for Scattering

The above method of calculating $f(l^{1/2})$ for screened potentials by means of the perturbation formula (3.1) was used in our original computations of stopping powers and cross sections. We have therefore reproduced that calculation in § 4. Shortly after having applied the formulae, we did, however, derive a much simpler method. We called it the magic formula, because its structure and accuracy was rather surprising. In the present chapter we introduce the magic formula and use it for a number of comparative studies. We shall find that it gives quite closely the same results as found in § 3 and § 4.

Power Potentials

As a starting-point, we consider again the perturbation formula for scattering by power law potentials, i. e. eq. (3.6). We note that, since the deflection is $\theta = \gamma_s b k_s p^{-s} a^{s-1}$, it is proportional to the potential $V_s(R)$ itself (cf. eqs. (2.3) and (3.5)), taken at the distance $R = p$, and multiplied by $s \cdot \gamma_s$. Now, a multiplication by s is equivalent to a logarithmic differentiation, $-Rd/dR$, of the power law potential. Therefore, if γ_s may be approximated by a simple function of s , we should be able to obtain the right-hand side of eq. (3.6) by differentiation of the potential at the point $R = p$, or by integration. When looking for a simple approximation to γ_s , we can hardly avoid introducing a square root, because of the asymptotic behaviour given in Table 1, i. e. $\gamma_s \rightarrow (\pi/2s)^{1/2}$ for $s \rightarrow \infty$. We must also demand that the approximation is accurate for $s = 1$, where $\gamma_s = 1$. Let us compare two fairly accurate approximations of this type, denoted as γ'_s and γ''_s ,

$$\gamma'_s = \frac{1}{s} \sqrt{\frac{3s-1}{2}}, \quad (5.1)$$

and

$$\gamma''_s = \sqrt{\frac{\pi}{2s+1}}. \quad (5.2)$$

Both of the functions represent rather well the asymptotic behaviour of γ_s for $s \rightarrow \infty$. When $s = 1$, we find $\gamma'_1 = 1$, which is the correct value, whereas $\gamma''_1 = 1.023$, i. e. slightly too large. It is of course an advantage that Rutherford scattering ($s = 1$) is obtained exactly. The behaviour of the ratios γ'_s/γ_s and

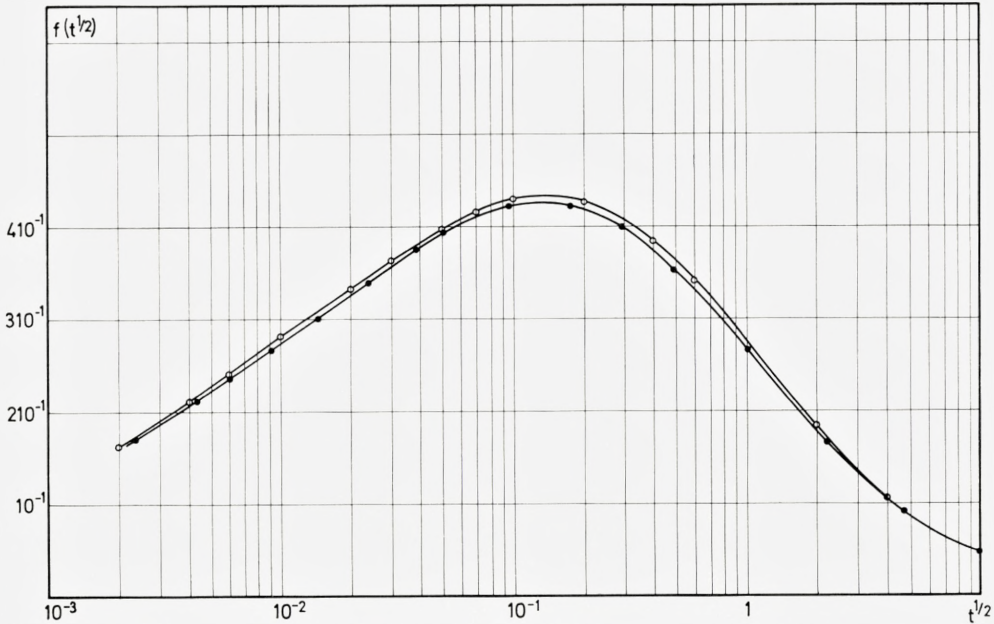


Fig. 5. Check of error in magic formula applied to Thomas-Fermi potential. Curve with open circles reproduces $f(t^{1/2})$ as a function of $t^{1/2}$ from Fig. 1. Curve with full circles is calculated from magic formula, eqs. (5.4) and (5.5).

γ''_s/γ_s is stated in Table 3. It is apparent that γ'_s gives a superior fit—within $1^0/0$ —in the important interval $1 \leq s \leq 4$, and γ'_s coincides with γ_s not merely for $s = 1$, but also for $s = 3$.

TABLE 3.
Accuracy of γ'_s , (5.1), and γ''_s , (5.2).

s	1	1.5	2	2.5	3	4	5	6	∞
γ'_s/γ_s	1.000	1.009	1.007	1.002	1.000	0.995	0.992	0.990	0.977
γ''_s/γ_s	1.023	1.016	1.009	1.007	1.004	1.003	1.002	1.002	1

The decisive feature, however, is the way in which s enters in the two functions. The significant quantity is $s \cdot \gamma_s$, as shown above, and γ'_s has the property that $(s\gamma'_s)^2 = (3s - 1)/2$, which corresponds simply to one differentiation. The quantity $(s\gamma''_s)^2 = \pi s^2/(2s + 1)$, on the contrary, is of a type requiring one integration and two differentiations, and is therefore quite

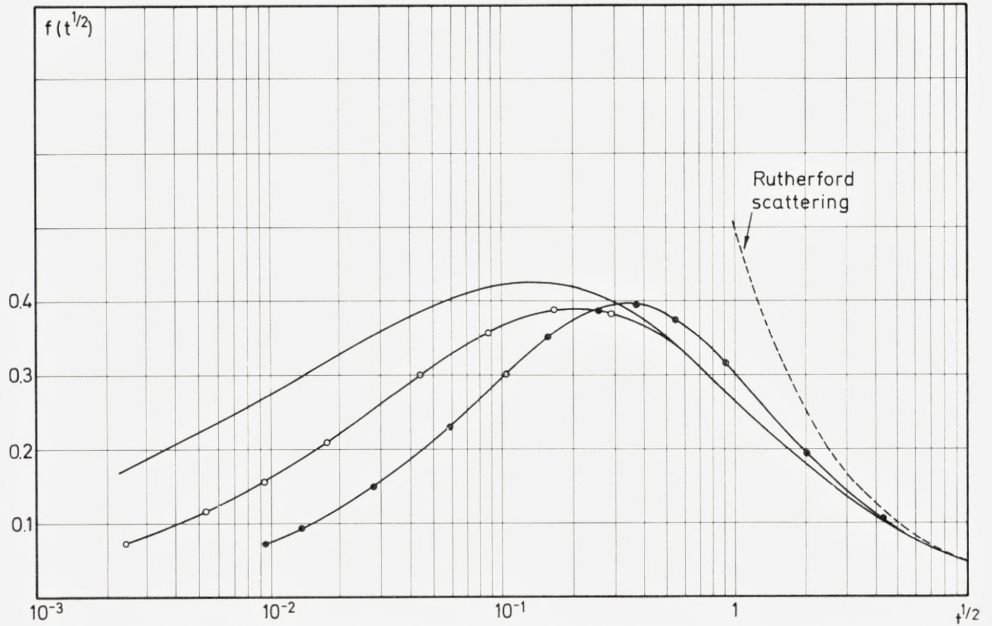


Fig. 6. Comparison of reduced differential cross sections for three screened Coulomb potentials. Ordinate is $f(t^{1/2}) = 2t^{3/2}(d\sigma/dt)(\tau a^2)^{-1}$, abscissa is reduced deflection $t^{1/2} = \epsilon \sin \theta / 2$. Full-drawn curve corresponds to Thomas Fermi potential, curve with open circles to Lenz-Jensen potential, and curve with full circles to Bohr potential, (2.11).

complicated. Although we might have made the numerical values of γ_s'' as accurate as those of γ_s' by introducing a constant factor, this would not improve upon the innate complication belonging to γ_s'' .

Magic Formula in Perturbation Limit

On the basis of γ_s' in eq. (5.1), we are then led to a tentative perturbation formula for scattering, as deduced from power law potentials,

$$\frac{\theta^2}{4} = -\frac{3}{4(M_0 v^2)^2} p^{1/3} \frac{d}{dp} \{V^2(p) p^{2/3}\}. \quad (5.3)$$

We have seen that, in so far as γ_s' may be considered equal to γ_s , the formula (5.3) is equivalent to the perturbation formula (3.6) for power potentials. In particular, for $s = 1$ and $s = 3$ the two formulae coincide; the error in θ is less than 1% when $s \leq 6$, and less than $\sim 2\%$ when s is large.

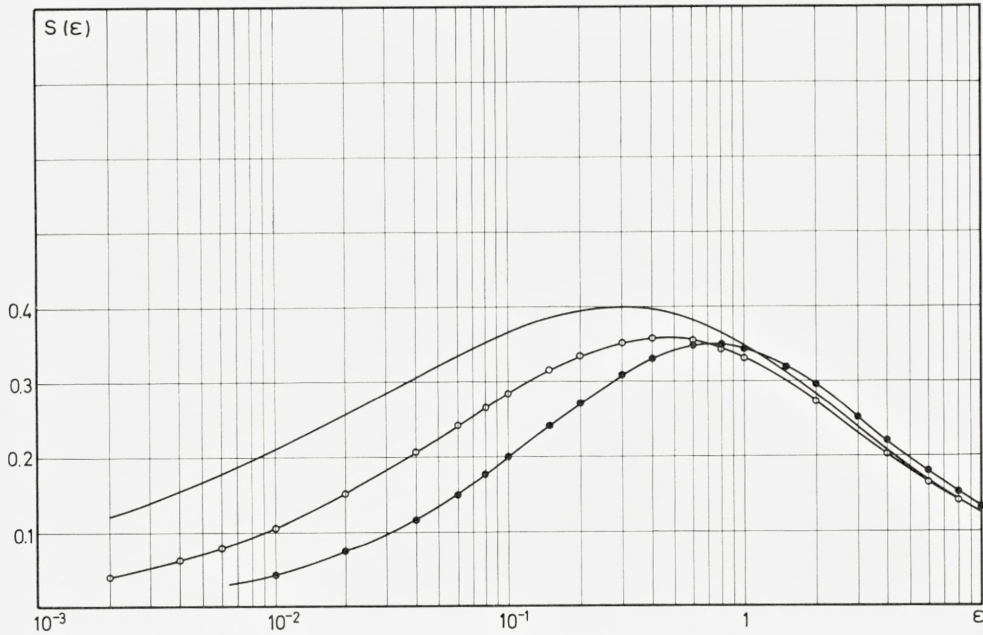


Fig. 7. Comparison of reduced stopping cross section, $s(\epsilon)$, for three screened Coulomb potentials, calculated from curves in Fig. 6. Full-drawn curve corresponds to Thomas-Fermi potential, open circles to Lenz-Jensen potential, and full circles to Bohr potential.

We shall show presently that—in the general case of screened Coulomb potentials—the formula (5.3) rather faithfully reproduces the original perturbation formula (3.1). The advantage of eq. (5.3) is that only one differentiation is necessary, whereas eq. (3.1) demands one differentiation and one integration. The magic formula (5.3) is therefore primarily an alternative way of calculating scattering by small angles, the advantage being great simplicity in both analytical and numerical treatments.

Magic Formula Applied to Wide Angles

We can immediately generalize the perturbation formula (5.3) by introducing the wide angle extrapolation (3.9). We replace $\theta^2/4$ in eq. (5.3) by $\sin^2\theta/2$, and the impact parameter p by $(p^2 + p_0^2)^{1/2}$, where $p_0 = p_0(E)$. We confine the treatment to the basic case of a screened Coulomb potential given by eq. (2.8), i.e. $V(R) = Z_1 Z_2 e^2 u(R/a)/R$. By changing to reduced variables, we then arrive at a formulation of eq. (5.3) which includes wide angles,

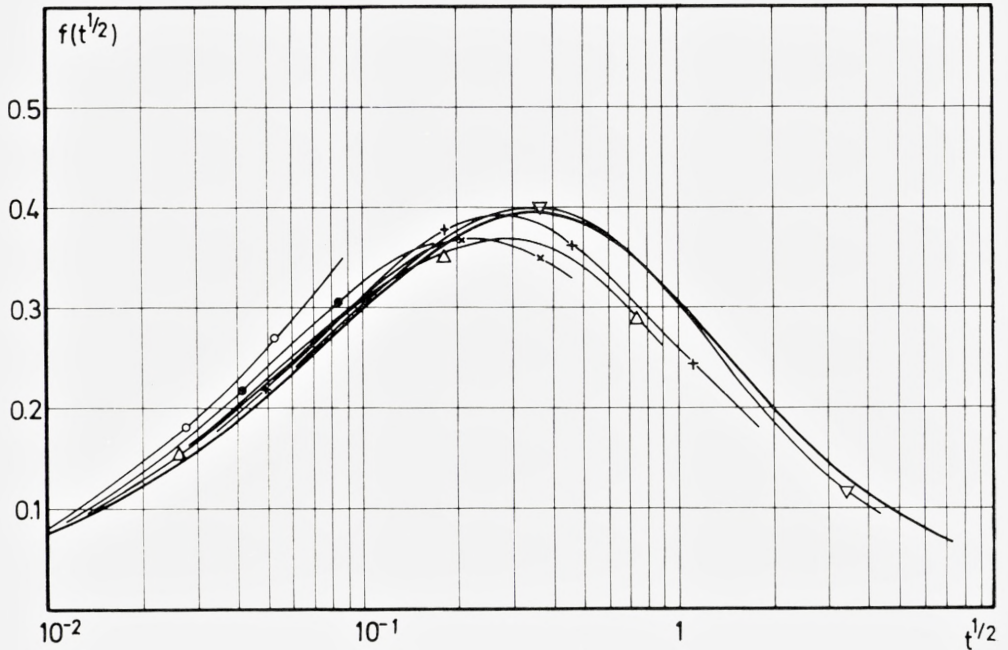


Fig. 8. Comparison between exact calculations (EVERHART et al.⁴⁾ and present formulae for Bohr potential, in a $f(t^{1/2})$ vs. $t^{1/2}$ -plot. Full-drawn curve is calculated from magic formula. The six separate curves are Everhart's calculations, for $\varepsilon = 0.089$ (\circ), $\varepsilon = 0.177$ (\bullet), $\varepsilon = 0.443$ (\times), $\varepsilon = 0.89$ (\triangle), $\varepsilon = 1.77$ ($+$), and $\varepsilon = 4.43$ (∇).

$$t = \varepsilon^2 \sin^2 \frac{\theta}{2} = -\frac{3}{16} \xi^{1/3} \frac{d}{d\xi} \{u^2(\xi) \xi^{-4/3}\}, \quad (5.4)$$

which connects t with the variable $\xi = (p^2/a^2 + p_0^2/a^2)^{1/2}$, by means of a differentiation. According to the definition of $f(t^{1/2})$, eq. (4.2), we find this function from eq. (5.4) by one further differentiation,

$$f(t^{1/2}) = -\frac{2t^{3/2}}{dt/d(\xi^2)}. \quad (5.5)$$

The formulae (5.4) and (5.5) represent the magic formula in the case of wide angle extrapolation for repulsive potentials.

Fig. 5 gives a comparison between the direct calculation of $f(t^{1/2})$ for the Thomas-Fermi potential, as given in Fig. 1, and a calculation by means of the magic formula. The deviations in the cross section are seen to be less

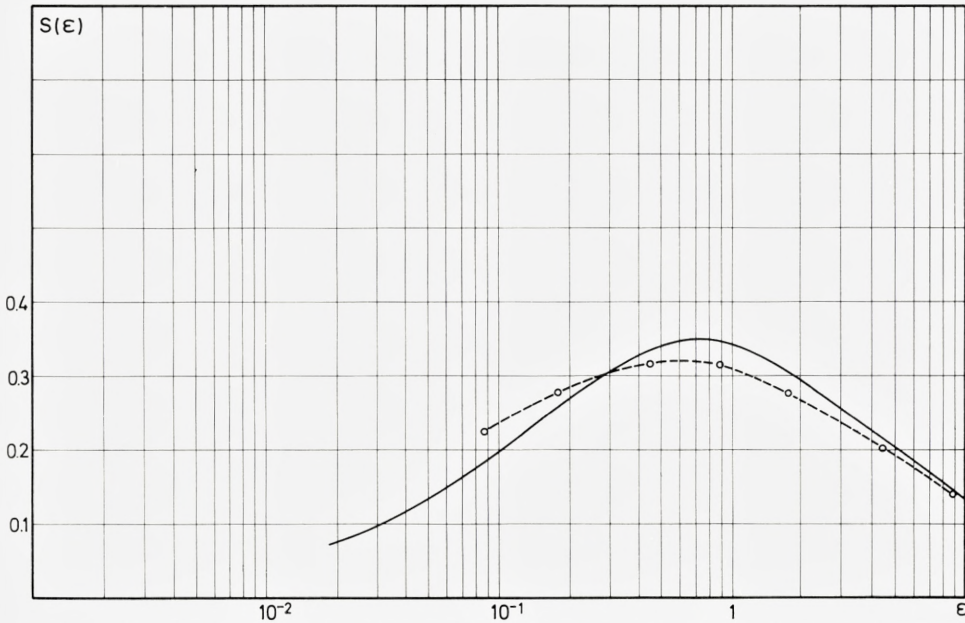


Fig. 9. Reduced stopping cross section $s(\epsilon)$ for Bohr potential. Comparison between exact calculations (dashed curve), and magic formula (full-drawn curve).

than $\sim 3\%$, which is a completely satisfactory agreement in the present connection.

Because of the simplicity of the magic formula and its equivalence to the direct calculations, we use it for a number of comparisons. Thus, in Fig. 6 we compare $f(t^{1/2})$ -curves for the Thomas-Fermi, the Lenz-Jensen, and the Bohr potentials. The Bohr potential leads to too low cross sections at low t (i.e. low ϵ or low θ), and to slightly too high cross sections at $t \sim 1$.

Fig. 7 gives a comparison of the reduced stopping cross section, (4.8), in the three cases represented in Fig. 6. The curves exhibit a similar behaviour as in Fig. 6, with too low stopping cross sections for the Bohr potential at low ϵ .

Numerical calculations of scattering by simple screened potentials, like the Bohr potential and the Thomas-Fermi potential, have been performed by EVERHART et al.⁴⁾, ROBINSON²⁰⁾, and others. The calculations lead to the differential cross section (2.10), depending on two parameters, ϵ and $\sin\theta/2$. In Fig. 8 we compare Everhart's calculations of scattering in the Bohr potential with our one-parameter curve. Everhart's curves are shown for

six values of ε ; each curve ends at $t^{1/2} = \varepsilon$, corresponding to backward scattering for the ε -value in question. As expected, the deviations from our curve is—in general—largest at backward scattering.

In Fig. 9 is shown the stopping cross section for the Bohr potential, as calculated in the present treatment and from Everhart's cross sections. We may emphasize again that, if it were desirable, one could, e.g., modify the present $f(t^{1/2})$ so as to give the stopping curve of Everhart's calculations (cf. p. 20).

In conclusion, we wish to express our gratitude to many colleagues and friends for their kind interest in the present work. We are particularly grateful to SUSANN TOLDI for patient assistance in the preparation of the paper.

*Institute of Physics
University of Aarhus.*

References

- 1) J. BIERSACK: Reichweiten schwerer Teilchen I: Neutrale Atome in isotroper Bremssubstanz, Hahn-Meitner-Institut für Kernforschung, HMI-B37 (1964).
- 2) N. BOHR: The Penetration of Atomic Particles through Matter. *Mat. Fys. Medd. Dan. Vid. Selsk.* **18**, no. 8 (1948).
- 3) A. ERDÉLYI, W. MAGNUS, F. OBERHETTINGER, and F. G. TRICOMI: Higher Transcendental Functions I. McGraw-Hill (1953).
- 4) E. EVERHART, G. STONE, and R. J. CARBONE: Classical Calculation of Differential Cross Section for Scattering from a Coulomb Potential with Exponential Screening. *Phys. Rev.* **99**, 1287 (1955).
- 5) B. FASTRUP, P. HVELPLUND, and C. A. SAUTTER: Stopping Cross Section in Carbon of 0.1–1.0 MeV Atoms with $6 \leq Z_1 \leq 20$. *Mat. Fys. Medd. Dan. Vid. Selsk.* **35**, no. 10 (1966).
- 6) O. B. FIRSOV: Interaction Energy of Atoms for Small Nuclear Separations. *Sovj. Phys. JETP* **5**, 1192 (1957); Calculation of the Interaction Potentials of Atoms, *ibid.* **6**, 534 (1958); Scattering of Ions by Atoms, *ibid.* **7**, 308 (1958).
- 7) P. GOMBÁS: Die Statistische Theorie des Atoms und ihre Anwendungen. Springer Verlag, Wien (1949); cf. also P. GOMBÁS: *Handbuch der Physik*, Bd. XXXVI (1956).
- 8) D. HEINRICH: Näherungsmethoden zur Berechnung der klassischen elastischen Streuung zweier Teilchen. *Ann. d. Physik*, 7. Folge, **13**, 284 (1964).
- 9) G. LEIBFRIED and T. PLESSER: The Convergence Behaviour of Expansions in the Classical Collision Theory. *Z. f. Physik* **187**, 411 (1965).
- 10) G. W. LEHMANN and K. A. SHAPIRO: Approximate Analytic Approach to the Classical Scattering Problem. *Phys. Rev.* **120**, 32 (1960).
- 11) J. LINDHARD and M. SCHARFF: Energy Dissipation by Ions in the keV Region. *Phys. Rev.* **124**, 128 (1961).
- 12) J. LINDHARD, M. SCHARFF, and H. E. SCHIÖTT: Range Concepts and Heavy Ion Ranges. *Mat. Fys. Medd. Dan. Vid. Selsk.* **33**, no. 14 (1963).
- 13) J. LINDHARD, V. NIELSEN, M. SCHARFF, and P. V. THOMSEN: Integral Equations Governing Radiation Effects. *Mat. Fys. Medd. Dan. Vid. Selsk.* **33**, no. 10 (1963).
- 14) J. LINDHARD and V. NIELSEN: Nuclear Collisions and Ionization Fluctuations in Charged Particle Detectors. *Phys. Lett.* **2**, 209 (1962).
- 15) J. LINDHARD and P. V. THOMSEN: Sharing of Energy Dissipation between Electronic and Atomic Motion. "Radiation Damage in Solids". IAEA, Vienna, Vol. 1, 65 (1962).

- 16) H. E. SCHIÖTT: Range-Energy Relations for Low-Energy Ions. *Mat. Fys. Medd. Dan. Vid. Selsk.* **35**, no. 9 (1966).
- 17) J. LINDHARD: Thomas-Fermi Approach and Similarity in Atomic Collisions. *NAS-NRC Publ.* 1133, 1 (1964).
- 18) PH. LERVIG, J. LINDHARD, and V. NIELSEN: Quantal Treatment of Directional Effects for Energetic Charged Particles in Crystal Lattices. *Nucl. Phys.* **A96**, 481 (1967).
- 19) J. LINDHARD: Influence of Crystal Lattice on Motion of Energetic Charged Particles. *Mat. Fys. Medd. Dan. Vid. Selsk.* **34**, no. 14 (1965).
- 20) M. T. ROBINSON: Tables of Classical Scattering Integrals for the Bohr, Born-Meyer, and Thomas-Fermi Potentials. ORNL-3493 (1963).
- 21) J. W. SHELDON: Use of the Statistical Field Approximation in Molecular Physics. *Phys. Rev.* **99**, 1291 (1955).
- 22) P. SIGMUND and J. B. SANDERS: Spatial Distribution of Energy Deposited by Ion Bombardment. *Conf. on Application of Ion Beams to Semiconductor Technology*, Grenoble (1967).
- 23) F. T. SMITH, R. P. MARCHI, and K. G. DEDRICK: Impact Expansions in Classical and Semi-Classical Scattering. *Phys. Rev.* **150**, 79 (1966).



J. H. BARTLETT

MOTION UNDER A PERIODIC CUBIC FORCE

Det Kongelige Danske Videnskabernes Selskab
Matematisk-fysiske Meddelelser **36**, 11



Kommissionær: Munksgaard
København 1968

Synopsis

In order to ascertain the effects of non-linearities, a study has been made of the simple differential equation $\ddot{x} + p(t) x^3 = 0$, where $p(t)$ is a periodic square wave function of time. Integration was at first accomplished by the use of the Runge-Kutta method, but accuracy limited only by the computer capacity can be achieved by the construction of a table of elliptic functions.

When the time t is increased by one period, any point P of the (x, \dot{x}) phase plane is transformed into a point $T(P)$, defining a mapping of the phase plane into itself. The motion is rotatory when p is positive and hyperbolic when p is negative, so that iteration of T can result in wrinkling. As the distance from the origin increases, the motion becomes faster, and $T(P)$ becomes infinite. That is, a particle can go to infinity in a finite time.

The equation has an infinite number of periodic solutions, or the mapping has an infinite number of fixed points. For the $p(t)$ which we have chosen, there is at least one fixed point on the x -axis and on the \dot{x} -axis for each T^n ($n = 1, 2, \dots$), and a fixed point for T^{n+1} lies closer to the origin than one for T^n . These fixed points P , plus their transforms $T^k P$ ($k = 1 \dots n-1$) are apparently all that exist. A table is given of some fixed points with n small.

The inner part of the plane is rather stable, in the sense that particles have only a small chance of reaching infinity. If there is an invariant region around an elliptic fixed point for T^n , it may be found by obtaining the invariant curves issuing from the hyperbolic fixed points for T^n .

Introduction*

Although non-linear differential equations have been studied extensively in connection with the dynamics of a particle, most of the literature has been devoted to systems where the Hamiltonian does not depend explicitly on time. However, the design of high-energy accelerators and the resolution of stability questions in celestial mechanics call for the development of adequate theory for Hamiltonians which are periodic in time. Basic existence theorems concerning invariant curves have been advanced recently by ARNOL'D (1) and by MOSER (2), but further work is apparently required before one has effective and practical methods of computation. In this paper, we shall discuss in detail the solution of a simple non-linear equation, with special reference to the location of the fixed points and to stability of solutions.

For one degree of freedom, the motion may be represented by the equation $\ddot{x} + p(t) f(x) = 0$, where $p(t)$ is periodic with period τ . For simplicity, we shall assume p to be a square wave, namely $p = p_0$ for $-\frac{\tau}{4} < t \leq \frac{\tau}{4}$ and $p = -p_0$ for $\frac{\tau}{4} < t \leq \frac{3\tau}{4}$, and $p_0 > 0$. If $f(x) = x$, the theory is well-known and given by FLOQUET (3). The equation with $f(x) = x + ax^3$ has been integrated numerically, for various initial conditions, by WRIGHT and POWELL (4) and discussed with the aid of perturbation theory (small values of "a") by MOSER (5). However, this work was very limited in extent, and a conversation with Dr. MOSER had as its subject the desirability of a theory for large values of x (or "a"). Subsequently, the author decided to neglect the linear term, to set $f(x) = x^3$, and to integrate with no reliance on perturbation theory. Such procedure brings out the effects due to the non-linearity of the system.

The Mathieu-Hill Equation

Before taking up the non-linear equation, it is necessary to review the linear case, where $f(x) = x$, because the literature is somewhat scattered. Our treatment will be based mainly on the work of COURANT and SNYDER (6).

* This work was reported in part to the USSR Mathematical Congress at Leningrad on July 5, 1961.

The Mathieu-Hill equation to be considered is

$$\frac{d^2x}{dt^2} + p(t)x = 0 \quad (1)$$

where $p(t)$ is defined as above.

Let the transformation T through one period be written

$$\left. \begin{aligned} x(\tau) &= M_{11}x(0) + M_{12}\dot{x}(0) \\ \dot{x}(\tau) &= M_{21}x(0) + M_{22}\dot{x}(0). \end{aligned} \right\} \quad (2)$$

This is a linear transformation of the phase plane (x, \dot{x}) into itself. It transforms the initial point $(1, 0)$ into (M_{11}, M_{21}) , and $(0, 1)$ into (M_{12}, M_{22}) . The coefficients M_{ij} must be obtained by actual integration of (1) for one period ($t = 0$ to $t = \tau$).

Since the Wronskian of the 2 solutions $(1, 0)$ and $(0, 1)$ is constant and initially unity, the matrix M has determinant 1, and can be taken to be

$$M: \begin{pmatrix} \cos \sigma & \beta \sin \sigma \\ -(1/\beta) \sin \sigma & \cos \sigma \end{pmatrix} \quad (3)$$

since $p(t) = p(-t)$. If $|\cos \sigma| \leq 1$, then σ is real and Equations (2) may be written

$$\left. \begin{aligned} x(\tau) &= x(0) \cos \sigma + \beta \dot{x}(0) \sin \sigma \\ \beta \dot{x}(\tau) &= -x(0) \sin \sigma + \beta \dot{x}(0) \cos \sigma. \end{aligned} \right\} \quad (4)$$

This shows that T just rotates the vector $(x, \beta \dot{x})$ through an angle σ , the magnitude of which is determined by $p(t)$ alone and not by the initial values of x and $\beta \dot{x}$. If we just consider the points $t = n\tau$, $n = \text{integer}$, the quantity $x^2 + \beta^2 \dot{x}^2$ is constant. When σ is real, β is real, the locus of the vector (x, \dot{x}) , for $t = n\tau$, is an ellipse, and the origin is called an *elliptic fixed point*. If $n\sigma = 2\pi m$, with m and n integers, the initial point P and the companion points TP , T^2P , etc. will be fixed under T^n . If $n\sigma \neq 2\pi m$, repeated application of T generates more and more points on the ellipse.

When $|\cos \sigma| > 1$, σ is imaginary, and β must be imaginary also, since M_{12} is real. Put $\sigma = i\psi$ and $i\beta = \gamma$, a real quantity. Equation (4) becomes

$$\left. \begin{aligned} x(\tau) &= x(0) ch \psi + \gamma \dot{x}(0) sh \psi \\ \gamma \dot{x}(\tau) &= x(0) sh \psi + \gamma \dot{x}(0) ch \psi. \end{aligned} \right\} \quad (5)$$

For the points $t = n\tau$, the quantity $x^2 - \gamma^2 \dot{x}^2$ is constant, and the locus consists of the branches of a hyperbola. For this case, the origin is called a *hyperbolic* fixed point.

The asymptotes to the hyperbolas are given by $x = \gamma \dot{x}$ and $x = -\gamma \dot{x}$. If the initial point P is on the first asymptote, then the map TP will also be, but the distance from the origin will have been stretched by the factor $\lambda_1 = ch\psi + sh\psi$, as we see by substitution into (5). Similarly, the distance from the origin to a point on the second asymptote will be shrunk, the factor now being $\lambda_2 = ch\psi - sh\psi$.

If $\dot{x}(0) = 0$, then Equation (4) yields $\cos \sigma = x(\tau)/x(0)$. Consequently, if $x \neq 0$, $\dot{x} = 0$ is a fixed point, we can test whether it is elliptic or hyperbolic by seeing how a point on the x -axis maps under T . If $|x(\tau)| < |x(0)|$, the fixed point is elliptic; if $|x(\tau)| > |x(0)|$, the fixed point is hyperbolic.

The x -axis is mapped into $x(\tau) = x(0) ch\psi$, $\gamma \dot{x}(\tau) = x(0) sh\psi$, the first equation giving $ch\psi$, and the second γ , assuming that the mapping has been done numerically. The stretch factors λ_1 and λ_2 follow immediately from $ch\psi$.

The Cubic Equation

Let us now consider the equation

$$\frac{d^2x}{dt^2} + p(t)x^3 = 0 \quad (6)$$

where $p(t)$ has period τ and

$$p = p_0 \quad \text{for} \quad -\frac{\tau}{4} < t \leq \frac{\tau}{4}, p_0 > 0,$$

$$p = -p_0 \quad \text{for} \quad \frac{\tau}{4} < t \leq \frac{3\tau}{4}.$$

As in the case of the Mathieu-Hill equation, the important thing is to find the transformation T , or how the (x, \dot{x}) plane maps into itself when t is increased by the period τ . This mapping depends only on the initial values of x and \dot{x} , and not on t . For the Mathieu-Hill equation, conclusions about stability are immediate, and depend only on the value of σ , so that an elliptic point is stable and a hyperbolic point unstable. However, for the cubic equation and other similar non-linear equations, the mapping is not simple and conclusions about stability are more difficult to reach. Hyperbolic

points are obviously unstable, while ARNOLD and MOSER (loc. cit.) have presented proofs that elliptic points are stable if certain criteria are satisfied. For any given differential equation, one must examine the mapping to find out whether these conditions are in fact met.

If extremely high accuracy is not necessary, integration by the Runge-Kutta method is simple and expeditious. Our first results were obtained in this way, but these have been later improved by the use of Jacobian elliptic functions, in a manner to be discussed presently.

A table of these functions is stored on a computer, and the integration reduces to looking up these functions and their inverses in the table. The accuracy is then limited by the number of bits which can be stored in a computer location.

First Integration

When $p = p_0$, the first integral of Eq. (6) is

$$\dot{x}^2 + (p_0/2)x^4 = (p_0/2)x_0^4 \quad (7a)$$

where x_0 is the intercept on the x -axis.

When $p = -p_0$, and there is an intercept on the x -axis at x_1 , the first integral of Eq. (6) is

$$\dot{x}^2 - (p_0/2)x^4 = -(p_0/2)x_1^4. \quad (7b)$$

When $p = -p_0$, and there is an intercept on the \dot{x} -axis, the first integral is

$$\dot{x}^2 - (p_0/2)x^4 = (p_0/8)a^4 \quad (7c)$$

where a is a real constant.

The transition from (7b) to (7c) occurs when

$$\dot{x} = \pm (p_0/2)^{1/2}x^2. \quad (8)$$

If this condition is satisfied initially, the motion will be along a parabola passing through the origin. Otherwise, the motion is along a quasi-ellipse (7a), or a quasi-hyperbola (7b or 7c).

Reduction to Standard Form

In Equation (7a), let $x = zx_0$. Then

$$\dot{z}^2 = (p_0/2)x_0^2(1 - z^4). \quad (9a)$$

In Equation (7b), let $x = x_1/z$. Then

$$z^2 = (p_0/2)x_1^2(1 - z^4). \quad (9b)$$

Finally in Equation (7c), let $x^2 = a^2w^2/2$ and $w^2 = (1-z)/(1+z)$. Since $w\dot{w} = -\dot{z}/(1+z)^2$, we obtain

$$z^2 = (p_0/2)a^2(1 - z^4). \quad (9c)$$

These equations all have the same form, and differ only in the parameter which enters.

Jacobian Elliptic Functions

Since the integration of Equations (9) involves Jacobian elliptic functions with parameter $k = (1/2)^{1/2}$, we enumerate for future reference some of the properties of these functions.

$$sn u = u - \frac{1}{4}u^3 + \frac{11}{160}u^5 \dots \quad (10a)$$

$$cn u = 1 - \frac{1}{2}u^2 + \frac{1}{8}u^4 - \frac{3}{80}u^6 \dots \quad (10b)$$

$$dn u = 1 - \frac{1}{4}u^2 + \frac{3}{32}u^4 \dots \quad (10c)$$

$$d sn u = cn u dn u du \quad (10d)$$

$$d cn u = - sn u dn u du \quad (10e)$$

$$2d dn u = - sn u cn u du \quad (10f)$$

$$cn^2u + sn^2u = 1 \quad (10g)$$

$$dn^2u + \frac{1}{2}sn^2u = 1 \quad (10h)$$

$$d^2 cn u/du^2 = - cn^3u \quad (10i)$$

$$\frac{d^2}{du^2} \frac{sn u}{1 - cn u} = \frac{1}{2} \left(\frac{sn u}{1 - cn u} \right)^3. \quad (10j)$$

The functions $sn u$ and $cn u$ may be regarded as distorted sines and cosines, with period $4K = 7.41629871$. The function $dn u$ is even, and also symmetric about $u = K$, with $dn^2K = \frac{1}{2}$. Note that $cn(2K - u) = -cn u$. Also

$$D \operatorname{sn}(a+b) = \operatorname{sn} a \operatorname{cn} b \operatorname{dn} b + \operatorname{sn} b \operatorname{cn} a \operatorname{dn} a \quad (10k)$$

$$D \operatorname{cn}(a+b) = \operatorname{cn} a \operatorname{cn} b - \operatorname{sn} a \operatorname{sn} b \operatorname{dn} a \operatorname{dn} b \quad (10l)$$

$$D \operatorname{dn}(a+b) = \operatorname{dn} a \operatorname{dn} b - \frac{1}{2} \operatorname{sn} a \operatorname{sn} b \operatorname{cn} a \operatorname{cn} b \quad (10m)$$

where

$$D = 1 - \frac{1}{2} \operatorname{sn}^2 a \operatorname{sn}^2 b. \quad (10n)$$

Furthermore,

$$\left. \begin{aligned} \operatorname{sn} i v \operatorname{cn} v &= i \operatorname{sn} v, & \operatorname{cn} i v \operatorname{cn} v &= 1, \\ \operatorname{dn} i v \operatorname{cn} v &= \operatorname{dn} v. \end{aligned} \right\} \quad (10p)$$

Second Integration

The integral of Eq. (9a) is

$$z = \operatorname{cn}(p_0^{1/2} x_0 t) \quad (11)$$

as may be verified by using (10e), (10g), and (10k). Thus, if the motion starts on the x -axis at x_0 and is of duration t , the final point (quasi-elliptic motion) will be at

$$\left. \begin{aligned} x &= x_0 \operatorname{cn}(p_0^{1/2} x_0 t) = x_0 \operatorname{cn} u \\ \dot{x} &= -p_0^{1/2} x_0^2 \operatorname{sn} u \operatorname{dn} u \\ u &= p_0^{1/2} x_0 t. \end{aligned} \right\} \quad (12)$$

with

If the motion starts on the x -axis at x_1 and is quasi-hyperbolic, the final point will be at

$$\left. \begin{aligned} x &= x_1 / \operatorname{cn} u \\ \dot{x} &= p_0^{1/2} x_1^2 \operatorname{sn} u \operatorname{dn} u / \operatorname{cn}^2 u \\ u &= p_0^{1/2} x_1 t. \end{aligned} \right\} \quad (13)$$

with

Finally, if quasi-hyperbolic motion starts on the $+\dot{x}$ -axis, the point at time t will be at

$$\left. \begin{aligned} x &= (a^2/2)^{1/2} (1 - \operatorname{cn} u) / \operatorname{sn} u \\ &= (a^2/2)^{1/2} \operatorname{sn} u / (1 + \operatorname{cn} u) \\ \dot{x} &= (p_0/2)^{1/2} a^2 \operatorname{dn} u / (1 + \operatorname{cn} u) \\ u &= p_0^{1/2} a t. \end{aligned} \right\} \quad (14)$$

with

If the motion starts from a point not on either axis, the appropriate value of the parameter (x_0, x_1 , or a) must first be found from Equation (7), and the time from the axis to the initial point can be calculated by solving Eq. (12), (13), or (14). This gives immediately the time from the axis to the final point, since the duration of the motion is presumed to be given. The coordinates of the final point can now be calculated directly from Eq. (12), (13), or (14).

In what follows, it will be convenient to denote quasi-elliptic mapping for time $\tau/4$ by e , and quasi-hyperbolic mapping for this time by h . Also, from now on, we shall omit the term "quasi".

Scale

The values of p_0 and of τ can be fixed quite arbitrarily. Inspection of (12) shows that the motion depends essentially on $u = p_0^{1/2}x_0t$, so that if we select p_0 and t , then x_0 may be calculated from u . Powell and Wright (4) chose $p_0 = e/3$, where $e = 0.1$, and the quarter period $\tau/4 = 1.5$. In our calculations, it has been convenient to modify this slightly, taking $p_0 = 0.037$ and $\tau/4 = 1.5$.

General Properties of the Motion

Symmetry and Reversal

If $x(t)$ is a solution of Equation (6), so are $x(-t)$, $-x(t)$, and $-x(-t)$. The motion may be reversed by replacing (x, \dot{x}) by $(x, -\dot{x})$. An equivalent reverse motion is $(-x, \dot{x})$. To reverse the motion, reflect in the x -axis or the \dot{x} -axis.

Elliptic Motion

If the motion is elliptic for a time $\tau/4$, the x -axis maps into the curve $e(x)$. This starts as a cubic from the origin, since $x = x_0$ and $\dot{x} \cong -p_0x_0^3\tau/4$, and then turns into a curve which spirals outward and clockwise, traversing one quadrant each time that $p_0^{1/2}x_0\tau/4$ increases by K . The first intercept on the \dot{x} -axis will be, by (12), at $\dot{x} = -(p_0/2)^{1/2}x_0^2$, where $x_0 = 4K/p_0^{1/2} = 6.4259$, since $u = K$ for $x = 0$.

Under elliptic motion, the time to traverse one quadrant from the x -axis is $K/x_0p_0^{1/2}$, and therefore the outer parts of the plane are rotated faster than the inner parts.

If x_0 is fixed, the points reached by elliptic motion lie on the oval described by (7a) and (12), and only differ by the value of the parameter u , which will be called the *phase*. Under elliptic motion, the phase difference between 2 points on the above oval remains constant. Since the \dot{x} -axis is described by $u = -K$, the map $e(\dot{x})$ will also be a curve which spirals outward and clockwise, each point on it lagging in phase by the amount K behind a corresponding point on $e(x)$. For small values of \dot{x} , the locus $e(\dot{x})$ is given by $x = \dot{x}_0\tau/4$, or a straight line.

Hyperbolic Motion

If the motion is hyperbolic for a time $\tau/4$, the x -axis maps into the curve $h(x)$, which starts out from the origin as a cubic, namely $x = x_0$ and $\dot{x} \cong p_0\dot{x}^3\tau/4$. The maximum value of u equals K , and if $v = K - u$ is small, Equation (13) yields

$$\dot{x} \sim (p_0/2)^{1/2}x^2 \quad (15)$$

and so the cubic approaches this parabola asymptotically from below as $u \rightarrow K$.

The corresponding map of the \dot{x} -axis, $h(\dot{x})$, starts out from the origin as a straight line $x = \dot{x}_0\tau/4$. Equation (14) shows that x becomes infinite when $u = 2K$ and also that $x^2 = (a^2/2)(1 - cn u)/(1 + cn u)$ and

$$\dot{x} = 2(p_0/2)^{1/2}x^2 dn u/(1 - cn u).$$

But, as $u \rightarrow 2K$, this last equation becomes

$$\dot{x} \rightarrow (p_0/2)^{1/2}x^2$$

so that the straight line changes into a curve $h(\dot{x})$ which also approaches the parabola (15) asymptotically, but from above.

Under hyperbolic motion, a finite point (not the origin) will move to infinity in a finite time t_0 . If the point starts at x_1 on the x -axis, then from (13) we have $t_0 = K/p_0^{1/2}x_1$. If the point starts from the \dot{x} -axis, then from (14) $t_0 = 2K/p_0^{1/2}a$, where $a^2(p_0/2)^{1/2} = 2\dot{x}_0$. It should then be possible to fix a value for t_0 , and to find a curve C in the (x, \dot{x}) plane such that any point on this curve will just reach infinity in the time t_0 .

Part of curve C may be regarded as generated by points leaving the x -axis and travelling for time $(K/p_0^{1/2}x_1) - t_0$. If $v = p_0^{1/2}x_1t_0$, then

and

$$\left. \begin{aligned} x &= x_1/cn(K-v) = \sqrt{2}x_1dnv/snv \\ &= (2/p_0)^{1/2}v\,dnv/t_0snv \\ \dot{x} &= (2/p_0)^{1/2}v^2cnv/t_0^2sn^2v. \end{aligned} \right\} \quad (16)$$

(The formula for \dot{x} is obtained from Equation (13) by noting that $sn(K-v) = cnv/dnv$ and $dn(K-v) = \sqrt{1/2}dnv$).

Now equation (7c) will reduce formally to (7b) if we put $a = (1+i)x_1$. The remainder of curve C, that generated by points leaving the \dot{x} -axis, can then be found by setting $u = (1+i)v$ and finding what Equations (16) become in terms of u . Making use of Equations (10k)–(10p) and the relation

$$(2dn^2v - isn^2v)/(1 + icn^2v) = 1 - i,$$

we find

$$\left. \begin{aligned} \frac{2v\,dnv}{snv} &= \frac{u(1+cnu)}{snu} = \frac{u\,snu}{1-cn u}, \\ \frac{v\,cnv}{snv\,dnv} &= \frac{u\,dnu}{snu}, \end{aligned} \right\} \quad (17a)$$

and

$$\frac{2v^2cnv}{sn^2v} = \frac{u^2dnu}{1-cn u}. \quad (17b)$$

Consequently, substituting (17a) and 17b) in (16), we have

with

$$\left. \begin{aligned} x &= (2/p_0^{1/2})u\,snu/2t_0(1-cn u) \\ \dot{x} &= (2/p_0^{1/2})u^2dnu/2t_0(1-cn u) \\ u &= p_0^{1/2}a\,t_0. \end{aligned} \right\} \quad (18)$$

(These formulas can also be obtained by using $2K-u$ instead of u in the arguments of Equations (14)).

Equations (16) and (18) represent together a smooth curve. It has a companion, obtained by changing x to $-x$ and \dot{x} to $-\dot{x}$. Any point outside of these two curves will, under hyperbolic motion, reach infinity in time less than t_0 . For the present problem, the maximum time that hyperbolic motion takes place continuously is one half-period, so that we shall set $t_0 = \tau/2 = 3$. All points which can reach infinity in time less than this will be called primarily unstable, and the above curves mark the boundary of primary instability. They are shown in Figure 1. The x -intercept has

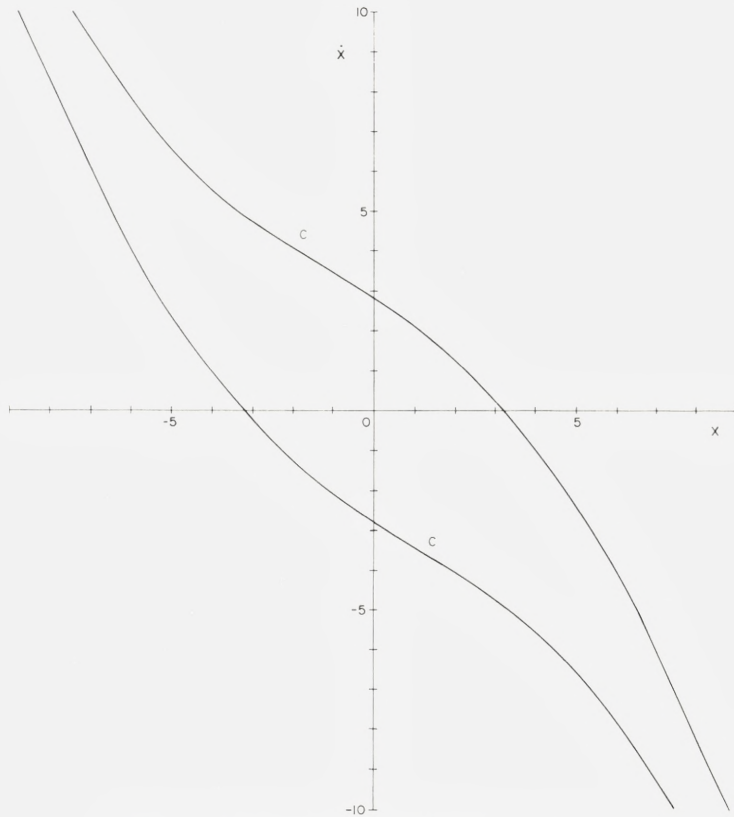


Figure 1. Primary Instability Boundary C , (\dot{x} vs x).

magnitude $K/3p_0^{1/2} = 3.21296$, while the \dot{x} -intercept has magnitude $(2/p_0)^{1/2}(K/t_0)^2 = 2.8082$.

The behavior of Equation (16) or (18) as $x \rightarrow \infty$ is readily obtained. From (16),

$$\dot{x} = (p_0/2)^{1/2} x^2 \operatorname{cn} v / \operatorname{dn}^2 v.$$

Letting $u \rightarrow 2K$, we have $x \rightarrow \infty$ and

$$\dot{x} = -(p_0/2)^{1/2} x^2. \quad (15a)$$

In the limit, curves C approach either this parabola or that described by (15) with $x < 0$. (When there is no ambiguity, we shall just say “the parabola”).

The boundary between the two parts of curve C is marked by the 2 points obtained by setting $x_1 = 0$, or $v = 0$, or $u = 0$. Equation (16) then gives $x = (2/p_0)^{1/2}/t_0$ and $\dot{x} = (p_0/2)^{1/2}x^2$. The motion, as a function of t_0 , is along the parabola, inward if $\dot{x}/x < 0$ and outward if $\dot{x}/x > 0$. The velocity is proportioned to x^2 and is thus faster the farther out we are. Knowing the initial x , we can calculate the initial t_0 , add an increment Δt_0 , and then obtain the final value of x .

Hyperbolic motion, which has this parabolic motion as a special case, is thus faster the farther out in the plane the points are.

The combined motion, which is always such as to preserve area in the phase plane, is rotatory half the time and hyperbolic for the other half. The inward hyperbolic motion ($\dot{x}/x < 0$) compresses toward the origin, and the outward hyperbolic motion ($\dot{x}/x > 0$) pulls away from the origin, in a rough manner of speaking. Wrinkling is the result.

Combined Motion (small x_0)

Let the motion start at a small value of x_0 on the x -axis, and be elliptic for the time $t_0 = \tau/4$, hyperbolic for time $\tau/2$ and elliptic for time $\tau/4$. We wish to find the locus of the end point $e h^2 e (x_0) = T_e(x_0)$. Let $x_a =$ abscissa after time $\tau/4$ from x_0 , and $t_1 =$ time from x_a along the hyperbolic part to the axis at x_1 . The values of x will be taken so small as to be approximately constant. From Equations (12) and (13),

$$\left. \begin{aligned} x_a &= x_0 \operatorname{cn}(p_0^{1/2} x_0 t_0) = x_1 / \operatorname{cn}(p_0^{1/2} x_1 t_1) \\ &\simeq x_0 - \frac{1}{2} p_0 x_0^3 t_0^2 \simeq x_1 + \frac{1}{2} p_0 x_1^3 t_1^2 \end{aligned} \right\} \quad (19)$$

and

$$\dot{x}_a \simeq -p_0 x_0^3 t_0 \simeq -p_0 x_1^3 t_1. \quad (20)$$

If $\lambda = p_0 x_0^2$, then, from Equation (19)

$$x_1 \simeq x_0 - \lambda x_0 t_0^2 = x_0(1 - \lambda t_0^2)$$

and from Equation (20)

$$(t_1/t_0) = (x_0/x_1)^3 \simeq 1 + 3\lambda t_0^2$$

or

$$t_1 - t_0 = 3\lambda t_0^3 = 3p_0 x_0^2 t_0^3.$$

This is the time required for the hyperbolic motion from $he(x_0)$ to x_1 . The time for the (elliptic) motion to go from the x -axis to $T_e(x_0)$ is very

closely twice this. Substituting in Equation (20), the final value of \dot{x} will be $\dot{x}_f = -p_0 x_0^3 (6p_0 x_0^2)(\tau/4)^3 = -6(\tau/4)^3 p_0^2 x_0^5$.

The mapping $e h^2 e$ thus, for small x_0 , displaces a point on the x -axis downwards by an amount proportional to x_0^5 . Calling this mapping temporarily $T(x_0)$, it is obvious that $T^2(x_0)$ will, for small positive x_0 , lie below $T(x_0)$, and so on. This mapping is then a clockwise twist of the plane, the twist increasing with distance from the origin.

Fixed Points

A transformation T will in general carry one point P of the plane into another point $T(P)$, but there do exist special points, called *fixed* points, such that $T(P) = P$. The corresponding solutions of the differential equation are *periodic*, since T refers to the change due to a replacement of t by $t + \tau$. (The motion is to start in the middle of a sector, with p positive or negative). Let the symbol (n/m) signify that a point is fixed under T^n , and that the origin has been encircled exactly m times. As will be shown below, the points $(1/1)$, which are fixed under T , lie either on the x -axis or the \dot{x} -axis.

The Transformation $T = e h^2 e(x_0)$

As x_0 increases, the curve $e(x_0)$ spirals outward and clockwise, intersecting the parabola when $cn^4 u = 1/2$ i. e. when $x_0 = 2.037$. At this stage $he(x_0)$, which starts out from the origin as a fifth-power downwards, has turned and reached the parabola. Further increase of x_0 puts $e(x_0)$ across the parabola, and with it $he(x_0)$. The curve $e(x_0)$ reaches the \dot{x} -axis when $x_0 = 6.426$. On the other hand, $h^{-1}(\dot{x})$, for $\dot{x} < 0$, starts out as a straight line downward and to the right, eventually approaching the parabola asymptotically, so that it will intersect $e(x_0)$, and does so for $x_0 = 3.414$ (calculated). At this point, the motion is symmetric with respect to the \dot{x} -axis, so that $e h^2 e(x_0) = -x_0$, which means that this value of x_0 is fixed under T^2 . We also see that $T(x_0)$ has a spiral nature and has reached the negative x -axis. The next important event that occurs is that $e(x_0)$ intersects the primary instability boundary (P. I. B.) (see Figure 1), so that $h^2 e(x_0)$ becomes infinite. What happens is that $h^2 e(x_0)$ approaches the parabola in the second quadrant, with the magnitude of x increasing as x_0 does. The subsequent elliptic motion becomes faster and faster, with $e h^2 e(x_0)$ intersecting the $+x$ -axis and spiralling to infinity. If the value of x for which this inter-

section first takes place is x_1 , then $T(x_0) = x_1$, and the points x_0 and x_1 are fixed under T^2 , and classified as $(2/2)$. We thus obtain a whole series of fixed points as x_0 approaches the limiting value where $e(x_0)$ intersects the P.I.B. Later, however, as the parabola in the third quadrant is approached, $e(x_0)$ emerges from this instability region, crosses the parabola and then enters the region again. (The gap contains the point $e(1/1)$, see below).

Location of Points Fixed under $(1/n)$

Periodic motion under T consists of 2 parts, one elliptic and the other hyperbolic, each for time $\tau/2$.

(a) Let the elliptic part intersect the x -axis at x_0 , and the hyperbolic part intersect it at x_1 . From Equations (7a) and (7b), their common points have $2\dot{x}^2 = (p_0/2)(x_0^4 - x_1^4)$. Consequently, *the orbit is symmetric about the x -axis*, and the fixed points lie on the x -axis, at x_0 and at x_1 , respectively. If x_0 is positive and small enough so that $e(x_0)$ lies in the first quadrant ($x > 0$, $\dot{x} < 0$) then $he(x_0)$ will lie below the x -axis, since the hyperbolic motion is at lesser x than the elliptic motion and hence slower. Consequently $T(x_0) \neq x_0$ and x_0 cannot be a fixed point for T under these circumstances. If x_0 increases so that $e(x_0)$ is in the second quadrant, $he(x_0)$ still lies below the x -axis and x_0 is not a fixed point for T . When, however, x_0 is large enough so that $e(x_0)$ is in the third quadrant, the hyperbolic motion is at first toward the $(-x)$ -axis and the time to go to this axis increases from zero, when $e(x_0)$ is on the $(-x)$ -axis, to infinity when $e(x_0)$ is on the parabola $\dot{x} = (p_0/2)^{1/2}x^2$. For some value of x_0 in between, $he(x_0)$ will be on the $(-x)$ -axis. There is then a fixed point $(1/1)$ at this value of x_0 . Actual calculation shows that $e(x_0)$ is not far from the parabola, so that we may take it at the parabola if we want a rough estimate for x_0 . For such an intersection, $2x^4 = x_0^4$, or $cn u = \pm 2^{-1/4}$ and $u = 0.58778, 3.12037$, etc. Corresponding values of x_0 are 2.037, 10.814, 14.889, etc. The *fixed point* $(1/1)$ therefore *lies a little below* $x_0 = 14.889$. The fixed points $(1/n)$ are located approximately at $x_0 = 2.037 + 12.852 n$, ($n = 1, 2 \dots$).

(b) Let the elliptic part intersect the x -axis at x_0 , and the hyperbolic part intersect the \dot{x} -axis as given by Equation (7c) with $x = 0$. From (7a) and (7c), the common points have $2x^4 = x_0^4 - \frac{1}{4}a^4$. *The orbit is symmetric about the \dot{x} -axis*, with fixed points at $\dot{x} = \pm (p_0/2)^{1/2}x_0^2$ and $\dot{x} = \pm (p_0/8)^{1/2}a^2$, for $n = 1$. A rough lower estimate, obtained by intersecting the ellipse with

the parabola above, gives $x_0 = 2.037 + 6.426 = 8.463$. Thus, there is a fixed point $(1/1)$ on the \dot{x} -axis lying somewhat above $\dot{x} = (p_0/2)^{1/2}x_0^2 = 9.74$. (Actual calculation shows it to be at about 10.26). The fixed points $(1/n)$ on the \dot{x} -axis are at values corresponding to $x_0 = 8.463 + (n-1) 12.852$.

More accurately, if a point P on the x -axis is fixed under T , then $he(P)$ must also lie on the x -axis, say at $x = x_1$ (positive or negative). Then, if we find the intersections of $e(x)$ with $h^{-1}(x)$ or $h^{-1}(-x)$, the fixed points are determined. The curve $e(x)$ spirals out from the origin, lying below $h^{-1}(x)$ in the first quadrant, and then intersecting $h^{-1}(-x)$ and $h^{-1}(x)$ alternately (third, fifth, etc. quadrants) and yielding fixed points $(1/n)$ with n a positive integer. At large distances h^{-1} is asymptotic to the parabolas P of Equation (15) or (15a). If the reflection of P in the x -axis is denoted by \bar{P} , then $e(\bar{P})$ will spiral around and intersect the x -axis near all the above fixed points $(1/n)$.

Conjecture

The above types of symmetry are found in general, and seem essential for periodic solutions of this differential equation. No rigorous proof has been devised, but our experience leads us to believe that *all the fixed points P of the equation $\ddot{x} + px^3 = 0$, such that $T^n P = P$ ($n = \text{integer}$), lie either on the x - or \dot{x} -axis, or are transforms ($TP, T^2P \dots$) of other fixed points which do.*

Successive Transformations $T^n(x)$

The curve $T(x)$ starts from the origin and spirals clockwise, intersecting the x -axis first at $-x_2$ and then at $+x_1$, with $|x_1| > |x_2|$. If x_a is the point which maps into $-x_2$, i. e. $T(x_a) = -x_2$, then $T^{-1}(x_a) = -x_2$, by symmetry, and $T^2(x_a) = T(-x_2) = x_a$. Consequently, x_a is a fixed point for T^2 as is $-x_2$. But $he(x)$ intersects $(he)^{-1}(-x)$ the first time on the $-\dot{x}$ -axis, everything is symmetric, and so $x_a = x_2$. Two neighboring curves $T^n(x)$ and $T^{n+1}(x)$ will intersect when $T^{n+1}(x_b) = T^n(x_c)$, or $T(x_b) = x_c$. But then, by symmetry as above, x_b must be fixed under T^2 and $x_c = \pm x_b$. If we require that both x_b and x_c be positive, then they will be equal. Thus, $T^n(x)$ and $T^{n+1}(x)$, with $x > 0$, intersect for the first time at the fixed point $(1/1)$.

Let us consider successive mappings Tx, T^2x, T^3x , where $0 \leq x \leq x_2$. Tx spirals clockwise to $-x_2$, T^2x spirals clockwise inside $T(x)$ to $+x_2$, T^3x inside T^2x to $-x_2$, etc. The operation T rotates the end of the curve by π each time. T^3x crosses the positive x -axis for some value $x_3 < x_2$, which is the fixed point $T^3x_3 = x_3$. Likewise, T^4x lies inside T^3x , and so the fixed

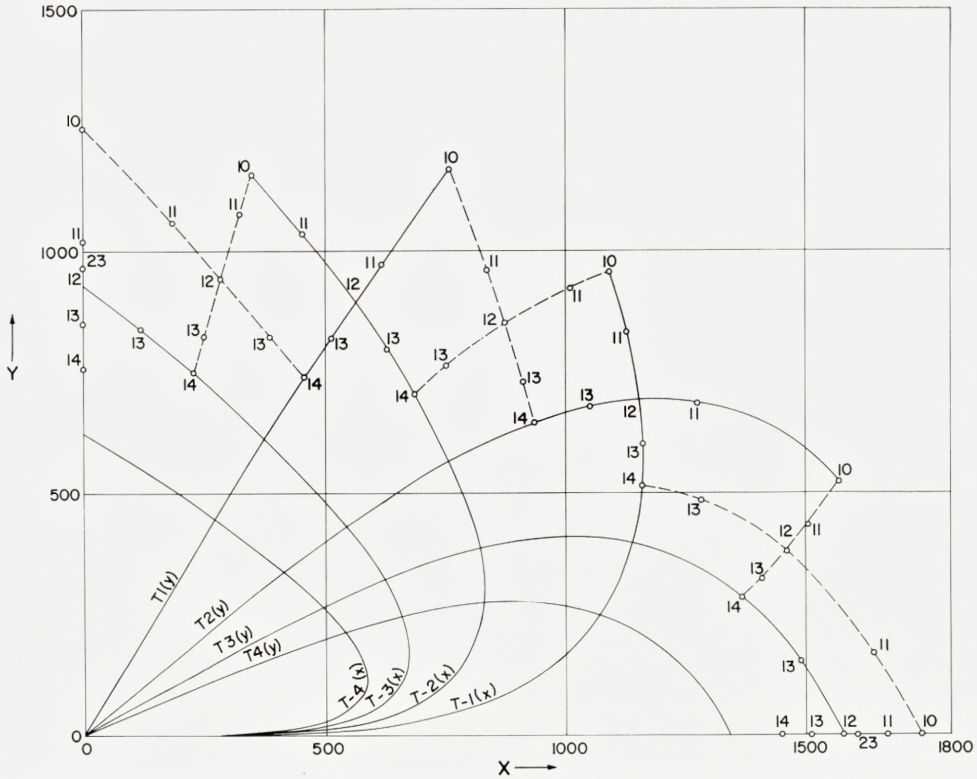


Figure 2. Fixed Points for $n = 10$ to $n = 14$ ($y = \dot{x}$ vs. x). Vertical Scale: $10^4 \dot{x}$, Horizontal Scale: $10^3 x$. Also mappings $T^{-n}(x)$ and $T^n(y)$ for $n = 1$ to $n = 4$.

point $T^4 x_4 = x_4$ will have $x_4 < x_3$. Thus we have an infinite number of isolated fixed points along the $+x$ -axis, at least one for each value of n . (Similar reasoning applies to the \dot{x} -axis).

Now it can happen, as n becomes larger, that wrinkles develop in the curve $T^n x$ and that this will have more than one intersection with the $+x$ -axis. Insertion of just one wrinkle will result in 3 intersections, i. e. $T^n(x_\alpha) = x_1$, $T^n(x_\beta) = x_2$, and $T^n(x_\gamma) = x_3$, where $x_\alpha < x_\beta < x_\gamma$. If these intersections are all distinct, then, since $T^n(x)$ cannot cross itself, either $x_1 < x_2 < x_3$ or $x_1 > x_2 > x_3$. In the first case, $x_1 = x_\alpha$, $x_2 = x_\beta$, $x_3 = x_\gamma$ and all the points are fixed under T^n . In the second case, $x_1 = x_\gamma$, $x_2 = x_\beta$, and $x_3 = x_\alpha$, so that only the middle point is fixed under T^n , and the outer points are fixed under T^{2n} .

Location of Points Fixed under $(n/1)$

A systematic search for points fixed under T^n can be made by looking at the mapping. First find where $T^n(x_a, \dot{x})$ intersects $x = x_a$ and plot the locus of such intersections. Then find where $T^n(x, \dot{x}_b)$ intersects $\dot{x} = \dot{x}_b$ and plot the corresponding locus. Intersections of the two loci give the fixed points. Such a search was made in the early stages of this work, and led to the observation that all the fixed points so obtained lay either on the x -axis or the \dot{x} -axis or were transforms of points which do.

Figure 2 shows, for $n = 10, 11, 12, 13$ and 14 , where the fixed points ($x > 0, \dot{x} = y > 0$) lie, and in addition how the x and y axes map for $n = 1, 2, 3$, and 4 . (Here T is defined as $e h^2 e$). The point $(23/2)$ is also shown.

A survey of some of the fixed points for low values of n was made by the Runge-Kutta method, for $p_0 = .037$ and period 6, and the results are tabulated below. If p is initially positive (first quarter-period), we deal with the basic transformation $T = e h^2 e$, while if p is initially negative, the basic transformation is $T = h e^2 h$.

TABLE I: Fixed points

<i>x-axis, $T = e h^2 e$</i>							
<i>n</i>	2	3	4	5	6	7	8
<i>x</i>	3.4143	3.1823	2.387	2.338	2.1086	2.058	1.9106
<i>n</i>	9	10	11	12			
<i>x</i>	1.8506	1.736	1.667	1.5777			
 <i>\dot{x}-axis, $T = e h^2 e$</i>							
<i>n</i>	2	3	4	5	6	7	8
<i>\dot{x}</i>	9.6012	.4591	.3775	.3579	.3088	.1639	.1545
<i>n</i>	9	10	11	12			
<i>\dot{x}</i>	.1464	.1259	.1021	.09339			
 <i>x-axis, $T = h e^2 h$</i>							
<i>n</i>	2	3	4	5	6	7	8
<i>x</i>	3.7968	2.1534	2.0564	1.6558	1.6276	1.5061	1.478
<i>n</i>	9	10	12				
<i>x</i>	1.4046	1.375	1.2926				

\dot{x} -axis, $T = h e^2 h$

n	2	3	4	5	6	7	8
\dot{x}	1.355	1.082	.931	.2294	.2151	.2016	.1780
n	12						
\dot{x}	.09545						

Regions of Stability

Even though a study of the mapping near a fixed point immediately reveals whether this point is *elliptic or hyperbolic*, a further investigation is needed to ascertain whether or not an elliptic point is *stable*. ARNOL'D (1) and MOSER (2) claim that, if a mapping satisfies certain criteria near the fixed point, there exists an invariant curve around the fixed point such that no particle inside this curve can get outside; i. e. that the fixed point is stable. We shall now show how one can construct such a curve for the differential equation in question, if the curve exists.

Let us consider the points which are fixed under T^n . There will be a set of elliptic points ranged around the origin. Around each such point, if we are close enough so that the mapping is linear, any point P is mapped by T^n , T^{2n} , etc., into other points which lie on an ellipse. As the distance from the fixed point to P is increased, these ellipses swell out to meet corresponding ovals from neighboring fixed points. Their meeting place, roughly speaking, is marked by a hyperbolic fixed point. Thus, as we go round the origin, elliptic and hyperbolic points alternate, and the two pairs of characteristic lines from two neighboring hyperbolic points bend into invariant curves (I. C.'s) which enclose the elliptic point between them.

Let us now examine more closely the region between a hyperbolic point H_1 (for T^n) and its neighbor $T(H_1) = H_2$. Denote by α_1 and α_2 the I.C.'s for which the motion is away from H_1 and H_2 respectively, and by β_1 and β_2 the I.C.'s for which the motion is toward these points, as shown in Figure 3.

In practise, one can construct α_1 by taking points very close to H_1 and subjecting them repeatedly to the transformation T^n . The other invariant curves can be constructed in similar fashion.

Let α_1 and β_2 intersect at A_2 , and α_2 and β_1 at B . The curve $H_1 \alpha_1 A_2 \beta_2 H_2 \alpha_2 B \beta_1 H_1$ will be regarded as a bounding curve, and points inside which do not get outside under repeated transformations by T^n will comprise a *stable region* under T^n .

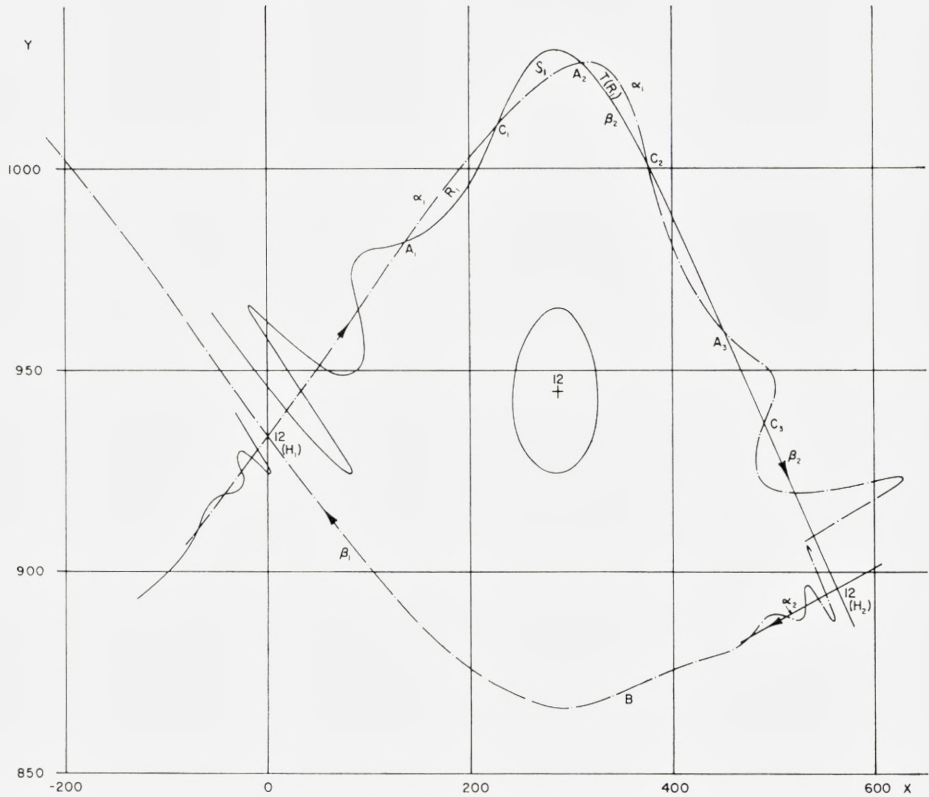


Figure 3. Invariant Curves from Hyperbolic Fixed Points H_1 and H_2 for $n = 12$ ($y = \hat{x}$ vs. x). An elliptic fixed point for $n = 12$, together with an approximate trajectory around it, is also shown. Vertical Scale: $10^4 \hat{x}$, Horizontal Scale $10^3 x$.

The nature of the invariant curve is such that oscillations of increasing amplitude develop. The point A_2 maps into $A_3 = T^n(A_2)$ on β_2 . A point just inside A_2 must map into a point just inside A_3 . Therefore, the curve α_1 , which has crossed β_2 at A_2 , must cross back between A_2 and A_3 , say at C_2 . Repeated application of T^n to A_3 gives a sequence of points A_4, A_5 etc., such that the distances A_n, A_{n+1} are reduced each time by roughly a constant factor (the "stretch" factor mentioned earlier). Since area must be preserved, the amplitude of oscillation must increase each time to offset the compression against α_2 . The end result is that *roughly one half of the points on α_1 near H_1 "escapes", and the other half approaches α_2 .*

As β_2 proceeds backwards from A_2 , it next crosses α_1 at $C_1 = T^{-n}(C_2)$ and then at $A_1 = T^{-n}(A_2)$. The region R_1 between β_2 and α_1 , from A_1 to C_1 ,

maps under T^n into a corresponding region between β_2 and α_1 from A_2 to C_2 . Thus points inside the bounding curve have gotten outside, or escaped. *The complete region of escape is composed of R_1 and the corresponding area R_2 between α_2 and β_1 , plus all of their maps under repeated application of T^{-n} .* At the same time that these particles are escaping, those from S_1 and S_2 , and their maps under T^{-n} , are entering.

One may say that an I.C. has an inside and an outside, and that a point on the outside always stays there. However, points inside the I.C. α_1 can get outside β_2 , as we have just seen. We have tacitly assumed that particles in $T(R_1)$ escape, when as a matter of fact they pile up on the I.C. from H_2 corresponding to α_1 . But some of these stay outside and some go in, with the chances about even. There is continual fluctuation across the boundary, and in the long run, if it is just a question of T^n alone, no particles will escape from its sphere of influence, if they are initially inside the bounding curve.

If, however, a particle is in such an area as $T(R_1)$, which is outside the bounding curve β_2 for T^{11} , say, it may simultaneously be in a region of escape for T^{10} . Thus it may be handed on to outer regions until it hits our region of primary instability and escapes finally to infinity. The combined probability of leaking out altogether may not be very great. More to the point is the question as to how much fluctuation a particle will undergo in general, and whether or not it will cross the bounding curve for T^n .

The determination of how stable a particle is depends naturally on our definition of stability. If we wish to know what domains particles can reach from infinity, we need only apply $T^n e$ to the reflection of the curve of primary instability. The result of this, in our case, is that few particles penetrate as far as the region of the T^{11} fixed points. As n increases, the probability gets smaller and smaller. If, however, we desire to know how many particles leave the domain primarily governed by T^n and come under the primary influence of T^{n-1} , we have merely to find the invariant curves of both transformations*, and then to see when the fluctuations, of the T^n I.C.'s are enough to intersect with the T^{n-1} I.C.'s.

This method does not lean at all on criteria of continuity as advanced by ARNOL'D and MOSER, but shows that the "invariant region" associated with a given transformation has as its boundary sections of the invariant curves issuing from the hyperbolic fixed points of this transformation.

* A similar remark holds for any T^m , $m \neq n$, but is of lesser significance when m is not close to n .

Acknowledgements

This work was conceived in 1956 at the Courant Institute for Mathematical Studies, while the author was on leave from the University of Illinois. It was supported at first by the University of Illinois Research Board, and later by the National Aeronautics and Space Administration (Grant No. NSG 280-63). The ideas on stability were crystallized during the summer of 1966, while the author was visiting the Copenhagen Observatory.

In addition to the previously mentioned discussion with Dr. J. MOSER, there were valuable talks with Dr. D. J. BOURGIN, who stressed the importance of ascertaining the mappings in the phase plane.

The author is very grateful for the above financial support and for the hospitality accorded him by Professor A. REIZ, Director of the Copenhagen Observatory, and by the USSR Academy of Sciences.

*Department of Physics, University of Alabama,
University, Alabama.*

References

- (1) V. I. ARNOL'D, Uspekhi mat. nauk, 18, 92–192 (1963).
 - (2) J. MOSER, Nachrichten Akad. Wiss. Göttingen (Math-phys.) (1962), 1–20.
 - (3) G. FLOQUET, Ann. Ec. Norm. (2) 13, 47 (1883).
 - (4) J. L. POWELL and R. S. WRIGHT, MURA report RW/JLP – 4 (1955).
 - (5) J. MOSER, Nachrichten Akad. Wiss. Göttingen (Math-phys.) (1955), 87–120.
 - (6) E. D. COURANT and H. S. SNYDER, Annals of Physics 3, 1–48 (1958).
-

ASGER AABOE

SOME LUNAR AUXILIARY TABLES
AND RELATED TEXTS FROM
THE LATE BABYLONIAN PERIOD

Det Kongelige Danske Videnskabernes Selskab
Matematisk-fysiske Meddelelser **36**, 12



Kommissionær: Munksgaard
København 1968

Synopsis

The present texts are concerned with a family of functions (Φ , F, G, Λ , X) from Babylonian lunar theory according to System A, all of them but X in evidence in the published corpus of texts, and each having the anomalistic month as its period. Rules for converting values of Φ into corresponding values of the other functions were under control, though they lacked motivation, but only the significance of F and G was known.

A text published by NEUGEBAUER in 1957 (the Saros text) and Text E below made it possible to identify all of these functions with reasonable certainty as well as to make astronomical sense of their established relations. Thus, for a given syzygy the associated values of the five functions have the following significance, beginning with the two that have long been identified:

daily progress of moon	= F°
length of preceding month	= $29d + GH$
length of subsequent 223 months	= $6585d + \Phi H$
length of preceding 12 months	= $354d + \Lambda H$
difference between a constant year and preceding 12 months	= X^d .

All of these functions, save perhaps F, are artificial; they are first approximations, reflecting only the variation in lunar velocity, and resting on the preliminary assumption that syzygies are evenly distributed in longitude. G and, as I have discovered since this manuscript went to press, also Λ receive corrections for solar anomaly.

It appeared that when the values of Φ were to be used, the zig-zag function representing Φ was truncated at effective extrema (F was treated similarly).

Texts A, B, C, D below give evidence of aberrant Φ -G relations. Text F presents several variants of the function F, all truncated at the same values. Finally, a fragment joining the Saros text is published together with the relevant parts of the old text.

Introduction

The present texts,¹ all in the British Museum, and all from unscientific excavations in Babylon, are concerned with Column Φ , in the terminology of ACT,² and related functions from Babylonian lunar theory.

Column Φ is a linear zig-zag function whose parameters are

$$\begin{array}{ll}
 M = 2,17, 4,48,53,20 & p = \frac{1,44,7}{1,51,35} = 0;55,59,6, \dots \\
 m = 1,57,47,57,46,40 & P = \frac{1,44,7}{7,28} = 13;56,39,6, \dots \\
 d = 2,45,55,33,20 & \Pi = 7,28P = 1,44,7
 \end{array}$$

where d is the difference corresponding to one synodic month. The period underlying Φ is the anomalistic month; indeed, Column Φ is exactly in phase with the unabbreviated Column F which represents daily lunar progress or, if one wishes, lunar velocity in degrees per day.

In a lunar ephemeris according to System A, Column Φ follows immediately upon the opening column listing year and month. It is a matter of experience, that Φ can be continued from one System A ephemeris to any other representing the same lunar phenomenon (either new or full moon); the corresponding families are called Φ_1 and Φ_2 , respectively. Φ can thus be used for dating a text, and it is singularly useful for this purpose since it, when listed monthly, repeats itself exactly only after some 500 years (6247 months, to be precise). The dates I have affixed to the first four texts below

¹ A grant from the National Science Foundation enabled me to spend the summer of 1963 in London, studying cuneiform astronomical texts, among them the ones published here, in the British Museum; part of my subsequent work was supported by another NSF grant.

The texts are published through the courtesy of the Trustees of the British Museum.

I owe a particular debt of gratitude to Professor ABRAHAM SACHS of Brown University: not only did he contribute directly to the present paper by giving me a transcription of Text F, but he patiently made himself available for checking difficult readings as well as for discussion of the issues as they arose.

² ACT = O. NEUGEBAUER, *Astronomical Cuneiform Texts*, London, 1955.

are to be taken in this sense, i.e., they rest on the assumption that the Φ -values in these texts are connectible to the System A ephemerides in ACT.

Φ 's only rôle in the fully developed System A scheme of the Seleucid period is to serve as the base for computing Column G, which denotes the excess over 29 days of a synodic month. G is a first approximation, taking into account only the variation in lunar velocity. It is convenient to describe G in terms of a linear zig-zag function \hat{G} whose parameters are

$$\begin{aligned} M &= 5; 4,57, 2,13,20^{\text{H}} \\ m &= 2; 4,59,45,11, 6,40^{\text{H}} \\ d &= 0;25,48,38,31, 6,40 \end{aligned}$$

where the units are large hours³ and the difference corresponds to one synodic month.

\hat{G} has the same period (the anomalistic month) as Φ and F , but is out of phase with them, so that the maximum of \hat{G} occurs slightly after the minimum of Φ . G agrees with \hat{G} on stretches of its ascending and descending branches, but is of a more complicated character and smoother appearance near its extrema which are

$$\begin{aligned} M &= 4;56,35,33,20 \\ m &= 2;40 \end{aligned}$$

again in large hours.

The values of G near its extrema are derived from those of Φ according to a scheme which is given in tabular form in ACT, page 60. This scheme is the subject of several procedure texts (e.g., ACT No. 205, 206, 207, 207a, 207b), and it is followed in the System A ephemerides.

The texts **B**, **C**, **D** below do not agree with this scheme. The disagreement cannot be due to faulty interpolation, for in one case (Text **B**, Obverse, line 20) the Φ -value is precisely in the ACT interpolation scheme, and in another (Text **C**, line 7) the Φ -value should imply that G be equal to \hat{G} which it is clearly not. Even the assumption that all three texts are consistent does not provide a sufficient base for reconstructing an underlying scheme.

These three texts are not the sole evidence for aberrant Φ -G relations. ACT No. 207ca is a procedure text which gives a variant of the usual scheme. Even though I have recently joined a fragment to this text⁴, it seems unlikely that it can be brought in agreement with the present texts.

³ 1 day = 6 large hours (H) = 6,0 (time) degrees. The large hour (= 1,0 time degrees) is a modern unit devised to avoid the use of Babylonian time degrees which often might necessitate comments.

⁴ B. M. 40611 (81-4-28, 156) joins the upper edge of ACT No. 207ca. A photograph of the rejoined tablet may yield readings which are not yet possible. This text will be published together with some other additions to ACT.

The rules for converting Φ into G are presented without motivation, even in the ACT procedure texts, so all that Φ is used for in the ephemerides is essentially to locate a given moment within the anomalistic month, a task for which F might, incidentally, seem more naturally suited.⁵ It is, therefore, very possible to compute a System A lunar table without knowing what Φ represents, and the precise meaning of Φ , and its original rôle, remained

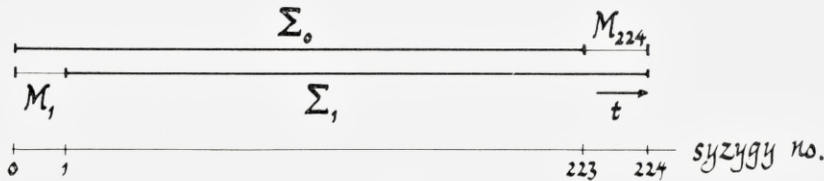


Fig. 1.

prominent among the unsolved problems in the ACT material. It was not until NEUGEBAUER in 1957 published a difficult procedure text – I shall call it the Saros text⁶ – that the discussion of this problem rose above mere guessing, as we now can see.

It appeared, entirely unexpectedly, that Φ has to do with the behaviour of the moon at 18-year intervals (more precisely, at intervals of 223 synodic months, the “Saros” period).⁷ The crucial relation was, as NEUGEBAUER rightly pointed out, that the monthly difference for Φ is the same as the difference in G-values 223 months apart, at least when Φ and G go from one linear branch to another of the same kind. This settled first that Φ measures time in large hours,⁸ as does G. Second, when we disregard the restriction of Φ and G to branches of the same kind, this relation suggests that the difference between Φ and the length of 223 months (or one Saros) is constant. This may be seen by the following argument. Let Σ_0 and Σ_1 be the lengths of two Saroi, Σ_1 beginning one month later than Σ_0 ; let further M_1 be the month preceding Σ_1 and M_{224} that following Σ_0 (my choice of indices anticipates, that the length of a Saros is associated with its initial syzygy, and that of a month with its final syzygy). We then have (see Figure 1)

⁵ There is, in fact, a procedure text (ACT No. 208) giving rules for transforming F into G.

⁶ O. NEUGEBAUER, “Saros” and Lunar Velocity in Babylonian Astronomy. Mat. Fys. Medd. Dan. Vid. Selsk. 31, no. 4 (1957). I shall refer to it as the Saros paper.

⁷ I shall here employ “Saros” to mean 223 synodic months. For a history of the use of “Saros” see O. NEUGEBAUER, *The Exact Sciences in Antiquity*. 2nd edition. Providence: Brown University Press, 1957, p. 141 ff.

⁸ Thus, e. g., $M_\Phi = 2;17,4,48,53,20^H$.

$$\begin{aligned}
 \Sigma_1 - \Sigma_0 &= M_{224} - M_1 \\
 &= (29^d + G_{224}) - (29^d + G_1) \\
 &= G_{224} - G_1.
 \end{aligned}$$

Thus, if the relation

$$G_{224} - G_1 = \Phi_1 - \Phi_0$$

holds throughout, as suggested by the Saros text, then

$$\Sigma_1 - \Sigma_0 = \Phi_1 - \Phi_0$$

or

$$\Sigma - \Phi = \text{constant.}$$

It is, therefore, a reasonable hypothesis that even as G is the excess over 29^d of a synodic month, so Φ is the excess over a whole number of days of 223 synodic months, taking into account only the effect of a variable lunar velocity. In his recent book,⁹ B. L. VAN DER WAERDEN states this hypothesis and proceeds to show that it implies several of the established relations of Φ to F and G . He further mentions in passing, that in order to have agreement between Φ and the fine-structure of G one must assume that, whenever its values are to be used, Φ be truncated near its maximum and its minimum.

Text **E** relates Φ to Column A , which was already known from ACT No. 207d and 207e, though its significance was dark, and to the new Column X , as I call it. This text turns out to be the first in which the values of Φ are in active use, and VAN DER WAERDEN's assumption is happily confirmed in that Φ appears truncated at the values 2;13,20 and 1;58,31,6,40. The structure of the text shows further that the difference in Φ over 12 months is the same as the difference in A for 223 months. Thus it follows that A indicates the length of 12 consecutive months. Its values are such that I believe it denotes the excess of a 12 month interval over a whole number of days (this can be negative). If this is so, it is possible to interpret Column X as the variable epect, that is, the difference (in days) between a year of constant length and the variable length of 12 months, ignoring all effects but that of lunar anomaly.

The technique displayed in Text **E** can be used, with obvious modifications, to construct a table for converting Φ into G ; this I did and reached excellent, though not complete, agreement with the ACT scheme. The agreement is good enough, though, to make it perfectly clear that the rule suggested by the Saros text (the difference in G for 223 months is the same as the difference in Φ for one month) holds without any restriction, if Φ is truncated. This was

⁹ B. L. VAN DER WAERDEN, *Anfänge der Astronomie*. Grossingen, 1966, p. 148 ff.

the only assumption used in the argument above, so it can no longer be doubted that Φ measures the Saros and A the 12 month year, even as G measures the month.

A and G can thus be derived from Φ and an initial value for each, and the derivation makes astronomical, as well as arithmetical, sense. It still remains to be explained how the initial values were determined; I can, however, show that they are independently chosen, or at least not related in the obvious way.

Once it was realised that 2;13,20 and 1;58,31,6,40 are the effective extrema of Φ , several passages in previously known texts became significant, and I shall here draw attention to some of them.

ACT No. 200, Section 5, is concerned with the relations between F and Φ . It first gives the parameters for the standard, unabbreviated Column F :

$$\begin{aligned} M &= 15;56,54,22,30^{0/d} \\ m &= 11; 4, 4,41,15 \\ d &= 0;42 \end{aligned}$$

It then relates that to M_Φ corresponds M_F , and to m_Φ corresponds m_F . Thus, of course, one can determine the constants in the relation

$$F = c_1\Phi + c_2.$$

In fact, the text later gives $c_1 = 15,11,15$.

But after this we are told that to

$$\Phi = 2,13,20 \quad \text{corresponds } F = 15$$

and to

$$\Phi = 1,58,31,6,40 \quad \text{corresponds } F = 11;15.$$

It used to appear unmotivated to single out these pairs of values (they are, of course, in agreement with the conversion rule), but now this passage suggests strongly that the effective extrema of F are 15 and 11;15, which, as we shall see, is so.

In three, I suspect rather old, lunar texts¹⁰ we do indeed find Φ and F truncated at 2,13,20 and 15, respectively. These texts have, however, no opportunity to do similarly near the minima; this is not odd, for while it is impossible to avoid reaching values in excess of 2;13,20 and 15, when

¹⁰ These lunar texts will be published shortly by A. SACHS and myself.

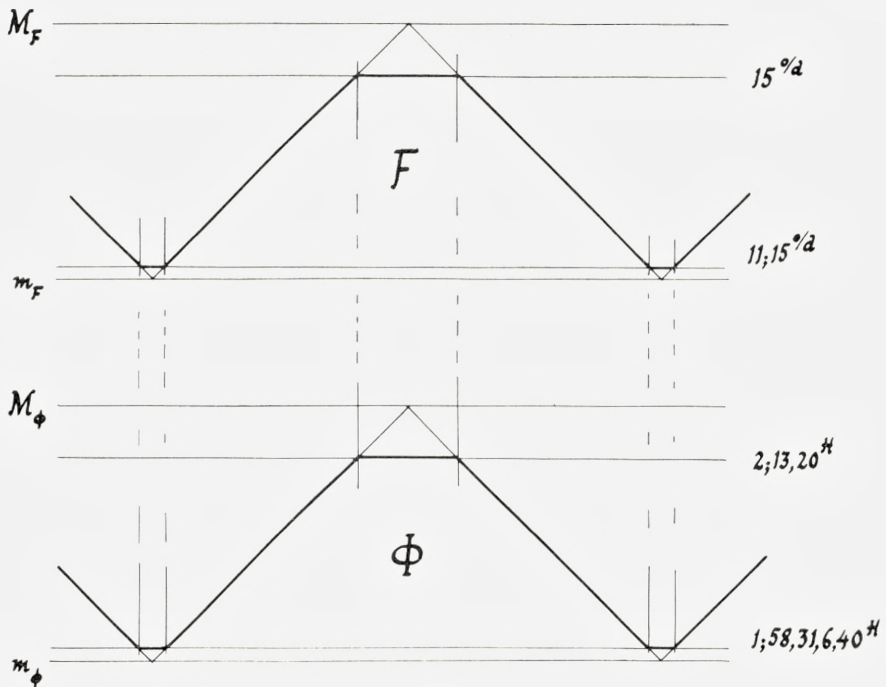


Fig. 2.

proceeding in monthly steps, 1;58,31,6,40 and 11;15 are so near the minima that it is certainly not always that these values would come into play.

In a table of effective Φ -values, 2,13,20 is thus very conspicuous; it is, therefore, not surprising that it appears that the number 2,13,20 is used in procedure texts as a proper name for Column Φ . NEUGEBAUER lists in ACT I, page 212, several curious usages of 2,13,20, all of which make sense if for "2,13,20" we simply read "Column Φ ".

In particular, ACT No. 204, Section 6, begins with the statement (Reverse, line 9): 2,13,20 šá u₄-1-kam aná u₄-14-kam aná šu-šu-ú 3[0 . . .]

Neglecting the final number, this may then be translated:

Column Φ for the 1st day to (Column Φ for) the 14th day for you to transform or, more freely, using the terminology for Φ for new and full moon:

To transform Φ_1 into Φ_2 .

The number following this sentence, broken off but for its beginning, must then be

$$20,39,48,53,20 = 15 \cdot d_{\Phi^*}$$

where

$$d_{\Phi^*} = 1,22,39,15,33,20$$

is the difference corresponding to 1 tithi¹¹ for Φ^* , the “daily” Φ (see ACT I, page 45).

As indicated, NEUGEBAUER reads 3[0 . . .], and PINCHES’s hand copy (LBAT¹² No. 96) shows three corner wedges with a slightly larger space between the second and third than between the first and second. This agrees well with the restoration 20,39,48,53,20.

The passage can then be rendered thus, following NEUGEBAUER’s restoration from line 10 and on:

⁹To transform Φ_1 into Φ_2 . 20,39,48,53,20

¹⁰add and subtract. That which exceeds 2,17,4,48,53,20 from 2,17,4,48,

¹¹53,20 subtract. That which goes below 1,57,47,57,46,40 to 1,57,

¹²47,57,46,40 add and put it down . . .

The rule works, of course. As an example, consider the following value of Φ_1 corresponding to S.E. 194, VII (ACT No. 13, Obverse, line 8)

	1,59,33,31, 6,40	
Augmented by:	20,39,48,53,20	
it is	2,20,13,20.	
This exceeds	2,17, 4,48,53,20	(= M_{Φ})
by	3, 8,31, 6,40	
which, subtracted from M_{Φ} , yields	2,13,56,17,46,40	

and this is precisely the value for Φ_2 corresponding to S.E. 194, VIII (ACT No. 13, Reverse, line 8).

Incidentally, the values 2,13,20 and 1,58,31,6,40 are assumed by Φ_2 on both an ascending and a descending branch. M_{Φ} is a value belonging to Φ_2 , while m_{Φ} belongs to Φ_1 . That the extrema are assumed implies symmetry in the sense that a value occurring on an ascending branch also occurs on a descending branch (thus it happens, that Φ_2 in Text **B** in part overlaps with ACT No. 1, but in reversed order).

Text **F** is a procedure text offering certain anomalies. It is concerned with several variants of Column F, all truncated at 15 and 11;15. One of the variants has, curiously enough, the same period as Column F in System B, while another probably has that of the standard Column F of System A.

¹¹ 1 synodic month = 30 tithis.

¹² LBAT = A. J. SACHS (ed.), *Late Babylonian Astronomical and Related Texts, copied by T. G. Pinches and J. N. Strassmaier*. Brown University Press, Providence, 1955.

Finally, I have joined yet a small fragment to Neugebauer's Saros text. This and the adjoining parts of the old text are published at the end of this paper, together with a discussion of a few of the old passages which can now be understood in the light of the above results about Φ .

Before presenting the texts themselves, I shall briefly argue, that the identification of Φ as the excess of 223 synodic months over a whole number of days implies that Φ is in phase with F.¹³ The argument proceeds from the fact, that 239 anomalistic months are slightly longer than 223 synodic months. Since the progress, l_a , in longitude of the moon in one anomalistic month is constant, its progress, L_a , in 239 anomalistic months (a constant time T_a) is also constant. We now assume, that we are dealing with syzygies (either conjunctions or oppositions of the moon) distributed evenly in respect of *longitude*, and are then concerned with the variation in the corresponding time intervals induced by a variable lunar velocity. Let the constant progress of the moon from one syzygy to the next be l_s , and its progress in 223 synodic months be the constant amount $L_s (= 223 l_s)$.

Consider now a certain syzygy S_0 (see Figure 3). Associated with S_0 are values of Φ and F, say, Φ_0 and F_0 . When the moon after 223 synodic months (of variable length) reaches the syzygy S_{223} , it will have travelled the distance L_s ; let the corresponding time be T_s . We then have:

$$T_s = 6585^d + \Phi_0^H.$$

If from S_{223} we go L_a back in longitude, we shall reach a point which precedes S_0 by the amount l , where

$$l = L_a - L_s.$$

The constant l is small, but positive.

The corresponding time:

$$t = T_a - T_s$$

is variable, but small (and positive); we may, therefore, assume that the moon's velocity during t is F_0 . We then have

$$t = \frac{l}{F_0},$$

so

$$\begin{aligned} \frac{l}{F_0} &= T_a - T_s \\ &= T_a - 6585^d - \Phi_0. \end{aligned}$$

¹³ This argument is, in essence, one given me by Dr. JOHN BRITTON in 1965, when he was still my student. It happens to be virtually identical with the one which later appeared in v. D. WAERDEN'S book (cf. note 9).

Introducing the constant

$$c = T_a - 6585^d,$$

i.e., the excess of 239 anomalistic months over a whole number of days, we get the relation between Φ and F:

$$(1) \quad \frac{l}{F} = c - \Phi,$$

where l and c are constants.

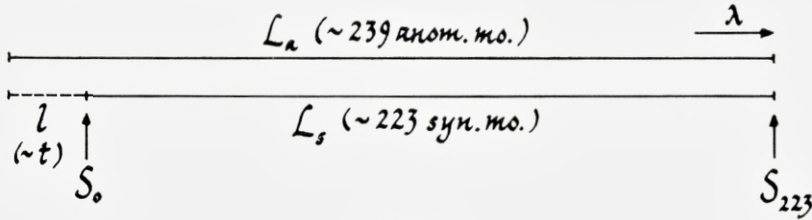


Fig. 3.

From (1) it follows immediately, that when Φ assumes its maximum then so does F, and analogously for their minima. Thus Φ and F are in phase.

If one chooses to represent the periodic functions Φ and F by zig-zag functions, the relation (1) cannot, of course, hold exactly.

To test whether the relation (1) may have been envisaged by the Babylonian astronomers, I introduced into it two pairs of Φ and F-values. It was here natural to pick the effective extrema, viz.

$$\Phi = 2;13,20^H \quad F = 15^{0/d}$$

and

$$\Phi = 1;58,31,6,40^H \quad F = 11;15^{0/d}.$$

These values yielded:

$$c = 2;57,46,40^H$$

and

$$l = 1;51, 6,40^0$$

It is remarkable, that all these parameters, including c and l , are very simple regular numbers.

Further, the value for c implies a value for the anomalistic month, for c is the excess over 6585^d of 239 anomalistic months. This value is $27^d;33,15,43,22,30, \dots$ which compares rather well with the value given in the Saros text, viz., $27^d;33,16,30$.

Though the agreement is not perfect, it still establishes beyond any doubt that the integral number of days is 6585 , as I have tacitly assumed. Thus one would look in vain for a direct connexion between the mean values (or

initial values) of Φ and G , for any reasonable mean value of G would imply a length of 223 months far in excess of 6585^d. It is well known that G is so adjusted that no correction to the month length is necessary when the solar progress is 30⁰ per month, and that the correction (Column J) is negative on the arc of low solar velocity. Thus the mean value of G is high, and it is not strictly true that the length of the Saros, as used in the argument on page 6, is

$$\sum_{i=1}^{223} (29^d + G_i).$$

However, since the argument only turns on differences in Φ and in G , it is independent of the mean values, and so is still valid.

Texts A, B, C, D

Text A: B. M. 36994 (= 80-6-17, 738).

Contents: Φ_2 for S.E. 6, I-IX.

Transcription: Table 1.

Photograph: Plate I.

TABLE 1.

		Φ_2	(\hat{G}_2)
S.E. 6, I II III IV V VI VII VIII IX X	1.	[2, 11, 2, 35][33][20]	3, 12, 51, 51, 6, 40
		[2, 11, 3, 48, 31, 6][40]	2, 47, 3, 12, 35, 33, 20
		[2, 16, 34, 26, 40]	2, 21, 14, 34, 4, 26, 40
		[2, 14, 49, 15, 38][20]	2, 14, 33, 34, 48, 53, 20
	5.	2, 12, 3, 20	2, 40, 22, 13, 20
		2, 9, 17, 24, 26, 40]	3, 6, 10, 51, 51, 6, 40
		2, 6, 31, 28][53, 20]	3, 31, 59, 30, 22, 13, 20
		2, 3, 48, 33, 20]	3, 57, 48, 8, 53, 20
		[2, 2, 59][37, 46, 40]	4, 23, 36, 47, 24, 26, 40
	10.	[1, 58, 13, 42, 13, 20]	4, 49, 25, 25, 55, 33, 20

Text A: BM 36994.

This is a flake with left and, perhaps, top edge preserved. There is no room for an initial date column, so the text is not a fragment of an ephemeris. In the transcription I have supplied the corresponding values of \hat{G}_2 .

Text B: B. M. 36824 (= 80-6-17, 563) + 37222 (= 80-6-17, 976).

Contents: Obverse: Φ_2 , G_2 for S.E. 35, I to S.E. 36, X.

Reverse: Φ_1 , G_1 for S.E. 35, XI to S.E. 37, I.

Transcription: Table 2.

Photograph: Plate I.

TABLE 2.

		Φ_2	G_2			
S.E. 35,	Obv.	I	[2, 1, 13] 4, 13, 20	[4, 44, 28, 8, 53, 20]		
		II	[2, 3] 59, 37 [46, 40]	[4, 18, 39, 30, 22, 13, 20]		
		III	[2, 6] 45, 33, 20	[3, 52, 50, 51, 51, 6, 40]		
		IV	[2, 9] 31, 28, 53, 20	3 [27, 2, 13, 20]		
		V	[2, 12] 17, 24, 26, 40	3, [1, 13, 34, 48, 53, 20]		
		VI	[2, 15] 3, 20	2 [//////////]		
		VII	[2, 16] 20, 22, 13, 20	2 [//////////]		
		VIII	[2, 13] 34, 26, 40	2 [//////////]		
		IX	[2, 10, 48, 3] 6, 40	2 [//////////]		
		X	[2, 8, 2, 3] 33, 20	3, 17, 49, 8, 8, [3, 20]		
		XI	[2, 5, 13] 40	3, 43, 37, 46, 40		
		XII	[2, 2, 30] 44, 26, 40	4, 9, 26, 25, 11, 6, 40		
		36,	I	[1, 59] 44, 48, 53, 20	4, 35, 15, 3, 42, 13, 20	
				[1, 58, 37] 2, 13, 20	4, 56	
				II	[2, 1, 2] 2, 57, 46, 40	4, 43, 1, 43, 42, 13, 20
				III	[2, 4] 8, 53, 20	4, 17, 13, 5, 11, 6, 40
				IV	[2, 6, 5] 4, 48, 53, 20	3, 51, 24, 26, 40
				V	[2, 9, 40] 44, 26, 40	3, 25, 35, 48, 8, 53, 20
20,	I	[2, 12, 2] 6, 40	2, 59, 47, 9, 37, 44, 40			
		[2, 15, 12, 3] 33, 20	2, 45, 2, 13, [20]			
		[2, 16, 11, 1] 40	2, 40			
		[2, 13, 25, 11, 6] 40	2, 40			

		Φ_1	G_1		
S.E. 35,	Rev.	XI	[2, 10, 59, 4, 26, 40]	[3] 13, 24, 41, 28, 53, 20	
		XII	[2, 13, 45]	[//] 4, 2 [//////////]	
		36,	I	[2, 16, 30, 55, 33, 20]	2 [//] 23 [//////////]
				[2, 14, 52, 46, 40]	2, 40 blank
				[2, 12, 6, 51, 16, 40]	2, 40, .9 [//////////]
		II	[2, 9, 20, 55, 33, 20]	3, 5, 38, 1, 28, 53, 20	
		III	[2, 6, 35] blank	3, 31, 26, 40	
		IV	[2, 3, 49, 4] 26, 40	3, 57, 15, 18, 31, 6, 40	
		V	[2, 1] 3, 8 [53, 20]	[4, 23, 3, 57, 2, 13, 20]	
		VI	[1, 58, 17] 13, 20	[//////////]	
		IX	[2, 0, 4] 37, 46 [40]	[//////////]	
		X	[2, 2] 50 [33, 20]	[4, 29, 24, 11, 51, 6, 40]	
		XI	[2, 5] 36, 28, 53, 20	[4, 3, 35, 33, 20]	
		XII	[2, 8] 22, 24, 26 [40]	[3, 37, 46, 54, 48, 53, 20]	
		37,	I	[2, 11] 18, [20]	[3, 11, 58, 16, 17, 46, 40]

Text B: BM 36824.

Though M.B. 37222 joins B.M. 36824, its reverse is destroyed. No edges are preserved. At the end of obverse, line 14, a trace of a vertical ruling is preserved; after it the beginning of a sign is just visible. The sign is unidentifiable, but clearly not a number; thus the G-column was not followed by another $\Phi - G$ pair.

The reverse is in a wretched state, yet I feel reasonably confident of my restoration¹⁴ since it was done without a view to dates, which turned out to match those of the obverse well. However, all readings that cannot be controlled by computations are very tentative.

The entries for which G differs from \hat{G} , and most of which are at odds with the standard conversion rules, are collected with similar values from Texts C and D in Table 5.

Critical Apparatus.

Rev. 2. Reading very uncertain; there is even a possibility that the number may agree with

$$\hat{G} = 2,47,36,2,57,46,40$$

and so this entry is omitted from Table 5.

Rev. 5. As noted in the transcription, the G-value is written 2,40,,9, . . . , where “.” represents the separation sign consisting of two diagonal wedges, to distinguish it from 2,49, . . .

Text C: B.M. 37203 (= 80-6-17, 956).

Contents: G_2 for S.E. 39, X to S.E. 40, IV.

Transcription: Table 3.

Photograph: Plate I.

TABLE 3.

		(Φ_2)	G_2
S.E. 39, \bar{X}	1.	2, 7, 22, 35, 33, 20	3, 4[7, 5, 11, 6, 40]
\bar{X}_1		2, 10, 8, 31, 6, 40	3, 21, [16, 32, 35, 33, 20]
\bar{X}_2		2, 12, 54, 26, 40	2, 55, 27, 54, 4, 26[40]
\bar{X}_2		2, 15, 40, 22, 13, 20	2, 41, 12, 11, 15[////]
40, I	5.	2, 15, 43, 20	[2, 40]
\bar{I}		2, 12, 57, 24, 26, 40	[2], 40, 25, 39, 7, 13, 20
\bar{II}		2, 10, 11, 28, 53, 20	[2, //] 19, 45, 11, 6, 40
\bar{IV}		2, 7, 25, 33, 20	[3, 23, 34] 48, 53, 20

Text C: BM 37203.

¹⁴ My restoration of these four texts was greatly facilitated by a table giving an entire number period of the functions $\Phi_1, \Phi_2, \hat{G}_1$, and \hat{G}_2 . This table was executed by the Yale Computer according to the program of Miss VIVIAN REICH.

This text is a small flake. The photograph suggests that the left edge is preserved, but an unbiased inspection showed that the tablet rather was broken along a vertical ruling. I have supplied the corresponding values of Φ_2 in the transcription.

Text D: B.M. 37600 (= 80-6-17, 1357).

Contents: Φ_2 , G_2 for S.E. 42, XII to S.E. 43, V.

Transcription: Table 4.

Photograph: Plate I.

The text is a small fragment with only one side, and no edges, preserved.

These four texts are unique in several respects. First it is clear that they are not fragments of standard System A ephemerides, even though the functions Φ and G progress in monthly steps. In the ephemerides, Φ and G are separated by several columns, while they are juxtaposed in Text **B** and **D**. Text **A** has no space for an initial column of dates, and Text **C** shows so many similarities to Text **D**, in its style of writing, in the dates, and in its deviations from the standard $\Phi - G$ scheme, that I should not be surprised if these two fragments came from the same tablet.

Second, the dates of these texts are very early; as said, my dating of them rests on the assumption that their Φ -values can be continued to the ACT material. The range of dates is from S.E. 6 to S.E. 43 (i.e., from 306 to 269 B.C.). The earliest lunar ephemeris in ACT (No. 1) is from S.E. 124, but an auxiliary table (No. 70), gives latitudes of full moons for at least S.E. 49 to 60.^{14a}

Third, the values of G near its extrema differ from those derived from the standard ACT scheme. I have collected the aberrant pairs of values in Table 5

TABLE 4.

		Φ_2	G_2
S.E. 42, \overline{XII}	I.	[1, 59, 32, 35, 33, 20]	[//////] 40 [//////]
\overline{XII}_2		[2, 2, 18, 31, 6, 40]	[4, 34, 23, 12, 35, 3, 20]
43, \overline{I}		[2, 5, 4, 20] 40	4, 8, 34, 34, 4, 40]
\overline{II}		[2, 7, 50, 22] 13, 20	3, 42, 45, 55, 3, 20]
\overline{III}	S.	[2, 10, 36, 7, 46, 40]	3, 16, 57, 17, 2, 18, 20]
\overline{IV}		[2, 13, 22, 3, 20]	2, 53, 17, 23, 30]
\overline{V}		[2, 16, 8, 8, 3, 20]	[//////] [//////]

Text D: BM 37600.

^{14a} See now the note added in proof at the end of this paper.

TABLE 5.

	Φ	G_{text}	G_{ACT}	\hat{G}	
<i>Text B, Obv.</i>	14.	1,58,37, 2,13,20†	4,56	4,56	5, 1, 3, 42, 13, 20
	20.	2,15,12,35,33,20†	2,45, 2,13,[20]	2,40,53,20	2,33,58,31, 6,40
	21.	2,16,11, 6,40 †	2,40	2,40	2, 8, 7,52,35,33,20
	22.	2,13,25,11, 6,40†	2,40	2,40	2,27,38,16,17,46,40
<i>Rev.</i>	3.	2,16,30,55,33,20†	2[0]23[0]////	2,40	2,21,47,24,26,40
	4.	2,14,52,46,40 †	2,40	2,40	2,14, 0,44,26,40
	5.	2,12, 6,57, 6,40†	2,40,9[0]////	2,43, 7,57,46, 40	2,39,49,22,57,46,40
<i>Text C</i>	4.	2,15,40,22,13,20†	2,41,12,11,15[33,20]	2,40, 7,46,40	2,29,39,15,33,20
	5.	2,15,43,20 †	2,40	2,40	2, 6, 8,53,20
	6.	2,12,57,24,26,40†	[2]40,25,39, 7,13,20	2,40,27,24,26,40	2,31,57,31,51, 6,40
	7.	2,10,11,28,53,20†	[2,0]19,45,11, 6,40	$G = \hat{G}$	2,57,46,10,22,13,20
<i>Text D</i>	1.	1,59,32,35,33,20†	[0]////40 [0]////	4,55,51, 6,40	5, 0,11,51, 6,40
	6.	2,13,22,13,20 †	2,53,27,23,3[0]	2,51,13,20	2,51, 8,38,31, 6,40

together with the G-values expected from ACT and the values of \hat{G} . Most of the evidence concerns the situation near the minimum of G, and here the variants appear generally larger than the expected values. It is out of the question that the deviations are caused by faulty interpolation in the standard conversion table, for in one case (Text **B**, Obv. 20) the Φ -value is precisely in the ACT scheme, and in another (Text **C**, line 7) the Φ -value should imply that $G = \hat{G}$, which it is not.

The evidence is so scant and fragmentary that I could not comfortably reconstruct an underlying scheme, even assuming that the texts are consistent.

It is ironic, but perhaps to be expected, that this new evidence for variant $\Phi - G$ relations appears precisely at the moment when we have learned to control the standard scheme. Yet it confirms my feeling that Babylonian astronomical activities were more varied and diffuse than the ACT material would lead us to believe.

Text E

Text E: B.M. 36311 (= 80-6-17, 37) + B.M. 36593 (= 80-6-17, 321).

Contents: Φ , A , and X .

Transcription: Tables 6 and 7.

Photograph: Plates II and III.

Colophon: invocation in lower left corner of upper edge:

[ina a-mat ^{de}]n u ^{de}gašan-ja liš-lim

= at the command of the deities Bēl and Bēlti, may it go well.

Description of Text.

This tablet is large; when unbroken it was about $6\frac{1}{2}$ inches wide and 7 inches high. The top edge and the right edge are almost complete; a small piece of the left edge remains, while the bottom edge is destroyed, though the restoration shows that only a few lines are missing. The four columns continue from the obverse over the bottom edge to the reverse. Horizontal alignment is carefully observed, and horizontal rulings are preserved. There were 62 lines to each side, the reverse spilling over onto the top edge.

The text is a copy, for the scribe wrote *hi-bi* (i.e., broken) thrice in the upper right corner. He could easily have restored the missing signs, had he so chosen, for the fourth column, as the third, is symmetrical about the bottom edge, so its beginning on the obverse is identical, in opposite order, with its end on the reverse, which is preserved.

At the end of Obverse II,1 after a number which must have been 2,13,20 one may read *šá* [*si-*]*man* (concerning the time). NEUGEBAUER has already drawn attention to a parallelism between the usage of "2,13,20" and of *si-man*.¹⁵

In the last column the scribe left an unusually large space between the initial 10 (or 11) and the remaining one or two digits. One might well wonder if the initial digits should be read with the others at all, were it not for the fact that the initial 10 changes to 11 precisely when required by the difference of 54 in the third digit (Obverse IV, 43–44).

Critical Apparatus.

Obv. II, 9. 2,10,57,46,40: 46 looks like 45.

Obv. II,16. [2],8,53,20: 53 looks like 52.

Obv. III,10. 3,44,5[3,20]: erasure between 44 and 53.

Obv. III,13. 3,36: 36 looks like 56.

Obv. III,42. [1,6,36],17,46,40: 17 damaged, might be read 45.

Obv. IV. *hi-bi* is written after the initial 10 in lines 3,4, and 6.

Rev. II,21. [...]6,40 should be 2,7,44,48,53,20; the scribe may have copied the corresponding number in III,21 in error.

Rev. IV, 2. 11,11,3[9]: a faint trace remains of what may have been a vertical wedge rather than the diagonal wedges expected for 9.

The separation sign consisting of two diagonal wedges, transcribed as “.”, is used three times (Obv. IV,44, Rev. III,28, and Rev. III,35) to denote

¹⁵ ACT I, p. 212; see also his Saros paper.

Text E.

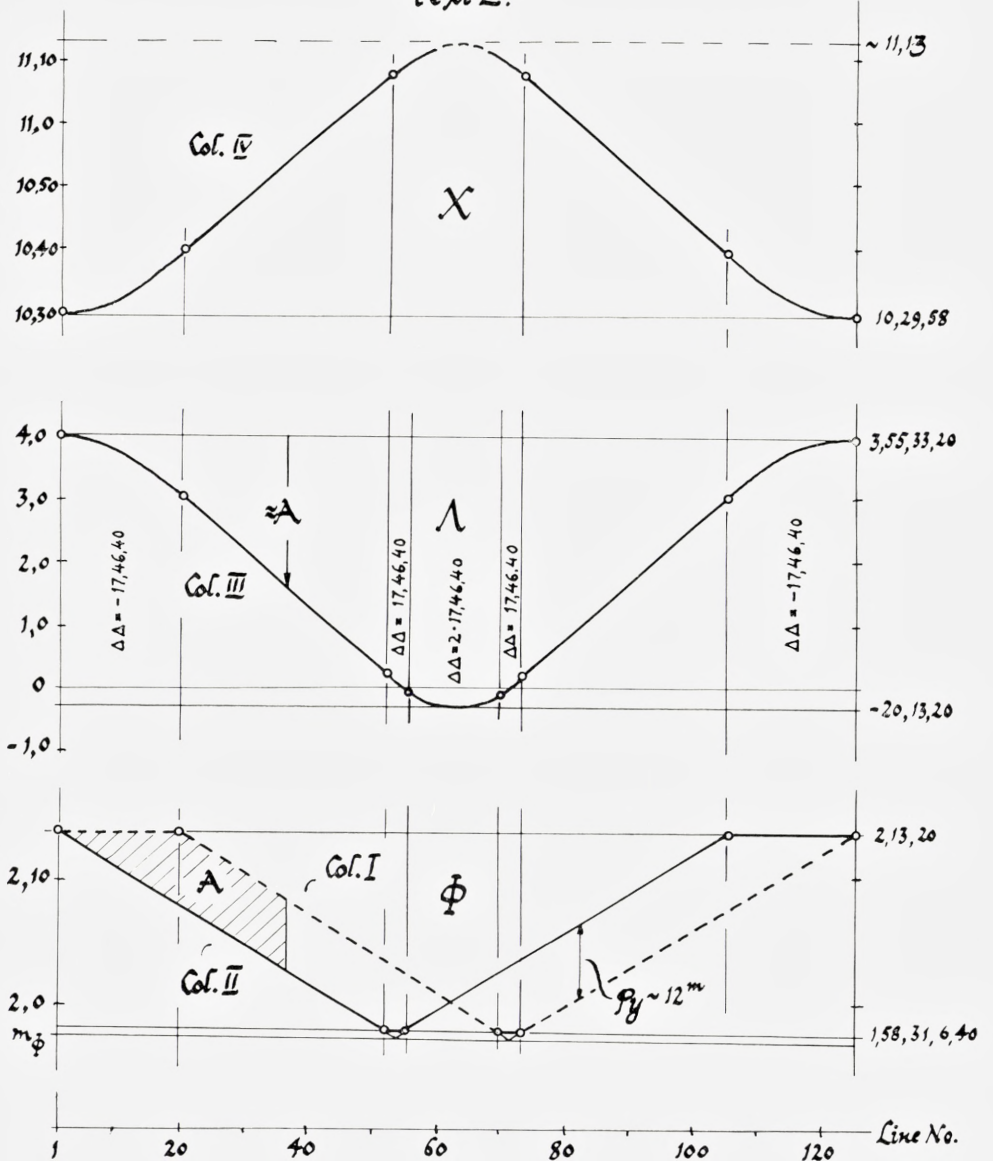


Fig. 4.

0, i.e., an empty sexagesimal place. In Rev.IV,56 and 57, the entries are written 10,30,.7 and 10,30,. [1] to distinguish them from 10,37 and 10,31, respectively.

Astronomical Commentary.

The first two columns of Text **E** concern Φ , the third Δ , which is known from ACT Nos. 207d and 207e, and the fourth X , as I call it, which is found here for the first time. Two parameters for Φ play a fundamental rôle in the relations between Φ and Δ . One is the increment of Φ from ascending branch to ascending branch corresponding to 12 months (one "year"):

$$\varphi_y = 12 \cdot d_\Phi - 2 \Delta_\Phi = -0;5,22,35,33,20^H,$$

and the other is Φ 's increment, again from ascending branch to ascending branch, corresponding to 223 months (one Saros):

$$\varphi_s = 223 \cdot d_\Phi - 16 \cdot 2 \Delta_\Phi = -0;0,17,46,40,0^H.$$

φ_s is a well-known parameter, and it plays a prominent rôle in the Saros text. φ_y was identified by NEUGEBAUER in ACT No. 207d, but its significance for Δ was not yet understood.

The uncovering of the table's structure proceeds from a crucial relation between the entries in the first three columns. The relation is, that the difference between the second and the first column is the line by line difference of the third, or more precisely (using $I(n)$ to mean the entry in Column I, line n , and similarly for the other columns)

$$II(n) - I(n) = III(n+1) - III(n). \quad (3.1)$$

Relation (3.1) holds exactly throughout the text. (In modern language, Column III measures very nearly the area A between the graphs of Columns I and II – but for a constant – as suggested in Figure 4).

Now, on most of the obverse we find that the first two columns, both of which present Φ values, obey the relation

$$I(n+1) - I(n) = II(n+1) - II(n) = \varphi_s, \quad (3.2)$$

and that further

$$II(n) - I(n) = \varphi_y. \quad (3.3)$$

Thus, where (3.2) and (3.3) are valid, they imply

TABLE 6.

	I	II	III	IV
1.	[2, 13, 20]	[2, 13, 20]	3, 55, 33, 20	1.
	[2, 13, 20]	[2, 13, 20]	3, 55, 33, 20	
	[2, 13, 20]	2, [12, 44], 26, 40	3, 55, 15, 33, 20	10, 30, 17
	[2, 13, 20]	2, 12, 26, 40	3, 54, 40	10, 30, 77
5.	[2, 13, 20]	2, 12, 8, 53, 20	3, 53, 46, 40	10, 30, 167
	[2, 13, 20]	2, 11, 51, 6, 40	3, 52, 35, 33, 20	10, 30, 287
	[2, 13, 20]	2, 11, 33, 20	3, 51, 6, 40	10, 30, 437
	[2, 13, 20]	2, 11, 15, 33, [20]	[3, 49, 20]	10, 31, 1
	[2, 13, 20]	2, 10, 57, 46, 40	[3, 47, 15, 33, 20]	10, 31, 24
10a	[2, 13, 20]	2, 10, 40	3, 44, 5, [3, 20]	10, 31, 48
	[2, 13, 20]	2, 10, 22, 13, 20	[3, 42, 13, 20]	10, 32, 15
	[2, 13, 20]	2, 10, 4, 26, 40	3, 39, [15, 33, 20]	10, 32, 45
	[2, 13, 20]	2, 9, 46, 40	3, 36	10, 33, [18]
	[2, 13, 20]	[3, 9, 28, 53, 20]	[3, 32, 26, 40]	10, 33, [54]
15.	[2, 13, 20]	[3, 9, 11, 6, 40]	[3, 28, 35, 33, 20]	10, 34, 33
	[2, 13, 20]	[3, 8, 53, 20]	[3, 24, 26, 40]	10, 35, 15
	[2, 13, 20]	[3, 8, 35, 33, 20]	[3, 20]	10, 36
	[2, 13, 20]	[3, 8, 17, 46, 40]	[3, 15, 15, 33, 20]	10, 36, 48
	[2, 13, 20]	[3, 8]	3, 10, 13, 20	10, 37, 39
20.	[2, 13, 4, 48, 53, 20]	[3, 7, 42, 13, 20]	3, 4, [53, 20]	10, 38, 33
	[2, 12, 47, 2, 13, 20]	[3, 7, 24, 216], 40	2, 59, [30, 44], 26, 40	10, 39, 27
	[2, 12, 29, 15, 33, 20]	[2, 7, 6, [40]]	2, 54, 8, [8, 53, 20]	10, 40, 21
	[2, 12, 11, 28, 53, 20]	[2], 6, 48, 53, 20	2, 48, [15], 33, 20	10, 41, 15
	[2, 11, 53, 42, 13, 20]	[2], 6, 31, 6, 40	2, 43, [22], 57, 46, 40	10, 42, 9
25.	[2, 11, 35, 55, 33, 20]	[2], 6, 13, 20	2, 38, [0], 22, 13, 20	10, 43, 3
	[2, 11, 18, 8, 53, 20]	[2, 5, 55, 33, 20]	2, 32, [37], 46, 40	10, 43, 57
	[2, 11, 0, 22, 13, 20]	[2, 5, 37, 46, 40]	2, 27, [15], 11, 6, 40	10, 44, 51
	[2, 10, 42, 35, 33, 20]	[2, 5, 20]	2, 21, [5], 35, 33, 20	10, 45, 45
	[2, 10, 24, 48, 53, 20]	[2, 5, 2, 13, 20]	2, 16, [30]	10, 46, 39
30.	[2, 10, 7, 2, 13, 20]	[2, 4, 44], 6, 40	2, 11, [7, 2], 4, 26, 40	10, 47, 33
	[2, 9, 49, 15, 33, 20]	[2, 4, 26, 40]	2, 5, [44], 48, 53, 20	10, 48, 27
	[2, 9, 31, 28, 53, 20]	[2, 4, 8, 53, 20]	[2, 0, 22, 13, 20]	10, 49, 21
	[2, 9, 13, 42, 13, 20]	[2, 3, 51, 6, 40]	[1, 53, 59, 37, 46, 40]	10, 50, 15
	[2, 8, 55, 55, 33, 20]	[2, 3, 33, 20]	1, 49, 37, 2, 13, 20	10, 51, 9
35.	[2, 8, 38, 8, 53, 20]	[2, 3, 15, 33, 20]	1, 44, 14, 26, 40	10, 52, 3
	[2, 8, 20, 22, 13, 20]	[2, 2, 57, 46, 40]	1, 38, 51, 51, [6], 40	10, 52, 57
	[2, 8, 2, 35, 33, 20]	[2, 2, 40]	1, 33, 29, 15, 33, 20	10, 53, 51
	[2, 7, 44, 48, 53, 20]	[2, 2, 22, 13, 20]	1, 28, 6, 40	10, 54, 45
	[2, 7, 27, 2, 13, 20]	[2, 2, 4, 26, 40]	[1, 2], 24, 4, 26, 40	10, 55, 39
40.	[2, 7, 9, 15, 33, 20]	[2, 1, 46, 40]	[1, 1], 21, 28, 53, 20	[10], 56, 33
	[2, 6, 57, 28, 53, 20]	[2, 1, 28, 53, 20]	[1, 11, 53, 53, 20]	[10], 57, 27
	[2, 6, 33, 42, 13, 20]	[2, 1, 11, 6, 40]	[1, 6, 36], 17, 46, 40	10, 58, 21
	[2, 6, 15, 55, 33, 20]	[2, 0, 53, 20]	[1, 1, 13, 42, 13, 20]	10, 59, 9
	[2, 5, 58, 8, 53, 20]	[2, 0, 35, 33, 20]	[5], 57, 1, 6, 40	11, ., 9
45.	[2, 5, 40, 22, 13, 20]	[2, 0, 17, 46, 40]	[5], 0, 28, [31, 6, 40]	11, 1, 3
	[2, 5, 22, 35, 33, 20]	[2]	[4, 5, 5, 55, 33, 20]	11, 1, 57
	[2, 5, 4, 48, 53, 20]	[1, 59, 42, 13, 20]	[3], 43, 20	11, 2, 51
	[2, 4, 47, 2, 13, 20]	[1, 59, 24, 26, 40]	[3], 4, 20, 44, [6, 40]	11, 3, 45
	[2, 4, 29, 15, 33, 20]	[1, 59, 6, 40]	[3, 58, 8, [53, 20]]	11, 4, 39
50.	[2, 4, 11, 28, 53, 20]	[1, 58, 48, 53, 20]	23, 35, [3, 20]	11, 5, 33
	[2, 3, 53, 42, 13, 20]	[1, 58, 31, 6, 40]	18, 12, 5, [7, 46, 40]	11, 6, 27
	[2, 3, 35, 55, 33, 20]	[1, 58, 31, 6, 40]	[12, 50, 22, 13, 20]	11, 7, 21
	[2, 3, 18, 8, 53, 20]	[1, 58, 31, 6, 40]	[7, 45, 33, 20]	[11], 8, 12
	[2, 3, 0, 22, 13, 20]	[1, 58, 31, 6, 40]	[1, 58, 31, 6, 40]	[11], 9
55.	[2, 2, 42, 35, 33, 20]	[1, 58, 31, 6, 40]	[1, 30, 44, 26, 40 tab]	[11], 9, 45]
	[2, 2, 24, 48, 53, 20]	[1, 58, 31, 42, 13, 20]	[5, 42, 13, 20]	[11], 10, 27]
	[2, 2, 7, 2, 13, 20]	[1, 58, 51, 28, 53, 20]	[9, 33, 20]	[11], 11, 6]
	[2, 1, 49, 15, 33, 20]	[1, 59, 9, 15, 33, 20]	[12, 48, 53, 20]	[11, 11, 39]
	[2, 1, 31, 28, 53, 20]	[1, 59, 27, 2, 13, 20]	[15, 28, 53, 20]	
60.	[2, 1, 13, 42, 13, 20]	[1, 59, 44, 48, 53, 20]	[17, 33, 20]	
	[2, 0, 55, 55, 33, 20]	[2, 0, 2, 35, 33, 20]	[19, 2, 13, 20]	
	[2, 0, 38, 8, 53, 20]	[2, 0, 20, 22, 13, 20]	[19, 55, 33, 20]	destroyed

TABLE 7.

	I	II	III	IV	
-3	[2, 0, 20, 22, 13, 20]	[2, 0, 38, 8, 53, 20]	[20, 13, 20]	destroyed	-3
	[2, 0, 2, 35, 33, 20]	[2, 0, 55, 55, 33, 20]	[19, 55, 33, 20]		
0.	[1, 57, 44, 48, 53, 20]	[2, 1, 13, 42, 13, 20]	[19, 2, 13, 20]		0.
	[1, 57, 27, 2, 13, 20]	[2, 1, 31, 28, 53, 20]	[17, 33, 20]		
	[1, 57, 9, 15, 33, 20]	[2, 1, 49, 15, 33, 20]	15, 28, 53, 20]	[////////]	
	[1, 58, 57, 28, 53, 20]	[2, 2, 7, 2, 13, 20]	12, 48, 53, 20]	11, 11, 39]	
	[1, 58, 33, 42, 13, 20]	[2, 2, 24, 48, 53, 20]	9, 33, 20]	11, 11, 6	
	[1, 58, 31, 6, 40]	[2, 2, 42, 35, 33, 20]	5, 42, 13, 20]	[11, 11, 6	
5.	[1, 58, 31, 6, 40]	[2, 3, 0, 22, 13, 20]	1, 30, [44, 26, 40] tab	11, 10, 27	5.
	[1, 58, 31, 6, 40]	[2, 3, 18, 8, 53, 20]	2, 58, [31, 6], 40 tab	11, 9, 45	
	[1, 58, 31, 6, 40]	[2, 3, 35, 55, 33, 20]	7, 45, 33, 20]	11, 9	
	[1, 58, 31, 6, 40]	[2, 3, 53, 42, 13, 20]	12, [50, 22, 13, 20]	11, 8, 12	
	[1, 58, 48, 53, 20]	[2, 4, 11, 28, 53, 20]	18, [12, 57, 7, 46, 40]	11, 7, 21	
10.	[1, 59, 6, 40]	[2, 4, 39, 15, 33, 20]	23, 35, 33, 20]	11, 6, 27	
	[1, 59, 24, 26, 40]	[2, 4, 47, 2, 13, 20]	[28, 58, 8, 53, 20]	11, 5, 33	10.
	[1, 59, 42, 13, 20]	[2, 5, 4, 48, 53, 20]	34, 20, 44, 26, 40]	11, 4, 39	
	[2]	[2, 5, 22, 35, 33, 20]	39, 43, 20]	11, 3, 45	
	[2, 0, 17, 46, 40]	[2, 5, 40, 2, 13, 20]	45, 5, 55, 33, 20]	11, 2, 51	
15.	[2, 0, 35, 33, 20]	[2, 5, 58, 8, 53, 20]	50, 28, 31, 6, 40]	11, 1, 57	15.
	[2, 0, 53, 20]	[2, 6, 15, 55, 33, 20]	55, 51, 6, 40]	11, 1, 3	
	[2, 1, 11, 6, 40]	[2, 6, 33, 42, 13, 20]	1, 1, 13, 42, 13, 20]	[11, 0], 9	
	[2, 1, 28, 53, 20]	[2, 6, 57, 28, 53, 20]	1, 6, 36, 17, 46, 40]	10, 59, 15	
	[2, 1, 46, 40]	[2, 7, 19, 15, 33, 20]	1, 11, 58, 53, 20]	10, 58, 21	
20.	[2, 2, 4, 26, 40]	[2, 7, 27, 2, 13, 20]	1, 17, 21, 28, 53, 20]	10, 57, 27	
	[2, 2, 22, 13, 20]	[2, 7, 27, 2, 13, 20]	1, 22, 44, 4, 26, 40]	10, 56, 33	20.
	[2, 2, 40]	[2, 8, 2, 35, 33, 20]	1, 28, 6, 40]	10, 55, 39	
	[2, 2, 57, 46, 40]	[2, 8, 20, 22, 13, 20]	1, 33, 29, 15, 33, 20]	10, 54, 45	
	[2, 3, 33, 20]	[2, 8, 38, 8, 53, 20]	1, 38, 51, 51, 6, 40]	10, 53, 51	
25.	[2, 3, 57, 6, 40]	[2, 8, 55, 55, 33, 20]	1, 44, 14, 26, 40]	10, 52, 57	25.
	[2, 4, 8, 53, 20]	[2, 9, 13, 42, 13, 20]	1, 49, 37, 2, 13, 20]	10, 52, 3	
	[2, 4, 26, 40]	[2, 9, 31, 28, 53, 20]	1, 54, 57, 37, 46, 40]	10, 51, 9	
	[2, 4, 44, 26, 40]	[2, 9, 49, 15, 33, 20]	2, - 22, 13, 20]	10, 50, 15	
30.	[2, 5, 2, 13, 20]	[2, 10, 7, 2, 13, 20]	2, 5, 44, 48, 53, 20]	10, 49, 21	
	[2, 5, 20]	[2, 10, 24, 48, 53, 20]	2, 11, 7, 24, 26, 40]	10, 48, 27	30.
	[2, 5, 37, 42, 13, 20]	[2, 10, 42, 35, 33, 20]	2, 16, 30]	10, 47, 33	
	[2, 5, 35, 33, 20]	[2, 11, 0, 22, 13, 20]	2, 21, 52, 35, 33, 20]	10, 46, 39	
	[2, 6, 13, 20]	2, 11, 18, 8, 53, 20]	2, 27, 15, 11, 6, 40]	10, 45, 45	
35.	[2, 6, 31, 6, 40]	2, 11, 35, 55, 33, 20]	2, 32, 37, 26, 40]	10, 44, 51	35.
	[2, 6, 48, 53, 20]	2, 11, 53, 42, 13, 20]	2, 38, - 22, 13, 20]	10, 43, 3	
	[2, 7, 6, 40]	2, 12, 11, 28, 53, 20]	2, 43, 22, 57, 46, 40]	10, 42, 9	
	[2, 7, 24, 26, 40]	2, 12, 29, 15, 33, 20]	2, 48, 45, 33, 20]	10, 41, 15	
40.	[2, 7, 42, 13, 20]	[2, 12, 47, 2, 13, 20]	2, 54, 8, 8, 53, 20]	10, 40, 21	
	[2, 8]	[2, 13, 4, 48, 53, 20]	2, 59, 30, 44, 26, 40]	10, 39, 27	40.
	[2, 8, 17, 46, 40]	[2, 13, 20]	[3], 4, 53, 20]	10, 38, 33	
	[2, 8, 35, 33, 20]	2, 13, 20]	3, 10, 13, 20]	10, 37, 39	
	[2, 8, 53, 20]	2, 13, 20]	3, 15, 15, 33, 20]	10, 36, 48	
45.	[2, 9, 11, 6, 40]	2, 13, 20]	3, 20]	10, 36	
	[2, 9, 28, 53, 20]	2, 13, 20]	3, 24, 26, 40]	10, 35, 15	
	[2, 9, 46, 40]	2, 13, 20]	3, 28, 35, 33, 20]	10, 34, 33	45.
	[2, 10, 4, 26, 40]	2, 13, 20]	3, 32, 26, 40]	10, 33, 54	
	[2, 10, 22, 13, 20]	2, 13, 20]	3, 36]	10, 33, 18	
	[2, 10, 40]	2, 13, 20]	3, 39, 15, 33, 20]	10, 32, 45	
50.	[2, 10, 57, 46, 40]	2, [13, 20]	3, 42, 13, 20]	10, 32, 15	
	[2, 11, 15, 33, 20]	[2, 13, 20]	3, 44, 53, 20]	10, 31, 48	50.
	[2, 11, 33, 20]	[2, 13, 20]	3, 47, 15, 33, 20]	10, 31, 24	
	[2, 11, 51, 6, 40]	[2, 13, 20]	3, 49, 20]	10, 31, 1	
	[2, 12, 8, 53, 20]	[2, 13, 20]	3, 51, 6, 40]	10, 30, 43	
55.	[2, 12, 26, 40]	[2, 13, 20]	3, 52, 35, 33, 20]	10, 30, 28	55.
	[2, 12, 44, 26, 40]	[2, 13, 20]	3, 53, 46, 40]	10, 30, 16	
	[2, 13, 2, 13, 20]	[2, 13, 20]	3, 54, 40]	10, 30, -7	
	[2, 13, 20]	[2, 13, 20]	3, 55, 15, 33, 20]	10, 30, [1]	
	[2, 13, 20]	[2, 13, 20]	3, 55, 33, 20]	[0, 29, 58]	

- (i) that to move one line down means to advance 223 months, and
- (ii) that to go horizontally from Column I to Column II means to advance 12 months.

Further, if we allow for truncation of Φ at 2,13,20 and 1,58,31,6,40 and for reflexion in M_Φ and m_Φ , it is readily shown that (i) and (ii) hold throughout the text.

The relation (3.1) therefore states that the difference in \mathcal{A} for 223 months is the same as the difference in Φ for 12 months. It is therefore possible to

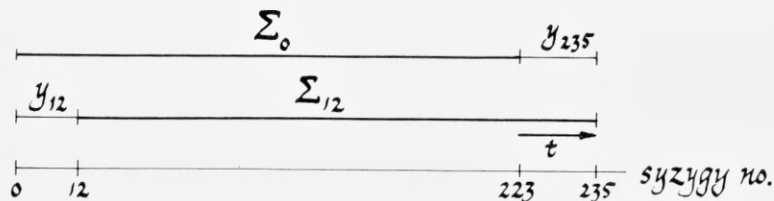


Fig. 5.

give an argument completely similar to the one above (p. 5) for Φ and G showing first, that \mathcal{A} is measured in large hours and second, that the difference between the length of 12 months and \mathcal{A} is constant.

First, we learn from ACT Nos. 207d and 207e that the \mathcal{A} -value given in III(n) is associated with the Φ -value in II(n) and not with that in I(n). Now we know that the value of G associated with a given syzygy refers to the preceding month, so the derivation of the Φ - G scheme to be given later shows that the value of Φ associated with a syzygy measures the following Saros (as we have already used). We shall then show that the difference between the value of \mathcal{A} associated with a given syzygy (via a Φ -value) differs by a constant from the length of the preceding 12 months.

Let Σ_{12} be a Saros beginning 12 months after the Saros Σ_0 ; let further y_{235} be the length of the 12 months following Σ_0 and y_{12} be the length of the 12 months preceding Σ_{12} . We then have (see Figure 5)

$$\Sigma_{12} - \Sigma_0 = y_{235} - y_0.$$

But we have, that

$$\Sigma_{12} - \Sigma_0 = \Phi_{12} - \Phi_0,$$

so since, (as shown by the structure of our tablet and the association of \mathcal{A} with syzygies as in ACT)

$$\Phi_{12} - \Phi_0 = \mathcal{A}_{235} - \mathcal{A}_{12}$$

we have

$$y_{235} - y_{12} = A_{235} - A_{12}$$

or

$$y - A = \text{constant.}$$

The values of A are such that it appears reasonable that A is the excess in large hours of 12 months over a whole number of days; I shall return to this point below after discussing the $\Phi - G$ relations further.

A may be negative. In the text, only the situation where A goes through zero increasingly is preserved (Rev. III, 5 and 6); the last negative value is followed by "lal", and the first positive by "tab".

In Table 8, I have displayed the structure of the first three columns of Text **E**. A few remarks suffice to show how it (or rather the table in ACT consisting in essence of Columns II and A) was constructed. First, both φ_y and φ_s are negative when Φ goes from one *increasing* branch to another; it is therefore clear, that the Φ -values in Column II must belong to increasing branches until line 54; thus I have designated them with arrows pointing upwards.

Second, we recall that the values of A are associated with the values of Φ given in Column II of this text.

The table is readily constructed from (i) and (ii) above. We begin in Column II with the value 2,13,20[†]. The corresponding value in Column I is found by subtracting φ_y from 2,13,20 and reflecting in M_Φ (φ_s is negative). We obtain the value given in the parenthesis of Column I, line 1, of Table 8; since this is larger than 2,13,20 the effective value of I(1) is 2,13,20. Columns I and II now proceed with a difference per line of φ_s , supplied with the appropriate sign; where values exceed 2,13,20, we write 2,13,20. As long as Column I remains constant at 2,13,20, while Column II increases by φ_s per line, the quantity

$$\text{II}(n) - \text{I}(n) = \Delta A$$

will decrease by 0;0,17,46,40 per line, i.e., the second difference of A is constant and equal to φ_s .

From line 20 to line 50, Columns I and II run parallel, so ΔA is constant and equal to φ_y .

In line 51, Column II reaches the value 1,58,31,6,40. If we proceed with the difference of φ_s , and reflect in m_Φ , we get the values given in the parentheses. As long as these are below 1,58,31,6,40, Column II remains constant at this value. This means, that ΔA increases by 0;0,17,46,40 per line, or that $\Delta \Delta A$ is constant and equal to $-\varphi_s$. From line 56, Column I decreases by

TABLE 8.

	I	II	II-I = ΔΛ	Λ
1.	2, 13, 20 (2, 15, 27, 2, 13, 20)	2, 13, 20 ↑	0	3, 55, 33, 20
	2, 13, 20 (2, 15, 44, 48, 53, 20)	2, 13, 2, 13, 20 ↑	- 17, 46, 40	3, 55, 33, 20
	2, 13, 20 (2, 16, 2, 35, 33, 20)	2, 12, 44, 26, 40 ↑	- 35, 33, 20	3, 55, 15, 33, 20
	2, 13, 20 (2, 16, 20, 22, 13, 20)	2, 12, 26, 40 ↑	- 53, 20	3, 54, 40
5.	2, 13, 20 (2, 16, 38, 8, 53, 20)	2, 12, 8, 53, 20 ↑	- 1, 11, 6, 40	3, 53, 46, 40
	2, 13, 20 (2, 16, 55, 55, 33, 20)	2, 11, 51, 6, 40 ↑	- 1, 28, 53, 20	3, 52, 35, 33, 20
	2, 13, 20 (2, 16, 55, 55, 33, 20)	2, 11, 33, 20 ↑	- 1, 46, 40	3, 51, 6, 40
	2, 13, 20 (2, 16, 38, 8, 53, 20)	2, 11, 15, 33, 20 ↑	- 2, 4, 26, 40	3, 49, 20
	2, 13, 20 (2, 16, 20, 22, 13, 20)	2, 10, 57, 46, 40 ↑	- 2, 22, 13, 20	3, 47, 15, 33, 20
10.	2, 13, 20 (2, 16, 2, 35, 33, 20)	2, 10, 40 ↑	- 2, 40	3, 44, 53, 20
	2, 13, 20 (2, 15, 44, 48, 53, 20)	2, 10, 22, 13, 20 ↑	- 2, 57, 46, 40	3, 42, 13, 20
	2, 13, 20 (2, 15, 27, 2, 13, 20)	2, 10, 4, 26, 40 ↑	- 3, 15, 33, 20	3, 39, 15, 33, 20
	2, 13, 20 (2, 15, 9, 15, 33, 20)	2, 9, 46, 40 ↑	- 3, 33, 20	3, 36
	2, 13, 20 (2, 14, 51, 28, 53, 20)	2, 9, 28, 53, 20 ↑	- 3, 51, 6, 40	3, 32, 26, 40
15.	2, 13, 20 (2, 14, 33, 42, 13, 20)	2, 9, 11, 6, 40 ↑	- 4, 8, 53, 20	3, 28, 35, 33, 20
	2, 13, 20 (2, 14, 15, 55, 33, 20)	2, 8, 53, 20 ↑	- 4, 26, 40	3, 24, 26, 40
	2, 13, 20 (2, 13, 58, 8, 53, 20)	2, 8, 35, 33, 20 ↑	- 4, 44, 26, 40	3, 20
	2, 13, 20 (2, 13, 40, 22, 13, 20)	2, 8, 17, 46, 40 ↑	- 5, 2, 13, 20	3, 15, 15, 33, 20
	2, 13, 20 (2, 13, 22, 35, 33, 20)	2, 8 ↑	- 5, 20	3, 10, 13, 20
20.	2, 13, 4, 48, 53, 20	2, 7, 42, 13, 20 ↑	- 5, 22, 35, 33, 20	3, 4, 53, 20
	2, 12, 47, 2, 13, 20	2, 7, 24, 26, 40 ↑	- 5, 22, 35, 33, 20	2, 59, 30, 44, 26, 40
50.	2, 4, 11, 28, 53, 20	1, 58, 48, 53, 20 ↑	- 5, 22, 35, 33, 20	+ 23, 35, 33, 20
	2, 3, 53, 42, 13, 20	1, 58, 31, 6, 40 ↑	- 5, 22, 35, 33, 20	+ 18, 12, 57, 46, 40
	2, 3, 35, 55, 33, 20	1, 58, 31, 6, 40 (1, 58, 13, 20) ↑	- 5, 4, 48, 53, 20	+ 12, 50, 22, 13, 20
	2, 3, 18, 8, 53, 20	1, 58, 31, 6, 40 (1, 57, 55, 33, 20) ↑	- 4, 47, 2, 13, 20	+ 7, 45, 33, 20
	2, 3, 0, 22, 13, 20	1, 58, 31, 6, 40 (1, 57, 58, 8, 53, 20) ↑	- 4, 29, 15, 33, 20	+ 2, 58, 31, 6, 40
55.	2, 2, 42, 35, 33, 20	1, 58, 31, 6, 40 (1, 58, 15, 55, 33, 20) ↓	- 4, 11, 28, 53, 20	- 1, 30, 44, 26, 40
	2, 2, 24, 48, 53, 20	1, 58, 33, 42, 13, 20 ↓	- 3, 51, 6, 40	- 5, 42, 13, 20
	2, 2, 7, 2, 13, 20	1, 58, 51, 28, 53, 20 ↓	- 3, 15, 33, 20	- 9, 33, 20
	2, 1, 49, 15, 33, 20	1, 59, 9, 15, 33, 20 ↓	- 2, 40	- 12, 48, 53, 20
	2, 1, 31, 28, 53, 20	1, 59, 27, 2, 13, 20 ↓	- 2, 4, 26, 40	- 15, 28, 53, 20
60.	2, 1, 13, 42, 13, 20	1, 59, 44, 48, 53, 20 ↓	- 1, 28, 53, 20	- 17, 33, 20
	2, 0, 55, 55, 33, 20	2, 0, 2, 35, 33, 20 ↓	- 53, 20	- 19, 2, 13, 20
	2, 0, 38, 8, 53, 20	2, 0, 20, 22, 13, 20 ↓	- 17, 46, 40	- 19, 58, 33, 20
	2, 0, 20, 22, 13, 20	2, 0, 38, 8, 53, 20 ↓	+ 17, 46, 40	- 20, 13, 20

$\Delta\Delta\Lambda = -17, 46, 40$
 $\Delta\Delta\Lambda = 17, 46, 40$
 $\Delta\Delta\Lambda = 2 \cdot 17, 46, 40$

0;0,17,46,40, while Column II increases by the same amount per line. Thus $\Delta\Delta\Lambda$ is constant, and equal to $-2\varphi_8$.

Λ is therefore completely determined from Φ and its initial value 3;55,33,20.

φ_s and φ_y are so related, that Columns I and II are symmetrical in the sense that Column II as a whole, counting both obverse and reverse, is the same as Column I reversed. Thus \mathcal{A} is symmetrical about the first line of the reverse. It may also be noted that in Column I of Table 8 the values in the parentheses are symmetrical about M_Φ .

Because of these symmetry properties, one side of the text suffices to display the entire scheme. Thus I have given only the obverse (plus one line) in Table 8; the presence of the first half of Column I compensates for the absence of the last half of Column II. From Column II, line 63, we go to Column I, line 61. Two changes should be observed, first, that the Φ -value now belongs to a descending branch, and second, that the \mathcal{A} -value associated with a Φ -value in Column I is now found one line lower. These properties of the $\Phi - \mathcal{A}$ scheme may well have some bearing on the structure of the actual $\Phi - G$ scheme, as we shall see below.

Before I finish the discussion of \mathcal{A} , it is well to consider the $\Phi - G$ relations, where one may readily apply the technique displayed in Text **E** with but slight and obvious modifications. This I have done in Table 9.^{15a} The fundamental relation is, that the monthly difference in Φ (the Saros) is the same as the "Sarosly" difference in G (the month). Columns A and B contain Φ -values; the effective values are truncated at 2,13,20 above and 1,58,31,6,40 below, while the untruncated values are given in parentheses. The parameter which replaces φ_y is

$$\varphi_m = d_\Phi = 0;2,45,55,33,20,$$

i.e., the monthly difference in Φ on an ascending branch. As before, the line by line difference for both Column A and Column B is φ_s (with appropriate sign) except where modified by necessary reflexions and truncations. Thus, to move horizontally from Column A to Column B is to advance one month in time, and to move one line down corresponds to 223 months. If n denotes the line number, the table is constructed so that

$$G(n+1) - G(n) = B(n) - A(n),$$

which simply expresses the fundamental relation.

Thus G is in principle completely determined from Φ and initial value.

There is excellent, though not complete, agreement between this theoretical scheme and the one extracted from procedure texts and ephemerides in ACT. More precisely, the constructed scheme deviates in two respects from that in ACT. The first anomaly is, that in four instances (lines 57–60) the generated

^{15a} ACT No. 207 cd may be a small fragment of just such a table.

descending, for the greater part), is assigned the G-value in line $(n + 1)$. This is precisely what we should have expected if Table 9, were it continued, had turned out to be symmetrical in the same senses as the table for A , but that is not so. The reason is, of course, that φ_m and φ_s do not bear to each other as pleasant a relation as do φ_y and φ_s .

It is, therefore, very tempting to believe, that the $\Phi - G$ scheme, though for the greater part generated in a strict fashion, is modelled in its entirety after the $\Phi - A$ scheme. The first anomaly – the four aberrant values near the maximum – would then be the result of an attempt to symmetrise the G-values (it may be noted, that the actual differences in G are simple combinations of the expected ones). The second anomaly would then simply constitute the justification of the first.

It is natural to search for a direct connexion between A and G. The result is disappointing. First, if for a given value of Φ one compares the corresponding value of A with the sum of the appropriate 12 values of G, one does not get exact agreement modulo a whole number of days. Next, it is reasonable to seek a corollation between the initial values of A and G, and I believe they are extrema. I therefore took 12 consecutive monthly G-values, symmetrically disposed about G's maximum, and similarly 12 about its minimum, added them, and obtained

$$\sum_{i=1}^{12} (29^d + G_i) = 355^d + 3;32,21,43,42,13,20^H \tag{i}$$

and

$$\sum_{i=1}^{12} (29^d + G_i) = 355^d - 0;43,20,59,15,33,20^H. \tag{ii}$$

These two values must be the extrema of sums of the duration of 12 consecutive months, or very nearly so. The two values, $3;32, \dots^H$ and $-0;43, \dots^H$, fall short of the respective extrema of A by about $0;23^H$. Still, the difference between (i) and (ii) is very close indeed to the amplitude of A , but then that is only to be expected since both G and A are completely determined by Φ but for an additive constant, if we ignore the slight adjustments of G near its maximum.

I can therefore safely conclude that if I am right in identifying A with the excess of 12 months over a whole number of days, then the initial values of G and A are chosen independently of each other. Further, the purpose of A is clearly not to serve as a check for G.

For this reason, corroborated by the analogous situation for Φ and G,

the high values of G are no obstacle to assuming that A is the excess of 12 months, not over 355^d , but rather over 354^d , i.e.,

$$12 \text{ months} = 354^d + A^H.$$

Indeed, 12 mean synodic months amount to about

$$354^d + 2;12, \dots^H,$$

and $2;12, \dots$ is not far from a reasonable mean value of A . Further, the value 354 (but not 355) opens a possibility for interpreting Column X , as we shall see directly.

Column X , the fourth column of Text **E**, is in structure very like Column A (see Figure 4). The function is symmetrical in the same sense as A ; near its extrema it has sections with constant second difference (of ± 3 and, if my reconstruction is right, in part of ± 6), and in between a linear stretch (with constant difference of ± 54). The non-linear parts of X near its extrema are shown separately in Tables 10 and 11.

Table 10 exhibits one irregularity of X near its minimum. The second difference, here usually 3, is once 1 and then 5 whereupon it becomes 3 again. In the appended columns I have displayed what X would be if the second difference remained constant at 3. The resulting minimum is more pleasant, viz., 10,30,0 versus 10,29,58.

Unfortunately, the maximum of X and its neighbouring values are destroyed. Thus the values in Table 11 are largely restored. My restoration rests on the assumption of a doubling (to 6) of the second difference in analogy with the case of A . This assumption is plausible, for it generates the correct number of lines and makes X symmetrical about its maximum.

X appears here for the first time. I believe that it can be identified as the epact measured in days corresponding to A , i.e., the variable difference between a constant year and the variable length of 12 months.

Indeed, Figure 4 suggests that X is a complement to A ; more precisely, if A is converted into days and added to X interpreted as days (so that, e.g., its maximum is $11;12,54^d$) this sum, i.e.,

$$\frac{1}{8}A + X,$$

is very nearly constant throughout the text. Assuming my reconstructed extrema for X , these values all lie between $11;9,15,33,20^d$ and $11;9,31,46,40^d$. Interpreting A as above, we get:

TABLE 10.

TABLE 11.

Obv.21 = Rev.39

X	ΔX	$\Delta\Delta X$				
10,39,27						
10,38,33	-54		X if constant $\Delta\Delta$			
10,37,39	-54	0				
10,36,48	-51	3				
10,36	-48	3				
10,35,15	-45	3				
10,34,33	-42	3				
10,33,54	-39	3				
10,33,18	-36	3				
10,32,45	-33	3				
10,32,15	-30	3				
10,31,48	-27	3		10,31,48		
10,31,24	-24	3		10,31,24	-24	
10,31,1	-23	1		10,31,3	-21	3
10,30,43	-18	5		10,30,45	-18	3
10,30,28	-15	3		10,30,30	-15	3
10,30,16	-12	3		10,30,18	-12	3
10,30,7	-9	3		10,30,9	-9	3
10,30,1	-6	3		10,30,3	-6	3
10,29,58	-3	3	10,30	-3	3	

Obv.50 = Rev.10

X	ΔX	$\Delta\Delta X$			
11,5,33					
11,6,27	54				
11,7,21	54	0			
11,8,12	51	-3			
11,9	48	-3			
11,9,45	45	-3			
11,10,27	42	-3			
11,11,6	39	-3			
11,11,39	33	-6			
11,12,6	27	-6			
11,12,27	21	-6			
11,12,42	15	-6			
11,12,51	9	-6			
11,12,54	3	-6			
11,12,51	-3	-6			

$$12^m + X = 354^d + \frac{1}{6}A + X = 365;9, \dots^d$$

which is very near a value for the year, though too small. However, the text B. M. 36712¹⁶ gives evidence for a year length of 6,5;10^d.

I believe that the slight variation of

$$\varepsilon = \frac{1}{6}A + X$$

is the result of rounding, not of X 's values, but of its parameters. On the linear stretch, constancy of the quantity ε would require that ΔX , but for its sign, should be

$$\frac{1}{6}\Delta A = 0;0,53,45,55,33,20$$

while we find

$$\Delta X = 0;0,54,$$

and on the stretch of constant second difference, $\Delta\Delta X$ should be

$$\frac{1}{6}\Delta\Delta A = 0;0,2,57,46,40$$

while in fact

¹⁶ A. SACHS and O. NEUGEBAUER, *A Procedure Text Concerning Solar and Lunar Motion: B. M. 36712*. Journal of Cuneiform Studies X, 1956, pp. 131-135.

$$\Delta\Delta X = 0;0,3,$$

and analogously where the second difference is doubled. This serves further to explain, that the transitions from constant second to constant first difference do not happen exactly in the same lines for A and for X . Once the decision to limit the number of sexagesimal places of X was made, the handsome arithmetical structure of X must have been deemed more important than the constancy of the generated year length.

Text F

Text F: B.M. 36775 (= 80-6-17, 512).

Contents: Procedure text for variants of Column F.

Photograph: Plate IV.

Description of Text.

This tablet is about 4 inches wide and $2\frac{1}{2}$ inches high. Not much clay is missing, but the surface is damaged, particularly that of the obverse. The writing is divided into sections by horizontal rulings. Traces of a few signs are left here and there in the destroyed section; thus the obverse clearly did not begin with line 1'.

Transcription.

Obverse

Section 1.

- 1'. [. . .] 15 lal [.] 15 t[a]
 2'. [. . .] 2,45 zi-m[a.] t[a.] ki-i al 11,15
 3'. [. . .] tab-ma 2,11 [.] 2,15 gar-an

Section 2.

- 4'. [.] 1ta1 [.] 46,52,30
 5'. [.] gab-bi šá al-la 15 dir 15 e-šú
 6'. [mim-ma šá al 11,15 lal-ú 11,15 e-šú 42 šá] itu 1,21,39,22,30
 7'. [šá mu 2,20,37,30 šá 14 itu 23,15 šá 9 mu-m] eš 4,30 šá 18 mu-meš
 8'. [.] zi blank gal (?)
 9'. [.] blank

Section 3.

- 10'. [.] 11,15 zi
 11'. [.] an ta 15 ta
 12'. [.] gar-an ki-i al 15 dir
 13'. [.] gar-an ki-i al 15 lal 2,141 [. . .]

Reverse

1. [.] 13,5,9,22,30 [.]
2. [.] DU (?) 11, 15¹ lal (?) 42,11,15 [.]

Section 4.

3. [t]a 15,44,31,52,30 en 10,58,23,26,15 itu
4. [ana itu] 42,11,15 tab u lal lib-bu-ú šá itu-meš ta-ba-nu-ú
5. [. . .] gab-bi šá al-la 15 dir 15 e-šú mim-ma šá al 11,15
6. [lal-]ú 11,15 e-šú 42,11,15 šá itu 1,22,1,52,30 šá mu
7. [2,] 20,37,30 šá 14 itu 23,26,(15) šá 9 mu 4,41,15 šá 18
8. [mu] 4,11 šal-meš zi-šú kur-ád ta [1]5,4,4,31,52,30
9. [en 10,]50,23,26,15 4,54,[8,26,15] BAL (?) meš sar

Section 5.

10. [ana tar-ša 2,1]3,20 15 zi ana tar-ša [1,58,31,6,40 11,15 zi]
11. [ta 15,56],54,22,30 en [11,4,4,41,15]

Rest destroyed.

Critical Apparatus.

- Obv. 2'.]2,45 : 3,45 certainly possible
- Rev. 3. 10,58,23,26,15 : error for 10,50,23,26,15. The correct value, but for the initial 10, is given in Rev. 9.
- Rev. 6. 1,22,1,52,30 written like 1,23,52,30.
- Rev. 7. 23,26, the difference for 9 years, should be 23,26,15.

Translation.

I shall translate only Section 4, the best preserved section; Section 2 is for the greater part restored after the pattern of Section 4, and the remaining sections are so badly damaged that the numbers in them only made sense in isolation.

Section 4.

- Rev. 3. From 15,44,31,52,30 to 10,58,23,26,15 (error for 10,50,23,26,15) month.
4. [by month] 42,11,15 add and subtract; exactly as when (?) you make up (?) months.
 5. . . . whenever it exceeds 15, call it 15. Whenever it is smaller than 11,15,
 6. call it 11,15. 42,11,15 per month, 1,22,1,52,30 per year,

7. [2,]20,37,30 per 14 months, 23,26 (error for 23,26,15) per 9 years, 4,41,15 per 18
 8. [years.] 4,11 completely¹⁷ restores its velocity. From [1]5,44,31,52,30
 9. [to 10,]50,23,26,15 4,54, [8,26,15 . . .]

Commentary.

Section 4 is concerned with a hitherto unattested variant of Column F, the lunar velocity. I shall call it F'. Its parameters are:

$$\begin{array}{ll}
 M = 15;44,31,52,30^{0/d} & P = 13;56,40 = \frac{4,11}{18} \\
 m = 10;50,23,26,15 & II = 4,11 \\
 \Delta = 4;54, 8,26,15 & Z = 18 \\
 d = 0;42,11,15 & \mu = 13;17,27,39,22,30
 \end{array}$$

where d is the difference corresponding to one synodic month. The period is precisely that of Column F in System B (the abbreviated and the unabbreviated Column F have the same period), but none of the other parameters is found elsewhere. The monthly difference 0;42,11,15 is larger than the usual difference of 0;42 for F in System A. Incidentally, 42,11,15 is regular.

Several of these parameters are given in the text. M and m are found in Rev. 3, and again in Rev. 8 and 9. The erroneous value for m in Rev. 3 was an obstacle to understanding the text, but fortunately it appears correctly in Rev. 9. I believe that Δ was given in Rev. 9, and I have restored the number accordingly. II appears in Rev. 8.; one would expect a noun after 4,11, such as months or steps, but no convincing candidate corresponding to *šal* could be found. The value of d is found in Rev. 4 and 6. Though its period agrees with System B, F' is truncated at precisely the same values as F in System A, viz., 15 and 11;15. In Rev. 5 and 6 the truncation process is clearly described.

This section further gives the change in F' (without sign) corresponding to various time intervals. In Rev. 6 the monthly difference d is repeated, followed by the difference corresponding to one year. *Year* must mean 12 months here, for

$$2 \Delta - 12d = 1;22,1,52,30$$

which is the value of the text. Next is given the difference for 14 months

$$14d - 2 \Delta = 0;2,20,37,30$$

¹⁷ The phonetic reading of *šal-meš* was suggested to me by Professor J. J. FINKELSTEIN in a conversation on York Street. It is without precedent in the astronomical literature. My thanks are further due to Professor FINKELSTEIN for kindly checking several of these tablets for me while he was in the British Museum in 1966.

which, but for the initial 2, is found at the beginning of Rev. 7. Since 14 months is only slightly larger than

$$P = 13;56,40$$

this is a good checking parameter for F' (as are the corresponding values for F and Φ).

9 years must here mean 111 synodic months, for

$$8 \cdot 2 \Delta - 1,51 \cdot d = 0;23,26,15$$

which is the number written in Rev. 7, though the scribe omitted the final 15.

Finally, the difference for 18 years, i.e., 223 synodic months, is given, viz.,

$$16 \cdot 2 \Delta - 3,43 \cdot d = 0;4,41,45.$$

We shall now turn our attention to Section 2 which I have restored after the pattern of Section 4. The phrase in Obv. 6', describing truncation at 15, and the word *zi* (= velocity) in Obv. 8' identify the subject of this passage as a Column F variant. The difference 4,30 corresponding to 18 years suggests the parameters of the usual, unabbreviated Column F of System A, for which

$$d_F = 0;42$$

$$\Delta_F = 4;52,49,41,15,$$

and with these values:

$$16 \cdot 2 \Delta_F - 3,43 \cdot d_F = 0;4,30$$

(this is the difference corresponding to 17,46,40 for Φ). These parameters further serve to explain the number in Rev. 7' as the difference corresponding to one year (12 months), for

$$2 \Delta_F - 12 \cdot d_F = 1;21,39,22,30.$$

The differences corresponding to the other time intervals become:

$$\text{for 14 months:} \quad 14 \cdot d_F - 2 \Delta_F = 0;2,20,37,30$$

$$\text{for 9 years:} \quad 8 \cdot 2 \Delta_F - 1,51 \cdot d_F = 0;23,15$$

and I have restored the passage accordingly. It should be noted that the difference for 14 months is the same for F and F'.

These parameters depend only on d and Δ , so they give no information about the extrema. I do not believe that Section 2 deals with the standard

Column F from System A, for in Obv. 5', where the ending of the minimum is expected, we find [. . .]46,52,30 which does not agree with

$$m_F = 11;4,4,41,15$$

nor, for that matter, with

$$M_F = 15,56,54,22,30.$$

Thus I expect that Section 2 presents a variant of F which agrees with the standard function in d , Δ , and therefore P , but not in μ . Even so, this variant is also truncated at the usual values of 15 and 11;15 though, strictly speaking, only the truncation at 15 is described in the preserved part.

All I can safely say about the other sections is that they are concerned with variants of F. In Section 1 we find the characteristic values 15 and 11;15, while I can make no sense of the remaining few and fragmentary numbers.

In Section 3 the two characteristic values occur again, as well as z_i . The number 13,5,9,22,30 in Rev. 1 is too small to be a mean value of lunar velocity. In Rev. 2 we find 42,11,15 which is the monthly difference of F'.

In Section 5, Rev. 10, occurs the expression *ana tar-ša* which is the standard terminology for transforming one function into another¹⁸ (*ana tar-ša* (a) (b) means: opposite (a) (put down) (b)). I have restored the line to be identical with Obv. I, 18 of ACT No. 200, where the section in question treats of the transformation of Φ into F. It was natural to restore M_F and m_F in Rev. 11., since the preserved numbers agree with the ending of M_F .^{18a} These restorations are obviously not very secure, yet it is a possibility that Section 5 is concerned with the standard Column F of System A which, of course, is in phase with Φ .

It is unusual to find variants of functions or models juxtaposed in one text (other examples are ACT Nos. 812 and 813 which present various methods for Jupiter). The purpose of the text is not clear to me, nor is the astronomical justification of truncating variants of F at the same values.

The importance of Text F is that it furnishes direct evidence for the truncation of F, giving us the technical terminology for this process. Strictly speaking, it contains the only direct evidence for the truncation below at 11;15, for only rarely is an F-value smaller than 11;15, and the truncation of Φ at 1,58,31,6,40 had to be inferred from the structure of Δ and G.^{18b}

¹⁸ cf. ACT II, p. 494.

^{18a} There is now a text (B.M. 36722 + 40082) in which it appears that Col. F is truncated at the values 15;25,54,22,30 and 11;25,4,4[1,15]; since the endings agree with those of the extrema, it is not entirely excluded that these effective extrema should be restored here. This text will be published as Text K in O. NEUGEBAUER and A. SACHS, *Some Atypical Astronomical Texts II* in the Journal of Cuneiform Studies.

^{18b} This is no longer so (see the note added in proof at the end of this paper).

Additions and Comments to the Saros Text

In the present section I shall first present those passages of NEUGEBAUER'S Saros text which are affected by the small fragment I joined to it. Unfortunately, the new piece adds but little to our understanding of this difficult text; indeed, in several cases it merely confirms NEUGEBAUER'S restorations.

Next, I shall discuss some hitherto obscure parts of this text which can now be understood in light of the knowledge gained from Text E. It was particularly the fact that Φ is truncated at 2,13,20 and 1,58,31,6,40 that enabled me to make sense of some of the numbers which previously lacked motivation.

To republish the entire text seemed absurd, so in the following I shall presuppose a familiarity with NEUGEBAUER'S publication.

B.M. 37484 (= 80-6-17,1241) joins B.M. 36705 (= (80-6-17,437) + (80-6-17,458)).

Photograph: Plate V.

The small fragment (at most $1\frac{1}{4}$ inches either way) joins the upper right corner of the obverse (= lower right corner of the reverse). Part of the right edge is preserved, and the fragment is near the top edge. It appears, that NEUGEBAUER'S Section 1 has a predecessor which I shall call Section 0 to avoid renumbering the sections, and similarly for the line numbers.

Transcription.

Obverse.

Section 0.

- 1. [.] ù 2[0]

Section 1.

0. [.] 1,5,4,22,30 DU-*ma*
1. [.2,13],20 *a-na* 1,58,31,6,40 m[u . . .]
2. [.]E-*ma* 14,48,53,20 mu-m[eš . .] 17,46,40 *taš-pil-tú*
3. *šá* 18 mu-meš *šá* E-*ma* 13,39,35,36[. .]6,15 *šu-ú*

Section 2.

4. 17,46,40 a-rá 9,20 DU-*ma* 2,45,55,3[3,20 . .]. . . 13,46,38,15 me
5. ta *muḫ-ḫi* zi *sin* gal en *muḫ-ḫi* zi *sin* tur . . .[. . .] etc.

Reverse.

Section 15.

32. *a-na tar-ši* 2,17,4,48,53,20 2,15,31,6,35,33,20
 33. [*a-na t*] *ar-ši* 2, . . ., 59,15,33,20 4,46,42,57,46,40
 34. [*a-na tar-ši* 1,57,4] 7,57,46,40 5,15,28,23,37,46,40
 35. [.] blank *bī-ri-šū-nu*
 36. [.] 1,22,57,46,40] [. . .]
 Rest destroyed.

Critical Apparatus.

- Obv. – 1. 2[0]: *sin* and *šamaš* both possible.
 Obv. 1. 40 m[u. . .] written on the edge.
 Obv. 4. 13,46,38,15 is preceded by what looks like a high diagonal wedge and two corner wedges. The final 5 and “me” are on the edge.
 Rev. 35. From the blank space with a ruling above it NEUGEBAUER concluded that a new section began here. The position of *bī-ri-šū-nu* contradicts this.
 Rev. 36. The reading of this number is very tentative. It is, however, unlikely that this is the first line of a new section.

Commentary.

In Obv. 2 and 3 we now have the statement, that *17,46,40 is the difference for 18 years*, which was the basis for our understanding of Φ .

The number 1,5,4,22,30 in Obv. 0, which also occurs farther down in Obv. 9, is, as NEUGEBAUER pointed out, the result of dividing Δ_{Φ} by 17,46,40. I shall return to it below where it will be called *N*.

In Obv. 1 we find 1,58,41,6,40, which is the effective minimum of Φ , so I have restored the effective maximum, 2,13,20, just preceding it. The number 14,48,53,20 in Obv. 2 can now be explained as the difference between 2,13,20 and 1,58,31,6,40, i.e., the effective amplitude of Φ ; I shall return to it below where it will be called δ_2 . I do not understand why these numbers are denominated years,¹⁹ nor can I make sense of the number in Obv. 3 beginning 13,39,35, . . .²⁰.

In Section 2, Obv. 4 and 5, we now read: *13,46,38,15 days from high velocity of the moon to low velocity of the moon.*

¹⁹ The meaning *line* of mu does not seem to help.

²⁰ It may be a value for half the sidereal month, but I cannot make it fit the context.

13;46,38,15 days is indeed half the anomalistic month; this value is found in Obv. 6 converted into large hours, as NEUGEBAUER recognised.

In Section 15, Rev. 32, 33, and 34, the new fragment confirms NEUGEBAUER'S restoration of the endings of the numbers, and shows further that nothing else was written in these lines. In Rev. 34 we now have the word *bi-ri-šú-nu* (= the distance (arc) between them), which may refer to lunar elongation. Even so, I cannot explain the numbers in this section beyond what NEUGEBAUER already has done. So far the new fragment.

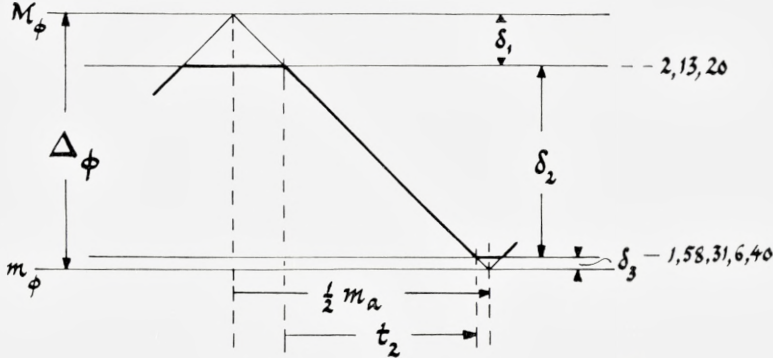


Fig. 6.

The recognition of Φ 's effective extrema makes it possible to explain a few more numbers in the Saros text, particularly those in Section 3.

Consider a branch of Φ , subdivided at 2,13,20 and 1,58,31,6,40 (see Figure 6). We introduce

$$\begin{aligned} \delta_1 &= M_\Phi - 2;13,20 &&= 0;3,44,48,53,20^H \\ \delta_2 &= 2;13,20 - 1;58,31,6,40 &&= 0;14,48,53,20^H \\ \delta_3 &= 1;58,31,6,40 - m_\Phi &&= 0;0,43,8,53,20^H \end{aligned}$$

so

$$\delta_1 + \delta_2 + \delta_3 = \Delta_\Phi = 0;19,16,51,6,40.$$

If we now proceed along the branch of Φ in steps of length 0;0,17,46,40, as we did in Text E, we find, dividing the δ 's by 0;0,17,46,40, that the corresponding number of steps are:

from M_Φ to 2;13,20 :	$n_1 = 12;38,45$	steps
from 2;13,20 to 1;58,31,6,40 :	$n_2 = 50$	steps
from 1;58,31,6,40 to m_Φ :	$n_3 = 2;25,37,30$	steps
and from M_Φ to m_Φ :	$N = n_1 + n_2 + n_3 = 1,5;4,22,30$	steps.

The number N occurs in Obv. 9, and now in Obv. 0, and was correctly explained by NEUGEBAUER.

Section 3 contains n_1 , n_2 , and n_3 and instructs us to multiply them by 17,46,40. The results, which are not given, are δ_1 , δ_2 , and δ_3 .²¹

In Obv. 9, 10, and 11, the length of half the anomalistic month (in large hours) is divided by N , yielding

$$t = \frac{1,22;39,49,30^H}{1,5;4,22,30} = 1;16,13,10,11,24,36^H,$$

as NEUGEBAUER recognised though, as he points out, the division is not executed quite correctly. If we now consider again the branch of Φ , i.e., the true Φ -function whose period is the anomalistic month, then t is the time it takes to move one step of length 0;0,17,46,40 along this branch.

The time t_2 it takes to travel from 2;13,20 to 1;58,31,6,40 is thus:

$$t_2 = n_2 \cdot t = 50 \cdot t = 1,3;30,58,29,30,30^H$$

which is the number preserved in Rev. 3 (what NEUGEBAUER read as “ $\frac{1}{2}$ ” is “*ina* 1” written closely so the horizontal wedge of *ina* intersects the vertical 1, and where he read “?48” one should read 58).

²¹ NEUGEBAUER carries out these multiplications and gives the results on page 18 of the Saros paper (there are, unfortunately, two errors in the printing: 3,44,50,53,20 should be 3,44,48,53,20 (= δ_1) and 48,8,53,20 should be 43,8,53,20 (= δ_3)).

It is remarkable that several of the parameters of Φ are simple multiples of 17,46,40. Thus, e.g.,

$$\begin{aligned} 2;13,20 &= 7,30 \cdot 0;0,17,46,40 \\ 1;58,31,6,40 &= 6,40 \cdot 0;0,17,46,40. \end{aligned}$$

For the constants c and l mentioned above on page 11 we also have

$$\begin{aligned} c &= 10,0 \cdot 0;0,17,46,40 \\ l &= 6,15 \cdot 0;0,17,46,40 \end{aligned}$$

though l , of course, is measured in degrees.

Yale University
New Haven, Connecticut, U. S. A.

Added in Proof

Just after the manuscript of this paper went to the printer I came across two texts in the British Museum that contain additional information about F and Δ .

The first text (BM 36961 (= 80-6-17,702)) is a fragment containing remnants of three columns. What is of interest here is that the second is the abbreviated Column F of System A whose parameters are:

$$M = 15;57 \qquad d = 0;42$$

$$m = 11;4$$

and it is truncated at 15 and 11;15. Since the first line has 14;40 \downarrow , the effective minimum 11;15 actually appears in line 6. The effective maximum 15 occurs thrice (in lines 12-14). It is worthy of note that on the upper edge is visible ^{1]} *Se-lu-ku*, so the practice of truncating F was certainly known in Seleucid times.

The second text (BM 40094 (= 81-2-1,59)) is of considerable interest. It is a fragment of an ephemeris for consecutive new moons; though the date column is destroyed, I can say with confidence, on the basis of internal evidence, that the text covers the three years from S.E.-8, XII to S.E.-5, XII. Thus it antedates the oldest hitherto known lunar ephemeris (ACT No. 1) by 132 years. It can further be shown, again on indirect, but secure evidence, that solar longitudes not only were computed according to the well-known System A scheme, but also that they are continuable on the ACT texts, and similarly for Column Φ . What is of particular concern here is that this text contains a Column Δ (month by month)-this is the first time Δ has been encountered in an ephemeris-and following this a column (I call it Column Y) giving corrections for solar anomaly to Δ . Y is related to J (the analogous correction of G) by the rule that the monthly difference in Y is the 12-monthly difference in J. Further, Column Y, as Column J, is 0 on the fast arc. It is presently not out of the question that the connexion between the initial values (or mean values) of G and Δ is to be found here, and that it rests on the decision that both J and Y be 0 on the arc of high monthly progress of the sun.

PLATES



Text A



Text B, Obv.

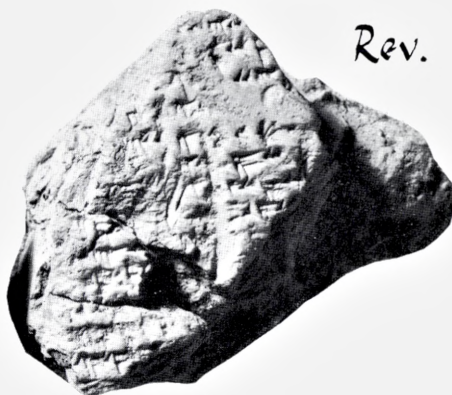


Text C



Rev.

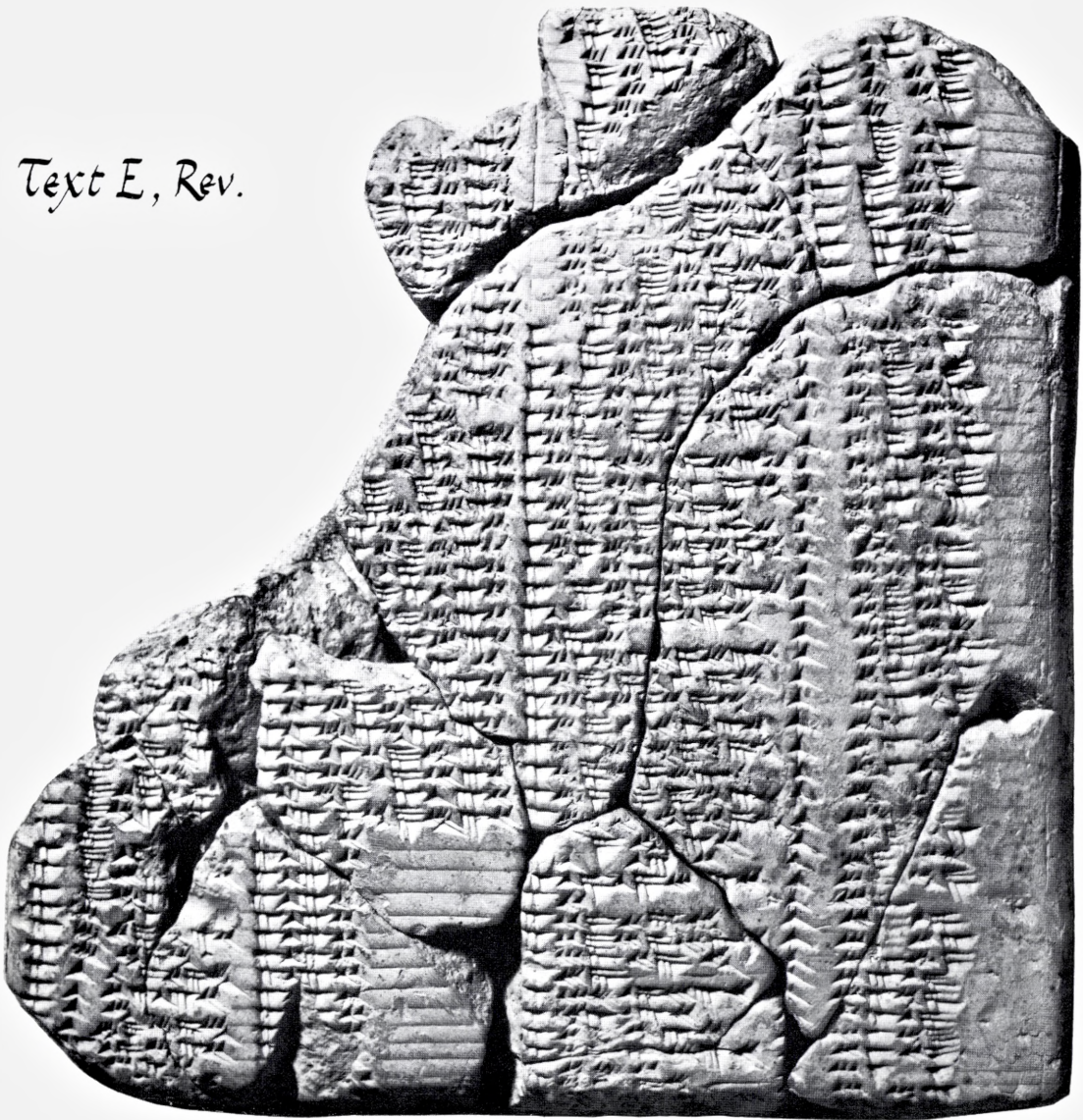
Text D





Text E, Obv.

Text E, Rev.



Obv.



Rev.

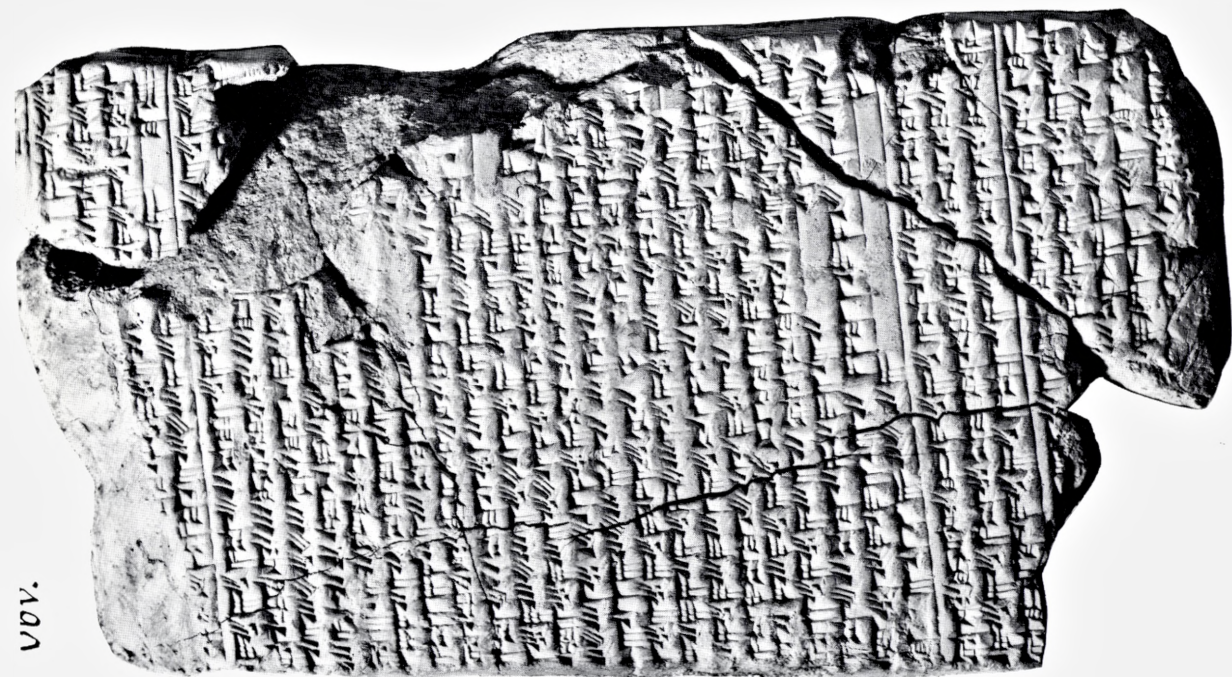


Text F



No. V.

B.M. 36705.



No. VV.

ESKO SUHONEN

ON THE ENERGY
TRANSFER BY MATERIAL PARTICLES
AND RADIATION IN A GENERAL
RELATIVISTIC GAS

Det Kongelige Danske Videnskabernes Selskab
Matematisk-fysiske Meddelelser **36**, 13



Kommissionær: Munksgaard

København 1968

Synopsis

A general relativistic form of the energy transfer equation is developed for material particles interacting with a spherically symmetric and static medium. Using the relativistic expressions of the energy density and the pressure in the different statistics, the radial energy flow is obtained from the transfer equation for Maxwellian particles, bosons and fermions as a diffusion approximation. The thermal conductivity of ionization electrons is derived for a medium consisting of only one kind of nuclei. The equations of the energy transfer by photons and neutrinos are obtained in the special case of massless energy carriers. The condition of no net energy flow is found to lead to Tolman's law of thermodynamical equilibrium. The mean absorption coefficient of material particles is introduced and an approximative method for the calculation of this coefficient is given analogously to the Rosseland mean opacity.

1. Introduction

In order to investigate the state of matter in the interior of dense stars, it is necessary to derive the energy transfer by radiation as well as by material particles. In most cases the energy transfer by material particles or the thermal conductivity accounts only for a negligible proportion of the energy transfer. But under certain conditions the conductivity of the electron gas plays an important role, particularly in the white dwarf stars⁽¹⁾.

The discovery of the quasistellar radiosources in the past few years has given support to the theory of relativistic astrophysics. The relativistic methods are necessary because of those special circumstances which are probably present in these radio sources⁽²⁾. The radiative energy transfer has been studied both in the static⁽³⁾ and in the time-dependent⁽⁴⁾ radially symmetric medium in a general covariant way. But the general relativistic problem of the conductive energy transfer seems to be unexplored.

In this paper the energy transfer by material particles is examined by the same method as for the radiative transfer problem. The treatment is restricted to the radially symmetric and static case. We also limit ourselves to the case of energy flow due to identical particles which are interacting with the external medium while their interactions with each other are neglected. Further, the study is restricted to the condition that the gas is close to thermodynamical equilibrium.

After some auxiliary equations the transfer equation is presented in section 2. In section 3 the energy density, the radial energy flow and the pressure of the particles carrying the energy are introduced and the transfer equation is expressed as a relation between these quantities. By using the relativistic expressions for the energy density and the pressure in the different statistics, the radial energy flow is found proportional to the gradients of the thermal and the chemical potentials, in chapter 3A for Maxwellian particles and in chapter 3B for fermions and bosons.

The thermal conductivity of ionization electrons which are interacting with a medium consisting of only one kind of nuclei is derived in chapter 4A.

In chapter 4B the expressions of the radiative energy transfer and the neutrino diffusion are obtained in the special case of massless energy carriers. The mean absorption coefficient of material particles is introduced, and an approximative method for the calculation of this coefficient is given for electrons, photons and neutrinos in section 5.

2. Transport equation

We shall study a stream of identical particles, which at a definite point is characterized by a four-dimensional elementary solid angle $\delta\Omega$, a space-like direction N and an intensity I_Ω (in dimension $\frac{|\text{energy}|}{|\text{area}| |\text{time}|}$). The elementary solid angle $\delta\Omega$ is given by

$$\delta\Omega = \sinh^2 \xi \delta\xi \delta\omega, \quad (1)$$

where $\delta\omega$ is the three-dimensional solid angle in the local rest-system of the external medium with which the particles are interacting. The number ξ denotes a pseudoangle which measures the angle between the unit tangent of nearly parallel world lines in $\delta\Omega$ and the four-velocity vector of the medium.

The metric of the radially symmetric and static medium has the form

$$ds^2 = -e^{\lambda(r)} dr^2 - r^2 (dv^2 + \sin^2 v d\varphi^2) + e^{\mu(r)} c^2 dt^2. \quad (2)$$

We denote the space-like unit vector in the radial direction by N_r and the time-like unit vector in the direction of time by U . In the metric (2) they have the following contravariant components:

$$\left. \begin{aligned} N_r^\alpha &= \left\{ e^{-\frac{1}{2}\lambda}, 0, 0, 0 \right\} \\ U^\alpha &= \left\{ 0, 0, 0, e^{-\frac{1}{2}\mu} \right\}. \end{aligned} \right\} \quad (3)$$

Now we let θ denote the angle between N and N_r . The vectors N , N_r and U then have the properties:

$$\left. \begin{aligned} N \cdot N &= N_r \cdot N_r = -1 \\ U \cdot U &= 1 \\ N \cdot U &= N_r \cdot U = 0 \\ N \cdot N_r &= -\cos \theta. \end{aligned} \right\} \quad (4)$$

We assume that the particle paths are geodesics except in the regions where scatterings occur. The geodesics-approximation is good, if we idealize the scattering processes as point interactions. This is a rather useful approximation, even for electrons in an ionized medium. The electromagnetic interactions between the electrons and between electrons and nuclei cancel on a large scale the effect of each other. We can then write for the particles the equations of motion between scattering regions in the form

$$U_{\Omega} \cdot (\nabla U_{\Omega}) = 0, \quad (5)$$

where

$$U_{\Omega} = U \cosh \xi + N \sinh \xi \quad (6)$$

is the four-velocity vector of the particles belonging to the solid angle $\delta\Omega$ and ∇U_{Ω} is the covariant gradient of U_{Ω} .

Taking the scalar product of eq. (5) and the vector U , we obtain

$$U_{\Omega} \cdot (\nabla U_{\Omega}) \cdot U = U_{\Omega} \cdot \nabla \cosh \xi - U_{\Omega} \cdot (\nabla U) \cdot U_{\Omega} = 0. \quad (7)$$

Since we have assumed the situation to be static, the operator $U \cdot \nabla$ applied to any scalar function is equal to zero. When this is taken into account, eq. (7) is reduced to the form

$$\sinh \xi N \cdot \nabla \cosh \xi = U_{\Omega} \cdot (\nabla U) \cdot U_{\Omega}. \quad (8)$$

Taking the gradient of U in component form, we get the equation

$$N \cdot \nabla \cosh \xi = -\frac{1}{2} \frac{d\mu}{dr} e^{-\frac{\lambda}{2}} \cosh \xi \cos \theta. \quad (9)$$

Performing similar calculations by multiplying eq. (5) scalarly by N_r , we obtain the result

$$N \cdot \nabla \cos \theta = \frac{1}{2} e^{-\frac{\lambda}{2}} \left(\frac{2}{r} - \frac{d\mu}{dr} \frac{\cosh^2 \xi}{\sinh^2 \xi} \right) \sin^2 \theta, \quad (10)$$

where we have also made use of eq. (9).

The energy-momentum for the stream under consideration is

$$\delta T_{\Omega} = c^2 \varrho_{\Omega} U_{\Omega} U_{\Omega} \delta \Omega, \quad (11)$$

where ϱ_{Ω} is the density of the rest mass of the particles in the solid angle $\delta\Omega$. In writing eq. (11) we have ignored the interactions of particles with each

other. The quantity $-cU \cdot \delta T_{\Omega} \cdot N$ describes the energy flux in the direction N per unit proper time in the rest-system defined by U . This energy flux is also equal to $I_{\Omega} \delta \Omega$. Then we have

$$\begin{aligned} I_{\Omega} \delta \Omega &= -cU \cdot \delta T_{\Omega} \cdot N \\ &= c^3 \varrho_{\Omega} \sinh \xi \cosh \xi \delta \Omega, \end{aligned}$$

so that

$$\varrho_{\Omega} = \frac{I_{\Omega}}{c^3 \sinh \xi \cosh \xi}. \quad (12)$$

Substitution of eq. (12) into eq. (11) yields the expression for δT_{Ω}

$$\delta T_{\Omega} = \frac{I_{\Omega} U_{\Omega} U_{\Omega} \delta \Omega}{c \sinh \xi \cosh \xi}. \quad (13)$$

The covariant divergence of $\frac{1}{c} \delta T_{\Omega}$ describes the generation of momentum per unit time and unit volume. The U -component of this vector expresses the generation of energy in mass units. We define the coefficients of absorption and emission x_{Ω} and j_{Ω} , such that the energy flux absorbed from the beam and emitted into it by the medium is respectively $x_{\Omega} \varrho_0 I_{\Omega} \delta \Omega$ and $\frac{1}{4\pi} j_{\Omega} \varrho_0 \delta \Omega$, where ϱ_0 is the proper mass density of the external medium. The gain of energy must balance the loss at every point, so that in energy units we have the equation

$$c(\nabla \cdot \delta T_{\Omega}) \cdot U = -x_{\Omega} \varrho_0 I_{\Omega} \delta \Omega + \frac{1}{4\pi} j_{\Omega} \varrho_0 \delta \Omega. \quad (14)$$

Inserting δT_{Ω} from eq. (13) into the left side of eq. (14), we obtain

$$c(\nabla \cdot \delta T_{\Omega}) \cdot U = \nabla \cdot \left(\frac{I_{\Omega} U_{\Omega} \delta \Omega}{\sinh \xi} \right) - \frac{I_{\Omega} \delta \Omega}{\sinh \xi \cosh \xi} U_{\Omega} \cdot (\nabla U) \cdot U_{\Omega}. \quad (15)$$

The first term on the right side can be developed as follows:

$$\nabla \cdot \left(\frac{I_{\Omega} U_{\Omega} \delta \Omega}{\sinh \xi} \right) = U \cdot \nabla \left(\frac{\cosh \xi}{\sinh \xi} I_{\Omega} \delta \Omega \right) + \frac{\cosh \xi}{\sinh \xi} (\nabla \cdot U) I_{\Omega} \delta \Omega + \nabla \cdot (I_{\Omega} N \delta \Omega),$$

where the first term is equal to zero, since the situation is static. The second term vanishes too, which we can see by computing $\nabla \cdot U$ from eq. (3). We have then

$$\nabla \cdot \left(\frac{I_{\Omega} U_{\Omega} \delta \Omega}{\sinh \xi} \right) = \nabla \cdot (I_{\Omega} N \delta \Omega). \quad (16)$$

Substituting eqs. (8) and (16) into eq. (15) and then further into eq. (14), we obtain the equation of the energy transfer

$$\left. \begin{aligned} \nabla \cdot (I_{\Omega} N \delta \Omega) = & - \left(x_{\Omega} \varrho_0 + \frac{1}{2} \frac{d\mu}{dr} e^{-\frac{1}{2}\lambda} \cos \theta \right) I_{\Omega} \delta \Omega \\ & + \frac{1}{4\pi} j_{\Omega} \varrho_0 \delta \Omega. \end{aligned} \right\} \quad (17)$$

3. Radial Energy Flow

We restrict our examination to the very nearly isotropic case. Instead of working with the function I_{Ω} , we want to express eq. (17) by the moments of this function. The energy density, the energy flux in the direction N_r and the gas pressure are given by the formulas

$$\left. \begin{aligned} E_{\Omega} &= U \cdot \delta T_{\Omega} \cdot U = \frac{1}{c} \frac{\cosh \xi}{\sinh \xi} I_{\Omega} \delta \Omega \\ H_{\Omega} &= -c U \cdot \delta T_{\Omega} \cdot N_r = I_{\Omega} \cos \theta \delta \Omega \\ P_{\Omega} &= N_r \cdot \delta T_{\Omega} \cdot N_r = \frac{1}{c} \frac{\sinh \xi}{\cosh \xi} I_{\Omega} \cos^2 \theta \delta \Omega. \end{aligned} \right\} \quad (18)$$

Now we introduce the quantities E_{ξ} , H_{ξ} , P_{ξ} and I_{ξ} , belonging to particles of the same ξ , by the expressions

$$\left. \begin{aligned} E_{\xi} &= \sinh^2 \xi \int E_{\Omega} d\omega \\ H_{\xi} &= \sinh^2 \xi \int H_{\Omega} d\omega \\ P_{\xi} &= \sinh^2 \xi \int P_{\Omega} d\omega \\ I_{\xi} &= \sinh^2 \xi I_{\Omega}. \end{aligned} \right\} \quad (19)$$

Substituting eq. (18) into eq. (19), we have the following integrals:

$$\left. \begin{aligned} E_{\xi} &= \frac{1}{c} \frac{\cosh \xi}{\sinh \xi} \int I_{\xi} d\omega \\ H_{\xi} &= \int I_{\xi} \cos \theta d\omega \\ P_{\xi} &= \frac{1}{c} \frac{\sinh \xi}{\cosh \xi} \int I_{\xi} \cos^2 \theta d\omega. \end{aligned} \right\} (20)$$

In order to construct the appropriate relation between the integrals (20) we need the auxiliary equation

$$\left. \begin{aligned} \nabla \cdot (I_{\Omega} N \cos \theta \delta \Omega) &= \Delta \cdot (I_{\xi} N \cos \theta \delta \xi \delta \omega) \\ &= \cos \theta \nabla \cdot (I_{\Omega} N \delta \Omega) + I_{\xi} \delta \xi \delta \omega N \cdot \nabla \cos \theta \end{aligned} \right\} (21)$$

which, after using eqs. (10) and (17), can be written in the form

$$\left. \begin{aligned} \nabla \cdot (I_{\xi} N \cos \theta \delta \xi \delta \omega) &= - \left(x_{\xi} \varrho_0 + \frac{1}{2} \frac{d\mu}{dr} e^{-\frac{\lambda}{2}} \cos \theta \right) I_{\xi} \cos \theta \delta \xi \delta \omega \\ &+ \frac{1}{4\pi} j_{\xi} \varrho_0 \cos \theta \delta \xi \delta \omega + \left(\frac{1}{r} - \frac{1}{2} \frac{d\mu}{dr} \frac{\cosh^2 \xi}{\sinh^2 \xi} \right) e^{-\frac{\lambda}{2}} I_{\xi} \sin^2 \theta \delta \xi \delta \omega. \end{aligned} \right\} (22)$$

We have applied the following definitions in eq. (22)

$$\left. \begin{aligned} x_{\xi} &= x_{\Omega} \\ j_{\xi} &= \sinh^2 \xi j_{\Omega}. \end{aligned} \right\} (23)$$

Integrating eq. (22) over all three-dimensional solid angles and taking into account the radial symmetry and the expressions (20), we get the relation

$$\left. \begin{aligned} \nabla \cdot \left(N_r \frac{\cosh \xi}{\sinh \xi} P_{\xi} \delta \xi \right) &= \left(\frac{1}{r} \frac{\sinh \xi}{\cosh \xi} - \frac{1}{2} \frac{d\mu}{dr} \frac{\cosh \xi}{\sinh \xi} \right) e^{-\frac{\lambda}{2}} E_{\xi} \delta \xi \\ &- \frac{\varrho_0}{c} x_{\xi} H_{\xi} \delta \xi - \left(\frac{1}{r} \frac{\cosh \xi}{\sinh \xi} - \frac{1}{2} \frac{d\mu}{dr} \frac{\cosh \xi}{\sinh^3 \xi} \right) e^{-\frac{\lambda}{2}} P_{\xi} \delta \xi. \end{aligned} \right\} (24)$$

The divergence in eq. (24) can be evaluated using the component representation (3) of the vector N_r and the expression

$$\frac{d\xi}{dr} = -\frac{1}{2} \frac{d\mu}{dr} \frac{\cosh \xi}{\sinh \xi} \quad (25)$$

which is obtained from eq. (9). After a simple calculation we get

$$\left. \begin{aligned} \nabla \cdot \left(N_r \frac{\cosh \xi}{\sinh \xi} P_\xi \delta \xi \right) &= \frac{2}{r} e^{-\frac{\lambda}{2}} \frac{\cosh \xi}{\sinh \xi} P_\xi \delta \xi \\ + \frac{1}{2} \frac{d\mu}{dr} e^{-\frac{\lambda}{2}} \frac{\cosh^3 \xi}{\sinh^3 \xi} P_\xi \delta \xi + e^{-\frac{\lambda}{2}} \frac{\cosh \xi}{\sinh \xi} \frac{d(P_\xi \delta \xi)}{dr} \end{aligned} \right\} \quad (26)$$

Inserting eq. (26) in eq. (24), we find

$$\left. \begin{aligned} \frac{d(P_\xi \delta \xi)}{dr} &= \left(\frac{1}{r} \frac{\sinh^2 \xi}{\cosh^2 \xi} - \frac{1}{2} \frac{d\mu}{dr} \right) E_\xi \delta \xi - \frac{\varrho_0}{c} e^{\frac{\lambda}{2}} \frac{\sinh \xi}{\cosh \xi} x_\xi H_\xi \delta \xi \\ &\quad - \left(\frac{3}{r} + \frac{1}{2} \frac{d\mu}{dr} \right) P_\xi \delta \xi. \end{aligned} \right\} \quad (27)$$

Now we introduce the integrals

$$\left. \begin{aligned} E &= \int_0^\infty E_\xi \delta \xi \\ H &= \int_0^\infty H_\xi d\xi \\ P &= \int_0^\infty P_\xi d\xi \end{aligned} \right\} \quad (28)$$

which represent the total energy density due to the particles we consider, the total radial energy flow defined as the flux of energy relative to the particle stream, and the total gas pressure due to these particles. We further define the mean absorption coefficient x of material particles analogously to the Rosseland mean opacity⁽⁵⁾ by

$$xH = \int_0^\infty \frac{\sinh \xi}{\cosh \xi} x_\xi H_\xi d\xi, \quad (29)$$

which we analyze in section 5.

The integration over the quantity ξ in eq. (27) gives the equation

$$\left. \begin{aligned} \frac{dP}{dr} = \frac{1}{r} \int_0^\infty \frac{\sinh^2 \xi}{\cosh^2 \xi} E_\xi \delta \xi - \frac{1}{2} \frac{d\mu}{dr} E - \frac{\varrho_0}{c} e^{\frac{\lambda}{2}} x H \\ - \left(\frac{3}{r} + \frac{1}{2} \frac{d\mu}{dr} \right) P. \end{aligned} \right\} \quad (30)$$

We have worked with moments of the intensity function rather than the intensity itself in deriving eq. (30). Because of that we need an independent auxiliary equation. It is then customary to use the diffusion approximation, where the statistical expressions of the energy density and the gas pressure in thermal equilibrium are applied. We shall eliminate the quantities E and P from eq. (30) in the case of relativistic Boltzmann-statistics and quantum statistics in chapters 3A and 3B respectively. The quantities belonging to quantum statistics have an index d .

3A. Radial Energy Flow due to Relativistic Boltzmann-particles

The basic assumption of the relativistic kinetic theory is the equal a priori probabilities of equal cells $\delta v \delta \Omega$, where δv is the volume element which the tangential vectors of geodesics intersect orthogonally in the four-dimensional elementary solid angle $\delta \Omega$. The cell $\delta v \delta \Omega$ is invariant under general space-time coordinate transformations⁽⁶⁾. The statistical, special relativistic expressions of the energy density and the pressure first derived by F. JÜTTNER⁽⁷⁾ are then valid also in the general theory of relativity.*

In a relativistic Boltzmann-gas consisting of material particles of proper mass m , the following relations are valid⁽⁷⁾:

$$\left. \begin{aligned} E &= 3P + \frac{\gamma}{\tau} K_1(\tau) \\ P &= \frac{\gamma}{\tau^2} K_2(\tau) \end{aligned} \right\} \quad (31)$$

where we denote

* This is physically obvious, because the general relativistic effects are negligible in small distances of the mean free paths of particles.

$$\left. \begin{aligned} \tau &= \frac{mc^2}{kT} \\ \gamma &= 4\pi mc^2 \left(\frac{mc}{h} \right)^3 e^{\frac{\psi + mc^2}{kT}} \end{aligned} \right\} \quad (32)$$

Further, the functions $K_n(\tau)$ are modified Bessel functions of the second kind; k is the Boltzmann constant, h the Planck constant, T is temperature measured in the rest frame of the medium and ψ is the chemical potential. The expressions (31) are derived for thermal equilibrium, but they are also valid to a high degree of accuracy when the gas is close to equilibrium. We recall the definition of $K_n(\tau)$ ⁽⁸⁾

$$K_n(\tau) = \frac{\tau^n}{1 \cdot 3 \cdots (2n - 1)} \int_0^\infty e^{-\tau \cosh \xi} \sinh^{2n} \xi d\xi \quad (33)$$

and two recurrence relations for them

$$\left. \begin{aligned} nK_n(\tau) - \tau \frac{dK_n(\tau)}{d\tau} &= \tau K_{n+1}(\tau) \\ K_{n+1}(\tau) - K_{n-1}(\tau) &= \frac{2n}{\tau} K_n(\tau) \end{aligned} \right\} \quad (34)$$

For the quantity E_ξ we get from eqs. (28), (31) and (33) the expression

$$E_\xi = \gamma e^{-\tau \cosh \xi} \sinh^2 \xi \cosh^2 \xi \quad (35)$$

which, substituted in the first term of the right side of eq. (30), gives

$$\frac{1}{r} \int_0^\infty \frac{\sinh^2 \xi}{\cosh^2 \xi} E_\xi d\xi = \frac{\gamma}{r} \int_0^\infty e^{-\tau \cosh \xi} \sinh^4 \xi d\xi = \frac{3}{r} P. \quad (36)$$

By use of eqs. (31), (33), (34) and (36) we obtain from eq. (30)

$$\left. \begin{aligned} -\frac{\rho_0}{c} e^{\frac{\lambda}{2}} xH &= \frac{dP}{dr} + 2 \frac{d\mu}{dr} P + \frac{1}{2} \frac{d\mu}{dr} \frac{\gamma}{\tau} K_1(\tau) \\ &= \frac{K_2(\tau)}{\tau^2} \frac{d\gamma}{dr} + \frac{\gamma}{\tau^3} \left[\tau \frac{dK_2(\tau)}{d\tau} - 2K_2(\tau) \right] \frac{d\tau}{dr} + \frac{1}{2} \frac{d\mu}{dr} \frac{\gamma}{\tau} \left[\frac{4}{\tau} K_2(\tau) + K_1(\tau) \right] \\ &= \frac{K_2(\tau)}{\tau^2} \frac{d\gamma}{dr} + \frac{\gamma k}{mc^2} K_3(\tau) e^{-\frac{\mu}{2}} \frac{d\left(T e^{\frac{\mu}{2}} \right)}{dr} \end{aligned} \right\} \quad (37)$$

The expression of $\frac{d\gamma}{dr}$ can be written in the form

$$\frac{d\gamma}{dr} = -\frac{\gamma(\psi + mc^2)}{kT^2} e^{-\frac{\mu}{2}} \frac{d\left(Te^{\frac{\mu}{2}}\right)}{dr} + \frac{\gamma}{kT} e^{-\frac{\mu}{2}} \frac{d\left[(\psi + mc^2)e^{\frac{\mu}{2}}\right]}{dr} \quad (38)$$

which, substituted into eq. (37), yields the result

$$H = -\frac{\gamma k}{mc\rho_0 x} e^{-\frac{\lambda+\mu}{2}} \left\{ \left[K_3(\tau) - \left(1 + \frac{\psi}{mc^2}\right) K_2(\tau) \right] \frac{d\left(Te^{\frac{\mu}{2}}\right)}{dr} + \frac{T}{mc^2} K_2(\tau) \frac{d\left[(\psi + mc^2)e^{\frac{\mu}{2}}\right]}{dr} \right\}. \quad (39)$$

The radial energy flow has been separated into two parts to remove differences of relativistic thermal and chemical potentials in the gas. Because the chemical potential is also a function of the temperature and the density of the gas, the first term in eq. (39) is not the total expression of the heat flow, but the other term will give a contribution to it.

3B. Radial Energy Flow due to Bosons and Fermions

In the relativistic quantum statistics, the following relations are valid⁽⁹⁾:

$$\left. \begin{aligned} E_{\xi a} &= \cosh \xi u_a \\ P_{\xi a} &= \frac{1}{3} \frac{\sinh^2 \xi}{\cosh \xi} u_a, \end{aligned} \right\} \quad (40)$$

where the distribution function u_a is

$$\left. \begin{aligned} u_a &= \frac{\gamma_a \cosh \xi \sinh^2 \xi}{\exp\left[-\frac{\psi}{kT} + \tau(\cosh \xi - 1)\right] + \eta} \\ \gamma_a &= 4\pi mc^2 \left(\frac{mc}{h}\right)^3 \end{aligned} \right\} \quad (41)$$

and η is equal to +1 for Fermi-Dirac-gas and -1 for Bose-Einstein-gas.

Using eq. (25), we obtain from eq. (40)

$$\left. \begin{aligned} \frac{dP_{\xi a}}{dr} = & -\frac{1}{6} \frac{d\mu}{dr} \left(\frac{1}{\cosh \xi} + \cosh \xi \right) u_a - \frac{1}{6} \frac{d\mu}{dr} \sinh \xi \frac{\partial u_a}{\partial \xi} \\ & + \frac{1}{3} \frac{\sinh^2 \xi}{\cosh \xi} \left(\frac{\partial u_a}{\partial T} \frac{dT}{dr} + \frac{\partial u_a}{\partial \psi} \frac{d\psi}{dr} \right). \end{aligned} \right\} \quad (42)$$

Insertion from eqs. (40) and (42) into eq. (30) gives the equation

$$\left. \begin{aligned} -\frac{\rho_0}{c} e^{\frac{\lambda}{2}} x_a H_a = & \frac{1}{3} \frac{d\mu}{dr} \int_0^\infty \cosh \xi u_a d\xi - \frac{1}{6} \frac{d\mu}{dr} \int_0^\infty \sinh \xi \frac{\partial u_a}{\partial \xi} d\xi \\ & + \frac{1}{3} \int_0^\infty \frac{\sinh^2 \xi}{\cosh \xi} \left(\frac{\partial u_a}{\partial T} \frac{dT}{dr} + \frac{\partial u_a}{\partial \psi} \frac{d\psi}{dr} \right) d\xi + \frac{1}{6} \frac{d\mu}{dr} \int_0^\infty \frac{\sinh^2 \xi}{\cosh \xi} u_a d\xi. \end{aligned} \right\} \quad (43)$$

From eq. (41) we have for $\frac{\partial u_a}{\partial \xi}$ and $\frac{\partial u_a}{\partial T}$ the expressions:

$$\left. \begin{aligned} \frac{\partial u_a}{\partial \xi} = & -\frac{\tau \sinh \xi \exp \left[-\frac{\psi}{kT} + \tau(\cosh \xi - 1) \right]}{\exp \left[-\frac{\psi}{kT} + \tau(\cosh \xi - 1) \right] + \eta} u_a + \left(\frac{\sinh \xi}{\cosh \xi} + 2 \frac{\cosh \xi}{\sinh \xi} \right) u_a \\ \frac{\partial u_a}{\partial T} = & \frac{\tau}{T} \left(\cosh \xi - 1 - \frac{\psi}{mc^2} \right) \frac{\exp \left[-\frac{\psi}{kT} + \tau(\cosh \xi - 1) \right]}{\exp \left[-\frac{\psi}{kT} + \tau(\cosh \xi - 1) \right] + \eta} u_a. \end{aligned} \right\} \quad (44)$$

Substituting the expression

$$\left. \begin{aligned} \sinh \xi \frac{\partial u_a}{\partial \xi} + \frac{\sinh^2 \xi}{\cosh \xi} T \frac{\partial u_a}{\partial T} = & \left(\frac{\sinh^2 \xi}{\cosh \xi} + 2 \cosh \xi \right) u_a \\ - \frac{\left(\tau + \frac{\psi}{kT} \right) \exp \left[-\frac{\psi}{kT} + \tau(\cosh \xi - 1) \right]}{\exp \left[-\frac{\psi}{kT} + \tau(\cosh \xi - 1) \right] + \eta} \frac{\sinh^2 \xi}{\cosh \xi} u_a, \end{aligned} \right\} \quad (45)$$

obtained from eq. (44) into eq. (43), we get after grouping the terms

$$\begin{aligned}
 -\frac{\varrho_0}{c} e^{\frac{\lambda}{2}} x_a H_a &= \frac{1}{3} \left(\frac{dT}{dr} + \frac{T}{2} \frac{d\mu}{dr} \right) \int_0^\infty \frac{\sinh^2 \xi}{\cosh \xi} \frac{\partial u_a}{\partial T} d\xi \\
 + \frac{1}{3kT} \left[\frac{d\psi}{dr} + \frac{1}{2} (\psi + mc^2) \frac{d\mu}{dr} \right] &\int_0^\infty \frac{\exp \left[-\frac{\psi}{kT} + \tau(\cosh \xi - 1) \right]}{\exp \left[-\frac{\psi}{kT} + \tau(\cosh \xi - 1) \right] + \eta} \frac{\sinh^2 \xi}{\cosh \xi} u_a d\xi
 \end{aligned}$$

from which

$$\begin{aligned}
 H_a &= -\frac{c\gamma_a}{3} \frac{\tau e^{-\frac{\lambda+\mu}{2}}}{\varrho_0 T x_a} \left\{ \frac{d \left(T e^{\frac{\mu}{2}} \right)}{dr} \int_0^\infty \frac{\left(\cosh \xi - 1 - \frac{\psi}{mc^2} \right) \exp \left[-\frac{\psi}{kT} + \tau(\cosh \xi - 1) \right]}{\left(\exp \left[-\frac{\psi}{kT} + \tau(\cosh \xi - 1) \right] + \eta \right)^2} \sinh^4 \xi d\xi \right. \\
 &\quad \left. + \frac{T}{mc^2} \frac{d \left[(\psi + mc^2) e^{\frac{\mu}{2}} \right]}{dr} \int_0^\infty \frac{\exp \left[-\frac{\psi}{kT} + \tau(\cosh \xi - 1) \right]}{\left(\exp \left[-\frac{\psi}{kT} + \tau(\cosh \xi - 1) \right] + \eta \right)^2} \sinh^4 \xi d\xi \right\}. \quad (46)
 \end{aligned}$$

4A. Electronic Heat Conductivity

As an important special case of energy transfer by material particles we examine in this chapter the electronic heat conductivity. We limit ourselves to the case with energy flow due to ionization electrons which are interacting with a medium consisting of only one kind of nuclei of proper mass M and atomic number Z .

In order to obtain an expression of thermal conductivity from eq. (39) or eq. (46) we have to find a relation between the expressions $d[(\psi + mc^2)e^{\mu/2}]/dr$ and $d(Te^{\mu/2})/dr$. We regard the medium as a perfect fluid, whose energy-momentum tensor is given by

$$(T_0)_\alpha^\beta = \left(\varrho + \frac{p_0}{c^2} \right) u_\alpha u^\beta - g_\alpha^\beta \frac{p_0}{c^2}, \quad (47)$$

where ϱ is the total mass-energy density, p_0 is the pressure in the medium, and g_α^β are the components of the metric tensor.

From the covariant conservation law

$$\nabla \cdot T^0 = 0 \quad (48)$$

we have in the metric (2) the equation

$$\frac{1}{c^2} \frac{dp_0}{dr} + \frac{1}{2} \left(\varrho + \frac{p_0}{c^2} \right) \frac{d\mu}{dr} = 0. \quad (49)$$

The medium consisting of nuclei is a Boltzman-gas also when the electron gas is weakly degenerate. The equations of state are

$$\left. \begin{aligned} \varrho + \frac{p_0}{c^2} &= \frac{\gamma_0}{\tau_0} K_3(\tau_0) \\ p_0 &= \frac{\gamma_0 c^2}{\tau_0^2} K_2(\tau_0) = \frac{c^2}{\tau_0} \varrho_0, \end{aligned} \right\} \quad (50)$$

where we denote

$$\left. \begin{aligned} \gamma_0 &= 4\pi M \left(\frac{Mc}{h} \right)^3 e^{\frac{\psi_0 + Mc^2}{kT}} \\ \tau_0 &= \frac{Mc^2}{kT}. \end{aligned} \right\} \quad (51)$$

The chemical potential of nuclei is given⁽¹⁰⁾ by

$$e^{\frac{\psi_0}{kT}} = \left(\frac{h^2}{2\pi M k T} \right)^{3/2} \frac{\varrho_0}{M}. \quad (52)$$

Comparing this with

$$e^{\frac{\psi}{kT}} = \left(\frac{h^2}{2\pi m k T} \right)^{3/2} \frac{Z \varrho_0}{M}, \quad (53)$$

which is the expression of the chemical potential in a non-degenerate electron gas, we find the relation

$$\psi_0 = \psi - kT \log \left[\left(\frac{M}{m} \right)^{3/2} Z \right]. \quad (54)$$

Substituting the expressions (50) into eq. (49) and using the first eq. (34), we obtain

$$\frac{K_2(\tau_0)}{\tau_0^2} \frac{d\gamma_0}{dr} + \frac{\gamma_0 K_3(\tau_0)}{\tau_0 T} \frac{dT}{dr} + \frac{1}{2} \frac{\gamma_0 K_3(\tau_0)}{\tau_0} \frac{d\mu}{dr} = 0. \quad (55)$$

Using eqs. (51) and (54), we get from eq. (55) after simple calculations

$$= \left[\frac{\psi + mc^2}{T} - \frac{Mc^2}{T} \frac{K_3(\tau_0)}{K_2(\tau_0)} \frac{T \left(\frac{\partial \psi}{\partial T} + \frac{\partial \psi}{\partial \varrho_0} \frac{d\varrho_0}{dT} \right) - \psi - mc^2}{T \left(\frac{\partial \psi}{\partial T} + \frac{\partial \psi}{\partial \varrho_0} \frac{d\varrho_0}{dT} \right) - \psi - Mc^2} \right] \frac{d \left[(\psi + mc^2) e^{\frac{\mu}{2}} \right]}{dr}. \quad (56)$$

The quantity $\frac{d\varrho_0}{dT}$ can further be derived as a function of T and ϱ_0 . We obtain from eqs. (50) and (51) the expression

$$\frac{d\varrho_0}{dT} = \frac{T \frac{\partial \psi}{\partial T} - \psi - Mc^2 - kT + Mc^2 \frac{K_3(\tau_0)}{K_2(\tau_0)}}{T \left(\frac{Mc^2}{\gamma_0 K_2(\tau_0)} - \frac{\partial \psi}{\partial \varrho_0} \right)}. \quad (57)$$

Insertion of ψ from eq. (53) yields

$$\frac{d\varrho_0}{dT} = \frac{\left(\frac{K_3(\tau_0)}{K_2(\tau_0)} - 1 \right) \tau_0 - \frac{5}{2}}{T \left(\frac{\tau_0}{\gamma_0 K_2(\tau_0)} - \frac{1}{\varrho_0} \right)}. \quad (58)$$

Substituting eqs. (53) and (56) into eq. (39), the equation of the radial heat flow reduces to the form

$$H = -A \frac{d \left(T e^{\frac{\mu}{2}} \right)}{dr}, \quad (59)$$

where

$$A = \frac{4\pi km^3 c^4}{h^3 \varrho_0 x} e^{\frac{\psi + mc^2}{kT}} e^{-\frac{\lambda + \mu}{2}} \left. \begin{array}{l} \\ \\ \left[K_3 \left(\frac{mc^2}{kT} \right) - K_2 \left(\frac{mc^2}{kT} \right) \frac{MK_3 \left(\frac{Mc^2}{kT} \right)}{mK_2 \left(\frac{Mc^2}{kT} \right)} \frac{\left(\frac{T}{\varrho_0} \frac{d\varrho_0}{dT} - \frac{mc^2}{kT} - \frac{3}{2} \right)}{\left(\frac{T}{\varrho_0} \frac{d\varrho_0}{dT} - \frac{Mc^2}{kT} - \frac{3}{2} \right)} \right] \end{array} \right\} \quad (60)$$

is the expression of thermal conductivity of a non-degenerate electron gas.*

The chemical potential of a degenerate electron gas can be derived⁽¹⁰⁾ from the integral equation

$$F\left(\frac{\psi_d}{e^{kT}}\right) = \frac{4}{\pi^{\frac{1}{2}}} \int_0^\infty \frac{x^2 dx}{\exp\left(-\frac{\psi_d}{kT} + x^2\right) + 1} = \left(\frac{h^2}{2\pi mkT}\right)^{\frac{3}{2}} \frac{Z\varrho_0}{M}. \quad (61)$$

For small values of $e^{\psi_d/kT}$ we have the expansion

$$F\left(\frac{\psi_d}{e^{kT}}\right) = \frac{\psi_d}{e^{kT}} - \frac{2\psi_d}{2^{3/2}} + \frac{3\psi_d}{3^{3/2}} - \frac{4\psi_d}{4^{3/2}} + \dots \quad (62)$$

From eqs. (61) and (62) we obtain

$$\frac{\psi_d}{e^{kT}} = \left(\frac{h^2}{2\pi mkT}\right)^{3/2} \frac{Z\varrho_0}{M} + \frac{1}{2^{3/2}} \left(\frac{h^2}{2\pi mkT}\right)^3 \frac{Z^2 \varrho_0^2}{M^2} + \dots \quad (63)$$

Repeating the calculations from eq. (54) to eq. (60), using eq. (46) instead of eq. (39) and eq. (63) instead of eq. (53), we obtain the expression of heat flow due to a weakly degenerate electron gas

$$H_d = - \left\{ \frac{4\pi m^5 c^8 e^{-\frac{\lambda + \mu}{2}}}{3kh^3 \varrho_0 T^2 x_d} \int_0^\infty \frac{A_{\xi d} \exp\left[-\frac{\psi_d}{kT} + \frac{mc^2}{kT} (\cosh \xi - 1)\right]}{\exp\left[-\frac{\psi_d}{kT} + \frac{mc^2}{kT} (\cosh \xi - 1)\right] + 1} \right\} d\left(Te^{\frac{\mu}{2}}\right) \frac{dr}{dr}, \quad (64)$$

* The relativistic law of heat-diffusion (59), which agrees with the expression for the heat flow derived by C. ECKART⁽¹¹⁾, includes the gradient of the quantity $Te^{\mu/2}$ instead of the temperature gradient of the classical case. The dependence on the metrics is due to inertia of the heat. In the classical limit eq. (59) reduces to Fourier's law of heat conduction.

where we denote

$$A_{\xi d} = \frac{MK_3 \left(\frac{Mc^2}{kT} \right) \left[\left(\frac{T}{\varrho_0} \frac{d\varrho_0}{dT} - \frac{3}{2} \right) \frac{1 + \frac{1}{2^{1/2}} \left(\frac{h_2}{2\pi mkT} \right)^{3/2} \frac{Z\varrho_0}{M}}{1 + \frac{1}{2^{3/2}} \left(\frac{h^2}{2\pi mkT} \right)^{3/2} \frac{Z\varrho_0}{M}} - \frac{mc^2}{kT} \right]}{mK_2 \left(\frac{Mc^2}{kT} \right) \left(\frac{T}{\varrho_0} \frac{d\varrho_0}{dT} - \frac{3}{2} - \frac{Mc^2}{kT} \right) \cosh \xi - \sinh^4 \xi} \exp \left[-\frac{\psi_d}{kT} + \frac{mc^2}{kT} (\cosh \xi - 1) \right] + 1 \quad (65)$$

and $\frac{d\varrho_0}{dT}$ is the same function (58) of T and ϱ_0 as in the case of a non-degenerate electron gas.

From eqs. (59) and (64) we get as a special case of no net energy flow due to a non- or weakly degenerate electron gas the general law⁽¹²⁾

$$Te^{\frac{\mu}{kT}} = T\sqrt{g_{44}} = \text{constant} \quad (66)$$

for a relativistic fluid in thermal equilibrium.

The expressions of thermal conductivity of a semi- or strongly degenerate electron gas can be derived only with numerical methods.

4B. Radiative Energy Transfer and Neutrino Flux

The radiative energy transfer is obtained in the limiting case of the energy transfer by material particles. The calculations up to eq. (30) are valid for a photon gas, if the expressions $m \cosh \xi$ and $m \sinh \xi$ are changed to $h\nu/c^2$, where ν denotes the frequency in the rest-system defined by the vector U . Eq. (30) then takes the form

$$\frac{dP_f}{dr} = \left(\frac{1}{r} - \frac{1}{2} \frac{d\mu}{dr} \right) E_f - \frac{\varrho_0}{c} e^{\frac{\lambda}{2}} x_f H_f - \left(\frac{3}{r} + \frac{1}{2} \frac{d\mu}{dr} \right) P_f, \quad (67)$$

where the mean absorption coefficient of photons or the Rosseland mean opacity x_f is defined by

$$x_f H_f = \int_0^\infty x_\nu H_\nu d\nu. \quad (68)$$

Using the isotropic approximation

$$E_f = 3P_f = aT^4, \quad (69)$$

where a is the radiation pressure constant, we obtain from eq. (67) the equation of the radiative energy transfer

$$H_f = -\frac{acT^3}{3\rho_0 x_f} e^{-\frac{\lambda+\mu}{2}} \frac{d\left(Te^{\frac{\mu}{2}}\right)}{dr} \quad (70)$$

agreeing with the corresponding results in references 3 and 4.

We notice that the condition of no net radiation yields the same law (66) of thermal equilibrium as when the equilibrium is established by the thermal conductivity of electrons.

The energy transfer by neutrinos is obtained similarly as the radiative energy transfer, if one assumes almost isotropic neutrino distribution. The only modification which must be done is the change of the radiation constant to the constant $7/8a$, since the energy density of an isotropic neutrino gas is not aT^4 , but $7/8aT^4$ ⁽¹³⁾. Defining the mean absorption coefficient of neutrinos by

$$x_n H_n = \int_0^\infty x_{n\nu} H_{n\nu} d\nu, \quad (71)$$

we get the equation of the neutrino flux

$$H_n = -\frac{7acT^3}{6\rho_0 x_n} e^{-\frac{\lambda+\mu}{2}} \frac{d\left(Te^{\frac{\mu}{2}}\right)}{dr}. \quad (72)$$

Because the interactions of neutrinos and antineutrinos with matter are generally different, the Rosseland mean must be taken as the average of that for neutrinos x_n^+ and for antineutrinos x_n^- or⁽¹⁴⁾.

$$\frac{2}{x_n} = \frac{1}{x_n^+} + \frac{1}{x_n^-}. \quad (73)$$

Eq. (67), which has been derived using an isotropic approximation, can not be applied to the case of a purely radial outward-moving neutrino flow. A purely radial neutrino emission has been used by C. W. MISNER⁽¹⁵⁾ to describe a flux of neutrinos produced in the deep interior of a supernova.

5. Mean Absorption Coefficient

Eqs. (59), (64), (70) and (72) for the radial energy flow contain as a parameter the mean absorption coefficient derived in eq. (29) for material particles, in eq. (68) for photons and in eq. (71) for neutinos. In this section we give an approximative method for the calculation of this coefficient. The procedure is the same⁽¹⁶⁾ as in computing the Rosseland mean opacity from monocromatic absorption coefficients.

First we want to eliminate $\delta\xi$ from eq. (27). Since we are concerned with the radially symmetric and static case, we have from eqs. (3) and (4)

$$N \cdot \nabla \cosh \xi = e^{-\frac{\lambda}{2}} \cos \theta \frac{d(\cosh \xi)}{dr}. \quad (74)$$

Comparing eqs. (9) and (74), we find the relation

$$\frac{1}{\cosh \xi} \frac{d(\cosh \xi)}{dr} = -\frac{1}{2} \frac{d\mu}{dr}. \quad (75)$$

For another stream of particles having the same space-like direction N but a little different pseudo-angle ξ , eq. (75) can be applied in the form

$$\frac{1}{\cosh \xi + \delta(\cosh \xi)} \frac{d[\cosh \xi + \delta(\cosh \xi)]}{dr} = -\frac{1}{2} \frac{d\mu}{dr}. \quad (76)$$

Subtracting eq. (75) from eq. (76) and using eq. (25), we get

$$\frac{d(\delta\xi)}{dr} = \frac{1}{2} \frac{d\mu}{dr} \frac{\delta\xi}{\sinh^2 \xi}. \quad (77)$$

Elimination of $\delta\xi$ from eq. (27) by means of eq. (77) yields

$$\left. \begin{aligned} \frac{dP_\xi}{dr} &= \frac{1}{r} \frac{\sinh^2 \xi}{\cosh^2 \xi} E_\xi - \frac{1}{2} \frac{d\mu}{dr} E_\xi - \frac{\varrho_0 x_\xi}{c} e^{\frac{\lambda}{2}} \frac{\sinh \xi}{\cosh \xi} H_\xi \\ &\quad - \frac{1}{2} \frac{d\mu}{dr} \frac{\cosh^2 \xi}{\sinh^2 \xi} P_\xi - \frac{3}{r} P_\xi. \end{aligned} \right\} \quad (78)$$

Dividing this equation by $\frac{\sinh \xi}{\cosh \xi} x_\xi$ and integrating over the quantity ξ , we obtain

$$\left. \begin{aligned} -\frac{\varrho_0}{c} e^{\frac{\lambda}{2}} H &= -\frac{1}{r} \int_0^\infty \frac{\sinh \xi}{\cosh \xi} \frac{E_\xi}{x_\xi} d\xi + \frac{1}{2} \frac{d\mu}{dr} \int_0^\infty \frac{\cosh \xi}{\sinh \xi} \frac{E_\xi}{x_\xi} d\xi \\ + \int_0^\infty \frac{\cosh \xi}{\sinh \xi} \frac{1}{x_\xi} \frac{dP_\xi}{dr} d\xi &+ \frac{1}{2} \frac{d\mu}{dr} \int_0^\infty \frac{\cosh^3 \xi}{\sinh^3 \xi} \frac{P_\xi}{x_\xi} d\xi + \frac{3}{r} \int_0^\infty \frac{\cosh \xi}{\sinh \xi} \frac{P_\xi}{x_\xi} d\xi. \end{aligned} \right\} \quad (79)$$

We shall eliminate the quantities E_ξ and P_ξ from eq. (79) separately for a non- and weakly degenerate electron gas and for a photon and neutrino gas analogously to the calculations in chapter 3B.

5A. Mean Absorption Coefficient of Non- and Weakly Degenerate Electron Gas

From eqs. (28), (31), and (33) we obtain for a non-degenerate electron gas the relations

$$\left. \begin{aligned} E_\xi &= \cosh \xi u \\ P_\xi &= \frac{1}{3} \frac{\sinh^2 \xi}{\cosh \xi} u, \end{aligned} \right\} \quad (80)$$

where we denote

$$u = \gamma e^{-\tau \cosh \xi} \cosh \xi \sinh^2 \xi. \quad (81)$$

Using eq. (80) we can write eq. (79) in the form

$$\left. \begin{aligned} -\frac{\varrho_0}{c} e^{\frac{\lambda}{2}} H &= \frac{1}{3} \int_0^\infty \left(\frac{1}{\cosh \xi} + \cosh \xi \right) \frac{d\xi}{dr} \frac{u}{x_\xi} d\xi \\ + \frac{1}{3} \int_0^\infty \left(\frac{\partial u}{\partial \xi} \frac{d\xi}{dr} + \frac{\partial u}{\partial T} \frac{dT}{dr} + \frac{\partial u}{\partial \psi} \frac{d\psi}{dr} \right) \frac{\sinh \xi}{x_\xi} d\xi &+ \frac{2}{3} \frac{d\mu}{dr} \int_0^\infty \frac{\cosh^2 \xi}{\sinh \xi} \frac{u}{x_\xi} d\xi. \end{aligned} \right\} \quad (82)$$

Substitution of the expression

$$\sinh \xi \frac{\partial u}{\partial \xi} + \frac{\sinh^2 \xi}{\cosh \xi} T \frac{\partial u}{\partial T} = \frac{\sinh^2 \xi}{\cosh \xi} \left(1 - \tau - \frac{\psi}{kT} \right) u + 2 \cosh \xi u \quad (83)$$

into eq. (82) yields

$$\left. \begin{aligned} -\frac{\varrho_0}{c} e^{\frac{\lambda}{2}} H &= \frac{4}{3} \int_0^\infty \cosh \xi \frac{d\xi}{dr} \frac{u}{x_\xi} d\xi - \frac{1}{3} \left(\tau + \frac{\psi}{kT} \right) \int_0^\infty \frac{\sinh^2 \xi}{\cosh \xi} \frac{d\xi}{dr} \frac{u}{x_\xi} d\xi \\ &+ \frac{1}{3} \int_0^\infty \frac{\sinh \xi}{x_\xi} \frac{\partial u}{\partial \psi} \frac{d\psi}{dr} d\xi - \frac{1}{3} \int_0^\infty \left(\frac{\sinh^2 \xi}{\cosh \xi} T \frac{dT}{dr} - \sinh \xi \frac{dT}{dr} \right) \frac{\partial u}{\partial T} \frac{1}{x_\xi} d\xi \\ &+ \frac{2}{3} \frac{d\mu}{dr} \int_0^\infty \frac{\cosh^2 \xi}{\sinh \xi} \frac{u}{x_\xi} d\xi. \end{aligned} \right\} \quad (84)$$

Taking into account eq. (25), we obtain from eq. (84)

$$\left. \begin{aligned} -\frac{\varrho^0}{c} e^{\frac{\lambda}{2}} H &= \\ \frac{1}{3} e^{-\frac{\mu}{2}} \left\{ \frac{d \left(T e^{\frac{\mu}{2}} \right)}{dr} \int_0^\infty \frac{\sinh \xi}{x_\xi} \frac{\partial u}{\partial T} d\xi + \frac{1}{kT} \frac{d \left[(\psi + mc^2) e^{\frac{\mu}{2}} \right]}{dr} \int_0^\infty \frac{\sinh \xi}{x_\xi} u d\xi \right\}. \end{aligned} \right\} \quad (85)$$

Making insertion of $u, \frac{\partial u}{\partial T}$ and the relation (56) into eq. (84), and denoting

$$\left. \begin{aligned} A_\xi &= \frac{\cosh \xi - \frac{MK_3 \left(\frac{Mc^2}{kT} \right) \left(\frac{T}{\varrho_0} \frac{d\varrho_0}{dT} - \frac{3}{2} - \frac{mc^2}{kT} \right)}{mK_2 \left(\frac{Mc^2}{kT} \right) \left(\frac{T}{\varrho_0} \frac{d\varrho_0}{dT} - \frac{3}{2} - \frac{Mc^2}{kT} \right) \sinh^4 \xi, \\ &\exp \left[-\frac{\psi}{kT} + \frac{mc^2}{kT} (\cosh \xi - 1) \right] \end{aligned} \right\} \quad (86)$$

we finally get

$$H = - \left\{ \frac{4\pi m^5 c^8}{3kh^3 \varrho_0 T^2} e^{-\frac{\lambda + \mu}{2}} \int_0^\infty \frac{A_\xi \cosh \xi}{x_\xi \sinh \xi} d\xi \right\} \frac{d \left(T e^{\frac{\mu}{2}} \right)}{dr}. \quad (87)$$

Comparing eqs. (59) and (60) with eq. (87) we find the following expression for the mean absorption coefficient of a non-degenerate electron gas:

$$\frac{1}{x} = \frac{\frac{1}{3} \left(\frac{mc^2}{kT} \right)^2 \int_0^\infty \frac{A_\xi \cosh \xi}{x_\xi \sinh \xi} d\xi}{K_3 \left(\frac{mc^2}{kT} \right) - K_2 \left(\frac{mc^2}{kT} \right) \frac{MK_3 \left(\frac{Mc^2}{kT} \right) \left(\frac{T}{\varrho_0} \frac{d\varrho_0}{dT} - \frac{3}{2} - \frac{mc^2}{kT} \right)}{mK_2 \left(\frac{Mc^2}{kT} \right) \left(\frac{T}{\varrho_0} \frac{d\varrho_0}{dT} - \frac{3}{2} - \frac{Mc^2}{kT} \right)}. \quad (88)$$

The calculations for the mean absorption coefficient of a weakly degenerate electron gas are similar to the ones made above. We shall give only the final results. The equation of thermal conductivity of a weakly degenerate electron gas is

$$H_d = \left\{ \frac{4\pi m^5 c^8}{3kh^3 \varrho_0 T^2} e^{-\frac{\lambda + \mu}{2}} \int_0^\infty \frac{A_{\xi d} \exp \left[-\frac{\psi_d}{kT} + \frac{mc^2}{kT} (\cosh \xi - 1) \right]}{x_{\xi d} \left[\exp \left[-\frac{\psi_d}{kT} + \frac{mc^2}{kT} (\cosh \xi - 1) \right] + 1 \right]} \frac{\cosh \xi}{\sinh \xi} d\xi \right\} \frac{d \left(T e^{\frac{\mu}{2}} \right)}{dr}. \quad (89)$$

For the absorption coefficients $x_{\xi d}$ and x_ξ the following relation is valid⁽¹⁷⁾

$$x_{\xi d} = \bar{\eta} x_\xi = \left\{ 1 - \frac{1}{\exp \left[-\frac{\psi_d}{kT} + \frac{mc^2}{kT} (\cosh \xi - 1) \right] + 1} \right\} x_\xi, \quad (90)$$

where $\bar{\eta}$ is the probability that the final state after a scattering of an electron is free. Inserting eq. (90) into eq. (89), it reduces to the form

$$H_d = - \left\{ \frac{4\pi m^5 c^8}{3kh^3 \varrho_0 T^2} e^{-\frac{\lambda + \mu}{2}} \int_0^\infty \frac{A_{\xi d} \cosh \xi}{x_\xi \sinh \xi} d\xi \right\} \frac{d \left(T e^{\frac{\mu}{2}} \right)}{dr}. \quad (91)$$

The expression for the inverse value of the mean absorption coefficient for a weakly degenerate electron gas is

$$\frac{1}{x_d} = \frac{\int_0^{\infty} \frac{A_{\xi d}}{x_{\xi}} \frac{\cosh \xi}{\sinh \xi} d\xi}{\int_0^{\infty} A_{\xi d} d\xi}. \quad (92)$$

5B. Mean Absorption Coefficient of Photons and Neutrinos

The relativistic Rosseland mean opacity has been studied by K. A. HÄMEEN-ANTTILA⁽¹⁶⁾. For the sake of completeness, the calculation is now outlined starting from the theory of material particles. In the special case of $mc^2 \cosh \xi \rightarrow h\nu$ and $mc^2 \sinh \xi \rightarrow h\nu$, we obtain from eqs. (25) and (77) the corresponding relations

$$\frac{d\nu}{dr} = -\frac{1}{2} \frac{d\mu}{dr} \nu \quad (93)$$

$$\frac{d(\delta\nu)}{dr} = -\frac{1}{2} \frac{d\mu}{dr} \delta\nu. \quad (94)$$

With the quantities now measured per unit frequency interval, eq. (27) can be written in the form

$$\frac{d(P_{\nu} \delta\nu)}{dr} = \left(\frac{1}{r} - \frac{1}{2} \frac{d\mu}{dr} \right) E_{\nu} \delta\nu - \frac{\varrho_0}{c} e^{\frac{\lambda}{2}} x_{\nu} H_{\nu} \delta\nu - \left(\frac{3}{r} + \frac{1}{2} \frac{d\mu}{dr} \right) P_{\nu} d\nu. \quad (95)$$

Elimination of $\delta\nu$ by means of eq. (94) gives

$$\frac{dP_{\nu}}{dr} = \left(\frac{1}{r} - \frac{1}{2} \frac{d\mu}{dr} \right) E_{\nu} - \frac{\varrho_0}{c} e^{\frac{\lambda}{2}} x_{\nu} H_{\nu} - \frac{3}{r} P_{\nu}. \quad (96)$$

Dividing this equation by x_{ν} and integrating over ν , we get

$$-\frac{\varrho_0}{c} e^{\frac{\lambda}{2}} H_f = -\left(\frac{1}{r} - \frac{1}{2} \frac{d\mu}{dr} \right) \int_0^{\infty} \frac{E_{\nu}}{x_{\nu}} d\nu + \frac{3}{r} \int_0^{\infty} \frac{P_{\nu}}{x_{\nu}} d\nu + \int_0^{\infty} \frac{1}{x_{\nu}} \frac{dP_{\nu}}{dr} d\nu. \quad (97)$$

The classical laws of black body radiation

$$\left. \begin{aligned} E_\nu &= \frac{4\pi}{c} B_\nu \\ P_\nu &= \frac{4\pi}{3c} B_\nu \\ B_\nu &= \frac{2h\nu^3}{c^2} \frac{1}{\exp\left(\frac{h\nu}{kT}\right) - 1} \end{aligned} \right\} \quad (98)$$

can be calculated from eqs. (40) and (41) in the special case of photons, after putting ψ_a equal to zero and multiplying the expressions with 2 because of the polarization of photons. Insertion of eq. (98) into eq. (97) yields

$$-\frac{\varrho_0}{c} e^{\frac{\lambda}{2}} H_f = \frac{2\pi}{c} \frac{d\mu}{dr} \int_0^\infty \frac{B_\nu}{x_\nu} d\nu + \frac{4\pi}{c} \int_0^\infty \frac{1}{x_\nu} \left(\frac{\partial B_\nu}{\partial \nu} \frac{d\nu}{dr} + \frac{\partial B_\nu}{\partial T} \frac{dT}{dr} \right) d\nu. \quad (99)$$

Using eq. (93) and the expression

$$3B_\nu = \nu \frac{\partial B_\nu}{\partial \nu} + T \frac{\partial B_\nu}{\partial T}, \quad (100)$$

we get, after grouping the terms,

$$-\frac{\varrho_0}{c} e^{\frac{\lambda}{2}} H_f = \frac{\pi}{3c} e^{-\frac{\mu}{2}} \frac{d\left(Te^{\frac{\mu}{2}}\right)}{dr} \int_0^\infty \frac{1}{x_\nu} \frac{\partial B_\nu}{\partial T} d\nu. \quad (101)$$

Comparing eqs. (70) and (101), we find the following expression for the mean absorption coefficient of photons:

$$\frac{1}{x_f} = \frac{\pi}{acT^3} \int_0^\infty \frac{1}{x_\nu} \frac{\partial B_\nu}{\partial T} d\nu. \quad (102)$$

Differentiation of the expression for the total energy density of black body radiation

$$\frac{4\pi}{c} \int_0^{\infty} B_\nu d\nu = aT^4 \quad (103)$$

with respect to T and the insertion into eq. (102) gives another representation for $\frac{1}{x_f}$:

$$\frac{1}{x_f} = \frac{\int_0^{\infty} \frac{1}{x_\nu} \frac{\partial B_\nu}{\partial T} d\nu}{\int_0^{\infty} \frac{\partial B_\nu}{\partial T} d\nu}. \quad (104)$$

Eqs. (102) and (104) for the Rosseland mean opacity are just the same as in classical astrophysics⁽⁵⁾.

The mean absorption coefficient of neutrinos is obtained similarly as the Rosseland mean opacity by using Fermi-Dirac statistics instead of Bose-Einstein statistics. We get the expression

$$\frac{1}{x_n} = \frac{\int_0^{\infty} \frac{1}{x_{\nu n}} \frac{\partial B_{n\nu}}{\partial T} d\nu}{\int_0^{\infty} \frac{\partial B_{n\nu}}{\partial T} d\nu}, \quad (105)$$

where

$$B_{n\nu} = \frac{2h\nu^3}{c^2} \frac{1}{\exp\left(\frac{h\nu}{kT}\right) + 1} \quad (106)$$

is the Fermi-Dirac distribution function for massless particles.

Acknowledgment

The author wishes to thank Professor K. A. HÄMEEN-ANTTILA for suggesting the problem and for many helpful discussions. He is also much indebted to Professor C. W. MISNER and especially to Professor C. MØLLER for reading the manuscript and for valuable advice.

References

1. T. D. LEE, *Astrophys. J.* **111**, 625 (1950).
2. I. ROBINSON, A. SCHILD and E. L. SCHUCKING: *Quasi-Stellar Sources and Gravitational Collapse* (University of Chicago Press, Chicago, 1965).
3. K. A. HÄMEEN-ANTTILA and E. ANTTILA, *Ann. Acad. Sci. Fennicae, Ser. A. VI*, No 191 (1966).
4. R. W. LINDQUIST, *Ann. Phys.* **37**, 487 (1966).
5. S. ROSSELAND: *Theoretical Astrophysics* (Clarendon Press, Oxford, 1936), p. 110.
6. K. A. HÄMEEN-ANTTILA, *Ann. Acad. Sci. Fennicae, Ser. A. VI*, No 251 (1967).
7. F. JÜTTNER, *Ann. Phys. (Leipzig)* **34**, 856 (1911); **35**, 145 (1911).
8. G. N. WATTSON: *Theory of Bessel Functions*, (Cambridge University Press, London, 1958) pp. 76–77.
9. F. JÜTTNER, *Z. Phys.* **47**, 542 (1928).
10. K. HUANG: *Statistische Mechanik II* (Bibliographisches Institut, Mannheim, 1966), pp. 72, 100–103.
11. C. ECKART, *Phys. Rev.* **58**, 919 (1940).
12. R. C. TOLMAN: *Relativity, Thermodynamics and Cosmology* Clarendon Press, Oxford, 1962) p. 313.
13. L. D. LANDAU and E. M. LIFSHITZ: *Statistical Mechanics* (Pergamon Press, London, 1958), p. 326.
14. R. A. SCHWARTZ, *Ann. Phys.* **43**, 42 (1967).
15. C. W. MISNER, *Phys. Rev.* **137**, B 1360 (1965).
16. K. A. HÄMEEN-ANTTILA, *Ann. Acad. Sci. Fennicae, Ser. A. VI*, No 192 (1966).
17. D. H. SAMPSON, *Astrophys. J.* **129**, 734 (1959).

J. A. CHRISTIANSEN

SEVEN ESSAYS RELATING
TO THE STEREOCHEMISTRY OF
CYCLOHEXANE AND ITS VICINAL
DI-DERIVATIVES

Det Kongelige Danske Videnskabernes Selskab
Matematisk-fysiske Meddelelser **36**, 14



Kommissionær: Munksgaard
København 1968

CONTENTS

	Page
1. Introduction	3
2. The Configuration of Baeyer's Hexahydrogenated Phthalic Acids	5
3. On the Possibilities of Separation of Racemic Mixtures of Vicinal Derivatives of Cyclohexane with two Equal Substituents	8
4. Mohr's Assumption Concerning the Ease of Conversion of the Sachse Hexa- gon. Assignment of Configurations to Vicinal Cyclohexanediols	12
REFERENCES 1-4	15
5. Transition State and Work of Activation at the Inversion of the Sachse (Chair) Hexagon	16
REFERENCES 5	24
6. A Hypothesis on the Cause of Coalescence of Multiplets in NMR Spectra of Cyclohexane and Related Compounds at Increasing Temperatures	25
REFERENCES 6	28
7. Hypotheses on Tautomerism of Conformational Isomers of Vicinal Derivati- ves of Cyclohexane	29
REFERENCES 7	33

Introduction

The accepted assignment of configurations to vicinal *di*-derivatives of cyclohexane dates back to a renowned paper by WERNER and CONRAD (1899)¹. In the same paper the two authors believed to have decided the competition between BAEYER's² planar and SACHSE's^{3,4} puckered (chair-) form of cyclohexane in favour of the former.

About two decades later MOHR⁵ revived SACHSE's brilliant idea with the exception that he (M.) assumed the conversion of the two SACHSE-hexagons into each other to be fast. In that form SACHSE's idea has survived to the present day. However, if one scrutinizes WERNER and CONRAD's paper, it appears that they uncautiously replaced BAEYER's names from 1890² of the two isomers of his hexahydro phthalic acid, maleinoidic and fumaroidic, respectively by *cis*- and *trans*-. From BAEYER's paper it is clear that he chose his names to express that the maleinoidic isomer could easily be dehydrated and the fumaroidic one only with difficulty. BAEYER carefully uses these names throughout his paper and only once he mentions in passing *cis*- and *trans*-. But if, in a contest between BAEYER's and SACHSE's hexagons, one replaces maleinoidic and fumaroidic by *cis*- and *trans*-, one has already implied the validity of BAEYER's planar form because SACHSE's chair form permits a *cis*(*ea*) and a *trans*(*ee*) configuration in which the distances between the two sites are equal (in the ideal models) and small enough to permit the formation of a five-membered ring coupled to the six-membered one. The *trans*(*aa*) form can not be expected to react at all in that way. The fact is that WERNER and CONRAD found that the fumaroidic isomer of BAEYER's acids could be separated into optical antipodes while the maleinoidic could not. This is certainly not sufficient evidence to denote the former as *trans*- and the latter as *cis*-. But, if MOHR's assumption be accepted, the *cis*(*ea*) form must be a racemic equilibrium mixture of its two optical antipodes and the isomer which can be separated into enantiomers was believed to be a mixture of the two *trans*-forms.

When MOHR wrote his paper, it was impossible, for lack of experimental data, to estimate the work of activation for the conversion in question, which is necessary to prove or to disprove the validity of his assumption. This assumption differed radically from SACHSE's, which he (S.) admittedly arrived at by intuition, namely, that his chair-model, on account of mechanical resistances, was rigid. But, after the surge of papers on RAMAN and a little later on infrared spectra which began in the thirties, estimates became possible, at least in principle. The present author^{6, 7} has tried to perform such estimates, and his result is, that it is difficult, to say the least, to avoid the conclusion that SACHSE was right and MOHR wrong. Furthermore, a study of the conditions for the separability of the enantiomers by the method of diastereomers showed that the *cis*(ea) enantiomers must be much easier to separate than the *trans*(ee) and *trans*(aa) ones.⁸

Generally, all experiments known to the writer can, so far as he can see, more naturally be interpreted to mean that BAEYER's fumaroidic acid is *cis*(ea) and that the maleinoidic acid is *trans*(ee). Of course, different kinds of experiments have different weights, but in some of them the situation seems to be so clear, that the opposite assignment, the current one, cannot be maintained.

The whole problem has so many fascinating aspects that the writer has found it convenient for the reader and for himself to treat them separately in a number of essays. A group of such essays is published on the following pages.

2. The Configuration of Baeyer's Hexahydrogenated Phtalic Acids

In 1890 A. BAEYER² published an extensive paper in which he reported a great number of experimental results on the reduction products of phtalic acid obtained by his coworkers. In the same paper he presents his well known opinion that the hexahydrogenated benzene ring is plane, an opinion which most probably has been enhanced by his veneration for his old master KEKULÉ. Among many other facts BAEYER reports the discovery of two different hexahydrogenated phtalic acids, one melting between 182 and 192°C and another melting in the interval 215 to 221°C. The former loses water very easily, already just above the melting point. The latter, the isomer with the higher melting point, can be dehydrated, but only by use of a strongly dehydrating reagent. BAEYER's coworker whom he, as always, took great care to mention by name, used acetyl-chloride. Referring to the somewhat similar properties of maleic and fumaric acid he named them respectively maleinoid and fumaroid. Somewhere in the paper he mentions in passing the prefixes *cis* and *trans* but it is characteristic for BAEYER and his time that throughout the paper he speaks only about the maleinoidic and the fumaroidic acid, thus referring only to the factual properties of the two isomers and not to any hypotheses concerning their configuration as implied in the prefixes *cis* and *trans*.

In the same year, 1890, H. SACHSE published³ the first of his two renowned papers on the strainless carbon skeleton in alicyclic compounds, the most important examples being cyclohexane and its derivatives. The second one appeared⁴ in 1892, but SACHSE did not live to follow up his discovery of the strainless six-rings and to defend his ingenious ideas. He died in 1893, 31 years old. His first paper was abstracted in *Chemisches Centralblatt* by the organic chemist J. WAGNER. The abstract is short and, to say the least, very cool. The second paper was abstracted by W. NERNST who was the junior of SACHSE by two years. His abstract is longer and one gets the impression, that NERNST has seen the importance and the difficulties of SACHSE's model.

For example he emphasizes that SACHSE's model in contrast to BAEYER's permits two monosubstitutes of cyclohexane, while only one was (and is) known.

After that it seems that silence fell upon SACHSE's idea and BAEYER's plane model was generally accepted as true. However, in 1899 the problem was taken up by A. WERNER in cooperation with H. E. CONRAD¹. They believed to be able to settle the conflict between BAEYER's and SACHSE's views experimentally by using the following argument: If BAEYER is right, the *cis*-form of his hexahydro phthalic acid must be optically inactive and the *trans*-form active that is that isomer which can be separated into optical antipodes must be the *trans*-form. But if SACHSE is right it is the *cis* acid which has this property. (The two authors seem to have overlooked the fact that also the molecules of the *trans*-forms of BAEYER's acids are asymmetric if SACHSE's model (chair-form) is accepted). Now, what WERNER and CONRAD found was, that BAEYER's fumaroidic acid could be separated into optical antipodes and the maleinoidic not. But, unfortunately, they were less cautious than BAEYER and translated the latter's designations, which are free from hypotheses, into *trans*- and *cis*, expressions which refer to the middle plane of the molecule.

As well known a maleinoidic isomer of a dibasic acid must have the property of being able to loose water very easily, while the corresponding fumaroidic one looses water only with difficulty or not at all. When we say that the former has its two COOH groups near to each other and the latter far, or further, from each other, it is of course a hypothesis, but a hypothesis which is so well founded that its validity hardly can be doubted. If therefore we knew that BAEYER's planar form of cyclohexane were the right one we should certainly be justified in using WERNER's assignment of *cis*- and *trans*- to maleinoidic and fumaroidic respectively. But, unfortunately, according to SACHSE's (chair) model there are, at vicinal C-atoms, one pair of *cis*-positions but two pairs of *trans*-positions, one (*aa*) and one (*ee*) This complicates the assignment as the distance between the *cis*(*ea*) sites in the (ideal) SACHSE model is exactly the same as that between the *trans*(*ee*) ones. Consequently, when we identify maleinoidic with *cis*- and fumaroidic with *trans*- we imply the validity of BAEYER's model, which means that the two authors in their proof have assumed what they intended to prove. Today, however, we know, with a probability approaching certainty, that SACHSE's model is the right one, and by reverting WERNER and CONRAD's argument we might therefore draw the conclusion from their experiments, that it is BAEYER's fumaroidic acid which is *cis*-.

The difficulty is, however, that not only the *cis* form but also the two *trans* forms are asymmetric. But, as will be shown later, we must expect that the difference in solubility between diastereomers which have been formed from a pair of *cis* enantiomers will be much greater than that between diastereomers formed from a pair of *trans* enantiomers.

The two authors express the result of their experiments in a strikingly cautious way. On the second page of their paper they say: “. . . so spricht das Resultat, unter Berücksichtigung der positiven Ergebnisse bei der Transsäure, doch dafür, dass die Annahme stabiler räumlicher Lagerungen der Hexamethylenkohlenstoffe nicht sehr wahrscheinlich ist. “It must be remembered that “der Transsäure” means “der fumaroide Säure”. It is not quite evident what the authors mean by “stabile räumliche Lagerungen” but most probably the expression refers to the fact that SACHSE’s model in contrast to BAEYER’s is strainless.

One can only guess at the reason for this cautiousness, but it is certain, that contemporary chemists took WERNER and CONRAD’s experiments as a proof that BAEYER was right, and it seems also certain that nobody observed the flaw in the logic of their argument. The proof of the former statement is that MEYER and JACOBSEN in their renowned LEHRBUCH der Organischen Chemie, Zweiter Band, ERSTER TEIL (1902) p. 860 use BAEYER’s model and do not spend a single word on SACHSE’s. In contrast to this one finds in the same volume p. 63 a rather detailed description of SACHSE’s now nearly forgotten model of benzene. It may be mentioned in this connection, that it appears from articles in Chemiker Zeitung (1893) that professor MEYER highly venerated his deceased colleague and his work.

Before continuing the later history of SACHSE’s model we shall discuss the assignment of configurations (*cis*-, *trans*-) to BAEYER’s fumaroidic and maleinoidic hexahydrogenated phtalic acids by means of WERNER and CONRAD’S experiments from another point of view.

3. On the Possibilities of Separation of Racemic Mixtures of Vicinal Derivatives of Cyclohexane with two Equal Substituents

In stead of considering WERNER and CONRAD'S experiments from the viewpoint of the possibility of optical activity of BAEYER'S two acids one may discuss which of them may be expected to be best suited for separation by means of the difference in solubility in symmetric solvents, of their salts with an asymmetric base.

To investigate the conditions for the solubilities being different one must study the possibilities for interaction between the solvent molecules and those of the diastereomers.

In cyclohexane and its derivatives there are on the "surface" of the molecule twelve sites, namely 2×3 axial and 2×3 equatorial sites which are occupied either by hydrogen atoms or by substituents. In between there are twelve empty sites where solvent molecules may accommodate themselves. It must be such solvent molecules which mainly determine the interaction between the diastereomers and the solvent and therefore the solubility of the former in the latter.

Now, unfortunately, it is nearly impossible to illustrate the situation by means of drawings of the molecular models. In stead of that one must use some sort of projection from which the relative position of ligands and empty sites can be seen qualitatively. Table 1 represents a kind of "Mercator's Projection" in which the 24 empty and occupied sites are tabulated in four lines corresponding to the two groups of axial and two groups of equatorial sites, and in six columns corresponding to the six carbon atoms. It will be seen that there are around each ligand four empty sites, one above, one below, one to the left and one to the right. Now, an asymmetric ligand may be compared with a screw. As well known a screw has the property that its two ends are alike while there is a difference between its left and its right sides. This is true also for some kinds of asymmetric molecules, but for others there is only a qualitative and not an exact likeness between the two ends.

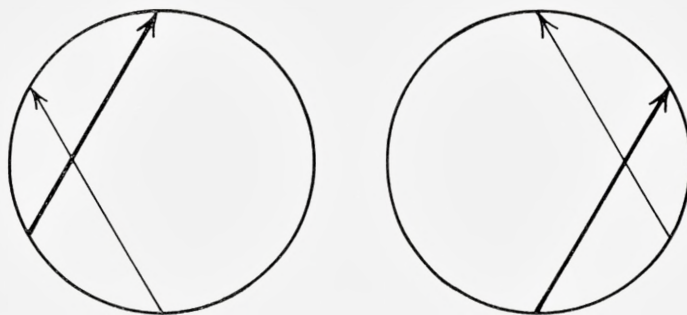


Fig. 1.

The figure to the left is meant to represent a fictive asymmetric molecule consisting of a regular cylinder provided with electrical permanent dipoles on both endfaces. Heavily drawn dipoles are meant to be nearest to the eye, if they are thinly drawn they are meant to be more distant. The "molecule" has the property of a lefthanded screw in so far as a screw-like motion of the upper dipole will cause its direction to coincide with that of the lower. The arrows point against the negative ends of the dipoles (by convention). When the translation is from the upper to the lower, end the rotation is to the left.

The figure to the right represents the same "molecule" turned through 180° around a vertical axis in the plane of the paper. It is seen that the negative ends of the two arrows point to the same side when the model is regarded, e.g. from the left, whether or not it is turned upside down. That it has the same screw-property seen from both ends is a matter of course.

For example, they may both contain dipoles, but the dipoles may be of different strength. However, the difference between the two sides is much more pronounced, as can be seen *e.g.* from fig. 1 where the left hand side is negative whether or not the model is turned upside down. If the upper and the lower ends of the asymmetric substituent are not equal, the two sites at the upper and the lower end of that substituent are not exactly equivalent, but the forces emanating from its two ends are still similar. They may for example both be dipole forces, which are not very different from each other. But the forces from the two sides, left and right, are qualitatively different and stronger than those from the ends. Consequently the difference between left and right around an asymmetric substituent is much more pronounced than that between above and below.

In the diagrams or "projections" Table 1 the empty sites are marked by asterisks and the asymmetric substituent is symbolized by the letter Z, because this letter has the same property in a plane as a screw has in space: it looks alike whether it is seen from below or from above, while there is a marked difference between sites which are to the left or to the right of it.

As the three isomers, *cis(ea)*, *trans(ee)* and *trans(aa)* are all asymmetric, the three corresponding pairs of diastereomers with a common asymmetric substituent cannot be equal that is, there must be differences between the

TABLE 1.

Vicinal Derivatives of the SACHSE Model of Cyclohexane With Two Equal Asymmetric Substituents

3 2 1 6 5 4 3	3 2 1 6 5 4 3
* * * * * *	* * * * * *
<i>a</i> * Z * H * H *	<i>a</i> * H * H * Z *
<i>e</i> H * Z * H * H	<i>e</i> H * H * Z * H
<i>e</i> * H * H * H *	<i>e</i> * H * H * H *
<i>a</i> H * H * H * H	<i>a</i> H * H * H * H
* * * * * *	* * * * * *
cis (<i>ea</i>)	
3 2 1 6 5 4 3	3 2 1 6 5 4 3
* * * * * *	* * * * * *
<i>a</i> * H * H * H *	<i>a</i> * H * H * H *
<i>e</i> H * Z * H * H	<i>e</i> H * H * Z * H
<i>e</i> * Z * H * H *	<i>e</i> * H * H * Z *
<i>a</i> H * H * H * H	<i>a</i> H * H * H * H
* * * * * *	* * * * * *
trans (<i>ee</i>)	
3 2 1 6 5 4 3	3 2 1 6 5 4 3
* * * * * *	* * * * * *
<i>a</i> * Z * H * H *	<i>a</i> * H * H * Z *
<i>e</i> H * H * H * H	<i>e</i> H * H * H * H
<i>e</i> * H * H * H *	<i>e</i> * H * H * H *
<i>a</i> H * Z * H * H	<i>a</i> H * H * Z * H
* * * * * *	* * * * * *
trans (<i>aa</i>)	

TABLE 2.

Empty Sites
in Diastereomers of Vicinal Disubstituted Cyclohexane

cis(<i>ea</i>)	
<i>a</i> 1 above Z(<i>e</i>), R	<i>a</i> 5 above Z(<i>e</i>), L
<i>e</i> 2 below Z(<i>a</i>), L	<i>e</i> 4 below Z(<i>a</i>), R
trans (<i>ee</i>)	
<i>e</i> 2 above Z(<i>e</i>), L	<i>e</i> 4 above Z(<i>e</i>), R
<i>e</i> 1 below Z(<i>e</i>), R	<i>e</i> 5 below Z(<i>e</i>), L
trans (<i>aa</i>)	
<i>a</i> 1 above H(<i>e</i>), R	<i>a</i> 5 above H(<i>e</i>), L
<i>a</i> 2 below H(<i>e</i>), L	<i>a</i> 4 below H(<i>e</i>), R

diastereomers in each pair. The question is in which pair the difference in solubility is most pronounced. Now, as the solubility must be determined mainly by the location of the empty sites, where solvent molecules may locate themselves, and as differences in solubility must be expected to arise mainly from differences in location of the empty sites which are nearest to the asymmetric substituents, we must try to enumerate these differences by means of the "projections". This has been done in table 2.

As will be seen, one of the diastereomers is to the left, and the corresponding one to the right. Inspection of table 1 shows that, only empty sites in lines containing the symbol Z are different from those in their diastereomers that is, there are, in each pair of diagrams, only two lines to consider. Each site is indicated by the character of its line, axial (*a*) or equatorial (*e*), followed by the number of its column, which is the same as the number of the carbon atom in question.

For each site there are in table 2 two entries. Concerning the first one *e.g.* "above Z(*e*)" means that the empty site in question is in the same column but above an equatorial asymmetric substituent Z.

Concerning the second entry, R means that the empty site in question is to the right of an asymmetric substituent in the same line and similarly to the left if the entry is L.

In the *cis(ea)* pair of diastereomers it is seen that all four entries are different in the two members of the pair. All these differences may be called major because of the decisive difference between equatorial and axial positions.

In the case of the *trans(ee)* isomer, the difference between the diastereomers is much less. As will be seen, the only difference between the sites *e2* and *e5* is that, one is above and the other one below an equatorial Z. Similarly, the only difference between *e1* and *e4* is, that the former is below and the latter above an equatorial Z. Thus there are in this case only two differences between the diastereomers, and these differences are, according to what was said before, much less pronounced than the four differences in the *cis* case.

In the *trans(aa)* case the difference between the diastereomers is still less: It must be immaterial whether the site in question is above or below a hydrogen atom. Therefore, if only sites which are neighbours to asymmetric substituents are taken into account there is no difference between the diastereomers. It is only when forces between an empty axial site in the lower half of the molecule and an axial asymmetric substituent in the same column but in the upper half are taken into account, that a difference can be assumed to exist. Such forces must however be very weak, and as the

situation concerning the empty axial site besides Z in the upper half of the molecule, is the same the difference between the *trans(aa)* diastereomers must be very small indeed.

In this way we arrive at the result that the difference in solubility of the diastereomers is much greater in the *cis(ea)*- than in the *trans(ee)*-case and that the difference in the latter case is again greater than that in the *trans(aa)*-case.

AS NOW WERNER and CONRAD succeeded in separating diastereomers of BAEYER's fumaroidic acid but were unable to separate diastereomers prepared from his maleinoidic acid, one can hardly avoid the conclusion that the former must be the *cis*-form and the latter one of the *trans*-forms, or a mixture of both. This is just the opposite of the result arrived at by the two authors, whose assignment of configurations to the two acids has been accepted by all chemists up till now.

4. Mohr's Assumption Concerning the Ease of Conversion of the Sachse Hexagon.

Assignment of Configurations to Vicinal Cyclohexanediols

After the commencement of the 20'th century silence fell again upon SACHSE's idea, and it was so late as in 1918 that MOHR⁵ saw the advantage of SACHSE's model as compared to BAEYER's, and his paper paved the road for its general acceptance by chemists. Many new chemical findings, most of them being due to W. HÜCKEL⁹ and his coworkers, gave more and more experimental support to the chair conformation of the SACHSE-hexagon until finally X-ray and electronic diffraction experiments provided us with practically certain proofs of its validity. As one of the leaders, or as the leader, of the latter kind of experimental work O. HASSEL¹⁰ (Oslo) should be mentioned, so much more as a great part of the work in his laboratory was carried out under the extremely difficult conditions prevailing in Norway during world war II.

Nevertheless, a fate of misunderstanding or of missing appreciation of the strength of SACHSE's arguments seemed still to cling to his fundamental work.

In the two papers^{3,4}, particularly in the one from 1892, SACHSE emphasizes that strong mechanical forces (due to the deformation of valency angles) must resist the conversion ("Version" as proposed by SACHSE) of one of the chair forms into the other one and also the conversion of a boat form into

the chair form and *vice versa*. To get an explanation of the circumstance which was at that time considered to be a fact, that the SACHSE model gave room for too many isomers, MOHR⁵ simply reversed SACHSE's statement and assumed that the conversions in question could easily take place. MOHR seems to have been under the impression, that the only or at least the main forces which tend to hinder the said conversions are those arising from rotations around single bonds. This is certainly not true, as angular deformations must give an essential contribution to what we nowadays may denote as the work of activation. In this connection it may be of interest to note that SACHSE's first paper appeared only about one year after ARRHENIUS's¹¹ renowned work on the dependence of the velocity of chemical reactions on temperature, the paper in which the concept energy of activation is introduced. The present author has tried to calculate the work of activation for the conversion of the two chair forms into each other, as a sum of two contributions one from the rotations around single valence bonds and one from the deformation of valency angles^{6,7}. He arrived at the result, that the work in question was large enough to prevent, practically speaking, the conversion at not extremely high temperatures. However, after the publication of MOHR's paper, chemists accepted his assumption of easy conversion without further discussion.

Today, when one looks back at the situation in 1918 it seems a little surprising that MOHR was so convinced that SACHSE's model permitted too many isomers. The background for this remark is the following: Originally two and only two isomers of 1,2 cyclohexanediol were known, one which melted at 99°C and one with m.p. 104°C. But in 1908 SABATIER with his coworker MAILHE¹² tried his method of catalytic hydrogenation on catechol and obtained an isomer of vicinal cyclohexanediol with m.p. 75°C. It is true that H. LEROUX¹³ two years later reported that the low melting isomer could be formed by dissolving the two higher melting ones and evaporation, from which he concluded that the former was a chemical combination of the two latter.

However, LEROUX's report, which may have released a sigh of relief from contemporary chemists, is contained in a few lines which are part of a comprehensive paper on hydrogenation products of naphthalene- β -diols. In this paper he describes three isomers which he denotes as *cis*-naphtanediol- β (m.p. 160°C), *cis-trans* naphtanediol- β (m.p. 141°C) and (*cis* + *cis-trans*) naphtanediol- β (m.p. 125°C). The latter can be formed by mixing solutions of the two higher melting isomers and evaporating, and LEROUX emphasizes that it cannot be fractionated back into the two others. He considers it to be

a compound of the two, notwithstanding the fact that a determination of the molecular weight gave him 177 g/mol (calculated for a single molecule 170 g/mol). He does not report any m.w. determination of the low melting cyclohexane diol. These results may not prove with certainty the existence of the three isomers permitted by the SACHSE models, but much less do they prove the non-existence of a third isomer.

It is thus seen that in the case of the cyclohexanediol the number of isomers may agree with that predicted by the SACHSE model.

As mentioned in the foregoing, two vicinal cyclohexane diols have been known for a long time, one with the melting point 104°C and another with melting point 99°C. The former can be separated into optical antipodes and the latter not.¹⁴

On this basis the 104° diol has been believed to be the *trans*-form and the other one the *cis*-form. The argument for this assignment is the following: According to MOHR'S hypothesis the conversion of the SACHSE hexagon takes place very easily and it is therefore impossible to separate the two enantiomeric *cis*-forms from each other, as they are transformed into each other by the conversion of the SACHSE hexagon, in other words the lower melting diol should be a racemic *cis*-mixture. On the other hand, by the same conversion one of the two *trans*-forms must be transformed into the other one, or, in other words, the *trans*-form is an equilibrium mixture of *trans*(aa) and *trans*(ee), both of which are asymmetric and therefore separable into optical antipodes.

According to the considerations in the foregoing paragraphs this is improbable and, apart from that, it is seen that the whole argument rests on the validity of MOHR'S assumption, that the work of activation for the conversion in question is small and the conversion therefore rapid. The validity of this assumption has been discussed by the writer in a note⁶ and the result was that the work of activation must be rather high and the conversion therefore slow. Consequently conversion of the Sachse (chair) hexagon does not prevent the separation of the two enantiomeric *cis*-forms.

In consideration of the importance of the question of the work of activation it will be discussed in more detail in the next essay.

References to Essays 1-4

1. WERNER, A., and CONRAD, H. E., Ber. **32**. (1899) 3046.
2. BAEYER, A., Ann. d. Chem. **258** (1890) 145.
3. SACHSE, H., Ber. **23** (1890) 1363.
4. SACHSE, H., Z. physik. Chem. **10** (1892) 228.
5. MOHR, E., J. prakt. Chem. **98** (1918) 315.
6. CHRISTIANSEN, J. A., Nature **211** (1966) 184.
7. Same author, Danske Vids. Selsk.
8. Same author, Danske Vids. Selsk.
9. W. HÜCKEL. Theoretische Grundlagen der organischen Chemie, Leipzig, Erste Auflage (1931) and later editions.
10. O. HASSEL and coworkers. Acta Chemica Scandinavica Vol. **1** (1947) with references to earlier publications.
11. ARRHENIUS, SV., Z. physik. Chem. **4** (1889) 226.
12. SABATIER, P., and MAILHE, C. R. **146** (1908) 1154.
13. LEROUX, H. Ann. de chim. et de phys. 8^{ieme} ser. **21** (1910) 541.
14. BÖESEKEN, J., VAN GIFFEN, J., and DERX, Rec. trav. chim. **39** (1920) 183.

5. Transition State and Work of Activation at the Inversion of the Sachse (Chair) Hexagon

For reasons mentioned in a note in *NATURE* it is assumed that all intermediates between the two Sachse (chair) hexagons can be inscribed on the surface of a regular hexagonal prism, and that their angles and their sides are all equal, the sides being constant in length. Consequently the transition form is assumed to be BAEYER's planar regular hexagon. The work of activation for the inversion ("Version" as SACHSE named it) of one of the SACHSE (chair) forms into the other one is then calculated, *a.* at 176.2 kJ/mol (directly from the frequency 384.1 cm^{-1} in the Raman spectrum of cyclohexane) and *b.* at about 173 kJ/mol (indirectly by adding 101.4 kJ/mol calculated from the methane frequency 1520 cm^{-1} to six times PITZER's maximum for the work of twisting the C-C bond in ethane. This means that SACHSE was right when he intuitively deemed it to be difficult or impossible to invert his puckered hexagon, the reason being mechanical resistances.

In a note in *Nature*¹ it was pointed out that it is hardly possible to avoid the conclusion that the transition state between the two (congruent) forms of SACHSE's (chair) model^{2,3} of cyclohexane must be BAEYER's planar model of the same substance. When this is taken for granted the work of activation for the conversion of one of the two forms into the other one can be calculated by classical mechanics.

It is assumed that the molecule behaves as a system of atoms bound to each other by bonds of constant length, so that only the deformation of the bond angles determine the potential energy of the molecule in a given configuration.

When BAEYER's "Spannungshypothese" is taken into account, it is seen that the two SACHSE forms are at minima of the potential energy and therefore stable. They are separated by the BAEYER form which is at a maximum and

unstable. The difference between the two extreme values of the potential energy must then be the required work of activation.

From the standpoint of quantum theory it might be argued that this difference must be the difference between two "eigenvalues" of the energy of the molecule. But this is not so certain as it sounds. Many years ago the present writer and H. A. KRAMERS wrote a paper on chemical kinetics⁴. In this paper KRAMERS pointed out that the active state (as it was called at that time) might not be a state in the quantum-theoretical sense of the word.

A few years later J. FRANCK⁵ drew attention to a phenomenon observed by V. HENRI⁶ who named it "Prädissociation". HENRI observed that lines in a band spectrum often became diffuse and the more so the shorter their wavelength. He interpreted the phenomenon as a beginning dissociation, a predissociation.

FRANCK explained the phenomenon by means of potential curves, corresponding to the force-field which produced the vibrations in question. FRANCK's theory is described *e.g.* in the book of his coworker H. SPONER⁵: *Molekulspektren und ihre Anwendung auf chemische Probleme* vol. II. In the meantime HEISENBERG's uncertainty relation had come to light and following FRANCK, SPONER uses this to connect the breadth of the diffuse lines with the life-time of at least one of the two states involved in the quantum-jump in question. As the life of the transition state must be very short indeed its state must be very ill defined. This is the same result as that maintained by KRAMERS several years before the advent of quantum-mechanics. It is clear that this uncertainty in the quantum mechanical definition of the transition state prevents a contradiction between that and the classical mechanical one, Consequently it must be permissible to calculate the work of activation in the classical way.

Calculation of the work of activation in the SACHSE hexagon.

We consider a particle of mass m which is located relative to the rest of the molecule at a certain equilibrium position. Let the displacement of the particle in a certain direction from the equilibrium position be x . Assuming the validity of HOOKE's law the force in the x direction will then be

$$F_x = - Dx \tag{1}$$

where D is the restoring force at unit displacement of the particle in the direction considered. We have from the law of motion

$$m(d^2/dt^2)x = - Dx \tag{2}$$

(2) describes a vibration with frequency ν connected to D by the equation

$$m(2\pi\nu)^2 = D. \quad (3)$$

Thus, if m is known and the frequency ν has been measured, D can be calculated. Furthermore, if z is the displacement in a direction which is perpendicular to that of x and the force constant D is independent of the direction, the force in the z direction becomes

$$F_z = - Dz. \quad (4)$$

If the forces from (1) and (4) are the only ones which act on the particle its potential energy V is given by

$$2V = D(x^2 + z^2). \quad (5)$$

Now, in the chair form of the SACHSE model of cyclohexane the six carbon nuclei are at the corners of what might be called a quasiregular hexagon, meaning a hexagon in which all the sides and all the angles are equal and which can be inscribed on the surface of a regular hexagonal prism. If the angles are equal to the tetrahedral angle

$$\omega = \arccos(-1/3) \quad (6)$$

the hexagon will, according to BAEYER's hypothesis, be strainless, but it is strained at all other values of the angle. The arguments in the note referred to above make it natural or even necessary to assume that also the strained forms of the hexagon have the property of being quasiregular.

If this be granted there is only one deviation from the tetrahedral angle to take into account, but this is not the only stress which contributes to the restoring force represented by D .

Years ago PITZER^{7,8} showed that there is in ethane a difference between the potential energies of the molecule in the two positions named "eclipsed" and "staggered" of the pair of valency triades. PITZER estimated this difference at about 3 kcal or about 12 kJ. If therefore we calculate D from the RAMAN spectrum of cyclohexane (the vibration in question is inactive in the IR-spectrum) we have already included both kinds of stress in our calculations. This was pointed out by LANGSETH and BAK⁹ in their paper on the RAMAN spectra of cyclohexane and some deuterated cyclohexanes. However, for the application of the spectra to the determination of the restoring force it is unfortunate that neither LANGSETH and BAK nor other investigators of the cyclohexane spectrum have assigned types of vibrations to the different,

surprisingly few, RAMAN lines. For the calculation of the work of activation relating to the transition from one chair form of the SACHSE hexagon into the other one we are interested in that type of vibrations during which the hexagon remains quasiregular.

We shall assume that the RAMAN frequency to be assigned to that type of vibration is 384.1 cm^{-1} , the lowest one found by LANGSETH and BAK in their investigation, and in agreement with that found by a number of other authors. By comparison with their tables of RAMAN lines in the spectra of deuterated cyclohexanes it can be concluded with certainty that there are no lines with lower RAMAN shifts than the one at 384.1 cm^{-1} hidden in the strong light from the exciting mercury line. That the assignment is correct is admittedly a guess, but it is a guess which yields the lowest possible value of the work of activation which is compatible with the RAMAN spectrum.

The numerical value of D is to be calculated from (3). For this calculation the value of m is needed. We may at once replace m for one molecule by the molar mass. However, the vibrational movement of the molecule is more complicated than that on which equation (3) is based, and it is therefore not so easy to assign a certain value to m , but as a crude approximation it may be assumed that the CH^2 group vibrates as an entirety, and that its entire mass is located in the carbon nucleus. Using this approximation we get the value of D by putting m equal to 14 g. This and the wave number 384.1 molar from LANGSETH and BAK's paper yields, by insertion in (3),

$$D = 7.332 \times 10^{28} \text{ g/s}^2. \quad (7)$$

Fig. 2 is intended to illustrate the calculations of the displacements x and z which are the same for all six CH^2 groups.

It shows the regular hexagonal prism on whose surface the quasiregular hexagon is inscribed, the prism being viewed from the side. Its upper end face contains the three uppermost corners of the hexagon and the lower endface the three other ones. The height of the prism may be denoted by h and its largest radius by r . If a is the side length of the SACHSE hexagon we then get

$$r = a\sqrt{2(1 - \cos\omega)}/3 \quad (8)$$

$$h = a\sqrt{(1 + 2\cos\omega)}/3. \quad (9)$$

From (8) and (9) we get in the first approximation for the displacements x and z caused by the deformation α of the angle ω

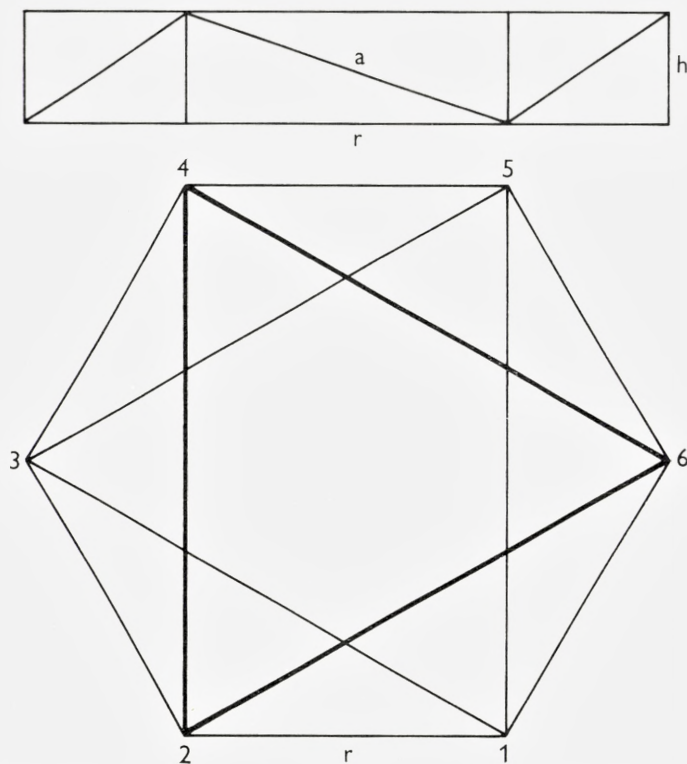


Fig. 2.

The drawing shows a regular hexagonal prism, with a SACHSE hexagon inscribed on its surface, in horizontal and in vertical projection respectively. The C-atoms in the corners are numerated as usual in hydrocarbon-chemistry but with C_6 in stead of O_5 . The height of the prism is $a/3$ if a is the length of the side in the SACHSE-hexagon. The length of the side of the hexagon in vertical projection is then $2a\sqrt{2}/3$. The triangle drawn with thick lines connects the three uppermost C-atoms, 6, 2, and 4, and the one drawn thinly connects the three lower ones. The triangles are helpful in visualizing the possible ways in which the SACHSE-hexagon can be deformed.

$$x = \alpha(d/d\omega)r \quad (10)$$

and

$$z = \alpha(d/d\omega)h \quad (11)$$

In connection with (11) it must be remembered that a certain decrease of the six tetrahedral angles displaces the upper endface of the prism upwards by a certain amount and its lower endface downwards by the same amount. Consequently the six radial and the six axial displacements will cancel each other and there will result neither a displacement of the center of gravity

nor a rotation of the SACHSE hexagon, conditions which necessarily must be fulfilled for any permitted type of internal motion of the molecule.

Insertion of $\omega = \arccos(-1/3)$ in (10) and (11) yields

$$x^2 = a^2\alpha^2/9 \quad (12)$$

and

$$z^2 = 8a^2\alpha^2/9. \quad (13)$$

Consequently

$$2V = A\alpha^2 \quad (14)$$

where

$$A = Da^2. \quad (15)$$

From many sources it is known that a , the C-C distance, is very nearly $1.54 \cdot 10^{-8}$ cm. Insertion of this and (7) in (15) yields

$$A = 1739 \text{ kJ/radian}^2 \quad (16)$$

for one "mol of angles".

If α is taken to be the difference between 120° and the tetrahedral angle

$$\alpha = 0.1838 \text{ radian}. \quad (17)$$

Insertion of (16) and (17) in (14) yields

$$2V = 58.72 \text{ kJ} \quad (18)$$

where V is the work required to increase one angle from the tetrahedral value to 120° plus the work required to twist one pair of valency triades from its most favorable into its least favorable position. For the total work of activation of the SACHSE hexagon G^* we thus get

$$G^* = 6V = 176.2 \text{ kJ/mol}. \quad (19)$$

When it is remembered that RT at 300°K equals 2.5 kJ/mol it is seen that the conversion of the hexagon must be extremely slow at ordinary temperatures. This disagrees completely with the assumption originally introduced by MOHR, that the conversion is fast enough to make the two states tautomeric whenever they have been made different by substitution of at least one of the twelve hydrogen atoms by some other atom or radical. Even today MOHR's assumption is generally accepted and it is therefore desirable or necessary to look for other ways of calculating G^* .

It is evidently the force constant which measures the angular restoring force of the aliphatic C-C-C angle which is decisive. Let the force constant

be denoted by B . As the C–C and the C–H bonds are both two-electronic we may expect them to have about the same “stiffness” or about the same B . Now, according to H. SPONER¹⁰ there is in methane a vibration with the wave number 1520 cm^{-1} which she ascribes to a synchronous vibration of the four C–H bonds of such a kind that they do not effect the position of the carbon nucleus. She gives the distance C–H at $1.1\ 10^{-8}\text{ cm}$.

With $m = 1.008\text{ g/mol}$ we get from (3) and (15)

$$D = 8.266\ 10^{28}\text{ g/s}^2 \quad (20)$$

and

$$B = 1001\text{ kJ/mol rad}^2. \quad (21)$$

With these values we get for the work of distortion of six angles through 0.1838 radian

$$6V = 101.40\text{ kJ/mol} \quad (22)$$

To get the work of activation in question we must add to this about 72 kJ/mol which is the work required to twist six pairs of valency triades from the staggered into the eclipsed position. In this way we get

$$G^* = 173.4\text{ kJ/mol} \quad (23)$$

On account of the different approximations which we have used the close agreement between the results (23) and (19) may be fortuitous but so much seems to be certain that the conversion in question must be very slow indeed. Qualitatively the same result was arrived at in the authors note in *Nature*¹ but quantitatively there is a marked difference. In the note, WESTHEIMER's¹¹ value $8 \times 10^{-12}\text{ erg/radian}^2$ was used for the *molecular* constant A in (14). This lead to the the value 48.84 kJ for the *molar* value of $6V$, which is a little less than half of that from (22). WESTHEIMER's value is nearly identical with that given by KAARSEMAKER and COOPS¹² who have $7.97\ 10^{-12}\text{ erg/rad}^2$ molecule.

For this value they refer to T. P. WILSON's paper¹³ on the IR and RAMAN spectra of cyclobutane. From his spectra WILSON has calculated a number of force constants which are tabulated in his Table V. Among these constants is a constant f_γ which relates to deviations from the C–C–C angle (90°). The table gives for this constant $0.767\ 10^{-11}\text{ erg/radian}^2$, but it has a footnote saying: “The interaction constants given here are taken from matrix expressions for the potential energy. For use in the quadratic form of this quantity they should be multiplied by 2”. It is not clear to the present author whether

or not the footnote means that, when the potential energy V is given by $2V = A\gamma^2$, A should equal $2f_\gamma$. If that is so the difference between the value of V derived from the spectra of cyclohexane and methane on one side and that derived from the cyclobutane spectrum on the other side would practically disappear.

At any rate, all three ways of calculating the activation potential lead qualitatively to the same result, that SACHSE was right when he maintained, by intuition, that the inversion in question ("Version" as he named it), on account of mechanical resistances, does not take place. This however leaves us with the necessity to explain the old puzzle, why fewer isomers of substituted cyclohexanes have been found than are permitted by the model.

Post Scriptum

Some months ago ANET and BOURN¹⁴ objected against my note in *Nature* that I had not taken a paper by K. S. PITZER and coworkers¹⁵ into account. These authors calculated the height of the potential barrier between a SACHSE chair form and one of the boat forms of cyclohexane at about 14 kcal/mol. They based this calculation on the existence of a line at 231 cm^{-1} in the spectrum of the substance in question. They state, however, that a line of this frequency had been found, neither in the infrared nor in the RAMAN spectrum and that it "was selected to fit the experimental entropy of cyclohexane". To the present writer this seems to be an insecure foundation on which to build far reaching conclusions. Furthermore, I am in agreement with PITZER and coworkers when, in the foregoing, I have assigned the RAMAN frequency at 384.1 cm^{-1} (PITZER has 382 cm^{-1}) to a motion leading from one chair conformation through the BAEYER planar form to the other chairform. If that be accepted, there are in the motion six angular strains acting on six C-atoms. On the other hand, in the motion to which PITZER and coworkers assign the frequency 231 cm^{-1} there are two angular strains acting on one C-atom. To me this would suggest that the latter type of motion corresponds to a vibration whose frequency is greater and not less than that of the former. The present writer, therefore, does not believe that his calculations can be upset by PITZER and coworkers considerations.

References

1. CHRISTIANSEN, J. A., *Nature* **211**, (1966) 184.
2. SACHSE, H., *Ber.* **23**, (1890) 1363.
3. SACHSE, H. *Z. physik. Chem.* **10**, (1892) 203.
4. CHRISTIANSEN, J. A., and KRAMERS, H. A. *Z. physik. Chem.* **104**, (1923) 451.
5. SPONER, H. *Molekülspektren und ihre Anwendung auf chemische Probleme*. II. J. Springer, Berlin (1936).
6. HENRI, V., and TEVES, M. C. *Nature* **114**, (1924) 894.
7. PITZER, K. S., *Science* **101**, (1945) 672.
8. PITZER, K. S. *Discussions, Faraday Society* **10**, (1951) 66.
9. LANGSETH, A., and BAK, B., *J. Chem. Physics* **8**, (1940) 403.
10. SPONER, H., Ref. 5. vol. I. Tabelle 13. p. 82.
11. WESTHEIMER, F. H. in *Steric Effects in Organic Chemistry* edit. by Newman, M. S. (1956) 533.
12. KAARSEMAKER, S., and COOPS, J. *Rec. Trav. chim.* **71**, (1952) 261.
13. WILSON, T. P. *J. Chem. Physics.* **11**, (1943) 369.
14. ANET, F. A. L., and BOURN, A. J. R. *J. Amer. Chem. Soc.* **89**, (1967) 760.
15. BECKETT, C. W., PITZER, K. S., and PITZER, R. *J. Amer. Chem. Soc.* **69**, (1947) 2488.

6. A Hypothesis on the Cause of Coalescence of Multiplets in NMR Spectra of Cyclohexane and Related Compounds at Increasing Temperatures

It is assumed that the coalescence of signals due to equatorial and axial protons is caused by the onset at higher temperatures of angular vibrations of the C-H bonds. Calculations based on the HERZFELD-EYRING expression for the rate constant of unimolecular reactions at the coalescence temperatures of $C_6D_{11}H$ and $C_5H_{10}O$ agree with this assumption.

The generally accepted explanation of the well known phenomenon of coalescence at increasing temperatures, of doublets or multiplets in the n.m.r. spectrum of cyclohexane into a singlet is that the interconversion of the two SACHSE chair forms of that compound becomes so fast at the coalescence temperature that the slightly different signals from the axial and the equatorial protons merge into one. To the writers knowledge however, it has never been proved that this conversion is the only possible cause of the coalescence. If it were, there would be a hopeless clash between the work of activation calculated from optical spectra on one side and that calculated from from the n.m.r. spectra on the other side.^{1,2}

Now, it is well known that vibrations of not too low frequency are "frozen" at low temperatures and may be "thawed" at higher ones. It is also known that C-H bonds, *e.g.* in cyclohexane, perform angular vibrations whose frequency can be read from the optical (infrared or RAMAN-) spectra of the compound in question. The protons bound to the C-atoms behave like spinning tops and in classical physics one should say, that they perform a precessing motion, when they are placed in the magnetic field of the n.m.r. spectrograph. In the language of quantum mechanics somewhat different expressions are used but the difference is so small that the writer may be permitted to use the older language. The precession is a motion in which the axis of the spinning proton performs a conical motion whose frequency depends on the strength of the magnetic field.

At available field strengths it is so low that it can come into resonance with radio waves which are fed into the spectrograph and whose frequency, usually 40 or 60 MHz, is fixed. Whenever resonance between the variable frequency of precession and the fixed radio-frequency obtains, a peak will appear on the screen of the spectrograph.

At low temperatures the protons in cyclohexane and similar compounds are known to produce double or multiple peaks which in all probability is due to the existence of both equatorial and axial bonds in the molecule. If now the two kinds of C–H bonds are excited to angular vibrations it seems probable that the directions of the spin axes of the two kinds of protons are perturbed so much that their frequencies of precession become equal, *e.g.* so that both kinds of spin axes become perpendicular to the threefold rotational symmetry axis of the molecule. It is natural to suppose that the condition for the perturbation to be strong enough to extinguish the difference between equatorial and axial protons is that the molecule sufficiently often during one revolution of the precessing spin axis takes up an energy-quantum, *e.g.* once for each C-atom in the SACHSE hexagon.

The probability pro second, w , for this to happen can easily be calculated if we accept the HERZFELD-EYRING value of the pre-exponential factor and if the frequency ν of the vibration in question is known. The familiar expression is

$$w = (kT/h) \exp(-h\nu/kT) \quad (1)$$

where T must be understood as the coalescence temperature. On account of the resonance the frequency of revolution of the precessing spin axis equals the radiofrequency f which is characteristic of the spectrograph and therefore known. The quantity to be determined is then, according to the preceding text w/f , which is the number of "hits" during one revolution of the precessing spin axis. We calculate the frequency ν from the wave number 1445.1 cm^{-1} which LANGSETH and BAR³ determined from the RAMAN spectrum of cyclohexane. This frequency must in all probability be assigned to the angular vibrations of the C–H bond. ANET and BOURN⁴ chose a particularly clear-cut example for their recent investigation, namely the substance $\text{C}_6\text{D}_{11}\text{H}$, where only one nucleus, the proton, has a spin. For this substance they determined the coalescence temperature at $-61,4^\circ\text{C} = 211,75^\circ\text{K}$. With $2,9978 \cdot 10^{10} \text{ cm/s}$ for the speed of light and $h/k = 4,7984 \cdot 10^{-11} \text{ s.deg}$ we get from (1)

$$w = 18,707 \cdot 10^7 \text{ s}^{-1} \quad (2)$$

The radio-frequency in ANET and BOURN'S spectrograph was $f = 6.10^7 \text{ s}^{-1}$ and consequently

$$w/f = 3,118 \quad (3)$$

Another recent example is that investigated by GATTI, SEGRE and MORANDI⁵. Their object was tetrahydropyrane, $\text{C}_5\text{H}_{10}\text{O}$, and their experimental methods are somewhat similar to those of ANET and BOURN. They found a coalescence temperature at $-65^\circ\text{C} = 208,15^\circ\text{K}$. With the same value of ν as that used above one gets

$$w = 15,467 \cdot 10^7 \text{ s}^{-1} \quad (4)$$

and

$$w/f = 2,578. \quad (5)$$

That the ratio w/f (3) is just above three at the coalescence-temperature may mean that the molecule is hit about three times for each revolution of the precessing spin axis by a quantum $h\nu$ and that this is enough to secure that the single C-H bond is set in vibration. This might seem to agree with the fact that the mother-substance, cyclohexane, has a three-fold symmetry-axis and that it therefore has, so to speak, three equivalent compartments. This is however not sufficient because the molecule has also three two-fold symmetry axes which means that there should be six and not only three equivalent ways in which it can be hit, corresponding to the fact, that the six C atoms are equivalent if we ignore the difference between the two possible directions of the three-fold symmetry axis of cyclohexane. It follows that to secure that the single C-H bond in $\text{C}_6\text{D}_{11}\text{H}$ is excited to vibration the molecule should be hit six times. We learn therefore from the experimentally determined value 3,12 of w/f that w means the number of times the molecule is hit from one side pro second and that it must be multiplied by two to get the whole number of "hits" pro second. Similarly the number of hits which is necessary to extinguish the difference between equatorial and axial protons in tetrahydropyrane is, according to the experiments, 5,16 for each turn of the precessing spin axes, while the expected value is five.

To test the validity of these considerations, the coalescence-temperatures for the same substances should be determined at other radio-frequencies, *e.g.* 40 MHz in stead of 60, but unfortunately the present writer is unable to do this as he retired some nine years ago. But it seems important to him if someone else would undertake the job. It would not only be important to know whether or not the ratio w/f is independent of the radio-frequency, but if so, the result would be a rather strong proof of the validity of the HERZFELD-

EYRING value for the preexponential factor in the expression for the unimolecular velocity-constant in reaction kinetics. It goes without saying that the clash concerning the work of activation for the conversion of the two forms of the SACHSE chair hexagon into each other, calculated on one hand from optical and on the other hand from n.m.r. spectra would disappear simultaneously.

References

1. CHRISTIANSEN, J. A., *Nature* **211**, (1966) 184.
2. CHRISTIANSEN, J. A., *Kgl. Danske Vid. Selsk.* this issue p. 16.
3. LANGSETH, A., BAK, B., *J. Chem. Physics* **8**, (1940) 403.
4. ANET, F. A. L., and BOURN, A. J. R., *J. Amer. Chem. Soc.* **89**, (1967) 760.
5. GATTI, G., SEGRE, A. L., and MORANDI, C., *J. Chem. Soc. B*, (1967) 1203.

7. Hypotheses on Tautomerism of Conformational Isomers of Vicinal Derivatives of Cyclohexane

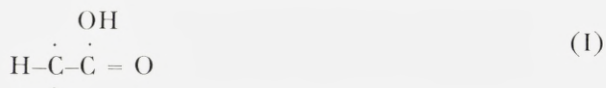
The fact that SACHSE's rigid model of cyclohexane permits „too many" isomers must be caused by some sort of tautomerism. As calculations based on spectral evidence of work of activation have corroborated that SACHSE's hexagon is rigid, the flexibility must be caused by changes in some of the angles in the hexagon. Such changes can be brought about *e.g.* by displacement of a H-atom geminal to a carboxyl-group or by displacement of a proton geminal to a hydroxyl group. In both cases the corresponding ring-angle will change from about the tetrahedric angle to about 120° . In that case experiments with models of the space-filling type show that mutual transformations of the two *trans* forms, (*ee*) and (*aa*), of vicinal disubstituted compounds must be relatively easy while racemization of the *cis* (*ea*) forms is difficult.

The classical objection against the rigid chair form of the SACHSE model of cyclohexane is that it permits more isomers than are actually known. For example, it permits two monosubstitutes, one axial (*a*) and one equatorial (*e*), while no cases of more than one substance of the composition of a monosubstitute are known. Concerning vicinal disubstituted cyclohexanes the model permits three isomers, apart from enantiomers, namely *trans*(*aa*), *trans*(*ee*) and *cis*(*ea*). However, only two vicinal dicarboxylic acids derived from cyclohexane are known. Concerning vicinal diols the situation is more complicated. As a matter of fact three different substances of that kind have been isolated, two with melting points at respectively 104°C and 99°C and one which melts at 75°C .

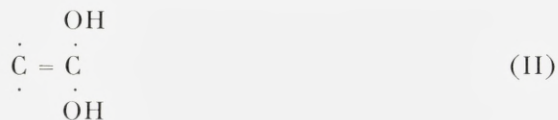
The latter was prepared by SABATIER and MAILHE by catalytic hydrogenation of catechol¹. LEROUX² found that a substance with the same melting point could be prepared from a mixed solution of the two former ones and he believed it to be a compound of them.

However, so far as known to the present author a determination of the molecular weight of the 75° diol has never been performed, and this is necessary before LEROUX's assumption can be finally accepted. The need for a determination of the m.w. of the 75° diol is so much more needed as LEROUX himself by catalytic hydrogenation of a certain naphthalene diol got three isomers of which the low melting one could be prepared from a mixed solution of the two others, in analogy with his results for the cyclohexane derivatives. Here, however, he performed a m.w. determination and found that the low melting compound was a monomer.

In his paper from 1918 MOHR³ took it for granted that only two disubstituted and one monosubstituted cyclohexane were known and he assumed therefore that the mutual conversion of the two chair forms of the SACHSE model was fast enough to make some of the isomers pairwise tautomeric. That tautomerism must occur seems certain enough but, as shown in a preceding paper, an easy conversion of the two chair forms into each other can hardly be the explanation. In the search for other explanations we may begin with the cyclohexane monocarboxylic acid. The configuration around the carbon atom which is implied in the substitution is usually assumed to be the one indicated by (I)



But, many years ago, ASCHAN^{4,5} explained certain reactions in camphor chemistry by assuming an enolization of the carboxylgroup as indicated by (II)



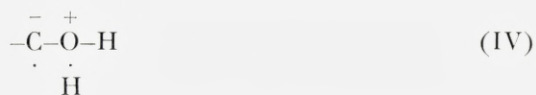
From many investigations of different kinds it has been concluded that the directions of two single and one double bond around a carbon atom form angles of about 120° with each other. If we now build models corresponding to (I) and (II) of cyclohexane carboxylic acid from atomic models of the STUART BRIEGLER type it turns out that the one corresponding to (I) is rigid but that the one corresponding to (II) is flexible in so far as the $\text{C}=\text{C}(\text{OH})_2$ group can be turned relative to the rest of the molecule between two extreme positions which correspond roughly to the equatorial and the axial positions respectively. The movement is not free from resistance but it can be per-

formed without breaking the ring, while a similar movement is impossible with the model corresponding to (I). Consequently, when one of the two hydrogen atoms in (II) migrates back into the position indicated by (I) it depends on chance whether it becomes fixed axially or equatorially. In this way the tautomerism of the (*a*) and (*e*) forms of the monocarboxylic acid may be understood.

The case of the monosubstituted hydroxy derivative is somewhat different, but it may nevertheless be treated in a similar way: The tertiary proton in (III)



may migrate to the OH group which thus acts as a base as indicated in (IV)



By this exchange of charges both the carbon and the oxygen atom become nitrogen isosters and may be expected to have three valency bonds each⁶. As these bonds must be expected to form angles of approximately 120° with each other, the situation may be much the same as that described above in the case of the monocarboxylic acid, that is, the (*e*) and the (*a*) forms may be expected to be tautomeric. The case of vicinal disubstituted cyclohexanes is more complicated. Experiments with the STUART-BRIEGLEB models show that, if two neighbouring carbon atoms in the ring have double bonds pointing outwards, the ring becomes even more flexible than in the case of the monosubstitute, in so far as these carbon atoms can then be turned relative to each other in opposite directions, but not in the same direction. In one of the extreme positions where the substituents have been turned as far as possible relative to each other they approach the *trans*(*aa*) conformation and in the other extreme position they approach the *trans*(*ee*) form. When now the migratory hydrogen atoms return to their normal sites on the ring carbon atoms it depends on chance which one of the two conformations will result, and we may therefore understand that the two *trans*-forms are mutually tautomeric.

But to transform one of the *cis*(*ea*) forms into its mirror image the two substituents must be moved to the same side and experiments with the model shows this to be impossible. Therefore we cannot expect that racemization of the optical antipodes is easy.

Concerning the *trans*-forms of the vicinal dicarboxylic acid the model

shows that there is a difficulty. It seems that steric hindrance must prevent the two $=C(OH)_2$ groups in passing by each other. This is, however, probably of no great consequence because the two colliding HO groups, one from each of the two enolized carboxyl groups can change over from one carbon atom to the other by small changes in their electronic clouds and without large displacement of the nuclei. The two diagrams (V) are intended to show the situation. If the relative movements of the two groups and the distribution of the valencies are as shown to the left the two groups cannot pass each other. If however the valency clouds around the two oxygen atoms are rearranged so as to produce the valency distribution indicated to the right the movement can continue in the same direction as before the two groups met, without mutual hindrance.



Of course the two diagrams are schematic, but a comparison with the model shows it to be more realistic than such diagrams usually are. It must be understood that the diagrams are intended to visualize the positions and the movements of the enolized carboxylic groups seen from the outside of a model whose axis is vertical. In this way tautomerism between the two *trans* forms can be understood, but, as mentioned before, to transform the enantiomeric *cis* forms into each other, the trivalent atomic models must be turned in the same direction, which is difficult or impossible. Therefore even enolization of the carboxyl group cannot lead to a racemization of one of the optical antipodes of the *cis* compound. In case the compound considered is a vicinal cyclohexane diol the transition state may be one in which two tertiary protons have been displaced as indicated in (IV) so that we get two neighbouring negatively charged nitrogen isosters, which again may be assumed to be centers for three single bonds. The situation is then about the same as in the case of the cyclohexane dicarboxylic acid, and we are led to expect tautomerism between the two *trans* forms but not between the enantiomeric *cis* forms.

The activation potential may be expected to be twice the work necessary to transform (III) into (IV) where one proton has been displaced. Similarly,

the work of activation for the transformation of the two *trans* forms of the dicarboxylic acids into each other may be expected to be twice the difference between the potential energies of (II) and (I), where a hydrogen atom has been displaced. As this may be expected to be less, than when a proton is displaced it seems natural that it is possible to isolate two *trans* forms of the diol, but not of the dicarboxylic acid.

References

1. SABATIER, P., and MAILHE, C. r. **146**, (1908) 1154.
 2. LEROUX, H., *Ann. de Chim. et Phys.* [8] **21**, (1910) 541.
 3. MOHR, E., *J. prakt. Chem.*, [2] **98**, (1918) 315.
 4. ASCHAN, O., *Liebigs Ann.* **387**, (1912) 17.
 5. HÜCKEL, W., *Theoretische Grundlagen der organischen Chemie*, Erster Band. Leipzig (1931) 256.
 6. CHRISTIANSEN, J. A., *J. Coll and Interface Science* **22**, (1966) 2.
-

ESKO SUHONEN

GENERAL RELATIVISTIC
FLUID SPHERE AT MECHANICAL
AND THERMAL EQUILIBRIUM

Det Kongelige Danske Videnskabernes Selskab
Matematisk-fysiske Meddelelser **36**, 15



Kommissionær: Munksgaard
København 1968

Synopsis

The field equations of general relativity for a static fluid sphere composed of ideal gas and radiation are solved numerically under the assumption that the fluid is at thermal equilibrium throughout a configuration. The law of thermal equilibrium is used in the general relativistic form.

1. Introduction

Only few solutions describing the static gravitational field inside a spherical mass distribution are known. This is caused by the complicated non-linear character of the field equations. In order to ensure solutions in terms of known functions, one has been obliged to pay more attention to a mathematical simplification than to a physical situation. Therefore the resulting solutions, derived by R. C. TOLMAN⁽¹⁾, M. WYMAN⁽²⁾ and B. KUCHOWICZ⁽³⁾, are not of much physical interest.

A more satisfactory procedure is to use an equation of state as an auxiliary equation. The system of equations can then be solved only numerically. The simplest cases are the relativistic generalizations of the classical polytropic, standard and isothermal fluid spheres. A polytropic fluid sphere where the pressure and energy density are connected by a power law, has been examined by R. F. TOOPER^(4, 5). He has also examined a standard model where the ratio of the gas pressure to the total pressure is constant throughout a configuration⁽⁶⁾. A fluid sphere obeying an isothermal equation of state has been studied by M. L. MEHRA⁽⁷⁾. However, it appears that there are some errors in MEHRA's paper. MEHRA has not taken into account the microscopic kinetic energy of the gas. The law of thermal equilibrium has been used in the classical form. The boundary conditions are not satisfactory, either.

In the present paper a relativistic treatment for a fluid sphere where the matter is at thermal equilibrium, is given again. The proper temperature of the fluid as measured by local observers is not constant throughout a sphere, but varies with gravitational potential according to the general relativistic law of thermal equilibrium⁽⁸⁾. The conditions under which thermal equilibrium might arise are not examined in this paper. The dynamical stability of a relativistic 'isothermal' sphere is not investigated, either.

In section 2 the general relativistic equations of mechanical equilibrium are given for a spherically symmetric, static system. Using the relativistic, statistical expressions for the pressure and energy density⁽⁹⁾, the equations

of state are derived for a mixture of ideal gas and radiation in section 3. The equations of mechanical equilibrium are transformed in a suitable dimensionless form in section 4. In section 5 the radius, mass, and pressure distribution are expressed in terms of dimensionless variables. The equilibrium equations have been integrated numerically, and results are given and discussed in section 6.

2. Equations of Mechanical Equilibrium

Any time-independent, spherically symmetric general relativistic metric can be transformed to the standard form

$$ds^2 = -e^\lambda dr^2 - r^2(d\vartheta^2 + \sin^2\vartheta d\varphi^2) + e^\nu c^2 dt^2, \quad (1)$$

where the functions e^λ and e^ν depend on the radial coordinate r only. Assuming the expression for the energy-momentum tensor

$$T_j^i = \left(\varrho + \frac{P}{c^2} \right) u_j u^i - \frac{P}{c^2} g_j^i, \quad (2)$$

where quantities u^i , p and ϱ are the fluid 4-velocity, pressure and total mass density, respectively, the gravitational field equations reduce in the metric (1) to

$$e^{-\lambda} \left(\frac{1}{r} \frac{d\nu}{dr} + \frac{1}{r^2} \right) - \frac{1}{r^2} = \frac{8\pi G}{c^4} P \quad (3)$$

$$\frac{1}{2} e^{-\lambda} \left\{ \frac{d^2\nu}{dr^2} + \frac{1}{2} \left(\frac{d\nu}{dr} - \frac{d\lambda}{dr} \right) \left(\frac{d\nu}{dr} + \frac{2}{r} \right) \right\} = \frac{8\pi G}{c^4} P \quad (4)$$

$$e^{-\lambda} \left(\frac{1}{r} \frac{d\lambda}{dr} - \frac{1}{r^2} \right) + \frac{1}{r^2} = \frac{8\pi G}{c^2} \varrho. \quad (5)$$

Here G is the Newtonian gravitational constant. Setting eqs. (3) and (4) equal to each other and making use of eq. (5), lead to the relation

$$\frac{dp}{dr} + \frac{1}{2} (\varrho c^2 + p) \frac{d\nu}{dr} = 0. \quad (6)$$

Relation (6) follows also from the conservation of the energy-momentum. Eqs. (3), (5) and (6) are the relativistic conditions for mechanical equilibrium which, together with an equation of state, form the full set for determination of e^λ , e^ν , p and ϱ as functions of the coordinate r .

3. Equations of State

The total pressure and the total mass density of a fluid sphere consisting of ideal gas and radiation are

$$p = p_g + p_r \quad (7)$$

$$\varrho = \varrho_g + \varrho_r, \quad (8)$$

where quantities belonging to ideal gas and radiation are denoted with indexes g and r .

A relativistic ideal gas consisting of identical particles has the following equations of state⁽⁹⁾

$$p_g + \varrho_g c^2 = \frac{\gamma}{\tau} K_3(\tau) \quad (9)$$

$$p_g = \frac{\Re}{\mu} \varrho_0 T = \frac{\gamma}{\tau^2} K_2(\tau). \quad (10)$$

Here we denote

$$\tau = \frac{\mu c^2}{\Re T}; \quad (11)$$

$K_n(\tau)$ are modified Bessel functions of the second kind; γ is a coefficient depending on nature constants and on the chemical potential; \Re is the gas constant; μ is the mean molecular weight; ϱ_0 is the rest-mass density, and T is the proper temperature measured in a fluid comoving system of coordinates. Using the recurrence relation

$$K_3(\tau) = K_1(\tau) + \frac{4}{\tau} K_2(\tau), \quad (12)$$

we obtain from eqs. (9) and (10) the expression for $\varrho_g c^2$:

$$\left. \begin{aligned} \varrho_g c^2 &= \frac{\gamma}{\tau} K_1(\tau) + \frac{3\gamma}{\tau^2} K_2(\tau) \\ &= \left(\frac{K_1(\tau)}{K_2(\tau)} + \frac{3}{\tau} \right) \varrho_0 c^2. \end{aligned} \right\} \quad (13)$$

The pressure and energy density of radiation are expressed by

$$p_r = \frac{1}{3} \varrho_r c^2 = \frac{1}{3} a T^4, \quad (14)$$

where a is the radiation constant.

For a mixture of ideal gas and radiation we get from eqs. (7), (8), (10), (13) and (14) the equations of state

$$p + \varrho c^2 = \frac{4}{3} a T^4 + \left(\frac{K_1(\tau)}{K_2(\tau)} + \frac{4}{\tau} \right) \varrho_0 c^2 \quad (15)$$

$$p = \frac{1}{3} a T^4 + \frac{\mathfrak{R}}{\mu} \varrho_0 T. \quad (16)$$

4. Equations of Mechanical Equilibrium in Dimensionless Form

From the general relativistic law of thermal equilibrium⁽⁸⁾

$$T(g_{44})^{1/2} = T e^{y/2} = \text{constant} \quad (17)$$

we obtain a relation

$$\frac{dy}{dr} = - \frac{2}{T} \frac{dT}{dr} \quad (18)$$

which, substituted in eq. (6), gives

$$\frac{dp}{dr} - \frac{(\varrho c^2 + p)}{T} \frac{dT}{dr} = 0. \quad (19)$$

Inserting expressions (15) and (16) in eq. (19), we obtain after a simplification

$$\frac{1}{\varrho_0} \frac{d\varrho_0}{dr} - \frac{1}{T} \left(3 + \tau \frac{K_1(\tau)}{K_2(\tau)} \right) \frac{dT}{dr} = 0. \quad (20)$$

Eq. (20) is difficult to integrate due to the presence of functions $K_1(\tau)$ and $K_2(\tau)$. However, in the case of large argument τ , we have a convenient approximation for $K_n(\tau)$ ⁽¹⁰⁾:

$$K_n(\tau) = \left(\frac{\pi}{2\tau}\right)^{1/2} e^{-\tau} \left\{ 1 + \frac{4n^2 - 1}{8\tau} + \frac{(4n^2 - 1)(4n^2 - 3)}{2!(8\tau)^2} + \dots \right\}, \quad (21)$$

from which

$$\frac{K_1(\tau)}{K_2(\tau)} \approx 1 - \frac{3}{2\tau}. \quad (22)$$

This approximation can be used for all constituents of the fluid below the limit $T = 10^9$ degrees where $\tau = 5.9$ for electrons and positrons. For all constituents except electrons and positrons, extension (21) is valid for $T < 10^{12}$ degrees. But in any case we must restrict the treatment to temperatures below $2 \cdot 10^9$ degrees, because above this limit the neutrino emission carries so much energy away that equilibrium is disturbed⁽¹¹⁾.

Using expression (22), eq. (20) becomes

$$\frac{1}{\varrho_0} \frac{d\varrho_0}{dr} - \frac{1}{T} \left(\frac{3}{2} + \tau \right) \frac{dT}{dr} = 0, \quad (23)$$

which can be integrated to give

$$\varrho_0 = AT^{3/2} e^{-\mu c^2 / \Re T}. \quad (24)$$

The constant A of integration is determined by initial conditions. Denoting the rest mass density and the proper temperature at the centre by ϱ_{0e} and T_c , we obtain

$$\frac{\varrho_0}{\varrho_{0e}} = \left(\frac{T}{T_c} \right)^{3/2} e^{-\frac{\mu c^2}{\Re} \left(\frac{1}{T} - \frac{1}{T_c} \right)}. \quad (25)$$

Eq. (5), which can be written also in the form

$$\frac{d(re^{-\lambda})}{dr} = 1 - \frac{8\pi G}{c^2} \varrho r^2, \quad (26)$$

can be integrated only formally because the distribution of the energy density is unknown. We define a new function $M(r)$ by

$$M(r) = \int_0^r 4\pi \varrho r^2 dr. \quad (27)$$

Function $M(r)$ represents the total mass arising from the density ϱ and from the gravitational field, inclosed by the sphere of coordinate radius r . Integrating eq. (26), we get

$$e^{-\lambda} = 1 - \frac{2GM(r)}{c^2 r}. \quad (28)$$

In terms of function M , eq. (26) becomes

$$\frac{dM}{dr} = 4\pi\varrho r^2. \quad (29)$$

Substituting the expression of density ϱ from eqs. (13), (14) and (22) in eq. (29), we obtain

$$\frac{dM}{dr} = \frac{4\pi r^2}{c^2} \left\{ \alpha T^4 + \left(1 + \frac{3}{2\tau} \right) \varrho_0 c^2 \right\}. \quad (30)$$

Insertion of eqs. (18) and (28) in eq. (3) gives

$$-\frac{2}{r} \left(1 - \frac{2GM}{c^2 r} \right) \frac{1}{T} \frac{dT}{dr} + \frac{1}{r^2} \left(1 - \frac{2GM}{c^2 r} \right) - \frac{1}{r^2} = \frac{8\pi G}{c^4} P. \quad (31)$$

Using the expression

$$P = \frac{c^2}{12\pi r^2} \frac{dM}{dr} - \left(\frac{1}{3} - \frac{1}{2\tau} \right) \varrho_0 c^2 \quad (32)$$

obtained from eqs. (15), (16), (22) and (29), eq. (31) becomes

$$\left(1 - \frac{2GM}{c^2 r} \right) \frac{r}{T} \frac{dT}{dr} + \frac{GM}{c^2 r} + \frac{G}{3c^2} \frac{dM}{dr} - \frac{4\pi G}{c^2} \left(\frac{1}{3} - \frac{1}{2\tau} \right) \varrho_0 r^2 = 0. \quad (33)$$

A change of variables

$$r = \frac{x}{B} \quad (34)$$

$$v(x) = \frac{B^3 M(r)}{4\pi\varrho_0 c}, \quad (35)$$

where

$$B = \left(\frac{\pi G \varrho_0^2 c}{P_c} \right)^{1/2} \quad (36)$$

puts eqs. (30) and (33) in dimensionless form. Substituting new variables x and v in eqs. (30) and (33), we obtain the following first order differential equations

$$\frac{dv}{dx} = x^2 \left\{ \frac{\alpha T^4}{\varrho_{0c} c^2} + \left(1 + \frac{3\Re T}{2\mu c^2} \right) \frac{\varrho_0}{\varrho_{0c}} \right\} \quad (37)$$

$$\left(\frac{\varrho_{0c} c^2}{4p_c} - \frac{2v}{x} \right) \frac{x^2 dT}{T dx} + v + \frac{x dv}{3 dx} - \left(\frac{1}{3} - \frac{\Re T}{2\mu c^2} \right) \frac{\varrho_0}{\varrho_{0c}} x = 0. \quad (38)$$

Using eq. (37), eq. (38) can be written also in the form

$$\left(\frac{1}{C} - \frac{2v}{x} \right) \frac{x^2 dT}{T dx} + v + \frac{\alpha T^4}{3\varrho_{0c} c^2} x^3 + \frac{\Re T}{\mu c^2 \varrho_{0c}} x^3 = 0, \quad (39)$$

where we denote

$$C = \frac{4p_c}{\varrho_{0c} c^2} = 4 \left(\frac{\alpha T_c^4}{3\varrho_{0c} c^2} + \frac{\Re T_c}{\mu c^2} \right). \quad (40)$$

In terms of variables x and v , the following expression for the metric component $|g_{11}| = e^\lambda$ is found from eq. (28)

$$e^\lambda = \left(1 - 2C \frac{v}{x} \right)^{-1}. \quad (41)$$

5. Physical quantities

The element of spatial distance measured with a standard measuring-rod is given by⁽¹²⁾

$$dl^2 = \left(g_{ij} - \frac{g_{4i} g_{4j}}{g_{44}} \right) dx^i dx^j. \quad (42)$$

In the metric (1), the metric components g_{4i} are equal to zero, and the physical distance from the centre to a point with radial coordinate r is from eqs. (34), (41) and (42),

$$R = \int_0^r e^{\lambda/2} dr = \frac{1}{B} \int_0^x \left(1 - 2C \frac{v(x)}{x} \right)^{-1/2} dx \quad (43)$$

or measured in units of the radius of the sun $R_\odot = 6.96 \cdot 10^{10}$ cm

$$\frac{R}{R_{\odot}} = 4.71 \cdot 10^2 \left(\frac{C}{\varrho_0 c} \right)^{1/2} \int_0^x \left(1 - 2C \frac{v(x)}{x} \right)^{-1/2} dx, \quad (44)$$

where we have also used eqs. (36) and (40). For the mass inside a sphere of the radius r we obtain from eqs. (35) and (36) the expression

$$M = \frac{4p_c^{3/2}}{\pi^{1/2} G^{3/2} \varrho_0 c^2} v(x) = 2.22 \cdot 10^8 M_{\odot} \frac{C^{3/2}}{\varrho_0 c^{1/2}} v(x), \quad (45)$$

where $M_{\odot} = 1.985 \cdot 10^{33} g$ is the mass of the sun. The expression for the pressure distribution

$$\left. \begin{aligned} \frac{p}{p_c} &= \frac{4}{C} \left(\frac{\alpha T^4}{3\varrho_0 c^2} + \frac{\Re T}{\mu c^2} \frac{\varrho_0}{\varrho_0 c} \right) \\ &= \frac{1}{C} \left(1.13 \cdot 10^{-3} \frac{T^4}{\varrho_0 c} + 3.70 \cdot 10^{-5} \frac{T}{\mu} \frac{\varrho_0}{\varrho_0 c} \right) \end{aligned} \right\} \quad (46)$$

is found from eqs. (16) and (40).

6. Numerical Results and Discussion

Eqs. (37) and (39) were integrated numerically under the initial conditions $v(0) = 0$ and $T(0) = T_c$ using the Runge-Kutta method. The molecular weight was taken to be 0.5, corresponding to purely hydrogen configurations. Simultaneously with the determinations of functions $v(x)$ and $T(x)$ integral (43) for the physical radius R was calculated. The values of the radial metric component $|g_{11}| = e^{\lambda}$, mass and normalized pressure were obtained from eqs. (41), (45) and (46). For the calculation of the metric component $g_{44} = e^{\nu}$ from eq. (17), it was assumed that, far from the centre, the relation $|g_{11}| = 1/g_{44}$ is valid.

Numerical results in an appropriate case are shown graphically in Fig. 1. The physical radius R is used as the independent variable, so that the geometrical effects arising from the presence of gravitating matter have been taken into account in preparing the graphs.

The behaviour of the results differs in several respects from the corresponding classical case. In spite of thermal equilibrium, the proper temperature measured in a fluid comoving system of coordinates, decreases monotonically as a function of radius. The matter is concentrated more mark-

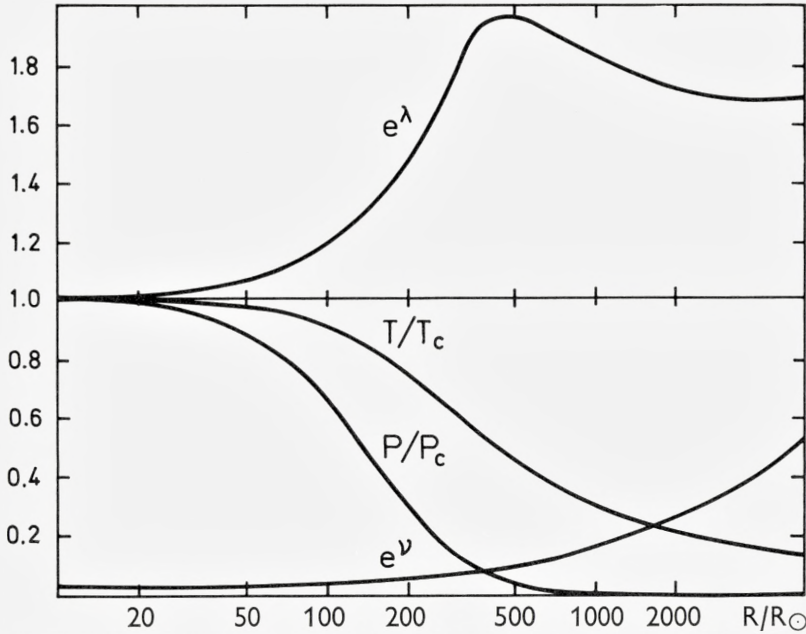


Fig. 1. Metric components, temperature and pressure as functions of the physical radius, when central temperature $T_c = 10^9$ degrees.

edly toward the centre than in a classical isothermal sphere. The normalized pressure and total density fall off rapidly in an outward direction. The metric components e^{λ} and e^{ν} differ strongly from their Euclidian values. The radial component $|g_{11}| = e^{\lambda}$ increases from its minimum value unity at the centre to the first and highest maximum, goes down to the lowest minimum, and then oscillates moderately. The time component e^{ν} is always less than unity, and is a monotonically increasing function of radius.

In Tables 1 and 2 the values of the radius, mass and normalized temperature and pressure are given, corresponding to the first maximum and second minimum of e^{λ} for three central temperatures. Eqs. (37) and (39) include besides the central temperature T_c , the central rest mass density ρ_{0c} as another parameter. The rest mass density originates from the gas pressure term in the expression of the total pressure. The ratio of gas pressure to radiation pressure decreases very rapidly as a function of radius. Even in cases where gas pressure dominates over radiation pressure at the centre, it is negligible quite soon outside the centre. This is caused by an exponential decrease of the rest mass density with respect to the proper temperature, which is found in eq. (25). For this reason, the metric tensor

TABLE 1. Radius, mass, normalized temperature and pressure corresponding to the first maximum of e^λ .

T_c	R/R_\odot	M/M_\odot	T/T_c	P/P_c	e^λ
10^8	$4.8 \cdot 10^4$	$4.4 \cdot 10^9$	0.45	0.041	1.965
$5 \cdot 10^8$	$2.0 \cdot 10^3$	$1.8 \cdot 10^8$	0.45	0.041	1.965
10^9	$4.8 \cdot 10^2$	$4.4 \cdot 10^7$	0.45	0.041	1.965

TABLE 2. Radius, mass, normalized temperature and pressure corresponding to the second minimum of e^λ .

T_c	R/R_\odot	M/M_\odot	T/T_c	P/P_c	e^λ
10^8	$3.0 \cdot 10^5$	$2.2 \cdot 10^{10}$	0.18	$1.0 \cdot 10^{-4}$	1.690
$5 \cdot 10^8$	$1.2 \cdot 10^4$	$9.1 \cdot 10^8$	0.18	$1.0 \cdot 10^{-4}$	1.690
10^9	$3.0 \cdot 10^3$	$2.2 \cdot 10^8$	0.18	$1.1 \cdot 10^{-4}$	1.690

components and physical parameters are nearly independent of the central rest mass density.

It is seen from tables 1 and 2 that the maximum and minimum values of the metric component e^λ and the corresponding values of the normalized temperature and pressure are independent of the central temperature. The physical radius and mass are approximately inverse to the square of the central temperature. This is valid, not only for the maximum and minimum values of e^λ , but everywhere. Because of the similar feature of the graphs for different central temperatures, we have shown the results graphically only in one special case.

The condition of thermal equilibrium leads to very massive configurations. Such fluid spheres extend to infinity, like classical isothermal models. However, it might be possible to develop theoretical models of a moderately long time-scale where the inner parts are at mechanical and thermal equilibrium, but the outer layers are away from equilibrium. The radial pulsations at the surface should correspond to a "stellar wind".

References

- 1) R. C. TOLMAN, *Phys. Rev.* **55**, 364 (1939).
 - 2) M. WYMAN, *Phys. Rev.* **75**, 1930 (1949).
 - 3) B. KUCHOWICZ, Report, Univ. Warsaw, Dept. of Radiochemistry (1966).
 - 4) R. F. TOOPER, *Astrop. J.* **140**, 434 (1964).
 - 5) R. F. TOOPER, *Astrop. J.* **142**, 1541 (1965).
 - 6) R. F. TOOPER, *Astrop. J.* **143**, 465 (1966).
 - 7) M. L. MEHRA, *Acta Phys. Austr.* **25**, 1 (1967).
 - 8) R. C. TOLMAN: *Relativity, Thermodynamics and Cosmology* (Clarendon Press, Oxford, 1962) p. 313.
 - 9) J. L. SYNGE: *The Relativistic Gas* (North-Holland Publishing Company, Amsterdam, 1957) pp. 34–36.
 - 10) G. N. WATSON: *Theory of Bessel Functions* (Cambridge University Press, London, 1944) p. 202.
 - 11) F. HOYLE and W. A. FOWLER, *Nature* **197**, 533 (1963).
 - 12) C. MØLLER: *The Theory of Relativity* (Clarendon Press, Oxford, 1952) p. 238.
-

C. MØLLER

GIBBS' STATISTICAL MECHANICS IN THE THEORY OF RELATIVITY

Det Kongelige Danske Videnskabernes Selskab
Matematisk-fysiske Meddelelser **36**, 16



Kommissionær: Munksgaard
København 1968

Synopsis

Recent investigations in relativistic thermodynamics have shown that the momentum and energy of transferred heat in a thermodynamical process transform as the components of a four-vector under Lorentz transformations, in striking contrast to the ideas of the early formulation of relativistic thermodynamics of sixty years ago. In the present paper it is shown that the results of the new formulation are supported in all details by a relativistic generalisation of Gibbs' classical statistical mechanics.

1. Introduction and Survey

In a most interesting paper by H. OTT from 1963 [1], it was shown that the old relativistic treatment of thermodynamical processes by PLANCK and others [2] contained an error which led to a wrong transformation formula for the heat energy transferred in a process. In pre-relativistic thermodynamics, the first law expresses the law of conservation of energy when heat energy is involved in the process. In relativity theory, this law has to be supplemented by a similar law of conservation of momentum. Thus, in an arbitrary system of inertia S , we have four conservation equations*

$$\Delta G_i = \Delta I_i + \Delta Q_i, \quad i = 1,2,3,4 \quad (1.1)$$

with

$$\left. \begin{aligned} \Delta G_i &= \{\Delta \mathbf{G}, -\Delta H/c\} \\ \Delta I_i &= \{\Delta \mathbf{I}, -\Delta A/c\} \\ \Delta Q_i &= \{\Delta \mathbf{Q}, -\Delta Q/c\}. \end{aligned} \right\} \quad (1.2)$$

Here, $\Delta \mathbf{G}$ and ΔH are the changes of the momentum \mathbf{G} and energy H of the thermodynamic body in a process leading from one equilibrium state to another such state. $\Delta \mathbf{I}$ is the mechanical impulse, i.e. the time integral of the mechanical forces acting on the body, while ΔA is the work performed by these forces during the process. Consequently, ΔQ is the heat energy transferred to the body in the process (definition!) and $\Delta \mathbf{Q}$ is the corresponding momentum transferred along with the heat supply.

In his paper, quoted above, OTT clearly pointed out that the error in the old treatments is due to a wrong expression for the mechanical work performed by the external forces. However, his argument and his results were not universally recognized and his paper gave rise to a large number

* Latin indices run from 1 to 4, Greek indices from 1 to 3. The metric tensor in Minkowski space has signature +2 and the usual summation convention is made.

of mutually contradicting papers on the subject [3]. Therefore in a recent paper [4], the present author considered once more in all details the simple case of thermodynamical processes in a fluid enclosed in a container of changeable volume. If we assume that the fluid cannot withstand shear, the external force on the fluid is simply the normal pressure from the walls of the container. Since the pressure is a relativistic scalar, it is easy in this case to write down the transformation equations for the quantities ΔG_i and ΔI_i . Then, the transformation laws for the quantities ΔQ_i follow from (1.2). The main results obtained in reference 4 are the following. In general, neither ΔG_i nor ΔI_i will transform like the components of 4-vectors under Lorentz transformations. Nevertheless, the differences $\Delta G_i - \Delta I_i$, i.e. *the ΔQ_i are the covariant components of a 4-vector, the four-momentum of supplied heat*. This result, which in reference 4 was proved for a fluid only, has been shown by BREVIK [5] and by SÖDERHOLM [6] to be valid for any elastic body and for any thermodynamical process leading from one equilibrium state to another such state of the body.

Further it was shown in reference 4 that the four-momentum of supplied heat for an infinitesimal *reversible* process is proportional to the four-velocity

$$V_i = \{\gamma\mathbf{v}, -\gamma c\}, \quad \gamma = (1 - v^2/c^2)^{-1/2} \quad (1.3)$$

of the body:

$$dQ_i^{\text{rev}} = \frac{dQ_{\text{rev}}^0}{c^2} V_i, \quad (1.4)$$

where dQ_{rev}^0 is the transferred heat energy measured in the rest system S^0 of the body. The fourth component of (1.4) gives

$$dQ^{\text{rev}} = \frac{dQ_{\text{rev}}^0}{\sqrt{1 - v^2/c^2}}. \quad (1.5)$$

As regards the second law of thermodynamics, it is generally agreed that the entropy S is a relativistic invariant,

$$S = S^0, \quad (1.6)$$

i.e. and, in the rest system, we have

$$dS^0 = \frac{dQ_{\text{rev}}^0}{T^0} \quad (1.7)$$

where T^0 is the proper temperature as measured in the rest system. If one wants a similar equation

$$dS = \frac{dQ_{\text{rev}}}{T} \quad (1.8)$$

to hold in any other system of inertia, one finds by (1.5–8) that the so defined temperature T is connected with the proper temperature T^0 by ORT's formula

$$T = \frac{T^0}{\sqrt{1 - v^2/c^2}}. \quad (1.9)$$

Thus, T is not an invariant but rather the fourth component of a time-like vector

$$T_i = \frac{T^0}{c} V_i \quad (1.10)$$

the 'temperature 4-vector' introduced by ARZÉLIÈS [7]:

$$T = T^4 = -T_4 \quad (1.11)$$

Obviously the norm of this vector is equal to the invariant proper temperature T^0 , since

$$\sqrt{-T_i T^i} = T^0. \quad (1.12)$$

Thus, instead of using a single quantity T , defined by (1.9), for the characterization of the thermodynamic state (together with 'extensive' quantities like the volume etc.) it seems more appropriate in an arbitrary system of inertia to use the four components of the temperature 4-vector T_i for this purpose. Only in the rest system S^0 where the spatial components $T_i^0 = 0$ we are left with a single quantity $T_4^0 = -T^0$ as in classical thermodynamics. This point of view was carried through in a recent paper [8] in which also a generally relativistic formulation was given which in a very simple way leads to Tolman's condition for thermal equilibrium in a large body under the influence of its own gravitational field.

However, in the case of an *irreversible* process the formulation of the second law leads to unnecessary complications in this scheme. In the rest system S^0 we have, for an irreversible process,

$$dS^0 > \frac{dQ^0}{T^0}, \quad (1.13)$$

but in an arbitrary system of inertia S , (1.13) is *not* equivalent to

$$dS > \frac{dQ}{T}, \quad (1.14)$$

a relation which is simply not true. This is connected with the fact that the 4-vector dQ_i for irreversible processes is not proportional to V_i in general. However, we get a very simple general formulation of the second law if we, instead of the temperature 4-vector T_i , introduce the reciprocal temperature 4-vector θ^i defined by

$$\theta^i = \theta^0 V^i, \quad \theta^0 = (T^0)^{-1} \quad (1.15)$$

which has the norm

$$\theta = \sqrt{-\theta_i \theta^i} / c = \theta^0. \quad (1.16)$$

Then, the second law in an arbitrary system S takes the form

$$dS \geq -\theta^i dQ_i, \quad (1.17)$$

where the equality sign holds for reversible processes only. In the latter case, where dQ_i is of the form (1.4), (1.17) is identical with (1.7) (or (1.8)) and, for an irreversible process, we have

$$-\theta^i dQ_i = -\theta^{0i} dQ_i^0 = -\frac{c}{T^0} dQ_4^0 = \frac{dQ^0}{T^0}$$

so that (1.17) is equivalent to (1.13). In the form (1.17), the second law can immediately be taken over into the general theory of relativity and the results obtained in reference 8, in particular Tolman's equilibrium conditions, follow immediately.

The considerations in references 4 and 8 were purely thermodynamical, but it is clear that the results quoted in this section should be obtainable also by means of a relativistic generalization of Gibbs' statistical mechanics in which the thermodynamic properties of a macroscopic system in thermal equilibrium is described as mean values in a canonical ensemble. A *reversible* process is then described by a succession of canonical ensembles with varying values for the parameters that characterize the ensemble. In this way it is possible to derive all the earlier mentioned thermodynamic properties of the systems, in particular the transformation properties of ΔG_i , ΔI_i and ΔQ_i , from statistical mechanical considerations, and this is the subject of the present paper.

In view of the generality of the properties in question, it is sufficient to treat a highly simplified model like an ideal gas of equal particles enclosed in a container. Since the particles do not interact in this case, the particles move independently of each other in the field of force originating from the walls of the container and possibly from other external sources. In the next section we shall, therefore, start by considering a one-particle system, which is then easily generalized to the case of n identical particles. It will be shown that the equations of motion can be written in the Hamiltonian form in any system of inertia, but the Hamiltonian will in general not be a constant of the motion. Section 3 contains a short survey of the properties of relativistic phase-spaces, such as Liouville's theorem in an arbitrary Lorentz system and the relativistic invariance of the volume of phase-space. In section 4 we consider ensembles of mechanical systems in the phase-space of an arbitrary Lorentz system. In particular, the relativistic invariance of the probability density and the general form of the latter for a *canonical* ensemble are considered.

The following section contains a derivation of the transformation properties of the mean values of the canonical four-momentum, the forces, the rate of work, and the 'probability exponential' in a canonical ensemble. In section 6 we give a statistical description of a reversible process and a calculation of the mechanical impulse and work is carried out, by which typical relativistic effects are clearly brought out. We shall also obtain a statistical expression for the four-momentum of supplied heat in a reversible process. Finally, in the last section, a number of theorems are derived which allow to calculate mean values of important physical quantities by differentiations of a function that is closely related to the free energy of thermodynamics.

2. Lagrangian and Hamiltonian Form of the Equations of Motion in the Case when the Field of Force is Static in a Certain System of Inertia S^0

The motion of a particle of constant rest mass m subjected to a force \mathfrak{F} in any system of inertia S is generally given by Minkowski's equations

$$\frac{dp_i}{d\tau} = F_i, \quad i = 1, 2, 3, 4, \quad (2.1)$$

where

$$d\tau = dt\sqrt{1 - u^2/c^2} \quad (2.2)$$

is the proper time,

$$p_i = \{\mathbf{p}, -E/c\} = \left\{ \frac{m\mathbf{u}}{\sqrt{1 - u^2/c^2}}, -\sqrt{m^2c^2 + p^2} \right\} \quad (2.3)$$

is the four-momentum and

$$F_i = \left\{ \frac{\mathfrak{F}}{\sqrt{1 - u^2/c^2}}, -\frac{(\mathfrak{F} \cdot \mathbf{u})/c}{\sqrt{1 - u^2/c^2}} \right\} \quad (2.4)$$

the four-force.

We shall now in particular consider the case where the force \mathfrak{F}^0 is static in a certain system S^0 and derivable from a potential $U^0(\mathbf{x}^0)$ which is independent of t^0 , i. e.

$$F_i^0 = \left\{ \begin{array}{l} \mathfrak{F}^0 = -\text{grad } U^0 \\ -\frac{\partial U^0}{\partial \mathbf{x}^0}, \left(\frac{\partial U^0}{\partial \mathbf{x}^0} \cdot \mathbf{u}^0/c \right) \end{array} \right\} / \sqrt{1 - u^{02}/c^2}. \quad (2.5)$$

$U^0 = U^0(\mathbf{x}^0, a)$ may depend on a number of constant parameters (a_l) which characterize the external sources of the force. For a particle in a container of volume V^0 without other external forces, the potential energy U^0 is constant and shall be chosen equal to zero inside V^0 and $+\infty$ outside. In the presence of external forces like static electric or magnetic fields, $U^0 \neq 0$ will be varying inside the container. The parameters (a) determine the strength of the external forces as well as the form and the volume of the container. For constant (a) and varying \mathbf{x}^0

$$-dU^0 = -\frac{\partial U^0(\mathbf{x}^0, a)}{\partial \mathbf{x}^0} d\mathbf{x}^0$$

is equal to the work performed on the particle during a displacement $d\mathbf{x}^0$. For fixed values of \mathbf{x}^0 (and \mathbf{p}^0), the increase of the potential energy by a change (da_l) of the external parameters is

$$d_{(a)}U^0 = \sum_l \frac{\partial U^0(\mathbf{x}^0, a)}{\partial a_l} da_l \quad (2.6)$$

which must be interpreted as the work performed on the system by a change of the configuration of the surrounding systems.

For fixed (a), the three equations (2.1) with $i = 1, 2, 3$ in the system S^0 are the Euler equations of the variational principle

$$\left. \begin{aligned} \delta \int L^0 dt^0 &= 0 \\ L^0 &= -mc^2 \sqrt{1 - u^{02}/c^2} - U^0(\mathbf{x}^0), \end{aligned} \right\} \quad (2.7)$$

i. e.

$$\frac{d}{dt} \left(\frac{\partial L(\mathbf{u}^0, \mathbf{x}^0)}{\partial \mathbf{u}^0} \right) = \frac{\partial L(\mathbf{u}^0, \mathbf{x}^0)}{\partial \mathbf{x}^0}. \quad (2.8)$$

The canonical momentum \mathbf{P}^0 corresponding to the Lagrangian (2.7) is

$$\mathbf{P}^0 = \frac{\partial L^0(\mathbf{u}^0, \mathbf{x}^0)}{\partial \mathbf{u}^0} = \mathbf{p}^0, \quad (2.9)$$

i. e. in S^0 the canonical momentum is identical with the linear momentum \mathbf{p}^0 . The corresponding Hamiltonian

$$\xi^0 = \mathbf{P}^0 \cdot \mathbf{u}^0 - L^0 = E^0 + U^0(\mathbf{x}^0) = c \sqrt{m^2 c^2 + p^{02}} + U^0(\mathbf{x}^0) \quad (2.10)$$

is equal to the total energy of the particle in the external field. The Hamiltonian equations

$$\frac{d\mathbf{p}^0}{dt^0} = - \frac{\partial \xi^0(\mathbf{p}^0, \mathbf{x}^0)}{\partial \mathbf{x}^0}, \quad \frac{d\mathbf{x}^0}{dt^0} = \frac{\partial \xi^0(\mathbf{p}^0, \mathbf{x}^0)}{\partial \mathbf{p}^0} \quad (2.11)$$

are equivalent to the equations (2.8) or to (2.1) with $i = 1, 2, 3$. ξ^0 is a constant of the motion

$$\frac{d\xi^0}{dt^0} = - \frac{\partial L^0(\mathbf{u}^0, \mathbf{x}^0)}{\partial t^0} = 0 \quad (2.12)$$

which is equivalent to the fourth equation (2.1) in S^0 . The equation (2.6) may also be written

$$d_{(a)} U^0 = \sum_l \frac{\partial \xi^0(\mathbf{p}^0, \mathbf{x}^0, a)}{\partial a_l} da_l = d_{(a)} \xi^0. \quad (2.6')$$

We shall now consider the motion of the particle with respect to an arbitrary system of inertia S . Let \mathbf{v} be the velocity of S^0 with respect to S . Then, the corresponding four-velocity V_i is given by (1.3) and for simplicity we shall assume that the connection between the coordinates in S and S^0 is given by a Lorentz transformation without rotation of the spatial axes. If we treat $U^0(\mathbf{x}^0)$ as an invariant scalar it may also be regarded as a function of coordinates $x^i = \{\mathbf{x}, ct\}$ in S .

$U(x, a)$ then denotes the function obtained from $U^0(\mathbf{x}^0, a)$ by eliminating \mathbf{x}^0 by means of the Lorentz transformation connecting S and S^0 , i. e.

$$U(x, a) = U(\mathbf{x}, t, a) = U^0(\mathbf{x}^0, a). \quad (2.13)$$

In the present case, the four-force (2.4) is easily seen to have the form of a 'Lorentz force', i. e.

$$F_i = F_{ik} U^k / c^2 \quad (2.14)$$

where

$$U^i = \left\{ \frac{\mathbf{u}}{\sqrt{1 - u^2/c^2}}, \quad \frac{c}{\sqrt{1 - u^2/c^2}} \right\} \quad (2.15)$$

is the four-velocity of the particle, and the antisymmetric tensor F_{ik} is given by

$$F_{ik} = \frac{\partial U(x)}{\partial x^i} V_k - \frac{\partial U(x)}{\partial x^k} V_i. \quad (2.16)$$

Since $F_{ik} U^k$ is a 4-vector, the validity of the expression (2.14) for F_i follows from the remark that it reduces to the expression (2.5) for F_i^0 in the system S^0 where $V_i^0 = -c\delta_{i4}$. Introduction of (2.16) into (2.14) gives

$$F_i = \frac{V_k U^k}{c^2} \frac{\partial U}{\partial x^i} - \frac{V_i}{c^2} \frac{dU}{d\tau}. \quad (2.17)$$

Therefore, if we define a new 4-vector P_i by

$$P_i = p_i + \frac{V_i}{c^2} U(x, a), \quad (2.18)$$

the equations (2.1) may be written

$$\frac{dP_i}{d\tau} = K_i \quad (2.19)$$

with

$$K_i = \frac{V_k U^k}{c^2} \frac{\partial U(x)}{\partial x^i}. \quad (2.20)$$

Since $V^{0i} = c\delta_4^i$, i. e.

$$\frac{\partial U(x)}{\partial x^i} V^i = \frac{\partial U^0(\mathbf{x}^0)}{\partial x^{0z}} V^{0z} = 0, \quad (2.21)$$

the 4-vector K_i is orthogonal to V^i , i. e.

$$K_i V^i = 0. \quad (2.22)$$

If we put

$$P_i = \{ \mathbf{P}, -\xi/c \} \quad (2.23)$$

we get from (2.18,3) and (1.3)

$$\left. \begin{aligned} \mathbf{P} &= \mathbf{p} + \gamma \mathbf{v} U(\mathbf{x})/c^2 \\ \xi &= E + \gamma U(\mathbf{x}) \end{aligned} \right\} \quad (2.24)$$

Then we get from (1.3), (2.15,20,22)

$$K_i = \left\{ \frac{\mathfrak{K}}{\sqrt{1-u^2/c^2}}, -\frac{(\mathfrak{K} \cdot \mathbf{v})/c}{\sqrt{1-u^2/c^2}} \right\} \quad (2.25)$$

with

$$\mathfrak{K} = -(1 - (\mathbf{v} \cdot \mathbf{u})/c^2) \gamma \frac{\partial U(\mathbf{x}, t)}{\partial \mathbf{x}}. \quad (2.26)$$

For $i = 1, 2, 3$ the equations of motion (2.19) are now

$$\frac{d\mathbf{P}}{dt} = \mathfrak{K} \quad (2.27)$$

which are the Euler equations of the variational principle

$$\delta \int L dt = 0 \quad (2.28)$$

with the Lagrangian

$$L(\mathbf{u}, \mathbf{x}, t) = -mc^2 \sqrt{1-u^2/c^2} - (1 - \mathbf{v} \cdot \mathbf{u}/c^2) \gamma U(\mathbf{x}, t). \quad (2.29)$$

For, by differentiating with respect to \mathbf{u} , we get

$$\frac{\partial L(\mathbf{u}, \mathbf{x}, t)}{\partial \mathbf{u}} = \mathbf{p} + \frac{\mathbf{v}}{c^2} \gamma U(\mathbf{x}, t) \equiv \mathbf{P}$$

on account of (2.24), and by differentiation with respect to \mathbf{x}

$$\frac{\partial L(\mathbf{u}, \mathbf{x}, t)}{\partial \mathbf{x}} = -(1 - \mathbf{v} \cdot \mathbf{u}/c^2) \gamma \frac{\partial U(\mathbf{x}, t)}{\partial \mathbf{x}} = \mathfrak{K} \quad (2.30)$$

on account of (2.26). Thus, \mathbf{P} in (2.23) is the canonical momentum and \mathfrak{K} may be called the canonical force. The corresponding Hamiltonian is

$$\begin{aligned} \mathbf{P} \cdot \mathbf{u} - L &= \mathbf{p} \cdot \mathbf{u} + (\mathbf{v} \cdot \mathbf{u})\gamma U(x)/c^2 + mc^2\sqrt{1 - u^2/c^2} + (1 - \mathbf{v} \cdot \mathbf{u}/c^2)\gamma U(x) \\ &= E + \gamma U(\mathbf{x}, t) = \tilde{\xi}. \end{aligned} \quad (2.31)$$

Hence, the quantity $\tilde{\xi}$ in (2.24) which together with the canonical momentum \mathbf{P} defines the 'canonical' four-momentum vector (2.23) is equal to the total energy of the particle in the external field. Therefore, $\gamma U(\mathbf{x}, t)$ may be interpreted as the potential energy. In contrast to $U^0(\mathbf{x}^0)$ and ξ^0 , both U and $\tilde{\xi}$ are time-dependent and $\tilde{\xi}$ is not a constant of the motion. From (2.19) with $i = 4$ we get, by (2.23,25)

$$\frac{d\tilde{\xi}}{dt} = \mathfrak{K} \cdot \mathbf{v} = -(1 - \mathbf{v} \cdot \mathbf{u}/c^2)\gamma \left(\mathbf{v} \cdot \frac{\partial U(\mathbf{x}, t)}{\partial \mathbf{x}} \right) = -\frac{\partial L(\mathbf{u}, \mathbf{x}, t)}{\partial t} \quad (2.32)$$

on account of (2.21,26,29). The equations (2.27,32) may be comprised in the four-component equation

$$\frac{dP_i}{dt} = \frac{\partial L(\mathbf{u}, \mathbf{x})}{\partial x^i} = -(1 - \mathbf{v} \cdot \mathbf{u}/c^2)\gamma \frac{\partial U(x)}{\partial x^i} \quad (2.33)$$

on account of (2.30).

If we eliminate the velocity \mathbf{u} in (2.31) by means of (2.24), $\tilde{\xi} = \tilde{\xi}(\mathbf{P}, \mathbf{x}, t)$ appears as a function of \mathbf{P} and \mathbf{x} and the equations of motion may be written in the Hamiltonian form

$$\frac{d\mathbf{P}}{dt} = -\frac{\partial \tilde{\xi}(\mathbf{P}, \mathbf{x}, t)}{\partial \mathbf{x}}, \quad \frac{d\mathbf{x}}{dt} = \frac{\partial \tilde{\xi}(\mathbf{P}, \mathbf{x}, t)}{\partial \mathbf{P}}. \quad (2.34)$$

On account of the relation [9]

$$\frac{\sqrt{1 - u^2/c^2}}{\sqrt{1 - u^{02}/c^2}} = \gamma(1 - \mathbf{v} \cdot \mathbf{u}/c^2) = \frac{1}{\gamma(1 + \mathbf{v} \cdot \mathbf{u}^0/c^2)}, \quad (2.35)$$

the variational principle (2.7,28) is invariant. For, by (2.29,2,7), we get

$$Ldt = \frac{Ld\tau}{\sqrt{1 - u^2/c^2}} = \frac{L^0d\tau}{\sqrt{1 - u^{02}/c^2}} = L^0dt^0.$$

The preceding considerations are easily generalized to a gas of n non-interacting particles of mass m subjected to the same external force. In this case the Lagrangian L_g is simply the sum of the Lagrangian functions (2.29) for each particle, i. e.

$$\left. \begin{aligned} L_g &= \sum_{r=1}^n L^{(r)}(\mathbf{u}^{(r)}, \mathbf{x}^{(r)}, t) \\ L^{(r)} &= -mc^2 \sqrt{1 - u^{(r)2}/c^2} - (1 - \mathbf{v} \cdot \mathbf{u}^{(r)}/c^2) \gamma U(\mathbf{x}^{(r)}, t). \end{aligned} \right\} \quad (2.36)$$

The corresponding Hamiltonian is

$$\mathfrak{H}_g = \sum_{r=1}^n \mathfrak{H}^{(r)}(\mathbf{P}^{(r)}, \mathbf{x}^{(r)}, t). \quad (2.37)$$

The suffix g indicates that the quantity in question refers to the system as a whole. This case is therefore a trivial generalization of the one-body problem and, in the following section, we shall first consider the statistical mechanics of a single particle and afterwards make the generalization to the n -body system. Let P_i^g denote the sum of the canonical four-momenta of all particles in the gas, i. e.

$$P_i^g = \sum_r P_i^{(r)}(\mathbf{p}^{(r)}, \mathbf{x}^{(r)}, t, a) = \sum_{r=1}^n p_i^{(r)} + \frac{V_i}{c^2} \sum_{r=1}^n U(\mathbf{x}^{(r)}, t, a). \quad (2.38)$$

It depends on the external parameters (a) as well as on the coordinates and momenta. For constant values of the latter quantities an increase (da_l) of the a 's changes the quantity P_i^g by an amount

$$d_{(a)} P_i^g = \sum_l \frac{\partial P_i^g}{\partial a_l} da_l = \frac{V_i}{c^2} \sum_{r=1}^n \sum_l \frac{\partial U(\mathbf{x}^{(r)}, t, a)}{\partial a_l} da_l. \quad (2.39)$$

3. The Structure of Relativistic Phase-spaces

In classical statistical mechanics one introduces the important notion of a 'phase-space' which for a one-particle system is a space of six dimensions where every phase-point corresponds to a definite mechanical state of the system. However, in a relativistic theory it is convenient to introduce a separate phase-space $\Sigma(S)$ for each system of reference S . Each mechanical state is pictured as a point in $\Sigma(S)$ with the six coordinates (\mathbf{P}, \mathbf{x}) . The 'state-points' are moving according to the Hamiltonian equations (2.34),

which determine the curve (the phase-track) in $\Sigma(S)$ described by a state-point $(\mathbf{P}(t), \mathbf{x}(t))$ in the course of the time t .

On account of the Hamiltonian form of the equations of motion in every system S , Liouville's theorem holds in every $\Sigma(S)$ although ξ in general is time dependent. Thus, if $\Omega(t_0)$ is the region in $\Sigma(S)$ which is occupied by state points at the time t_0 and $\Omega(t)$ the region occupied by the same state-points at the time t , then the volumes of the two regions are equal, i. e.

$$\left. \begin{aligned} V_{\Omega(t)} &\equiv \iiint_{\Omega(t)} d\mathbf{P}d\mathbf{x} = \iiint_{\Omega(t_0)} d\mathbf{P}d\mathbf{x} \equiv V_{\Omega(t_0)}; \\ d\mathbf{P}d\mathbf{x} &\equiv dP_x dP_y dP_z dx dy dz. \end{aligned} \right\} \quad (3.1)$$

(In every $\Sigma(S)$ the volume is defined in the same way as in a Euclidean space with Cartesian coordinates).

In S^0 where ξ^0 is independent of t^0 the phase-tracks are fixed curves in $\Sigma(S^0)$. This is not the case in S where the direction of a phase-track passing through a fixed point is given by the 'phase velocity' $\left(\frac{d\mathbf{P}}{dt}, \frac{d\mathbf{x}}{dt}\right)$ which by (2.34) is seen to be time dependent.

Instead of the canonical variables (\mathbf{P}, \mathbf{x}) we may also use the non-canonical variables

$$\xi_\mu \equiv (p_x, p_y, p_z, x, y, z) \quad (3.2)$$

as 'coordinates' of the phase points. From the 'transformation' equations (2.24)

$$\mathbf{P} = \mathbf{p} + \mathbf{v}\gamma U(x)/c^2 \quad (3.3)$$

it is easily seen that the corresponding Jacobian determinant is equal to unity, i. e.

$$J = \frac{d(\mathbf{P}, \mathbf{x})}{d(\mathbf{p}, \mathbf{x})} = 1. \quad (3.4)$$

Thus, by Jacobi's theorem the volume of a region Ω may also be written

$$V_\Omega = \iiint_{\Omega} d\mathbf{p}d\mathbf{x}, \quad d\mathbf{p}d\mathbf{x} = \prod_{\mu=1}^6 d\xi_\mu. \quad (3.5)$$

In the new coordinates, Liouville's theorem (3.1) takes the form

$$V_{\Omega(t)} = \iiint_{\Omega(t)} d\mathbf{p}d\mathbf{x} = \iiint_{\Omega(t_0)} d\mathbf{p}d\mathbf{x} = V_{\Omega(t_0)}. \quad (3.6)$$

The equations (3.1,6) show that the volume $V_{\Omega(t)}$ occupied by the state-points which lie inside a region $\Omega(t)$ at time t is independent of t . Further this volume is relativistically invariant in the following sense. Consider the state-points which at the time t^0 in S^0 are situated inside a region $\Omega^0(t^0)$ of $\Sigma(S^0)$. The same state-points are moving through $\Sigma(S)$ of another system S according to the equations (2.34). At the time t their simultaneous positions will span a region $\Omega(t)$. Then

$$V_{\Omega^0(t^0)} \equiv \iiint_{\Omega^0(t^0)} d\mathbf{p}^0 d\mathbf{x}^0 = \iiint_{\Omega(t)} d\mathbf{p} d\mathbf{x} = V_{\Omega(t)} \quad (3.7)$$

independently of the choice of t^0 and t . The proof of this theorem is a little intricate and, for simplicity, we shall consider the special case (which does not spoil the generality of the proof), where Ω^0 and Ω are infinitesimal and the relative velocity \mathbf{v} of S and S^0 is

$$\mathbf{v} = \{v, 0, 0\}. \quad (3.8)$$

A state-point which at the time t passes through a point $\xi_\mu = (\mathbf{p}, \mathbf{x})$ in $\Sigma(S)$ will in $\Sigma(S^0)$ go through a point $\xi_\mu^0 = (\mathbf{p}^0, \mathbf{x}^0)$ at a time t^0 given by the Lorentz transformation

$$\left. \begin{aligned} p_x^0 &= \gamma[p_x - vE/c^2], & p_y^0 &= p_y, & p_z &= p_z^0 \\ x^0 &= \gamma[x - vt], & y^0 &= y, & z^0 &= z \end{aligned} \right\} \quad (3.9)$$

$$t^0 = \gamma[t - vx/c^2]. \quad (3.10)$$

Here we have made use of the 4-vector character of $p_i = \{\mathbf{p}, -E/c\}$. Since $E = c\sqrt{m^2c^2 + p^2}$, the equations (3.9) represent a non-linear transformation

$$\xi_\mu^0 = f_\mu(\xi_\nu, t) \quad (3.11)$$

which defines a certain one to one correspondence of the points in $\Sigma(S^0)$ and $\Sigma(S)$. On account of the relation

$$\frac{\partial E}{\partial \mathbf{p}} = \frac{c^2 \mathbf{p}}{E} = \mathbf{u}, \quad (3.12)$$

the partial derivatives $\frac{\partial \xi_\mu^0}{\partial \xi_\nu} = \frac{\partial f_\mu(\xi, t)}{\partial \xi_\nu}$ are given by the matrix

$$\frac{\partial f_{\mu}}{\partial \xi_{\nu}} = \begin{pmatrix} \gamma(1 - vu_x/c^2) - \gamma vu_y/c^2 - \gamma vu_z/c^2 & 0 & 0 & 0 & 0 & 0 \\ 0 & 1 & 0 & 0 & 0 & 0 \\ 0 & 0 & 1 & 0 & 0 & 0 \\ 0 & 0 & 0 & \gamma & 0 & 0 \\ 0 & 0 & 0 & 0 & 1 & 0 \\ 0 & 0 & 0 & 0 & 0 & 1 \end{pmatrix} \quad (3.13)$$

Now, consider the state-points in $\Sigma(S)$ which at the time t are passing through the phase points inside an infinitesimal parallelepiped $\Omega(t)$ spanned by six infinitesimal vectors along the ‘coordinate axes’, i. e.

$$\left. \begin{aligned} d^{(1)}\xi_{\mu} &= (dp_x, 0, 0, 0, 0, 0) \\ d^{(2)}\xi_{\mu} &= (0, dp_y, 0, 0, 0, 0) \\ &\dots\dots\dots \\ &\dots\dots\dots \\ d^{(6)}\xi_{\mu} &= (0, 0, 0, 0, 0, dz) \end{aligned} \right\} \quad (3.14)$$

or

$$\left. \begin{aligned} d^{(\alpha)}\xi_{\mu} &= \delta_{\mu}^{\alpha} d\xi_{\alpha}, \quad \alpha = 1, 2, 3, 4, 5, 6 \\ &(\text{no summation over } \alpha!) \\ d\xi_{\alpha} &= (dp_x, dp_y, dp_z, dx, dy, dz). \end{aligned} \right\} \quad (3.15)$$

The volume of this region is given by the determinant

$$dV_{\Omega(t)} = |d^{(\alpha)}\xi_{\mu}| = |\delta_{\mu}^{\alpha} d\xi_{\alpha}| = \prod_{\alpha=1}^6 d\xi_{\alpha} = \mathbf{dpdx}. \quad (3.16)$$

In the mapping of $\Sigma(S)$ on $\Sigma(S^0)$, defined by (3.9) or (3.11), the region $\Omega(t)$ corresponds to a region $\Omega^0(t^0, t^0 + dt^0)$ in $\Sigma(S^0)$ which is spanned by the six infinitesimal ‘vectors’

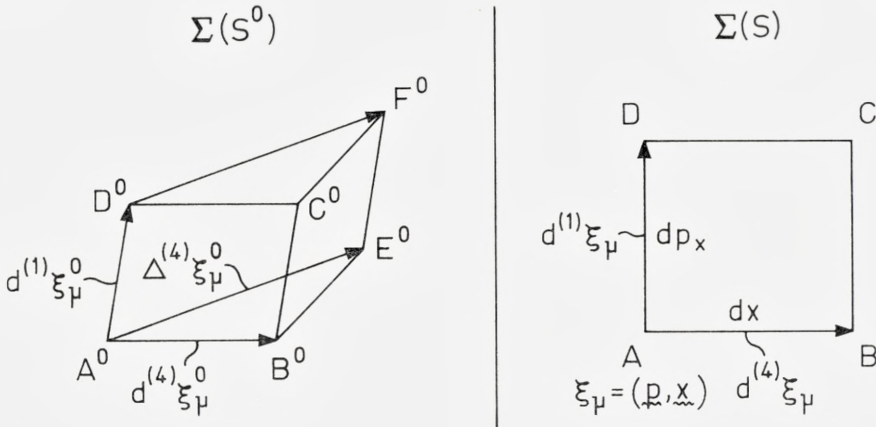
$$d^{(\alpha)}\xi_{\mu}^0 = \sum_{\nu} \frac{\partial f_{\mu}(\xi, t)}{\partial \xi_{\nu}} d^{(\alpha)}\xi_{\nu} = \frac{\partial f_{\mu}}{\partial \xi_{\alpha}} d\xi_{\alpha}, \quad (3.17)$$

on account of (3.15). The volume of this region is given by the determinant

$$dV_{\Omega^0(t^0, t^0 + dt)} = \left| \frac{df_{\mu}}{\partial \xi_{\alpha}} d\xi_{\alpha} \right| = J \prod_{\alpha=1}^6 d\xi_{\alpha} = J dV_{\Omega(t)} \quad (3.18)$$

where the Jacobian J is the determinant of the matrix (3.13), i. e.

$$J = \frac{d(\mathbf{p}^0, \mathbf{x}^0)}{d(\mathbf{p}, \mathbf{x})} = \gamma^2(1 - vu_x/c^2). \quad (3.19)$$



In the 2-dimensional picture above the region $\Omega(t)$ in $\Sigma(S)$ is represented by the inside of the rectangle $ABCD$ with sides dx and dp_x , the vectors $d^{(1)}\xi_\mu$ and $d^{(4)}\xi_\mu$ being represented by the lines \overrightarrow{AD} and \overrightarrow{AB} , respectively. The corresponding vectors $d^{(1)}\xi_\mu^0$ and $d^{(4)}\xi_\mu^0$ in $\Sigma(S^0)$, as given by (3.17), are represented by the lines $\overrightarrow{A^0D^0}$ and $\overrightarrow{A^0B^0}$, and the region $\Omega^0(t^0, t^0 + dt^0)$ is the inside of the parallelogram $A^0B^0C^0D^0$.

According to (3.18,19) the volume $dV_{\Omega^0(t^0, t^0 + dt^0)}$ of this region is *not* equal to the volume $dV_{\Omega(t)}$ of $\Omega(t)$. However, the points inside $\Omega^0(t^0, t^0 + dt^0)$ are *not* the positions in $\Sigma(S^0)$ of the state points in $\Omega(t)$ at the same time t^0 , since the passage time, for the points along the lines parallel to A^0B^0 , according to (3.10) vary linearly from t^0 to $t^0 + dt^0$ with

$$dt^0 = -\frac{\gamma v}{c^2} dx \tag{3.20}$$

which is negative. During the time $|dt^0| = \frac{\gamma v}{c^2} dx$, the points on the line B^0C^0 are displaced by a displacement vector $\delta\xi_\mu^0$ which, if we neglect small terms of the second order, is given by

$$d\xi_\mu^0 = \left(\frac{d\mathbf{p}^0}{dt^0} |dt^0|, \frac{d\mathbf{x}^0}{dt^0} |dt^0| \right) = \left(-\frac{\partial \xi_\mu^0}{\partial \mathbf{x}^0} \frac{\gamma v dx}{c^2}, \frac{\gamma v \mathbf{u}^0}{c^2} dx \right). \tag{3.21}$$

In the picture this constant vector is represented by $\overrightarrow{B^0E^0}$ or $\overrightarrow{C^0F^0}$. The state-points, which at the time $t^0 + dt^0 = t^0 - \frac{\gamma v}{c^2} dx$ were in B^0 and C^0 , will

at the time t^0 be in the positions E^0 and F^0 , respectively, and the whole line B^0C^0 will be displaced to E^0F^0 . Thus, the region $\Omega^0(t^0)$ which at the time t^0 is occupied by the state points inside $\Omega(t)$ is in the figure above represented by the parallelogram $A^0E^0F^0D^0$ spanned by the vectors $\overrightarrow{A^0D^0}$ and $\overrightarrow{A^0E^0}$, i.e. by the vectors $d^{(1)}\xi_\mu^0$ and $d^{(4)}\xi_\mu^0 + \delta\xi_\mu^0 = \Delta\xi_\mu^0$. Therefore, in the 6-dimensional phase space the region $\Omega^0(t^0)$ is spanned by the six vectors

$$\Delta^{(\omega)}\xi_\mu^0 = \{d^{(1)}\xi_\mu^0, d^{(2)}\xi_\mu^0, d^{(3)}\xi_\mu^0, \Delta\xi_\mu^0, d^{(5)}\xi_\mu^0, d^{(6)}\xi_\mu^0\} \quad (3.22)$$

with

$$\left. \begin{aligned} \Delta^{(4)}\xi_\mu^0 &= \Delta\xi_\mu^0 = d^{(4)}\xi_\mu^0 + \delta\xi_\mu^0 = \frac{\partial f_\mu}{\partial \xi_4} dx + \delta\xi_\mu^0 \\ &= \left(-\frac{\partial \xi^0}{\partial x^0} \frac{\gamma v}{c^2}, -\frac{\partial \xi^0}{\partial y^0} \frac{\gamma v}{c^2}, -\frac{\partial \xi^0}{\partial z^0} \frac{\gamma v}{c^2}, \gamma \left(1 + \frac{vu_x^0}{c^2} \right), \frac{\gamma vu_y^0}{c^2}, \frac{\gamma vu_z^0}{c^2} \right) dx \end{aligned} \right\} \quad (3.23)$$

on account of (3.17,21,13). The other vectors $\Delta^{(\omega)}\xi_\mu^0$ are given by (3.17,13). The volume of the region spanned by the vectors (3.22) is

$$dV_{\Omega^0(t^0)} = |\Delta^{(\omega)}\xi_\mu^0|$$

for which one easily gets the value

$$dV_{\Omega^0(t^0)} = \gamma^2(1 - vu_x/c^2)(1 + vu_x^0/c^2)d\mathbf{p}d\mathbf{x}$$

or, on account of (2.35) and (3.8,16),

$$dV_{\Omega^0(t^0)} = d\mathbf{p}d\mathbf{x} = dV_{\Omega(t)}. \quad (3.24)$$

Since dV_Ω is invariant under arbitrary spatial rotations, it is obvious that (3.24) holds for an arbitrary system S (arbitrary \mathbf{v}). Thus, for two arbitrary Lorentz systems S and S' we have

$$dV_{\Omega(t)} = dV_{\Omega'(t')}. \quad (3.25)$$

The generalization of these results to a system of n non-interacting particles is trivial. The phase spaces $\Sigma(S)$ are $6n$ -dimensional, and as the coordinates of the phase-points we may take the $6n$ variables

$$\xi_\mu = (\mathbf{p}^{(1)}, \mathbf{x}^{(1)}, \dots, \mathbf{p}^{(n)}, \mathbf{x}^{(n)}, \dots, \mathbf{p}^{(n)}, \mathbf{x}^{(n)}). \quad (3.26)$$

If the volume of a region Ω in $\Sigma(S)$ is defined by

$$V_{\Omega} = \int_{\Omega} \dots \int_{\Omega} \prod_{\mu=1}^{6n} d\xi_{\mu} = \int_{\Omega} \dots \int_{\Omega} d\mathbf{p}^{(1)} d\mathbf{x}^{(1)} \dots d\mathbf{p}^{(n)} d\mathbf{x}^{(n)} \quad (3.27)$$

it is obvious that Liouville's theorem (3.6) as well as the relativistic invariance of dV_{Ω} , i. e. equation (3.24) holds also for a gas of n particles.

4. Statistical Ensembles of Mechanical Systems in the Phase-Space $\Sigma(\mathcal{S})$ of an Arbitrary Lorentz System \mathcal{S} . Canonical Ensembles

Let us start by considering an arbitrary ensemble of one-particle systems. In $\Sigma(\mathcal{S})$ the distribution of the state-points of the ensemble is described by a probability density $\mathfrak{P}(\mathbf{p}, \mathbf{x}, t)$ which in general depends explicitly on the time. The number of systems which at the time t are lying inside an infinitesimal region $\Omega(t)$ of volume $dV_{\Omega(t)}$ at the place (\mathbf{p}, \mathbf{x}) is then by definition

$$N\mathfrak{P}(\mathbf{p}, \mathbf{x}, t)dV_{\Omega(t)}, \quad (4.1)$$

where N is the total number of systems in the ensemble ($N \rightarrow \infty$). At a different time t_0 the same number of state-points is given by

$$N\mathfrak{P}(\mathbf{p}_0, \mathbf{x}_0, t_0)dV_{\Omega(t_0)} \quad (4.2)$$

where

$$dV_{\Omega(t_0)} = dV_{\Omega(t)} \quad (4.3)$$

on account of (3.6). Thus, (4.1,2) gives

$$\mathfrak{P}(\mathbf{p}_0, \mathbf{x}_0, t_0) = \mathfrak{P}(\mathbf{p}, \mathbf{x}, t) \quad (4.4)$$

which shows that $\mathfrak{P}(\mathbf{p}, \mathbf{x}, t)$ is a constant of the motion, i. e.

$$\frac{d\mathfrak{P}(\mathbf{p}, \mathbf{x}, t)}{dt} = \frac{\partial \mathfrak{P}(\mathbf{p}, \mathbf{x}, t)}{\partial \mathbf{x}} \cdot \mathbf{u} + \frac{\partial \mathfrak{P}(\mathbf{p}, \mathbf{x}, t)}{\partial \mathbf{p}} \cdot \frac{d\mathbf{p}}{dt} + \frac{\partial \mathfrak{P}(\mathbf{p}, \mathbf{x}, t)}{\partial t} = 0. \quad (4.5)$$

By integration over the whole phase-space we get for all t

$$\iint \mathfrak{P}(\mathbf{p}, \mathbf{x}, t) d\mathbf{p} d\mathbf{x} = 1. \quad (4.6)$$

All these relations hold for any Lorentz system. In the phase-space $\Sigma(\mathcal{S}')$ of another system \mathcal{S}' , the state-points given by (4.1) occupy at a time t' an infinitesimal region $\Omega'(t')$ around the point $(\mathbf{p}', \mathbf{x}')$, where $(\mathbf{p}', \mathbf{x}', t')$ and

$(\mathbf{p}, \mathbf{x}, t)$ are connected by the Lorentz transformation leading from S to S' . On account of (3.25) the volume $dV_{\Omega'(t')}$ of this region is equal to $dV_{\Omega(t)}$. Therefore, since the number (4.1) of systems is also equal to

$$N\mathfrak{F}'(\mathbf{p}', \mathbf{x}', t')dV_{\Omega'(t')}, \quad (4.7)$$

where $\mathfrak{F}'(\mathbf{p}', \mathbf{x}', t')$ is the probability density in $\Sigma(S')$, we may conclude that the probability density is a relativistic invariant, i.e.

$$\mathfrak{F}(\mathbf{p}, \mathbf{x}, t) = \mathfrak{F}'(\mathbf{p}', \mathbf{x}', t') \quad (4.8)$$

where the arguments in the two functions are connected by the Lorentz transformation $S \rightarrow S'$.

The mean value of any physical quantity $F(\mathbf{p}, \mathbf{x}, t)$ like the energy \mathfrak{E} or the canonical momentum \mathbf{P} is, at the time t , given by

$$\langle F(\mathbf{p}, \mathbf{x}, t) \rangle = \iint F(\mathbf{p}, \mathbf{x}, t) \mathfrak{F}(\mathbf{p}, \mathbf{x}, t) d\mathbf{p} d\mathbf{x}. \quad (4.9)$$

For a system of n non-interacting particles, the probability density $\mathfrak{F}_g(\xi_\mu, t)$ in the 6 n -dimensional phase-space $\Sigma(S)$ is the product of the probability densities in the 6-dimensional phase-spaces of the separate particles

$$\mathfrak{F}_g(\xi_\mu, t) = \prod_{r=1}^n \mathfrak{F}^{(r)}(\mathbf{p}^{(r)}, \mathbf{x}^{(r)}, t). \quad (4.10)$$

We shall now in particular consider the case where the ensemble is canonically distributed in S^0 . Such an ensemble represents an adequate description of our knowledge about the mechanical state of a gas in a container at rest in S^0 and in thermal equilibrium with a heat reservoir of given temperature T^0 . For an ideal gas each of the particles in the gas will then be canonically distributed with a probability density

$$\mathfrak{F}^0(\mathbf{p}^0, \mathbf{x}^0) = e^{(\varphi^0 - \theta^0 \mathfrak{E}^0(\mathbf{p}^0, \mathbf{x}^0, a))/k} \quad (4.11)$$

where k is Boltzmann's constant and $\theta^0 = 1/T^0$ is the reciprocal of the proper temperature T^0 .

$$\varphi^0 = \varphi_p^0 + \varphi_q^0 \quad (4.12)$$

are phase-independent quantities defined by

$$\left. \begin{aligned} e^{-\varphi^0/k} &= \iint e^{-\theta^0 \mathfrak{E}^0/k} d\mathbf{p}^0 d\mathbf{x}^0, \\ e^{-\varphi_p^0/k} &= \int e^{-\theta^0 E^0/k} d\mathbf{p}^0, \quad e^{-\varphi_q^0/k} = \int e^{-\theta^0 U^0(\mathbf{x}^0, a)/k} d\mathbf{x}^0. \end{aligned} \right\} \quad (4.13)$$

These equations determine $\varphi^0 = \varphi^0(\theta^0, a)$ as a function of θ^0 and the external parameters (a) which define the thermodynamical state of the system in S^0 . The thermodynamical significance of φ^0 is given by the relation

$$F^0 = n\varphi^0/\theta^0 = \Phi^0/\theta^0 \tag{4.14}$$

where F^0 is the free energy of the gas in the rest System S^0 (see § 5).

While \mathfrak{P}^0 in S^0 is independent of t^0 the probability density \mathfrak{P} in S is time dependent. Since the canonical four-momentum P_i is a 4-vector we have

$$P_i V^i = P_i^0 V^{0i} = -\xi^0. \tag{4.15}$$

Thus, if we introduce the 4-vector (1.15,16)

$$\theta^i = \theta^0 V^i = \theta V^i \tag{4.16}$$

we get, on account of the invariance of the probability density expressed by (4.8) with $S' = S^0$,

$$\mathfrak{P}(\mathbf{p}, \mathbf{x}, t) = e^{(\varphi + \theta^i P_i)/k}, \tag{4.17}$$

where

$$\varphi = \varphi^0 \tag{4.18}$$

is an invariant.

In the general system S the thermodynamical state is determined by the four parameters θ^i together with the external parameters (a_i). The expression (4.17) is closely related to expressions used by MAZUR and LURÇAT and by BARUT [10].

5. The Mean Values of the Energy and the Canonical Momentum and their Transformation Properties

The mean values in question are, in a system S ,

$$\left. \begin{aligned} \langle \xi \rangle &= \iint \xi(\mathbf{p}, \mathbf{x}, t) \mathfrak{P}(\mathbf{p}, \mathbf{x}, t) d\mathbf{p} d\mathbf{x}, \\ \langle \mathbf{P} \rangle &= \iint \mathbf{P}(\mathbf{p}, \mathbf{x}, t) \mathfrak{P}(\mathbf{p}, \mathbf{x}, t) d\mathbf{p} d\mathbf{x}, \end{aligned} \right\} \tag{5.1}$$

where the integrations are to be performed at constant time. From these expressions it would seem that $\langle \xi \rangle$ and $\langle \mathbf{P} \rangle$ are time dependent. However,

a calculation of the integrals (5.1) will show that these quantities are independent of t for a canonical ensemble with \mathfrak{F} given by (4.17).

Let us again for simplicity arrange it so that the velocity of S^0 with respect to S is

$$\mathbf{v} = \{v, 0, 0\} \quad (5.2)$$

in which case the equations (3.9) are valid. In order to perform the integrations in (5.1) it is convenient for constant t to introduce the quantities $\mathbf{p}^0, \mathbf{x}^0$ defined by (3.9) as new variables of integration. The inverse transformations of (3.9) are (for constant t)

$$\left. \begin{aligned} p_x &= \gamma[p_x^0 + vE^0/c^2], & p_y &= p_y^0, & p_z &= p_z^0 \\ x &= vt + x^0/\gamma, & y &= y^0, & z &= z^0. \end{aligned} \right\} \quad (5.3)$$

According to Jacobi's theorem we have then to replace $d\mathbf{p} d\mathbf{x}$ by

$$d\mathbf{p}d\mathbf{x} = Jd\mathbf{p}^0d\mathbf{x}^0. \quad (5.4)$$

Here J is the Jacobian determinant corresponding to (5.3) which is easily seen to be

$$J = \frac{d(\mathbf{p}, \mathbf{x})}{d(\mathbf{p}^0, \mathbf{x}^0)} = 1 + vE_x^0/c^2 = 1 + v p_x^0/E^0. \quad (5.5)$$

J in (5.5) is of course the reciprocal of the determinant (3.19) (comp. (2.35)). Since P_i is a 4-vector and $\mathbf{P}^0 = \mathbf{p}^0$ we have

$$\mathfrak{H} = \gamma[\mathfrak{H}^0 + v p_x^0]$$

and, because of the invariance of the probability density, the first integral in (5.1) becomes

$$\langle \mathfrak{H} \rangle = \iint \mathfrak{F}^0(\mathbf{p}^0, \mathbf{x}^0) \gamma(\mathfrak{H}^0 + v p_x^0) (1 + v p_x^0/E^0) d\mathbf{p}^0 d\mathbf{x}^0. \quad (5.6)$$

Here we have made use of the time independence of \mathfrak{F}^0 .

In the next section we shall consider a case where the probability density $\mathfrak{F}^0(\mathbf{p}^0, \mathbf{x}^0, t^0)$ is t^0 -dependent. In applying the formula (5.6) one has then in $\mathfrak{F}^0(\mathbf{p}^0, \mathbf{x}^0, t^0)$ for the argument t^0 to substitute the expression (3.10), which by means of (5.3) may be written

$$t^0 = \gamma[t - vx/c^2] = t/\gamma - vx^0/c^2. \quad (5.7)$$

However, in the present case we get from (5.6)

$$\langle \xi \rangle = \gamma \left[\langle \xi^0 \rangle^0 + v \langle p_x^0 \rangle^0 + \left\langle \frac{v \xi^0}{E^0} p_x^0 \right\rangle^0 + \left\langle \frac{v^2 p_x^{02}}{E^0} \right\rangle^0 \right], \quad (5.8)$$

where $\langle \rangle^0$ denotes the mean value over the ensemble (4.11) in $\Sigma(S^0)$. Since $\xi^0 = c\sqrt{m^2 c^2 + p^{02}} + U^0(\mathbf{x}^0)$ and E^0 depend on the squares of p_x^0, p_y^0 and p_z^0 only and the integration over these variables goes from $-\infty$ to $+\infty$, where $\xi^0 = +\infty$ and $\mathfrak{P}^0 = 0$, it is obvious that

$$\left. \begin{aligned} \langle p_x^0 \rangle^0 &= \langle p_y^0 \rangle^0 = \langle p_z^0 \rangle^0 = 0 \\ \langle p_x^0 p_y^0 \rangle^0 &= \langle p_x^0 p_z^0 \rangle^0 = \left\langle \frac{\xi^0 p_x^0}{E^0} \right\rangle^0 = 0. \end{aligned} \right\} \quad (5.9)$$

Further, as

$$\frac{c^2 p_x^{02}}{E^0} = p_x^0 \frac{\partial E^0}{\partial p_x^0} = p_x^0 \frac{\partial \xi^0}{\partial p_x^0}, \quad (5.10)$$

we get by partial integration

$$\left. \begin{aligned} \left\langle \frac{c^2 p_x^{02}}{E^0} \right\rangle^0 &= \iint p_x^0 \frac{\partial \xi^0}{\partial p_x^0} e^{(\varphi^0 - \theta^0 \xi^0)/k} \mathbf{d}p^0 \mathbf{d}\mathbf{x}^0 \\ &= -\frac{k}{\theta^0} \iint p_x^0 \frac{\partial \mathfrak{P}^0}{\partial p_x^0} \mathbf{d}p^0 \mathbf{d}\mathbf{x}^0 = kT^0 \iint \mathfrak{P}^0 \mathbf{d}p^0 \mathbf{d}\mathbf{x}^0 = kT^0. \end{aligned} \right\} \quad (5.11)$$

Hence,

$$\langle \xi \rangle = \gamma \left[\langle \xi^0 \rangle^0 + \frac{v^2}{c^2} kT^0 \right]. \quad (5.12)$$

Similarly we get from the second equation (5.1), remembering that

$$P_x = \gamma [p_x^0 + v \xi^0 / c^2], \quad P_y = P_y^0, \quad P_z = P_z^0, \quad (5.13)$$

$$\left. \begin{aligned} \langle P_x \rangle &= [\langle \xi^0 \rangle^0 + kT^0] \gamma v / c^2 \\ \langle P_y \rangle &= \langle P_z \rangle = 0 \end{aligned} \right\} \quad (5.14)$$

on account of (5.9,11).

For a gas of n non-interacting particles, the equations (5.12,14) hold for each particle separately and, by multiplying these equations by n , we get the corresponding formulae for the mean values of the total energy and canonical momentum of the gas. Thermodynamically, these quantities are to be identified with the energy and momentum of the gas, i. e.

$$\left. \begin{aligned} H &= \langle \mathfrak{S}_g \rangle = n \langle \mathfrak{S} \rangle, & H^0 &= \langle \mathfrak{S}_g^0 \rangle^0 = n \langle \mathfrak{S}^0 \rangle^0 \\ \mathbf{G} &= \langle \mathbf{P}_g \rangle = n \langle \mathbf{P} \rangle, & \mathbf{G}^0 &= \langle \mathbf{P}_g^0 \rangle^0 = n \langle \mathbf{P}^0 \rangle^0 \\ G_i &= \langle P_i^g \rangle = n \langle P_i \rangle, & G_i^0 &= \langle P_i^{g0} \rangle^0 = n \langle P_i^0 \rangle^0. \end{aligned} \right\} \quad (5.15)$$

The justification for this identification lies in the fact that the fluctuations of these quantities normally are completely negligible for large n of the order of the number of particles in a ponderable amount of gas. It is perhaps a little surprising that \mathbf{G} is identified with the mean value of the *canonical* momentum and not with that of the linear momentum. However, it should be noted that the potential $U^0(\mathbf{x}^0)$ of a particle in S^0 will represent a momentum $\gamma v \langle U^0 \rangle^0 / c^2$ in S and, according to (2.24), this is just the difference between the mean values of the canonical and the linear momenta. In the case where there are no other external fields than the forces from the walls, $\langle U^0 \rangle^0$ is zero and there is then no difference between $\langle \mathbf{P} \rangle$ and $\langle \mathbf{p} \rangle$.

From (5.12,14,15) we now get for the momentum and energy of the gas

$$\left. \begin{aligned} \mathbf{G} &= [H^0 + nkT^0] \gamma \mathbf{v} / c^2 \\ H &= \left[H^0 + \frac{v^2}{c^2} nkT^0 \right] \gamma \end{aligned} \right\} \quad (5.16)$$

holding for any direction of v . This may also be written

$$\left. \begin{aligned} G_i &= \frac{H^0}{c^2} V_i + g_i \\ g_i &= \left\{ \frac{nkT^0}{c^2} \gamma v_i, -\frac{nkT^0}{c^2} \frac{v^2 \gamma}{c} \right\}. \end{aligned} \right\} \quad (5.17)$$

The quantity g_i (and hence G_i) is *not* a 4-vector, but it satisfies in any system S the relation

$$\text{i. e.} \quad \left. \begin{aligned} g_i V^i &= 0, \\ G_i V^i &= -H^0. \end{aligned} \right\} \quad (5.18)$$

Since F_i is a 4-vector we have, in the case (5.2), the following transformation formula for the mechanical force \mathfrak{F} and the rate of mechanical work $\mathfrak{F}\mathbf{u}$:

$$\left. \begin{aligned}
 \tilde{\mathfrak{F}}_x &= \frac{\tilde{\mathfrak{F}}_x^0 + v(\tilde{\mathfrak{F}}^0 \cdot \mathbf{u}^0)/c^2}{1 + v u_x^0/c^2}, & \tilde{\mathfrak{F}}_y &= \frac{\tilde{\mathfrak{F}}_y^0}{\gamma[1 + v u_x^0/c^2]} \\
 \tilde{\mathfrak{F}}_z &= \frac{\tilde{\mathfrak{F}}_z^0}{\gamma[1 + v u_x^0/c^2]}, & \tilde{\mathfrak{F}}^0 &= -\frac{\partial U^0(\mathbf{x}^0)}{\partial \mathbf{x}^0} \\
 \tilde{\mathfrak{F}} \cdot \mathbf{u} &= \frac{\tilde{\mathfrak{F}}^0 \cdot \mathbf{u}^0 + v \tilde{\mathfrak{F}}_x^0}{1 + v u_x^0/c^2}.
 \end{aligned} \right\} \quad (5.19)$$

Similarly, we get for the canonical force (2.25,26)

$$\left. \begin{aligned}
 \mathfrak{K}_x &= \frac{\mathfrak{K}_x^0}{1 + v u_x^0/c^2}, & \mathfrak{K}_y &= \frac{\mathfrak{K}_y^0}{\gamma[1 + v u_x^0/c^2]} \\
 \mathfrak{K}_z &= \frac{\mathfrak{K}_z^0}{\gamma[1 + v u_x^0/c^2]}, & \mathfrak{K}^0 &= -\frac{\partial U^0(\mathbf{x}^0)}{\partial \mathbf{x}^0} \\
 \mathfrak{K} \cdot \mathbf{v} &= \frac{\mathfrak{K}^0 \cdot \mathbf{v}}{1 + v u_x^0/c^2} = \frac{\mathfrak{K}_x^0 v}{1 + v u_x^0/c^2}.
 \end{aligned} \right\} \quad (5.20)$$

The mean value of $\tilde{\mathfrak{F}}^0 = \mathfrak{K}^0$ over the ensemble (4.11) is

$$\left. \begin{aligned}
 \langle \tilde{\mathfrak{F}}^0 \rangle^0 &= \langle \mathfrak{K}^0 \rangle^0 = - \iint \frac{\partial U^0(\mathbf{x}^0)}{\partial \mathbf{x}^0} e^{(q^0 - \theta^0 E^0 - \theta^0 U^0)/k} d\mathbf{p}^0 d\mathbf{x}^0 \\
 &= \frac{k}{\theta^0} \iint \frac{\partial}{\partial \mathbf{x}^0} (e^{(q^0 - \theta^0 E^0 - \theta^0 U^0)/k}) d\mathbf{p}^0 d\mathbf{x}^0 = 0
 \end{aligned} \right\} \quad (5.21)$$

since \mathfrak{K}^0 vanishes outside the container. Similarly, we find

$$\langle \tilde{\mathfrak{F}}^0 \cdot \mathbf{u}^0 \rangle^0 = \langle \mathfrak{K}^0 \cdot \mathbf{v} \rangle^0 = 0. \quad (5.22)$$

By means of Jacobi's theorem and (5.4,5,19,20) we get, therefore, for the mean values of the forces and the rates of work in the system S

$$\left. \begin{aligned}
 \langle \tilde{\mathfrak{F}} \rangle &= \langle \mathfrak{K} \rangle = 0 \\
 \langle \tilde{\mathfrak{F}} \cdot \mathbf{u} \rangle &= \langle \mathfrak{K} \cdot \mathbf{v} \rangle = 0.
 \end{aligned} \right\} \quad (5.23)$$

Although the mean value of the total external force acting on the system is zero in a canonical ensemble, as one should expect for a thermodynamical system at rest and in thermal equilibrium in S^0 , we get of course in general a non-zero result if we take the mean value over this quantity when the

position of the particle is fixed or confined to a finite region ω^0 in space. Then we get in S^0 , instead of (5.21),

$$\left. \begin{aligned} \langle \mathfrak{F}^0 \rangle_{\omega^0}^0 &= \langle \mathfrak{S}^0 \rangle_{\omega^0}^0 = \int e^{(\varphi^0 - \theta^0 E^0)/k} d\mathbf{p}^0 k T^0 \int_{\omega^0} \frac{\partial e^{-\theta^0 U^0(\mathbf{x}^0)/k}}{\partial \mathbf{x}^0} d\mathbf{x}^0 \\ &= k T^0 \int_{\sigma^0} e^{-\theta^0 U^0(\mathbf{x}^0)/k} \mathbf{n} d\sigma^0 \bigg/ \int e^{-\theta^0 U^0(\mathbf{x}^0)/k} d\mathbf{x}^0, \end{aligned} \right\} \quad (5.24)$$

where the integral in the numerator is taken over the surface σ^0 of ω^0 and \mathbf{n} is an outward normal to the surface element $d\sigma$. The volume integral in the denominator in (5.24) follows from (4.13). In the case where the forces from the walls of the container are the only external forces present, we have

$$U^0(\mathbf{x}^0) = \left\{ \begin{array}{ll} 0 & \text{inside the container} \\ +\infty & \text{outside the container} \end{array} \right\} \quad (5.25)$$

and the denominator becomes

$$\int e^{-\theta^0 U^0/k} d\mathbf{x}^0 = \mathfrak{Q}^0 \quad (5.26)$$

where \mathfrak{Q}^0 is the rest volume of the container.

Now let us for ω^0 take a small cylinder with end surfaces $d\sigma_1^0$ and $d\sigma_2^0$ lying immediately inside and outside the container wall, respectively. (Actually we have to think of the wall as consisting of a thin transition layer inside which the potential rises rapidly but continuously from the value 0 at $d\sigma_1^0$ to a very large value at $d\sigma_2^0$.) Then, we get from (5.24) in the case (5.25)

$$\langle \mathfrak{F}^0 \rangle_{\omega^0}^0 = \langle \mathfrak{S}^0 \rangle_{\omega^0}^0 = k T^0 d\sigma_1^0 \mathbf{n}_1 / \mathfrak{Q}^0 \quad (5.27)$$

where \mathbf{n}_1 is the inward normal of the container wall. When multiplied by the number n of particles and divided by $d\sigma_1^0$ (5.27) gives the normal pressure p^0 of the wall on the gas. Hence,

$$p^0 = nkT^0 / \mathfrak{Q}^0. \quad (5.28)$$

When U^0 is given by (5.25) the pressure is the same everywhere, the thermodynamical body is homogeneous. On the other hand, when $U^0(\mathbf{x}^0) \neq 0$ inside the container, the pressure varies as $e^{-\theta^0 U^0/k}$, where U_1^0 is the value of the

potential U^0 at the place considered. If the considerations leading to (5.24,27) are carried through in the system S one easily finds by means of (5.19) that the pressure is an invariant, i.e.

$$p = p^0. \tag{5.29}$$

In the homogeneous case (5.25) where (5.28) holds the equations (5.16) may also be written

$$\left. \begin{aligned} \mathbf{G} &= [H^0 + p^0 \mathfrak{S}^0] \gamma \mathbf{v} / c^2 \\ H &= \left[H^0 + \frac{v^2}{c^2} p^0 \mathfrak{S}^0 \right] \gamma \end{aligned} \right\} \tag{5.30}$$

which are the equations for a thermodynamical fluid from which we started our considerations in reference 4.

Finally we shall consider the statistical analogue of the thermodynamical entropy S . If we put

$$\mathfrak{P} = e^\eta, \quad \mathfrak{P}^0 = e^{\eta^0}, \tag{5.31}$$

then the invariance of the probability density entails the invariance of the 'probability exponential' η , i.e.

$$\eta(\mathbf{p}, \mathbf{x}, t) = \eta^0(\mathbf{p}^0, \mathbf{x}^0) \tag{5.32}$$

where the arguments in these functions are connected by the equations (5.3). Hence

$$\langle \eta \rangle = \langle \eta^0 \rangle^0. \tag{5.33}$$

This also follows by means of Jacobi's theorem and (5.4,5) which gives

$$\begin{aligned} \langle \eta \rangle &= \int \int \eta \mathfrak{P} d\mathbf{p} d\mathbf{x} = \int \int \eta^0 \mathfrak{P}^0 (1 + v p_x^0 / E^0) d\mathbf{p}^0 d\mathbf{x}^0 \\ &= \langle \eta^0 \rangle^0 + v \langle \eta^0 p_x^0 / E^0 \rangle^0. \end{aligned}$$

By the arguments leading to (5.9) it follows that the last term in this expression is zero so that (5.33) follows. (5.33) holds for every particle and from (4.10) we get for the mean value of the probability exponential for a gas of n particles

$$\left. \begin{aligned} \eta_g &= \ln \mathfrak{P}_g \\ \langle \eta_g \rangle &= n \langle \eta \rangle = n \langle \eta^0 \rangle^0 = \langle \eta_g^0 \rangle^0. \end{aligned} \right\} \tag{5.34}$$

According to classical statistical mechanics the entropy S^0 of the gas in the rest system is

$$S^0 = -k\langle \eta_g^0 \rangle^0 = -kn\langle \eta_l^0 \rangle^0 \quad (5.35)$$

and, since the entropy is a relativistic invariant, (5.34) shows that the entropy S in an arbitrary system of inertia must be given by

$$S = -k\langle \eta_g \rangle = -kn\langle \eta_l \rangle. \quad (5.36)$$

For a canonical ensemble (4.17),

$$\eta_l = \ln \mathfrak{K} = (\varphi + \theta^i P_i)/k.$$

Hence

$$S = -nq - n\theta^i \langle P_i \rangle \quad (5.37)$$

or, by (5.15),

$$\left. \begin{aligned} \Phi &= -\theta^i G_i - S \\ \Phi &= n\varphi. \end{aligned} \right\} \quad (5.38)$$

Although G_i is not a 4-vector, $\theta^i G_i$ is an invariant. For we have, by (5.18) and (4.16),

$$\theta^i G_i = -\theta^0 H^0 = -H^0/T^0. \quad (5.39)$$

On account of the invariance of the entropy, (5.38) may then be written

$$\Phi = \Phi^0 = \frac{H^0 - T^0 S^0}{T^0} = F^0/T^0 \quad (5.40)$$

in accordance with (4.14).

In the present section we have considered the statistical expressions for the thermodynamic state functions G_i , p and S which are functions of θ^i and (a) . The change of these quantities in a process connecting two equilibrium states of the body is obtained by simple differentiation. However, we shall also consider quantities like $\Delta \mathbf{I}$ and ΔA (the mechanical impulse and the work) that are not absolute differentials and which therefore depend on the character of the process. In the next section we shall in particular consider processes which are reversible.

6. Statistical Description of a Reversible Process. The Mechanical Impulse and Work. The Four-Momentum of Supplied Heat

Consider a reversible thermodynamical process connecting to equilibrium states (θ^i, a_l) and $(\theta^i + \Delta\theta^i, a_l + da_l)$ and let us for the moment assume that the rest system S^0 is fixed during the process, which means that the velocity

\mathbf{v} of the thermodynamical body with respect to S is constant. Then, the change of θ^i is due solely to a change in the temperature T^0 of the amount ΔT^0 . Now, a process is reversible if it is performed so slowly that the system may be considered going through a succession of equilibrium states with temperatures $T^0(t^0)$ and external parameters $a_i(t^0)$, which are ‘infinitely’ slowly varying monotonic functions of the time t^0 . If τ^0 is the duration of the process we may assume that the temperature and the external parameters rise from the initial values (T^0, a_i) to the final values $(T^0 + \Delta T^0, a_i + \Delta a_i)$ in the time interval

$$0 \leq t^0 \leq \tau^0. \tag{6.1}$$

Experimentally, the body has during the process to be brought into contact with a ‘continuous’ succession of heat reservoirs of temperatures $T^0(t^0)$.

From classical statistical mechanics we know that the adequate statistical description of this process in the system S^0 is furnished by a ‘quasi-canonical’ ensemble with a probability density (for each particle) of the type

$$\mathfrak{P}^0(\mathbf{p}^0, \mathbf{x}^0, \theta^0(t^0), a(t^0)) = \exp\{(\varphi^0(\theta^0, a) - \theta^0(t^0)\xi^0(\mathbf{p}^0, \mathbf{x}^0, a(t^0)))/k\}. \tag{6.2}$$

Like $T^0(t^0)$ and $a(t^0)$,

$$\theta^0(t^0) = 1/T^0(t^0) \tag{6.3}$$

is also a slowly varying function in the interval (6.1) but constant outside, i. e.

$$\theta^0(t^0) = \left\{ \begin{array}{ll} \theta^0 & \text{for } t^0 \leq 0 \\ \theta^0 + \Delta\theta^0 & \text{for } t^0 \geq \tau^0. \end{array} \right\} \tag{6.4}$$

Since φ^0 is a function of θ^0 and (a) it will also be a function of t^0 in the interval (6.1). The condition for the correctness of this description is that τ^0 is extremely large compared with the period of the system, i. e.

$$\tau^0 \gg l^0/\langle u^0 \rangle^0, \tag{6.5}$$

where l^0 is the linear extension of the container and $\langle u^0 \rangle^0$ is the mean value of the particle velocity.

We shall now calculate the mean force and the mean rate of work on the particle in the general system S , and let us start by considering the case where the a ’s are kept constant during the process. As we shall see, this simple case exhibits already the typical new features introduced by the theory of relativity. In non-relativistic thermodynamics the mechanical work is zero in such a process and the change of the temperature is due solely

to the supply of heat energy. In a relativistic theory, this is still true in the rest system S^0 but, as was shown in detail in reference 4, in any other system S we have a finite impulse and a finite work performed by the external forces. We shall now calculate this effect from statistical mechanics.

For simplicity we shall start by assuming that the relative velocity \mathbf{v} is given by (5.2) so that (5.3) is the transformation connecting the phase-spaces $\Sigma(S)$ and $\Sigma(S^0)$. Then, using (5.19) and Jacobi's theorem (5.4,5), we get for the mean value of \mathfrak{F}_x at the time t in S

$$\langle \mathfrak{F}_x \rangle_t = \left. \iint \frac{\mathfrak{F}_x^0 + \frac{v}{c^2} (\mathfrak{F}^0 \cdot \mathbf{u}^0)}{1 + vp_x^0/E^0} \mathfrak{P}^0(\mathbf{p}^0, \mathbf{x}^0, \theta^0(t^0)) (1 + vp_x^0/E^0) d\mathbf{p}^0 d\mathbf{x}^0, \right\} \quad (6.6)$$

where \mathfrak{P}^0 is the distribution function (6.2) (with constant a 's). Here it must be remembered that $\theta^0(t^0)$ is a function of the variable

$$t^0 = t/\gamma - vx^0/c^2 \quad (6.7)$$

given by (5.7), which depends on the variable of integration x^0 . Hence

$$\langle \mathfrak{F}_x \rangle_t = \left. \begin{aligned} & \iint \left(-\frac{\partial U^0(\mathbf{x}^0)}{\partial \mathbf{x}^0} \right) \mathfrak{P}^0(\mathbf{p}^0, \mathbf{x}^0, \theta^0(t^0)) d\mathbf{p}^0 d\mathbf{x}^0 \\ & + v \iint \frac{(\mathfrak{F}^0 \cdot \mathbf{p}^0)}{E^0} \mathfrak{P}^0(\mathbf{p}^0, \mathbf{x}^0, \theta^0(t^0)) d\mathbf{p}^0 d\mathbf{x}^0. \end{aligned} \right\} \quad (6.8)$$

The last integral is obviously zero since \mathfrak{P}^0 as a function of (p_x^0, p_y^0, p_z^0) depends on the squares of these quantities only. Therefore, it follows from (5.20) that the mean values of \mathfrak{F}_x and \mathfrak{K}_x are equal. In order to calculate the first integral in (6.8) we remark that the quantity $k\mathfrak{P}^0/\theta^0$, in the present case where the a 's are constant, depends on the variable x^0 both through $U^0(\mathbf{x}^0)$, occurring in the exponential of the expression (6.2) for \mathfrak{P}^0 , and through $\theta^0(t^0)$. Therefore

$$k \frac{\partial \mathfrak{P}^0/\theta^0}{\partial x^0} = \mathfrak{P}^0 \left(-\frac{\partial U^0(\mathbf{x}^0)}{\partial x^0} \right) + k \frac{\partial (\mathfrak{P}^0/\theta^0)}{\partial \theta^0} \frac{\partial \theta^0(t^0)}{\partial x^0} \quad (6.9)$$

or, by means of the relation

$$\frac{\partial \theta^0(t^0)}{\partial x^0} = -\frac{\gamma v}{c^2} \frac{\partial \theta^0(t^0)}{\partial t} \quad (6.10)$$

following from (6.7),

$$k \frac{\partial \mathfrak{P}^0 / \theta^0}{\partial x^0} = \left(- \frac{\partial U^0}{\partial x^0} \right) \mathfrak{P}^0 - k \frac{\gamma v}{c^2} \frac{\partial \mathfrak{P}^0 / \theta^0}{\partial t}. \quad (6.11)$$

If we integrate this equation over the whole phase-space $\Sigma(S^0)$ the left hand side gives zero, while the integral of the first term on the right hand side is just the first term in (6.8). Hence

$$\langle \mathfrak{F}_x \rangle_t = \langle \mathfrak{R}_x \rangle_t = \frac{k\gamma v}{c^2} \frac{d}{dt} \iint \frac{\mathfrak{P}^0(\mathbf{p}^0, \mathbf{x}^0, \theta^0(t^0))}{\theta^0(t^0)} d\mathbf{p}^0 d\mathbf{x}^0. \quad (6.12)$$

Similarly we find, by means of (5.19,20),

$$\langle \mathfrak{F}_y \rangle_t = \langle \mathfrak{R}_y \rangle_t = 0, \quad \langle \mathfrak{F}_z \rangle_t = \langle \mathfrak{R}_z \rangle_t = 0 \quad (6.13)$$

which together with (6.12) may be written in the general vector form

$$\langle \mathfrak{F} \rangle_t = \langle \mathfrak{R} \rangle_t = \frac{k\gamma \mathbf{v}}{c^2} \frac{d}{dt} \iint \frac{\mathfrak{P}^0(\mathbf{p}^0, \mathbf{x}^0, \theta^0(t^0))}{\theta^0(t^0)} d\mathbf{p}^0 d\mathbf{x}^0. \quad (6.14)$$

In the same way we obtain for the mean mechanical effect

$$\langle \mathfrak{F} \cdot \mathbf{u} \rangle_t = \langle \mathfrak{R} \cdot \mathbf{v} \rangle_t = \frac{k\gamma v^2}{c^2} \frac{d}{dt} \iint \frac{\mathfrak{P}^0(\mathbf{p}^0, \mathbf{x}^0, \theta^0(t^0))}{\theta^0(t^0)} d\mathbf{p}^0 d\mathbf{x}^0. \quad (6.15)$$

For a gas of n particles, the expressions on the right hand sides of (6.14,15) have to be multiplied by n . For the impulse of the total mechanical force on the gas during a time interval $t_1 < t < t_2$ we get therefore

$$\left. \begin{aligned} \Delta \mathbf{I}(t_1, t_2) &= n \int_{t_1}^{t_2} \langle \mathfrak{F} \rangle_t dt \\ &= \frac{n\gamma \mathbf{v} k}{c} \left[\iint \mathfrak{P}^0(\mathbf{p}^0, \mathbf{x}^0, \theta^0(t_2^0)) / \theta^0(t_2^0) d\mathbf{p}^0 d\mathbf{x}^0 \right. \\ &\quad \left. - \iint \mathfrak{P}^0(\mathbf{p}^0, \mathbf{x}^0, \theta^0(t_1^0)) / \theta^0(t_1^0) d\mathbf{p}^0 d\mathbf{x}^0 \right]. \end{aligned} \right\} \quad (6.16)$$

where t_1^0 and t_2^0 are obtained from (6.7) by putting t equal to t_1 and t_2 , respectively. Now choose t_1 and t_2 so that $t_1^0 \leq 0$ and $t_2^0 \geq \tau^0$ for all values of x^0 inside the container. Then, $\theta^0(t_2^0)$ and $\theta^0(t_1^0)$ have the constant values $\theta^0 + \Delta\theta^0$ and θ^0 , respectively, in the two integrals in (6.16). Thus, we get for the mechanical impulse during the whole process

$$\Delta \mathbf{I} = \frac{n\gamma \mathbf{v}}{c^2} \left[\frac{k}{\theta^0 + \Delta\theta^0} - \frac{k}{\theta^0} \right] = \gamma \mathbf{v} \frac{nk\Delta T^0}{c^2}. \quad (6.17)$$

Similarly, by integration of (6.15), we obtain the total external work

$$\Delta A = \frac{\gamma v^2}{c^2} nk\Delta T^0. \quad (6.18)$$

Hence

$$\Delta I_i = \left\{ \frac{nk\Delta T^0}{c^2} \gamma \mathbf{v}, -\frac{nk\Delta T^0}{c^2} \frac{\gamma v^2}{c} \right\} = \Delta g_i, \quad (6.19)$$

where Δg_i is the change of the quantity g_i in (5.17) for the case of constant \mathbf{v} .

From (5.17) and (6.19) we see that the difference $\Delta G_i - \Delta I_i$ is a 4-vector which, according to (1.1), must be interpreted as the four-momentum of supplied heat:

$$\Delta Q_i = \Delta G_i - \Delta I_i = \frac{\Delta H^0}{c^2} V_i = \frac{\Delta \langle \xi_g^0 \rangle^0}{c^2} V_i = \frac{\Delta Q^0}{c^2} V_i \quad (6.20)$$

where

$$\Delta Q^0 = \Delta H^0 = \Delta \langle \xi_g^0 \rangle^0 \quad (6.20')$$

is the supplied heat in the rest system for constant (a).

The equation (6.20) is in agreement with the thermodynamical equation (1.4) derived in reference 4, but so far it has been derived from statistical mechanics only for the case where the a 's are kept constant during the process. However, it is easy to find statistical expressions for the work and the impulse arising from an infinitesimal reversible change of the external parameters (a). In the system S^0 , the work performed on a particle (for fixed $\mathbf{p}^0, \mathbf{x}^0$) by an increase (da_i) is given by (2.6,6'). The mean value of this quantity multiplied by n is to be identified with the work performed on the gas due to a change of the a 's, i.e.

$$dA^0 = n \langle d_{(a)} \xi_g^0 \rangle^0 = n \sum_l \left\langle \frac{\partial \xi_g^0}{\partial a_l} \right\rangle^0 da_l \quad (6.21)$$

or

$$dA^0 = \langle d_{(a)} \xi_g^0 \rangle^0 = \sum_l \left\langle \frac{\partial \xi_g^0}{\partial a_l} \right\rangle^0 da_l \quad (6.22)$$

where ξ_g^0 is the total Hamiltonian (2.37) of the gas.

In the homogeneous case (5.25), there is only one external parameter

for which we can take the rest volume \mathfrak{V}^0 . Since the work performed on a gas by a reversible increase $d\mathfrak{V}^0$ of the volume is

$$dA^0 = -p^0 d\mathfrak{V}^0, \tag{6.23}$$

a comparison with (6.21,22) gives

$$p^0 = -\left\langle \frac{\partial \xi_g^0}{\partial \mathfrak{V}^0} \right\rangle^0 = -n \left\langle \frac{\partial \xi^0(\mathbf{p}^0, \mathbf{x}^0, \mathfrak{V}^0)}{\partial \mathfrak{V}^0} \right\rangle^0, \tag{6.24}$$

an expression which also follows from (5.24) when one takes into account that the potential $U^0(\mathbf{x}^0)$ in the vicinity of the walls is a function of the normal distance to the wall.

On the analogy of (6.21,22), the impulse and work in S due to an increase (da_l) of the external parameters is equal to the mean value of the quantity $d_{(a)}P_i^g$ given by (2.39). Hence

$$\left. \begin{aligned} d_{(a)}I_i &= \langle d_{(a)}P_i^g \rangle = \sum_l da_l \left\langle \frac{\partial P_i^g(\xi, t, a)}{\partial a_l} \right\rangle = n \langle d_{(a)}P_i \rangle \\ &= n \sum_l da_l \left\langle \frac{\partial P_i(\mathbf{p}, \mathbf{x}, t, a)}{\partial a_l} \right\rangle = n \sum_l da_l \left\langle \frac{\partial U(x, a_l)}{\partial a_l} \right\rangle \frac{V_i}{c^2}. \end{aligned} \right\} \tag{6.25}$$

Since $\frac{\partial U}{\partial a_l}$ is a relativistic scalar, Jacobi's theorem (5.4,5) gives

$$\left\langle \frac{\partial U}{\partial a_l} \right\rangle = \left\langle \frac{\partial U^0}{\partial a_l} \right\rangle^0 = \left\langle \frac{\partial \xi_g^0}{\partial a_l} \right\rangle^0.$$

Thus, by (6.21,22,25),

$$d_{(a)}I_i = \frac{dA^0}{c^2} V_i = \frac{\langle d_{(a)}\xi_g^0 \rangle^0}{c^2} V_i, \tag{6.26}$$

which shows that this part of the mechanical 'impulse-work' dI_i is a 4-vector. For an *infinitesimal* reversible process the total expression for dI_i is obtained by combining (6.26) with the equation (6.19), i. e.

$$\left. \begin{aligned} dI_i &= dg_i + \frac{dA^0}{c^2} V_i \\ dg_i &= \left\{ \frac{nk dT^0}{c^2} \gamma \mathbf{v}, -\frac{nk dT^0 \gamma v^2}{c^2 c} \right\} \end{aligned} \right\} \tag{6.27}$$

for constant \mathbf{v} . Instead of (6.20) we now get in the general case

$$dQ_i = dG_i - dI_i = \frac{dH^0 - dA^0}{c^2} V_i = \frac{dQ^0}{c^2} V_i, \quad (6.28)$$

in complete agreement with (1.4). The statistical expression for the transferred heat energy in S^0 is, by (5.15) and (6.22),

$$dQ^0 = dH^0 - dA^0 = d\langle \mathfrak{S}_g^0 \rangle^0 - \sum_l da_l \left\langle \frac{\partial \mathfrak{S}_g^0}{\partial a_l} \right\rangle^0. \quad (6.29)$$

Since $dg_i \cdot V^i = 0$ we get from (6.27)

$$V^i dg_i = -dA^0 \quad (6.30)$$

which, by means of (1.2,3), gives

$$dA = \mathbf{v}d\mathbf{I} + dA^0 \sqrt{1 - v^2/c^2}. \quad (6.31)$$

The error made in the early treatments of relativistic thermodynamics consisted in replacing $d\mathbf{I}$ in this expression by $d\mathbf{G}$ instead of the correct replacement of $d\mathbf{I} = d\mathbf{G} - d\mathbf{Q}$ following from (1.1).

In the homogeneous case (5.25), where (5.28) and (6.23) are valid, we get from (6.27), (1.2,3) and (6.31)

$$\left. \begin{aligned} d\mathbf{I} &= \frac{\mathfrak{S}^0 d\mathfrak{p}^0}{c^2} \gamma \mathbf{v} \\ dA &= \frac{\mathfrak{S}^0 d\mathfrak{p}^0}{c^2} \gamma v^2 - \mathfrak{p} d\mathfrak{S}, \end{aligned} \right\} \quad (6.32)$$

where

$$\mathfrak{S} = \mathfrak{S}^0 \sqrt{1 - v^2/c^2}, \quad \mathfrak{p} = \mathfrak{p}^0 \quad (6.33)$$

is the volume and pressure in the system S . (6.32) is in agreement with the equations (66) and (72) in reference 4.

The equation (4.6), which for a canonical ensemble (4.17) reads

$$\iint e^{[\varphi + \theta^i P_i + \theta^i d_{(a)} P_i] / k} d\mathfrak{p} d\mathbf{x} = 1, \quad (6.34)$$

determines φ as a function of the state variables θ^i and (a) . Differentiation of this equation gives for infinitesimal increases $d\theta^i$, (da_i) of these variables

$$\iint (d\varphi + d\theta^i P_i + \theta^i d_{(a)} P_i) \mathfrak{S} d\mathfrak{p} d\mathbf{x} = 0$$

or

$$d\varphi + d\theta^i \langle P_i \rangle + \theta^i \langle d_{(a)} P_i \rangle = 0. \quad (6.35)$$

Further, by differentiation of the equation

$$k\langle \eta \rangle = \varphi + \theta^i \langle P_i \rangle \quad (6.36)$$

we get, using (6.35),

$$\left. \begin{aligned} kd\langle \eta \rangle &= d\varphi + d\theta^i \langle P_i \rangle + \theta^i d\langle P_i \rangle \\ &= \theta^i (d\langle P_i \rangle - \langle d_{(a)} P_i \rangle). \end{aligned} \right\} \quad (6.37)$$

Multiplying this equation with $-n$ we obtain, by (5.36), (5.15) and (6.25), for the change of the entropy S

$$dS = -\theta^i (dG_i - d_{(a)} I_i). \quad (6.38)$$

For the type of process considered here, where \mathbf{v} is constant, we have

$$\theta^i dg_i = \frac{1}{T^0} V^i dg_i = 0.$$

Thus, by means of (6.26–28),

$$dS = -\theta^i (dG_i - dI_i) = -\theta^i dQ_i \quad (6.39)$$

in accordance with the thermodynamical equation (1.17) for a reversible process. This may be regarded as a new proof of the statistical expression (5.36) for the entropy.

Finally, a few words about the process of *adiabatic acceleration* of the thermodynamic body, where the acceleration is performed 'infinitely' slowly and smoothly with constant (α) and without heat supply. In that case we may assume that the internal thermodynamic state is the same in the successive momentary rest systems S^0 of the container which means that H^0 and $\theta^0 = 1/T^0$ are constant during the process.

From (5.17), which also may be written

$$G_i = \frac{H^0 + nkT^0}{c^2} V_i + \frac{nkT^0}{c\gamma} \delta_{i4}, \quad (6.40)$$

we then get

$$\Delta G_i = \frac{H^0 + nkT^0}{c^2} \Delta V_i + \frac{nkT^0}{c} \delta_{i4} \Delta \gamma^{-1} = \Delta I_i \quad (6.41)$$

since there is no heat supply in this process. For an infinitesimal process of this type we have, since $V^i dV_i = 0$,

$$V^i dI_i = \frac{nkT^0}{c} V^4 d\gamma^{-1} = nkT^0 \gamma d\gamma^{-1}$$

or by (1.2,3)

$$dA = \mathbf{v}d\mathbf{I} - nkT^0 d\gamma^{-1} \quad (6.42)$$

which replaces (6.31) in this case. A detailed statistical derivation of (6.41) is most adequately obtained by replacing the successive rest systems by one smoothly accelerated system of coordinates such as the one introduced in chapter VIII, § 97, of reference 9. This requires a generalization of the statistical mechanics of the preceding sections to the case of accelerated systems of reference, a subject which we shall not go into here. However, in the next section we shall at least give a statistical derivation of the equation (1.17) for a process of adiabatic acceleration in which case (1.17) reduces to $dS = 0$.

7. Mean Values in a Canonical Ensemble

According to (4.10,17) a gas of n particles in thermal equilibrium is, in an arbitrary system of inertia S , described by the canonical probability density

$$\mathfrak{P} = e^{[\Phi + \theta^i P_i^g]/k}, \quad (7.1)$$

where

$$\left. \begin{aligned} P_i^g &= p_i^g + \frac{V_i}{c^2} U_g \\ p_i^g &= \sum_{r=1}^n p_i^{(r)}, \quad U_g = \sum_{r=1}^n U(\mathbf{x}^{(r)}, t, a). \end{aligned} \right\} \quad (7.2)$$

Thus, the 'total canonical momentum' P_i^g of the gas depends on the 'coordinates' (ξ_μ) (3.26) of the points in phase-space and on the parameters V^i and (a_i) of the thermodynamical state, i. e.

$$P_i^g = P_i^g(\xi_\mu, t, V^i, a). \quad (7.3)$$

The quantity Φ , which is connected with the free energy by (4.14, 18), is defined by the equation

$$\left. \begin{aligned} \int \dots \int e^{[\Phi + \theta^i P_i^g(\xi, t, V^i, a)]/k} d\xi &= 1, \\ d\xi &= d\mathbf{p}^{(1)} d\mathbf{x}^{(1)} \dots \dots d\mathbf{p}^{(n)} d\mathbf{x}^{(n)} \end{aligned} \right\} \quad (7.4)$$

or

$$e^{-\Phi/k} = \int \dots \int \exp[\theta^i P_i^g(\xi, t, V^i, a)] d\xi. \quad (7.5)$$

The variables θ^i and V^i are connected by (4.16). However, for the following development it is more convenient at the moment to regard the variables θ^i and V^i as independent of each other. For fixed V^i the quantity Φ , as defined by (7.5), appears then as a function $\Phi(\theta^i, V^i, a)$ of the independent variables θ^i and (a_l) , which may be partially differentiated with respect to θ^i or to a_l all other quantities being kept constant in these derivations.

By partial differentiation of (7.4) with respect to θ^i we then get

$$\int \dots \int \left(\frac{\partial \Phi(\theta^i, V^i, a)}{\partial \theta^i} + P_i^g \right) \mathfrak{P} d\xi = 0. \quad (7.6)$$

Thus, taking account of (7.1,4) and the relations (5.15) and (4.16),

$$G_i = \langle P_i^g \rangle = - \left[\frac{\partial \Phi(\theta^i, V^i, a)}{\partial \theta^i} \right]. \quad (7.7)$$

Here and in the following, a square bracket around a function of (θ^i, V^i, a) indicates that we have to put

$$\theta^i = \theta V^i = \theta^0 V^i \quad (7.8)$$

in this function.

Further partial differentiation of (7.6) with respect to θ^k gives

$$\int \dots \int \left\{ \frac{\partial^2 \Phi}{\partial \theta^i \partial \theta^k} + \frac{1}{k} \left(\frac{\partial \Phi}{\partial \theta^i} + P_i^g \right) \left(\frac{\partial \Phi}{\partial \theta^k} + P_k^g \right) \right\} \mathfrak{P} d\xi = 0 \quad (7.9)$$

or, if we put $\theta^i = \theta V^i$ in this equation and use (7.7),

$$\langle (P_i^g - \langle P_i^g \rangle) (P_k^g - \langle P_k^g \rangle) \rangle = -k \left[\frac{\partial^2 \Phi(\theta^i, V^i, a)}{\partial \theta^i \partial \theta^k} \right]. \quad (7.10)$$

In particular for $k = i$ we get the following simple expression for the square of the fluctuation $\sigma\{P_i^g\}$ of the quantity P_i^g :

$$\sigma^2\{P_i^g\} = -k \left[\frac{\partial^2 \Phi(\theta^i, V^i, a)}{\partial \theta^{i2}} \right]. \quad (7.11)$$

Similarly, the mean value of the probability exponential or the entropy may be expressed in terms of Φ and its first order derivatives. From (5.36,37) and (7.7), we get

$$\left. \begin{aligned} S &= -k\langle \iota_{ig} \rangle = -[\Phi + \theta^i \langle P_i^g \rangle] \\ &= -\left[\Phi(\theta^i, V^i, a) - \theta^i \frac{\partial \Phi(\theta^i, V^i, a)}{\partial \theta^i} \right]. \end{aligned} \right\} \quad (7.12)$$

Partial differentiation of (7.4) with respect to a_l (constant θ^i, V^i) gives

$$\int \dots \int \left(\frac{\partial \Phi}{\partial a_l} + \frac{\theta^i V_i}{c^2} \frac{\partial U_g}{\partial a_l} \right) \mathfrak{R} d\xi = 0. \quad (7.13)$$

Thus, putting $\theta^i = \theta V^i$ we get, since $\frac{\partial U_g}{\partial a_l}$ is invariant,

$$\left. \begin{aligned} \left\langle \frac{\partial U_g}{\partial a_l} \right\rangle &= \left\langle \frac{\partial U_g^0}{\partial a_l} \right\rangle_0 = \left\langle \frac{\partial \xi_g^0}{\partial a_l} \right\rangle_0 \\ &= \theta^{-1} \left[\frac{\partial \Phi(\theta^i, V^i, a)}{\partial a_l} \right] = \theta^{0-1} \frac{\partial \Phi^0(\theta^0, a)}{\partial a_l} \end{aligned} \right\} \quad (7.14)$$

where $\Phi^0(\theta^0, a) = nq^0(\theta^0, a)$ is the function defined by (4.13). In the homogeneous case, where the rest volume \mathfrak{R}^0 can be identified with the external parameter a , (5.29), (6.24) and (7.14) gives the following expression for the pressure

$$p = p^0 = -\theta^{-1} \left[\frac{\partial \Phi(\theta^i, V^i, \mathfrak{R}^0)}{\partial \mathfrak{R}^0} \right] = -\theta^{0-1} \frac{\partial \Phi^0(\theta^0, \mathfrak{R}^0)}{\partial \mathfrak{R}^0}. \quad (7.15)$$

From the preceding considerations it follows that all the thermodynamic functions of the system can be calculated by simple differentiations when the function $\Phi(\theta^i, V^i, a)$ is known. Also typically statistical quantities like the fluctuations of P_i^g may be obtained in this way. For reversible processes we may then also express quantities such as dI_i and dQ_i in terms of Φ and its derivations. For instance we get from (6.22,26) and (7.14)

$$\left. \begin{aligned} dA^0 &= \theta^{0-1} \sum_e \frac{\partial \Phi^0(\theta^0, a)}{\partial a_l} da_l \\ d_{(a)} I_i &= \left(\theta^{0-1} \sum_e \frac{\partial \Phi^0(\theta^0, a)}{\partial a_l} da_l \right) V_i / c^2. \end{aligned} \right\} \quad (7.16)$$

We shall now investigate the general structure of the function $\Phi(\theta^i, V^i, a)$. Although this function for $\theta^i = \theta V^i$ of course has the same value in every

Lorentz system, it is *not* a form-invariant function of the (independent) 4-vectors θ^i and V^i . Since

$$\theta^i P_i^g = \theta^i p_i^g + \frac{\theta^i V_i}{c^2} U_g \quad (7.17)$$

is a sum of two parts containing the momenta and coordinates separately, we may write

$$e^{-\Phi/k} = e^{-\Phi_p/k} e^{-\Phi_q/k}, \quad \Phi = \Phi_p + \Phi_q, \quad (7.18)$$

where

$$e^{-\Phi_p(\theta^i)/k} = \int \dots \int e^{\theta^i p_i^g/k} d\mathbf{p}^{(1)} \dots d\mathbf{p}^{(n)} \quad (7.19)$$

is a function of θ^i only, while

$$e^{-\Phi_q(\theta^i, V^i, a)} = \int \dots \int e^{\theta^i V_i U_g / k c^2} d\mathbf{x}^{(1)} \dots d\mathbf{x}^{(n)} \quad (7.20)$$

in general depends on all variables (θ^i, V^i, a) .

By partial differentiation of (7.19) with respect to θ^i we get, similarly as in (7.6,7), for the mean value of the linear four-momentum p_i^g

$$\langle p_i^g \rangle = - \left[\frac{\partial \Phi_p(\theta^i)}{\partial \theta^i} \right] \quad (7.21)$$

which may be interpreted as the 'bare' four-momentum of the gas. Similarly as in (7.11), the square of the fluctuation of the linear four-momentum is

$$\sigma^2\{p_i^g\} = -k \left[\frac{\partial^2 \Phi_p(\theta^i)}{\partial \theta^{i2}} \right]. \quad (7.22)$$

By subtraction of (7.7) and (7.21) and by using (7.2) and (7.18) we get for the 'four-momentum of the potential energy'

$$\frac{\langle U_g \rangle}{c^2} V^i = \frac{\langle U_g^0 \rangle^0}{c^2} V^i = - \left[\frac{\partial \Phi_q(\theta^i, V^i, a)}{\partial \theta^i} \right]. \quad (7.23)$$

Since $p_i^g = \sum_r p_i^{(r)}$ is the sum of the four-momenta of the separate particles we obtain from (7.19)

$$\Phi_p(\theta^i) = n \varphi_p(\theta^i) \quad (7.24)$$

where $\varphi_p(\theta^i)$ is given by

$$e^{-\varphi_p(\theta^i)/k} = \int e^{\theta^i p_i/k} d\mathbf{p}. \quad (7.25)$$

Here, both p_i and

$$\theta^i = \{\boldsymbol{\theta}, \theta^4\} \quad (7.26)$$

are time-like 4-vectors.

In the intergral (7.25) it is convenient as new variables of integration to introduce the components of the momentum vector \mathbf{p}^0 in a Lorentz system S^0 which has its time axis in the direction of θ^i . Then, the four-velocity of S^0 relative to S is

$$V^i = \theta^i/\theta = \{\mathbf{V}, V^4\} \quad (7.27)$$

which in S^0 has the components

$$V^{0i} = c\delta^{i4}. \quad (7.28)$$

Hence

$$\left. \begin{aligned} \theta^i p_i &= \theta V^i p_i = \theta V^{0i} p_i^0 = \theta c p_4^0 \\ &= -\theta E^0 = -\theta c \sqrt{m^2 c^2 + |\mathbf{p}^0|^2}. \end{aligned} \right\} \quad (7.29)$$

Since $d\mathbf{p}/E$ is known to be invariant under Lorentz transformations, the Jacobian corresponding to the transformation $\mathbf{p} \rightarrow \mathbf{p}^0$ is (comp. equation (2.35))

$$\frac{d(\mathbf{p})}{d(\mathbf{p}^0)} = \frac{E}{E^0} = V^4/c + (\mathbf{V} \cdot \mathbf{p}^0)/E^0 = \theta^4/c\theta + (\boldsymbol{\theta} \cdot \mathbf{p}^0)/\theta E^0 \quad (7.30)$$

on account of (7.27). Thus, (7.25) becomes

$$e^{-\varphi_p(\theta^i)/k} = \int e^{-\theta E^0/k} \frac{\theta^4}{\theta c} d\mathbf{p}^0 + \int e^{-\theta E^0/k} \frac{\boldsymbol{\theta} \cdot \mathbf{p}^0}{\theta E^0} d\mathbf{p}^0.$$

The last integral is obviously zero, so that $e^{-\varphi_p/k}$ is of the form

$$e^{-\varphi_p(\theta^i)/k} = \frac{\theta^4}{c\theta} e^{-f_p(\theta)/k}. \quad (7.31)$$

Here $f_p(\theta)$ is a function of the invariant norm

$$\theta = \sqrt{-\theta_i \theta^i}/c \quad (7.32)$$

defined by

$$e^{-f_p(\theta)/k} = \int e^{-\theta E^0/k} d\mathbf{p}^0 = (mc)^3 \iiint e^{-\frac{\theta mc^2}{k} \sqrt{1 + \xi^2 + \eta^2 + \zeta^2}} d\xi d\eta d\zeta. \quad (7.33)$$

A comparison of (7.33) with (4.13) shows that

$$\varphi_p^0(\theta^0) = f_p(\theta^0). \tag{7.34}$$

The function $f_p(\theta)$ defined by (7.33) may be expressed in terms of a Hankel function $H_2^{(1)}$ of the first kind and the second order with imaginary argument [11] in the following way:

$$\left. \begin{aligned} e^{-i_p(\theta)/k} &= (mc)^3 4\pi \int_0^\infty e^{-\frac{\theta mc^2}{k} \sqrt{1+u^2}} u^2 du \\ &= \frac{2\pi^2 m^2 ck}{i\theta} H_2^{(1)}(imc^2\theta/k). \end{aligned} \right\} \tag{7.35}$$

From (7.24,31) we get for the part Φ_p of Φ

$$\Phi_p(\theta^i) = n\varphi_p(\theta^i) = n \left(f_p(\theta) - k \ln \frac{\theta^4}{\theta c} \right). \tag{7.36}$$

This part is independent of the forces acting on the system, which have an influence only on the part Φ_q defined by (7.20).

For a system of non-interacting particles, where the potential is of the form (7.2), we have on the analogy of (7.24)

$$\Phi_q(\theta^i, V^i, a) = n\varphi_q(\theta^i, V^i, a) \tag{7.37}$$

with

$$e^{-\varphi_q/k} = \int e^{\theta^i V_i U(\mathbf{x}, t, a)/kc^2} d\mathbf{x}. \tag{7.38}$$

If we introduce the coordinates \mathbf{x}^0 of the rest system S^0 instead of \mathbf{x} as integration variables, we have in the integral (7.38), which is performed at constant t , to put

$$d\mathbf{x} = d\mathbf{x}^0 \sqrt{1 - v^2/c^2} = \frac{c}{V^4} d\mathbf{x}^0. \tag{7.39}$$

Thus, (7.38) may be written

$$e^{-\varphi_q(\theta^i, V^i, a)/k} = e^{-i_q(\mu, a)/k c/V^4}, \tag{7.40}$$

where $f_q(\mu, a)$, defined by

$$e^{i_q(\mu, a)/k} = \int e^{-\mu U^0(\mathbf{x}^0, a)/k} d\mathbf{x}^0, \tag{7.41}$$

is an invariant function of (a) and of the invariant variable

$$\mu = -\theta^i V_i / c^2. \quad (7.42)$$

A comparison of (7.41) with (4.13) shows that

$$\varphi_q^0(\theta^0, a) = f_q(\theta^0, a). \quad (7.43)$$

The quantity μ is positive for θ^i in the vicinity of the value (7.8). From (7.40,36,18) we finally get

$$\left. \begin{aligned} \Phi_q &= n \left(f_q(\mu, a) - k \ln \frac{c}{V^4} \right) \\ \Phi(\theta^i, V^i, a) &= n \left(f_p(\theta) + f_q(\mu, a) - k \ln \frac{\theta^4}{\theta V^4} \right) \end{aligned} \right\} \quad (7.44)$$

By means of this expression for Φ , we may now calculate the mean values of various physical quantities. For instance, by (7.7), the four-momentum G_i is obtained by differentiation of Φ with respect to θ^i and subsequently putting $\theta^i = \theta V^i$. Since

$$\frac{\partial \theta}{\partial \theta^i} = -\frac{\theta_i}{c^2 \theta}, \quad \frac{\partial \mu}{\partial \theta^i} = -V_i / c^2, \quad (7.45)$$

we get

$$\left. \begin{aligned} \frac{\partial \Phi}{\partial \theta^i} &= n \left(-f_p'(\theta) \theta^i / \theta - f_q'(\mu, a) V_i \right) / c^2 - nk \left(\frac{\delta_{i4}}{\theta^4} + \frac{\theta_i}{c^2 \theta^2} \right), \\ f_q'(\mu, a) &= \frac{\partial f_q(\mu, a)}{\partial \mu}. \end{aligned} \right\} \quad (7.46)$$

Thus, since

$$[\mu] = \theta = \theta^0, \quad (7.47)$$

$$G_i = - \left[\frac{\partial \Phi}{\partial \theta^i} \right] = n \left(f_p'(\theta^0) + f_q'(\theta^0, a) \right) V_i / c^2 + \frac{nk}{\theta^0} \frac{V_i}{c^2} + \frac{nk}{\theta^0 \gamma c} \delta_{i4} \quad (7.48)$$

which expresses G_i as function of the thermodynamical variables (V_i, a) and $\theta^0 = 1/T^0$. In the rest system where $V_i^0 = -c \delta_{i4}$, we get of course $\mathbf{G}^0 = 0$, and

$$H^0 = -c G_4^0 = n \left(f_p'(\theta^0) + f_q'(\theta^0, a) \right) \quad (7.49)$$

so that (7.48) may be written

$$G_i = \frac{H^0}{c^2} V_i + \frac{nkT^0}{c\gamma} \delta_{i4}, \quad (7.50)$$

in accordance with (6.40).

By further differentiation of (7.46) with respect to θ^i , we get from (7.11) an expression for the square of the fluctuation of P_i^g which obviously increases linearly with n . Since also the mean values, i.e. G_i , are linearly dependent on n we have for the ratio

$$\frac{\sigma\{P_i^g\}}{\langle P_i^g \rangle} = O(n^{-1/2}) \quad (7.51)$$

so that the fluctuations, generally speaking, become unimportant for macroscopic bodies. As mentioned earlier this is a general feature for all thermodynamic quantities.

When we put $V^i = \theta^i/\theta$ in $\Phi(\theta^i, V^i, a)$, we get a function $\Phi(\theta^i, a)$ of θ^i and (a) which, according to (7.44,42), is given by

$$\Phi(\theta^i, a) = [\Phi(\theta^i, V^i, a)] = n(f_p(\theta) + f_q(\theta, a)). \quad (7.52)$$

Thus, as a function of the thermodynamical state variables (θ^i, a) the quantity Φ is a function of the norm θ and (a) only:

$$\left. \begin{aligned} \Phi(\theta^i, a) &= f(\theta, a), \\ f(\theta, a) &= n(f_p(\theta) + f_q(\theta, a)). \end{aligned} \right\} \quad (7.53)$$

For the corresponding quantity Φ^0 in the rest system, defined by (4.10–13), we get by (7.34, 43)

$$\Phi^0(\theta^0, a) = n\varphi^0(\theta^0, a) = n(\varphi_p^0 + \varphi_q^0) = n(f_p(\theta^0) + f_q(\theta^0, a))$$

or

$$\Phi^0(\theta^0, a) = f(\theta^0, a). \quad (7.54)$$

Since $\theta = \theta^0$ is an invariant, (7.53, 54) show that

$$\Phi(\theta^i, a) = \Phi^0(\theta, a) = \Phi^0(\theta^0, a), \quad (7.55)$$

in accordance with (4.18).

As we have seen, the equation (7.7) allows us to calculate the four-momentum G_i by differentiating the function $\Phi(\theta^i, V^i, a)$ with respect to θ^i and afterwards using the relation (7.8). However, if we use (7.8) first in $\Phi(\theta^i, V^i, a)$, by which we obtain the function $\Phi(\theta^i, a)$ given by (7.53), and subsequently differentiate with respect to θ^i we get a quantity

$$P_i = - \frac{\partial \Phi(\theta^i, a)}{\partial \theta^i} \quad (7.56)$$

which, in contrast to G_i , is a 4-vector. In fact, from (7.53, 45, 8) we obtain

$$P_i = \frac{\partial f(\theta, a)}{\partial \theta} \frac{\theta_i}{c^2 \theta} = n(f'_p(\theta^0) + f'_q(\theta^0, a)) V_i / c^2$$

or, by means of (7.49),

$$P_i = \frac{H^0}{c^2} V_i. \quad (7.57)$$

P_i would be the four-momentum if the system were a free system.

In conclusion we shall convince ourselves that the expression (7.12) for the entropy is independent of V^i . From (7.46, 8, 53) we get

$$\left[\theta^i \frac{\partial \Phi}{\partial \theta^i} \right] = \theta n(f'_p(\theta) + f'_q(\theta, a)) = \theta f'(\theta, a) \quad (7.58)$$

and, hence, for the entropy (7.12)

$$S = -f(\theta, a) + \theta \frac{\partial f(\theta, a)}{\partial \theta}. \quad (7.59)$$

We see that this expression is independent of V^i , i. e.

$$S = S^0$$

in accordance with the invariance property of the entropy. Further it follows that S is unchanged, i. e.

$$dS = 0 \quad (7.60)$$

under an adiabatic acceleration, where θ and (a) are constant and only the variables V^i are changed. (7.60) is in accordance with the thermodynamic relation (1.17) for the process in question.

*The Niels Bohr Institute
and NORDITA*

References

1. H. OTT, Zs. f. Phys. **175**, 70 (1963).
2. M. PLANCK, Berl. Ber. p. 542 (1907); Ann. d. Phys. **76**, 1 (1908);
F. HASENÖHRL, Wien. Ber. **116**, 1391 (1907);
A. EINSTEIN, Jahrb. f. Rad. und El. **4**, 411 (1907) and numerous textbooks on relativity theory.
3. H. ARZELIÈS, Nuovo Cimento **35**, 792 (1965);
R. PENNEY, Nuovo Cimento **43** A, 911 (1966);
T. W. B. KIBBLE, Nuovo Cimento **41** B, 72, 83, 84 (1966);
A. GAMBA, Nuovo Cimento **37**, 1792 (1965); **41** B, 72 (1966);
H. ARZELIÈS, Nuovo Cimento **41** B, 81 (1966);
F. RÖHRLICH, Nuovo Cimento **45** B, 76 (1966);
L. DE BROGLIE, Compt. Rend. **262**, 1235 (1966);
A. STARNOSZKIEWICZ, Act. Phys. Pol. **29**, 249 (1966);
L. A. SCHMID, Nuovo Cimento **47** B, 1 (1967);
P. T. LANDSBERG, Proc. Phys. Soc. **89**, 1007 (1966).
4. C. MØLLER, Mat. Fys. Medd. Dan. Vid. Selsk. **36**, 1 (1967).
5. I. BREVIK, Mat. Fys. Medd. Dan. Vid. Selsk. **36**, 3 (1967).
6. L. SÖDERHOLM, The Transformation Properties of Momentum and Energy of the Heat Supplied to an Elastic System in a Process According to Special Relativistic Thermodynamics (1968) (to be published in Nuovo Cimento).
7. See the first paper by ARZELIÈS quoted in ref. 3.
8. C. MØLLER, Thermodynamics in the Special and the General Theory of Relativity (1967) in 'Old and New Problems in Elementary Particles', Academic Press, New York and London, 1968.
9. See, for instance, C. MØLLER, The Theory of Relativity, Oxford (1952), § 21, Eq. (56).
10. F. LURÇAT and P. MAZUR, Nuovo Cimento **31**, 140 (1964);
A. O. BARUT, Phys. Rev. **109**, 1376 (1958).
11. F. JÜTTNER, Ann. d. Phys. **34**, 856 (1911), which contains a relativistic treatment of an ideal gas in the rest system.

A. REIZ, J. OTZEN PETERSEN, AND P. M. HEJLESEN

A PRELIMINARY CALIBRATION OF
THE HERTZSPRUNG-RUSSELL DIAGRAM
IN TERMS OF MASS AND AGE
FOR POPULATION I MAIN-SEQUENCE STARS
OF 1.0-1.6 SOLAR MASSES

Det Kongelige Danske Videnskabernes Selskab

Matematisk-fysiske Meddelelser **36**, 17



Kommissionær: Munksgaard

København 1968

Synopsis

Three series of evolutionary tracks are derived for stars in the mass range 1.0–1.6 solar masses with chemical compositions given by $Z = 0.03$, $X = 0.60$ and 0.70 , respectively. The evolution is followed from the zero-age line until the secondary contraction begins. By means of these tracks the corresponding region of the HERTZSPRUNG-RUSSELL diagram is calibrated in terms of mass and age. Finally the accuracy of the calibration is discussed; it is concluded that mass and age determination for single main-sequence stars is considerably more difficult for spectral types later than about F0 than for stars of earlier types, and that this method can not be applied at all for spectral types later than about G0.

1. Introduction

Calibrations of the main-sequence band in terms of age and mass have been given by KELSALL and STRÖMGREN (1966) for B and A stars for several Population I chemical compositions. STRÖMGREN (1963) has derived ages of early type stars by means of such calibrations. For the later spectral types the calculation of the evolutionary tracks, on which age calibrations have to be based, is somewhat more complicated than for the early types. This is due to the fact that the structure of the stellar envelopes, especially of the ionization zones, has a considerable influence on the properties of the stellar models for lower effective temperatures, in contrast to the upper main-sequence, where the influence of the outer convection and ionization zones is negligible.

BAKER (1963) has calculated envelope models for stars with a mass in the range $0.00 \leq \log M/M_{\odot} \leq 0.20$ for the two Population I chemical compositions $Z = 0.03$, $X = 0.60$ and 0.70 , respectively. For the mass values $\log M/M_{\odot} = 0.00, 0.05, 0.10, 0.15$, and 0.20 , and both compositions, BAKER constructed two sets of envelope models, for $\alpha = 1$ and $\alpha = 2$ respectively, α being the mixing length in units of the local pressure scale height. Each set consists of 120 models in a network of $\log R/R_{\odot}$ and $\log L/L_{\odot}$ values with $\Delta \log R/R_{\odot} = 0.02$ and $\Delta \log L/L_{\odot} = 0.05$. The results for a family of models of the same chemical composition and the same α value are given in 5 tables, one for each mass value. One table supplies the values of $\log T$, $\log P$, $\log \rho$, and r/R_{\odot} at a certain point in the envelope model, for instance at a relative mass equal to 0.60.

The BAKER-tables form a basis for subsequent calculations of evolutionary tracks. Data found by interpolation in the tables fix the conditions for the boundary-value problems that have to be solved, i.e. the starting values for the inwards-running integrations. In the present computations, which were performed in the summer of 1965, we have used several of the BAKER-tables in the manner just described. For the chemical composition

$X = 0.70$ and $Z = 0.03$ we have considered both $\alpha = 1.0$ and $\alpha = 2.0$, while we have derived evolutionary tracks only for the case $\alpha = 2.0$ for the chemical composition given by $X = 0.60$ and $Z = 0.03$.

In Section 2 the procedure for model construction is described, and in Section 3 the main properties of the derived evolutionary tracks are analysed. The age calibrations based on these tracks are discussed in Section 4.

2. Model Construction

The evolutionary sequences are derived by means of a computer programme, which is essentially the same as the one described by REIZ and PETERSEN (1964), in particular the fitting procedure and the handling of the opacity tables are not altered. The physical variables $\ln P$, $\ln T$, $q = M(r)/M$, and $f = L(r)/L$ are obtained as function of $x = r/R$ by means of integration of the four basic differential equations from the bottom of the outer zone ($q = 0.60$) to a pre-assigned fitting-point, and from the centre to the fitting-point. The method of integration and the fitting procedure are precisely those described by REIZ and PETERSEN.

In computing the energy generation rate, the formulae given by REEVES (1965) for the pp and CN reactions are used directly, while the energy release due to changes in the stellar structure with time is neglected, as this term is known to have a negligible influence on the evolution of main-sequence models. The opacity values are determined by interpolation in tables giving $\log \kappa$ as function of $\log T$ and $\log \rho$ for a specific chemical composition defined by means of the relative contents of hydrogen (X) and heavy elements (Z). These tables were computed at the Institute for Space Studies, New York, by means of the procedure given by COX (1965), and made available to the Copenhagen Observatory by B. STRÖMGREN. Besides bound-free and free-free absorption, and electron scattering, which were included in the tables used by BAKER (1963), also bound-bound absorption (lines) is taken into account in the opacity tables used in the central parts of the present models.

In the equation of state non-relativistic, partial degeneracy is taken into account, using a Chebyshev expansion for the ratio of the Fermi-Dirac functions, as described by REIZ (1965). The corrections to the perfect gas law were, however, found to be small in all cases, amounting to at most a few per cent.

The values of the physical and astronomical constants are taken from

ALLEN (1955). All absolute magnitudes are therefore derived using $M_{\text{bol},\odot} = 4.62$. When comparison is made with results based on the more recent value $M_{\text{bol},\odot} = 4.72$ (ALLEN 1963) the difference in magnitude scale must be remembered.

3. Results of Calculations

For the original chemical composition $X = 0.70$ and $Z = 0.03$ two series of evolutionary tracks are derived with different assumptions for α . In one series the inwards-running integrations are started by means of second order interpolation in the BAKER-tables nos. 12–15 (for $\alpha = 1$), and in the other the tables nos. 26–30 ($\alpha = 2$) are used. Figure 1 shows these tracks in the $(\log T_e, M_{\text{bol}})$ diagram; the main characteristics of the models, together with similar information about a sequence of tracks derived for the original composition $X = 0.60$ and $Z = 0.03$ are summarized in Tables 1 and 2.

From Figure 1 it is seen that a gradual change in the evolutionary tracks occurs in the mass range covered by the present models. For the smaller mass values we find models with radiative cores, while the models of about 1.6 solar masses possess a convective core containing 12–16 per cent of the total mass in the homogeneous phase. Also the structure of the envelopes are rather different in the two cases. The heavier models have envelopes, in which the convective zones due to ionization of hydrogen and helium, are so shallow that they only have negligible influence on the structure of the whole star, whereas these zones for the models with about one solar mass have a considerable influence on the total radii of the models, and therefore also on the effective temperatures. The structure of the ionization zones is determined through the assumed value of the mixing length, i.e. by the efficiency of the convective energy transport. Comparing the cases $\alpha = 1$ and $\alpha = 2$, it is seen, that for large efficiency ($\alpha = 2$) relatively small radii are derived, and the difference is seen to increase with decreasing effective temperature. The difference in derived spectral class for models with $\alpha = 1$ and $\alpha = 2$ is negligible for spectral types earlier than about F0, but amounts to several subclasses near G0.

Both the form and the length of the evolutionary tracks in the $(\log T_e, M_{\text{bol}})$ diagram show a gradual change in the mass interval which is investigated. Roughly speaking we can say that the models with masses near 1.6 solar masses evolve as heavy main-sequence stars, while the model with 1.0 solar mass evolves as a low mass star. The main-sequence phase of the

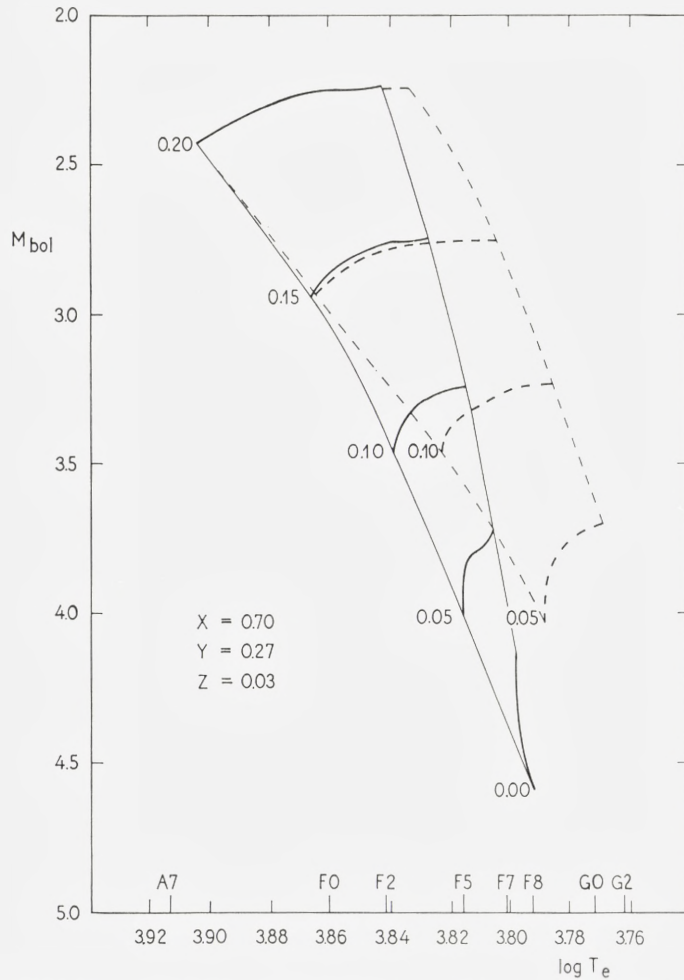


Figure 1. Evolutionary tracks for models with $X = 0.70$, $Y = 0.27$, and $Z = 0.03$ in the $(\log T_e, M_{\text{bol}})$ diagram. Full drawn curves correspond to models with $\alpha = 2$, while the dashed curves are for $\alpha = 1$. The zero-age line and the upper boundary of the main-sequence band (corresponding to $X_c \simeq 0.10$) are indicated by thin lines. The number attached to each sequence gives the logarithm of the mass in solar units.

model with 1.0 solar mass is characterized by an increase in luminosity with practically constant effective temperature, while the more massive models show a considerable decrease in effective temperature accompanied by a relatively small increase in luminosity. Similar results have been described by HALLGREN (1967) and IBEN (1967) for Population I models in the same mass range.

TABLE 1.

Evolutionary tracks for three groups of model sequences. The values of $B-V$ and M_V are derived using the bolometric corrections and the temperature scale published by HARRIS (1963).

$\log M/M_\odot$	$X = 0.70,$ Age (10^9 years)	$Y = 0.27,$ M_{bol}	$Z = 0.03,$ $\log T_e$	$\alpha = 1.0$ $B - V$	M_V
0.05	0.00	4.03	3.788	0.54	4.08
	0.30	4.01	3.788	0.54	4.06
	0.70	3.97	3.788	0.54	4.02
	1.10	3.92	3.788	0.54	3.97
	1.50	3.88	3.787	0.55	3.93
	1.90	3.84	3.786	0.55	3.89
	2.70	3.76	3.781	0.57	3.82
	3.00	3.74	3.778	0.58	3.80
	3.30	3.72	3.774	0.59	3.78
	3.50	3.71	3.771	0.60	3.77
	3.60	3.71	3.770	0.60	3.77
	3.70	3.70	3.768	0.61	3.77
	0.10	0.00	3.46	3.823	0.43
0.50		3.39	3.822	0.44	3.44
0.80		3.36	3.819	0.44	3.40
1.10		3.34	3.815	0.45	3.38
1.30		3.32	3.812	0.46	3.36
1.50		3.30	3.809	0.47	3.34
1.70		3.28	3.807	0.48	3.32
1.90		3.26	3.802	0.50	3.30
2.05		3.25	3.799	0.50	3.30
2.20		3.24	3.795	0.52	3.29
2.35		3.24	3.791	0.53	3.29
2.45		3.23	3.787	0.55	3.28
2.55		3.24	3.784	0.56	3.30
0.15	0.00	2.93	3.864	0.32	3.00
	0.10	2.93	3.863	0.32	3.00
	0.30	2.91	3.860	0.33	2.98
	0.50	2.87	3.857	0.34	2.95
	0.90	2.81	3.849	0.35	2.87
	1.10	2.79	3.843	0.37	2.85
	1.30	2.77	3.834	0.39	2.82
	1.40	2.76	3.830	0.41	2.81
	1.50	2.75	3.825	0.42	2.80
	1.60	2.75	3.819	0.43	2.79

(to be continued)

TABLE 1 (continued).

$\log M/M_{\odot}$	$X = 0.70,$ Age (10^9 years)	$Y = 0.27,$ M_{bol}	$Z = 0.03,$ $\log T_e$	$\alpha = 1.0$ $B - V$	M_V
	1.70	2.75	3.812	0.46	2.79
	1.80	2.74	3.805	0.49	2.78
0.20	0.00	2.43	3.904	0.22	2.54
	0.10	2.41	3.902	0.22	2.52
	0.20	2.39	3.900	0.23	2.50
	0.30	2.38	3.896	0.24	2.48
	0.45	2.35	3.891	0.25	2.45
	0.60	2.33	3.886	0.26	2.42
	0.75	2.30	3.880	0.28	2.38
	0.85	2.29	3.873	0.29	2.37
	0.95	2.27	3.868	0.31	2.34
	1.05	2.24	3.862	0.33	2.31
	1.15	2.25	3.850	0.36	2.31
	1.21	2.25	3.844	0.37	2.31
	1.26	2.24	3.839	0.38	2.29
	1.31	2.25	3.832	0.40	2.30
$\log M/M_{\odot}$	$X = 0.70,$ Age (10^9 years)	$Y = 0.27,$ M_{bol}	$Z = 0.03,$ $\log T_e$	$\alpha = 2.0$ $B - V$	M_V
0.00	0.00	4.59	3.792	0.53	4.64
	0.60	4.54	3.793	0.53	4.59
	1.20	4.51	3.794	0.52	4.56
	1.80	4.46	3.795	0.52	4.51
	2.40	4.40	3.796	0.52	4.45
	3.00	4.34	3.797	0.51	4.39
	3.30	4.32	3.797	0.51	4.37
	3.60	4.29	3.797	0.51	4.34
	3.90	4.26	3.797	0.51	4.31
	4.20	4.22	3.797	0.51	4.27
	4.40	4.19	3.798	0.51	4.24
	4.60	4.16	3.798	0.51	4.21
	4.80	4.14	3.797	0.51	4.19
0.05	0.00	4.01	3.816	0.45	4.05
	0.30	3.98	3.817	0.45	4.02
	0.70	3.95	3.816	0.45	3.99
	1.50	3.87	3.816	0.45	3.91

(to be continued)

TABLE 1 (continued).

$\log M/M_{\odot}$	$X = 0.70,$ Age (10^9 years)	$Y = 0.27,$ M_{bol}	$Z = 0.03,$ $\log T_e$	$\alpha = 2.0$ $B - V$	M_V
	1.90	3.83	3.815	0.45	3.87
	2.20	3.81	3.814	0.46	3.85
	2.50	3.80	3.812	0.46	3.84
	2.80	3.79	3.811	0.47	3.83
	3.00	3.78	3.810	0.47	3.82
	3.20	3.77	3.808	0.48	3.81
	3.40	3.74	3.806	0.48	3.78
	3.50	3.72	3.806	0.48	3.76
0.10	0.00	3.46	3.839	0.38	3.51
	0.20	3.44	3.839	0.38	3.49
	0.50	3.41	3.838	0.39	3.46
	0.80	3.37	3.837	0.39	3.42
	1.10	3.33	3.835	0.40	3.38
	1.40	3.31	3.832	0.40	3.36
	1.60	3.29	3.830	0.41	3.34
	1.80	3.28	3.827	0.42	3.33
	2.00	3.26	3.824	0.43	3.31
	2.20	3.26	3.821	0.44	3.31
	2.40	3.25	3.817	0.45	3.29
	2.55	3.24	3.814	0.46	3.28
	2.60	3.24	3.814	0.46	3.28
	2.65	3.22	3.814	0.46	3.26
0.15	0.00	2.94	3.866	0.31	3.01
	0.10	2.93	3.866	0.31	3.00
	0.30	2.90	3.864	0.32	2.97
	0.50	2.88	3.862	0.32	2.95
	0.70	2.85	3.859	0.33	2.93
	0.90	2.83	3.855	0.34	2.89
	1.10	2.79	3.851	0.35	2.85
	1.30	2.77	3.846	0.37	2.83
	1.50	2.75	3.840	0.38	2.80
	1.60	2.76	3.836	0.39	2.81
	1.70	2.76	3.832	0.40	2.81
	1.80	2.75	3.828	0.41	2.80
	1.85	2.74	3.827	0.42	2.79
0.20	0.00	2.43	3.904	0.22	2.54
	0.10	2.41	3.902	0.22	2.52
	0.30	2.37	3.897	0.24	2.47

(to be continued)

TABLE 1 (continued).

$\log M/M_{\odot}$	$X = 0.70,$ Age (10^9 years)	$Y = 0.27,$ M_{bol}	$Z = 0.03,$ $\log T_e$	$\alpha = 2.0$ $B - V$	M_V
	0.50	2.35	3.890	0.25	2.44
	0.70	2.31	3.883	0.27	2.40
	0.85	2.28	3.876	0.29	2.36
	1.00	2.26	3.866	0.31	2.33
	1.10	2.26	3.858	0.33	2.33
	1.20	2.25	3.850	0.36	2.31
	1.27	2.25	3.845	0.37	2.31
	1.31	2.24	3.843	0.37	2.30
$\log M/M_{\odot}$	$X = 0.60,$ Age (10^9 years)	$Y = 0.37,$ M_{bol}	$Z = 0.03,$ $\log T_e$	$\alpha = 2.0$ $B - V$	M_V
0.00	0.00	3.70	3.850	0.36	3.76
	0.40	3.66	3.848	0.36	3.72
	0.80	3.61	3.846	0.37	3.67
	1.20	3.57	3.842	0.38	3.63
	1.40	3.55	3.840	0.38	3.61
	1.60	3.53	3.838	0.39	3.58
	1.75	3.52	3.835	0.40	3.57
	1.90	3.51	3.833	0.40	3.56
	2.00	3.50	3.831	0.41	3.55
	2.10	3.48	3.830	0.41	3.53
0.05	0.00	3.20	3.877	0.28	3.28
	0.20	3.18	3.875	0.29	3.26
	0.40	3.15	3.873	0.29	3.23
	0.60	3.11	3.870	0.30	3.19
	0.80	3.07	3.866	0.31	3.14
	0.90	3.07	3.864	0.32	3.14
	1.00	3.06	3.861	0.33	3.13
	1.10	3.05	3.858	0.33	3.12
	1.20	3.05	3.854	0.34	3.11
	1.30	3.04	3.851	0.35	3.10
	1.40	3.03	3.847	0.36	3.09
	1.50	3.02	3.844	0.37	3.08
	1.57	2.99	3.843	0.37	3.05
	1.64	2.97	3.842	0.38	3.03

(to be continued)

TABLE 1 (continued).

$\log M/M_{\odot}$	$X = 0.60,$ Age (10^9 years)	$Y = 0.37,$ M_{bo1}	$Z = 0.03,$ $\log T_e$	$\alpha = 2.0$ $B - V$	M_V
0.10	0.00	2.72	3.912	0.20	2.84
	0.10	2.69	3.911	0.20	2.81
	0.30	2.65	3.906	0.22	2.76
	0.70	2.58	3.891	0.25	2.68
	0.80	2.56	3.887	0.26	2.65
	1.00	2.54	3.872	0.30	2.62
	1.10	2.54	3.863	0.32	2.61
	1.13	2.53	3.862	0.32	2.60
	1.18	2.50	3.859	0.33	2.57
0.15	0.00	2.18	3.952	0.12	2.36
	0.10	2.18	3.947	0.13	2.35
	0.20	2.17	3.942	0.14	2.33
	0.30	2.14	3.937	0.15	2.30
	0.40	2.11	3.932	0.16	2.26
	0.50	2.09	3.925	0.17	2.23
	0.60	2.06	3.918	0.19	2.19
	0.67	2.05	3.910	0.21	2.17
	0.72	2.03	3.906	0.22	2.14
	0.77	2.03	3.900	0.23	2.13
	0.82	2.02	3.894	0.24	2.12
	0.85	2.00	3.892	0.25	2.10
	0.87	1.99	3.891	0.25	2.09
0.20	0.00	1.74	3.982	0.07	1.98
	0.10	1.71	3.977	0.08	1.93
	0.20	1.67	3.971	0.09	1.88
	0.30	1.62	3.965	0.10	1.82
	0.40	1.59	3.955	0.11	1.77
	0.45	1.57	3.949	0.12	1.74
	0.50	1.56	3.943	0.14	1.72
	0.55	1.54	3.935	0.15	1.69
	0.60	1.52	3.926	0.17	1.66
	0.63	1.50	3.921	0.18	1.63
	0.65	1.51	3.917	0.19	1.64

The model with the physical parameters $M = 1.12M_{\odot}$, $X = 0.70$, $Z = 0.03$, and $\alpha = 1$ is an interesting intermediate case. The first part of the evolutionary track is very nearly vertical in the diagram, but in the later part of the main-sequence stage the track turns to the right, and this happens

before the hydrogen is exhausted in the central region. HALLGREN and DEMARQUE (1966) have recently published a study of the evolution of a star with very nearly the same physical parameters; their results agree well with those of the present investigation. We note especially, that the central convective core, which in the homogeneous model contains 2.6 per cent of the total mass (see Table 2), first grows until it contains slightly more than 4 per

TABLE 2.
Characteristics of three model sequences.

$X = 0.70, Z = 0.03, \log M/M_{\odot} = 0.05, \alpha = 1.0$							
Age (10^9 years)	X_c	q_c	f_c	$\log R/R_{\odot}$	$\log L/L_{\odot}$	$\log T_c$	$\log \varrho_c$
0.00	0.700	0.026	0.230	0.064	0.230	7.198	1.993
0.30	0.666	0.028	0.253	0.069	0.241	7.204	2.009
0.70	0.619	0.033	0.297	0.077	0.256	7.212	2.032
1.10	0.571	0.036	0.326	0.087	0.277	7.222	2.055
1.50	0.519	0.039	0.344	0.097	0.297	7.231	2.077
1.90	0.457	0.041	0.397	0.107	0.309	7.241	2.110
2.70	0.319	0.042	0.468	0.132	0.339	7.265	2.182
3.00	0.265	0.040	0.497	0.142	0.347	7.275	2.213
3.30	0.194	0.041	0.538	0.154	0.354	7.288	2.257
3.50	0.144	0.039	0.562	0.162	0.358	7.299	2.292
3.60	0.116	0.038	0.561	0.166	0.361	7.305	2.315
3.70	0.087	0.036	0.560	0.170	0.364	7.313	2.344

$X = 0.70, Z = 0.03, \log M/M_{\odot} = 0.20, \alpha = 1.0$							
Age (10^9 years)	X_c	q_c	f_c	$\log R/R_{\odot}$	$\log L/L_{\odot}$	$\log T_c$	$\log \varrho_c$
0.00	0.700	0.116	0.777	0.153	0.873	7.279	1.883
0.10	0.670	0.115	0.786	0.160	0.881	7.282	1.889
0.20	0.639	0.114	0.795	0.169	0.887	7.285	1.897
0.30	0.606	0.112	0.803	0.178	0.892	7.288	1.905
0.45	0.555	0.105	0.809	0.192	0.902	7.294	1.918
0.60	0.497	0.097	0.816	0.209	0.912	7.300	1.934
0.75	0.433	0.090	0.826	0.228	0.925	7.307	1.952
0.85	0.385	0.084	0.834	0.242	0.928	7.312	1.969
0.95	0.333	0.078	0.842	0.257	0.935	7.319	1.988
1.05	0.276	0.073	0.856	0.275	0.949	7.326	2.009
1.15	0.211	0.067	0.867	0.295	0.943	7.335	2.043
1.21	0.169	0.063	0.875	0.308	0.943	7.342	2.068
1.26	0.131	0.060	0.881	0.319	0.946	7.349	2.093
1.31	0.090	0.056	0.885	0.332	0.945	7.359	2.128

(to be continued)

TABLE 2 (continued).

$X = 0.70, Z = 0.03, \log M/M_{\odot} = 0.10, \alpha = 2.0$							
Age (10^9 years)	X_c	q_c	f_c	$\log R/R_{\odot}$	$\log L/L_{\odot}$	$\log T_c$	$\log \rho_c$
0.00	0.700	0.061	0.477	0.074	0.458	7.232	1.971
0.20	0.668	0.064	0.502	0.080	0.468	7.237	1.983
0.50	0.618	0.068	0.538	0.089	0.481	7.244	2.001
0.80	0.566	0.071	0.576	0.099	0.495	7.252	2.020
1.10	0.512	0.064	0.576	0.110	0.510	7.260	2.040
1.40	0.445	0.061	0.597	0.121	0.521	7.269	2.067
1.60	0.395	0.058	0.601	0.128	0.526	7.275	2.088
1.80	0.342	0.058	0.631	0.136	0.533	7.283	2.113
2.00	0.284	0.054	0.653	0.145	0.538	7.292	2.141
2.20	0.220	0.052	0.677	0.153	0.540	7.302	2.177
2.40	0.148	0.048	0.699	0.161	0.542	7.315	2.223
2.55	0.088	0.045	0.709	0.169	0.546	7.329	2.273
2.60	0.067	0.043	0.704	0.172	0.549	7.336	2.297
2.65	0.044	0.040	0.674	0.175	0.556	7.345	2.335

cent of the mass, when the hydrogen content at the centre is about 30 per cent, and thereafter decreases again. Although the convective core only contains a few per cent of the mass, a considerable fraction of the total luminosity is generated in the core. From Table 2 this fraction is seen to increase from 0.23 in the homogeneous stage to 0.56 when the central hydrogen content is 0.15. This is, of course, due to the increasing temperature and density in the central region of the model.

It is interesting to note that a small central convective core is found, even though nearly all energy is generated by the pp reactions and not by the CN cycle. This seems to be due to the fact, that the detailed dependence of ε_{pp} on T gives a larger concentration of the energy generation towards the centre than the approximate law $\varepsilon_{pp} \approx T^4$, which has often been used in computations in the past. Therefore it is more probable that a convective central core will appear when the more realistic expression for ε_{pp} is used.

KELSALL and STRÖMGREN (1966) have calculated evolutionary tracks of models in the mass range $0.25 \leq \log M/M_{\odot} \leq 0.85$ for the chemical compositions investigated here. Comparing the zero-age lines derived by KELSALL and STRÖMGREN with the present ones, we find that ours are placed somewhat below those given by KELSALL and STRÖMGREN, the difference being 0^m10 for the chemical composition $X = 0.70, Z = 0.03$ and 0^m25 for $X = 0.60, Z = 0.03$. Also from the derived effective temperature

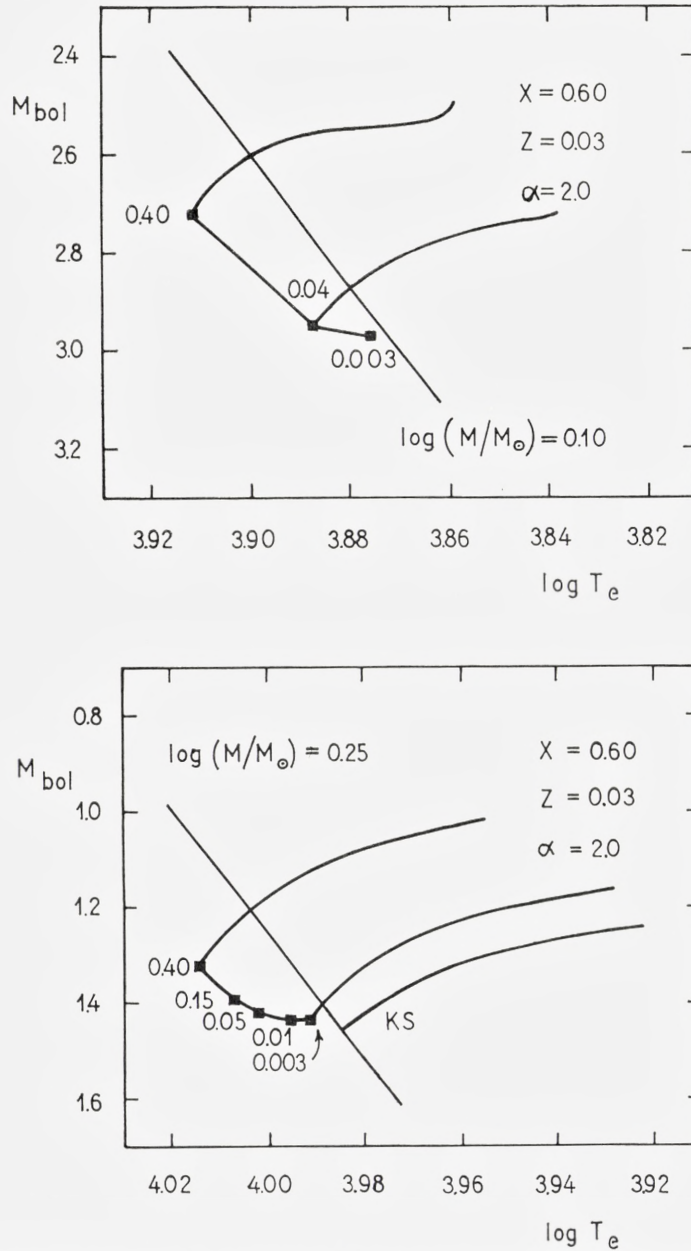


Figure 2-3. Evolutionary tracks of models with outer zones containing different fractions of the total mass. The numbers give the relative mass of the envelopes ($1-q_e$) with an opacity computed without the line contribution. The zero-age lines and the curve marked KS in Figure 2 are taken from KELSALL and STRÖMGREN (1966). Both the luminosity and the effective temperature are seen to decrease with decreasing relative mass of the envelope. The absolute magnitudes given by KELSALL and STRÖMGREN have been corrected by -0.10 (c. f. Section 2).

TABLE 3.

Calibration of the main-sequence band for three groups of model sequences.

$\log M/M_{\odot}$	$X = 0.70,$ $\log T_e$	$Y = 0.27,$ $\log \text{Age}$	$Z = 0.03,$ X_c	$\alpha = 1.0$ M_{bol}	ΔM_{bol}
0.05	3.785	9.331	0.423	3.82	0.26
	3.780	9.448	0.300	3.75	0.42
	3.775	9.509	0.214	3.73	0.53
	3.770	8.813	0.128	3.71	0.63
0.10	3.820	8.813	0.556	3.34	0.16
	3.815	9.047	0.500	3.33	0.24
	3.810	9.165	0.431	3.30	0.35
	3.805	9.252	0.347	3.27	0.47
	3.800	9.300	0.286	3.25	0.57
	3.795	9.340	0.225	3.24	0.66
	3.790	9.375	0.160	3.23	0.76
	3.785	9.402	0.099	3.23	0.85
0.15	3.860	8.527	0.641	2.91	0.07
	3.855	8.840	0.551	2.84	0.20
	3.850	8.961	0.486	2.81	0.30
	3.845	9.024	0.434	2.79	0.39
	3.840	9.071	0.388	2.78	0.46
	3.835	9.110	0.347	2.77	0.54
	3.830	9.145	0.304	2.76	0.61
	3.825	9.178	0.256	2.75	0.69
	3.820	9.200	0.220	2.74	0.76
	3.815	9.219	0.185	2.75	0.83
	3.810	9.237	0.147	2.75	0.91
	0.20	3.900	8.350	0.643	2.39
3.895		8.524	0.595	2.37	0.17
3.890		8.694	0.540	2.35	0.26
3.885		8.790	0.490	2.32	0.34
3.880		8.870	0.437	2.30	0.43
3.875		8.919	0.397	2.29	0.50
3.870		8.956	0.357	2.28	0.57
3.865		8.998	0.308	2.26	0.66
3.860		9.031	0.263	2.23	0.75
3.855		9.051	0.231	2.23	0.81
3.850		9.061	0.210	2.25	0.86
3.845		9.079	0.177	2.25	0.92
3.840		9.096	0.140	2.24	1.00
3.835		9.111	0.106	2.24	1.06

(to be continued)

TABLE 3 (continued).

$\log M/M_{\odot}$	$X = 0.70,$ $\log T_e$	$Y = 0.27,$ $\log \text{Age}$	$Z = 0.03,$ X_c	$\alpha = 2.0$ M_{bo1}	ΔM_{bo1}
0.05	3.815	9.288	0.437	3.82	0.21
	3.810	9.471	0.243	3.78	0.37
0.10	3.835	9.030	0.519	3.34	0.22
	3.830	9.200	0.399	3.29	0.38
	3.825	9.292	0.297	3.26	0.53
	3.820	9.348	0.210	3.26	0.66
	3.815	9.399	0.106	3.25	0.79
0.15	3.865	8.326	0.666	2.92	0.04
	3.860	8.824	0.556	2.86	0.18
	3.855	8.954	0.484	2.83	0.30
	3.850	9.061	0.404	2.79	0.43
	3.845	9.131	0.330	2.76	0.56
	3.840	9.176	0.267	2.75	0.69
	3.835	9.209	0.213	2.76	0.80
	3.830	9.243	0.147	2.75	0.92
0.20	3.900	8.146	0.638	2.38	0.10
	3.895	8.587	0.586	2.36	0.19
	3.890	8.699	0.538	2.35	0.27
	3.885	8.807	0.484	2.33	0.36
	3.880	8.884	0.431	2.30	0.46
	3.875	8.937	0.383	2.28	0.54
	3.870	8.979	0.339	2.26	0.62
	3.865	9.009	0.299	2.26	0.70
	3.860	9.033	0.264	2.26	0.78
	3.855	9.055	0.227	2.26	0.87
	3.850	9.081	0.181	2.25	0.97
	3.845	9.103	0.133	2.24	1.08
	0.00	$X = 0.60,$ $\log T_e$	$Y = 0.37,$ $\log \text{Age}$	$Z = 0.03,$ X_c	$\alpha = 2.0$ M_{bo1}
3.845		8.971	0.445	3.60	0.21
3.840		9.146	0.341	3.55	0.37
3.835		9.244	0.250	3.52	0.50
0.05	3.830	9.316	0.156	3.49	0.64
	3.875	8.229	0.562	3.18	0.05
	3.870	8.774	0.465	3.11	0.20

(to be continued)

TABLE 3 (continued).

$\log M/M_{\odot}$	$X = 0.60,$ $\log T_e$	$Y = 0.37,$ $\log \text{Age}$	$Z = 0.03,$ X_c	$\alpha = 2.0$ M_{bol}	ΔM_{bol}
	3.865	8.936	0.389	3.06	0.32
	3.860	9.013	0.336	3.06	0.42
	3.855	9.073	0.283	3.05	0.54
	3.850	9.124	0.228	3.04	0.66
	3.845	9.167	0.170	3.02	0.78
0.10	3.910	8.176	0.555	2.68	0.07
	3.905	8.519	0.496	2.64	0.17
	3.900	8.690	0.441	2.61	0.27
	3.895	8.792	0.396	2.59	0.36
	3.890	8.860	0.355	2.58	0.44
	3.885	8.922	0.305	2.55	0.53
	3.880	8.966	0.264	2.54	0.62
	3.875	8.993	0.233	2.54	0.69
	3.870	9.010	0.205	2.54	0.77
	3.865	9.035	0.171	2.54	0.85
	3.860	9.065	0.122	2.51	0.96
0.15	3.945	8.169	0.548	2.17	0.09
	3.940	8.370	0.505	2.16	0.18
	3.935	8.529	0.456	2.13	0.28
	3.930	8.638	0.407	2.10	0.37
	3.925	8.704	0.366	2.08	0.46
	3.920	8.759	0.325	2.06	0.55
	3.915	8.800	0.287	2.05	0.63
	3.910	8.829	0.255	2.04	0.70
	3.905	8.865	0.211	2.02	0.79
	3.900	8.887	0.180	2.03	0.86
	3.895	8.909	0.145	2.02	0.93
0.20	3.980	7.483	0.580	1.73	0.04
	3.975	8.187	0.530	1.70	0.14
	3.970	8.354	0.478	1.66	0.25
	3.965	8.476	0.427	1.62	0.36
	3.960	8.561	0.384	1.60	0.46
	3.955	8.606	0.347	1.58	0.54
	3.950	8.648	0.312	1.57	0.62
	3.945	8.684	0.276	1.56	0.71
	3.940	8.715	0.241	1.55	0.79
	3.935	8.740	0.208	1.54	0.87
	3.930	8.762	0.176	1.53	0.95
	3.925	8.782	0.144	1.52	1.03
	3.920	8.803	0.103	1.50	1.11

TABLE 4.
Age calibration for three groups of model sequences.

$\log M/M_{\odot}$	$X = 0.70,$		$Y = 0.27,$		$Z = 0.03,$		$\alpha = 1.0$	
	0.05		0.10		0.15		0.20	
$\log \text{Age}$	$\log T_e$	ΔM_{bol}	$\log T_e$	ΔM_{bol}	$\log T_e$	ΔM_{bol}	$\log T_e$	ΔM_{bol}
8.30...	3.900	0.09
8.35...	3.899	0.11
8.40...	3.898	0.12
8.45...	3.897	0.14
8.50...	3.859	0.09	3.896	0.16
8.55...	3.859	0.10	3.894	0.18
8.60...	3.858	0.12	3.893	0.20
8.65...	3.858	0.13	3.892	0.23
8.70...	3.822	0.09	3.857	0.15	3.890	0.26
8.75...	3.821	0.11	3.856	0.17	3.887	0.30
8.80...	3.820	0.12	3.855	0.20	3.884	0.35
8.85...	3.819	0.14	3.853	0.23	3.881	0.41
8.90...	3.819	0.16	3.851	0.27	3.877	0.48
8.95...	3.789	0.08	3.818	0.19	3.849	0.31	3.871	0.56
9.00...	3.789	0.10	3.816	0.21	3.846	0.36	3.865	0.67
9.05...	3.788	0.13	3.815	0.25	3.842	0.43	3.854	0.82
9.10...	3.788	0.15	3.813	0.29	3.836	0.52	3.839	1.01
9.15...	3.787	0.17	3.811	0.34	3.829	0.62
9.20...	3.787	0.19	3.808	0.40	3.820	0.76
9.25...	3.786	0.22	3.805	0.47	3.807	0.97
9.30...	3.785	0.25	3.800	0.57
9.35...	3.784	0.30	3.794	0.69
9.40...	3.782	0.35	3.785	0.84
9.45...	3.780	0.42
9.50...	3.776	0.51
9.55...	3.770	0.63

$\log M/M_{\odot}$	$X = 0.70,$		$Y = 0.27,$		$Z = 0.03,$		$\alpha = 2.0$	
	0.05		0.10		0.15		0.20	
$\log \text{Age}$	$\log T_e$	ΔM_{bol}	$\log T_e$	ΔM_{bol}	$\log T_e$	ΔM_{bol}	$\log T_e$	ΔM_{bol}
8.25...	3.900	0.10
8.30...	3.899	0.11
8.35...	3.899	0.12
8.40...	3.898	0.13
8.45...	3.897	0.15
8.50...	3.896	0.16
8.55...	3.863	0.09	3.895	0.19
8.60...	3.863	0.10	3.893	0.21

(to be continued)

TABLE 4 (continued).

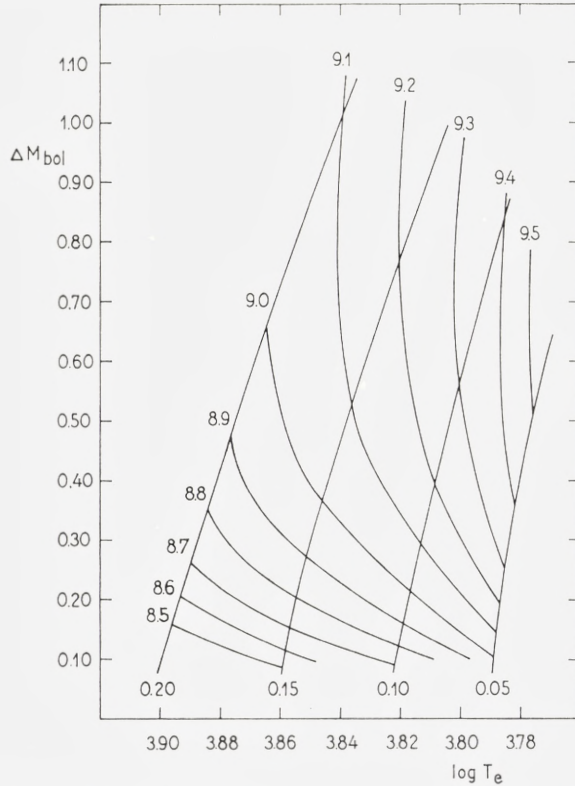
$X = 0.70,$			$Y = 0.27,$		$Z = 0.03,$		$\alpha = 2.0$		
$\log M/M_{\odot}$	0.05		0.10		0.15		0.20		
$\log \text{Age}$	$\log T_e$	ΔM_{bol}	$\log T_e$	ΔM_{bol}	$\log T_e$	ΔM_{bol}	$\log T_e$	ΔM_{bol}	ΔM_{bol}
8.65...	3.862	0.12	3.892	0.24	
8.70...	3.862	0.13	3.890	0.27	
8.75...	3.838	0.10	3.861	0.15	3.888	0.31	
8.80...	3.837	0.11	3.860	0.18	3.885	0.36	
8.85...	3.837	0.13	3.859	0.21	3.882	0.42	
8.90...	3.837	0.15	3.857	0.25	3.878	0.48	
8.95...	3.836	0.17	3.855	0.29	3.873	0.57	
9.00...	3.835	0.20	3.853	0.35	3.866	0.67	
9.05...	3.835	0.23	3.851	0.42	3.856	0.85	
9.10...	3.817	0.10	3.833	0.28	3.847	0.50	3.846	1.06	
9.15...	3.816	0.13	3.832	0.33	3.843	0.61	
9.20...	3.816	0.16	3.830	0.38	3.836	0.76	
9.25...	3.815	0.19	3.828	0.45	3.829	0.95	
9.30...	3.815	0.22	3.824	0.55	
9.35...	3.814	0.26	3.820	0.66	
9.40...	3.812	0.30	3.815	0.79	
9.45...	3.811	0.34	
9.50...	3.808	0.42	

$X = 0.60,$			$Y = 0.37,$		$Z = 0.03,$		$\alpha = 2.0$			
$\log M/M_{\odot}$	0.00		0.05		0.10		0.15		0.20	
$\log \text{Age}$	$\log T_e$	ΔM_{bol}	$\log T_e$	ΔM_{bol}	$\log T_e$	ΔM_{bol}	$\log T_e$	ΔM_{bol}	$\log T_e$	ΔM_{bol}
8.05...	3.976	0.12
8.10...	3.945	0.09	3.975	0.14
8.15...	3.944	0.10	3.974	0.16
8.20...	3.943	0.12	3.973	0.18
8.25...	3.909	0.09	3.943	0.13	3.972	0.20
8.30...	3.908	0.10	3.942	0.15	3.971	0.22
8.35...	3.908	0.11	3.940	0.17	3.970	0.26
8.40...	3.907	0.12	3.939	0.20	3.968	0.30
8.45...	3.874	0.09	3.907	0.14	3.938	0.22	3.966	0.34
8.50...	3.873	0.10	3.906	0.16	3.936	0.26	3.963	0.39
8.55...	3.873	0.11	3.904	0.19	3.934	0.29	3.960	0.46
8.60...	3.848	0.09	3.873	0.12	3.902	0.22	3.932	0.34	3.956	0.53
8.65...	3.848	0.10	3.872	0.14	3.900	0.25	3.929	0.39	3.950	0.63
8.70...	3.847	0.12	3.871	0.16	3.898	0.29	3.925	0.45	3.942	0.75
8.75...	3.847	0.13	3.870	0.19	3.896	0.33	3.921	0.54	3.933	0.91
8.80...	3.847	0.14	3.896	0.22	3.893	0.38	3.915	0.63	3.921	1.10

(to be continued)

TABLE 4 (continued).

log M/M_{\odot}	$X = 0.60,$		$Y = 0.37,$		$Z = 0.03,$		$\alpha = 2.0$			
	0.00		0.05		0.10		0.15		0.20	
log Age	log T_e	ΔM_{bol}	log T_e	ΔM_{bol}	log T_e	ΔM_{bol}	log T_e	ΔM_{bol}	log T_e	ΔM_{bol}
8.85 ...	3.846	0.16	3.868	0.25	3.891	0.43	3.907	0.75
8.90 ...	3.846	0.18	3.867	0.29	3.887	0.50	3.897	0.90
8.95 ...	3.845	0.21	3.864	0.34	3.881	0.60
9.00 ...	3.844	0.24	3.861	0.40	3.872	0.73
9.05 ...	3.843	0.28	3.857	0.49	3.862	0.91
9.10 ...	3.842	0.32	3.852	0.60
9.15 ...	3.840	0.37	3.847	0.73
9.20 ...	3.838	0.44	3.843	0.88
9.25 ...	3.835	0.51
9.30 ...	3.831	0.61

Figure 4. Mass and age calibration for $X = 0.70$, $Y = 0.27$, $Z = 0.03$, and $\alpha = 1$.

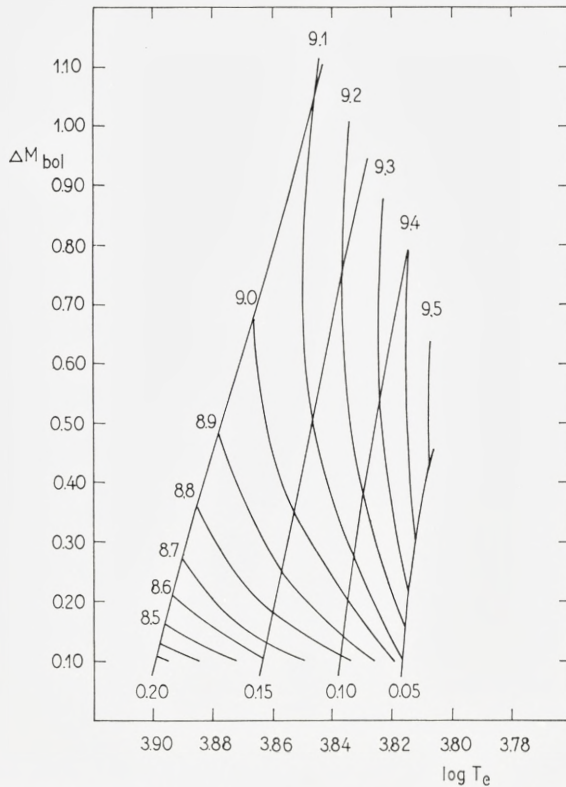


Figure 5. Mass and age calibration for $X = 0.70$, $Y = 0.27$, $Z = 0.03$, and $\alpha = 2$.

and the luminosity of the individual models it is evident that the present models can not be fitted directly to the sequence of models obtained by KELSALL and STRÖMGREN. If we estimate, where we should expect an evolutionary track for a model of a mass given by $\log M/M_{\odot} = 0.25$ to be located, by a rough extrapolation of the results derived for smaller masses, and make a comparison with the corresponding track as given by KELSALL and STRÖMGREN, we find that their models are somewhat less luminous than ours. This is probably due to the fact that different opacities have been used in the envelopes of the models in the two cases. The envelope opacities in our models (based on the BAKER-tables) do not include line opacities, and are therefore considerably smaller than those used by KELSALL and STRÖMGREN. We should expect, that the use of smaller envelope opacities would result in larger luminosity and higher effective temperature, and this is precisely the effect which is found.

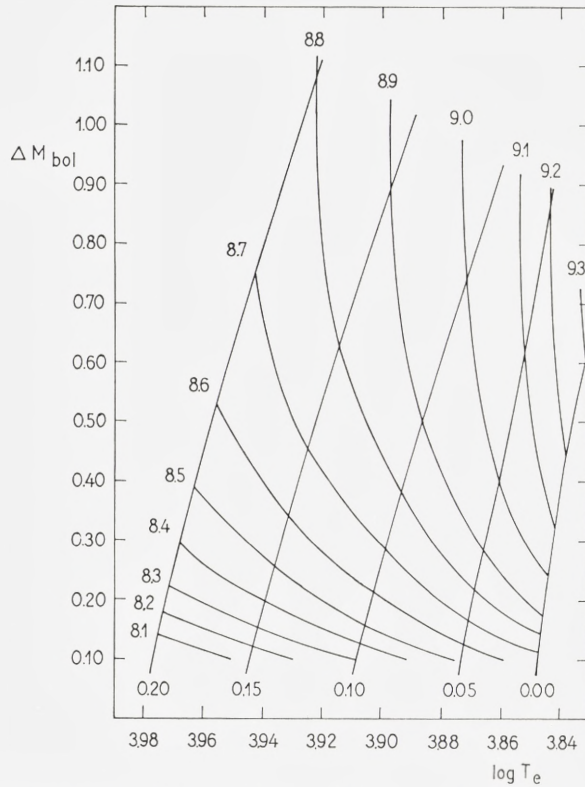


Figure 6. Mass and age calibration for $X = 0.60$, $Y = 0.37$, $Z = 0.03$, and $\alpha = 2$.

In order to investigate this matter in more detail we have constructed similar models in which the envelopes contain a much smaller part of the total mass, by means of the computer programmes described by PETERSEN (1966). The results are shown in Figures 2 and 3. The number attached to each sequence gives the relative mass of the envelopes with an opacity computed without the line contribution. It is seen that the luminosity does increase when the relative mass of the envelope increases, as was to be expected.

The calibration of the HERTZSPRUNG-RUSSELL diagram has been performed by means of second order interpolation in the data of the model sequences just described. Following KELSALL and STRÖMGREN (1966) we have, for equidistant values of $\log T_e$, computed ΔM_{bol} , defined as M_{bol} (zero-age line) $- M_{\text{bol}}$ (model sequence), using the zero-age models of the chemical composition in question, to derive M_{bol} for the zero-age line. In

order to facilitate the age calibration we have also calculated $\log T_e$ and ΔM_{bol} corresponding to the age values given by \log (Age in years) equal to 8.05, 8.10, up to the last model in the main-sequence stage ($X_c \approx 0.08$) for each evolutionary track. The results are given in Tables 3 and 4, and curves of equal mass and equal age in the $(\log T_e, \Delta M_{\text{bol}})$ diagram are shown in Figures 4, 5, and 6. From such figures the age and mass of a single main-sequence star can be derived, provided that observations can supply sufficiently accurate information about $\log T_e$, ΔM_{bol} , and the chemical composition of the star.

4. Discussion

Comparing Figures 4, 5, and 6 with the calibration diagrams for B and A stars in the paper by KELSALL and STRÖMGREN (*loc. cit.*) it is seen that the interval in ΔM_{bol} covered by a model sequence (curve of constant mass) becomes smaller for the later spectral types. This expresses the fact that the expected accuracy in the age determination, by a comparison of observations and the calibration curves, is higher for the early spectral types than for the later. And for spectral types later than about G0 this method for age determination of main-sequence stars clearly can not be applied at all, since the evolutionary tracks in the corresponding region of the HERTZSPRUNG-RUSSELL diagram follow the zero-age line, in contrast to the upper main-sequence, where the tracks are nearly perpendicular to this line.

In addition, also other effects tend to make the age determination for the later spectral types more difficult than for earlier types. The influence of differences in chemical composition becomes important for the later types because the value of ΔM_{bol} , that is derived from observations of a certain star, is dependent on the chemical composition, characterized by X and Z , determining which zero-age line one has to use. Consequently accurate determinations of mass and age can only be obtained if, for the sample of stars considered, the range of variation of X and Z is fairly limited. With regard to Z , selection of the sample of stars according to observations of a metal-content index may lead to a satisfactory solution. A discussion of this question is beyond the scope of the present investigation since the calculations have been carried out for one Z value only. With regard to the influence of variation in X , we conclude from our calculations that the effect on age determination is serious for the later spectral types unless the range

of variation of X is relatively small (less than 0.1), which may however well be the case.

We note in this connection that when ΔM_{bol} is determined spectroscopically, what matters in the context mentioned is the change of the relation between surface gravity and effective temperature with X .

Uncertainty concerning the appropriate value of the mixing length also contributes considerably to the uncertainty in the derived values of mass and age for the later types. From Figures 4 and 5 it is seen that this uncertainty is small for $\log T_e \geq 3.86$, but that it increases quickly for lower effective temperatures. For instance, for $\log T_e = 3.824$ and $\Delta M_{\text{bol}} = 0.54$ we will derive $\log M/M_\odot = 0.13$ and $\log(\text{Age in years}) = 9.16$ from Figure 4 (the case of $\alpha = 1$), while Figure 5 ($\alpha = 2$) gives the values 0.10 and 9.30 for the same quantities. Since the value of α is about 1.5 for main-sequence stars (see e.g. BAKER 1963) the realistic values of mass and age are probably intermediate between the values derived from Figures 4 and 5.

For earlier spectral classes, on the other hand, the interval in T_e covered by an evolutionary track is considerably larger and ΔM_{bol} , therefore, does not depend critically on the chemical composition, especially near the upper boundary of the main-sequence.

In view of above mentioned circumstances it seems unlikely that calibration of the present type (for stars with $X_c > 0.08$) can be utilized for accurate age determination for stars of spectral classes later than about F3. This means that the method considered here can only give reasonably accurate results for stars younger than about $2-3 \times 10^9$ years. Ages derived for spectral types later than about F3 will probably have only statistical significance.

It is noticeable that the isochrones in Figures 4, 5, and 6 are almost vertical in the upper part of the main-sequence band. Therefore any measure of effective temperature, for instance a colour index, is also an indicator of age in this part of the diagram. DENNIS (1966) has used this fact to derive ages for three groups of stars with $0.220 \leq \text{b-y} < 0.290$, $0.290 \leq \text{b-y} < 0.330$, and $0.330 \leq \text{b-y} \leq 0.390$, respectively, by means of the present age-calibration. He found, as would be expected, that the dispersion in the velocity perpendicular to the plane of the Galaxy for these three groups of stars increases with the derived ages.

Acknowledgements

The authors wish to thank Professor BENGT STRÖMGREN for stimulating discussions; one of them (A. R.) is grateful to the late Professor ROBERT J. OPPENHEIMER for his kind hospitality at the Institute for Advanced Study, where this work was begun. The calculations have been carried out by means of the GIER computer made available to the Copenhagen Observatory by the Carlsberg Foundation.

Copenhagen University Observatory

References

- ALLEN, C. W., 1955, *Astrophysical Quantities* (London, Athlone Press).
—, 1963, *Astrophysical Quantities* (London, Athlone Press).
BAKER, N., 1963, *Tables of Convective Stellar Envelope Models*, Goddard Institute for Space Studies, New York.
COX, A. N., 1965, *Stars and Stellar Systems*, Vol. 8, ed. L. H. ALLER and D. B. McLAUGHLIN (Chicago, Univ. of Chicago Press), Chapter 3.
DENNIS, T. R., 1966, *Ap. J.* *146*, 581.
HALLGREN, E. L. and DEMARQUE, P. R., 1966, *Ap. J.* *146*, 430.
—, 1967, *Ap. J.* *148*, 817.
HARRIS III, D. L., 1963, *Stars and Stellar Systems*, Vol. 3, ed. K. AA. STRAND (Chicago, Univ. of Chicago Press), Chapter 14.
IBEN, I., 1967, *Ap. J.* *147*, 624.
KELSALL, T. and STRÖMGREN, B., 1966, *Vistas in Astronomy*, Vol. 8, ed. A. BEER and K. AA. STRAND (New York, Pergamon Press), p. 159.
PETERSEN, J. O., 1966, *Publikationer og mindre Meddelelser fra Københavns Observatorium*, Nr. 186.
REEVES, H., 1965, *Stars and Stellar Systems*, Vol. 8, ed. L. H. ALLER and D. B. McLAUGHLIN (Chicago, Univ. of Chicago Press), Chapter 2.
REIZ, A., 1965, *The Observatory* *85*, 128.
— and PETERSEN, J. O., 1964, *Publikationer og mindre Meddelelser fra Københavns Observatorium*, Nr. 182.
STRÖMGREN, B., 1963, *Quart. J. Roy. Astron. Soc.* *4*, 8.

